Best Available Copy

20030204141

SECURITY CLASSIFICATION OF THIS PAGE

REPORT DOCUMENTATION PAGE

1a.	1b. RESTRICTIVE MARKINGS N/A
2a. AD-A208 927	3. DISTRIBUTION/AVAILABILITY OF REPORT unlimited
2b. N/A	
4. PERFORMING ORGANIZATION REPORT NUMBER(S) N/A	5. MONITORING ORGANIZATION REPORT NUMBER(S) N/A
6a. NAME OF PERFORMING ORGANIZATION University of California	6b. OFFICE SYMBOL (If applicable) N/A
7a. NAME OF MONITORING ORGANIZATION OSD/SDIO/TA Technology Application Program	
6c. ADDRESS (City, State, and ZIP Code) Beckman Laser Institute & Medical Clinic 1002 Health Sciences Road East Irvine, California 92715	7b. ADDRESS (City, State, and ZIP Code) OSD/SDIO/TA Washington, D.C. 20301-7100
8a. NAME OF FUNDING/SPONSORING ORGANIZATION Strategic Defense Initiative Organization	8b. OFFICE SYMBOL (If applicable)
9. PROCUREMENT INSTRUMENT IDENTIFICATION NUMBER N00014-86-k-0115	
8c. ADDRESS (City, State, and ZIP Code) Washington, D.C. 20301-7100	10. SOURCE OF FUNDING NUMBERS: PROGRAM ELEMENT NO. / PROJECT NO. / TASK NO. / WORK UNIT ACCESSION

11. TITLE (Include Security Classification)
Biomedical Studies with the Free Electron Laser (U)

12. PERSONAL AUTHOR(S)
Michael W. Berns

13a. TYPE OF REPORT	13b. TIME COVERED	14. DATE OF REPORT (Year, Month, Day)	15. PAGE COUNT
Final	FROM 2/1/86 to 1/31/88	5/15/89	5

16. SUPPLEMENTARY NOTATION

17. COSATI CODES			18. SUBJECT TERMS (Continue on reverse if necessary and identify by block number)
FIELD	GROUP	SUB-GROUP	Free Electron Laser, autoradiography

19. ABSTRACT (Continue on reverse if necessary and identify by block number)

See Summary of Work Completed Pages 3-5.

DTIC ELECTE JUN 06 1989 S D H

DISTRIBUTION STATEMENT A
Approved for public release
Distribution Unlimited

20. DISTRIBUTION/AVAILABILITY OF ABSTRACT	21. ABSTRACT SECURITY CLASSIFICATION
☒ UNCLASSIFIED/UNLIMITED ☐ SAME AS RPT ☐ DTIC USERS	U
22a. NAME OF RESPONSIBLE INDIVIDUAL Nick Montanarelli /Michael Marron	22b. TELEPHONE (Include Area Code) (202) 693-1556 / 22c. OFFICE SYMBOL OSD/SDIO T/TA

DD FORM 1473, 84 MAR — 83 APR edition may be used until exhausted. All other editions are obsolete. SECURITY CLASSIFICATION OF THIS PAGE

Best Available Copy

Best Available Copy

FINAL TECHNICAL REPORT

Biomedical Studies with the Free Electron Laser

Contract Period: 2/1/86-2/1/88
Contract No.
Contractee: Beckman Laser Institute and Medical Clinic
Principal Investigator: Michael W. Berns, Ph.D.

89 6 05 159

Best Available Copy

TABLE OF CONTENTS

1. Summary of Work

2. Index of Technical Reports (Progress Report 4/15/88)

3. Index of Publications: 26 abstracts of work presented
23 published papers

Accession For
NTIS GRA&I ☑
DTIC TAB ☐
Unannounced ☐
Justification
By
Distribution/
Availability Codes
Dist | Avail and/or Special
A-1

SUMMARY OF WORK COMPLETED

The original objectives of this project were to initiate studies on the University of California Santa Barbara Free Electron Laser (wavelength range 1 micron to 1 millimeter) and explore the potential biological and medical effects and applications in this wavelength range. Following initiation of the studies, it was realized rather quickly that the limitations of current FEL technology (not only for the Santa Barbara FEL) would really restrict the studies for the contract period to a wavelength range of 100-200 micrometers on the FEL. After full discussions with the contract monitor (C. Houston), a much broader ranger of contract objectives was outlined as secondary "spinoff" goals of this project (see attachment A to this summary). These goals were consistent with those projected for other SDIO MFEL funded sites (Utah and Harvard, in particular). Work on these secondary goals involved studies in the following areas: (1) laser plus dye photosensitization of cancer, (2) laser tissue interactions for the study of atherosclerosis, (3) pulsed laser effects on the eye, (4) laser application in genetic engineering and cell proliferation, (5) pulsed laser surgery, and (6) pulsed laser mutagenesis. Over 22 papers and 24 abstracts have been published as a direct result of the studies funded from this contract (see attachments in appendix 3).

The primary studies on the FEL were conducted at two wavelengths, 165 and 200 micrometers. These were the first studies in the world conducted in this wavelength range on live biological material. The publication resulting in the journal Photochemistry and Photobiology (46:165-167, 1987) was the first such study published. This study demonstrated a clear effect of the 200 micrometer FEL wavelength on DNA synthesis in a subpopulation of growing epithelial cells from the kidney of the rat kangaroo. In addition to demonstrating a new phenomenon that can be extrapolated to other biological systems, these studies also established the protocol and parameters for the use of the far IR FEL in biomedicine. Parameters such as beam profile and fluence were determined in addition to the actual logistics of conducting the experiments. The first three experimental series were conducted by remote control with the cells contained within the laser room and monitored by video. The latter series of experiments were conducted in a user room where the FEL beam was transmitted via reflectors from the laser vault. The results of all of these experiments is included in the progress report dated 4/15/88 and is included in section 2., Technical Reports. The overall conclusion of these experiments was that the two different IR FEL wavelengths tested could be used to affect either RNA or DNA

selectively: 165 micrometers affected RNA synthesis and 200 micrometers affected DNA. This finding could have far reaching implications for both the study of nucleic acids in vivo and in vitro, and possibly for the selective manipulation of these molecules (and their synthesis) in living systems. Of particular importance is gaining an adequate understanding of the nature of the phenomena. Further studies are being conducted to elucidate the biological (cellular) nature of the observations as well as the physical-chemical basis for them. These are major objectives of the current contract.

The secondary objectives of the contract were to study laser tissue/cellular effects with the ultimate determination of optimal laser parameters for a biomedical FEL. The over 40 papers and abstracts published as a result of this contract funding are included in Section 3 of this report. Below are listed the general highlights of these studies. Please refer to the appropriate article/abstract for further detail.

1. Dye plus laser photosensitization of cancer. Significant progress was made in elucidating the fundamental photophysical and structural basis for tumor destruction by this method. The mechanism appears to be singlet oxygen mediated. The subcellular target sites vary depending upon the type of photosensitizer used (chlorins for lysosomes, porphyrins for mitochondria etc). At the tumor level, the destruction appears to involve breakdown of the tumor vasculature.

2. Laser effects on atherosclerotic disease: In this area a variety of studies were conducted in which CW and pulsed lasers were examined with respect to their potential to remove plaque from blood vessels either surgically or non-surgically through a catheter. The most promising results have come with the pulsed excimer laser operating at 308 nm. However, other studies using pulsed IR wavelengths from the Erbium:YAG laser at 2.9 microns show promise because of the ability to cut hard calcified bone. This result would suggest that an FEL emitting in the near and mid-IR region might be effective for this application. These wavelengths might have advantage over the excimer UV wavelengths because of the reduced risk of mutagenesis.

3. Pulsed laser studies in the eye. Pulsed frequency doubled YAG laser (532) was investigated for its potential to perform retinal surgery. The characteristics of single pulses versus a train of pulses were examined in rabbit eyes. The results suggest that a rapidly pulsing doubled YAG laser can be effective in producing controlled retinal burns. In another study, the pulsed 193 nm excimer laser was investigated for its potential to produce controlled, precise ablation on the cornea. These studies involved light and electron microscopic analysis of acute and long term lesions. In addition, the

first study demonstrating a thermal component to the ablation process of a pulsed excimer laser was conducted and published. This study employed thermal camera which was purchased with contract funds and will provide valuable data in the future on pulsed laser effects.

4. Genetic and cell motility experiments. Studies with pulsed frequency doubled, tripled, and quadrupled YAG laser wavelengths were undertaken in order to manipulate cell genetics and cell motility. These studies resulted in the demonstration of laser-induced gene insertion, and laser microsurgery of the subcellular cytoskeleton. In addition to producing valuable information on the nature of pulsed laser effects on cells, these studies also revealed important information in cell biology and genetics. Furthermore, the studies demonstrated a major future role for pulsed laser effects in the manipulation of cells and tissues. Since the FEL will be a pulsed mode laser system, studies of this type are invaluable for the future assessment of FEL application.

5. Pulsed laser tissue surgery. Pulsed infrared and ultraviolet lasers were used to study the potential of these laser parameters for the controlled ablation of hard tissue. Of particular interest was the use of these lasers for bone surgery and removal of hard methacrylate bone cement. They were also investigated for removal of atherosclerotic plaque (see previous discussion). The results were presented at several meetings and in several research articles.

6. Pulsed laser mutagenesis. Very few studies have been conducted elucidating the mutagenic effect of pulsed lasers. We have published a definitive study examining the 193 and 308 nm wavelengths from the excimer laser. These studies showed a clear mutagenic potential of both of these wavelengths and compared them to a standard mutation source. Though most of the effects were believed to be a result of single photon absorption, multiphoton events could not be ruled out entirely. It was also observed that even though mutagenesis was detected in the several assay systems used, the amount of mutagenesis was 1-3 orders of magnitude less than standard mutation sources. Notwithstanding, it is still of importance to define the levels of mutagenesis when pulsed lasers are being used and, in particular, to determine if high fluences and peak powers can best result in multiphoton-induced mutagenesis.

In summary, considerable progress was made in achieving the primary goal of this contract: studies on the biological effects/potential of the FEL. Enormous progress was made in the secondary objectives, which focused on elucidating the mechanisms and effects of pulsed lasers on tissue. This information will be important in the overall consideration of FEL design.

FEL PROJECTS - BERNS Best Available Copy A

1. Characterization of Far IR (25-200 um) FEL wavelengths on cell growth, DNA, & RNA synthesis.

2. Determination of wavelength dependency of cellular effects (action spectrum analysis of Far IR FEL) in order to elucidate the basic mechanisms of photon interaction (Photon - Photon interactions).

3. Elucidation of usual parameters (using conventional lasers) desirous in an FEL for basic biological studies.

(a) cell structure/function
(b) cellular diagnostics
(c) tissue biophysics/optics
(d) non-linear multiphoton events.
(e) optical levitation

4. Elucidation of laser parameters (using conventional lasers) desirous in an FEL for medical and veterinary treatment/diagnosis.

(a) laser angioplasty

(b) Photodynamic therapy / diagnosis

(c) hard tissue (bone) surgery

(d) pulsed laser ablation of eye (corneal) tissue

(e) analysis of laser tissue - interaction bi-products (safety)

Best Available Copy

SECURITY CLASSIFICATION OF THIS PAGE

REPORT DOCUMENTATION PAGE

1a. REPORT SECURITY CLASSIFICATION U	1b. RESTRICTIVE MARKINGS N/A
2a. SECURITY CLASSIFICATION AUTHORITY N/A	3. DISTRIBUTION/AVAILABILITY OF REPORT unlimited
2b. DECLASSIFICATION/DOWNGRADING SCHEDULE N/A	
4. PERFORMING ORGANIZATION REPORT NUMBER(S) N/A	5. MONITORING ORGANIZATION REPORT NUMBER(S) N/A
6a. NAME OF PERFORMING ORGANIZATION University of California 6b. OFFICE SYMBOL (If applicable) N/A	7a. NAME OF MONITORING ORGANIZATION OSD/SDIO/TA Technology Application Program
6c. ADDRESS (City, State, and ZIP Code) Beckman Laser Institute & Medical Clinic 1002 Health Sciences Road East Irvine, California 92715	7b. ADDRESS (City, State, and ZIP Code) OSD/SDIO/TA Washington, D.C. 20301-7100
8a. NAME OF FUNDING/SPONSORING ORGANIZATION Strategic Defense Initiative Organization 8b. OFFICE SYMBOL (If applicable)	9. PROCUREMENT INSTRUMENT IDENTIFICATION NUMBER N 0014-87-K-0431
8c. ADDRESS (City, State, and ZIP Code) Washington, D.C. 20301-7100	10. SOURCE OF FUNDING NUMBERS PROGRAM ELEMENT NO. / PROJECT NO. / TASK NO. / WORK UNIT ACCESSION NO.

11. TITLE (Include Security Classification)
Biomedical Studies with the Free Electron Laser (U)

12. PERSONAL AUTHOR(S)
Michael W. Berns

13a. TYPE OF REPORT	13b. TIME COVERED	14. DATE OF REPORT (Year, Month, Day)	15. PAGE COUNT
Progress	FROM 2/1/87 TO 1/31/88	4/15/88	5

16. SUPPLEMENTARY NOTATION

17 COSATI CODES			18. SUBJECT TERMS (Continue on reverse if necessary and identify by block number)
FIELD	GROUP	SUB-GROUP	Free Electron Laser, autoradiography

19. ABSTRACT (Continue on reverse if necessary and identify by block number)

see attached abstract on following page

20. DISTRIBUTION/AVAILABILITY OF ABSTRACT ☒ UNCLASSIFIED/UNLIMITED ☐ SAME AS RPT ☐ DTIC USERS	21. ABSTRACT SECURITY CLASSIFICATION U
22a. NAME OF RESPONSIBLE INDIVIDUAL Charles L. Houston, III, Captain, USAF	22b. TELEPHONE (Include Area Code) (202)693 1556 22c. OFFICE SYMBOL OSD/SDIO/TA

DD FORM 1473, 84 MAR 83 APR edition may be used until exhausted. SECURITY CLASSIFICATION OF THIS PAGE

PROGRESS REPORT

BIOMEDICAL STUDIES WITH THE FREE ELECTRON LASER

Contract Number:	N00014-86-K-0115
Contract Period.	2/1/87-1/31/88
Principal Investigator:	Michael W. Berns, Ph.D.
Contractor	University of California Irvine

ABSTRACT

The electrostatic VandeGraff FEL at the University of California, Santa Barbara was used to study the effects of infrared radiation on the synthesis of DNA and RNA in living vertebrate cells in culture. The laser was operated at wavelengths of 165 and 200 microns at power densities of 0.1 - 30 KW/cm^2. Cells were incubated in radioactive precursors to either DNA or RNA following exposure to the FEL and analyzed by light microscope autoradiography. The results indicated that the 200 um wavelength inhibited DNA but not RNA synthesis in a subpopulation of cells and the 165 micron wavelength inhibited RNA synthesis and not DNA synthesis. The statistical significance for the 200 micron wavelength studies was p = 0.05 and for the 165 micron wavelength studies p = 0.001 - 0.005.

PROJECT OBJECTIVES

The main objectives of this research are to determine if the FEL has unique biological effects and if these effects can be used (1) to shed light on basic biological processes, and (2) to develop clinical diagnostic and therapeutic procedures.

EXPERIMENTAL RESULTS

In our initial studies (Berns and Bewley, 1987), we demonstrated that the Santa Barbara FEL operating at 200 microns (100 W/cm^2/pulse) caused an inhibition of DNA synthesis in a statistically significant number of cells. This was one of the first experimental studies using the FEL on a living biological system. Subsequent studies with the same wavelength looking at RNA synthesis by uridine autoradiography indicated no effect on the cells, thus suggesting a selective effect of the 200 micron wavelength on double stranded nucleic acid (DNA). The statistical significance of these studies was at p = 0.05 level. These results were reported at the Seventh Annual Meeting of the American Society of Lasers in Surgery and Medicine in San Francisco (Berns, Bewley, Elias, and Jaccarino).

More recent studies have employed the Santa Barbara FEL operating at 165 microns with a pulse width of 1 us. The laser energy was approximately 1 mJ per pulse. The pulse repetition frequency was .33 Hz. The optical transport of the FEL provided a beam focused to a spot with a 1/e half-width of approximately 1 mm.

The culture chambers were placed with their window surfaces at the focus. Each window was covered by a mask with a 4 mm diameter aperture in it. The beam spot from the FEL was located to within ± 1 mm of the center of the aperture with the HeNe alignment beam provided. The energy per pulse of the beam was measured using a Laser Precision RYP 735 RF pyroelectric detector. The reflectivity of the detector element, as measured by Mayer et al., 1986 was accounted for in determining the absolute energy per pulse. A Mylar beam splitter in the path of the incident beam provided a reference signal that was used to monitor the energy per pulse during the experiment. The reference detector was a Molectron model P3-01 pyroelectric detector and was calibrated with the Laser Precision detector mentioned earlier. The power density per pulse at the center of the beam was typically 30 kw/cm^2. The transmission of the quartz windows was determined from the ratios of the sample and reference signals with the windows alternately placed into and removed from the sample beam path. The transmission of the window was found to be approximately 84%. The transmission of a window with cells on it and no adjacent fluid was measured similarly and did not vary from the simple window case to within the 1% accuracy of the measurement.

The cell cultures in this experimental series received either 50 or 100 pulses from the FEL. Cells were placed into a 37°C incubator immediately following exposure to the FEL and transported to Irvine where they were incubated in either tritiated thymidine (DNA precursor, 2.5 μCi/ml) or tritiated uridine (RNA precursor, 5 μCi/ml). The exposure to the nucleic acid precursor occurred up to 3 hours following exposure to the FEL and was for a duration of 12 hours for the uridine and 36 hours for the thymidine. The cells were then subjected to standard autoradiographic analysis in order to determine if the irradiated cells exhibited any alteration in DNA or RNA synthesis as compared to control populations. The control cells were cells in the irradiation chamber that were shielded from the FEL beam by the metal ring. The autoradiograms were scored blindly by a person not familiar with the experimental series. A second individual scored a random number of the experimental chambers in order to verify the accuracy of the first individual. The results indicated that at 165 microns RNA synthesis was inhibited and DNA synthesis was unaffected. The statistical significance of this study was high. $p = 0.001 - 0.0005$. The data for both the 200 μm and 165 micron studies are presented in the following table.

Though the dosimetric parameters for the two wavelengths used were not identical (due to technical difficulties with the FEL), the results are intriguing nonetheless. It appears that two different nucleic acids can be affected selectively as a function of wavelength. The nature of these effects, and whether or not an action spectrum of the response can be determined are subjects for future experimentation.

Cells With "Light" Radioactive Label

165 μm	100 pulses ($\bar{x}$ of 500 cells)	50 pulses ($\bar{x}$ of 500 cells)	
uridine experimental	359.20	388.6	
uridine control	327.26	348.3	p = .001-.005 ∴ sig. diff
thymidine experimental	43.7	39.2	
thymidine control	38.1	42.2	p = .09 - .11 ∴ no sig. diff.

200 μm	100 pulses ($\bar{x}$ of 100 cells)	100 pulses ($\bar{x}$ of 100 cells)	
uridine experimental	68.6	70.4	
uridine control	63.5	64	p = .6 - .7 ∴ no sig. diff.
thymidine experimental	70	74	
thymidine control	43	43	p = .05 ∴ sig. diff.

FUTURE GOALS

The major objectives of future studies are (1) to determine action spectra for the effects on both nucleic acids, (2) to determine if there is a relationship between the phase of the cell cycle and the observed response, (3) to employ additional biological assays such as protein synthesis and membrane transport assays.

Best Available Copy

REFERENCES

1. Mayer, A and F Keilman (1986) Far-infrared nonlinear optics. I $X^{(2)}$ near ionic resonance. Physical Review B. 33: 6954-6961.

2. Berns M. W. and W. Bewley (1987). Inhibition of nucleic acid synthesis in cells exposed to 200 micrometer radiation from the Free Electron Laser. Photochem. Photobiol. 46:165-167.

3. Berns, M. W., W. Bewley, L. R. Elias and V. Jaccarino. Biological studies of the Free Electron Laser. Presented at Seventh Annual Meeting of Amer. Soc. for Laser Medicine and Surgery Annual Meeting, San Francisco, CA, April 11-13, 1987 (a).

4. Berns, M. W. and W. Bewley. Differential inhibition of nucleic acid synthesis in tissue culture using the far infrared wavelengths of the Free Electron Laser. To be presented at Eighth Annual Meeting of Amer. Soc. for Laser Medicine and Surgery Annual Meeting, Dallas, Texas, April 25-27, 1988 (a).

Photodynamic Therapy of Human Malignant Melanoma Xenografts in Athymic Nude Mice[1,2]

J. Stuart Nelson,[3,4] Jerry L. McCullough,[5] Michael W. Berns[3,4,5,6]

While photodynamic therapy (PDT) for cutaneous malignancies including dermal recurrences of breast cancer and basal cell carcinomas has shown great promise, PDT of malignant melanoma has remained incompletely understood. A comparison study of the effects of PDT in human xenograft amelanotic and melanotic malignant melanoma in the athymic nude mouse model was performed. Twenty-four hours after ip administration of Photofrin II, the responses to total laser light doses of 25–300 J/cm^2 were evaluated by histologic examination. Animals were also sacrificed 24 hours after administration of Photofrin II without light, and their uptake and localization of hematoporphyrin derivative (HpD) for each tumor were measured and compared. The results indicate that human xenograft melanotic melanoma, despite the fact that it contains more HpD than does amelanotic melanoma, is far less responsive to PDT. This result appears to be due to the competing chromophore melanin, which may inhibit the photochemical reaction at several key points. [J Natl Cancer Inst 1988;80:56–60]

The basic concept for the use of PDT in the treatment of malignant tumors is that certain molecules can function as photosensitizers. The presence of these photosensitizers in certain cells thus makes these cells vulnerable to light at the appropriate wavelength and intensity. The action of these photosensitizers is generally to absorb photons of the appropriate wavelength sufficient to elevate the sensitizer to an excited state. The excited photosensitizer subsequently reacts with cellular oxygen and results in the production of active cytotoxic radicals leading to tumor destruction. While numerous compounds have been tested as selective photosensitizers of malignant cells, HpD has received the most attention as a selective-tumor-localizing photosensitizer (*1*).

While PDT can be used to reduce relatively large tumors, it appears to be especially advantageous in the treatment of thin superficial tumors easily accessible to light. Since photosensitizers have been used in dermatology to enhance the therapeutic effects of light in treating a wide variety of disorders including vitiligo and psoriasis, a logical extension of PDT would seem to be in the local treatment of malignant lesions involving the skin. While good results have been reported in the treatment of dermal recurrences of breast cancer and basal cell carcinomas (*2*), PDT of malignant melanoma has not been demonstrated.

The purpose of this study is to compare the effectiveness of PDT in causing selective tumor necrosis of human xenograft amelanotic and melanotic malignant melanoma in the athymic nude mouse model. Several reports have indicated that the histology, growth characteristics, biologic behavior, and response to chemotherapeutic agents and other treatment modalities of melanoma xenografts are maintained after serial transplantation in athymic nude mice (*3–5*). It is hoped that this type of study would relate to human clinical studies where some melanomas responded well and others did not.

Materials and Methods

Hematoporphyrin derivative. Photofrin II was obtained from Photomedica Inc., Raritan, NJ, as an aqueous solution at a concentration of 2.5 mg/ml and stored in the dark at −80°C until used. For in vivo experiments, Photofrin II was diluted 1:4 with 0.9% NaCl solution and injected ip.

Animal and tumor system. The congenitally athymic (*nu/nu*) mouse experimental model for human xenograft melanoma has been well described (*6*). Metastatic human amelanotic and melanotic melanoma was harvested fresh from surgical specimens. It was maintained in vivo by serial transplantation in athymic nude mice. For this experiment, tumors were harvested fresh from mice and minced with fine scissors. Transplanted tumors were initiated id in the flanks of each mouse by injecting 0.1 ml of small tumor fragments suspended in RPMI (Grand Island Biological Co., Grand Island, NY). Mouse tumors were allowed to reach a size of 5–7 mm, at which time treatment was started. At this size, the small tumor was homogeneously white and spontaneous tumor necrosis minimal or absent.

Procedure for photosensitization studies. When tumors were of the appropriate size (as indicated above), the animals were shaved in the tumor area and given ip injections of Photofrin II in doses equal to 10 mg/kg (body wt). The remainder of the experiment was done in the dark, including housing of the animals. Control tumor-bearing animals were those that received light without sensitizer and sensitizer without light. Twenty-four hours post injection of Photofrin II, the experimental animals were treated with the laser light delivery system (*see* below). The mouse was anesthetized with Ketamine HCl (Parke, Davis & Co., Detroit, MI) and covered with a metal shield with a circular hole exposing the tumor. Animals were sacrificed 24 hours after PDT

ABBREVIATIONS USED: HpD = hematoporphyrin derivative; PDT = photodynamic therapy.

[1] Received October 21, 1987; revised November 12, 1987; accepted November 24, 1987.

[2] Supported by Public Health Service grants RR-01192 from the Division of Research Resources, National Institutes of Health (NIH), and CA-32248 from the National Cancer Institute, NIH, and by the Office of Naval Research grant N00014-86-K-0115.

[3] Department of Surgery, University of California at Irvine, Irvine, CA 92717.

[4] Beckman Laser Institute and Medical Clinic, University of California at Irvine, 1002 Health Sciences Rd. East, Irvine, CA.

[5] Department of Dermatology, University of California at Irvine.

[6] The authors thank Mr. Glen Profeta and Mr. Jeffrey Andrews for their technical assistance.

by Halothane (Halocarbon Laboratories Inc., Hackensack, NJ) anesthesia. Tissue was excised immediately and fixed in 3% glutaraldehyde: 5% Formalin in phosphate buffer (pH 7.4). Samples were then dehydrated in graded alcohols, cleared in xylene, and embedded in paraffin. Six-micrometer sections were cut, stained with hematoxylin and eosin, cleared of paraffin in xylene, and dried. Sections were examined with an Axiomat microscope (Carl Zeiss, Inc., New York, NY) and photographed with Panatomic X film (Eastman Kodak Co., Rochester, NY).

Laser light delivery system. Laser irradiations were performed with a 770 DL argon dye laser system (Cooper Lasersonics, Santa Clara, CA). The dye used in the dye laser was DCM premixed laser dye (Cooper Lasersonics) with a tuning range of 610-690 nm. The dye laser was tuned to emit radiation at 630 ± 1 nm for the entire experiment. The wavelength was verified using a #5/354 UV monochromator (Jobin Yvon, Longjuneau, France). The radiation was then coupled into a 400-μm fused silica fiber optic by using a model 316 fiber optic coupler (Spectra-Physics, Inc., Mountain View, CA). The output end of the fiber was terminated with a microlens that focused the laser irradiation into a circular field of uniform light intensity. Laser irradiation emanating from the fiber was monitored with a Coherent model 210 power meter before, during, and after treatment. Mice were placed underneath an aperture that controlled the area of light illumination on the tumor site. The area of illumination was 1 cm^2 with a power density of 100 mW/cm^2.

Animals with either the human xenograft amelanotic or melanotic melanoma were treated with the following doses of light: 25, 50, 75, 100, 125, 150, 175, 200, 225, 250, 275, and 300 J/cm^2. Animals were sacrificed 24 hours after treatment, and their tumors removed for histopathologic analysis as described above.

Localization and uptake studies. Five animals with tumors of either amelanotic or melanotic melanoma, which were destined for localization and uptake studies, were sacrificed 24 hours post injection of doses of Photofrin II at 10 mg/kg. Tumors were excised and immediately frozen at −80°C until extraction procedures were performed. The extraction procedure used has been previously described by Kessel (*7*). Tumor tissue was quick thawed and weighed (≈300-600 mg wet wt). Extractions were carried out by disrupting tumor tissue in 2.5 ml sodium phosphate buffer (pH 3.5) with the use of a glass homogenizer. The homogenate was shaken for 5 minutes at 22°C with 2.5 volumes of 1:1 methanol-chloroform and subsequently centrifuged (1,000*g*, 10 min, room temperature). The lower fluorescent phase was removed and evaporated under nitrogen, the residue was taken up in 100 μl of methanol, and insoluble materials were removed by brief centrifugation (12,000*g*, 30 sec, room temperature). Porphyrin uptake was estimated from the absorbance of a 2-ml aliquot of the methanol extract scanned from 350 to 650 nm with the use of a Beckman DU-7 spectrophotometer. The porphyrin concentration of each tumor was determined by comparing its absorbance at 400 nm with a known concentration of Photofrin II (*8*). Absorption spectra were obtained in solution for each tumor, which showed a broad peak of maximal absorption between 380 and 420 nm. Values listed in table 1 are expressed in terms of microgram porphyrin per gram tumor tissue (wet wt).

Results

Histopathology. (*a*) Amelanotic melanoma: Gross and microscopic examination of tumors revealed no evidence of necrosis in control animals (light without sensitizer and sensitizer without light). Histologically, at total light doses of 75 J/cm^2 or more, there was 100% destruction of the tumor 24 hours after PDT (fig. 1). The tumor cells that were not completely disrupted showed nuclear pyknosis and karyorrhexis with only minimal preservation of the basic cellular outline in a sea of red blood cells and amorphous granular debris.

(*b*) Melanotic melanoma: In contrast to the amelanotic tumor, melanotic melanoma that received total doses of light equal to 75 J/cm^2 showed only superficial necrosis with hemorrhage to a depth of 2-3 mm below the surface of the tumor (≈30%-40% of the total tumor vol) (fig. 2). Deep to this damaged zone was normal-appearing tumor with intact vasculature. Tumors that received up to 150 J/cm^2 of light demonstrated necrosis to a depth of 4-5 mm (60%-80% of the tumor vol) with resistant tumor present at the base and periphery of the tumor. However, within this necrotic zone, isolated patches of normal-appearing tumor cells were observed to be present, indicating PDT-resistant tumor (fig. 3). Tumors that received 200-300 J/cm^2 showed complete necrosis to the base of the tumor centrally. At the anteroposterior and lateral margins of the tumor, histology confirmed viable nests of persistent tumor cells (fig. 4). This conclusion is based upon the histopathologic examination of a large number of sections and tumors and is not attributable to the way a particular section was cut.

Table 1. HpD tumor localization and uptake in human xenograft amelanotic and melanotic melanoma

Tumor	Uptake μg porphyrin/g tumor	Average μg porphyrin/g tumor	Increase from control
Control (non-HpD)			
Amelanotic	1.03	1.04	1.0
	1.05		
Melanotic	1.07	1.09	1.0
	1.11		
Amelanotic	7.28	7.44	7.15×
	7.67		
	7.58		
	7.36		
	7.31		
Melanotic	8.26	8.42	7.72×
	8.61		
	8.41		
	8.28		
	8.55		

Best Available Copy

Figure 1. Photomicrograph of human xenograft amelanotic melanoma tumor removed 24 hr after treatment with Photofrin II and 75 J/cm² of light. At this dose of light the entire tumor is destroyed by hemorrhagic necrosis. Originally, ×50.

Tumor localization and uptake. Animals were sacrificed and their tumors removed 24 hours post injection of 10 mg/kg of Photofrin II. The porphyrin was extracted and expressed in terms of microgram porphyrin per gram tumor (wet wt), and tumors were compared in terms of their increase over control non-HpD tumors. Control amelanotic tumors contained an average of 1.04 μg porphyrin/g tumor. Amelanotic tumors that received HpD had an average of 7.44 μg porphyrin or 7.15 times that of control tumors. Melanotic control tumors contained 1.09 μg porphyrin, while melanotic tumors that received HpD had an average of 8.42 μg porphyrin or 7.72 times that of control tumors (table 1).

Discussion

The usual treatment of primary malignant melanoma is surgical, and the first neoplasm treated experimentally with a laser "scalpel" was a malignant melanoma (9). Early laser experiments on malignant melanomas consisted of photoexcision and photocoagulation of both primary and metastatic lesions. The necrosis was eventually replaced by scars felt to be more cosmetically acceptable than those following scalpel or electrosurgery. However, the long-term findings from these studies were largely negative and unproductive (*10*). Within the next few months, numerous new nodules appeared along the borders of excision due to incomplete resection. PDT, since it may provide a greater degree of selectivity than other treatment modalities currently being applied to these cases, offered new hope in targeting those viable tumor cells that may tend to remain behind after conventional treatment.

An important parameter determining the extent of tumor necrosis produced by PDT is the penetrability of the necessary visible light through the tissue being irradiated. This penetration will be dependent on the reflection, scattering, transmission, and absorptive characteristics of the particular tissue being exposed. Since PDT is a photochemical reaction rather than a thermal ablative or coagulative process, the absorptive properties of the tissue that depend on the specific chromophores present in the absorbing tissue will obviously be important. The energy of the photon is absorbed by the chromophore, which can then transfer its energy by various mechanisms to the target molecule. In the case of PDT, tumor necrosis is thought to be produced by the energy transfer from the excited triplet state of the porphyrin to oxygen, producing singlet oxygen, which causes irreversible oxidation of some essential cellular component (*11*). If, however, another chromophore is present in the tissue that has a strong absorption band located at the particular wavelength used, this chromophore will compete with the photosensitizer for photons resulting in inefficient phototoxicity.

Melanin is a stable protein-polymer complex with a broad absorption spectrum over 250–1,200 nm (*12*). It is synthesized into the skin by melanocytes and is sometimes referred to as a "light

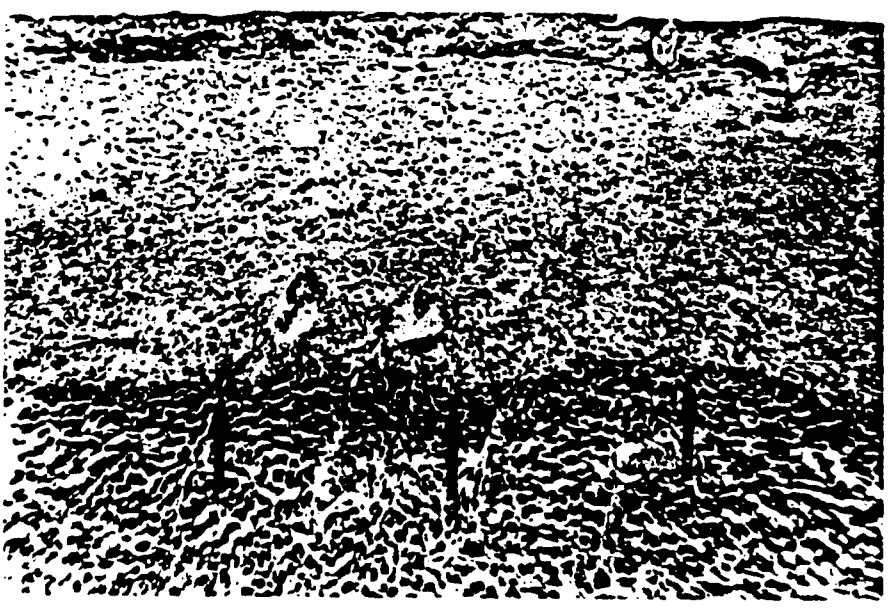

Figure 2. Photomicrograph of human xenograft melanotic melanoma tumor removed 24 hr after treatment with Photofrin II and 75 J/cm² of light. Note evidence of superficial hemorrhagic necrosis above the arrows. Deep to this damaged zone is normal-appearing tumor. Originally, ×80.

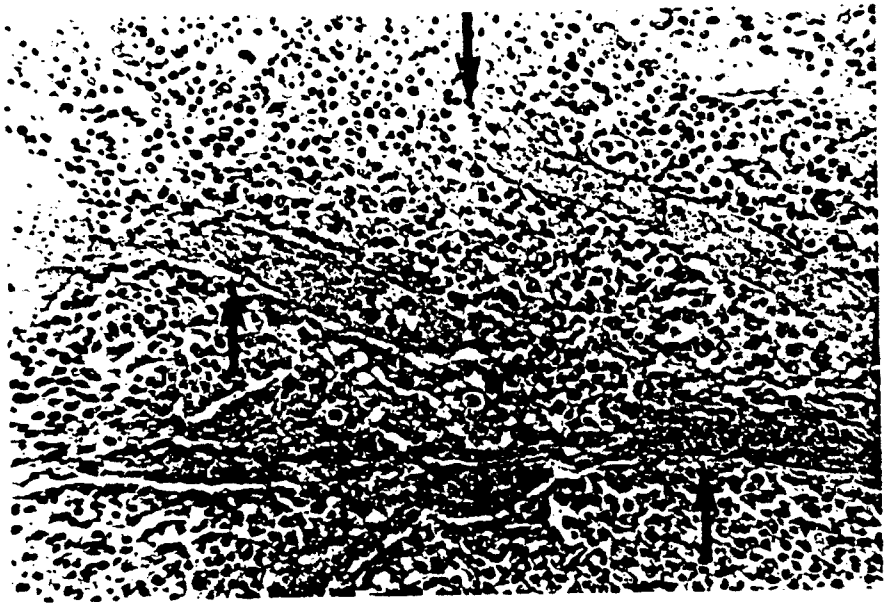

Figure 3. Photomicrograph of human xenograft melanotic melanoma tumor removed 24 hr after treatment with Photofrin II and 150 J/cm^2 of light. Note the large areas of hemorrhagic necrosis throughout the tumor at the tips of the arrows. However, within this necrotic zone isolated patches of normal-appearing tumor cells are present indicating PDT-resistant tumor. Originally, ×125.

absorbing mantle." Without melanin pigmentation of the skin, man could not tolerate exposure to the skin without fear of excessive sunburn. Malignant melanomas arise from melanocytes and can be pigmented or melanotic due to the massive accumulation of melanin, which imparts an intense black coloration to these lesions. Due to the fact that some melanocytes may be less well-differentiated and therefore produce less melanin, these malignant lesions may be nonpigmented or amelanotic.

Our study shows that human xenograft "nonmelanin pigmented" amelanotic melanoma is highly sensitive to PDT with HpD. Full thickness 100% tumor necrosis was observed following doses of HpD-PDT consisting of 10 mg/kg of Photofrin II and 630-nm red light treatments of 75 J/cm^2. Melanotic melanoma, which contains large quantities of the competing chromophore melanin, shows only superficial necrosis to a depth of 2-3 mm below the tumor surface by use of the same curative treatment parameters for amelanotic melanoma. Even with incident doses of light as high as 200-300 J/cm^2, small areas of viable tumor cells still persisted at the peripheral extremes of the tumor.

Using the methodology described by Kessel (*7*), we found that the total porphyrin accumulation of the melanotic melanoma 24 hours after injection of Photofrin II, as described above, was on the average 8.42 μg porphyrin/g tumor tissue. This was approximately 1 μg more porphyrin than was found to be present in the amelanotic melanoma (7.44 μg/g tumor tissue). This result would exclude the possibility of different tumor cell kinetics, such as uptake and retention of porphyrin as being the reason why amelanotic melanoma tumor responded well and melanotic melanoma did not.

Our study suggests that the presence of the melanin in melanotic melanoma will result in inefficient phototoxicity during PDT treatments. Protection by melanins against photodamage in model systems can occur by several mechanisms. Melanin may compete with the porphyrin for the absorption of photons or in the energy transfer process from the excited triplet state of the sensitizer to melanin instead of cellular oxygen. Furthermore, at least one study has suggested that melanin may in fact be a very effective quencher of singlet oxygen in aerobic photosensitization (*13*).

Extrapolation of the results to the human patient does involve some uncertainties, but further study on PDT with amelanotic melanoma seems promising and warranted. From a practical standpoint, PDT of melanotic melanoma may be useful in the elderly and debilitated patient who cannot tolerate extensive conventional surgery as an adjuvant to chemotherapy, immunotherapy, and radiotherapy. However, the risks at present of leaving viable tumor behind after PDT seem too high for patients who are operative candidates.

Figure 4. Photomicrograph of human xenograft melanotic melanoma tumor removed 24 hr after treatment with Photofrin II and 300 J/cm^2 of light. Note persistent viable nests of tumor cells between the arrows located at the lateral margin of this tumor. Above is hemorrhagic necrosis of the entire tumor. Below is connective tissue stroma outside of the tumor. Originally, ×210.

References

1. Dougherty T, Kaufman J, Goldfarb A, et al. Photoradiation therapy for the treatment of malignant tumors. Cancer Res 1978;38:2628–2635.
2. Dougherty T. Photoradiation therapy for cutaneous and subcutaneous malignancies. J Invest Dermatol 1981;77:122–124.
3. McCormick D, Wallace I, Kirk J, et al. The establishment and characterization of a cell line and mouse xenograft from a human malignant melanoma. Br J Exp Pathol 1983;64:103–115.
4. Povlsen C. Heterotransplants of human tumors in nude mice. Antibiot Chemother 1980;28:15–20.
5. Fogh J, Fogh JM, Orfeo T. One hundred and twenty-seven cultured human tumor cell lines producing tumors in nude mice. J Natl Cancer Inst 1977;59:221–226.
6. McCullough J, Newburger A, Gandbhir G. Melanoma: athymic nude mouse model. In: Maibach H, Lowe E, eds. Models in dermatology. New York and Basel: Karger, 1985:34–40.
7. Kessel D. In vivo fluorescence of tumors after treatment with derivatives of hematoporphyrin. Photochem Photobiol 1986;44:107–108.
8. Kessel D, Cheng M. Biological and biophysical properties of the tumor localizing component of hematoporphyrin derivative. Cancer Res 1985;45:3053–3057.
9. Goldman L. Laser treatment of melanoma. Laser cancer research. New York: Springer-Verlag, 1966.
10. Goldman L. Surgery by laser for malignant melanoma. J Dermatol Surg Oncol 1979;5:141–144.
11. Weishaupt K, Gomer C, Dougherty T. Identification of singlet oxygen as the cytotoxic agent in photoinactivation of a murine tumor. Cancer Res 1976;36:2326–2330.
12. Anderson R, Parrish J. Optical properties of skin. In: Regan D, Parrish J, eds. The science of photomedicine. New York: Plenum Press, 1982:147–194.
13. Sealy R, Sarna T, Wanner E, et al. Photosensitization of melanin: an electron spin resonance study of sensitized radical production and oxygen consumption. Photochem Photobiol 1984;40:453–459.

Reprinted from SPIE Vol. 908—Laser Interaction with Tissue
© 1988 by the Society of Photo-Optical Instrumentation Engineers Box 10 Bellingham, WA 98227-0010 USA

Corneal healing after excimer laser surface ablation

Neal L. Burstein, Ronald N. Gaster, Perry S. Binder[#],
Michael W. Berns[*], and Roy C. McCord[°]
Department of Ophthalmology and [*]Beckman Laser Institute,
University of California, Irvine;
[#]National Vision Research Institute,
San Diego, California;
[°]Gish Biomedical,
Santa Ana, California.

ABSTRACT

The special properties of far-uv light sources include tissue removal without major temperature rise and preparation of a surface well suited for cell locomotion and adherence. We have evaluated the use of the 193 nm excimer laser for large area surface ablation of the cornea. We have found that tissue removal can be accomplished with successful wound healing and corneal function by selecting the proper laser parameters.

Available data suggest that an ablative excimer laser of uniform and predictable beam power can supplant existing procedures for treating some corneal dystrophies, and preparing graft beds. The natural healing properties of the cornea aid in such procedures yet may make minor refractive change difficult to accomplish.

1. HISTORY OF ArF (193 nm) EXCIMER LASER USE IN THE CORNEA

Short-wavelength excimer lasers were first introduced to ophthalmology for deep cutting of the cornea by Trokel in 1983, working with IBM scientists Srinivasan and Braren.[1] They determined that precise removal of tissue could be accomplished without heating due to the direct breaking of organic molecular bonds by the far-ultraviolet light. Srinivasan found that an energy threshold for ablation exists below which no material is removed from a surface.[2] For polymethyl methacrylate plastic, this energy density is 10 mJ/cm^2/pulse of 14 ns. Above the threshold, efficiency of cutting increases rapidly until a fluence of 250 mJ/cm^2/pulse, then levels off sharply.

The 193 nm light source is 95% absorbed by a depth of 0.3 μm, and produces an oxygen-depleted surface of carbon radicals which can recombine and cross-link.[3] Therefore, deep corneal incisions with well-defined, compacted edges are produced, with most readily apparent damage confined to within 1 μm of the incision.[4] Loss of endothelial cells is observed directly beneath the incisions, however, perhaps due to shock waves.

In 1985, Serdarevic, Trokel and co-workers showed that a large area superficial corneal ablation could be used to remove infected tissue together with the infecting organisms.[5] They had success in treating keratitis caused by Candida albicans yeast. The wide area ablation was a new use of the laser as compared to deep incisions which characterized most early research. In that year also, several investigators in diverse laboratories confirmed that well controlled radial cuts would change refraction as did conventional radial keratotomy incisions.[6-8] These investigators as well as Trokel and co-workers confirmed that the 193 nm laser source removes tissue more efficiently than longer wavelengths and produces smoother walls.[9-11]

In May of 1986, our laboratory presented data to indicate that a moderately deep, large area ablation on the corneal surface would heal rapidly and could potentially be used to alter the refractive state of the cornea, using either a beam normal to the cornea or one which cut tangentially.[12] The advantages over radial keratotomy were several, including the use of a

cut 10% of stromal thickness to correct several diopters of spherical or cylindrical refractive error, compared to the 90% depth cuts required for radial keratotomy, as well as wound healing measured in days rather than years. In the past year and a half, we have attempted to define and solve the problem of optimizing corneal wound healing after large area excimer ablation. Our model has been the lamellar keratectomy, a simple type of tissue removal in rabbits and primates. These are results from these investigations.

2. HYPOTHESES AND GOALS FOR LARGE AREA ABLATION OF CORNEA

There are several criteria which must be satisfied for corneal wound healing following laser ablation in order to provide a technique which is an improvement over currently available procedures. Some of those basic to recovery of corneal health and function are listed here. We hypothesize that excimer laser ablation can meet these criteria better than currently accepted methods.

2.1 Production of a smooth surface for epithelial rehealing

The excimer laser produces a smooth and flat-surfaced vertical cut edge parallel to the beam.[4] It is important to remove the tissue of the curved cornea profile normal to the beam as well, so as to leave a surface of the same or similar curve which is microscopically smooth. Such a surface would promote epithelial wound healing and allow continued optical function. The energy profile of the beam needed to do this must be flat (optically neutral) at the target site, or vary in a carefully defined intensity distribution from edge to center for + or - dioptric modification. Even minor spatial perturbations in the beam must be avoided.

2.2 Epithelial closure.

Mechanical removal of a corneal layer (lamellar keratectomy) leaves a surface which is composed of loose collagen fibrils and packed bundles. Epithelial locomotion over such a surface is impeded so that a 6 mm diameter defect takes five days to close. The optimum rehealing of epithelium takes place over gently scraped or chemically denuded basal lamina, the surface the epithelium rests on, and takes only two days for a 6 mm diameter defect. Optimal closure of epithelium over the laser keratectomy should occur in minimal time.

2.3 Regrowth over margin of ablation.

Lamellar keratectomy produces a steep wound margin, and the behavior of stroma and of the covering epithelium at this margin is of considerable interest. This is a transition zone where major problems of mechanical locomotion, altered epithelial behavior, optical transition, and mechanical and tear film instability can occur. Observation of epithelial behavior over this zone will provide information necessary for prediction of epithelial rehealing and optical function.

2.4 Re-establishment of basal lamina and hemidesmosomes.

Bowman's layer in humans and primates is a thin apical stromal layer which is nearly structureless compared with deep stroma. It is removed by ablation and cannot be expected to reform. Once epithelial regrowth has occurred, the formation of significant adhesions (hemidesmosomes) to a freshly secreted substrate (basal lamina) are important for continued stability.

Best Available Copy

2.5 Optical characteristics of healed cornea.

A central optical zone slightly larger than the size of the pupil is required for visual function. The scotopic (dark-adapted) pupil size for humans is nominally 4 mm. Over the optical zone, all light impinging on the cornea from an object to be viewed must be focused to within ± 1/2 diopter for normal vision. This requires that any deviation from the normal corneal curvature result in a predictable, stable optical surface to produce refractive correction. The thickness of the epithelium, as well as the contour of the stroma after the obligatory swelling and thinning which accompany the initial phases of wound healing, are important in determining this correction.

The rehealed cornea must be clear, passing approximately 95% of light in the visible range to approximate normal function. Scatter can result from uneven surfaces between two layers of different refractive index, or from the buildup of scar tissue including de novo synthesis of disordered collagen, and large numbers of fibroblasts entering the wound site.

3. METHODS

3.1 Irradiation

The beam leaving the laser cavity is a rectangle of 7 x 22 mm of uneven intensity distribution. We found that the diverging beam, after travelling 340 cm, expanded to 12 x 75 cm. At this distance, it was possible to select a 6 mm diameter portion of the beam which was even in intensity distribution to within ± 5%. The fluence was 21 mJ/cm^2/pulse, only twice the threshold for material removal. A HeNe aiming beam was aligned in the selected portion of the excimer laser beam by means of a quartz plate at 45^o to the ArF beam (Figure 1). This greatly simplified head placement for exposure.

3.2 Aperture shield.

Fine particulate debris is found surrounding the edge of ablation sites, resulting from material blown from the surface, or from low energy ablation at the target margin. This observation has been described for polymethyl methacrylate targets.[2] We used a shield in order to prevent the deposition of such contaminants on the cornea, as well as to sharply define the ablation edge.

Shields were made of aluminum, a material which reflects far-uv light well, and were highly polished.[13] Thermocouple measurements made at a fluence of 150 mJ/cm^2/pulse showed that temperature plateau during long laser exposures was ambient + 10^o C, compared to a rise of 40^o C for copper (Figure 2). The shields were shaped to 8 mm radius for rabbits, and 6.5 mm for monkeys. They were of diameter sufficient to cover the cornea completely, and had a central 6 mm diameter aperture. A diaphrag n placed in front of the shield blocked the major portion of the laser beam from striking the lids or face.

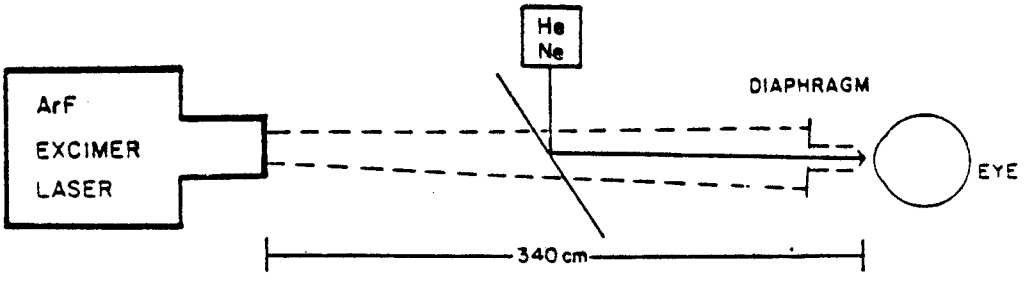

Figure 1. Distance broadened ablation beam

3.3 Corneal hydration and cleanliness.

Any object which is on the corneal surface at the time of ablation will produce a replicate shape in tissue as ablation occurs. Eyelashes, hair, and particulate debris must be kept completely clear of the ablation site in order to prevent unevenness in the resulting surface. Also, since the corneal stroma is between 75% and 80% water, and tends to swell by absorbing additional moisture, tissue hydration must be controlled to prevent locallized desiccation or imbibition from altering the ablative process.

We chose to leave the epithelium intact, and to allow the laser beam to remove the tear film and epithelium as a part of the ablative process. Great care was taken during the preparation of the eye to maintain the tear film and avoid contamination of the optical surface. A clean, sterile artificial tear solution was used frequently during anesthesia when the eye was open. The lids were taped shut while animals were anesthetized before and after the procedure to protect against corneal drying.

3.4 In vivo observations.

For evaluation of corneal clarity, a slit lamp was used. This biomicroscope with a narrow light beam allows visualization of scattered light from the cornea. For wound closure fluorescein was used, a fluorescent chemical which follows water and which does not penetrate the intact cornea. This diagnostic agent readily delineates epithelial defects by temporarily staining bare stroma.

The endothelial cell layer, a monolayer lining the inner corneal surface, is vital to corneal function since it must continually pump fluid to maintain corneal transparency. This layer cannot regenerate in humans or primates. They were viewed by specular microscopy, a technique developed by Maurice.[14] Photographs taken one week after ablation were evaluated for cell density. Corneal thickness was measured with the specular microscope by comparing the focus on the epithelium with that on the endothelium of the cornea.

3.5 Histology and electron microscopy.

Corneas were removed and fixed in buffered glutaraldehyde, dehydrated and embedded in epoxy resins. They were thin sectioned and stained with dyes for light microscopy, or with heavy metals for electron microscopy. Specimens were examined at one week, and one, two, or three months following excimer laser ablation.

4. RESULTS

4.1 Beam profile and exposure parameters

The unmodified ArF laser beam at a distance of 340 cm provided a profile across a 6 mm aperture which was uniform to within 5%.

At a fluence of 26 mJ/cm2/pulse, an exposure of 40 Hz for 100 seconds produced a uniform ablation. The total depth of the cut was approximately 80 µm, which is twice the depth of the epithelium alone. The surface initially had the appearance of ground glass, giving off a very even white specular reflection. Upon wetting with tear film, the surface immediately became nearly clear, with only a faint opalescence remaining, allowing the underlying iris to be viewed.

Long exposures of 150 seconds or more, or a high repetition rate of 100 Hz, caused a yellowish appearance to the tissue remaining after ablation, and delayed epithelial wound healing by at least one full day.

4.2 In vivo observations.

The epithelial margins were round and well defined and wound healing was rapid in all normal laser ablations through aluminum shields. Within 24 hours closure had commenced leaving a 3.8 to 4.2 mm diameter defect. By 48 hours corneas ablated 100 seconds or less showed complete epithelial closure with no staining of the stroma. Light punctate fluorescein staining was present in some cases at one week, indicating an unstable epithelial surface. Epithelial rehealing after excimer laser ablation was similar to that following epithelial removal alone, and less than half tha time of rehealing following lamellar keratectomy (Figure 3).[15]

Specular microscope pachymetry on day 3 showed thinning of 30 to 40 μm in the 100 second exposure group and swelling of 300 μm in the group exposed for 200 seconds. By four weeks, all ablated corneas were 20 μm thicker centrally than contralateral controls. Specular microscopy at three days in rabbits showed that the 100 second exposure group lost 17% of endothelial cell density, while the 200 second exposure corneas were too cloudy to provide cell counts. In primates, no endothelial loss was seen at one week after ablation, and both treated and control corneas had cell densities of 3100 cells/mm^2 or more.

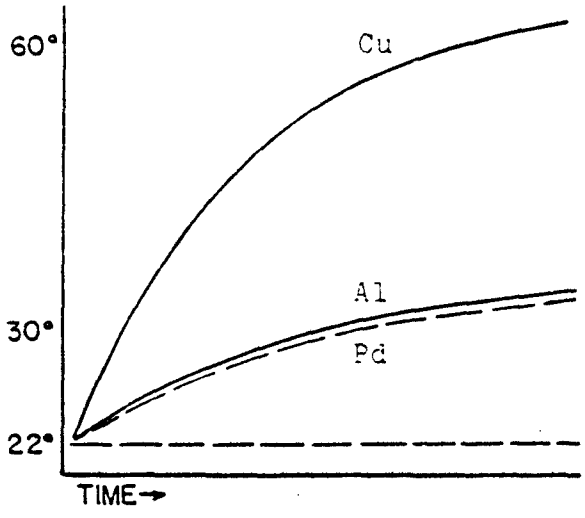

Figure 2. Cu, Al, Pd shield material.

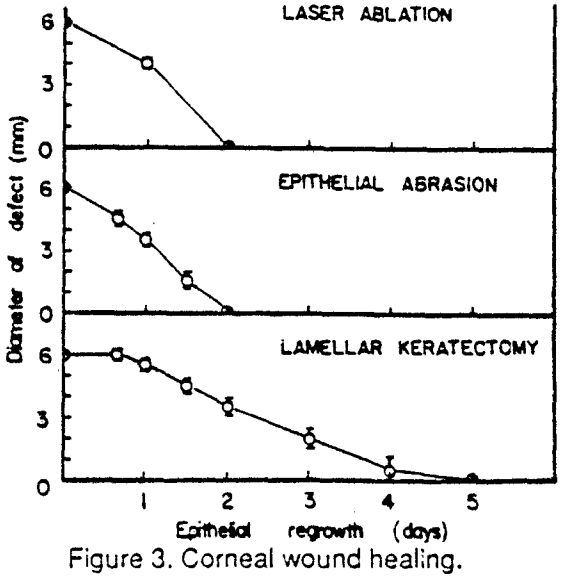

Figure 3. Corneal wound healing.

4.3 Histology and electron microscopy

The epithelium in the peripheral corneal areas was normal in appearance, with a total thickness of 5 to 7 cell layers. The central area of a shallow ablation had 4 to 5 layers of cells after one week. The basal lamina and hemidesmosomes were reformed at this time.

At the edge of the ablation site, there was often stromal swelling. In these cases, epithelium thickened over the swelling site, and remained thickened to over 10 cell layers in the bed of the ablation zone. Where slight thinning of stroma occurred at the edge of the ablation, the epithelium thickened to 9 to 11 layers and filled in the defect to maintain a smooth, unbroken epithelial surface. The rehealing epithelium filled small defects in the optical surface of the cornea, as well as the margins of shallow ablations, by forming an increased or decreased number of cell layers as required. This property of the epithelium helped to maintain the normal optical correction of the corneal surface. However, when the surface prepared by ablations had a large number of irregularities, the epithelial surface appears roughened also. Many cells were then seen to exfoliate by loosening abnormally

from the apical cell layer.

5. DISCUSSION

The healing of corneal epithelium, stroma, and endothelium after surface excimer laser ablation are determined largely by the parameters of the laser delivery system. These determine the potential risk of permanent corneal damage. Minimalization of stromal scarring and endothelial cell loss may make ablative tissue removal valuable as a clinical procedure. Numerous investigators have made recent contributions to wide area ablative corneal surgery by excimer laser.[16-22] An excellent review is available.[23] Following are some important considerations for future work.

5.1 Beam profile

Diverse techniques are being developed for delivery of a beam of even cross section. Some techniques, such as the present one and spatial filtering, produce great loss in beam intensity. Others under development may preserve beam power, allowing ablation at higher, more efficient fluence levels. For refractive procedures, a sudden loss of power to the system could result in a partially ablated cornea without a defined optical surface.

5.2 Heat and shock wave effects

Heating of tissue by laser irradiation can cause tissue damage, and delay wound healing. In the case of ultraviolet laser surface ablations, heating may result from transfer of energy residual to the breaking of chemical bonds. Localized heating of tissue at the ablation surface occurs at high pulse repetition rate and at high fluence. Prolonged exposures can allow heat conduction and temperature increases in underlying tissues. As the corneal thickness is reduced by ablation these effects could reach the endothelium.

Shock waves produced during exposure can damage cells at the site of impact and some distance away. Gases produced during cutting escaping from a confined space may cause mechanical damage to the endothelium either by flexing Descemet's or by producing shock waves. Such an effect may be responsible for the endothelial morphological alteration and the separation of membrane components which were observed in rabbits in the experiments described here. High exposures may exacerbate such damage.

5.3 Optimal wavelength

The optimal wavelength for laser ablation is still open to question. Currently, 193 nm seems ideal due to high ablation efficiency, accurate cutting, low mutagenicity [24,25], and the property of leaving smooth cut surface for corneal epithelial wound healing. Work is required in primates to determine the relative suitability of the 193 nm wavelength.

5.4 Shielding of beam

The shield method of delineating the corneal ablation zone as described herein has the advantages of simplicity, low cost, and accuracy. It may furthermore provide protection for surrounding tissue from gases including free radicals and particulate matter escaping the ablation zone. Optical methods of masking do not protect the wound margin and require that the eye be mechanically coupled to the optical system to prevent movement.

5.5 Clinical applications

Reis-Buckler's Syndrome is an opacification of the cornea involving the superficial

Best Available Copy

stroma, the basal lamina, and the epithelium. Cogan's (map, dot, fingerprint) dystrophy consists of intermittently appearing intraepithelial cysts of widely variable size, with basement membrane protruding into the epithelial cellular layers or becoming absent altogether. Recurrent erosion can be caused by fingernails, plant leaves and branches which damage epithelial basal lamina and prevent normal epithelial adhesion. Superficial corneal ablative technique may be useful in these and other cases where it is desirable to completely remove the epithelium and underlying basement membrane, leaving a surface which can be rapidly rehealed.

5.6 Elective refractive surgery

The use of the excimer laser to optically modify the corneal curvature for refractive purposes is an interesting possibility. At present, the extremely plastic response of the epithelium in healing wounds of various depths is a primary hindrance to this goal. Stromal swelling is uneven at varying depths, so that difficulty may be encountered in producing lenticule-like shapes cutting across lamellae.[26] In addition, the slight degree of endothelial damage observed may discourage the purely elective use of such procedures. It is likely that further experimentation will yield methods for overcoming these problems.

6. BIBLIOGRAPHY

1. Trokel SL, Srinivasan R, and Braren B: Excimer laser surgery of the cornea. Am J Ophthalmology 96:710, 1983.

2. Srinivasan R: Kinetics of the ablative photodecomposition of organic polymers in the far-ultraviolet (193 nm), J Vac Sci Tech B 1:923, 1983.

3. Lazare S, Hoh PD, Baker JM, and Srinivasan R: Controlled modifications of organic polymer surfaces by continuous wave far-ultraviolet (185 nm) radiation XPS studies. J Am Chem Soc 106:4288, 1984.

4. Marshall J, Trokel S, Rothery, and Shubert H: An ultrastructural study of corneal incisions induced by an excimer laser at 193 nm. Ophthalmology 92:749, 1985.

5. Serdarevic O, Darrell RW, Krueger RR, and Trokel SL: Excimer laser therapy for experimental candida keratitis. Am J Ophthalmol 99:534, 1985.

6. Puliafito CA, Steinert RF, Deutsch TF, Hillenkamp F, Dehm EJ, and Adler CM: Excimer laser ablation of the cornea and lens. Ophthalmology 92:741, 1985.

7. Aron-Rosa D, Carre F, Cassini P, Delacour M, Gross M, Lecour B, Olivio JC, and Timsit JC: Keratorefractive surgery with the excimer laser. Am J Ophthalmol 100:741, 1985.

8. Cotlier AM, Schubert HD, Mandell ER, and Trokel SL: Excimer laser radial keratotomy. Ophthalmology 92:206, 1985.

9. Kruger RR, and Trokel SL: Quantitation of corneal ablation by ultraviolet laser light. Arch Ophthalmol 103:1741, 1985.

10. Kruger RR, Trokel SL, and Schubert HD: Interaction of ultraviolet laser light with the cornea. Invest Ophthalmol Vis Sci 26:1455, 1985.

11. Marshall J, Trokel S, Rothery S, and Schubert H: An ultrastructural study of corneal incisions by an excimer laser at 193 nm. Ophthalmol 92:749, 1985.

12. Gaster RN, Berns MW, and Burstein, NL: Excimer Laser Interaction with the Cornea. Invest Ophthalmol Vis Sci 27(Suppl):92, 1986.

13. Gaster RN, Berns MW, Binder P, Giergiel J, Singer M, and Burstein NL: Corneal shield design for 193 nm excimer laser surgery of the cornea. Invest Ophthalmol Vis Sci 28(Suppl):109, 1987.

14. Maurice DM. Cellular membrane activity in the corneal endothelium of the intact eye. Experientia 24:1094, 1968.

15. Pfister RR and Burstein NL: The alkali burned cornea. I. Epithelial and stromal repair. Exp Eye Res 23:519, 1976.

16. Seiler T and Wollensak J: In vivo experiments with the excimer laser - Technical parameters and healing processes. Ophthalmologica 192:65, 1986.

17. Dehm EJ, Puliafito CA, Adler CM, Steinert RF: Corneal endothelial injury in rabbits following excimer laser ablation at 193 and 248 nm. Arch Ophthalmol 104:1364, 1986.

18. Srinivasan R, and Sutcliffe E: Dynamics of the ultraviolet laser ablation of corneal tissue. Am J Ophthalmol 103:470, 1987.

19. McDonald MB, Beuerman R, Falzoni W, Rivera L, and Kaufman HE: Refractive surgery with the excimer laser. Am J Ophthalmol 103:469, 1987.

20. Waring GO, Hanna K, Chastang JC, Pouliquen Y, Renard G, and Asfar L: A rotating slit delivery system for excimer laser photorefractive keratectomy. Invest Ophthalmol Vis Sci 28(Suppl):274, 1987.

21. McDonald M, Beuerman R, Falzoni W, Rivera L, and Kaufman H: Preliminary experience with the excimer laser for area ablation of rabbit corneas. Invest Ophthalmol Vis Sci 28(Suppl):275, 1987.

22. Mandel ER, Kreuger RR, Puliafito CA, and Steinert RF: Excimer laser large area ablation of the cornea. Invest Ophthalmol Vis Sci 28(Suppl):275, 1987.

23. Krauss JM, Puliafito C, and Steinert RF: Laser interactions with the cornea. Surv Ophthalmol 31:37, 1986. Ophthalmologica 192:65, 1986.

24. Nuss RC, Puliafito CA, and Dehm E: Unscheduled DNA synthesis following excimer laser ablation of the cornea in vivo. Invest Ophthalmol Vis Sci 28:287-294, 1987.

25. Trentacoste J, Thompson K, Parrish RK, Hajek A, Berman M, and Ganjei P: Mutagenic potential of a 193-nm excimer laser on fibroblasts in tissue culture. Ophthalmology 94:125, 1987.

26. Lee D and Wilson G: Non-uniform swelling properties of the corneal stroma. Curr Eye Res 1:457, 1981.

Lasers in Surgery and Medicine 8:22–29 (1988)

Effect of Laser-Heated Tip Angioplasty on Human Atherosclerotic Coronary Arteries

N. Charle Morcos, MD, PhD, Michael Berns, PhD, and Walter L. Henry, MD, FACC

Departments of Medicine (Cardiology Division) (N.C.M., W.L.H.), and Surgery (M.B.), and the Beckman Laser Institute (M.B.), University of California, Irvine

Effects of laser-heated-tip angioplasty on arteries is not fully understood. We report histology, ultrasound image properties, and vasoreactivity of human atherosclerotic cornary arteries after exposure to the laser-heated tip catheter. Segments of isolated human coronary arteries were obtained within 5–8 hours postmortem. Side branches were ligated and perfused with Krebs-Ringer solution. Coronary occlusions were recanalized during perfusion using a 1.5-mm tip heated twice with a 10 W argon laser for 10 seconds while two-dimensional 12-MHz ultrasound images were recorded. Images documented vessel recanalization and an increase in ultrasound refractile properties of vessel walls adjacent and 2–5 mm distal to the heated tip. Histologic studies showed charring along the neolumen and extensive coagulation pattern within the plaque. Vasoreactivity was assessed by measuring flow rate changes during perfusion with 100 ml of 10^{-5} M serotonin followed by washout with serotonin-free solution. Recanalized arteries showed a 50% increase in magnitude of vasospasm, which was persistent for 5 hours, compared to control atherosclerotic vessels, which relaxed within 30 minutes. In conclusion, laser-heated-tip-irradiated vessels demonstrated plaque coagulation, increased ultrasound refractile properties of plaque, and increased vasospasm, which persisted for several hours.

Key words: laser-heated tip, coronary artery, atherosclerosis, ultrasound image, vasoreactivity, thermal coagulation

INTRODUCTION

Cardiovascular applications of laser radiation have been investigated by several authors [Abela et al, 1982, 1985; Choy et al, 1982; Lee et al, 1983; McGuff et al, 1983]. Because of its optical properties, the laser beam can be delivered through silica or quartz optical fibres passed through catheters, and the energy can be localized at various sites within the arteries and veins [Abela and Conti, 1983]. Thus far, studies have concentrated on the immediate effect of laser energy on atherosclerotic tissue and the artery wall [Choy et al, 1982; Lee et al, 1983]. Abela and colleagues [1982] evaluated the three commonly available lasers, (the CO_2, Nd-YAG, and argon). An average energy level of 20–30 joules was generally effective to relieve vascular stenosis in the aorta and femoral arteris of live cholesterol-fed rabbits. The histologic appearance of tissue damage created by the three lasers was similar. In each case, three zones of damage were observed, consisting of an innermost zone of complete tissue vaporization, a second zone of thermal burning, and an outermost zone of diffuse tissue disruption presumed to be due to thermal spread. In its present state of development, intravascular laser treatment can be dangerous, and a better understanding of the energy ranges required to vaporize and focus the laser precisely is required. Having the laser beam heat a metal cap at the end of a catheter is an alternate approach to deliver controlled thermal energy with minimization of scat-

Accepted for publication November 12, 1987.

Address reprint requests to NC Morcos, MD, PhD, Division of Cardiology, Department of Medicine, University of California, Irvine, CA 92717.

© 1988 Alan R. Liss, Inc.

ter and tissue penetrance of uncontrolled light. The argon laser-heated laser probe has been found to have improved safety and efficacy compared with prior clinical studies with bare fiberoptic fibers [Choy et al, 1984; Ginsberg et al, 1985]. In a recent report by Cumberland et al [1986] 89% of femoropopliteal occlusions were successfully traversed by the laser probe. Initial clinical trials suggest the feasibility and potential of percutaneous coronary laser thermal angioplasty [Cumberland et al, 1986; Sanborn et al, 1986]. One of the potential problems in laser thermal damage is endothelial disruption, which has been shown to make the arterial wall susceptible to vasospasm. Vasospasm in the coronary arteries is a major factor in high-risk coronary artery disease such as rest angina [Hillis and Braunwald, 1978], preinfarction angina [Theroux et al, 1981], sudden cardiac death [Maseri et al, 1982], and myocardial infarction [Dalen et al, 1982].

While reports indicate minimal laser thermal damage to the intima and complete intimal repair in 5 days, there are no reports on vasomotor properties of irradiated regions. For instance, does a change in relative receptor densities or cellular structure occur and create a susceptible region for focal vasospasms or does the laser-treated zone lose its vasoactive receptors and hence maintain a relaxed vessel with a full patent lumen? One of the goals of the present study was to investigate changes in the vasoreactivity of atherosclerotic arteries obtained within 5–8 hours postmortem, perfused with oxygenated Ringer's solution, maintained viable, and exposed to laser-heated tip angioplasty for plaque ablation during perfusion. The changes in histology and ultrasound image properties before and after laser-heated-tip irradiation during perfusion have also been studied.

MATERIALS AND METHODS

Arterial Perfusion Model

A perfusion apparatus described previously by Morcos et al [1985] was utilized such that coronary artery segments of 2–3 cm in length and 0.5–2 mm in diameter were perfused under a constant pressure of 30 mm Hg (Fig. 1). Briefly, all coronary arteries were obtained within 5–8 hours postmortem at autopsy, were dissected free, and side branches were ligated with 6.0 silk sutures. The ends of each artery were cannulated and secured with 6.0 silk sutures on polyethylene tubing in a special holder. The holder was placed in a temperature-regulated bath at 37°C and its polyethylene tubing was connected to the inlets and outlets of the perfusion apparatus. The perfusate and

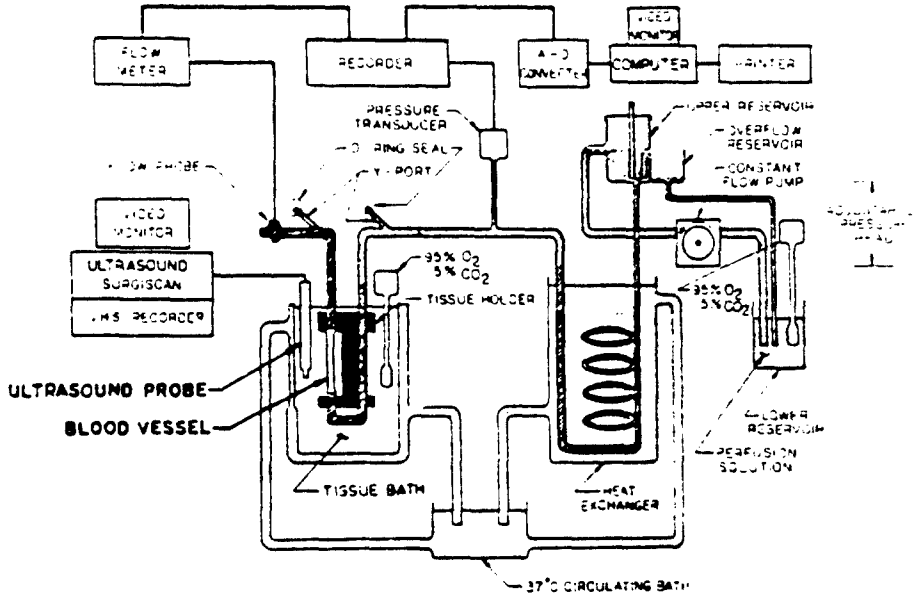

Fig. 1. Perfusion apparatus. Vessel segments, which were 2–3 cm in length and 1–2 mm in diameter, were mounted on the tubing of the artery holder. The holder was connected with perfusion tubing. The artery and holder were immersed in a temperature-controlled bath while being perfused intraluminally at constant pressure of 30 mm Hg. Perfusate and bath were Krebs-Ringer bicarbonate solution and continuously gassed with 95% O_2-5% CO_2. Imaging was performed by a 12-MHz ultrasound probe. Laser probe was introduced through Y-ports. Other experimental conditions were as described in "Materials and Methods."

Best Available Copy

bathing medium contained Krebs-Ringer bicarbonate solution of the following composition in mM: NaCl, 119.2; KCl, 4.9; $MgSo_4$, 1.2; KH_2PO_4, 0.44; $CaCl_2$, 1.3; $NaHCO_3$, 25; disodium ethylenediamine tetraacetic acid (EDTA), 0.03; ascorbic acid, 0.114 and glucose, 11.1; pH 7.34. Perfusate and bath were maintained at 37°C.

Pharmacologic Assessment of Vasoreactivity

To induce spasm, 100 ml of serotonin (5-HT) was introduced into the perfusate at a final concentration of 10^{-5} M. The serotonin solution was followed by a washout with 1 liter of serotonin-free Krebs solution to effect relaxation. Flow rate was measured continuously as a function of time. The flow rate at any time point was expressed as a percentage of normal flow rate (100%) prior to any interventions. Time = 0 is taken at the moment serotonin reached the artery in the perfusate.

Laser Instrumentation

An argon laser (Spectra Physics 171) was used to deliver radiation at a wavelength of 488 and 514 mm through a 300-mm core silica fiber to heat a metal cap, which was 1.5 mm diameter at its tip (Trimedyne Inc., Santa Ana, CA). After equilibrium of the mounted arterial segments in the perfusion apparatus, the heated-tip catheter was introduced through a Y-port with O-ring seal into the perfusion apparatus tubing in the presence of perfusate and advanced to the area of stenosis or occlusion under ultrasound visualization. Heated-tip angioplasty was performed by delivering two 10-second exposures of 10 W of argon laser energy with a 15-second interval to the metal tip. During the thermal radiation procedure the tip was continuously in motion to avoid adherence and/or localized superheating of the arterial wall. Following angioplasty the capped fiber was retracted, perfusion of the artery continued, and pharmacologic studies were performed.

Ultrasound Imaging

Ultrasound two-dimensional imaging of the arterial luminal diameter, arterial wall thickness, and outer diameter was performed continuously during the angioplasty and recorded on videotape. To image the arteries a two-dimensional 12-MHz ultrasound probe was placed into the perfusion bath within 1 cm from the artery wall. The probe was connected to a Biosound Surgiscan (Biosound, Indianapolis, IN) with video monitor and cursor bar with a joy stick. The Biosound device permitted measurements of arterial dimensions within 1/10 of a millimeter.

Histology Studies

At the end of irradiation and pharmacologic studies the mounted artery segments were fixed in 3% glutaraldehyde, embedded in paraffin, sectioned, and stained with hematoxylin and eosin. Histology was performed on a total of five recanalized segments.

Tissue

Human coronary arteries were obtained from the left anterior descending coronary artery and its tributaries within 5–8 hours postmortem. Atherosclerotic arteries were obtained from individuals who were over age 55 years. In this study, a total of nine atherosclerotic artery segments were used: four were diffusely atherosclerotic, and five contained a tight stenosis and were recanalized by laser-heated-tip irradiation. Histology and ultrasound imaging was performed on five of the recanalized vessels. Pharmacologic vasoreactivity was performed on three of the recanalized vessels.

RESULTS

Figure 2 shows histologic studies performed on representative sections of antherosclerotic coronary artery segment obtained from a 68-year-old male, which was irradiated by the heated-tip catheter during perfusion. The terminal segments of the artery were not thermally irradiated, and the tight occlusion was present in the central region.

Recanalization by thermal irradiation was performed in the proximal part of the occluding plaque, but the metal tip was not permitted to recanalize the distal section of the occlusion. In this manner, histologic assessment permitted visualization of the extent of original occlusion as shown in Figures 2C and 3D.

Sections from both ends of the segments show faint hematoxylin and eosin staining with preservation of structure in the intima and plaque (Fig. 2A,B, proximal end and 2F, distal end). In contrast, in central areas in the segments that were exposed to the heated tip, irradiation showed loss of structure and intense staining indicative of coagulation of the plaque and muscle matrix (Figs. 2D,E, 3A–D). Furthermore, at locations 2–3 mm distal to the heated tip, where the occluding plaque was still intact, the heat effects were observed as patchy intense staining indicative of coagulation in both the arterial wall and plaque. Also, along

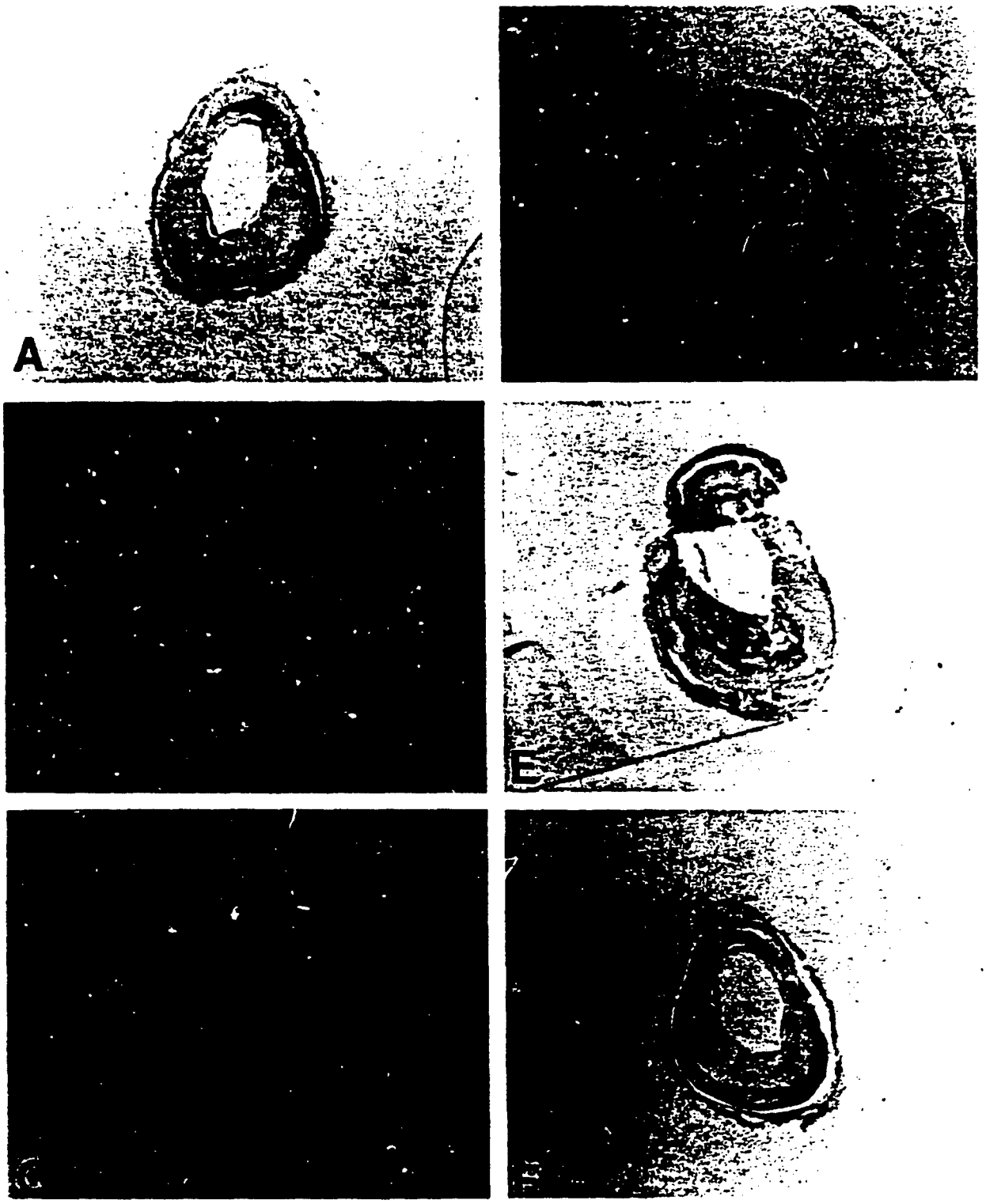

Fig. 2. Histology of representative occluded atherosclerotic coronary artery from proximal A to distal F ends after laser-heated-tip angioplasty. A: Proximal section. B: Narrowing of lumen prior to occlusion. C: Occluded central section. Laser heated tip (1.5 mm) was advanced through the distal end F. E: Recanalized section. D: Most proximal recanalized section. Laser-heated tip was not advanced beyond section C to maintain a portion of the occluding plaque. Magnification × 10. Histology on another four canalized vessels showed similar characteristics.

Best Available Copy

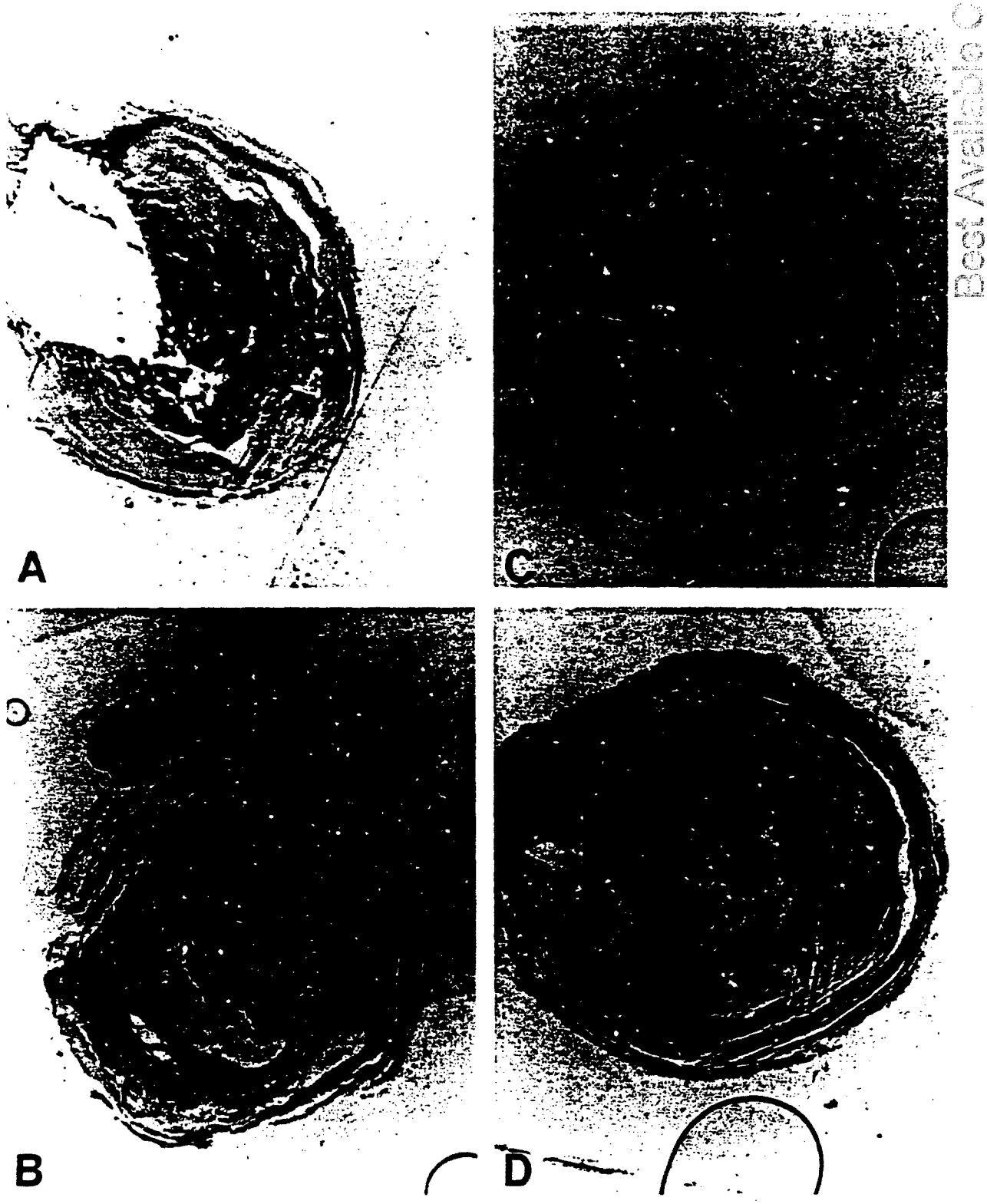

Fig. 3. Higher magnification of laser-heated-tip irradiated sections showing charring and intense red staining along to the heated-tip pathway. Recanalized sections shown as follows. A: Most distal. B: Intermediate. C: Most proximal. The red stain is more intense in the periphery of the neolumen and fades in areas near the outer periphery of the arterial wall. D: Most proximal section of spared unrecanalized plaque showing central intense staining located immediately adjacent to the advancing heated tip. Magnification ×24.

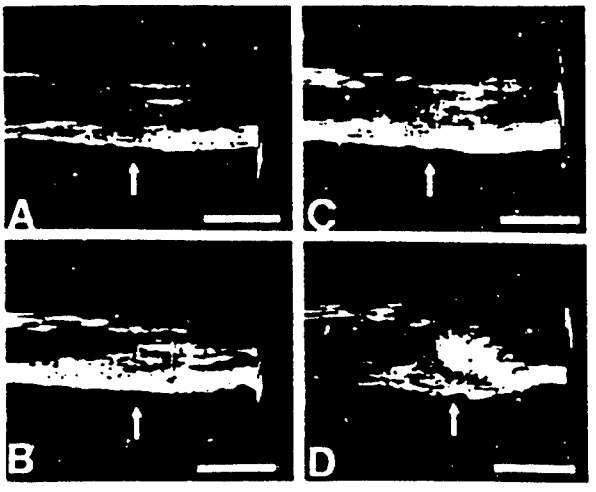

Fig. 4. Ultrasound images obtained from a representative vessel during laser-heated-tip angioplasty. A: Atherosclerotic artery with central occlusion appearing as soft density. B: Laser-heated tip activated and advanced from the distal right-hand section. Increase in refractile density of plaque and vessel wall observed at the site of occlusion and distal to it. C: Laser-heated tip advanced through plaque with increased refractile density. D: Laser-heated tip advanced proximally and sparing the most proximal end of the occluding plaque. Magnification ×3. Bar = 0.5 cm. Arrows indicate direction of ultrasound beam.

areas of direct contact between tissue and heated tip, a fine layer of charring is clearly observed along the neolumen (Fig. 3A–C).

Figure 4 shows a series of photographs obtained from the ultrasound-videotape recording during the heated-tip angioplasty of the vessel depicted in Figures 2 and 3. It is clear that prior to angioplasty, the occluded area represented plaque of soft density along the middle of the arterial segment as well as along the arterial walls. During exposure to heated tip irradiation, the plaque density became more refractile to the ultrasound beam and appeared as areas of high density on the monitor. These regions of high density in the ultrasound images persisted after termination of irradiation. The increased refractile density probably reflects an increase in crosslinking and binding of plaque and wall components equivalent to and corresponding to the coagulation pattern observed from the histologic sections.

Following complete recanalization, the pharmacologic vasoreactivity to serotonin of these thermally irradiated arteries was compared to the vasoreactivity of atherosclerotic arteries that were not thermally irradiated by the laser-heated tip. In Figure 5, the percentage of control flow rate is plotted versus time before, during and after transient exposure to the vasoactive agent, serotonin at 10^{-5} M, 100 ml. Another set of atherosclerotic arteries that were not occluded were not exposed to laser-heated-tip irradiation. In the non-irradiated vessels, vasospasm with resultant reduction in flow rate was observed immediately upon exposure of the artery to serotonin and resulted in a 63% reduction in flow rate. During the washout of serotonin, the flow rate gradually increased and reached normal values within 1 hour. In contrast, thermally irradiated arteries had increased sensitivity to serotonin. Upon exposure to serotonin, flow rate was greatly reduced by 90%. Furthermore, the reduction in flow rate was persistent for a period of over 6 hours. The sustained vasospasm could be relieved by intraluminal $MgSO_4$ at 5 mM. Such a concentration of $MgSO_4$ when introduced with the perfusate permitted vasorelaxation, and the flow increased to 90% of normal values.

DISCUSSION

Much success has recently been reported regarding recanalization of thrombosed and atherosclerotic arteries, particularly those arteries that are large and nontortuotous such as leg arteries. Smaller, tortuotous arteries, and particularly those located within a mobile matrix such as the coronary arteries in a beating myocardium, pose various challenges to the application of this advancing technology. Mechanical as well as heat-induced perforations have been high on the list of adverse reaction. However, aside from the technical problems for successful clinical applications of laser angioplasty, there are still many unanswered questions regarding the full effect of the laser on the irradiated tissues. Consequently, long-term changes and transformations occurring within such irradiated tissues must be fully studied. In the present study thermally induced coagulation of components of both plaque and arterial walls was observed in situ as a result of heated-tip angioplasty. Evidence for coagulation patterns correlated strongly with both the intense histologic staining and the increased ultrasound refractile density. These changes were evidence at distances of 2–3 mm away from the heated tip. Morcos and Henry [1987] showed that atherosclerotic arteries, in general, are more sensitive than normal arteries to vasoactive agents such as serotonin. In the presence of serotonin, atherosclerotic arteries that were not exposed to laser showed an

Best Available Copy

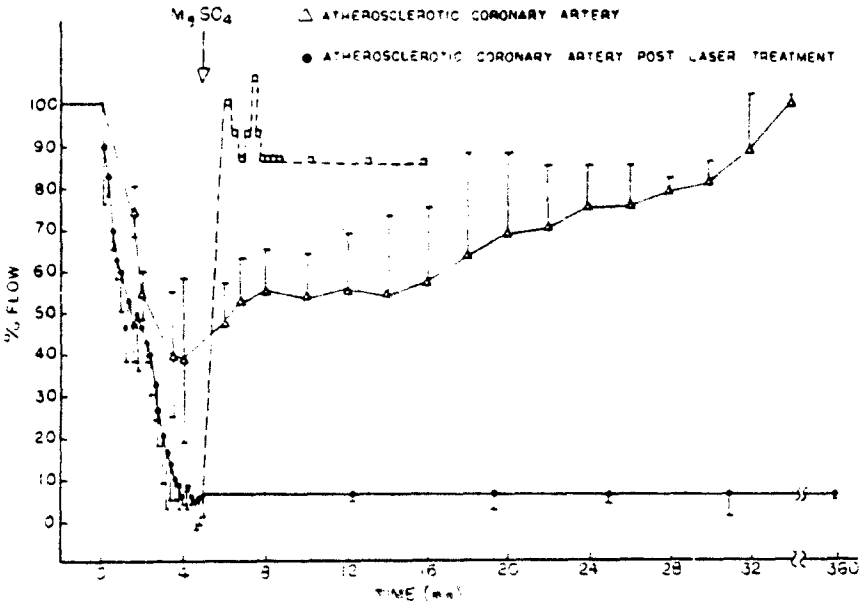

Fig. 5. Flow changes in atherosclerotic coronary arteries before and after laser-heated-tip angioplasty in response to limited exposure to serotonin. Serotonin, 100 ml at 10^{-5} M final concentration, was introduced intraluminally followed by washout with 1 liter of serotonin-free perfusate. Average of data from four atherosclerotic arteries. Average of data from three occluded and recanalized arteries. Differences between points on the two curves in the range 4–360 minutes is significant with a $P < .05$.

increased magnitude of flow reduction (63%) caused by vasospasm compared to arteries without atherosclerotic (22%) under similar experimental conditions of perfusion.

The pharmacologic vasoreactivity of irradiated vessels in patients is not clearly understood at present. It is generally realized, however, that individuals undergoing laser-heated-tip angioplasty in legs continue to experience pain for several days. The etiology of such pain may have several origins, including thermal burns to surrounding tissue or ischemic pain caused by hypersensitivity of the vessels to vasoactive substances that may be circulating in the blood, particularly under conditions of stress following angioplasty. Such substances would induce a reduction in blood flow through the recanalized area because of vasospasm. In the present study, two types of vasospasm were observed. One type was observed on the ultrasound videomonitor during thermal irradiation (Fig. 3B,C). The vessel walls contracted around the metal tip; however, such a spasm was relieved within 2 minutes after termination of thermal irradiation. The other type of vasospasm was drug-induced postangioplasty. In the present experiments sensitivity to the vasoactive agent serotonin was increased in irradiated vessels compared to non-irradiated vessels with a resultant 95% reduction in flow, which was persistent for a period of several hours. Interestingly, such sustained vasospasm was relieved by high concentrations of $MgSO_4$. It is conceivable that still lower concentrations of $MgSO_4$ as well as other vasodilating drugs may be equally effective in relieving postangioplasty vasospasm. The fact that the laser-irradiated vessels could maintain vasoreactivity is significant.

ACKNOWLEDGMENTS

The author wishes to express thanks to the Sheriff-Coroner of Orange County and the Orange County Sheriff-Coroner Forensic Science Faculty and Staff for assistance in obtaining autopsy specimens. This work was supported by grants from Intertherapy Inc. and the National Institutes of Health NIH RR 01192-08 and NIH HL 31318-04.

REFERENCES

Abela GS, Conti CR: Laser revascularization. J Cardiol Med 8:977–984, 1983.

Abela GS, Norman S, Cohen D, Feldman R, Geiser EA, Conti CR: Effects of carbon dioxide, Nd YAG, and argon laser

radiation on coronary atheromatous plaques. Am J Cardiol 50:1199–1205, 1982.

Abela GS, Crea F, Seegen JM, Franzini D, French A, Norman S, Feldman RL, Pepine CJ, Conti CR: The healing process in normal canine arteries and in atherosclerotic monkey arteries after transluminal laser irradiation. Am J Cardiol 56:983–988, 1985.

Choy DS, Stertzer S, Rotterdam HZ, Bruno MS: Laser coronary angioplasty: Experienced with 9 cadaver hearts Am J Cardiol 50:1209–1211, 1982.

Choy DS, Stertzer SH, Myler RK, et al: Human coronary laser recanalyzation. Clin Cardiol 7:377–381, 1984.

Cumberland DC, Starkey, R, Oakley GDG: Percutaneous laser assisted coronary angioplasty. Lancet 1:214, 1986.

Dalen JE, Ockene IS, Alpert JS: Coronary spasm, coronary thrombosis and myocardial infarction: A hypothesis concerning the pathophysiology of acute infarction. Am Heart J 104:1119–1124, 1982.

Ginsberg R, Wexler L, Mitchell RS, et al: Percutaneous transluminal angioplasty for treatment of peripheral vascular disease: Clinical exposure with 16 patients. Radiology 156:619–624, 1985.

Hillis, Braunwald E: Coronary artery spasm. N Eng J Med 299:695–702, 1978.

Lee G, Ikeda R, Herman I, Dwyer RM, Bass M, Hussein H, Kozina J, Mason DT: The qualitative effects of laser irradiation on human atherosclerotic disease. Am Heart J 105:885–889, 1983.

Maseri A, Severi S, Marzulla P: Role of coronary arterial spasm in sudden coronary ischemic death. Ann NY Acad Sci 382:204–127, 1982.

McGuff, PE, Bushnell O, Soroff HS, Deterling RA Jr: Studies of the surgical applications of laser (light amplification by simulated emission of radiation). Surg Forum 14:143–145, 1983.

Morcos NC, Henry WL: Vasoreactivity in isolated, perfused atherosclerotic coronary arteries. J Am Coll Cardiol 9:254A, 1987.

Morcos NC, Stupecky GJ, Purdy RE: Effect of arterial endothelium on sensitivity to 5-hydroxytryptamine. Proc West Pharmacol Soc 28:77–79, 1985.

Sanborn TA, Faxon DP, Kellet MA, et al: Percutaneous coronary laser thermal angiplasty. J Am Coll Cardiol 8:1431–1440, 1986.

Theroux P, Waters DD, Latour JG: Clinical manifestations and pathophysiology of myocardial ischemia with reference to coronary artery spasm and the role of slow channel calcium blockers. Am J Cardiol 48:69–74, 1981.

CHAPTER

32

INTRODUCTION TO LASER PHYSICS AND LASER-TISSUE INTERACTIONS

J. Stuart Nelson, William H. Wright, John Eugene, and Michael W. Berns

This chapter provides a brief description of the nature of the laser, how it works, and the fundamental mechanisms of its interaction with tissue. The appropriate and effective medical use of the laser depends upon an adequate appreciation of these principles.

To start, let us compare the laser with a light bulb (Fig. 32–1). The product of both is light, made up of packets of energy called photons. The laser and the light bulb differ in how their photons are organized. The light from a light bulb radiates in all directions, and there is a direct mathematical relationship between the loss of light intensity and the distance one moves away from the bulb. In the laser, the photons are emitted parallel (or nearly parallel) to and in phase with each other as they travel toward infinity. This property is known as coherence and explains why the light intensity of a laser does not decrease very much with distance. Indeed, this property has been used by scientists to send a laser beam to the moon and back. The laser beam can be highly collimated and focused to spot sizes as small as a single organelle within a living cell and into small-diameter fiberoptics that can be passed through biopsy ports in conventional endoscopes as well as catheters.[1]

Another feature of ordinary light (that from a light bulb) is that it is white or yellow-white in color, because it contains all the different colors and wavelengths in the visual portion of the electromagnetic spectrum and, hence, is polychromatic. A glass prism placed in front of a light bulb, will refract the different wavelengths and allow the constituent colors to be

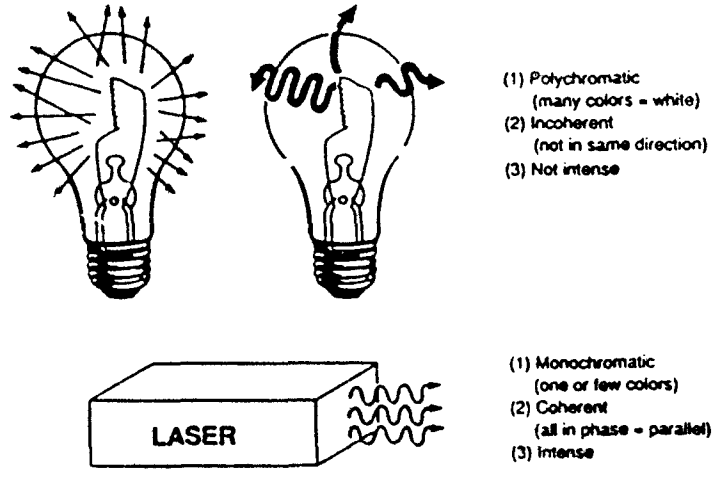

FIGURE 32–1. Characteristics of light from a conventional light bulb and from a laser.

seen. With the laser, the prism will produce light of one wavelength and one color. The light from the laser is therefore pure or monochromatic. This property, under some circumstances, allows for selective absorption of laser energy within the tissue—structures with high absorption at a laser wavelength can be selectively altered or destroyed.

A third difference between the two light sources is in their intensity. The number of photons per unit area of emission produced by the laser is much greater than for any other light source. In fact, millions more photons are emitted by a laser than by a comparable surface area of the sun. For example, peak powers of 10^{12} watts can be obtained with certain short-pulsed lasers. One can also vary the laser power over a large range and achieve quite different tissue effects. For example, a low-power laser may be used to gently heat a tissue, with perhaps the only change being an increase in metabolic rate, whereas a high-power pulsed laser may be used to achieve nonlinear optical effects (e.g., optical breakdown), causing explosions within the tissue.[2] In general, nonlinear effects are avoided in the design of therapies, and to date very high power densities are used only in ophthalmic surgery and in the destruction of urinary tract stones.

As a result of these three differences—coherence, monochromaticity, and intensity—the laser produces a highly unique form of electromagnetic radiation. Otherwise, the photons from the laser and the light bulb obey the same basic laws and principles governing their interaction with molecules and tissues.

BASIC LASER PRINCIPLES

The word *laser* is an acronym derived from *l*ight *a*mplification by the *s*timulated *e*mission of *r*adiation. The amplification of the stimulated emission of radiation is the actual physical process that goes on within the laser device.[3,4]

To understand the acronym, it is necessary to examine some basic atomic physics. Figure 32–2 illustrates two atoms existing in what is termed the ground state, the lowest possible energy level. If by some mechanism the electrons of these atoms are excited from the ground state by the input of energy, they move to a higher energy level called the excited singlet state. The source of this energy or "pumping system" can be electrical, chemical, radiofrequency waves, or light from a flashlamp or another laser. In the first laser built, in 1960, the energy used to excite the atoms inside the laser device was derived from a flashlamp. It is at that point in the process that the production of laser light can begin. When these atoms are in the excited singlet state, they will very quickly drop to an in-between, long-lived energy level called the metastable state. This state may last as long as a few seconds, as compared to 10^{-6} to 10^{-9} second for most excited states. This explains why some materials can go through the lasing process and others cannot. Only atoms and molecules with a metastable state in the energy structure can achieve what is called population inversion and undergo stimulated emission.

What happens next is a spontaneous event. Those atoms existing in the metastable state spontaneously, and by random action, return to the ground state with the loss of some energy. This loss of energy occurs in the form of light—the release of a photon. If the photon is in close proximity to another atom still in the metastable state (remember that the metastable state is long-lived, so that there are going to be many atoms still at that energy level at a given moment), it will collide (interact) with the other atom. This interaction stim-

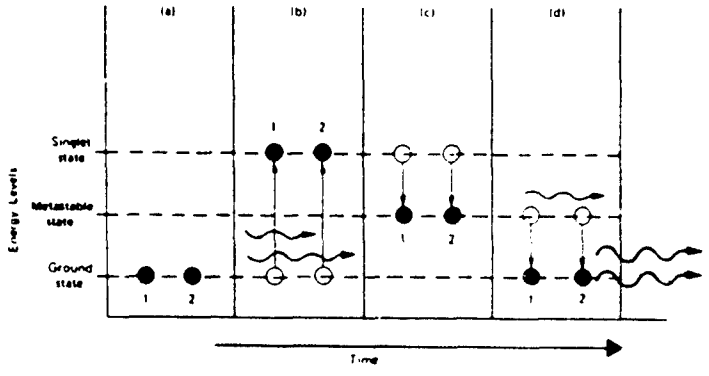

FIGURE 32–2. Energy transitions characteristic of atoms in stimulated emissions. A, Two ground-state atoms (1,2). B, Excitation to the singlet state. C, Transition to the metastable state. D, Atom 1 spontaneously drops to the ground state, emitting a photon that stimulates atom 2 also to drop to the ground state. Both photons from atom 1 and atom 2 have the same wavelength and travel parallel to each other and in phase.

ulates the second atom to return to its ground state and, in the process, emit another photon of light. This phenomenon is termed stimulated emission of radiation. It is a basic principle of physics that since both photons come from identical energy levels, they will be of the same wavelength (color) and will be moving parallel and in phase with each other (the property of coherence). Figure 32–2 illustrates the process of lasing: the stimulated emission of one photon by the action of another photon.

Figure 32–3 presents the foregoing on a much grander scale. Here the atoms in the lasing medium in the ground state are represented by open circles and those in the metastable

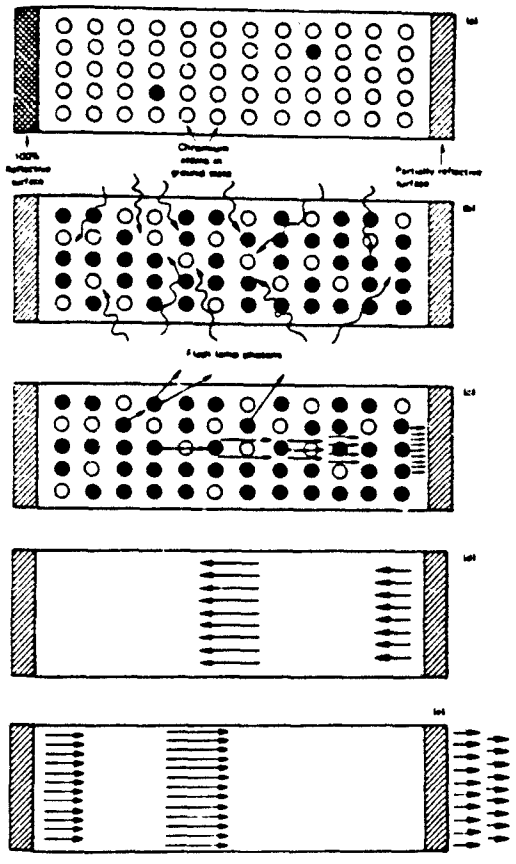

FIGURE 32–3. Schematic of ruby laser action illustrating photon cascade. A, Unstimulated ruby crystal; a few chromium atoms (closed circles) are spontaneously in the singlet or metastable state, but most are in the ground state (open circles). B, Energy input excites ground-state chromium atoms to the singlet state, whence they drop down to the metastable state (closed circles). C, Stimulated emission of excited atoms by photons of stimulated emitting atoms. D, Photon cascade is produced by reflection of reflecting ends; stimulated emission continues. E, Further photon cascade occurs and laser light passes out the partially reflective end.

FIGURE 32–4. Actual components of the first ruby laser, 1960. The pencil indicates the ruby crystal; the flashlamp is to the right of the crystal.

state by dark circles. Most of the atoms initially are in the ground state and are subsequently excited to the singlet state by a flash of light. They rapidly drop down to the metastable state. Following this event, spontaneous emission occurs as described above. The two emitted photons strike other atoms in the metastable state, causing them to emit photons in parallel and in phase with those already present. This results within a fraction of a second in an intense buildup of many photons, or photon cascade. If the laser cavity has opposing reflective surfaces, the photons will be oscillated through the medium at the speed of light, stimulating the emission of more photons. This buildup of intensity by oscillation between two reflecting surfaces results in the final process in lasing: amplification. By permitting the release of some photons by means of one partially reflective surface at one end of the cavity, the result is a bright, intense, monochromatic beam of light: a laser beam.

The first laser, built in 1960 by Theodore Maiman, used synthetic red ruby, which is a crystal of aluminum trioxide doped with chromium atoms. It is the chromium atoms inside the crystal lattice that go through the lasing process to produce the red light. The aluminum trioxide is merely a crystal structure that holds the chromium atoms in place. Figure 32–4 is a picture of the Maiman laser, a notably small apparatus with only three components: a ruby crystal, a flashlamp, and a cavity with

FIGURE 32–5. Free electron laser at the University of California, Santa Barbara.

two reflective mirrors. Figure 32–5 is an illustration of state-of-the-art laser technology, the free electron laser. This laser, which cost many millions of dollars to construct, may represent the future of laser technology because of its potentially broad wavelength tunability. Much engineering is still to be done to get this laser to a practical level, and research is under way on possible biomedical applications.

Figure 32–6A shows those regions in the electromagnetic spectrum where lasers can be utilized. It can be seen that lasers occupy a relatively small region of the entire spectrum. However, this portion is expanding with the development of the free electron laser, which eventually may be manipulated from the infrared to the ultraviolet portions of the spectrum.

Different kinds of lasers are identified by the type of material inside the device that undergoes the lasing process (e.g., the argon laser has argon gas as the lasing medium). There are four categories of lasing materials: solid, gas, liquid, and semiconductor. Examples of solid-state lasers are the ruby and YAG (yttrium-aluminum-garnet) lasers. Examples of gas lasers are the helium-neon, argon, and carbon dioxide lasers. Liquid lasers employ complex organic dyes such as rhodamine and coumarin in a solution or suspension. Semiconductor lasers use two layers of a semiconductor material such as gallium arsenide. It is possible to obtain lasing action from any of these materials provided their atomic structures have metastable states that permit the stimulated emission process to occur (Fig. 32–6B).

There are also ways to modify the wavelengths obtainable from lasers. Certain crystals, called nonlinear, asymmetric crystals, take photons from very intense light and, through an interaction of these photons with the crystal lattice, generate laser light with twice the frequency (half the wavelength) of the incident radiation. This is called frequency doubling or harmonic generation. These complicated physical processes can be used to double, triple, or quadruple the wavelengths from the primary laser source. If the primary laser is a tunable dye laser, it is possible to greatly increase the number of wavelengths available by passing the dye laser output through the nonlinear crystals (Fig. 32–7).

In summary, there is a wide range of lasers available for clinical use. The dye lasers, and in the future the free electron laser, can be precisely tuned to emit photons at wavelengths that match absorption peaks of tissue chromophores, thus permitting their selective destruction and subsequent tissue ablation.

DOSIMETRY

Laser light is a form of energy that is subject to certain fundamental physical laws defined by a set of equations. One needs to understand these relationships in order to properly use the laser as a medical tool.[7]

Laser light emitted from the standard medical device is generally characterized in terms of power, measured in watts. The energy

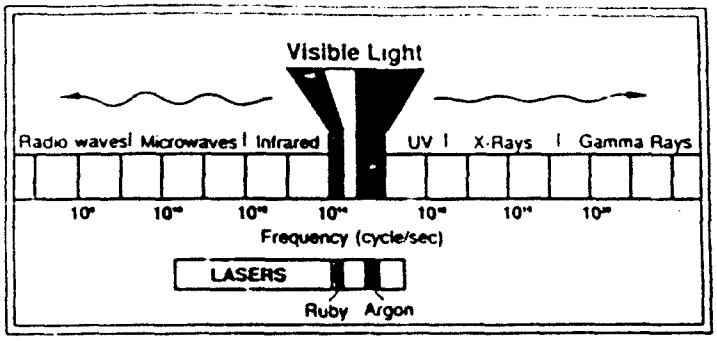

A

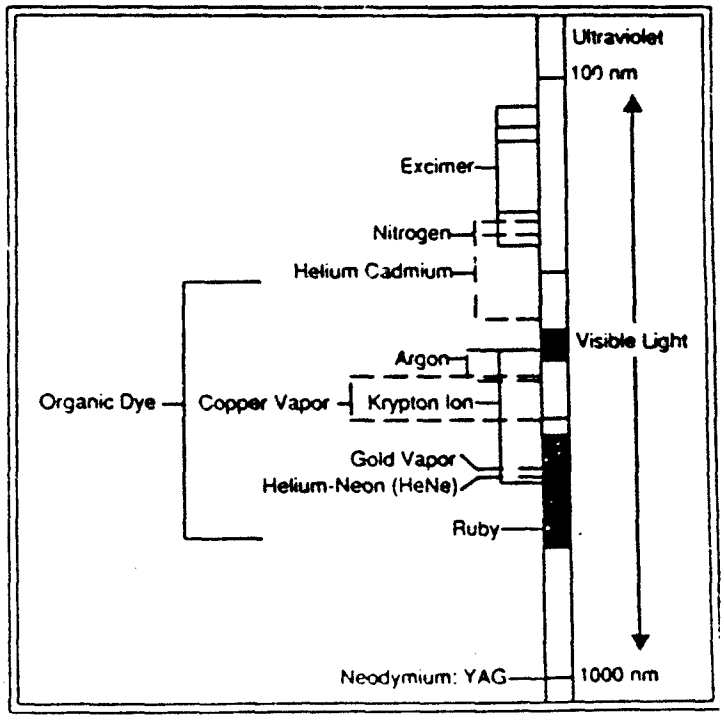

B

FIGURE 32–6. A, Comparison of various electromagnetic radiation sources. B, Types of lasers and their positions on the electromagnetic spectrum.

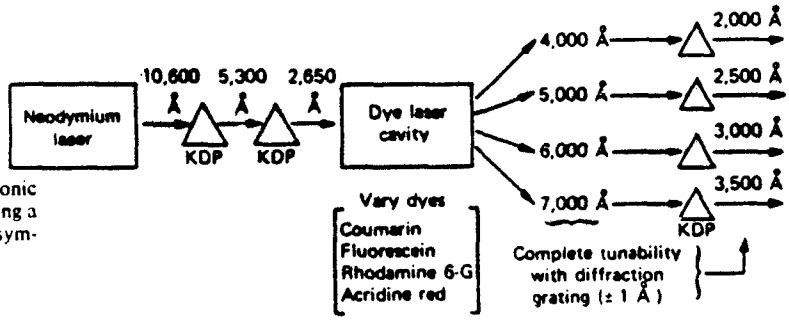

FIGURE 32–7. Second harmonic generation is produced by passing a Nd:YAG laser beam through asymmetric crystals.

Best Available Copy

(stated in joules) is defined as the power times the time interval during which it is emitted:

Energy (joules) = power (watts) × time (seconds).

For most commercially available lasers, the laser beam power density may be characterized by a gaussian curve in two dimensions (a gaussian spot). For this type of beam, the spot size (radius, r) is defined as the distance from the center of the beam to the point on the periphery where the power density is $1/e^2$ of that at the center (Fig. 32–8). The beam diameter is then twice the spot size. The power density or irradiance is then defined as the power applied per unit area of target tissue:

Power density = power (watts)/$\pi \times r^2$ (cm^2).

Fluence is defined as the energy applied to an area of target tissue:

Fluence = power density ($watts/cm^2$) × time (seconds) = $joules/cm^2$.

It can readily be appreciated that the effect of the laser beam on target tissue can be affected by any of three variables: power, spot size, and time. The effects of power and time are proportional, whereas that of spot size is an inverse square. If either the power or time is doubled, the fluence increases by a factor of two. However, if the spot size (radius) is decreased by a factor of two, the fluence will increase by a factor of four. Doubling the spot size will result in a fourfold reduction in the fluence (Fig. 32–9).

What does this mean with respect to tissue effects? If the clinical objective is to make an incision, the surgeon should use a very small spot with a high power density, because a laser

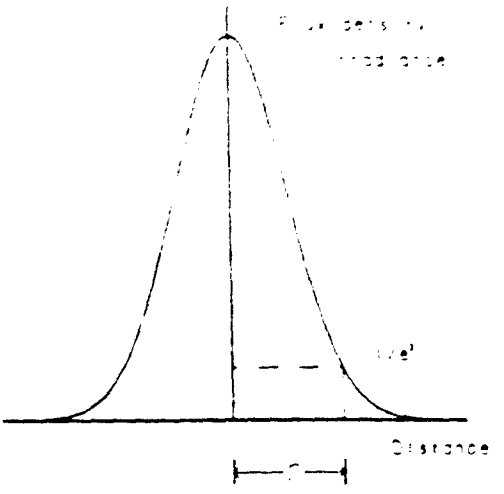

FIGURE 32–8. Laser beam profile.

with those characteristics will penetrate deeply into the tissues. However, if the intent is to ablate layer by layer from the surface, a larger spot size with a lower power density should be used (Fig. 32–10). This gives the physician a way to control the effect produced in the tissue by manipulating either the spot size or the power of the laser beam. It is very important to recognize this principle so that the physician will be able to achieve the desired clinical results.

A continuous wave (CW) laser may be differentiated from a pulsed laser, which provides bursts of energy. The CW laser undergoes very minimal fluctuation with time, creating a steady flow of radiation. A pulsed laser delivers its energy in the form of a single pulse or a train of pulses. The frequency or

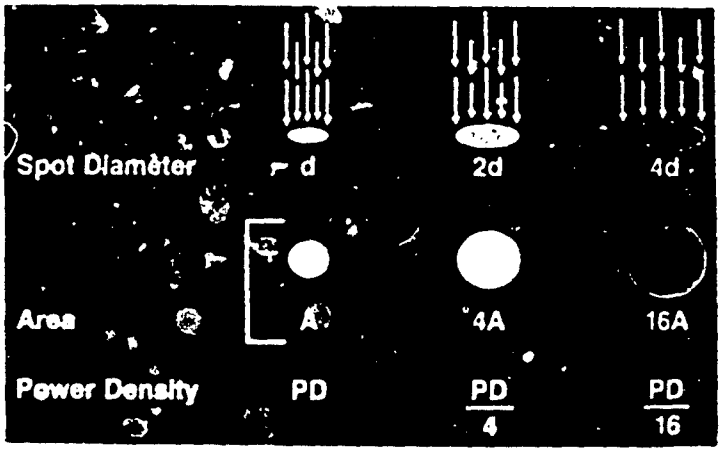

FIGURE 32–9. Spot size, area, and power density relationships.

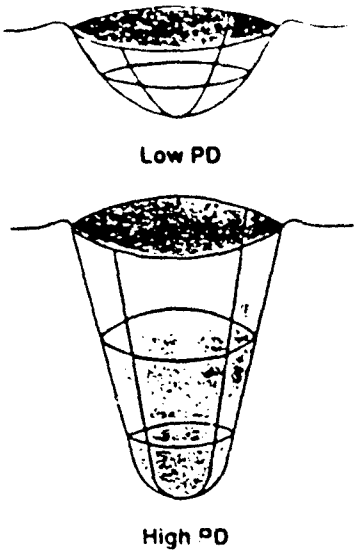

FIGURE 32–10. Relative crater configuration and volume as a function of power density (PD).

pulse repetition rate is the number of pulses emitted in 1 second. The duration of the pulse, or pulse width, is defined as the total time required for the pulse to rise from zero intensity, build to a maximum, and then fall to zero intensity again. An alternative definition for pulse width (used for short pulses) is the time between the 50 per cent points on the pulse curve. This is called full width at half maximum (FWHM; Fig. 32–11).

For each pulse, the energy, irradiance, and fluence are calculated as for the CW laser described above, noting that the laser is now on for a brief time. The average power produced by the train of pulses is determined by multiplying the pulse power by the pulse repetition rate and the pulse width:

Average power (watts)
= pulse power (watts)
× pulse repetition rate (1/seconds)
× pulse width (seconds).

The average irradiance and fluence are calculated in the same manner as described earlier.

Several methods of creating pulses of laser light are available, with pulse widths ranging from tenths of seconds to femtoseconds (10^{-15} second). Because these techniques can be quite complicated, especially in producing very short pulse widths, they are not discussed here.

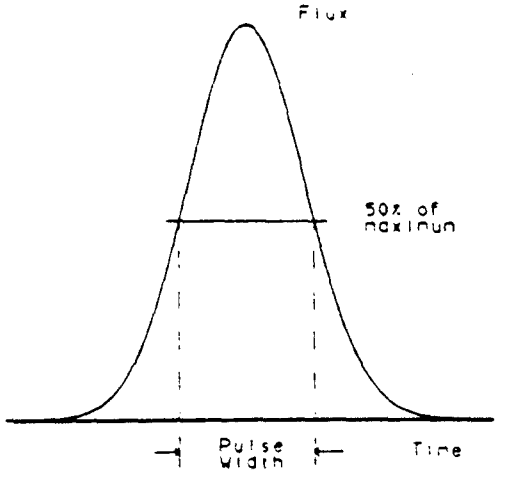

FIGURE 32–11. Full width at half maximum is defined as the time between the 50 percent maximum intensity points on the pulse curve.

LASER-TISSUE INTERACTIONS

How can this intense, pure beam of light be utilized? We recall that light from lasers follows the basic laws of photobiology. The one exception is for extremely short, intense laser pulses, where nonlinear events may occur. These events, such as multiphoton absorption, plasma generation, and ionization, occur as a function of photon intensity and were not observed until extremely short (nanosecond to picosecond) laser pulses were generated. It is important to recognize that the interactions of laser radiation with living tissue are complex phenomena influenced not only by laser parameters, such as power, spot size, time, and wavelength, but also by tissue properties (Fig. 32–12).[2]

If a laser beam is directed at a tissue, it may be reflected back to the source or to another undesired surface. Since tissues reflect light, their reflectance properties are important considerations. One must also be aware that instruments in the operative field may reflect the light and may create problems and health hazards for the patient or attending personnel.

If reflectance is adequately controlled and the light enters the tissue, the ultimate event affecting the tissue is absorption of the light. However, two things can happen other than absorption. The tissue itself can scatter the light. The light can literally bounce off particles and structures in the tissue and scatter to places where it is not wanted. Alternatively,

Best Available Copy

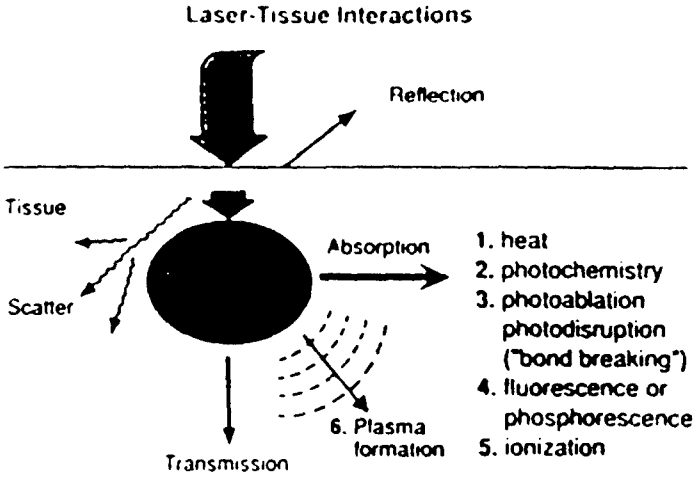

FIGURE 32–12. Types of laser-tissue interaction.

the light might be transmitted right through the tissue with only a minimal amount being absorbed. Since every tissue has reflective, scattering, and transmissive properties, understanding these tissue characteristics is an important aspect of knowing how to use the laser.

The process of absorption is the key to effective laser use. Without absorption, there is no tissue response. When photons enter the tissue, those that are not reflected, scattered, or transmitted are absorbed. Their energy is transferred to some other molecule or group of atoms in the tissue that is to be altered or changed. Where and how is this energy dissipated? Normally we think of lasers as producing heat, and in probably 80 per cent of clinical procedures using lasers, they are used for the production of some kind of local thermal event. However, as will be seen later, heat is just one way in which the energy of the photon can be dissipated (Fig. 32–12). The important point is that when photon energy is absorbed, the absorbing structure or tissue has to get rid of that energy in some way, and it is the manner in which this energy is dissipated that brings about the different biological effects that are useful clinically.

For light energy to be absorbed, it is necessary to have some absorbing molecule in the tissue. These molecules are generally referred to as chromophores. When light is absorbed by a chromophore, the photon energy becomes invested in the chromophore. In Figure 32–13 are plotted the absorption spectra of two common molecules that function as chromophores: hemoglobin and water. Hemoglobin has a very high absorption in the violet and blue-green portions of the spectrum. The absorption starts to decline in the red region of the spectrum; hemoglobin appears red because it does not absorb red light. This is the rationale for using an argon laser, which emits blue-green light, as the primary treatment for vascular lesions such as hemangiomas and port-wine stains. Hemoglobin absorbs the blue-green photon energy, which is converted to heat, which in turn destroys the blood vessel. This may not be as selective a process as anticipated because, even with selective absorption by the hemoglobin molecule, the heat that destroys the blood vessel (unless it is precisely confined just to this area), will radiate out in all directions and may still destroy the overlying skin layers or adjacent structures. Newer procedures are being developed with short-pulsed lasers, in which the energy is confined to a very short period of time, reducing the spread of the heat to surrounding structures.[6] Water, on the other hand, has no absorption in the visible portion of the spectrum and very minimal absorption in the near-infrared portion. However, further out in the infrared (past 2 μm) water has significant absorption. For this reason a carbon dioxide laser can have a direct effect on any tissue in the body. Proper use of a carbon dioxide laser can be compared clinically to performing a dermabrasion, because the laser gradually removes cells layer by layer by the volatilization of water present in the tissue. The photons of the neodymium:YAG (Nd:YAG) laser, on the other hand, are very poorly absorbed by hemoglobin, water, and other body pigments. This is why the Nd:YAG laser will penetrate much more deeply into tissue and affect a

Best Available Copy

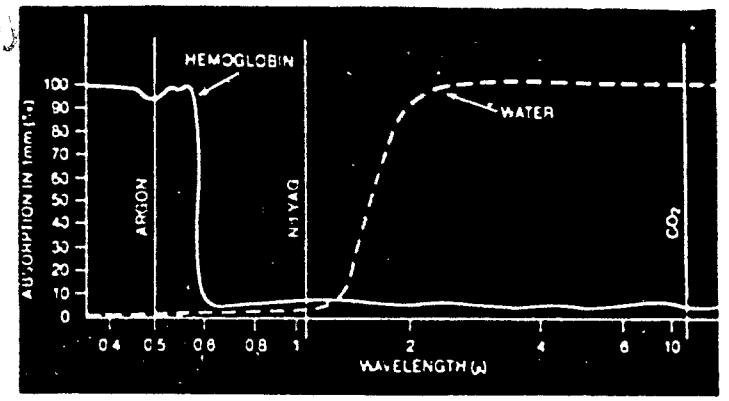

FIGURE 32–13. Absorption spectra of hemoglobin and water.

much greater volume of tissue than either the argon or the carbon dioxide laser.

In summary, selection of the correct laser for a particular clinical procedure requires an understanding of the absorptive as well as the reflective, scattering, and transmissive properties of the target tissue.[9]

HEAT

Given that one goal of laser therapy is the precise control of thermal energy, one must first understand the sequelae of tissue heating. Figure 32–14 shows the effect of a rise in temperature in a typical tissue being irradiated. As the temperature rises to between 37° and 60° C, the tissue starts to retract and conformational changes occur. At a temperature above 60° C, there is protein denaturation and coagulation. From 90° to 100° C, carbonization and burning of tissue occur. Above 100° C, the tissue is vaporized and ablated. Ideally from a clinical point of view, the physician should be able to confine the heating process to any one of these thermal ranges to produce the desired clinical result. Physicians experienced in laser therapy acquire the ability to discern these tissue changes visually so that the heating process can be stopped at the desired point. It is therefore important that physicians planning to use lasers take a basic course with hands-on tissue studies as well as complete a preceptorship with an instructor who has considerable experience with lasers and can help them develop the requisite skills.[10]

It is important to recognize that heat radiates in all directions around the crater produced by tissue vaporization. The result will be successive circumambient zones of car-

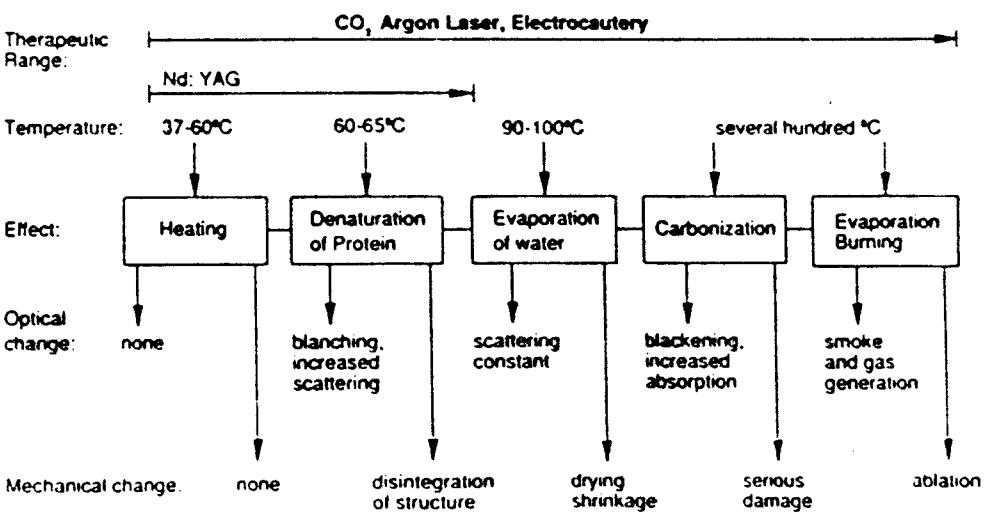

FIGURE 32–14. Thermal interactions of laser irradiation with biological tissues.

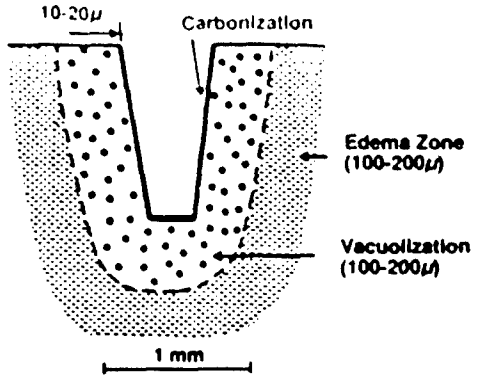

FIGURE 32–15. Zones of thermal damage following laser irradiation.

bonization, vacuolization, and edema as the heat is dissipated (Fig. 32–15). The zones of vacuolization and edema may be irreversibly affected and eventually become necrotic and slough off, or they may be repaired. The laser is not necessarily going to produce a nice, clean cut by vaporization while leaving all other tissues completely unaffected. The objective of many laser procedures is to minimize these other zones of thermal injury while maximizing tissue removal.

One way to maximize the [illegible] ment of heat is to use a pulsed laser with a pulse width on the order of the thermal relaxation time of the tissue. This is defined as the time it takes for a target structure to cool to one half its initial temperature. That is, the laser energy is invested in the target before much heat has diffused out of the target. Shorter pulse durations can confine the laser energy to progressively smaller targets. Longer pulses offer a more generalized heating and, therefore, less spatial selectivity."

PHOTOCHEMISTRY

Photon energy may also be dissipated by photochemistry. The basic concept of photochemistry is that certain molecules (natural or applied) can function as photosensitizers. The presence of these photosensitizers in certain cells makes them vulnerable to light at wavelengths absorbed by the chromophore. The excited photosensitizer subsequently reacts (transfers its energy) with a molecular substrate, such as oxygen, to produce highly reactive singlet oxygen, which causes irreversible oxidation of some essential cellular

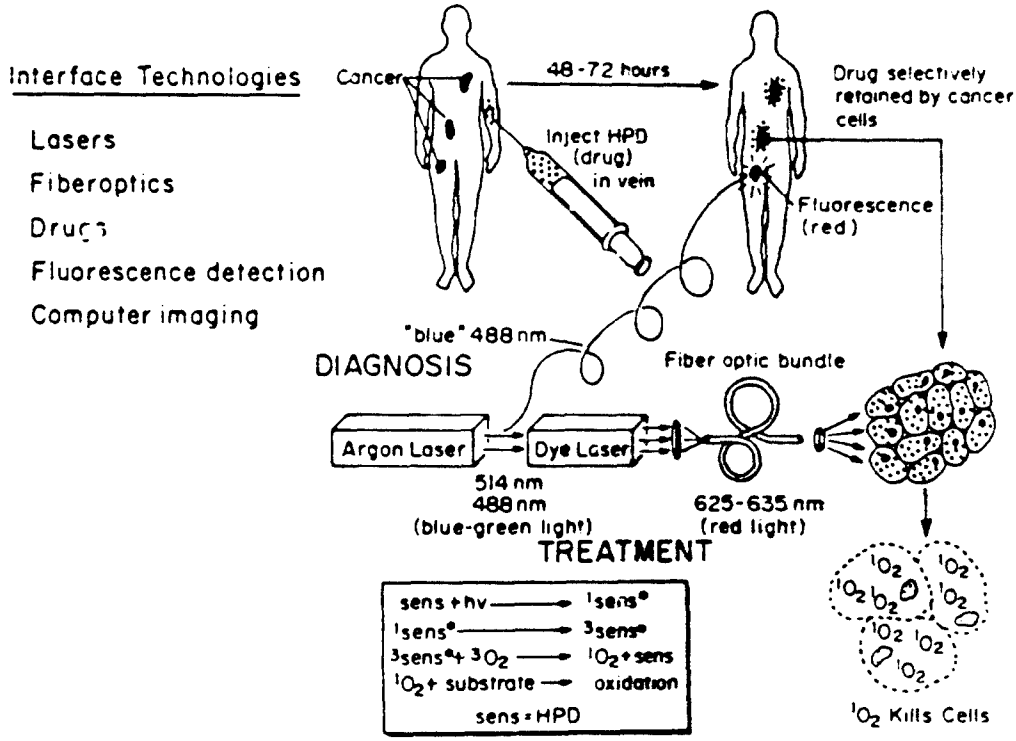

FIGURE 32–16. Scheme of photodynamic therapy for cancer using a laser and HPD injection.

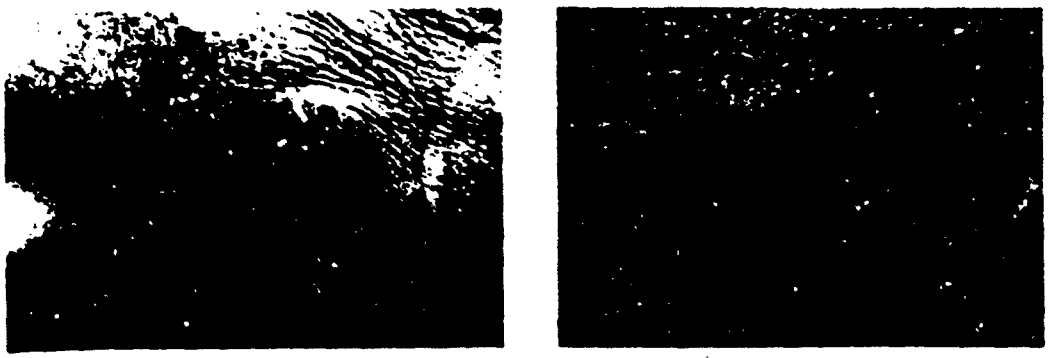

A B

FIGURE 32–17. Patient with superficial recurrence of breast cancer. A, before photodynamic therapy. B, 24 hours after treatment; note the black, necrotic tumor nodules.

component. All of this occurs without the generation of heat. The most common clinical use of this mechanism has been in the treatment of cancer after sensitization with hematoporphyrin derivative (HPD). Although the mechanism of HPD's preferential localization in malignant cells is uncertain, it is well established that the total time the HPD is retained in the malignant tissue is much longer than in nonmalignant tissue, from which it is generally cleared between 24 and 72 hours. As a result, there is a window of time in which one can exploit the differences in HPD concentration to bring about the selective photodegradation of malignant tissue (Fig. 32–16).

Clinically, photodynamic therapy is carried out by a two-step procedure. HPD is first administered intravenously in the range of 2 to 3 mg/kg body weight. After a delay of 24 to 72 hours to allow for the localization in malignant tissue, the tumor is irradiated with visible red light tuned to 630 nm. Shortly after light administration, the tumor becomes necrotic (usually within 24 hours), and when effectively treated, the tumor becomes a nonpalpable scab, which is usually sloughed off within a few days (Fig. 32–17). The high therapeutic ratio and relative lack of morbidity have made this potentially a very attractive form of therapy. Treatment parameters have been refined such that therapy can be undertaken with a reasonable expectation of good results in both animal and human trials. Although it can be used to eradicate relatively large tumors, it appears to be especially advantageous in the patient with a thin, superficial tumor easily accessible to light.[11]

This technique may also have application to vascular surgery. For example, Spears et al.[12] have described the selective photosensitization of atheromas with HPD, and Pollock et al.[13] have demonstrated that HPD-sensitized atheromas can be surgically excised (by endarterectomy) with less laser energy than nonsensitized atheromas. This could result in less perforation and damage to the underlying vessel wall.

FLUORESCENCE

Photon energy may be dissipated as the reemission of light. If this happens within 10^{-6} seconds after absorption, it is called fluorescence. The fluorescent photon is emitted as the excited atom returns to the ground state. However, because some energy is lost by collisions with other atoms in the excited state, the energy of the fluorescent photon is lower (and therefore the wavelength is longer) than the absorbed photon. How can this be used diagnostically?

It turns out that many of the photosensitizing dyes used to induce photochemistry are also fluorescent. If in the case of HPD, a 400 nm blue-violet light from a krypton laser is used with an appropriate filter and image intensifier, fluorescence can be observed in malignant tissue (Figure 32–18). It would then be possible to switch over to 630 nm red light and bring about the photochemical reaction to kill the cells containing the photosensitizer. This technique has a great deal of promise clinically and is being used in the detection of occult lung tumors and to determine the extent of superficial skin tumors as well as to delineate tumors

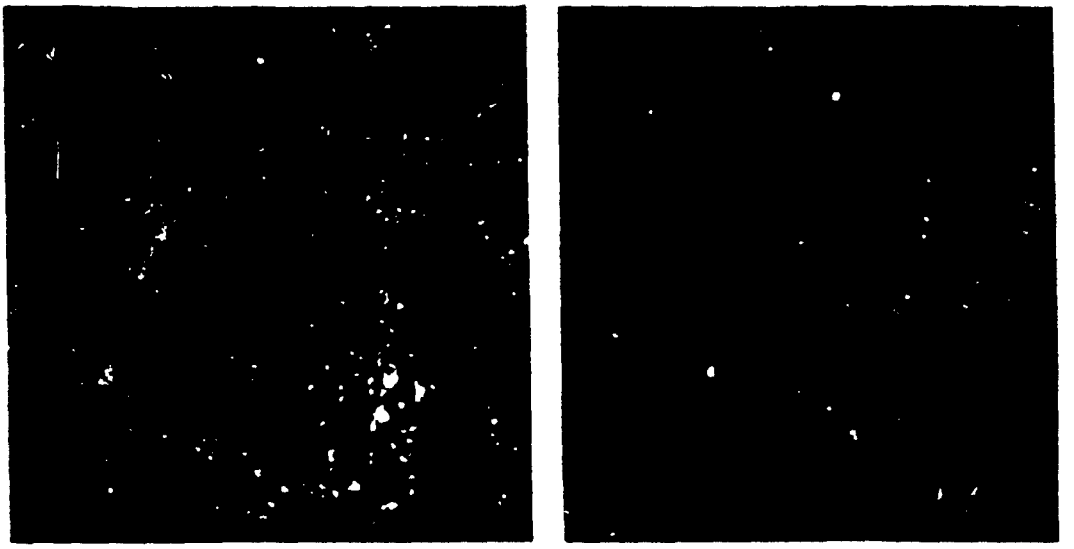

A B

FIGURE 32–18. Patient with recurrent breast carcinoma injected previously with HPD. Blue-violet 400 nm light from a krypton laser is used with appropriate filters, and red fluorescence can be observed in malignant cells. A, Before HPD injection; B, 48 hours after injection, red fluorescence is evident.

and dysplasia in the bladder.[14] If the image intensifiers presently under development become sensitive enough, it would theoretically be possible to detect just a few photons of light coming from a small group of cells or maybe even from a single malignant cell.

Intravascularly, laser-induced fluorescence is being developed to distinguish normal from diseased (atherosclerotic) vessels as well as to differentiate qualitatively and quantitatively the different classifications of plaque (see Chapter 46).

Laser-stimulated fluorescence can also be used analytically to scan large populations of cells that are passed through a laser beam in a cytofluorometer. In addition, lasers may be used to excite small microscopic regions of single cells to study the binding and movement of biologically important molecules.[15]

PHOTOABLATION

Photoablation occurs when pulsed, high-energy ultraviolet photons produced by an excimer laser are absorbed on the surface of an organic substrate.[16,17] Since ultraviolet radiation is absorbed intensely by most biological molecules, the penetration depths are only a few micrometers.[18] This combination of high absorption and high individual photon energy results in the direct transfer of energy within the absorbing molecule to the bonds that hold the molecule together. When the incoming ultraviolet energy exceeds the molecular bonding energy (the ablation threshold), the substrate will undergo random bond scission and be reduced to its atomic constituents. The rapid expansion created by this excitation and bond cleavage gives rise to the actual ejection of fragments at supersonic velocities—the ablation phenomenon. Although the question of heat generation in this process has not been resolved, it is clear that the tissue degradation process is by a nonthermal process.

This feature has been exploited experimentally to produce well-defined, nonthermal cuts of very small widths by excimer lasers at several ultraviolet wavelengths (argon fluoride, 193 nm; krypton fluoride, 248 nm; xenon chloride, 308 nm; xenon fluoride, 351 nm). This process may have many promising applications in ophthalmology, dermatology, vascular surgery, orthopedics, and neurosurgery, where precise athermal tissue removal would be highly desirable (Fig. 32–19).

IONIZATION

Ionization is the ejection of an electron from an atom, and it is generally felt that the individual photons generated from existing lasers do not have enough energy to cause the ab-

Best Available Copy

A

B

FIGURE 32–19. A, Incisional ablation of corneal stroma with 193 nm radiation from an excimer laser. B, Histology reveals a clean, nonthermal cut.

sorbing molecule to lose an electron. However, it is possible to have absorption of more than one photon simultaneously in a "multiphoton process."[19] This has been observed in solutions and in living cells, but in most present clinical situations ionization does not occur. With an x-ray laser (currently under development for military use), the photon energy would of course be high enough to cause the ejection of an electron.

PLASMA FORMATION

Plasma formation is the one laser-tissue interaction that does not obey the basic photobiological principle of reciprocity, which states that an effect is independent of the time period within which the photons are delivered (i.e., it is power dependent). With the advent of Q-switched (nanosecond) and short-pulsed, mode locked (picosecond) lasers, it has become possible to generate very high power densities (measurable in gigawatts per square centimeter) in focal spots of 25 to 50 microns. When these lasers are precisely focused on a small spot of tissue, unusual nonlinear events occur.[2] It is possible to generate a plasma, which is a gaseous cloud rich in free electrons. This plasma has sometimes been called the "fourth state of matter" because its properties are very different from those of solids, liquids, or gases. Because of the sudden production of an electrical field in 10^{-9} to 10^{-12} seconds, an intense acoustical shock wave is generated in the medium. This acoustic wave emanating from the focus carries potentially damaging kinetic energy and has been used clinically in the eye to remove secondary cataracts in the posterior capsule as well experimentally to fracture recalcitrant urinary calculi (Fig. 32–20).

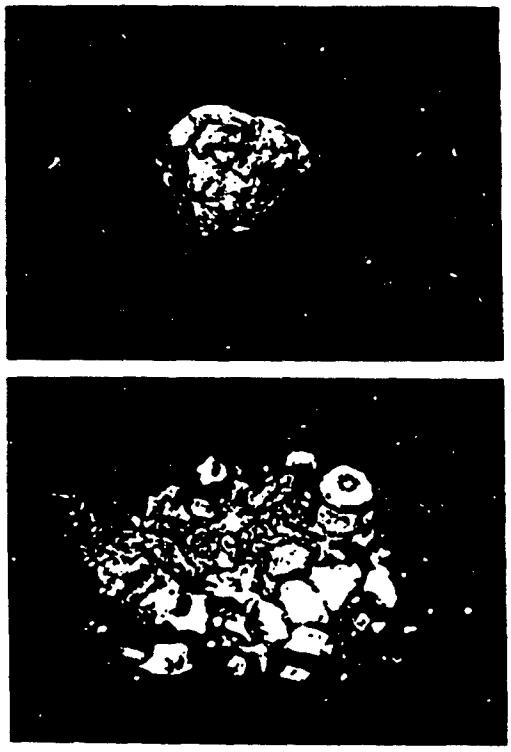

FIGURE 32–20. High power density from a short-pulsed laser produces an acoustical shock wave, destroying a urinary calculus. A, Prelaser; B, postlaser.

In summary, all the mechanisms discussed have biomedical applications. The most effective use of the laser requires an understanding of these different mechanisms.

TYPES OF LASERS

Argon Laser

The argon laser emits blue-green light at six different wavelengths, ranging from 457.9 to 514.5 nm, with 80 percent of the energy being contained in the 488 to 514.5 nm peaks. The device uses a very high electrical current passed through argon gas to excite the argon atoms into the singlet state. The argon laser operates on a continuous wave basis and is capable of average powers up to approximately 20 watts. Transmission of the light to the target is usually through a glass optical fiber that can be coupled to either an operating microscope or a handpiece or used directly through a variety of endoscopes.

The argon laser light has the ability to penetrate intact overlying skin or clear ocular structures to be primarily absorbed in tissue by the chromophores hemoglobin and melanin. If these chromophores are present, the argon laser photon energy is converted to heat, producing an area of thermal damage centered around the target chromophore structure.

The principal applications of the argon laser have been in the fields of ophthalmology, plastic surgery, and dermatology. One of the first major medical applications of lasers was the use of the argon laser in the treatment of diabetic retinopathy in the early 1970s. This disease is characterized by the excessive growth of blood vessels in response to hypoxia on the surface of the retina and into the vitreous. The result may be major hemorrhage and eventual retinal detachment, leading to a drastic reduction in visual acuity. In early studies, the laser was used to selectively destroy the newly proliferating blood vessels by focusing the laser directly on the blood vessel itself. However, this technique has given way to panretinal photocoagulation, which involves exposure of the entire, already ischemic retina rather than the new blood vessels themselves. The argon laser has also been used for a variety of other retinal vascular disorders including central retinal

vein occlusion, branch vein occlusion, Eales's disease, and senile macular degeneration.[20]

In plastic surgery and dermatology, the argon laser is the mainstay of treatment for multiple superficial or cutaneous vascular lesions, including port-wine stain, hemangioma, telangiectasia, senile angioma, and acne rosacea. The argon laser light is absorbed by hemoglobin in the dilated, ectatic capillaries of these lesions, causing thermal damage and thrombosis while sparing adjacent skin appendages. As the treatment site heals, fibrosis occurs and the targeted lesion is replaced. Good to excellent results with significant color change without scarring occur in 80 percent of cases. An ever-widening variety of benign pigmented cutaneous lesions are also amenable to argon laser treatment because of the presence of melanin. Argon laser treatment of decorative tattoos is a simple, efficient outpatient procedure using local anesthesia. The results are comparable to or minimally superior to conventional methods, which may be more time consuming or complicated.

Carbon Dioxide Laser

The carbon dioxide (CO_2) laser is currently the most frequently used surgical laser. This laser has a spectral emission in the middle to far-infrared portion of the spectrum at 10,600 nm (10.6 μm). The CO_2 laser is a gas laser that uses a mixture of carbon dioxide, nitrogen, and helium as the lasing medium. Excitation of the lasing medium is most commonly achieved by high-voltage electrical current. To obtain adequate energy transfer, an intermediary nitrogen atom is first excited, with the energy subsequently transferred to CO_2 atoms. After the CO_2 atom decays and emits infrared energy, the molecule is brought down to the ground state through collisions with the helium atoms. Light of this wavelength is not currently capable of fiberoptic transmission (although fiberoptics and hollow wave guides for the CO_2 laser are under intensive development) and must therefore be delivered to the tissue through an articulating arm that contains a series of reflecting mirrors terminating in a handpiece with a focusing lens. Since the CO_2 laser beam is invisible, a red helium-neon laser beam of very low intensity is employed as an aiming device in all commercial systems.

The CO_2 laser wavelength is highly absorbed by water. The absorption is so efficient that 98 percent of the incident energy is absorbed within approximately 0.01 mm of the impact point. This causes rapid, localized heat production, resulting in immediate boiling and vaporization of intracellular water within the tissue and, hence, tissue ablation.

Because all living tissue contains 70 to 90 percent water, the CO_2 laser has multiple applications in medicine and surgery.[21] The CO_2 laser may serve as a "light scalpel" for accomplishing incisional or excisional procedures involving infected or highly vascular lesions or in lesions located in a highly vascularized anatomic region. Here the beam diameter is reduced to its minimum possible size, usually in the range of 0.1 to 0.2 mm. The power output is relatively high, resulting in irradiance values in the range of 25,000 watts/cm^2. The actual depth of the incision will depend upon the power and the rate of movement of the beam across the tissue. The heat conducted to the surrounding tissue is capable of coagulating blood vessels up to 0.5 mm in diameter. Vessels larger than this may also be sealed with minimal damage by applying laser energy directly to the end of the severed vessel after it has been clamped. The beam has also been demonstrated to spontaneously seal lymphatic vessels, raising the possibility that the CO_2 laser may have a unique advantage in dealing with lesions that have a potential for lymphatic spread.

The CO_2 laser can also be used as a tool for the vaporization and ablation of multiple superficial lesions. Here the beam is applied to the tissue in a defocused, large spot size (2 to 5 mm) at low power, resulting in irradiances in the range of 150 to 500 watts/cm^2. When the laser is used in this manner, the final result is a broad but shallow zone of tissue ablation. In gynecology, CO_2 laser vaporization of precancerous lesions of the cervix, vagina, and vulva can be performed as an outpatient procedure under local anesthesia. Condyloma acuminatum is very effectively treated by CO_2 laser vaporization. Here the laser is of particular value in difficult-to-reach lesions or when surface contour must be preserved with minimal damage. Furthermore, high local temperatures sterilize and eliminate the virus from the field.[22]

In summary, the ubiquitous CO_2 laser has allowed many physicians to perform a large number of procedures on an outpatient basis that previously required hospitalization. Preliminary studies have suggested that there is a lower incidence of recurrence, less pain, faster healing, less scarring, and a lower risk of com-

plications following CO_2 laser surgery. However, these data are still very preliminary and not uniformly true for all patients and procedures.

YAG Laser

The YAG laser is a solid-state laser comprised of an yttrium-aluminum-garnet crystal doped with one of several elements that undergo flashlamp-excited stimulated emission. The most common doping element is neodymium (Nd), which emits primarily at 1.06 μm. However, it is also possible to optimize the Nd:YAG laser for 1.3 μm (which, because of a slightly better water absorption, is being experimented with for gentle tissue welding procedures).

The 1.06 micron YAG laser is constructed either as a heat-producing CW device for general surgical and endoscopic procedures, or as a short-pulsed (picosecond or nanosecond) device, used exclusively in ophthalmology for secondary cataract destruction via a plasma-generated shock wave.

Surgical application of the YAG is generally indicated when deep thermal coagulation of several centimeters or more is desired, for example, for the coagulation and necrosis of obstructions in the airways, the esophagus, or the urogenital tract. It is also used for the treatment of gastrointestinal bleeding. The fact that the 1.06 μm beam can be readily transmitted by conventional glass fiberoptics makes this laser particularly attractive for endoscopic procedures. However, because of the deeper penetration of this wavelength through tissue due to the absence of a strongly absorbing chromophore, this laser should be used with considerable caution by highly laser-experienced physicians.

The 1.06-μm YAG laser may also be used in combination with a solid sapphire crystal affixed to the end of the fiberoptic. This approach permits direct contact of the fiber with the tissue via the sapphire tip. A variety of tips with different geometries can focus the beam in such a way that tissue ablation can be achieved with desired geometries (incisional, radial, coagulation, etc.). In addition, it is suggested that this mode of application permits both some degree of surgical "touching," and better control of unwanted tissue scattering and transmission of the beam. The technique will undoubtedly have some application in general and vascular surgery, but it has yet to be fully defined (see Chapter 39).

Another type of YAG laser is the KTP frequency-doubled YAG. This device uses second harmonic generation (see section on "Basic Laser Principles") to generate 532 nm (green) laser light. These lasers can deliver up to 20 watts in continuous wave format and have been approved for many of the same procedures as the argon laser (vascular lesions) and the CO_2 laser (tissue ablation of lesions on the skin and in the gynecological, gastrointestinal, and urological tracts).

Finally, there are other YAG lasers that are doped with elements such as erbium (2.94 μm) and holmium (2.1 μm). Because these wavelengths are capable of fiberoptic transmission and are on the water absorption peaks, they may have considerable application in endoscopic surgery. They may, in fact, replace the CO_2 laser. In addition, these lasers can operate in a pulsed mode and produce tissue ablation by rapid volatilization of water, resulting in minimal thermal damage to surrounding tissue. These lasers are still considered experimental.

EXCIMER LASERS

The excimer laser produces coherent pulses of light at different ultraviolet wavelengths. (The word *excimer* is actually a contraction of "excited dimer" and pronounced similarly.) Initially, laser transitions were based on energy changes in the excited dimer Xe_2. Current excimer lasers use compounds of rare gases and halogens, which are excited complexes rather than excited dimers, but the name has persisted. Excimer output can be varied between 355 nm (near-ultraviolet) and 157 nm (far-ultraviolet) by changing the mixture of the gases.

The mechanism of action of the excimer laser differs from that of visible light and infrared lasers in that the ultraviolet photon energy is high enough to cause photodissociation, or the direct breaking of intramolecular bonds in polymeric chains without the production of heat. This produces sharp, clean cuts with little surrounding thermal tissue damage. Although ultraviolet laser pulses are energetic enough to break intramolecular bonds, there is considerable controversy over whether there is also a thermal component. Perhaps most of the energy of the ultraviolet

Best Available Copy

laser pulse goes into the thermal phase change associated with tissue vaporization. Ablated fragments are ejected from the tissue surface at supersonic velocities and carry most of the energy with them, leaving little energy to damage the surrounding tissue. Tight focusing of the laser beam increases the precision of the cut; defocusing seems to induce more diffuse thermal changes in tissue.

Excimer lasers are used in photochemistry to provoke photochemical reactions in research and production processes, including the enrichment of uranium. They are also being used to photoetch polymers—for example, to produce electronic circuits previously made by a photographic process. This etching ability has led to the suggestion that excimer lasers could have medical applications.[17]

There are four main research areas in which a clinical role for the excimer laser is being investigated. One of the most promising applications of this technology appears to be in the treatment of several ocular disorders, because of the potential for changing the eye's refractive power by precisely removing corneal tissue without generating secondary heat effects. Ablation of the corneal stroma with argon fluoride (193 nm) radiation has been shown to produce clean, nonthermal cuts. Long-term studies are needed, but the prospects for early clinical use for corrective refractive surgery seem good.

In dermatology, the extreme precision of the excimer laser may be better than that of the traditional scalpel for removing mass skin lesions. Krypton fluoride (248 nm) radiation has the ability to both cut tissue and coagulate blood. This is not possible at 193 nm, a wavelength that is highly absorbed by blood. Other uses include the selective ablation of subcutaneous chromophores, such as melanin, in pigmented lesions, but no clinical trials have started.

Vascular surgery is the most interesting but, at the same time, the most technically challenging application. Basic research has demonstrated that excimer lasers at several wavelengths can cut precise craters in vascular atheroma with minimal surrounding damage. The major thrust is now toward the development of a suitable fiberoptic system that can deliver 308 nm xenon chloride laser energy percutaneously to an obstructed blood vessel. It is very difficult to transmit any short laser pulse down a fiber; the shorter the pulse, the higher the peak pulse power. This high peak pulse power can cause disruption of the fiber at its proximal end. The problem is compounded with the excimer laser because the shorter and more useful wavelengths are increasingly absorbed by quartz, especially in the presence of impurities. Lengthening the wavelength used relaxes the fiber requirements, and it is now possible to transmit up to 40 mJ/pulse down fibers using xenon chloride (308 nm), which has been shown to produce ablation in human cadaver arteries (see Chapter 42).[23]

A final application of excimer lasers may be in orthopedics, where excimer lasers have been shown to produce clean cuts in bone and organic polymers such as polymethyl methacrylate, used in bone cement.

Although excimer laser research is proceeding quickly with an informed, multidisciplinary approach, major concerns that must be resolved before human work begins include the possible mutagenic or carcinogenic consequences of high-intensity ultraviolet radiation. Further investigations to address this important question are in progress.

Free Electron Laser

The last few years have seen dramatic improvements in the power and efficiency of free electron lasers. The fundamental principles of free electron lasers are now well understood, and theoretical predictions can accurately describe the performance of experimental devices.

In many ways, free electron lasers resemble microwave devices, such as traveling-wave tubes, more closely than they do conventional lasers. The gain medium consists of an electron beam moving at speeds close to the speed of light in a magnetic field. The magnetic field is arranged so that the electrons passing through it are deflected alternately left and right. Thus, the electrons execute a "wiggle" motion through the magnetic field (called the "wiggler"). Because the electrons slow down as they pass through the magnetic field, they lose a certain amount of energy, which they give up in the form of a photon. The wavelengths of the light obtained will depend upon the amount of electron energy dissipated as the beam passes through the magnetic field ($E = h\nu/\lambda$).

Because of the unique way in which free

electron lasers operate, they offer several advantages relative to conventional lasers:

1. They can be tuned to different wavelengths by varying the electron energy and the force of the magnetic field.
2. They produce excellent optical beam quality, close to the diffraction limit.
3. They can be operated at extremely high power. In conventional lasers, the power is limited by the rate at which waste heat can be removed by means of high-speed flow and other techniques. In free electron lasers, the waste heat resides in the electron beam and exits the optical region at nearly the speed of light. Some of this energy can actually be recovered and reused.

In the future, free electron laser research will focus on wavelengths not available from conventional lasers and variations in beam pulse structure. As better electron beam quality is achieved, it may be possible to operate free electron lasers at wavelengths as short as 10 nm in the near-x-ray part of the spectrum. As laser performance improves, increased emphasis will be given to the application of free electron lasers to a wide variety of problems in medicine and surgery.

LIMITATIONS

As with any new and technologically sophisticated medical modality, there are limitations. The limitations of the laser fall into several areas: (1) device based, (2) physician based, and (3) procedure based.

The device has to be reliable. It has to be well engineered in such a way that it is easy to operate and dependable with respect to laser output. For example, when the controls are set at 10 watts, 10 watts has to come out. If the beam is supposed to be gaussian in energy profile, the user has to be sure that it will always be that way. Unfortunately, even though the Food and Drug Administration regulates devices with respect to safety, design, and reliability, in actuality there are variations between devices from the same manufacturer and between manufacturers. In addition, depending upon the maintenance program and utilization profile (the number of different physicians using the laser, the frequency of use, and movement of the laser between rooms), the reliability of any given device may vary. As a result, both hospital- and office-based laser systems have to be regularly maintained and checked by a knowledgeable person with respect to its operational state. Unfortunately, this is rarely done in office practice and is inadequately handled by the biomedical engineering staff (if one exists) at most hospitals. On the positive side, most of the laser companies are aware of the problems with maintaining and operating their laser devices, and they are designing second- and third-generation machines that are more user friendly and reliable.

The physician-based limitations are focused around inadequate training and experience. The physician has to develop a good understanding of the biophysical tissue interaction principles discussed in this chapter. This cannot be accomplished by reading about them. Good hands-on training exercises on tissue and animal model systems as well as viewing of didactic videos and observation of laser-experienced physicians are essential. Familiarity with the specific laser model to be used in each procedure is also essential. Since many hospitals now have several different models of each laser type, a physician should become familiar with the controls and individual pecularities of the device that is going to be used. Finally, the physician should know when to use the laser and when not to. This knowledge comes both from experience in actually doing laser cases and from keeping current on the literature.

The procedure-based limitations are the most important considerations. The type of tissue to be exposed to the laser, the selection of laser parameters, and the clinical indications are all vital. For example, one would never attempt a cervical conization with a noncontact continuous wave YAG laser. The tissue penetration is too great, and it is impossible to achieve a clean incisional cut. However, very good results could be obtained with a tightly focused, superpulsed CO_2 laser or even a sapphire-tipped YAG laser. Similarly, one would never attempt retinal photocoagulation with a CO_2 laser because the water absorption in the cornea and vitreous would result in traumatic heating that would damage these structures. Therefore, the characteristics of the tissue and the medical indications are the determining factors in using (or not using) the laser. What it all finally comes down to is appropriate training, knowledge, and judgment on the part of the physician.

REFERENCES

1. Berns MW: Biological Microirradiation, Classical and Laser Sources. Englewood Cliffs, NJ, Prentice-Hall, 1974
2. Boulnois JL: Photophysical processes in recent medical laser developments: A review. Lasers Med Sci 1:47–66, 1986
3. Elion HA: Laser Systems and Applications. New York, Pergamon Press, 1967
4. Hitz CB: Understanding Laser Technology. Tulsa, OK, PennWell Publishing, 1985
5. O'Shea DC, Callen WR, Rhodes WT: Introduction to Lasers and Their Applications. Menlo Park, CA, Addison-Wesley Publishing, 1978
6. Siegman AE: Lasers. Mill Valley, CA, University Science Books, 1986
7. Sliney D, Wolbarsht M: Safety With Laser and Other Optical Sources. New York, Plenum Press, 1985
8. Anderson RR, Parrish JA: Selective photothermolysis: Precise microsurgery by selective absorption of pulsed radiation. Science 220:524–527, 1983
9. Nelson JS, Berns MW: Basic laser physics and tissue interactions. Contemp Dermatol 2:12–32, 1988
10. Bohigian GM: Lasers in medicine and surgery. JAMA 256:900–907, 1986
11. Dougherty TJ: Photosensitizers: Therapy and detection of malignant tumors. Photochem Photobiol 45:879–889, 1987
12. Spears JR, Serur J, Shropstire D, et al: Fluorescence of experimental plaques with hematoporphyrin derivative. J Clin Invest 71:395–399, 1983
13. Pollock ME, Eugene J, Hammer-Wilson M, Berns MW: Photosensitization of experimental atheromas by porphyrin. J Am Coll Cardiol 9:639–646, 1987
14. Benson RC, Farrow GM, Kinsey JH, et al: Detection and localization of in situ carcinoma of the bladder with hematoporphyrin derivative. Mayo Clin Proc 57:548–555, 1982
15. McGregor GM, Kapitza HG, Jacobson KA: Laser Focus 20:84–93, 1985
16. Srinivasan R: Ablation of polymers and biological tissue by ultraviolet lasers. Science 234:559–565, 1985
17. Trokel SL, Srinivasan R, Braren B: Excimer laser surgery of the cornea. Am J Ophthalmol 96:710–715, 1983
18. Parrish JA: Ultraviolet laser ablation. Arch Dermatol 121:599–600, 1985
19. Calmettes, PP, Berns MW: Laser-induced multiphoton processes in living cells. Proc Natl Acad Sci USA 80:7197–7199, 1983
20. L'Esperance FA: Ophthalmic Lasers. Photocoagulation, Photoradiation, and Surgery. St Louis, CV Mosby Company, 1983
21. Apfelberg DB: Evaluation and Installation of Surgical Laser Systems. New York, Springer-Verlag, 1986
22. Baggish, MJ: Laser surgery in gynecology. In Dixon JA (ed): Surgical Application of Lasers. Chicago, Year Book Medical Publishers, 1983, pp 102–145
23. Grundfest WS, Litvack F, Forrester JS, et al: Laser ablation of human atherosclerotic plaque without adjacent tissue injury. J Am Coll Cardiol 5:929–933, 1985
24. Apfelberg DB, Maser MR, Lash H, Flores F: Expanded role of the argon laser in plastic surgery. J Dermatol Surg Oncol 9:145–151, 1983
25. Bailin PL, Ratz JL: Uses of the carbon dioxide laser in dermatological surgery. In Ratz JL (ed): Lasers in Cutaneous Medicine and Surgery. Chicago, Year Book Medical Publishers, 1986, pp 73–104

Delayed Retinal Effects of the Frequency-Doubled YAG Laser (532 nm)

Marjorie A. Mosier,* Jean Champion,† Lih-Huei L. Liaw,† and Michael W. Berns†

In order to compare the retinal effects of the frequency-doubled YAG laser (532 nm) with those of argon laser, rabbit eyes were exposed to green YAG laser irradiation and processed for light and electron microscopic study at 24 hr, 2 weeks and 4 weeks. Detailed analysis was conducted on tissue exposed to 7.3 and 7.6 millijoules (mj). Response of the photoreceptors and retinal pigmented epithelium to green YAG was very similar to that described for argon laser over the same time period. By 2 weeks post-exposure, there was histologic evidence of partial recovery with absence of damaged, pycnotic photoreceptor nuclei, increased numbers of typical photoreceptor outer segment lamellae and repair of retinal pigmented epithelium. Four weeks after irradiation, normal-appearing photoreceptor nuclei were present although inner photoreceptor segments still showed mitochondrial damage. Outer segments at 4 weeks showed regular lamellar structures. We conclude that the frequency-doubled YAG laser is equivalent to the argon laser with respect to the production of thermal lesions in the retina. Its additional advantages include increased efficiency, portability, reliability and lack of absorption by macular xanthophyll pigment. Invest Ophthalmol Vis Sci 28:1298–1305, 1987

Although the argon laser (488 and 514 nm) has been widely used for the treatment of retinal disease, it has certain disadvantages. These include its inefficiency and resultant power loss, its considerable maintenance requirement, non-portability and the absorption of energy by macular xanthophyll pigment. These drawbacks, except for xanthophyll absorption, also apply to krypton green laser. An ideal replacement for these lasers would be an efficient, low-maintenance, portable laser using a wavelength absorbed only by pigment in the retinal epithelium and by hemoglobin. These features are present in the green YAG laser.

The frequency-doubled (532 nm) green YAG laser was first suggested as a possible replacement for the argon laser in 1971 by L'Esperance, who showed that the morphologic effects of the two lasers were similar.[1] In that study, an experimental prototype continuous wave laser was used to treat seven human eyes, later examined histologically. Puliafito reported preliminary experiments on rabbit and monkey eyes using the pulsed "green" YAG laser of Laserscope, Inc.[2] Simultaneously, we reported the short-term effects on rabbit eyes.[3] In both our studies and those of Puliafito, the gross morphology and light microscopic histology showed that the YAG and argon wavelengths produced similar lesions when a high repetition pulse rate and low peak powers were used.

Our early experiments used a Quantronix research laser (Quantronix Corp., Smithtown, NY) operating at 8–12 kHz with peak powers of 25–50 W.[4] Rabbit eyes were fixed for histologic analysis within 2 hr of laser exposure. Only subtle and probably insignificant differences were noted between the lesions produced by argon and green YAG lasers.

Support for the possibility of true equivalency of green YAG and argon laser effects requires studies of the late histopathologic response of irradiated tissue. The present study examines retinal lesions up to 1 month following exposure to green YAG laser and compares the changes to those seen following argon laser irradiation.

Materials and Methods

Animals

A total of 63 sites were irradiated in both eyes of five Dutch Cross rabbits. The animals were maintained pre- and postoperatively under standard conditions in the Animal Resource Facility, University of California, Irvine, and were anesthetized and sacrificed as described previously[4] and in accord with the ARVO Resolution on the Use of Animals in Research. Enucleation was performed at 24 hr, 2 weeks and 4 weeks postoperatively.

From the Departments of *Ophthalmology and †Surgery and Beckman Laser Institute and Medical Clinic, University of California, Irvine, California.

Supported in part by grants from Humphrey Instruments and CooperVision Inc., and NIH Grant RR01192.

Submitted for publication April 30, 1986.

Reprint requests: Marjorie A. Mosier, MD, Department of Ophthalmology, University of California, Irvine, CA 92717.

Best Available Copy

Fig. 1. Low power light microscopy of rabbit retina 24 hr after exposure to 532 nm (green) YAG laser (7.61 mj). The zone of thermal damage is sharply demarcated through all retinal layers (arrows) (×450).

Laser Exposure

The source of irradiation was the 532 nm beam from the Humphrey Instruments frequency-doubled YAG laser (Humphrey Instruments, San Leandro, CA). Measurements taken on the day preceding exposure indicated that the laser was operating at 12.8 kHz, with individual pulse durations of 400 nanoseconds. A 25 mm focal length lens was used to image the beam on the retina to a spot diameter of 200 μm. The total energy in each spot for this study ranged from 1.27 to 7.61 millijoules (mj). Detailed histology was conducted on exposures of 7.3 and 7.6 mj.

Histopathology

The eyes were enucleated, fixed and sectioned for both light and electron microscopic analysis as described previously.[4] Tissues containing 35 of the 63 lesions were embedded in plastic and prepared for sectioning and microscopic examination. Initial histopathologic analysis was performed on lesions produced with energies of 7.3 and 7.6 mj. This was chosen because previous experiments indicated that 7–12 mj produced clinically visible, equivalent lesions with both argon and the green YAG lasers.[4] The resulting lesions at 24 hr, 2 weeks and 4 weeks appeared similar to standard argon lesions by slit lamp examination. At least two lesions at each time point were examined by light microscopy, and one of each was further examined by electron microscopy.

Results

Threshold Lesion

Initial experiments were designed to determine the energy required to produce a visible blanching of the retina 50% of the time, ie, the threshold energy. This was determined to be 1.37 mj in a 200 μm-diameter spot.

Histopathology

Photographs of histopathological results are grouped into three sets: the 24-hr lesion is shown in Figures 1–3, the 2-week lesion in Figures 4–7 and the 4-week lesion in Figures 8–12.

24-hr Lesion

At 24 hr, the low power light micrograph (Fig. 1) demonstrates typical thermal photocoagulation histopathology. A zone of damage is clearly demarcated, extending from just below the inner neural layer and extending through photoreceptors and retinal pigmented epithelium (RPE). The dark-staining pycnotic photoreceptor nuclei are prominent, sharply separated from undamaged nuclei (Fig. 1, arrows). Inner and outer photoreceptor segments appear damaged and displaced by serous exudate. Severe intra-cellular disorganization of photoreceptor inner segments is shown by high magnification electron micrography (Fig. 2). Outer photoreceptor segments are highly dis-

Fig. 2. Electron micrograph of rabbit photoreceptor inner segments 24 hr after exposure to 532 nm YAG laser (7.61 mj) showing severe intracellular disorganization (×10,750).

organized as well and do not exhibit any of the orderly lamellar membrane stacks (Fig. 3). The RPE is highly disrupted with melanin granules interspersed with necrotic and vacuolar debris (Fig. 3). Loss of RPE integrity, separation from Bruch's membrane and loss of lamellar organization of photoreceptor outer segments are seen under high magnification electron microscopy (Fig. 3).

Fig. 3. High magnification electron micrograph of rabbit pigmented epithelium 24 hr after exposure to 532 nm YAG laser (7.61 mj), showing cellular disruption and separation from Bruch's membrane (arrow, right) (×10,500).

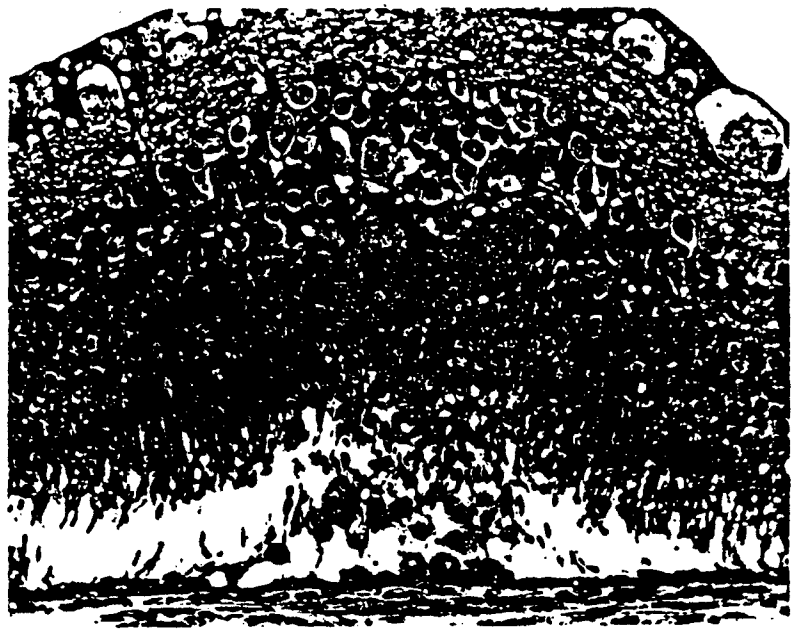

Fig. 4. Low power light microscopic appearance of rabbit retina 2 weeks after exposure to 532 nm YAG laser (7.3 mj). Zone of thermal damage is clearly demarcated (×450).

Two-Week Lesion

At 2 weeks, low power light microscopy shows considerable change. The zone of damage is still clearly demarcated (Fig. 4, arrow). Pycnotic photoreceptor nuclei are strikingly absent from this area and have been replaced by cellular debris and vacuolation (Fig. 5). The RPE appears somewhat less damaged than previously and is apposed to Bruch's membrane (Fig. 6). Photoreceptor outer segments are greatly disrupted in some areas (Fig. 6, arrow), but approach normal structure in others (Fig. 7). In the mitochondria-rich apex of inner segments, mitochondrial damage is evidenced by loss of many cristae, although outer membranes generally appear intact.

Four-Week Lesion

Considerable recovery in the lesion area has occurred at 4 weeks. The low power light micrograph

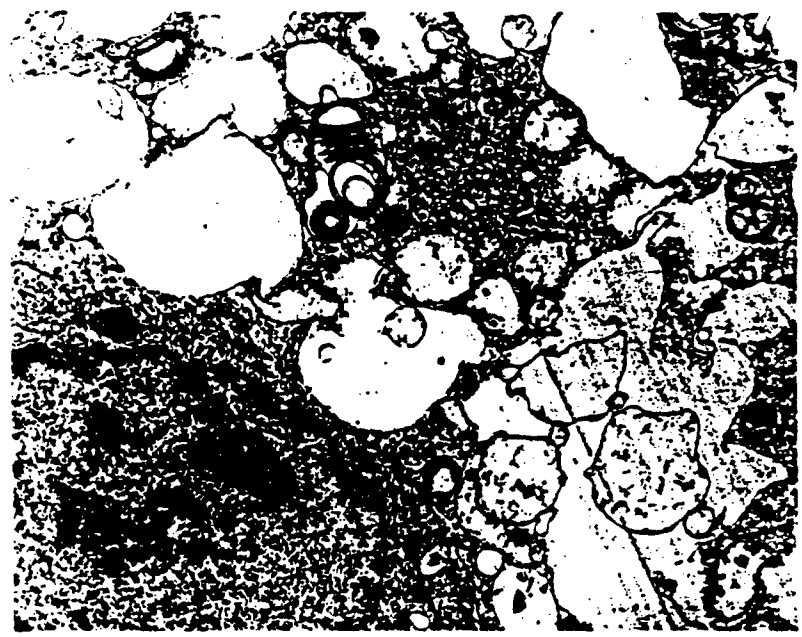

Fig. 5. Electron micrograph of rabbit photoreceptor nuclear zone 2 weeks after exposure to 532 nm YAG laser (7.3 mj), showing replacement of pyknotic nuclei with cellular debris and vacuolation (×10,800).

Fig. 6. Electron micrograph of rabbit retina 2 weeks after exposure to 532 nm YAG laser (7.3 mj). The pigmented epithelium is apposed to Bruch's membrane and shows moderate damage. Photoreceptor outer segments show focal disruption (arrow) (×5000).

demonstrates a buckling in the center of the lesion (Fig. 8, arrow), producing a separation of photoreceptor outer segments and RPE. Normal-appearing photoreceptor nuclei are adjacent to the damaged zone. The RPE appears normal and uniformly apposed to Bruch's membrane. Normal photoreceptor

Fig. 7. Electron micrograph of rabbit photoreceptor outer segments 2 weeks after exposure to 532 nm YAG laser (7.3 mj), showing significant recovery of normal lamellar structure (×5000).

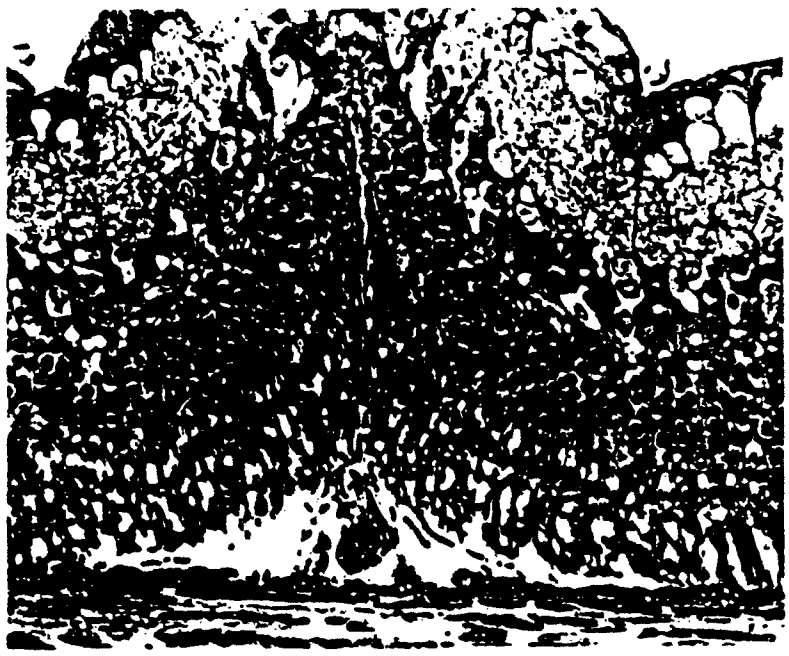

Fig. 8. Low power light micrograph of rabbit retina 4 weeks after exposure to 532 nm YAG laser (7.3 mj), showing buckling of center of lesion (arrow), with separation of photoreceptor outer segments from flat pigmented epithelium (×450)

outer segments are evident (Figs. 9–11). Photoreceptor nuclei appear normal by electron microscopy (Figs. 10 and 12). Mitochondria in photoreceptor inner segments show some disruption, suggesting that repair is not complete (Figs. 10 and 11).

Discussion

The severe tissue damage observed in the 24-hr samples underwent significant modulation by 2 weeks. At this point, the lesions showed absence of damaged cells from the zone of irradiation, along with repair and regeneration, or the inward movement of undamaged cells from the periphery of the lesion zone. A striking similarity is noted between this appearance and that reported for argon laser lesions. In 1973, Tso et al described 1–4-week argon lesions as follows: "One to four weeks after exposure, most of the pycnotic nuclei in the center of the lesions

Fig. 9. Electron micrograph of rabbit photoreceptor outer segments 4 weeks after exposure to 532 nm YAG laser (7.3 mj), showing normal lamellar structure (×44000)

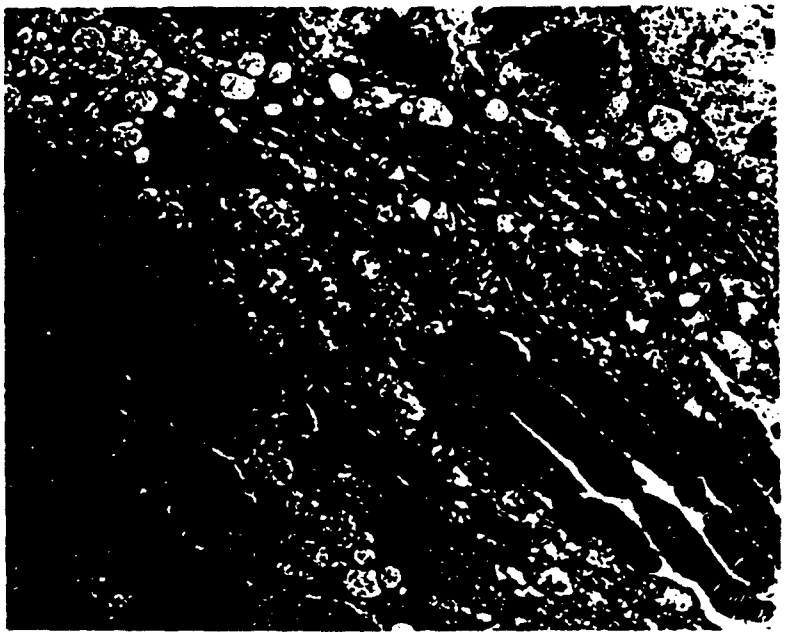

Fig. 10. Electron micrograph of rabbit photoreceptors 4 weeks after exposure to 532 nm YAG laser (~3 mj), showing normal-appearing nuclei and outer segments, but mitochondrial disruption (×4400)

were removed . . ." and: "Eight weeks after injury, repair and regeneration were most apparent".[5]

The present set of experiments shows that the histopathological response of the retina to green YAG laser is very similar to that described for the argon laser, both initially and over a 4-week period post-exposure. During that time, lesion development and repair in both types of laser injury occur in a similar manner. The disappearance of damaged photoreceptor nuclei and the return of relatively normal photoreceptors (as evidenced by normal nuclei and lamellar-patterned outer segments) bears a striking resemblance to the same events described for the argon laser in 1973 by Tso et al.[5] We conclude, therefore,

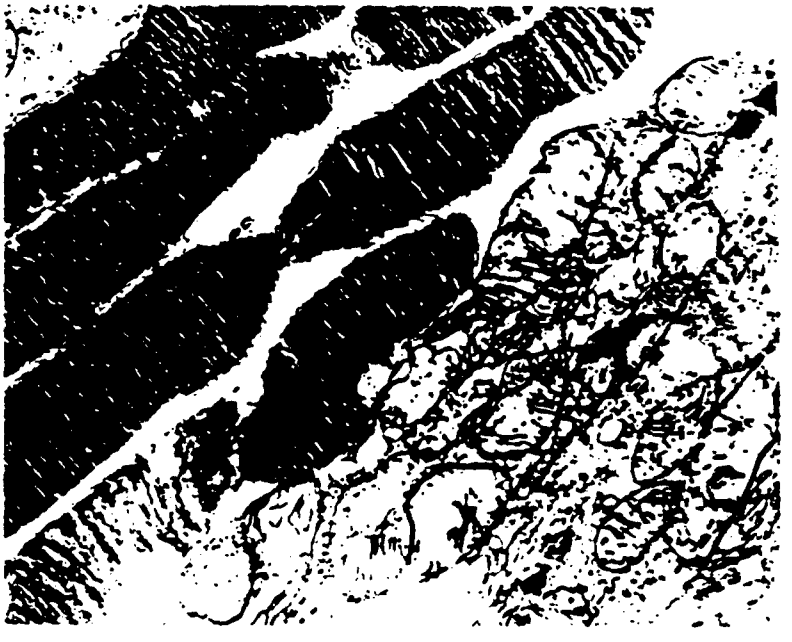

Fig. 11. High magnification electron micrograph of rabbit photoreceptors 4 weeks after exposure to 532 nm YAG laser (~3 mj), showing normal lamellar structure of outer segments but some disruption of inner segment mitochondria (×11,400)

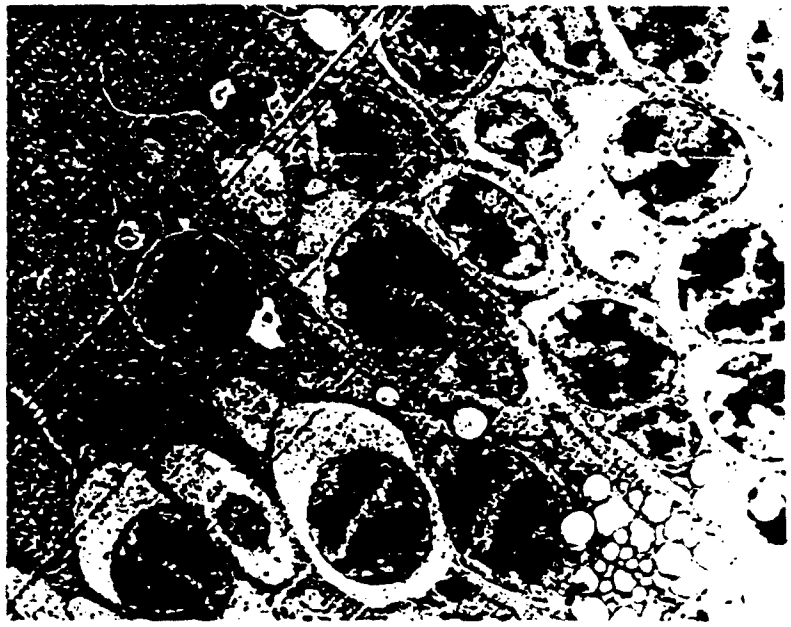

Fig. 12. Electron micrograph of rabbit photoreceptor nuclei 4 weeks after exposure to 532 nm YAG laser (7.3 mj), showing no effects of irradiation (×4400).

that the frequency-doubled YAG laser is equivalent to the argon laser with respect to the production of thermal lesions in the retina.

Key words: laser, retina, histopathology, YAG, green YAG

References

1 L'Esperance FA Jr: Clinical photocoagulation with the frequency-doubled neodymium yttrium-aluminum-garnet laser. Am J Ophthalmol 71:631, 1971

2 Puliafito CA, Adler CM, and Steinert RF: Experimental retinal photocoagulation with a frequency-doubled neodymium-YAG laser. ARVO Abstracts. Invest Ophthalmol Vis Sci 26(Suppl):38, 1985.

3 Moster MA and Berns MW: Retinal histopathologic effects of 532 nm (green) YAG laser: Comparison with argon. ARVO Abstracts. Invest Ophthalmol Vis Sci 26(Suppl) 38, 1985

4 Moster MA, Champion J, Liaw L-H, and Berns MW: Retinal effects of the frequency-doubled (532 nm) YAG laser: Histopathological comparison with argon laser. Lasers Surg Med 5:377, 1985.

5 Tso MOM, Wallow IHL, and Powell JO: Differential susceptibility of rod and cone cells to argon laser. Arch Ophthalmol 89:228, 1973

Photochemistry and Photobiology, Vol. 46, No. 5, pp. 829–835, 1987
Printed in Great Britain All rights reserved

0031-8655/87 $03.00+0.00
Copyright © 1987 Pergamon Journals Ltd

TUMOR DESTRUCTION IN PHOTODYNAMIC THERAPY

J. STUART NELSON[1], L.-H. LIAW[2] and MICHAEL W. BERNS[1,2]*
Departments of [1]Developmental and Cell Biology and [2]Surgery, and [2]Beckman Laser Institute and Medical Clinic, University of California, Irvine, 1002 Health Sciences Road East, Irvine, CA 92717, USA

(*Received* 2 *July* 1987; *accepted* 9 *July* 1987)

Abstract—The effects of photodynamic therapy (PDT) on the tumor microvasculature in the first few hours after treatment was studied at the light microscope (LM) and electron microscope (EM) levels in DBA/2Ha mice bearing SMT-F tumors. Animals received intraperitoneal injections of 10 mg kg^{-1} of Photofrin II and 24 h later tumors were treated with 100 J cm^{-2} of light (630 nm). Animals were sacrificed and their tumors removed at time 0, 30 min, 1, 2, 4, 8, 16 and 24 h after treatment. The results indicate that the effects of PDT are initially direct destruction of the microfibrils in the subendothelial zone of the tumor capillaries with subsequent tumor cell death secondary to hemorrhage and vascular collapse.

INTRODUCTION

Photodynamic therapy (PDT) using hematoporphyrin derivative (HpD) is a new approach to cancer treatment. Ever since Dougherty first suggested the use of HpD, a light-sensitizing tumor localizing porphyrin, plus light to bring about selective tumor necrosis, the medical applications of this new therapeutic modality have been pursued vigorously (Dougherty *et al.*, 1975, 1978).

HpD, a derivative of hematoporphyrin (Hp) prepared by the method of Lipson *et al.* (1961), is composed of a mixture of porphyrins. The components of the injected preparation responsible for the light induced cytotoxicity have not been chemically identified although a few reports have suggested that a hydrophobic component produces the greatest photosensitizing activity (Kessel, 1983). Damage to the cell membrane (Grossweiner, 1984), lysosomes (Tomnuki *et al.*, 1980), nuclear material (Foote, 1976) and mitochondria (Berns *et al.*, 1980) by HpD-PDT have been reported in the literature. The molecular mechanism leading to phototoxicity, though not conclusively established, is likely the production of singlet oxygen ($^1O_2$) as an active intermediate (Weishaupt *et al.*, 1976). This highly reactive molecule is subsequently capable of killing tumor cells through multiple interactions leading to oxidation of cellular components.

Despite all the work done in well defined cell culture systems, the relative contribution of the extracellular and intracellular HpD to the photodestruction of tumor tissue is still unknown. It is questionable how relevant *in vitro* studies are since the *in vivo* physiological milieu of the tumor cell such as blood supply, pH, oxygen tension, temperature and serum content of the medium immediately surrounding the cell obviously will be important. While HpD photosensitization has been exploited clinically for the treatment of solid tumors, there are still many determinants of this procedure which are incompletely understood.

One of the major unanswered questions associated with HpD-PDT is how these molecules are transported from the blood stream to the tumor tissue. Presumably HpD would have to interact with the vascular endothelium of the tumor tissue before passing into the surrounding perivascular tumor stroma. The effectiveness of tumor destruction is dependent upon an understanding of the parameters involved in this process. In order to fully appreciate the potential of HpD-PDT, it is necessary to characterize the role of the vasculature in bringing about the tumoricidal effect. This effect may be direct, such as destruction of the vasculature that nourishes the tumor.

Because of the complex nature of the role of the tumor vasculature in HpD-PDT, we have undertaken a series of experiments aimed at elucidating the effects of HpD-PDT on tumor microvasculature during the first few hours after phototherapy. We have employed a well defined murine tumor system and carefully examined the effects of HpD-PDT on the tumor vasculature at both the light microscope and electron microscope levels.

MATERIALS AND METHODS

Animal and tumor system. The following tumor system was used: a SMT-F (spontaneous mammary tumor) arising in the flank of a DBA/2Ha mouse (Pavelic *et al.*, 1978). All mice were 6–8 weeks old and weighed between 30 and 35 g at the time of treatment. When the tumors attained a size of 1–2 cm diameter, they were excised and minced with fine scissors in phosphate buffered saline (PBS). The resulting suspension of tumor cells was filtered through sterile gauze, washed twice in PBS and resuspended in RPMI media (GIBCO, Grand Island, NY) at a concentration of 5×10^7 viable cells ml^{-1}. Cell viability was assessed by the ability to resist cell lysis and exclude Trypan Blue dye (GIBCO). Tumors were initiated by injecting 0.1 ml of fresh tumor inoculum into the right flank of the mouse. The mouse tumors were generally

*To whom correspondence should be addressed.

palpable at 5 days and reached a size of 5–7 mm at 10–14 days at which time treatment was started. At this size, the small tumor was homogeneously white in color, [illegible] cross sectional or absent.

Hematoporphyrin derivative. Photofrin II obtained from Photomedica Inc., Raritan, NJ, was stored in the dark at 4° C until used. For treatment, the Photofrin II was diluted 1 : 4 with 0.9% NaCl solution and injected intraperitoneally.

Procedure. When tumors were of the appropriate size (as indicated above), the animals were shaved in the tumor area and given intraperitoneal injections of Photofrin II in doses equal to 10 mg kg^{-1} body weight. The remainder of the experiment was done in the dark, including housing of the animals. Control tumor-bearing animals were those that received light without Photofrin II. Twenty-four hours post injection, the experimental animals were treated with the laser light delivery system (see below). Previously published work by Dougherty (1975) has suggested that at 24 h, SMT-F tumors have their maximal uptake and retention of HpD. The mouse was anesthetized with Ketamine HCl (Parke-Davis) and covered with a metal shield with a circular hole exposing the tumor. Animals were sacrificed with Halothane (Halocarbon Laboratories, Inc., Hackensack, NJ) anesthesia at time 0, 30 min, 1, 2, 4, 8, 16 and 24 h after photodynamic therapy. Tissue was excised immediately and fixed in 4% glutaraldehyde (in sodium phosphate buffer at pH 7.4) for 2 h. The tissue was next rinsed with PBS and postfixed in 1% osmium (OsO_4) for 1 h at room temperature (18–20° C). Tissue was then rinsed with DDH_2O and stained *en bloc* for 2 h in Kellenberger's uranylacetate. Denydration was done with progressive ethanol–water in steps of 10 min each (30, 50, 70, 90, 100, 100%) and progressive ethanol–propyleneoxide in steps of 10 min each (30, 50, 70, 90, 100, 100%). Infiltration was started with propyleneoxide–epon 812 substitute (Polyscience Polybed 812) in steps of 30 min each (30, 50%), overnight (70%) and 60 min (100%). The mold was embedded and placed at 37° C overnight and then at 60° C in a vacuum oven for 48 h. The blocks were trimmed and sectioned (500 nm) for light microscopy using Richardson's stain and subsequently thin-sectioned (60 nm) for electron microscopy. A Phillips EM 300 (Amsterdam) electron microscope was used to examine the thin sections at 80 kV.

Laser light delivery system. Laser irradiations were performed with a Coherent (Palo Alto, CA) Innova 20 Argon ion laser stimulating a Coherent PRT-95 dye laser. The dye laser was tuned to emit radiation at 630 nm. The wavelength was verified using a Jobin Yvon #5-354 UV monochromator (Longjuneau, France). The radiation was focused into a 400 μm fused silica fiber optic using a Spectra-Physics (Mountain View, CA) Model 316 fiber optic coupler. The output end of the fiber was terminated with a microlens that focused the laser radiation into a circular field of uniform light intensity. Laser irradiation emanating from the fiber was monitored with a Coherent Model 210 power meter before and after treatment.

Mice were placed underneath an aperture that controlled the area of light illumination on the tumor site. The area of illumination was 1 cm^2. Total laser energy density was 100 J cm^{-2} with a power density of 150 mW cm^{-2}. A total of 40 light treated tumors were examined at different time-points post-irradiation (5 animals each at time 0, 30 min, 1, 2, 4, 8, 16 and 24 h).

RESULTS

Light microscopy

Control slides show the usual tumor architecture with multiple mitotic figures and easily discernible vessels. At 30 min and 1 h post PDT, there were no significant structural changes noted from control (Fig. 1a). At 2 h post PDT, the first structural change noted is the increased diameter of the capillary lumen as compared to controls (Fig. 1b). This conclusion is based upon the histopathological examination of a large number of sections and tumors and is not attributable to the way a particular section was cut. At 4 h, the capillaries are further engorged with distinct dark staining walls. In some areas the capillary wall is completely disrupted with red blood cells visible outside the lumen (Fig. 1c). By 8 h (results not shown) there is frank extravasation of red blood cells into the surrounding perivascular stroma. As time continues, the entire tumor becomes hemorrhagic.

Electron microscopy

Control ultrathin EM sections show the normal tumor microvasculature with the individual microfibrils (diameter 11 nm) in the subendothelial zone in the walls of the capillaries (Fig. 2a, inset). The fine structure of the capillary endothelium appears normal. The proliferatng tumor cells appear normal with numerous free and membrane-bound ribosomes contained in their cytoplasm (Fig. 2a). At 2 h post PDT, the microfibrils in the subendothelial zone of the capillary wall (Fig. 2b, inset) now appear much larger and with more spacing in between, when compared to controls (Fig. 2a, inset). These microfibrils now have a diameter averaging 15 nm. There also appears to be a 'halo' surrounding these microfibril subunits in the 2 h PDT tumors. The endothelial cells lining the capillary wall appear elongated and flat but are otherwise structurally normal as are the tumor cells in the surrounding perivascular stroma. By 4 h, the subendothelial zone of the capillary wall is filled with dense clumps of microfibrils (Fig. 2c,d) and in some areas completely disrupted with red blood cells visible outside the lumen (Figs. 2d and 3a). There are numerous large vacuoles in the cytoplasm of the endothelial cells indicative of impending cell death (Fig. 3a). Those tumor cells immediately adjacent to the capillaries are now showing the signs of cell death described above (Fig. 3b). Cells in the center of the tumor appear to be structurally intact (Fig. 4) except for some washout of the mitochondrial cristae. However, this was evident in controls (Fig. 4a) as well as experimentals (Fig. 4b). As time continues, the amount of hemorrhage increases with the entire tumor ultimately becoming a sea of red blood cells and amorphous granular debris.

DISCUSSION

Evidence that malignant tumors can be selectively destroyed by phototherapy with hematoporphyrin derivative has been well documented (Fornes *et al.*,

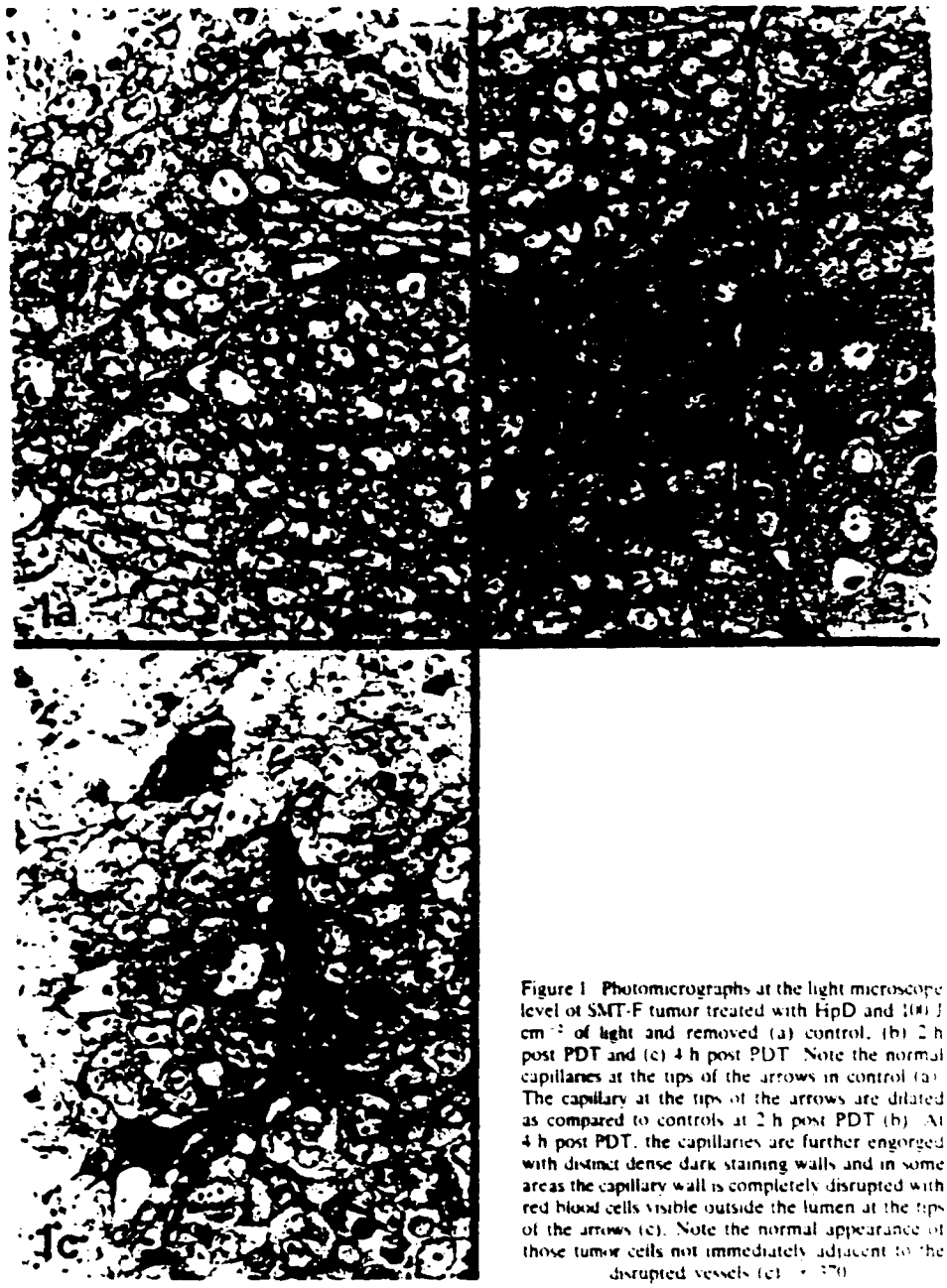

Figure 1 Photomicrographs at the light microscope level of SMT-F tumor treated with HpD and 100 J cm^{-2} of light and removed (a) control, (b) 2 h post PDT and (c) 4 h post PDT. Note the normal capillaries at the tips of the arrows in control (a). The capillary at the tips of the arrows are dilated as compared to controls at 2 h post PDT (b). At 4 h post PDT, the capillaries are further engorged with distinct dense dark staining walls and in some areas the capillary wall is completely disrupted with red blood cells visible outside the lumen at the tips of the arrows (c). Note the normal appearance of those tumor cells not immediately adjacent to the disrupted vessels (c). × 370.

1980; Dougherty *et al.*, 1981; Wile *et al.*, 1982; Dahlman *et al.*, 1983). Several researchers have suggested that damage to the tumor microvasculature brings about tumor necrosis. Castellani (1963) studied frog tongue and rat mesentery sensitized with hematoporphyrin and reported temporary stopping of blood flow, aggregation of red blood cells, vasodilatation and stasis. Oxygen radicals have been shown to cause vascular damage, and singlet oxygen may be similarly toxic to the tumor vasculature (Kontos *et al.*, 1983). Bugelski (1981) studied the distribution of isotopically labelled HpD using autoradiography and found that tritiated HpD was distributed at a ratio 5:1 in the surrounding perivascular stroma as compared to tumor cells. Starr (1986) using tumors grown in sandwich observation chambers showed that 3–15 min after treatment blood cells within the tumor began to disappear

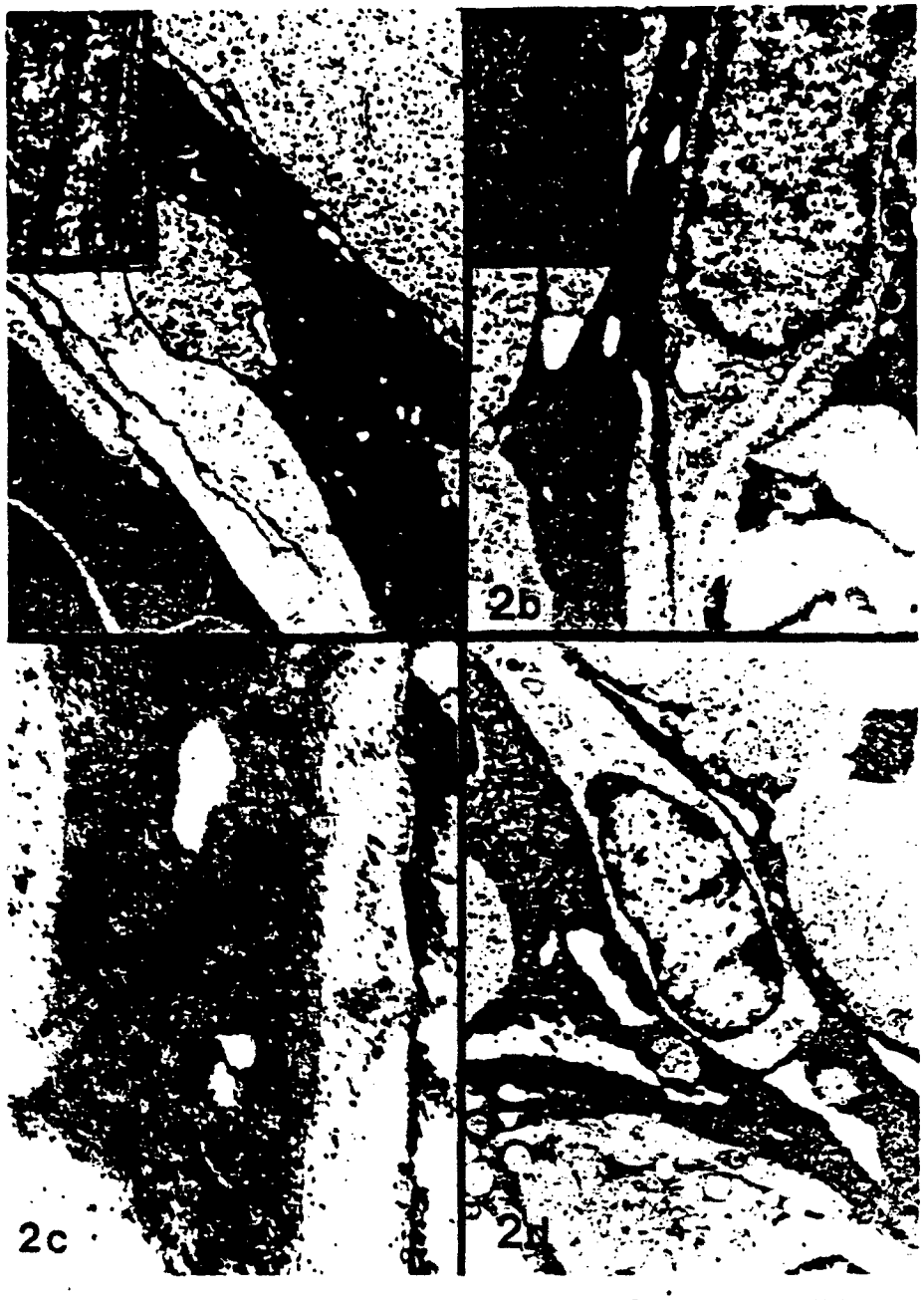

Figure 2. Photomicrographs at the electron microscope level of SMT-F tumor treated with HpD and 100 J cm^{-2} of light and removed (a) control, (b) 2 h post PDT and (c,d) 4 h post PDT. Note the individual microfibrils easily seen in the subendothelial zone of the capillary wall in control ultra thin sections (a). At 2 h post PDT the microfibrils appear much larger and with more spacing in between (b) when compared to controls (a). At 4 h post PDT, the subendothelial zone of the capillary wall is filled with dense clumps of microfibrils (c,d) and in some areas completely disrupted (d). (a,b) × 15 400; (c) × 40 800; (d) × 7 600. Inserts (a,b) are high power magnifications of the microfibrils in the subendothelial zone of the capillary walls. × 46 000

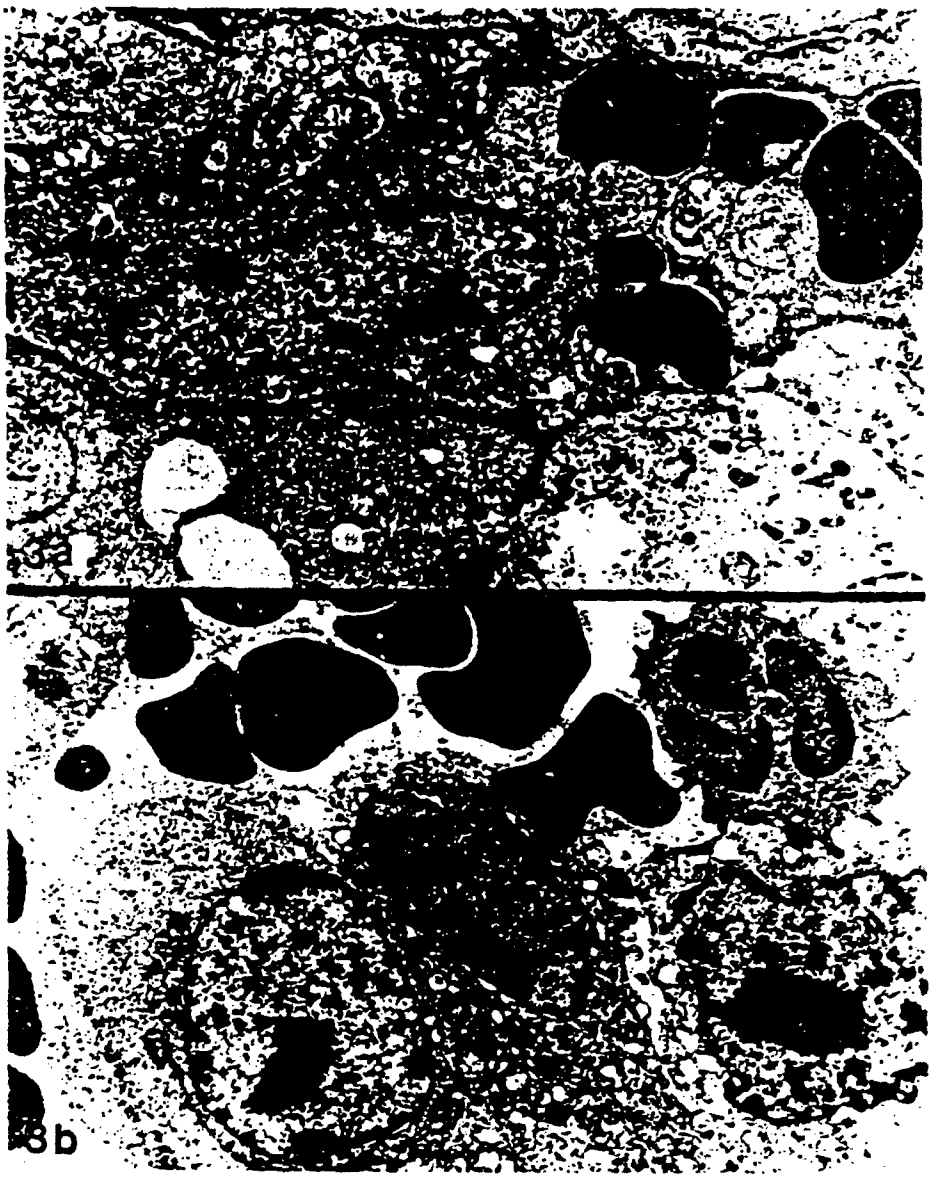

Figure 3. Photomicrographs at the electron microscope level of SMT-F tumor treated with HpD and 100 J cm^{-2} of light and removed 4 h after treatment (a,b). Note numerous large vacuoles in the cytoplasm of the endothelial cell outlined by the arrows with blood outside the capillary wall (a). Note hemorrhage into the surrounding perivascular stroma with varying degrees of tumor cell death depending on their proximity to the capillaries (b). × 7400

Within 2 h, a purplish discoloration appeared over the target area reminiscent of a hematoma with subsequent necrosis of tumor tissue. Bicher (1981) using oxygen electrode measurements, found experimental mouse tumors anoxic within 1 h after treatment, presumably due to vascular collapse. Selman (1984) using a bladder tumor model in a rat, found that PDT led to a rapid and sustained decrease in blood flow to the tumor. Henderson (1985) using tumor cell clonogenicity following PDT to assess *in vitro* colony formation, found that it was unaffected by PDT if the tumor tissue was excised and explanted immediately. If, however, tumor cells were left *in situ* following PDT for varying lengths of time (1–24 h), tumor cell death occurred rapidly and progressively implying that one of the major factors contributing to tumor destruction may be damage to the tumor circulation and the consequences of treatment-induced changes in tumor physiology. All these experiments add weight to the suggestion that

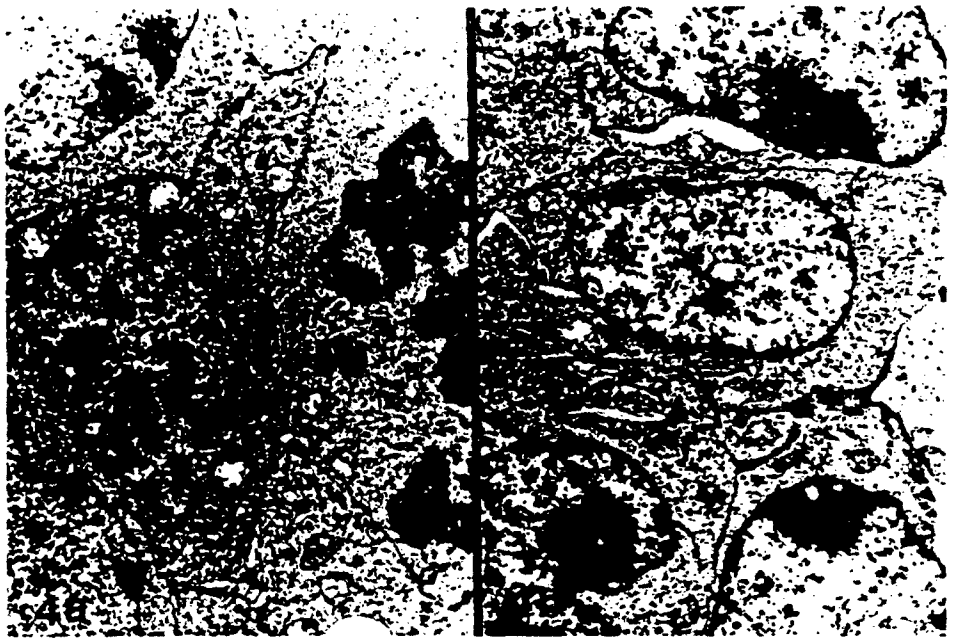

Figure 4. Photomicrographs at the electron microscope level of SMT-F tumor treated with HpD and 100 J cm^{-2} of light and removed (a) control and (b) 4 h post PDT. These tumor cells are deep within the tumor tissue away from the capillaries and all appear to be structurally intact even 4 h past PDT (b). × 8200.

tumor blood vessels may represent a highly vulnerable target for anti-tumor therapy. However, none were done at the level of the electron microscope and therefore the *in vivo* mechanisms responsible for vascular changes post PDT have remained incompletely understood.

Our investigation was conducted to determine the mechanisms and changes involved in the tumor vasculature responsible for the *in vivo* destruction of tumor tissue by PDT. Clearly many factors must be involved to produce the necrosis of a large tumor mass but our study demonstrates that the first observable signs of destruction occur in the subendothelial zone of the tumor capillary wall. The subendothelial zone of the capillary wall is a highly varied structure, both morphologically and chemically. Ultrastructurally, it is a complex composition of microfibrils, elastin, a collagen-type protein (referred to as collagen IV or AB) and other connective tissue elements, especially glycosaminoglycans. The microfibrils are electron-dense filaments oriented in a longitudinal direction to the long axis of the vessel and they maintain the structural integrity of the tiny capillary wall. This study shows that these structural subunits of the capillary wall lose their functional integrity and are ultimately destroyed within the first 2–4 h after phototherapy. We did note many normal appearing endothelial cells in areas where there were no distinct microfibrils visible suggesting that these microfibrillar hemorrhage, activation of intravascular components such as complement (a series of protein molecules that generate an impressive array of bioactive factors resulting in cell lysis) or hypoxia secondary to vascular collapse.

The results of our study are in close agreement with those recently reported by Berenbaum (1986) who while studying cerebral photosensitization found that the tumor capillaries were the primary site of damage in the brain at 2 h post PDT. Furthermore, those structures not immediately adjacent to the vasculature such as neurons and neuroglia appeared intact suggesting that the initial damage was not extravascular.

We conclude that the effects of photodynamic therapy leading to rapid tumor necrosis are not the result of direct tumor cell kill, but rather are secondary to destruction of the microfibrils in the subendothelial zone of the tumor capillary wall.

Acknowledgements—We thank Mr. William Wright and Mr Jeffrey Andrews for technical assistance and Mrs. Beverly Hyndman for her assistance in the preparation of the manuscript. This research was supported by NIH grants RR 01192 and CA 32248, and the Office of Naval Research grant No. N00014-86-K-0115.

REFERENCES

Berenbaum, M. C., G. W. Hall and A. D. Hayes (1986) Cerebral photosensitization by haematoporphyrin derivative. Evidence for an endothelial site of action. *Br. J. Cancer* 53, 81–89.

Berns, M. W., A. Dahlman, F. Johnson, R. Burns, D. Sperling, M. Guiltman, A. Siemens, R. Walter, W.

Wright, M Hammer-Wilson and A Wile (1982) *In vitro* cellular effects of hematoporphyrin derivative *Cancer Res* **42**, 2325–2329

Bicher, H I, F W Hetzel, P Vaupel and I S Sandhu (1981) Microcirculation modifications by localized microwave hyperthermia and hematoporphyrin photoradiation therapy *Bibliotheca Anatomica* **20**, 528–532

Bugelski, P J, C W Porter and T J Dougherty (1981) Autoradiographic distribution of hematoporphyrin derivative in normal and tumor tissue of the mouse *Cancer Res* **41**, 4606–4612

Castellani, A, G P Pace and M Concioli (1963) Photodynamic effect of haematoporphyrin on blood microcirculation *J Pathol Bacteriol* **86**, 99–102

Dahlman, A, A G Wile, R G Burns, G R Mason, F M Johnson and M W Berns (1983) Laser photoradiation therapy of cancer *Cancer Res* **43**, 430–434

Dougherty, T J, G B Grindey, K R Weishaupt and D Boyle (1975) Photoradiation therapy II *J Natl Cancer Inst* **55**, 115–120

Dougherty, T J, J E Kaufman, A Goldfarb, K R Weishaupt, D Boyle and A Mittleman (1978) Photoradiation therapy for the treatment of malignant tumors *Cancer Res* **38**, 2628–2635

Dougherty, T J, R E Thoma, D G Boyle and K R Weishaupt (1980) Interstitial photoradiation therapy for primary solid tumors in pet cats and dogs *Cancer Res* **41**, 401–404

Foote, C S (1976) Photosensitized oxidation and singlet oxygen: Consequences in biological systems In *Free Radicals in Biology* Edited by W A Pryor Vol II, pp 85–124 Academic Press, New York

Forrest, J J, P A Cowled, A S-Y Leong, A D Ward, R B Black, A J Blake and F J Jacka (1980) Phototherapy of human tumours using haematoporphyrin derivative *Med J Aust* **2**, 589–593

Grossweiner, L I (1984) Membrane photosensitization by hematoporphyrin and hematoporphyrin derivative In *Porphyrin Localization and Treatment of Tumors* Edited by D R Doiron and C J Gomer, pp 391–414 Liss, New York

Henderson, B W, S M Waldow, T S Mang, W R Potter, P B Malone and T J Dougherty (1985) Tumor destruction and kinetics of tumor cell death in two experimental mouse tumors following photodynamic therapy *Cancer Res* **45**, 572–576

Kessel, D and T C Chou (1983) Tumor-localizing components of the porphyrin preparation hematoporphyrin derivative *Cancer Res* **43**, 3442–3447

Kontos, H A and M L Hess (1983) Oxygen radicals and vascular damage In *Microcirculatory Injury* Edited by J J Spritzer), pp 365–375 Plenum Press, New York

Lipson, R E Baldes and A Olsen (1961) The use of a derivative of hematoporphyrin in tumor detection *J Natl Cancer Inst* **26**, 1–8

Pavelic, Z P, C W Porter, L M Allen and E Mihich (1978) Cell population kinetics of fast and slow-growing transplantable tumors derived from spontaneous mammary tumors of the DBA 2Ha-DD mouse *Cancer Res* **38**, 1533–1538

Selman, S H, R Keck, J E Kluane, M Kreimer-Birnbaum, P J Goldblat and S L Britton (1984) Blood flow in transplantable bladder tumors treated with hematoporphyrin derivative *Cancer Res* **44**, 1924–1927

Starr, W M, J P A Marijnissen, A van den Berg-Blok and H S Reinhold (1986) Destruction of rat mammary tumor and normal tissue microcirculation by hematoporphyrin derivative photoradiation observed in vivo in sandwich observation chambers *Cancer Res* **46**, 2532–2540

Tortinuki, W, T Miura and M Sera (1986) Lysosome destruction and apoperoxide formation due to active oxygen generated from hematoporphyrin on its irradiation *Br J Dermatol* **102**, 17–27

Weishaupt, K R, C J Gomer and T J Dougherty (1976) Identification of singlet oxygen as the cytotoxic agent in photoinactivation of a murine tumor *Cancer Res* **36**, 2326–2329

Wile, A W, A Dahlman, R G Burns and M W Berns (1985) Laser photoradiation therapy of [illegible] tumors sensitized with [illegible] *Lasers Med Surg* **2**, [illegible]

In Vitro Characterization of Monoaspartyl Chlorin e_6 and Diaspartyl Chlorin e_6 for Photodynamic Therapy[1,2]

W. Gregory Roberts,[3] *Fuu-Yau Shiau,*[4] *J. S. Nelson,*[3] *Kevin M. Smith,*[4] *Michael W. Berns*[4,5]

The characteristics of two new chlorin photosensitizers were studied in cell culture by determining phototoxicity, subcellular localization, and photophysical properties. Monoaspartyl chlorin e_6 (MACE) and diaspartyl chlorin e_6 (DACE) are new photosensitizers that show promise for use in photodynamic therapy. These chlorins are pure, monomeric compounds as determined by high-pressure liquid chromatography. Both compounds absorb substantially at a longer wavelength (664 nm) than does dihematoporphyrin ether-ester (DHE). Tumor diagnosis with the use of fluorescence should be facilitated due to the purity of the compounds and the single fluorescence emission peak. Phototoxicity dose-response curves of the sensitizers were completed using a standard clonogenic assay to determine cell viability. The chlorins showed good sensitizing capabilities with light. In addition, subcellular localization of MACE, DACE, and DHE was studied using fluorescence microscopy. Whereas DHE was located throughout the cytoplasm, the primary site of localization of the chlorins appeared to be in the lysosome. The results demonstrate that MACE and DACE are effective photosensitizing agents in vitro and compare favorably to DHE. [J Natl Cancer Inst 1988;80:330-336]

ABBREVIATIONS USED: ATCC=American Type Culture Collection; CCL = certified cell line; DACE = diaspartyl chlorin e_6; DHE = dihematoporphyrin ester-ether; FCS = fetal calf serum; HPD = hematoporphyrin derivative; HPLC = high-pressure liquid chromatography; MACE = monoaspartyl chlorin e_6; MEM = minimum essential medium; PBS = phosphate-buffered saline; PDT = photodynamic therapy.

[1]Received November 23, 1987; revised December 14, 1987, accepted December 29, 1987.

[2]Supported in part by Public Health Service grant CA-32248 and National Science Foundation grant CHE-86-19034.

[3]Department of Developmental and Cell Biology and Surgery, Beckman Laser Institute and Medical Clinic, University of California—Irvine, Irvine, CA 92715.

[4]Department of Chemistry, University of California—Davis, Davis, CA.

[5]The authors thank Marion Howard for her assistance with the cytotoxicity assay.

Porphyrin compounds, especially HPD, have shown great promise in treating cancers in animals (*1-3*) and humans (*4,5*). Photosensitization with a light of the appropriate wavelength and intensity can lead to a highly selective form of tumor eradication (*6,7*). Photodamage of the tumor requires irradiation of the sensitized tissue with light at a wavelength corresponding to the absorption bands of the photosensitizing agent (*8*). Since tumor tissue penetrance increases with wavelength (*9*), photosensitizers with absorption bands longer than 630 nm, currently used for HPD, would be more desirable for PDT. Photofrin II contains the tumor-localizing fraction of HPD, which has recently been identified as a combination of dihematoporphyrin ether and dihematoporphyrin ester DHE (*10*). At present, the efficacy of PDT with DHE is limited by the ability of 630-nm light to penetrate tissue and thus is primarily restricted to superficial tumors or the use of multiple fiber optic implants in larger implants. Chlorins are chlorophyll derivatives with a prominent absorbance band in the red region around 665 nm, which is red shifted about 25 nm in comparison to porphyrins (*11*).

Prior to determining the clinical efficacy of MACE and DACE, it is necessary to characterize the in vitro cytotoxicity and phototoxicity. In this study, absorbance and fluorescence spectra, in vitro subcellular localization, and dose-response curves were determined for MACE and DACE. Furthermore, comparing the phototoxicity and photophysical nature of the chlorins to that of an established photosensitizing agent, DHE, is a necessary prerequisite to their acceptance as an alternative to DHE-PDT.

Materials and Methods

Compounds. DACE (fig. 1A) and MACE (fig. 1B) were prepared and analyzed as follows: methyl pheophorbide-*a* was prepared by extraction from the alga *Spirulina maxima* (*12*). Alkaline degradation to give chlorin e_6 trimethyl ester was performed as described elsewhere (*13*). Chlorin e_6 was prepared from the corresponding trimethyl ester by hydrolysis in KOH-methanol-water (*14*). Di-*tert*-butyl aspartic acid (Sigma Chemical Co., St. Louis, MO) was attached to the chlorin e_6 following the method of Bommer and Burnham (*15*), except that the chlorin carboxylic function was activated as the acid chloride. Typically, a 75% yield of aspartyl chlorin *tert*-butyl esters was obtained and the ratio of products was around 75% MACE and 25% DACE. Structures were verified by nuclear magnetic resonance spectroscopy. Treatment with trifluoroacetic acid produced MACE and DACE, respectively, from their corresponding *tert*-butyl esters (*16*).

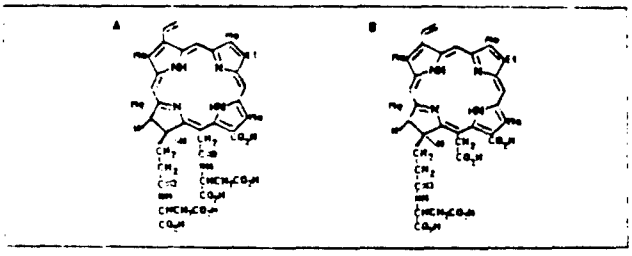

Figure 1. A) DACE (mol wt, 826) and B) MACE (mol wt, 711). A, B) Me = methyl, Et = ethyl.

Photofrin II was received from Photomedica Inc. (Raritan, NJ) as a dark brown solution at a concentration of 2.5 mg/ml in normal saline and was stored at −70°C. All compounds were diluted in culture medium as required for individual experiments.

Cells. PTK$_2$ cells, from an established rat kangaroo epithelial line (ATCC CCL 56; American Type Culture Collection, Rockville, MD), which has previously been used to determine in vitro effects of HPD (*17*), were grown in MEM (GIBCO, Grand Island, NY) supplemented with 0.292 mg L-glutamine/ml, 100 U penicillin G/ml, 100 μg streptomycin/ml, and 10% FCS (GIBCO).

We also used the established cell line CHO-K1 (Chinese hamster ovary cells, *Cricetulus griseus*, ATCC CCL 61). These cells were grown in MEM supplemented as described above.

HPLC analysis. Purity of material was established using analytical HPLC [Waters Associates model 6000A pump, Valco injector, Perkin Elmer LC55B variable wavelength detector set at 668 nm, Waters Associates Z module with C-18 reversed-phase 10-μm cartridge, flow rate of 2.5 ml/min of solvent with a linear gradient of 55% methanol and 45% phosphate buffer (pH 6.85, 0.01 *M*) through 100% methanol during 25 min]. The products were obtained as free acids by dilution of the trifluoroacetic acid mixtures with water, by extraction with dichloromethane, and by evaporation in air to give a residue recrystallized from tetrahydrofuran-*n*-hexane.

Absorption and fluorescence analysis. The absorption spectra of MACE, DACE, and DHE in 10% FCS were obtained using a Beckman DU-7 spectrophotometer. After cells were incubated 24 hours with 25 μg/ml of either the chlorins or DHE, washed three times with PBS, and sonicated, absorption spectra were obtained.

The fluorescence emission and excitation spectra of MACE, DACE, and DHE (2 μg/ml) in PBS plus 10% FCS were determined using an SLM 8000 spectrofluorometer. The emission spectra for the chlorins were scanned from 620 to 700 nm using an excitation wavelength of 400 nm. The emission spectrum for DHE was scanned from 590 to 750 nm by use of an excitation wavelength of 400 nm. The excitation spectrum was scanned from 350 to 560 nm with the use of an emission wavelength of 666 nm for the chlorins. The excitation spectrum of DHE was scanned from 340 to 600 nm with an emission wavelength of 635 nm.

Laser light delivery system. Laser irradiation was performed with a Cooper Lasersonics (Santa Clara, CA) 770DL argon dye laser system with 4-dicyanomethylene-2-methyl-6-(*p*-dimethyl amino-styryl)-4*H*-pyran dye. The laser was tuned to emit radiation at 630 nm for cells treated with DHE and to 664 nm for cells treated with the chlorins. Controls were irradiated at either 630 or 664 nm. Wavelengths were verified using a Jobin Yvon #5/354 UV monochromator (Longjumeau, France). The radiation from the dye laser was coupled into a 400-μm fused silica fiber optic that was terminated with a microlens that focused the laser radiation into a circular field of uniform light intensity. Laser irradiation emanating from the fiber optic was monitored with

Best Available Copy

a Coherent model 210 power meter before and after exposure. Total laser energy density was 10 J/cm² (4.2 min) with a power density of 40 mW/cm². Laser energy density and power density were selected based upon previous pilot studies.

Fluorescence microscopy. PTK_2 cells were grown on glass cover slips and incubated in the dark with one of the following: 25 μg/ml of either DHE, MACE, or DACE for 24 hours or the fluorochrome acridine orange [0.1% stock solution in PBS (pH 7.0)] for 5 minutes. The cells were washed repeatedly with fresh PBS prior to photography. An epifluorescence RA microscope (Zeiss) illuminated with a 50-W mercury lamp was used for all micrographs. Cells treated with DHE or the chlorins were photographed using a Zeiss BP405/8 exciter filter (a band-pass filter centered at 405 nm with a band width of 8 nm), chromatic beam splitter FT420 (Zeiss), and barrier filter LP590 (Zeiss). For acridine orange-treated cells, a cutoff exciter filter, G436; an FT510 beam splitter; and an LP515 barrier filter were used.

In vitro phototoxicity. CHO cells were plated in petri dishes at a density of 3×10^5 cells/dish. Twenty-four hours after seeding, cells were incubated with the appropriate sensitizer for 24 hours at various concentrations (0.5, 1, 5, 10, and 15 μg/ml). After incubation, 200 cells were replated into 60-mm-diameter petri dishes and allowed to attach for 4 hours, continuing incubation in presence of the drug. Immediately preceding irradiation, media with sensitizer were removed and replaced with fresh media. Cells were irradiated as described previously. Plates were allowed to incubate for 7 days after irradiation, at which time clones derived from individual surviving cells were washed with PBS and fixed with 100% methyl alcohol for 5 minutes. Clones were washed twice more with PBS and allowed to dry before staining with 0.5% crystal violet and 0.5% methylene blue. All procedures were performed in the dark or subdued light. Plating efficiency was determined from cells that received neither drug nor light. Controls consisted of cells that received either light alone (664 or 630 nm) or drug alone.

Results

HPLC analysis. Purity of the samples was determined by analytical HPLC shown in figure 2 and by HPLC comparison with an authentic sample (*15*).

Absorption and fluorescence spectra. The absorption spectra of MACE, DACE, and DHE in 10% serum are shown in figure 3. The significant absorption bands of the sensitizers (10 μg/ml) with the addition of 10% FCS were identical

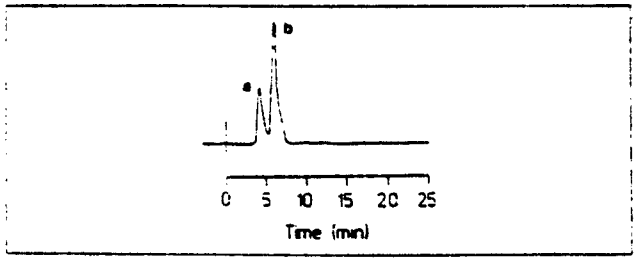

Figure 2. Analytical HPLC of an artificially produced admixture of DACE (a) and MACE (b)

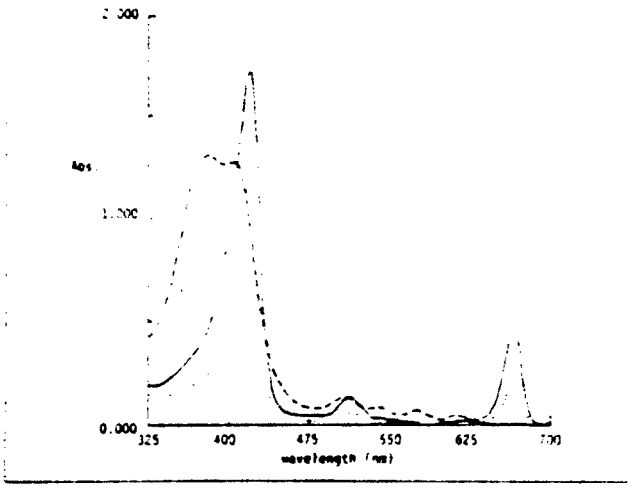

Figure 3. Absorption (Abs.) spectra of MACE (——), DACE (· · · ·), and DHE (- - -) in the presence of 10% FCS at a concentration of 10 μg/ml. ϵ_{664} for MACE = 3.8×10^4 L/mol·cm, ϵ_{664} for DACE = 2.3×10^4 L/mol·cm, and ϵ_{630} for DHE = 3.6×10^3 L/mol·cm.

to those obtained in cells (data not shown). The molar extinction coefficients at the therapeutic wavelengths are 3.8×10^4 L/mol·cm for MACE (664 nm) and 2.3×10^4 L/mol·cm for DACE (664 nm); for DHE (630 nm), ester-ether is one order of magnitude less at 3.6×10^3 L/mol·cm.

The fluorescence emission and excitation spectra of the two chlorins were very similar. The emission spectra of DACE and MACE had one peak (fig. 4A, 4B). However, the peak was at 669 nm for MACE and 667 nm for DACE. The fluorescence emission spectrum of DHE (fig. 4C) had three peaks: 620, 635, and 691 nm. All fluorescence intensities were normalized with respect to each other, with DHE having the lowest absolute intensity.

The fluorescence excitation spectrum for MACE (fig. 5B) exhibited peaks at 399 and 425 and a broad band centered at 510 nm, which correlated with the absorption spectrum (fig. 3). DACE exhibited only two peaks, a broad band centered at 417 nm and another at 570 nm (fig. 5A). The excitation spectrum of DHE had one large peak at 400 nm and smaller bands at 505, 538, and 578 nm (fig. 5C). The excitation spectra of DACE and DHE also correlated to their respective absorbance spectra. As with the emission spectra, the excitation spectra were normalized, with DHE yielding the lowest absolute intensity.

Subcellular binding. The cellular binding sites of MACE or DACE were examined by fluorescence microscopy. Figure 6C and 6D are fluorescence micrographs of PTK_2 cells incubated for 24 hours with MACE and DACE, respectively. Notice the discrete brightly staining regions in the cytoplasm and the lack of stain associated with the plasma membrane and nucleus. DHE (fig. 6A) exhibited diffuse staining throughout the cytoplasm. When the micrographs of chlorin-treated cells were compared to a micrograph of cells treated with a well-known lysosome-staining fluorochrome, such as acridine orange (fig. 6B), similar discrete brightly staining cytoplasmic inclusions were seen.

In vitro phototoxicity. Cell killing dose-response curves

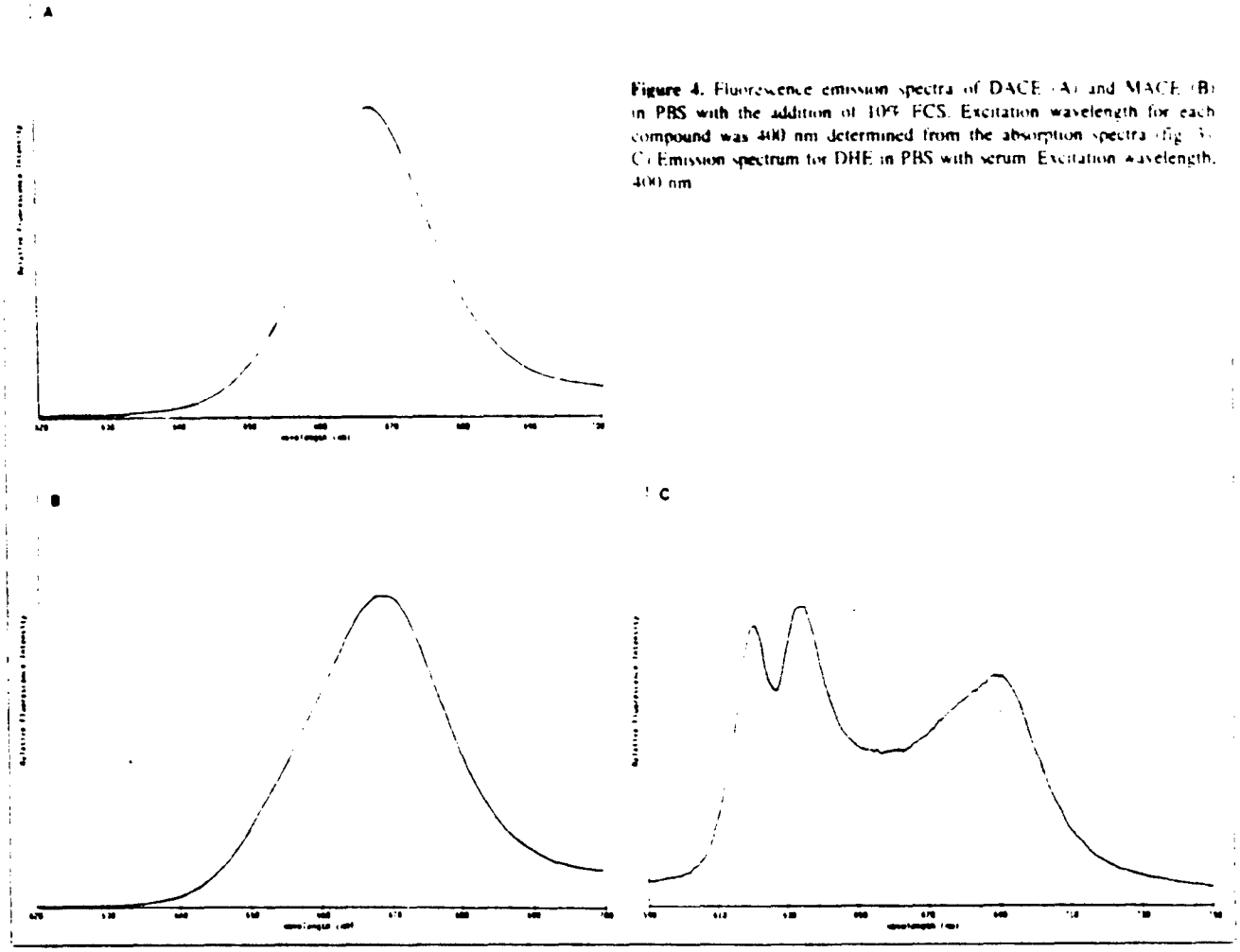

Figure 4. Fluorescence emission spectra of DACE (A) and MACE (B) in PBS with the addition of 10% FCS. Excitation wavelength for each compound was 400 nm determined from the absorption spectra (fig. 3). C) Emission spectrum for DHE in PBS with serum. Excitation wavelength, 400 nm.

with the use of a standard clonogenicity assay were determined for CHO cells after 24 hours of exposure to MACE, DACE, or DHE (fig. 7). This cell line was chosen because it is often used in clonogenicity assays due to its ability to form single-cell suspension (*18,19*). Virtually all the cells were killed by 5 μg/ml of DHE with 630-nm light, whereas 15 μg/ml of chlorin was needed to reach equivalent toxicities. The phototoxicities of the two chlorins were approximately equal, with the monoaspartyl derivative being slightly more effective. Each datum point represented the average of five petri dishes. Controls receiving only drug and no light showed little cytotoxicity with all the compounds. Even at the highest concentrations tested, less than 8% toxicity was seen. Cells exposed only to the irradiation with no photosensitizer showed less than 2% loss in viability. The chlorins were effective photosensitizers out to 670 nm.

Discussion

PDT with DHE has been limited in its effectiveness due to low tissue penetrance and minimal absorption at 630 nm. In addition, the heterogeneous nature of the porphyrin mixture has hindered elucidation of the mechanism behind PDT. The chlorins are known to have significant absorption bands at wavelengths longer than 650 nm, thereby increasing their tissue penetrance and potentially tumor photodestruction. Our study examined the absorption and fluorescence spectra, phototoxicity, cytotoxicity, and subcellular localization of two new monomeric photosensitizing compounds, MACE and DACE.

The HPLC analyses of the chlorins resulted in the elution of compounds with a single peak, suggesting that the chlorins are very pure. DACE appears to be slightly more hydrophilic than MACE, as determined by elution times.

Both compounds have significant absorbance at 664 nm. We noted a red shift of approximately 10 nm in the therapeutic band (664 nm) with the addition of cells or serum when compared to the compounds in PBS (data not shown). This is most likely due to drug binding to serum protein or membranes. As with porphyrins, the very intense Soret band (400-nm region) could be useful for the treatment of superficial diseases where deep penetration into the tissue is not desirable.

The fluorescence emission spectra for the chlorins have one peak around 668 nm, which does not shift when the microenvironment changes (data not shown), whereas DHE

Best Available Copy

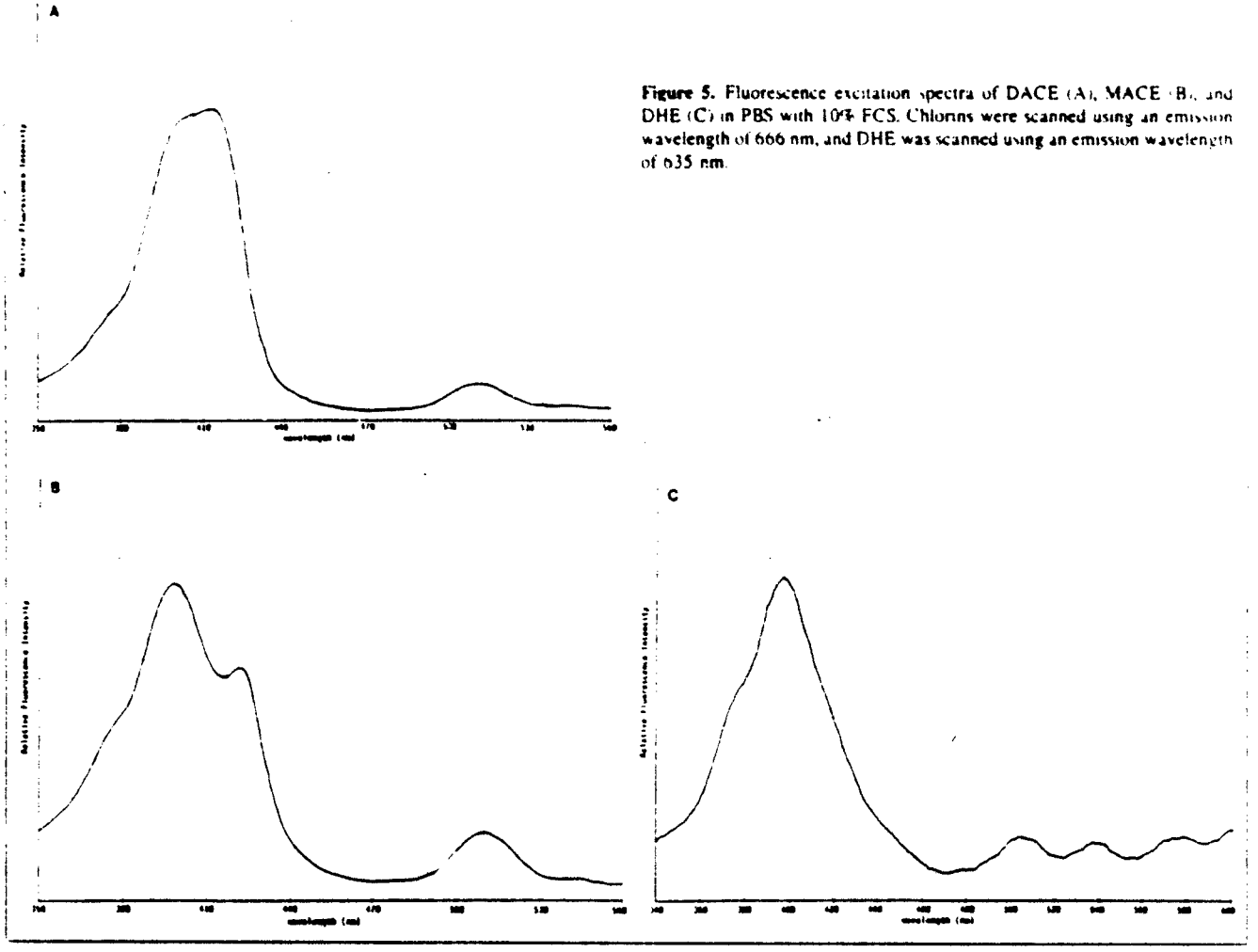

Figure 5. Fluorescence excitation spectra of DACE (A), MACE (B), and DHE (C) in PBS with 10% FCS. Chlorins were scanned using an emission wavelength of 666 nm, and DHE was scanned using an emission wavelength of 635 nm.

has three peaks at 620, 635, and 691 nm, which change in position and relative intensity when the serum concentration and/or pH is changed (Kimel S: personal communication). We believe that the single emission peak, purity, and in vitro stability of the chlorins could make them much easier compounds to use in the detection and treatment of tumors in vivo. Diagnostic fluorescence could only be attributed to the injected chlorin and directly correlates with molecular localization and therefore site of phototoxicity. However, the heterogeneous nature of HPD yields numerous fluorescent fractions, some of which are not significantly phototoxic.

The fluorescent micrographs provide insight into the possible differences in cellular uptake and organelle binding between the hydrophilic chlorins and the lipophilic DHE. Whereas DHE diffusely stains the cytoplasm, the chlorins are only found in cytoplasmic organelles that appear to be lysosomes. This conclusion is based upon seeing a similar pattern to that found in cells stained with acridine orange (a known lysosome-staining fluorochrome). Therefore, MACE and DACE are possibly more specific to a particular category of cellular organelles than is DHE. This hypothesis is consistent with the difference in relative hydrophobicities of the sensitizers [as can be determined from HPLC retention times of the chlorins compared to published retention times of HPD (*20*)].

The phototoxicity curves demonstrate that DHE is the more potent photosensitizer under the experiment conditions outlined above. However, it is also quite evident that both chlorin compounds are effective in vitro sensitizers; however, MACE is slightly more phototoxic. Note that an additional hydrophilic group on the chlorins results in decreased effectiveness. This finding is similar to results obtained with certain phthalocyanines (*21*). The difference in phototoxicity between the chlorins can be explained, in part, by the decrease in absorbance at 664 nm with DACE. In addition, cellular uptake is undoubtedly affected by the more hydrophilic nature of the diaspartyl compound. Although use of higher concentrations of the chlorins may be necessary to obtain equivalent phototoxicity, deleterious secondary side effects associated with DHE-PDT (such as skin photosensitization) are not present with the chlorin compounds [(22); unpublished results]. In addition, the chlorins are not cytotoxic unless activated with light at the highest concentration of sensitizer tested, suggesting that even higher concentrations can be used safely.

Our studies show that MACE and DACE are effective

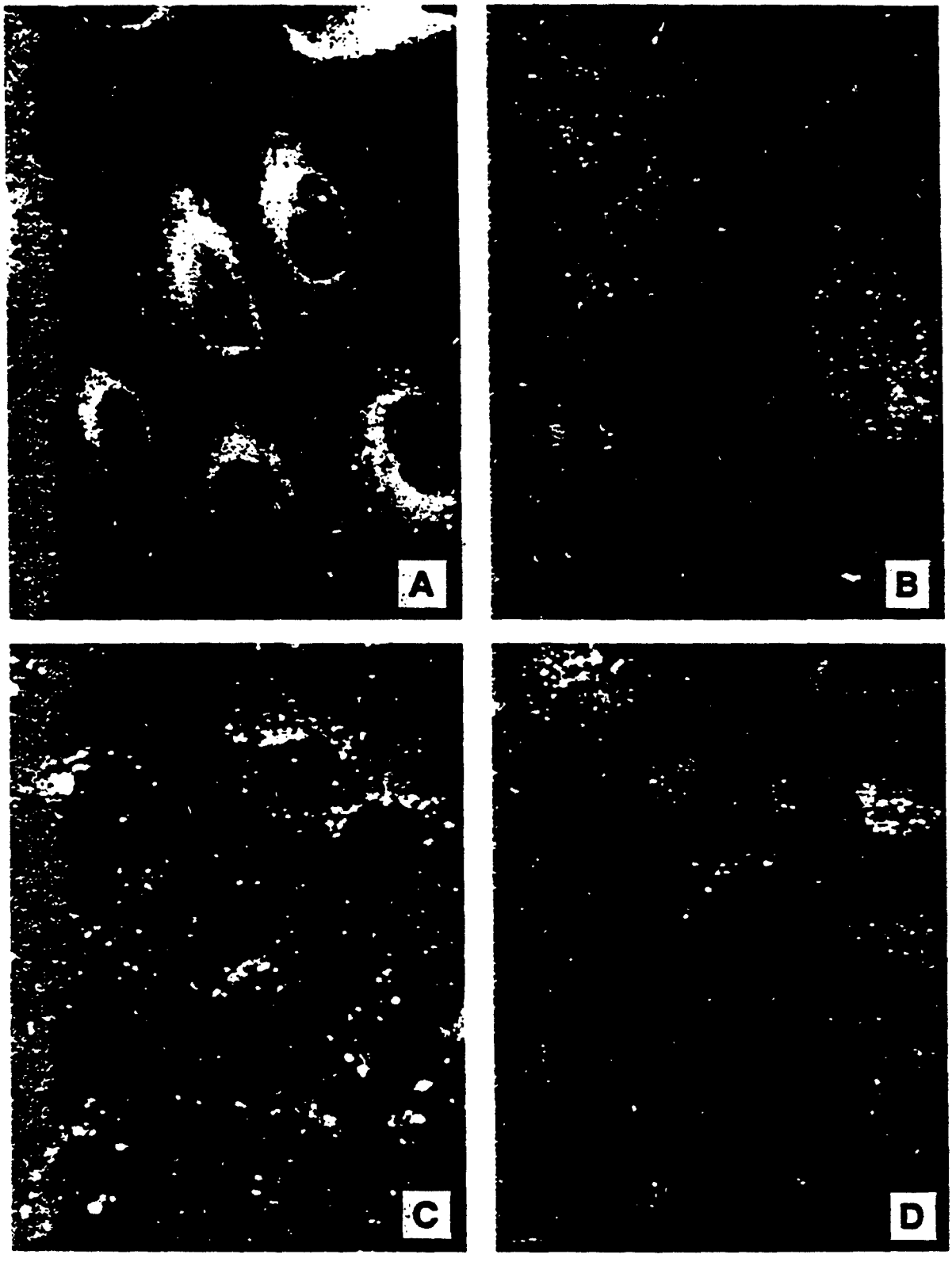

Figure 6. Fluorescence micrographs of PTK_2 cells incubated with DHE (25 μg/ml for 24 hr) (A); with acridine orange, a known lysosome-staining fluorochrome (B); with MACE (25 μg/ml for 24 hr) (C); and with DACE (25 μg/ml for 24 hr) (D). Notice the diffuse staining of cytoplasm in DHE-treated cells and the similarity between acridine orange-treated and chlorin-treated cells. Chlorins appear to be much more specifically localized. (A–D) × 630.

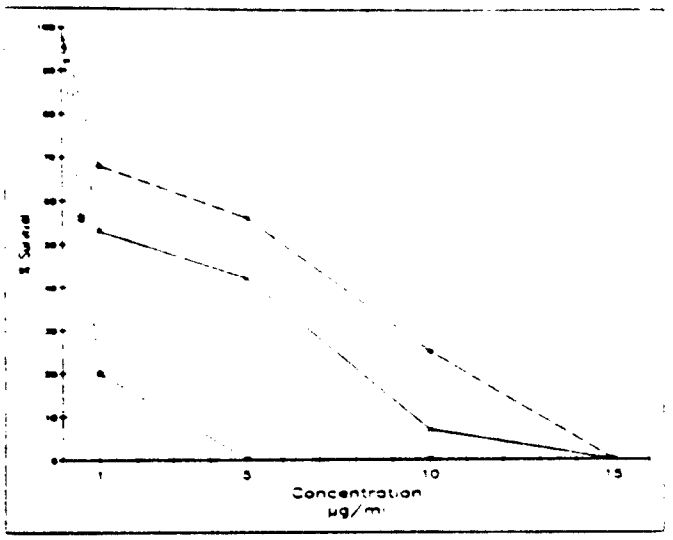

Figure 7. Dose-response curves of CHO cells incubated with DHE (□), MACE (×), or DACE (○) for 24 hr. After incubation and plating (200 cells/petri dish), cells were irradiated using an argon-pumped dye laser tuned to emit light at 630 nm for DHE-treated cells and at 664 nm for chlorin-treated cells. Viability was determined by a clonogenicity assay. Dark controls consistently had >95% survival.

photosensitizers in vitro and could provide an alternative to DHE. The greater tissue penetrance of the longer wavelength and the reduced residual skin photosensitivity give these compounds decided advantages over DHE. Furthermore, the chemical purity and single fluorescence emission band facilitate chemical analysis and characterization.

References

1. KESSEL D, CHOU T-H. Tumor localizing components of the porphyrin preparation hematoporphyrin derivative. Cancer Res 1983;43:1994-1999.
2. KESSEL D, CHENG M-L. Biological and biophysical properties of the tumor localizing component of hematoporphyrin derivative. Cancer Res 1985;45:3053-3057.
3. KESSEL D, CHENG M-L. On the preparation and properties of dihematoporphyrin ester, the tumor-localizing component of HPD. Photochem Photobiol 1985;4:277-282.
4. DAHLMAN A, WILE AG, BURNS RG, et al. Laser photoradiation therapy of cancer. Cancer Res 1983;43:430-434.
5. WILE AG, DAHLMAN A, BURNS RG, et al. Laser photoradiation therapy of cancer following hematoporphyrin sensitization. Lasers Surg Med 1982;2:163-166.
6. DOUGHERTY TJ. An overview of the status of photoradiation therapy. In: Doiron DR, Gomer CJ, eds. Porphyrin localization and treatment of tumors. New York: Alan R. Liss, 1984:75-87.
7. NELSON JS, WRIGHT WH, BERNS MW. Histopathological comparison of the effects of hematoporphyrin derivative on two different murine tumors using computer-enhanced digital video fluorescence microscopy. Cancer Res 1985;45:5781-5786.
8. GOMER CJ, DOIRON N, RUCKER N, et al. Action spectrum (620-640nm) for hematoporphyrin derivative induced cell killing. Photochem Photobiol 1984;39:365-368.
9. DOIRON DR. Photophysics of and instrumentation for porphyrin detection and activation. In: Doiron DR, Gomer CJ, eds. Porphyrin localization and treatment of tumors. New York: Alan R. Liss, 1984:41-73.
10. KESSEL D. Tumor localization and photosensitization by DHE and TPPS. Presented at the Clayton Foundation conference on photodynamic therapy. Manna del Rey, CA, February 15-19, 1987.
11. SMITH KM. General features of the structure and chemistry of porphyrin compounds. In: Smith KM, ed. Porphyrins and metalloporphyrins. Amsterdam: Elsevier, 1975.
12. SMITH KM, GOFF DA, SIMPSON DJ. Meso-substitution of chlorophyll derivatives: direct route for transformation of bacteriopheophorbides-d into bacteriopheophorbides-c. J Am Chem Soc 1985;107:4946.
13. KENNER GW, MCCOMBIE SW, SMITH KM. Pyrroles and related compounds. XXIV. Separation and oxidative degradation of chlorophyll derivatives. J Chem Soc [Perkin 1] 1973;21:2517-2523.
14. SMITH KM, FUJINARI EM, LANGRY KC, et al. Manipulation of vinyl groups in protoporphyrin. IX. Introduction of deuterium and ^{13}C labels for spectroscopic studies. J Am Chem Soc 1983;105:6638-6646.
15. BOMMER JC, BURNHAM BJ. European patent appl. EP 169,833. Chem Abstr 1986;105:133666e.
16. SCHEER H, KATZ JJ. In: Smith KM, ed. Porphyrins and metalloporphyrins. Amsterdam: Elsevier, 1975:319-514.
17. BERNS MW, DAHLMAN A, JOHNSON FM, et al. In vitro cellular effects of hematoporphyrin derivative. Cancer Res 1982;42:2325-2329.
18. GOMER CJ, SMITH D. Photoinactivation of Chinese hamster cells by hematoporphyrin derivative and red light. Photochem Photobiol 1980;32:341-348.
19. BEN-HUR E, ROSENTHAL I. Factors affecting the photokilling of cultured Chinese hamster cells by phthalocyanines. Radiat Res 1985;103:403-409.
20. SUN C-H, DUZMAN E, MELLOTT J, et al. Spectroscopic, morphologic, and cytotoxic studies on major fractions of hematoporphyrin derivative and photofrin II. Lasers Surg Med 1987;7:171-179.
21. BRASSEUR N, ALI H, LANGLOIS R, et al. Biological activities of phthalocyanines. V. Photodynamic therapy of EMT-6 mammary tumors in mice with sulfonated phthalocyanines. Photochem Photobiol 1987;45:581-586.
22. NELSON JS, ROBERTS WG, BERNS MW. In vivo studies on the utilization of mono-L-aspartyl chlorin (NPe6) in photodynamic therapy. Cancer Res 1987;47:4681-4685.

Reprinted from THE JOURNAL OF THORACIC AND CARDIOVASCULAR SURGERY, St. Louis
Vol. 93, No. 4, pp. 494-503, April, 1987. Printed in the U.S.A.
Copyright © 1987 by The C.V. Mosby Company

Comparison of continuous-wave lasers for endarterectomy of experimental atheromas

The standard surgical lasers, argon ion, neodymium–yttrium aluminum garnet, and carbon dioxide, are often operated as continuous wave lasers with specific uses. Clinical trials of laser therapy for arteriosclerotic cardiovascular disease are underway with all three lasers. Therefore, we compared these three lasers under controlled experimental conditions. A thoracoabdominal exploration was performed in 17 arteriosclerotic rabbits. The aorta was isolated, heparin administered, and multiple endarterectomies were performed in each rabbit with each of the lasers. A line of laser craters was created at the proximal and distal ends of an atheroma. Continuous-wave laser radiation was used to connect the craters and thereby form proximal and distal end points. The plaques were dissected free from the aorta with laser light and the end points were fused by laser. The aortas were removed for light microscopy and the animals were killed. The endarterectomy surfaces and end points were serially sectioned and graded according to light microscopic findings (1 = worst, 4 = best). Argon ion laser endarterectomy (N = 16) required 106 ± 10 J/cm². The surface score was 3.5 and end point score 3.4. Neodymium–yttrium aluminum garnet laser endarterectomy (N = 13) required 1,289 ± 115 J/cm² with a surface score of 2.4 ($p < 0.001$ from argon ion) and an end point score of 1.3 ($p < 0.001$ from argon ion). Carbon dioxide laser endarterectomy (N = 9) required 30 ± 5 J/cm² with a surface score of 2.0 ($p < 0.001$ from argon ion) and an end point score of 1.6 ($p < 0.001$ from argon ion). Perforation occurred in one of 16 argon ion studies (technical error, not laser), in 11 of 13 neodymium–yttrium aluminum garnet studies, and in six of nine carbon dioxide studies. This study demonstrates that of the currently available clinical continuous-wave lasers, the argon ion laser is superior for endarterectomy of experimental atheromas.

John Eugene, M.D. (by invitation), Marc E. Pollock, M.D. (by invitation), Stephen J. McColgan, M.D. (by invitation), Marie Hammer-Wilson, M.S. (by invitation), Michael W. Berns, Ph.D. (by invitation), and G. Robert Mason, M.D., Ph.D.,
Long Beach and Irvine, Calif.

Lasers that generate light as a continuous output of energy for a period of greater than 250 msec are known as continuous-wave (CW) lasers. The three standard surgical lasers, the argon ion, neodymium–yttrium aluminum garnet (Nd-YAG), and carbon dioxide lasers, can all be operated as CW lasers.[1] Because the lasers have different wavelengths, their light is absorbed to different degrees by different tissues and specific uses have evolved for each one. All of them have been proposed for use in the treatment of arteriosclerotic cardiovascular disease, and clinical trials have begun.[2-4] However, adequate comparative in vivo studies of their effect on arteriosclerotic vessels have not been performed. This study evaluates the laser-atheroma interaction of the standard surgical lasers in an experimental arteriosclerosis model by the gross and microscopic results of open laser endarterectomy.

From the Department of Surgery, Veterans Administration Medical Center, Long Beach, Calif., University of California, Irvine, Calif., and the Beckman Laser Institute and Medical Clinic.

Read at the Sixty-sixth Annual Meeting of The American Association for Thoracic Surgery, New York, N.Y., April 28-30, 1986.

Supported by National Institutes of Health Grants RRO 1192 and HL 31318.

Address for reprints: John Eugene, M.D., 5901 E. Seventh St. (112), Long Beach, Calif. 90822.

Best Available Copy

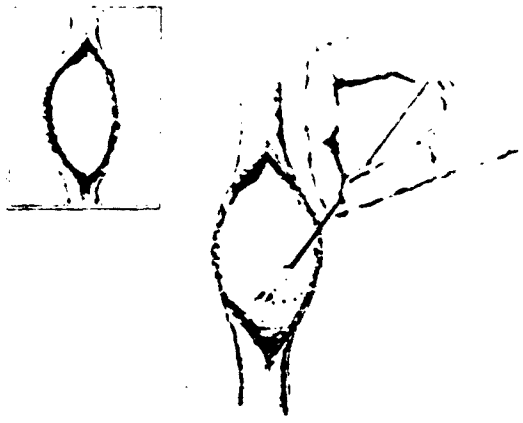

Fig. 1. *Inset* shows an arteriosclerotic rabbit aorta opened to expose an atheromatous plaque. A line of laser craters (approximately 0.5 mm) diameter is being created at one end of the plaque. The craters penetrate to the media.

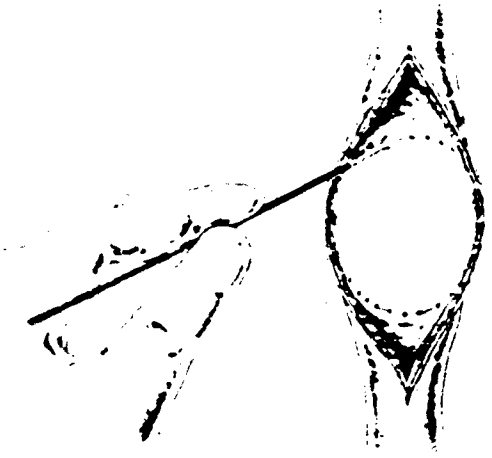

Fig. 2. The lines of laser craters are connected by CW laser radiation to loosen the plaque and form proximal and distal end points.

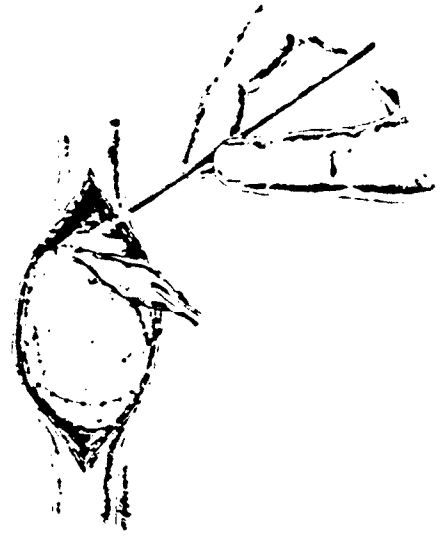

Fig. 3. The atheroma is elevated away from the media by CW laser radiation. The cleavage plane of the endarterectomy is being developed within the media by laser light.

Materials and methods

Arteriosclerotic New Zealand white rabbits were used in this study.[5] They received humane care in compliance with the "Principles of Laboratory Animal Care" formulated by the National Society for Medical Research and the "Guide for the Care and Use of Laboratory Animals" (NIH Publication No. 80-23, revised 1978). Under general anesthesia (intramuscular acepromazine 0.5 mg/kg, xylazine 30 mg/kg, and ketamine 50 mg/kg), 17 rabbits underwent balloon catheter trauma to the thoracoabdominal aorta. After recovery from anesthesia, they were begun on a 2% cholesterol diet and continued on this diet for 20 weeks. This regimen has been shown to produce significant arteriosclerosis in 86% of rabbits.[5] The arteriosclerosis is uniform throughout the traumatized aorta. The intima appears markedly thickened and discolored. The atheromas have a fibrous cap surrounding areas of inflammation, fatty infiltration, and microcalcification that often extend across the internal elastic lamina into the media.[5]

The arteriosclerotic rabbits were anesthetized (intramuscular acepromazine 0.5 mg/kg, xylazine 3 mg/kg, and ketamine 50 mg/kg), intubated, and ventilated with a small-animal respirator. Supplemental ketamine (50 mg/kg intravenously) was administered during the procedure to maintain anesthesia. A thoracoabdominal exploration was performed and the aorta was exposed. Heparin (3.0 mg/kg intravenously) was administered and proximal and distal vascular control was obtained. The aorta was opened to expose the atheromatous plaques. Open laser endarterectomy was performed by creating a line of laser craters with individual laser exposures at the proximal and distal ends of an atheroma. The lines of laser craters were connected by constant laser application to form proximal and distal end points and elevate the atheroma. Constant laser application was used to develop the proper cleavage

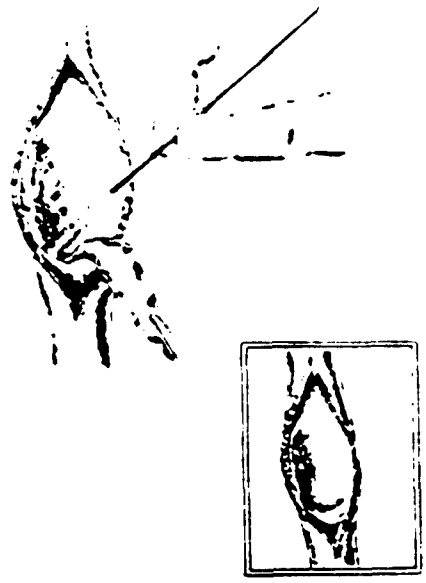

Fig. 4. The cleavage plane has been developed within the media by CW laser radiation, which allows the plaque to be dissected free from the artery. *Inset* shows the completed endarterectomy with the end points welded for a smooth transition from endarterectomy surface to intima.

plane just beneath the internal elastic lamina and to dissect the atheroma from the aorta. The end points were welded by additional laser exposure to provide a secure transition from endarterectomy surface to intima. Only laser light was used to perform the endarterectomies. The technique is illustrated in Figs. 1 to 4.

In Group I (seven rabbits) an argon ion laser (Innova 20, Coherent Inc., Palo Alto, Calif.) was used. Laser radiation was delivered through a 400 μm quartz optical fiber that was freshly cut for each experiment. Power was delivered at 1.0 W (producing a spot approximately 0.5 mm) and this was continuously monitored from the laser head. Power was also measured from the output end of the optical fiber at the beginning and conclusion of each endarterectomy with a Coherent power meter, Model 210. Energy delivered to the aorta was regulated by the duration of exposure, and this ranged from 1.0 second to 30 seconds (1.0 to 30 J per exposure).

In Group II (six rabbits) endarterectomy was performed with an Nd-YAG laser (Model 8000-3, Molectron Corporation, Santa Clara, Calif.). Laser radiation was delivered through a 600 μm quartz optical fiber with an integral aiming light. Power was delivered at 10 to 20 W depending on the tissue response to Nd-YAG radiation. Spot size was 0.6 to 0.8 mm. Power was continuously monitored from a built-in power meter. Energy delivered was regulated by the duration of exposure, and this ranged from 0.5 second to 30 seconds (10 to 300 J per exposure).

In Group III (four rabbits) a hand-held carbon dioxide laser (Model Systems LS 20-H, Directed Energy, Inc., Irvine, Calif.) was used. Power was delivered from the laser head directly at the aorta at an output of 10.0 W. Spot size was 0.2 to 0.4 mm. Exposure time was kept constant at 10 msec (0.1 J per exposure). Energy delivery was regulated by using rapid series of laser exposures to perform the steps of the endarterectomy.

After laser endarterectomy, the aortas were harvested and the animals were killed (barbiturate injection). The aortas were rinsed in Ringer's lactate solution and separated into surface and end point specimens under a dissecting microscope. The specimens were pinned flat on Teflon blocks, fixed in 3% glutaraldehyde in phosphate buffer at 4° C for 24 hours, and rinsed in phosphate buffer. They were dehydrated through an alcohol series, removed from the Teflon blocks, and embedded in paraffin. All specimens were serially sectioned at 6 μm and stained with hematoxylin and eosin.

The surfaces and end points were graded according to gross and light microscopic appearance. For the surface, 1 = perforation, 2 = wrong cleavage plane, 3 = rough surface, and 4 = smooth surface. For the end points, 1 = perforation, 2 = intimal flap, 3 = rough transition, and 4 = smooth transition. The specimens were examined independently by three of the authors and the results for each specimen were averaged to determine the final score. The scores for Groups I, II, and III were compared by the 4 by 3 contingency table and the Kruskal-Wallis test with tied midranks.[9] Differences amounting to a p value less than 0.05 were considered significant.

Results

A total of 16 endarterectomies were performed in Group I (argon ion laser), 13 endarterectomies in Group II (Nd-YAG laser), and nine endarterectomies in Group III (carbon dioxide laser).

The gross appearance of the argon ion laser endarterectomies was satisfactory. The surfaces were smooth and shiny without residual atheroma and the end points were fused. Perforation occurred at one distal end point as a result of a technical error (the tip of the fiber touched the artery) rather than the laser beam. The argon ion laser energy was well absorbed by the arteriosclerotic rabbit aortas and produced a uniform

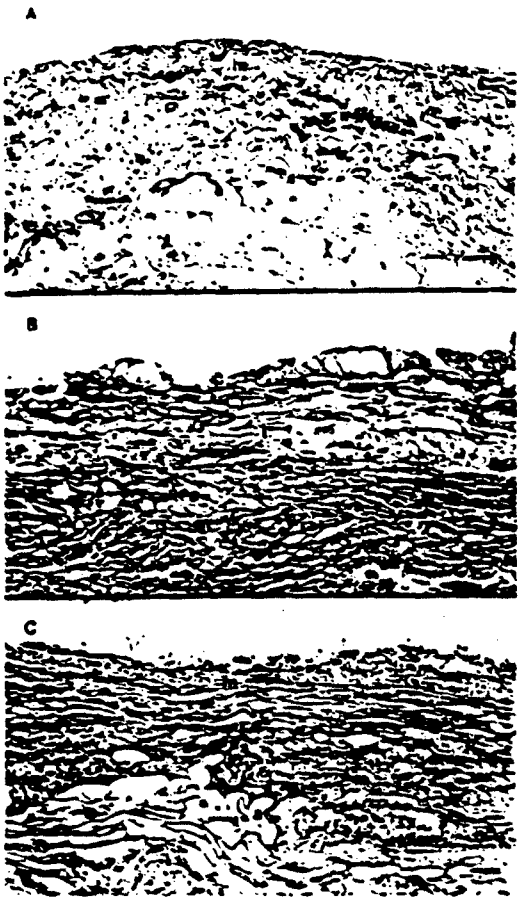

Fig. 5. Endarterectomy surfaces after open laser endarterectomy in arteriosclerotic rabbit aortas. *A*, Argon ion surface shows a smooth endarterectomy surface. The cleavage plane has been developed just beneath the internal elastic lamina. The architecture of the media and adventitia is undisturbed and there is no debris or thermal injury. *B*, Nd-YAG surface is rough and distorted. The cleavage plane is superficial to the internal elastic lamina leaving atheromatous intima. The surface shows extensive thermal injury manifested by charring and blistering. *C*, Carbon dioxide surface is uneven. The cleavage plane has been developed deep within the media almost to the adventitia. There is residual debris but no thermal injury. *i*, Intima. *m*, Media. *a*, Adventitia. Calibration bar = 50 μm (Hematoxylin and eosin stain).

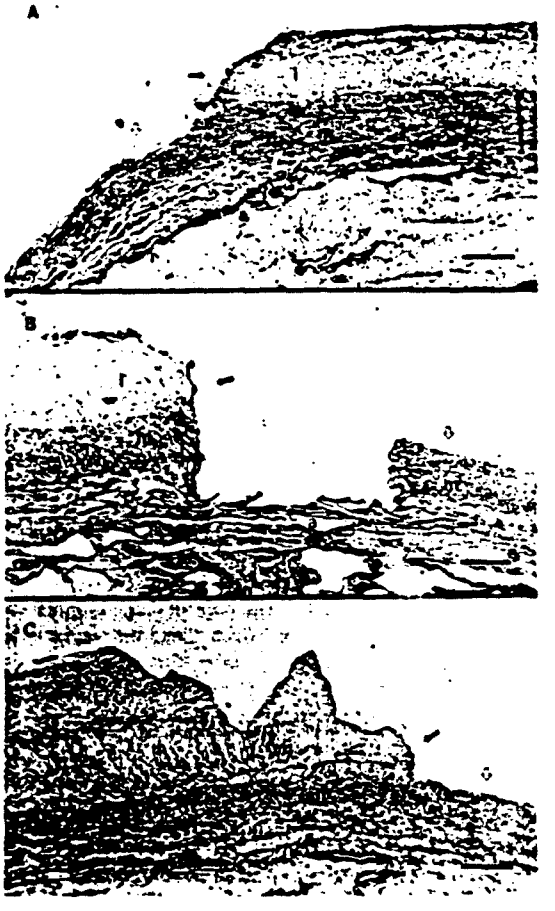

Fig. 6. Distal end points after open laser endarterectomy in arteriosclerotic rabbit aortas. *A*, Argon ion end point has a smooth tapered transition from intima to endarterectomy surface. The layers are fused and there are mild thermal changes along the surface manifested by carbonization and polymorphous lacunae. *B*, Nd-YAG end point is uneven and almost perforated. There is extensive thermal injury manifested by charring and distortion of tissue planes. *C*, Carbon dioxide end point is irregular and uneven. There are mild thermal changes manifested by surface carbonization. *Closed arrow*, Intimal surface. *Open arrow*, Endarterectomy surface. *i*, Intima. *m*, Media. *a*, Adventitia. Calibration bar = 100 μm (Hematoxylin and eosin stain).

depth of penetration that was predictable and controllable. There was no evidence of thermal damage to surrounding structures. Light microscopic examination of serial sections showed the cleavage plane to be just beneath the internal elastic lamina in all 16 experiments (Fig. 5, *A*). The end points were fused by phototherapy and nine of 16 showed a smooth transition from intima to endarterectomy surface (Fig. 6, *A*). An intimal flap was left in one experiment and this was detected only by microscopic examination.

The gross appearance of Nd-YAG laser endarterectomies was unsatisfactory. The surfaces were discolored

Table I. *Argon ion laser endarterectomy*

Experiment No.	Atherosclerosis	Power (W)	Surface area (cm²)	Energy density (J/cm²)	Surface score	End point score
1	Moderate	1.0	1.5	1,333	4	4
2	Moderate	1.0	1.4	1,429	4	4
3	Severe	1.0	1.0	2,000	4	4
4	Severe	1.0	1.75	1,143	4	4
5	Mild	1.0	1.2	1,250	4	4*
6	Mild-moderate	1.0	1.2	1,667	4	3
7	Moderate	1.0	1.84	1,087	4	4
8	Moderate	1.0	1.5	1,333	3	4
9	Mild-moderate	1.0	2.0	1,000	4	4
10	Mild-moderate	1.0	1.0	2,000	3	3
11	Moderate-severe	1.0	1.0	2,000	4	3
12	Moderate	1.0	2.7	1,000	4	4
13	Moderate-severe	1.0	2.0	1,431	3	2
14	Moderate-severe	1.0	1.6	1,429	3	4
15	Moderate-severe	1.0	2.9	1,170	4	4
16	Moderate-severe	1.0	3.12	220	4	4

*Technical error: fiber tip contacted surface.

and parched and the end points were charred. The Nd-YAG laser energy was not uniformly absorbed by rabbit aortas; rather, it was transmitted through the aorta so that it produced thermal damage to the adventitia and surrounding structures (inferior vena cava, bowel, and muscles). The unpredictable depth of laser beam penetration led to uneven endarterectomy surfaces and end points. Light microscopy revealed the wrong cleavage plane in six of 13 experiments (Fig. 5, *B*) and perforation at 11 of 13 end points (Fig. 6, *B*).

The gross appearance of carbon dioxide laser endarterectomies was generally satisfactory. Close inspection, however, revealed that fragments of intima and internal elastic lamina were left on the surfaces and there were small perforations at the end points. The carbon dioxide laser energy was so well absorbed by the arteriosclerotic rabbit aortas that the depth of laser beam penetration was unpredictable. The result was uneven dissection and frequent perforation. There was no evidence of thermal damage to surrounding structures. Light microscopy showed that the wrong cleavage plane was developed in five of nine surfaces (Fig. 5, *C*) and there were perforations at six of nine end points (Fig. 6, *C*).

Laser endarterectomy results are summarized in Tables I to III. The mean (± standard error of the mean) surface area of argon ion laser endarterectomy was 1.89 ± 0.23 cm² and required an average energy density of 106 ± 10 J/cm². The mean Nd-YAG laser endarterectomy surface area was 1.45 ± 0.16 cm² and required an average energy density of 1,289 ± 115 J/cm². The mean carbon dioxide laser endarterectomy surface area was 1.67 ± 0.11 cm² and required an average energy density of 30 ± 5 J/cm². Endarterectomy surface scores averaged 3.5 for Group I, 2.33 for Group II ($p < 0.001$ from Group I), and 2.0 for Group III ($p < 0.001$ from Group I). End point scores were 3.38 for Group I, 1.31 for Group II ($p < 0.001$ from Group I), and 1.56 for Group III ($p < 0.001$ from Group I).

Discussion

The argon ion laser (488 and 514.5 nm) is a CW laser with mixed wavelengths that are best absorbed by hemoglobin and melanin-pigmented tissue. It has been used to remove pigmented cutaneous lesions and to cauterize gastrointestinal bleeding sites. Its penetration in tissue is 1 to 2 mm. The Nd-YAG laser (1.06 μm) is a CW laser with a wavelength that is absorbed by tissue protein. It is used to ablate tumors, cauterize bleeding sites, and coagulate tissues. Its penetration in tissue is approximately 4 mm. The carbon dioxide laser (10.6 μm) is a CW laser whose beam is well absorbed by tissue water. It is used as a cutting instrument intraoperatively because its penetration in tissue is limited to 0.1 to 0.2 mm. The argon ion and Nd-YAG laser beams can be directed through commercially available optical fibers. There are no readily available optical fibers for the carbon dioxide laser, but several experimental fibers are being tested.[7-9]

Fiberoptic delivery makes it possible to direct laser energy through a catheter or angioscope to ablate atheromas at distant sites within arteries. Optical fibers can also be modified with metal caps[9, 10] or sapphire crystals[11] for specific recanalization or cutting purposes.

Best Available Copy

Table II. *Nd-YAG laser endarterectomy*

Experiment No.	*Atheroma*	*Power (W)*	*Surface area (cm²)*	*Energy (J)*	*Surface score*	*End points score*
	Moderate	10	1.2	1,706	3	1
2	Moderate	10	2.2	2,633	2	1
3	Moderate	10-20	1.1	1,072	2	3
4	Mild	10-20	1.0	890	3	3
5	Mild	10-20	1.0	681	3	1
6	Mild-moderate	10-20	1.2	1,255	2	1
7	Moderate-severe	10-20	1.5	2,755	2	1
8	Moderate-severe	10	1.4	1,408	2	1
9	Severe	10	1.2	1,553	3	1
10	Moderate	10	3.1	4,091	3	1
11	Severe	10-20	1.2	2,714	2	1
12	Moderate-severe	10-20	1.5	1,996	3	1
13	Moderate	10-20	1.2	1,690	1	1

Table III. *Carbon dioxide laser endarterectomy*

Experiment No.	*Atheroma*	*Power (W)*	*Surface area (cm²)*	*Energy (J)*	*Surface score*	*End points score*
1	Moderate-severe	10	2.0	92	2	1
2	Moderate-severe	10	1.6	91	1	3
3	Mild	10	1.6	51	2	1
4	Mild-moderate	10	1.8	73	3	1
5	Mild	10	1.17	36	1	1
6	Mild	10	1.3	26	2	1
7	Moderate	10	1.5	19	2	2
8	Moderate	10	2.0	29	3	3
9	Moderate-severe	10	2.1	42	2	1

For this reason most investigations of laser treatment for arteriosclerotic cardiovascular disease have been performed with the argon ion and Nd-YAG lasers and initial clinical trials were begun with these lasers.[12-14] Optical fibers may not be absolutely necessary, however. Livesay and associates[15,16] have shown that a carbon dioxide laser beam can be introduced into coronary arteries intraoperatively. Their technique is designed to recanalize diffusely diseased coronary arteries before bypass grafting. At this time clinical trials are in progress with these three different lasers without comparative in vivo data concerning their effects on arteriosclerotic arteries.

In the present study the three standard surgical lasers were compared by the results of open laser endarterectomy. Laser endarterectomy is a uniform method for the in vivo study of laser interactions with arteriosclerotic arteries.[5,17-19] With laser endarterectomy, all of the surgical uses of lasers (vaporization, cutting, dissection, coagulation, and welding) can be evaluated with one procedure under direct observation and vascular control. The technique of laser endarterectomy was developed with the argon ion laser because it produces a visible light that can be directed through an optical fiber. The visible light allowed us to be certain of the direction of the laser beam and the optical fiber allowed precise control of the beam for dissection. In arteriosclerotic rabbit aortas, the argon ion technique produces a better endarterectomy than the conventional surgical technique because the end points can be welded for an even transition.[18] Because consistently good results have been obtained with argon ion laser endarterectomy, it has become our standard for evaluating lasers for intravascular use.

Argon ion laser energy was well absorbed by arteriosclerotic rabbit aortas, and there was a predictable level of plaque penetration. The endarterectomy surfaces were all in the proper cleavage plane, they were smooth, and there was no thermal damage. The end points showed an even transition from surface to intima with mild thermal changes and no perforations. The Nd-YAG surfaces were uneven and usually within the wrong cleavage plane. There was extensive thermal injury along the endarterectomy surface and perforation

of most of the end points. The level of plaque penetration was unpredictable and power levels had to be changed frequently during the experiments to penetrate atheromas. As a result, very high energy levels were necessary to perform Nd-YAG laser endarterectomy. Carbon dioxide laser energy was very well absorbed by arteriosclerotic rabbit aortas as shown by the very low energy necessary to perform endarterectomy. The superior interaction between atheromas and carbon dioxide laser energy did not result in a superior endarterectomy because the beam could not be accurately directed without an optical fiber. An articulated arm may have helped to deliver the carbon dioxide laser beam in a steady fashion. We chose to use the hand-held carbon dioxide laser for this study because Livesay and associates[15, 16] have shown that it is easy to manipulate for endarterectomy.

The combination of predictable energy absorption and fiberoptic delivery led to an excellent endarterectomy with the argon ion laser. The poor laser-atheroma interaction of the Nd-YAG laser wavelength led to an endarterectomy that was uneven and destructive despite fiberoptic control. The lack of a fiberoptic delivery system for the carbon dioxide laser led to an unsatisfactory endarterectomy despite an excellent laser-atheroma interaction. Livesay and associates[15, 16] have modified this carbon dioxide laser with a hollow metal waveguide to direct the beam coaxially in coronary arteries. This limits the use of the carbon dioxide laser to short distances within straight arteries. Abela,[9] Sanborn,[10] and their associates have modified the optical fiber of the argon ion laser with a metallic tip to recanalize peripheral arteries. This system delivers heat only and eliminates the excellent laser-atheroma interaction of argon ion laser light.

Several investigators have considered CW lasers unsuitable for intravascular use because they cause some degree of thermal injury.[20, 21] They have proposed excimer lasers for the treatment of arteriosclerosis. This proposal is based on in vitro studies, however, because there are no data available on the effects of excimer lasers on arteriosclerotic arteries in vivo. Additionally there are no clinically available excimer lasers and there are significant problems to be overcome such as reliable optical fibers, toxic emission products, and the potential mutagenicity of ultraviolet light. Our data show that CW argon ion laser light can ablate atheroma without injury as long as low power is used in a carefully controlled fashion (open laser endarterectomy). Arteriosclerotic rabbit aortas resemble arteriosclerotic human coronary arteries in size (average diameter 1.5 mm) and texture (delicate, thin-walled) although rabbit arteriosclerosis is generally not as severe as human arteriosclerosis. Therefore, our data may represent the clinical response of human coronary artery disease to laser radiation. On the basis of the consistently good results of argon ion laser endarterectomy in the rabbit arteriosclerosis model, we recommend the argon ion laser for direct laser radiation of atheromas in clinical trials.

We wish to thank Jeffrey J. Andrews, B.A., Allison Oliva, B.S., Ron G. Tidwell, B.S., and William Wright, B.S., for technical assistance, Howard G. Tucker, Ph.D., and Arline Nakanishi, M.S., for statistical consultation, and Marian Berman for original drawings. R. L. Maxwell prepared the manuscript.

REFERENCES

1. Dixon JA. Lasers in surgery. Curr Probl Surg 1984;21:4-21.
2. Livesay JJ, Leachman DR, Hogan PJ, et al. Preliminary report on laser coronary endarterectomy in patients [Abstract]. Circulation 1985;72 (Pt 2):III302.
3. Geschwind HJ, Boussignac G, Teisseire B, Benhaiem N, Bittoun R, Laurent D. Conditions for effective Nd-YAG laser angioplasty. Br Heart J 1984;52:484-9.
4. Abela GS, Seeger JM, Barbieri E, et al. Laser angioplasty with angioscopic guidance in humans. J Am Coll Cardiol 1986;8:184-92.
5. Eugene J, McColgan SJ, Hammer-Wilson M, Berns MW. Laser endarterectomy. Lasers Surg Med 1985; 5:265-74.
6. Lehman EL. Non-parametrics. In: Statistical methods based on ranks. San Francisco: Holden-Day 1975:202-10.
7. Eldar M, Battler A, Neufeld HN, et al. Transluminal carbon dioxide-laser catheter angioplasty for dissolution of atherosclerotic plaques. J Am Coll Cardiol 1984;3:135-7.
8. Eldar M, Battler A, Gal D, et al. The effects of varying lengths and powers of CO_2 laser pulses transmitted through an optical fiber on atherosclerotic plaques. Clin Cardiol 1986;9:89-91.
9. Abela GS, Fenech A, Crea F, Conti CR. "Hot Tip": Another method of laser vascular recanalization. Lasers Surg Med 1985;5:327-35.
10. Sanborn TA, Faxon DP, Haudenschild CC, Ryan TJ. Experimental angioplasty: circumferential distribution of laser thermal energy with a laser probe. J Am Coll Cardiol 1985;5:934-8.
11. Daikuzono N, Joffee SN. Artificial sapphire probe for contact photocoagulation and tissue vaporization with the Nd:YAG laser. Med Instrum 1985;19:173-8.
12. Geschwind H, Baussignac G, Teissiere B, et al. Percutaneous transluminal laser angioplasty in man [Letter]. Lancet 1984;8381:844.
13. Choy DSJ, Stertzer SH, Myler RK, Marco J, Fournial G. Human coronary laser recanalization. Clin Cardiol 1984;7:377-81.

14. Ginsburg R, Wexler L, Mitchell RS, Profitt D. Percutaneous transluminal laser angioplasty for treatment of peripheral vascular disease: clinical experience with 16 patients. Radiology 1985;156:619-24.
15. Livesay JJ, Cooley DA. Laser coronary endarterectomy: proposed treatment for diffuse coronary atherosclerosis. Texas Heart Inst J 1984;11:276-9.
16. Livesay JJ, Johansen WE, Sutter LV, Klima T, Painvin GA, Follette DM. Experimental technique of laser coronary endarterectomy and its immediate effects on atherosclerotic plaques in cadaver hearts. Texas Heart Inst J 1984;11:280-5.
17. Eugene J, McColgan SJ, Hammer-Wilson M, Moore-Jeffries EW, Berns MW. Laser applications to arteriosclerosis: angioplasty, angioscopy and open endarterectomy. Lasers Surg Med 1985;5:309-20.
18. Eugene J, McColgan SJ, Pollock ME, Hammer-Wilson M, Moore-Jeffries EW, Berns MW. Experimental arteriosclerosis treated by conventional and laser endarterectomy. J Surg Res 1985;39:31-8.
19. Eugene J, McColgan SJ, Pollock ME, Hammer-Wilson M, Moore-Jeffries EW, Berns MW. Experimental arteriosclerosis treated by argon ion and neodymium-YAG laser endarterectomy. Circulation 1985;72 (Pt 2):II200-6.
20. Grundfest WS, Litvack IF, Goldenberg T, et al. Pulsed ultraviolet lasers and the potential for safe laser angioplasty. Am J Surg 1985;150:220-6.
21. Isner JM, Donaldson RF, Deckelbaum LI, et al: The excimer laser: gross, light microscopic and ultrastructural analysis of potential advantages for use in laser therapy of cardiovascular disease. J Am Coll Cardiol 1985;6:1102-9.

Discussion

DR. JAMES J. LIVESAY
Houston, Texas

Dr. Eugene and his co-authors have shown convincingly that CW lasers have thermal effects remote from the site of tissue ablation. We have also studied laser effects in animals as well as human cadaveric arteries.

The argon laser delivered to the human aorta with 2 W over 10 seconds causes vaporization or cutting of the plaque, resulting in a central crater. There is considerable thermal damage with vacuolization remote from the crater in the surrounding arterial wall. Undesirable thermal damage to the artery is produced with this method of laser application. This undesirable effect can be eliminated by using lasers with higher tissue absorption, such as the carbon dioxide laser or the excimer laser. A sharp, clean cut can be made in the arterial plaque by using a laser with characteristics of low penetrance and high absorption.

We have initiated the first United States clinical trial using the laser as an adjunct for coronary endarterectomy in a study approved by the Food and Drug Administration. To date, we have operated on 12 patients and have relieved arterial stenosis in 25 of 26 coronary arteries with the laser. Postoperative angiography has demonstrated patency in 95% of bypass grafts, 93% of bypassed arteries, and 76% of laser-treated arteries. The present limitations of this technology appear to be the need for better guidance systems and prevention of thrombosis in small vessels after endarterectomy.

Dr. Eugene, do you agree that the ideal laser for endarterectomy should cause a localized ablation of plaque? Second, do you believe the high incidence of perforation observed in your study could be related to the lack of guidance or control with your method of laser delivery?

DR. EUGENE *(Closing)*

I wish to thank Dr. Livesay for his comments and I wish to congratulate him on the fine results that he has thus far achieved in his clinical evaluation of laser endarterectomy.

Dr. Livesay, I think the perforations that occurred in our series of experiments were truly due to the laser-atheroma interaction. The operative procedure was standardized, the animal models were standardized, and we have considerable experience with performing this operation.

We believe the only variable that we were evaluating was the particular wavelength of the laser and that we were actually evaluating the lasers to determine the most appropriate laser-atheroma interaction.

In terms of a more precise guidance system, I think it is true that we do need something better, and new advances are being made in the technology. We can probably improve on laser endarterectomy, for example, by using sapphire crystals. The new guidance systems will probably require additional technology, and I do not know when that technology will become available.

The purpose of this study was to utilize available equipment, something that we have ready in any operating room right now. I would leave the new technological developments for another study.

ARTICLES

Mechanism of Tumor Destruction Following Photodynamic Therapy With Hematoporphyrin Derivative, Chlorin, and Phthalocyanine

J. Stuart Nelson, Lih-Huei Liaw, Arie Orenstein, W. Gregory Roberts, Michael W. Berns*

The effect of photodynamic therapy on the tumor microvasculature in the first few hours after treatment was studied at the light and electron microscopy levels. BALB/c mice with EMT-6 tumor received ip injections of hematoporphyrin derivative, chlorin, or phthalocyanine, and 24 hours later, the tumors were treated with light at 100 J/cm² at the appropriate therapeutic wavelength for each photosensitizer. Animals were killed and their tumors removed at time 0, 30 minutes, 1 hour, and 2, 4, 6, 8, 12, 16, and 24 hours after treatment. The results indicate that for all three sensitizers the effects of photodynamic therapy leading to rapid necrosis of tumor tissue are not the result of direct tumor cell kill but are secondary to destruction of the tumor microvasculature. The first observable signs of destruction occur in the subendothelial zone of the tumor capillary wall. This zone, composed of dense collagen fibers and other connective tissue elements, is destroyed in the first few hours after phototherapy. However, the ultrastructural changes seen in this zone are different for the hematoporphyrin derivative, compared with chlorin and phthalocyanine. Binding of photosensitizers to the elements in this zone as well as altered permeability and transport through the endothelial cell layer because of the increased intraluminal pressure may be key features of tumor destruction. [J Natl Cancer Inst 1988;80:1599–1605]

During the past several years, many photosensitizing porphyrins have been shown to be retained selectively in rapidly growing, solid tumors in humans and other mammals (*1*). The action of these photosensitizers is to absorb photons of the appropriate wavelength sufficient to elevate the sensitizer to an excited state. The excited photosensitizer subsequently reacts with a molecular substrate, such as oxygen, to produce singlet oxygen, which causes irreversible oxidation of some essential cellular component (*2*). Uncertainty arises as to the exact cellular targets of these excited intermediates, although damage to the cell membrane (*3*), mitochondria (*4*), lysosomes (*5*), and the nuclear material (*6*) have been reported.

Shortly after treatment, the tumor becomes necrotic (usually within 24 hr), and when effectively treated, the tumor becomes a nonpalpable scab that is usually sloughed within a few days. A wide variety of tumors with varying histologic types have been treated with photodynamic therapy (PDT) including cancers of the skin (*7*), female genital tract (*8*), esophagus (*9*), lung (*10*), bladder (*11*), eye (*12*), and breast (*13*), and head and neck squamous cell carcinomas (*14*). Treatment parameters have been refined such that therapy can be undertaken with a reasonable expectation of good results in both animal and human trials. Although PDT can be used to eradicate relatively large tumors, it appears especially advantageous to the patient with superficial early disease or early recurrence. In addition, previous surgery, radiation therapy, or chemotherapy does not preclude the use of PDT, and many of the clinical studies reported to date have been on patients who have not benefited from some or all other forms of therapy.

Received July 13, 1988; revised October 14, 1988; accepted October 18, 1988.

Supported in part by Public Health Service grants RR-01192 from the Division of Research Resources, and CA-32248 from the National Cancer Institute, National Institutes of Health, Department of Health and Human Services; and grant SDI084-88-C-0025 from the Department of Defense.

Department of Surgery, and the Beckman Laser Institute and Medical Clinic, University of California, Irvine, Irvine, CA.

We thank Dr. Kevin Smith, University of California at Davis, for providing the mono-L-aspartyl chlorin e_6, Jeffrey Andrews and Glen Profeta for their technical assistance in operating the lasers, and Ms. Elaine Kato for preparation of the manuscript.

**Correspondence to:* J. Stuart Nelson, M.D., Beckman Laser Institute and Medical Clinic, 1002 Health Sciences Road East, Irvine, CA 92715.

Best Available Copy

Despite these positive attributes, some of the fundamental mechanisms involved in this unique application of photochemotherapy remain incompletely understood. For example, it is still not known whether tumor destruction is a result of actual PDT phototoxic effects on the proliferating tumor cell or, as has been recently suggested, the result of damage produced to some other tumor elements, such as the microvasculature (*15*). Apparent internal hemorrhage and red cell extravasation are common findings after PDT, not only in most experimental animal tumors but in tumors in patients as well. With this in mind, our objective in this study was to examine the ultrastructural effects of several photosensitizers on the tumor microvasculature during the first few hours after phototherapy. We hope that this type of study will help elucidate the complex role of the tumor vasculature in PDT as well as provide a basic understanding of the mechanism of phototoxicity of potential new photosensitizers.

Materials and Methods

Animal and Tumor System

The EMT-6 experimental mammary tumor arising in the flanks of BALB/c mice was used. All mice were 6-8 weeks old and weighed between 30 and 35 g at the time of treatment. When the tumors attained a size of 1-2 cm in diameter, they were excised and minced with fine scissors in phosphate-buffered saline (PBS). This resulting suspension of tumor cells was filtered through sterile gauze, washed twice in PBS, and then resuspended in RPMI media (GIBCO, Grand Island, NY) at a concentration of 5×10^5 viable cells/mL. Viability of the cells was assessed by their ability to resist lysis and exclude Trypan Blue dye (GIBCO). We initiated the tumors by injecting 0.1 mL of fresh tumor inoculum into the right flank of mice. The mouse tumors were generally palpable at 5 days and reached a size of 5-7 mm by 10-14 days at which time we started the treatment. At this size, the small tumors were homogeneously white, with spontaneous tumor necrosis minimal or absent.

Photosensitizers

For all photosensitizers, a drug dose was chosen that would ensure complete tumor kill in all animals tested.

Photofrin II [(DHE); Photomedica, Inc., Raritan, NJ] was obtained as an aqueous solution at a concentration of 2.5 mg/mL and stored in the dark at −70 °C until used. For in vivo experiments, DHE was diluted 1:4 with 0.9% NaCl solution and injected ip in doses equal to 10 mg/kg body weight (*16*).

Mono-L-aspartyl chlorin e_6 (MACE) was received as a dark green powder, reconstituted in Dulbecco's PBS to a final concentration of 2.5 mg/mL, and stored in the dark at −70 °C until used (*17*). Prior to injection, MACE was diluted 1:4 with 0.9% saline solution and injected ip in doses equal to 10 mg/kg body weight (*18*).

Chloroaluminum sulfonated phthalocyanine [(CASPc); Ciba-Geigy Corp., Basel, Switzerland] was provided as a 300-mg/mL sample in water. It was diluted in Dulbecco's PBS to a final concentration of 2.5 mg/mL and stored in the dark at −70 °C until used. Prior to injection, CASPc was diluted 1:4 with 0.9% saline solution and then given ip in doses equal to 1 mg/kg body weight.

Experimental Procedure

When the tumors reached the appropriate size of 5-7 mm, the animals were shaved in the tumor area and given ip injections of the photosensitizer; the remainder of the experiment was done in the dark, including housing of the animals. Control tumor-bearing animals received light without photosensitizer and photosensitizer without light. Twenty-four hours after the injections, the animals were treated with a laser light delivery system. The mice were anesthetized with ketamine hydrochloride (Parke-Davis, Morris Plains, NJ) and covered with a metal shield with a circular hole exposing the tumor. Animals were killed with Halothane (Halocarbon Laboratories, Inc., Hackensack, NJ) at time 0, 30 minutes, 1 hour, and 2, 4, 6, 8, 12, 16, and 24 hours after exposure to the laser light. Tissue was excised immediately and placed in Karnovsky's fixative (2% paraformaldehyde; 3% glutaraldehyde), refrigerated overnight at 4 °C, and subsequently transferred to 0.1 *M* cacodylate buffer until electron microscopy embedding was performed. The tissue was postfixed in 1% osmium tetroxide in 0.1 *M* cacodylate buffer for 1 hour at room temperature (18 °C - 20 °C). Tissue was then rinsed with double distilled water and stained en bloc for 2 hours in Kellenberger's uranylacetate. Dehydration was done with progressive ethanol-water in 10-minute steps (30%, 50%, 70%, 90%, 100%, 100%) and progressive ethanol-propyleneoxide also in 10-minute steps. Infiltration was started with propyleneoxide-Epon 812 substitute [Poly/Bed 812 Embedding Media (Polysciences Inc., Warrington, PA)] in steps of 30 minutes each (30%, 50%), overnight (70%), and 60 minutes (100%). The mold was embedded, placed at 37 °C overnight, and then at 60 °C in a vacuum oven for 48 hours. The blocks were trimmed, sectioned (500 nm), and stained for light microscopy with Richardson's stain. The thin-sectioned (60 nm) blocks were subsequently examined with a Jeol 100C electron microscope at 80 kV.

Laser Light Delivery System

Laser irradiations were performed with a 770DL argon pumped dye laser system (Cooper Lasersonics, Santa Clara, CA) and DCM Premixed Laser Dye (Cooper Lasersonics) with a tuning range of 610-690 nm. The dye laser was tuned to emit radiation at 630 nm for DHE, 664 nm for MACE, and 675 nm for CASPc. We verified the wavelength to ± 1 nm by using a #5/354 UV monochromator (Jobin Yvon, Longjuneau, France). The radiation was then transferred with a Model 316 fiber optic coupler into a 400-μm fused, silica fiber optic (Spectra-Physics, Mountain View, CA). We terminated the output end of the fiber with a microlens that focused the laser radiation into a circular field of uniform light intensity. The laser irradiation that emanated from the fiber was monitored with a Coherent Model 210 power meter before, during, and after treatment.

Mice were then placed underneath an aperture that controlled the area of light illumination on the tumor site; the

area of illumination was 1 cm^2. Total laser energy density, 100 J/cm^2, had a power density of 100 mW/cm^2.

Results

Light Microscopy

Control (either light or drug alone) slides showed the usual tumor architecture with multiple mitotic figures and easily discernible vessels. At 30 minutes after PDT, no significant structural changes were noted from the control. At 1 hour afterward, the first structural change observed with all photosensitizers tested was the increased diameter of the tumor capillary lumen compared with controls. Of particular interest was the large diameter (swelling) of the erythrocytes in the swollen vessels. This conclusion was based on the histopathologic examination of all sections and tumors and was not attributable to the way a particular section was cut. At 2 hours, the capillaries were further engorged, and, over time, the capillary wall broke down with extravasation of erythrocytes into the surrounding perivascular tumor stroma with the tumor ultimately becoming completely hemorrhagic. This observation was made for all photosensitizers tested (fig. 1).

Electron Microscopy

Control ultrathin sections showed normal tumor microvasculature with the subendothelial zone densely packed with large amounts of collagen, elastic and reticular fibers, and background connective tissue elements, especially proteoglycans (fig. 2). Generally, the lumen of each tumor capillary was surrounded by three to four endothelial cells in junctional contact with each other. The tumor cells in the surrounding perivascular tumor stroma appeared structurally intact with large numbers of mitochondria, endoplasmic reticulum, and ribosomes. At 30 minutes after completion of PDT, there were no significant structural changes from controls noted in the microvasculature or the tumor cells.

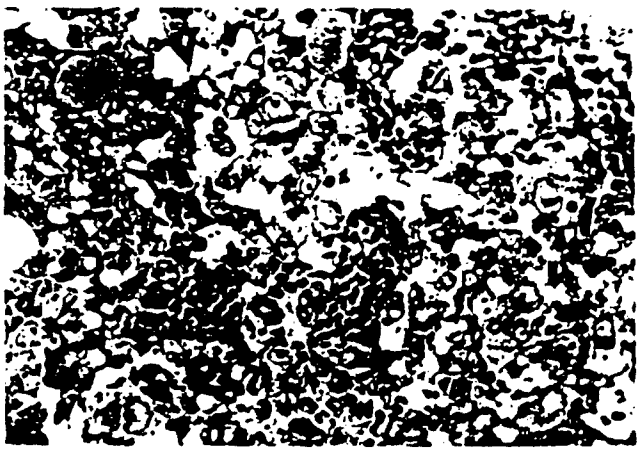

Figure 1. Photomicrograph of EMT-6 tumor removed 4 hr after treatment with photosensitizer and light at total dose of 100 J/cm^2. Note evidence of extravasation of erythrocytes into the surrounding perivascular tumor stroma (arrows). Originally: ×700.

Figure 2. Photomicrographs of control tumor (no photosensitizer, no light) showing normal tumor microvasculature (A) with the subendothelial zone (arrows) densely packed with large amounts of collagen, elastic and reticular fibers, and background connective tissue elements (B). Originally: A, ×6,000; B, ×28,100.

One hour after completion of PDT with MACE (fig. 3) and CASPc (fig. 4), injury to the subendothelial zone of the capillary wall was characterized by considerable edema and fragmentation of the collagen and fiber elements. The endothelial cells lining the capillary wall appeared elongated and flat compared with our controls with smooth luminal and abluminal surfaces but were otherwise structurally normal. The nuclei had the typical chromatin condensation along the nuclear envelope, normal rough endoplasmic reticulum, and membrane-bound lysosomes were evident in the cytoplasm. Erythrocyte swelling described above was also seen. By 2 hours post PDT, the background substance was essentially absent, and only a few fragmented collagen fibers remained in the subendothelial zone in the MACE- and CASPc-treated tumors (fig. 5).

One hour after completion of PDT with DHE, some of the ultrastructural changes in the subendothelial zone were strikingly different from those observed in tumors treated with MACE or CASPc. At 1 hour post PDT, the subendothelial zone was more darkly stained, and individual collagen fibers were no longer clearly distinguished (fig. 6). However,

Best Available Copy

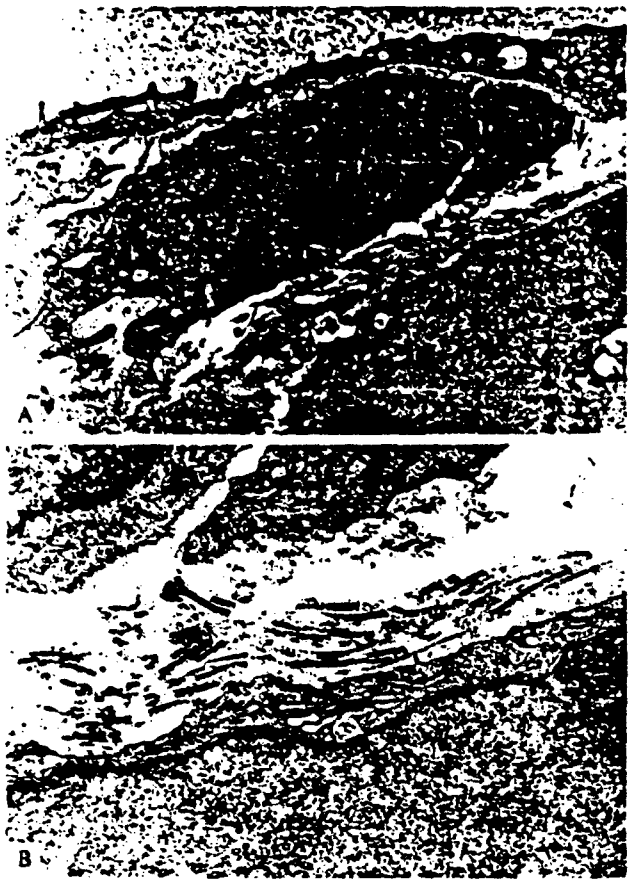

Figure 3. Photomicrographs of tumor removed 1 hr after treatment with MACE and light. Note in the subendothelial zone (arrows) the formation of considerable edema (A) and fragmentation of the collagen and other fiber elements (B). Originally: A, ×9,000; B, ×26,600.

as with the MACE- and CASPc-treated tumors, the vessels were swollen, erythrocytes were enlarged, and considerable edema was observed in the subendothelial zone. At 2 hours after treatment, the background substance in the subendothelial zone was essentially destroyed and replaced by edema, but numerous clusters still contained large amounts of fibers and fibrin that appeared to have coalesced. Furthermore, delineation of the characteristic periodicity and banding pattern of collagen fibers was difficult (fig. 7).

Beyond 2 hours posttreatment, the subendothelial zone was completely disrupted, although there was still some evidence of fibrin. Erythrocytes and plasma proteins were extravasated into the subendothelial zone and subsequently into the region of the tumor cells immediately adjacent to the microvasculature with the three photosensitizers tested (fig. 8). Tumor cells closer to the hemorrhage showed more signs of cell membrane damage and lysis. However, tumor cells distant from the microvasculature in the center of the tumor appeared to have their cell membranes structurally intact even 4 hours after PDT. In those cells, dispersion of the heterochromatin around the nuclear envelope was apparent as well as some increase in the number of cytoplasmic vacuoles (fig. 9). Beyond 4 hours, the amount of hemorrhage increased with the entire tumor ultimately becoming a sea of erythrocytes and amorphous granular debris.

Discussion

Although most investigators to date have focused their research on understanding the biochemistry, biophysics, and molecular biology of PDT on cancer cells in vitro, less attention has been paid to the in vivo tumor environment where the photochemistry leading to tumor necrosis occurs. However, it is apparent that the exact mechanism of PDT phototoxicity in vivo will have to be explained by the anatomy, physiology, and biochemistry of the whole tumor rather than on the basis of some special characteristic of malignant tumor cells. Once a molecule used for cancer detection or treatment is injected into the bloodstream, it must first be distributed throughout the vascular space. Because no molecule can reach tumor cells from the blood without passing through the microvascular wall, it seems reasonable that investigators should attempt to learn more about the role that this compartment plays in PDT.

Some progress has been made recently in our understanding how the microvasculature may be involved in the events leading to tumor necrosis. Several investigators (*19,20*) have

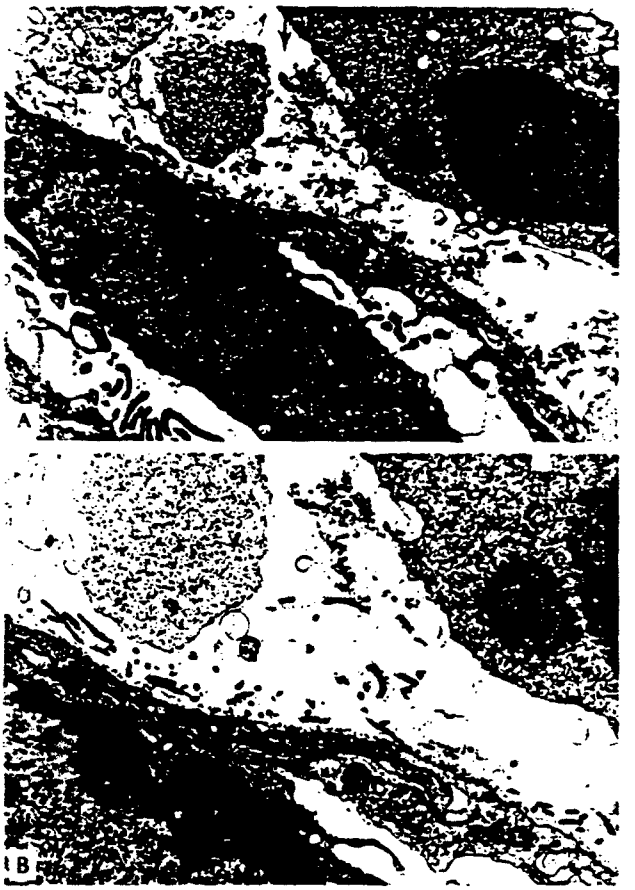

Figure 4. Photomicrographs of tumor removed 1 hr after treatment with CASPc and light. Note in the subendothelial zone (arrows) the formation of considerable edema (A) and fragmentation of the collagen and other fibers (B). Originally: A, ×15,000; B, ×26,600.

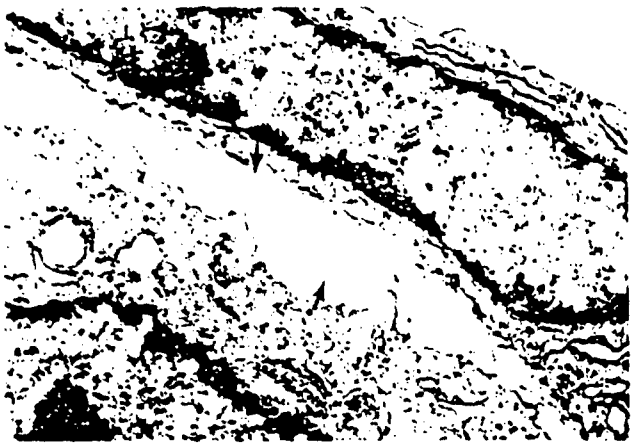

Figure 5. Photomicrograph of tumor removed 2 hr after treatment with MACE and light. Background substance was essentially absent and only a few fragmented collagen fibers remained in the subendothelial zone (arrows). Originally: ×24,400.

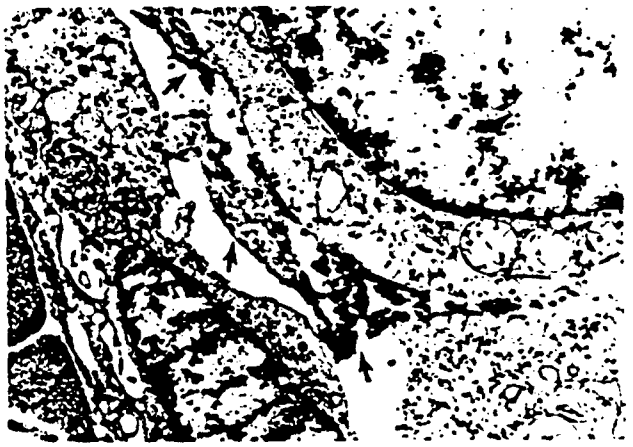

Figure 7. Photomicrograph of tumor removed 2 hr after treatment with DHE and light. Background substance in the subendothelial zone was essentially destroyed and replaced by edema, but note the presence of numerous clusters of fibers and fibrin that appeared to have coalesced (arrows). Furthermore, delineation of characteristic periodicity and banding pattern of collagen fibers was difficult. Originally: ×15,000.

shown that within a few minutes of light exposure, the significant decrease in the rate of blood flow through tumors is followed shortly thereafter by complete cessation. In addition, researchers in another study, using tumor cell clonigenicity following PDT to assess in vitro colony formation, found that it was unaffected by PDT if the tumor tissue was excised and explanted immediately. If, however, tumor cells were left in situ following PDT for varying periods, tumor cell death occurred rapidly and progressively as assayed by clonigenicity (*21*). Taken together, all these experiments suggest that the vascular compartment represents an important target for PDT and that more detailed studies should be undertaken.

Our objective in this study was to determine the ultrastructural changes seen in the tumor microvasculature in vivo in the first few hours after PDT. Clearly, many physiologic parameters of blood vessels, such as blood flow, pH, oxygen tension, temperature, and serum content, will be important. However, our study demonstrates that the first observable signs of destruction occur in the subendothelial zone of the tumor capillary wall. Blood vessels contain endothelial cells that are surrounded by a basement membrane, which may be damaged or missing in tumors (*22*). Adjacent to this is a subendothelial or interstitial compartment bounded by the basement membrane on one side and by the membranes of tumor cells on the other. Similar to normal blood vessels, the subendothelial zone of tumor vessels is composed predominantly of a dense collagen, elastic, and reticular fiber network. Interspersed within this cross-linked structure are the macromolecular polysaccharide constituents (proteoglycans and hyaluronate) that form a gellike background substance (*23*). This zone, which maintains the structural in-

Figure 6. Photomicrograph of tumor removed 1 hr after treatment with DHE and light. Note the presence of large numbers of dense dark staining clumps of fibers in the subendothelial zone (arrows). Individual collagen fibers were no longer clearly distinguished. Originally: ×28,900.

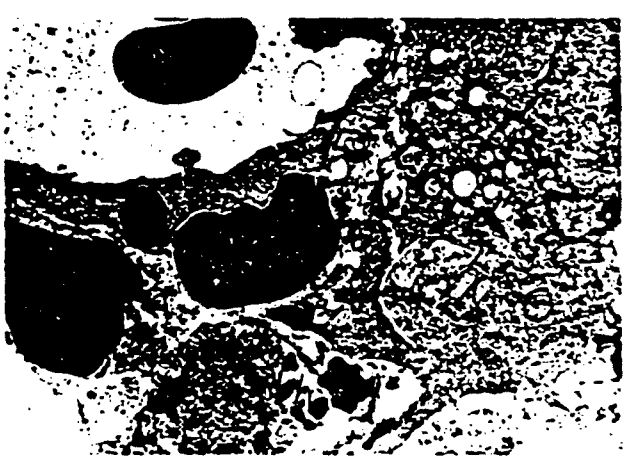

Figure 8. Photomicrograph of tumor removed 2 hr after treatment with CASPc and light. Subendothelial zone (arrows) was completely disrupted, although there was still some evidence of fibrin, with extravasation of red blood cells (rbc) into this area. Tumor cells (t) closer to this hemorrhage showed more signs of cell membrane damage. Originally: ×9,600.

Best Available Copy

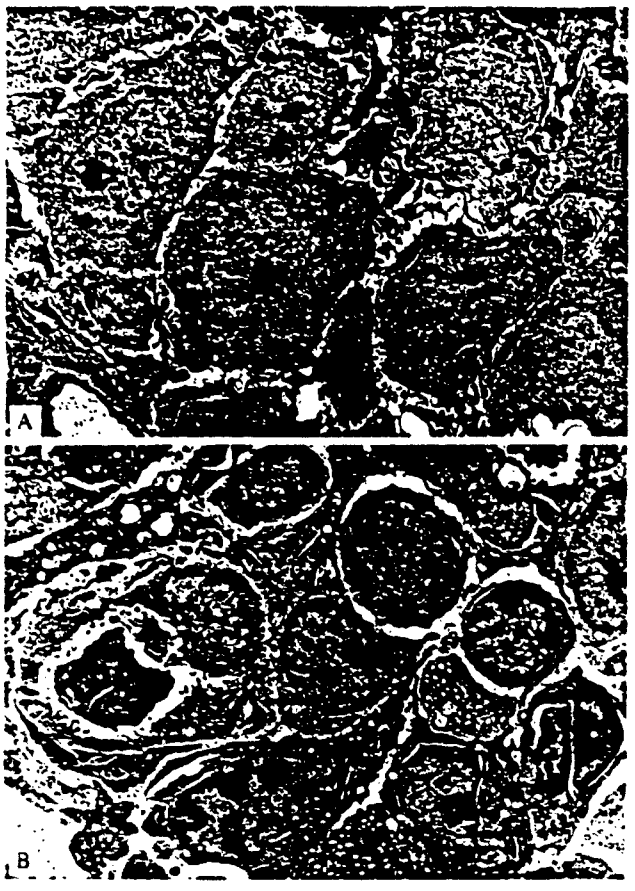

Figure 9. Photomicrographs of control tumor (A) and tumor removed 4 hr after treatment with MACE and light (B). Treated tumor cells distant from the microvasculature in the center of the tumor have their cell membranes structurally intact. Some dispersion of the hematochromatin can be seen around the nuclear envelope as well as some increase in the number of cytoplasmic vacuoles (B). Originally: A, ×3,600; B, ×6,000.

tegrity of the tumor capillary wall, was destroyed within the first 2 hours after phototherapy with all three photosensitizers tested. We did note many normal appearing endothelial cells in areas where there was significant damage to the fibers in the subendothelial zone. The normal ultrastructure of the endothelial cells was surprising because these cells were suspected of being primary target sites of the dye-sensitized photodynamic reaction. However, the fact that no structural alteration of the endothelial cells was observed does not mean that their membrane permeability or junctional contacts were unaffected. In fact, their unusually flattened and elongated appearance as soon as 1 hour after PDT (undoubtedly caused by swollen erythrocytes) could have resulted in membrane stretching and altered junctional contacts. This phase was followed shortly by edema in the subendothelial zone and, ultimately, diffuse hemorrhage into the surrounding perivascular stroma. Initially, tumor cells located away from the microvasculature appeared structurally intact after PDT. Over time, all tumor cells were ultimately destroyed as a consequence of hemorrhage, activation of intravascular component such as complement, or hypoxia secondary to vascular collapse.

Why is the subendothelial zone of the tumor microvasculature so important to successful PDT? Part of the answer may come from in vitro and in vivo studies that have shown that a stabilized polysaccharide network (proteoglycans and hyaluronate) enmeshed in collagen fibers offers considerable resistance to interstitial transport (*24,25*). Although the insoluble, collagen fibrous proteins impart structural integrity to a tissue, the polysaccharides are thought to govern the mass transfer characteristics of the tissue due to their high-charge density. The biologic and physicochemical properties of this zone combined may retard the movement of photosensitizing compounds from the vascular space into the tumor cells. That the tumor collagen is produced by the host and its synthesis is governed by the tumor cells are particularly noteworthy (*26*). If tumor growth depends on collagen production to the extent that it depends on neovascularization, this characteristic of tumors may be exploited in arresting such growth. Tumor collagen fibers also resemble the types of fibers seen in embryonic tissue and in wounds during healing. That these fibers, recently made in the neovascularization of tumors, would not be as highly cross-linked as those found in more mature tissues is to be expected. Furthermore, one study (*27*) has shown that newly formed collagen and perhaps elastin and fibrin as well have a substantially greater binding capacity for porphyrins than does mature collagen and may constitute potentially important binding sites for porphyrin localization and retention.

The reason for the different ultrastructural changes seen with DHE as opposed to MACE and CASPc is less clear, but some possible explanations are proposed. Due to the internal structure of collagen (a cylindrical molecule composed of three chains coiled in a ropelike fashion to form a triple helix), fibers will have space within them that is probably accessible to small molecules and ions. DHE is highly hydrophobic and tends to aggregate into large molecules of 200–300 components. MACE and CASPc are hydrophilic, smaller molecules that may be able, on the basis of size, to become intercalated inside the coiled collagen helix. Such action could lead to the breakdown and fragmentation of the collagen fibers from the inside as we saw in this experiment. DHE may be confined to the outside of the collagen fiber leading to the coalescence of large clumps of collagen fibers seen on examination with electron microscopy. Additionally, collagen contains three specific amino acids (glycine, hydroxylysine, and hydroxyproline) that may interact with the available carboxy groups on MACE and the sulfonated groups on CASPc. These biologic and physicochemical characteristics could explain the ultrastructural differences observed for the different photosensitizers. Further research in this area is needed.

In conclusion, the present study suggests that the effects of PDT leading to rapid tumor necrosis with DHE, MACE, and CASPc are not the result of direct tumor cell kill but are secondary to destruction of the collagen fibers and other connective tissue elements located in the subendothelial zone of the tumor capillary wall. Binding of photosensitizers to the elements in this zone as well as altered permeability and transport through the endothelial cell layer resulting from erythrocyte swelling and increased intraluminal pressure may

be key features of the dye-sensitized, photodynamic reaction leading to tumor destruction.

References

1 Dougherty TJ. Photosensitizers: therapy and detection of malignant tumors. Photochem Photobiol 1987;45:879-889.

2 Weishaupt KR, Gomer CJ, Dougherty TJ. Identification of singlet oxygen as the cytotoxic agent in photoinactivation of a murine tumor. Cancer Res 1976;36:2326-2329.

3 Gronsweiner LL. Membrane photosensitization by hematoporphyrin and hematoporphyrin derivative. In: Doiron DR, Gomer CJ, eds. Porphyrin localization and treatment of tumors. New York: Liss, 1984:391-404.

4 Berns MW, Dahlman A, Johnson F, et al. In vitro cellular effects of hematoporphyrin derivative. Cancer Res 1982;42:2325-2329.

5 Toriniki L, Miora T, Seiji M. Lysosome destruction and lipoperoxide formation due to active oxygen generated from hematoporphyrin on UV radiation. Br J Dermatol 1980;102:17-27.

6 Foote CS. Photosensitized oxidation and singlet oxygen: consequences in biological systems. In: Pryor WA, ed. Free radicals in biology, vol II. New York: Academic Press, 1976:85-124.

7 Dougherty TJ. Photoradiation therapy for cutaneous and subcutaneous malignancies. J Invest Dermatol 1981;77:122-124.

8 Rettenmaier MA, Berman ML, DiSaia PJ, et al. Gynecologic uses of photoradiation therapy. In: Doiron DR, Gomer CJ, eds. Advances in experimental medicine and biology, vol 170. New York: Liss, 1984:767-775.

9 Dougherty TJ. Photodynamic therapy (PDT) of malignant tumors. CRC Crit Rev Oncol Hematol 1984;2:83-116.

10 Hayata Y, Kato H. Applications of laser phototherapy in the diagnosis and treatment of lung cancer. Jpn Ann Thoracic Surg 1983;3:203-210.

11 Benson RC, Farrow GM, Kinsey JH, et al. Detection and localization of in situ carcinoma of the bladder with hematoporphyrin derivative. Mayo Clin Proc 1982;57:548-555.

12 Bruce BA. Evaluation of hematoporphyrin photoradiation therapy to treat choroidal melanoma. Lasers Surg Med 1984;4:59-64.

13 Dougherty TJ, Lawrence G, Kaufman GH, et al. Photoradiation in the treatment of recurrent breast carcinoma. J Natl Cancer Inst 1979;62:231-236.

14 Wile AG, Dahlman A, Berns RG, et al. Laser photoradiation therapy of cancer following hematoporphyrin sensitization. Lasers Surg Med 1982;2:163-168.

15 Nelson JS, Liaw L-H, Berns MW. Mechanism of tumor destruction in photodynamic therapy. Photochem Photobiol 1987;46:829-836.

16 Nelson JS, Wright WH, Berns MW. Histopathological comparison of the effects of hematoporphyrin derivative on two different murine tumors using computer enhanced digital video fluorescence microscopy. Cancer Res 1985;45:5781-5786.

17 Roberts WG, Shiau F-Y, Nelson JS, et al. In vitro characterization of monoaspartyl chlorin e_6 and diaspartyl chlorin e_6 for photodynamic therapy. J Natl Cancer Inst 1988;80:330-336.

18 Nelson JS, Roberts WG, Berns MW. In vivo studies on the utilization of mono-L-aspartyl chlorin (NPe6) for photodynamic therapy. Cancer Res 1987;47:4681-4685.

19 Selman SH, Kremer-Birnbaum M, Klaunig JE, et al. Blood flow in transplantable bladder tumors treated with hematoporphyrin derivative. Cancer Res 1984;44:1924-1927.

20 Star WM, Marijnissen HPA, van den Berg-Blok AE, et al. Destruction of rat mammary tumor and normal tissue microcirculation by hematoporphyrin derivative photoradiation observed in vivo in sandwich observation chambers. Cancer Res 1986;46:2532-2540.

21 Henderson BW, Waldow SM, Mang TS, et al. Tumor destruction and kinetics by tumor cell death in two experimental mouse tumors following photodynamic therapy. Cancer Res 1985;45:572-576.

22 Jain RK. Transport of macromolecules in tumor microcirculation. Biotechnol Res 1985;1:81-84.

23 Jain RK. Transport of molecules in the tumor interstitium: a review. Cancer Res 1987;47:3039-3051.

24 Comper WD, Laurent TC. Physiological function of connective tissue polysaccharides. Physiol Rev 1978;58:255-315.

25 Laurent TC. Structure, function and turnover of the extracellular matrix. Adv Microcirc 1987;13:15-34.

26 Gullino PM, Grantham FH. The influence of the host and the neoplastic cell population on the collagen content of a tumor mass. Cancer Res 1963;23:648-653.

27 Musser DA, Wagner JM, Datta-Gupta N. The interaction of tumor localizing porphyrins with collagen and elastin. Res Commun Chem Pathol Pharmacol 1982;36:251-259.

Lasers in Surgery and Medicine 8:10–17 (1988)

Phycocyanin: Laser Activation, Cytotoxic Effects, and Uptake in Human Atherosclerotic Plaque

N. Charle Morcos, MD, PhD, Michael Berns, PhD, and Walter L. Henry, MD, FACC

Department of Medicine, Division of Cardiology (N.C.M., W.L.H.), Department of Surgery (M.B.), and the Beckman Laser Institute (M.B.), University of California, Irvine

Phycocyanin is a phycobiliprotein with peak absorption at 620 nm. The laser activation, cytotoxic effects, and uptake into atherosclerotic plaque of phycocyanin was studied. Optimal activation was produced by argon dye laser at 0.5 W and a total energy dose of 300 J/cm^2 at 620 nm and 650 nm, irradiated through blood with a hematocrit of 8%. Activation was evidenced by reduction of optical density by 0.3 units at 340 nm caused by oxidation of the reduced nicotinamide adenine dinucleotide phosphate (NADPH) in a buffered reaction solution containing 0.1 mg/ml of phycocyanin. Cytotoxicity was evaluated by measuring viability of mouse myeloma cells in culture after incubation with phycocyanin (0.25 mg/ml) and irradiated by 300 J/cm^2 at 514 nm. After 72 hours post-treatment the cells showed 15% viability compared to 69% and 71% for control cells exposed to laser only or phycocyanin only, respectively. Atherosclerotic artery segments obtained within 5 hours postmortem were perfused with 0.1 mg/ml phycocyanin in oxygenated Krebs Ringer solution at 30 mm Hg for 5 minutes followed by washout with phycocyanin-free Krebs for 10 minutes. Artery sections examined histologically by light and fluorescence microscopy showed specific fluorescence localization within the plaque particularly at the elastic laminae and to a larger extent at the internal elastic lamina but not in the medial muscle layer. In conclusion, phycocyanin is a cytotoxic photosensitizer that exhibits specific binding to plaque and is activated at a wavelength minimally absorbed by blood. These properties suggest potential therapeutic use for plaque localization and regression.

Key words: laser, photodynamic activation, atherosclerosis, cytotoxicity

INTRODUCTION

The use of photochemicals (eg, hematoporphyrin and its derivatives [HPD]) as anti-cancer agents has been under investigation in humans and animals for quite some time [Dougherty et al, 1975, 1978, 1979]. HPD has been used in cancer treatment with varying degrees of success. It is readily taken up and is retained by malignant tissue [Auler and Bancer, 1942; Figge et al, 1948]. The drug is activated by visible light, and its cytotoxic effect is mediated mainly through the production of singlet oxygen [Kvello et al, 1980]. There have been several attempts particularly by Spears and colleagues [1983] to utilize this approach for clinical applications to atherosclerosis. Spears et al [1983] injected rabbits and monkeys that had developed experimentally induced plaques with HPD and showed selective fluorescence in diseased segments of aortas 48 hours later. Kessel and Sykes [1984] incubated segments of nonviable atherosclerotic human aortas in media containing HPD. The contents of the plaque were then extracted and analyzed by thin-layer chromatography for its hematoporphyrin content. These authors showed that plaque possibly contains hydrophillic sites that bind hematoporphyrin. Pollock et al [1987] recently showed photosensitization of experimental atheromas by

Accepted for publication October 29, 1987

Address reprint requests to N.C. Morcos, MD, PhD, Division of Cardiology, Department of Medicine, University of California, Irvine, CA 92717

© 1988 Alan R. Liss, Inc.

porphyrins. Unlike the rapid progress of investigations for photodynamic therapy in cancer, advances in the application of photodynamic therapy for plaque have been hampered for many reasons, which include 1) the absence of an animal model for plaque that resembles human atherosclerotic plaque, 2) the apparent slow dynamics and turnover of human plaque components, which necessitates prolonged observations for documentation of therapeutic effects, 3) the conditions for delivery of light to plaque necessitate a transluminal route through blood vessels for the laser fiber and light delivery through the blood field. Blood strongly absorbs visible light in the absorption range of HPD and therefore results in significant attenuation of the activating light.

In the study reported here we have attempted to overcome these problems. Human atherosclerotic coronary arteries that were obtained within 5 hours postmortem and were cannulated, perfused, and maintained pharmacologically viable [Morcos et al, 1985] provided a model in which to study viable human atherosclerotic plaque. We have studied a porphyrin-like compound, phycocyanin, that is a phycobiliprotein and has a peak absorption wavelength of 620 nm, which is at the periphery of the wavelength range for blood absorption. The study reported here describes the photodynamic activation, cytotoxic effects, selective uptake into the human atherosclerotic plaque, and the potential therapeutic value of phycocyanin.

MATERIALS AND METHODS

Phycocyanin, NADPH, and other enzymes were purchased from Sigma Co., St Louis.

Measurement of Phycocyanin Activation

Activation of phycocyanin was measured by the method of Boadaness and Chan [1977]. This method is based on measurement of singlet oxygen release in a solution of deuterium oxide saturated with oxygen, which contains the reduced form of nicotinamide adenine dinucleotide phosphate (NADPH). The reaction solution contained 0.1 mg/ml phycocyanin and was placed in sealed vials and submerged in a diluted and buffered blood solution with a hematocrit of 8%. Laser irradiation was performed at several wavelengths using a tunable argon dye laser (Spectra Physics 171) at 0.5 W and a total energy dose of 300 J/cm^2. Oxidation of NADPH to NADP+ by the released singlet oxygen resulted in loss of NADPH absorption at 340 nm. Estimation of enzymatically active NADP+ produced by photo-oxidation was determined by regeneration of NADPH at the end of the photodynamic activation as follows. After measurement of optical density of the remaining NADPH at the end of light exposure, $MgCl_2$ (10 mM), DL-isocitrate (2.43 mM), and NADPH-dependent isocitrate dehydrogenase (ICHD, 66 μg) were added to the irradiated mixture. After 10 minutes at room temperature in the dark, the absorbance at 340 nm was measured again and corrected for dilution additions. The change in absorbance was recorded as change in optical density, O.D. at 340 nm. In general, about 80% of the photo-oxidized nucleotide was in the form of enzymatically active NADP+. Samples were assayed in triplicate.

Cytotoxic Effects

Photodynamic cytotoxic effects were evaluated by measurement of viability of mouse myeloma cells X63-Ag 8.653 derived from mouse Balb/C Pk in culture. Cells were grown in RMPI-1640 with 10% fetal calf serum, 1.2 μM L-glutamine, 10,000 Units each of streptomycin, penicillin, and fungizone in a humidified atmosphere, 95% air, 5% CO_2 at 37°C. Cells were cultured to a density of 10^5 cells/ml in flasks containing 4 ml of medium. Four groups of culture flasks were tested namely: 1) control, 2) phycocyanin-treated alone, 3) laser-treated alone, and 4) phycocyanin- and laser-treated. Each group contained three flasks. Sterile phycocyanin solution was added to appropriate flasks to a final concentration of 2.5 mg/ml and allowed to incubate for 4 hours. At zero time, appropriate flasks were irradiated with laser at 514 nm to deliver a total dose of 300 J/cm^2 at room temperature (22°C). During irradiation, the temperature was measured by a thermistor and showed a 4°C increase. Viability was measured using Trypan Blue dye followed by counting using a hemacytometer at 0, 12, 24, 36, 48, and 72 hours. Viability was expressed as a percentage of the viability at T = 0. There was no change in viability during the 4-hour preincubation period with phycocyanin.

Tissues and Arterial Perfusion Model

Human coronary arteries were obtained from the left anterior descending coronary artery and its tributaries within 5 to 8 hours postmortem. Atherosclerotic arteries were obtained from individuals who were over 55 years old. In this study, a total of seven atherosclerotic artery segments were used. A perfusion apparatus described previously by Morcos et al [1985] was utilized such that coronary artery segments of 2–3 cm in length and 0.5–2 mm in diameter were perfused under a con-

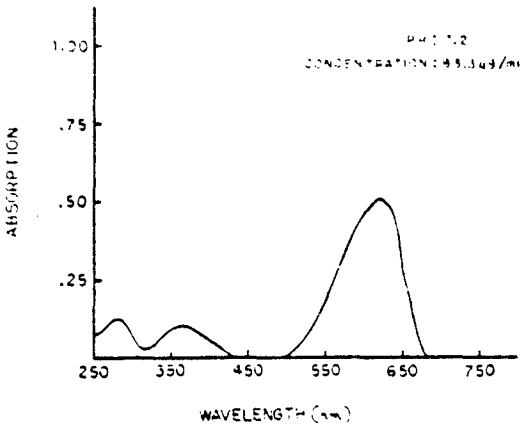

Fig. 1. Absorption spectrum of phycocyanin. Experimental conditions are indicated on the figure.

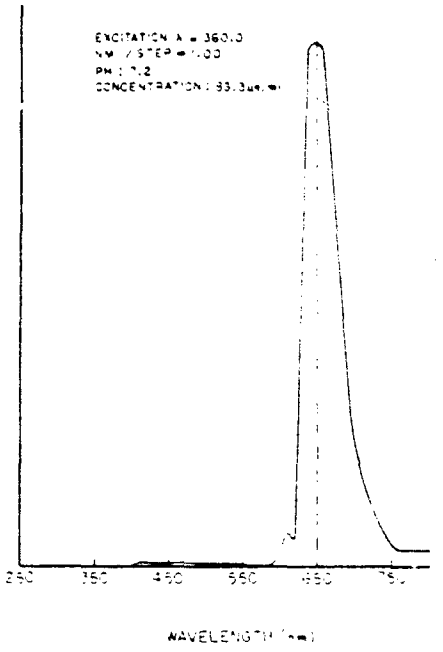

Fig. 2. Emission spectrum of phycocyanin. Experimental conditions are indicated on the figure.

stant pressure of 30 mm Hg. Briefly, all coronary arteries were dissected free, and side branches were ligated with 6.0 silk sutures. The ends of each artery were cannulated and secured with 6.0 silk sutures on polyethylene tubing in a special holder. The holder was placed in a temperature-regulated bath, and its polyethylene tubing was connected to the inlets and outlets of the perfusion apparatus. The perfusate and bathing medium contained Krebs-Ringer bicarbonate solution of the following composition in mM: NaCl, 119.2; KCl, 4.9; $MgSO_4$, 1.2; KH_2PO_4, 0.44; $CaCl_2$, 1.3; $NaHCO_3$, 25; disodium ethylenediamine tetraacetic acid (EDTA), 0.03; ascorbic acid, 0.114; and glucose, 11.1, pH 7.34. Perfusate and bath were maintained at 37°C.

To assess pharmacologic vasoreactivity of each artery segment, spasm was induced by introduction of 100 ml of serotonin (5-HT) into the perfusate at a final concentration of 10^{-5}. The serotonin solution was followed by a washout with 1 liter of serotonin-free Krebs solution to effect relaxation. Flow rate was measured continuously as a function of time. Flow rate reduction by approximately 50% was indicative of pharmacologic viability of the coronary artery segment.

Uptake of Phycocyanin in Perfused Coronary Arteries

Phycocyanin was introduced into the perfusate of isolated pharmacologically viable human atherosclerotic coronary arteries at a concentration of 0.1 mg/ml for 5 minutes. This was followed by washout with Phycocyanin-free Krebs-Ringer solution for 10 minutes.

Histology and Microscopy

At the end of the washout procedure, the mounted artery segments were fixed in 3% glutaraldehyde, embedded in paraffin, sectioned, and mounted for microscopy without exposure to any organic solvent. Light microscopy was performed as specified in the figure legends using either normal light or polarized light at 577 nm to enhance contrast caused by absorption by phycocyanin at 620 nm.

RESULTS

Spectral Properties of Phycocyanin

Phycocyanin is a blue pigment phycobiliprotein that is soluble in aqueous solutions. Its absorption is in the range of 441–664 nm with peak absorption at 620.5 nm (Fig. 1). Two other minor absorption peaks occur at 278.5 and 362.5 nm. The excitation spectrum generated using an emission wavelength of 835 nm occurs in the range of 470 to 620 nm with a peak at 580 nm (Fig. 2). Low-level excitation occurs between 300 and 420 nm. The emission spectrum using an excitation wavelength of 380 nm occurs in the range of 580–760

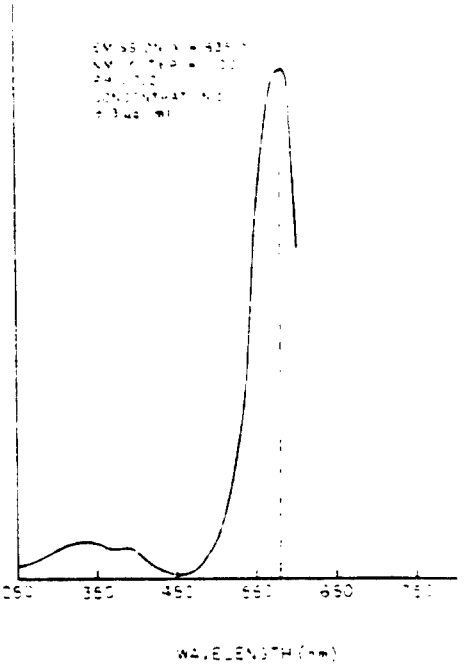

Fig. 3. Excitation spectrum of phycocyanin. Experimental conditions are indicated on the figure.

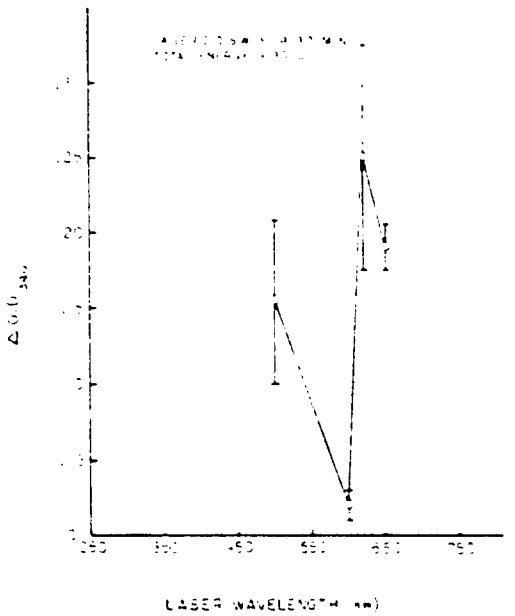

Fig. 4. Laser photodynamic activation of phycocyanin. Phycocyanin was in a reaction medium saturated with oxygen and containing deuterium oxide and NADPH. NADPH oxidation to NADP+ was measured by loss of absorption at 340 nm. Activation by argon laser was performed at 514, 600, 620, and 650 nm to deliver 300 J cm^2 directed toward the reaction vial through a blood solution with a hematocrit of 8%. The amount of enzymatically active NADP+ generated by photoradiation was measured by regeneration to NADPH by isocitrate dehydrogenase. The regenerated NADPH is reported as change in optical density (O.D. 340) in the figure. All measurements were performed on triplicate reaction mixtures. Concentrations and experimental conditions are as described in "Materials and Methods."

nm with a peak at 645 nm (Fig. 3). The high wavelength of absorption (620 nm) that occurs at the limit of one end of the spectrum for blood absorption enables phycocyanin to absorb light irradiated through blood.

Photodynamic Activation of Phycocyanin

The ability of phycocyanin to generate singlet oxygen and other oxidizing radicals was evaluated by measuring the oxidation of NADPH in the same reaction mixture as described in "Materials and Methods." Reaction mixtures were activated using the argon laser at 514, 600, 620, 650 nm. Sealed reaction vials were submerged in a larger vial containing blood with an 8% hematocrit. Reaction vials were irradiated through blood. The light dose was 300 J cm^2 measured away from the fiber at the position of the reaction mixture in absence of blood. Figure 4 shows the change in absorbance caused by NADPH oxidation resulting from photodynamic activation of phycocyanin. The peak activation occurred at laser wavelengths of 620–650 nm. Activation at 600 nm was 10% of that at 620 nm. However, activation at 514 nm was also present but to a lesser extent (58%) compared to the activation at 620 nm.

Cytotoxic Effects of Phycocyanin

Suspension cultures of mouse myeloma cells were exposed to laser light alone, phycocyanin alone, and both laser and phycocyanin (Fig. 5). A 4-hour preincubation period with phycocyanin was allowed prior to laser irradiation at 514 nm. Cells exposed to laser alone or phycocyanin alone showed a small loss of viability (approximately 8%) over a period of 72 hours. In contrast, cells exposed to photodynamic treatment lost 81% of their viability linearly over a period of 72 hours. The percentage of cells viable at 72 hours post-treatment was 79, 71, 69, and 15% for control, laser, phycocyanin, and photodynamically treated (laser and phycocyanin) cells, respectively. Laser irradiation was performed at room temperature (22°C). The temperature at the outside surface of the culture flasks receiving the light dose was

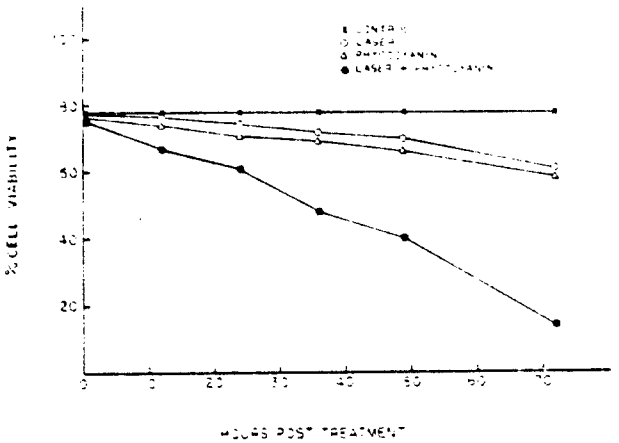

Fig. 5. Cytotoxicity of phycocyanin. Mouse myeloma were grown to a density of 10^5 or 10^6 cells/ml in 4-ml suspensions in RPMI-1640. Cells were preincubated with phycocyanin at 0.25 mg/ml for 4 hours. Argon laser irradiation at 514 nm was performed on appropriate flasks to deliver 300 J/cm^2. Control cells were not exposed to either phycocyanin or laser. Laser-treated cells were exposed to laser only, and phycocyanin-treated cells were exposed to phycocyanin only. All tests were performed in triplicate flasks. Cell viability was determined after initiation of laser treatment by counting cells showing uptake and cells not showing uptake of the dye trypan blue using a hemacytometer.

26°C, which is still lower than the temperature of culture incubation (37°C).

Uptake of Phycocyanin Into Human Atherosclerotic Plaque

Human atherosclerotic coronary artery segments were mounted, perfused with phycocyanin, then washed with phycocyanin-free perfusate. Vessels were processed for histology without the use of any organic solvents. Light and fluorescence microscopy of sections from these vessels are shown in Figure 6A and B. Figure 6A shows atherosclerotic plaque with fine blue particles within its body of the thickened intima. A large concentration of blue material was present at the internal elastic lamina (arrow). Figure 6B is a fluorescence image of the same field. Phycocyanin was present in the body of the plaque. It was concentrated along convoluted bands of different widths and different spacings between each other. These bands are possible elastic laminae within the plaque. The largest concentration of phycocyanin is at the internal elastic laminae (arrow), showing a broad band that has a highly intense fluorescence. Beyond this internal elastic laminae band, phycocyanin was dramatically absent from the media (dark zone).

Other vessels were treated similarly and were visualized using polarized light at 577 nm (Fig. 7). Since phycocyanin absorbs strongly in that range of wavelength, areas within the cross-section that contain phycocyanin appeared dark. In Figure 7, the thickened intima and plaque appeared dark, showing the presence of phycocyanin. The thin medial plaque muscle coat appeared relatively much lighter in color and demonstrated poor localization of the pigment.

DISCUSSION

In this study we describe the specific uptake and the mode of localization in viable human atherosclerotic coronary arteries of a photosensitizer, phycocyanin, which possesses photodynamic and cytotoxic properties.

Uptake of porphyrins, present in HPD, by atheromatous lesions in rabbit aorta in vitro was described by Spears et al [1983]. Later Kessel and Chou [1983], Kessel and Sykes [1984], and Pollock et al [1987] using chemical analysis showed accumulation of HPD in human aortic plaques obtained at autopsy. However, details of patterns of distribution of such material in the plaque are unknown. Furthermore, HPD has a peak wavelength of absorption that lies within the same wavelength range of absorption by blood. Phycocyanin described in this study is a deeply colored, highly fluorescent photoreceptor pigment obtained from blue-green, red, and crytomonad algae that contain a linear tetrapyrrol as the prosthetic group [Bennet and Siegelman, 1979]. Phycocyanin naturally occurs as large molecular weight aggregates that are attached to the photosynthetic membranes. They are closely linked to the chlorophyll-containing system for efficient energy transfer. It exists in two forms that are interconverted upon alternative exposure to red and far-red light with a peak absorption at 620.5 nm. We have taken advantage of this property since it represents peak absorption at the limit of the wavelength range for absorption of light by blood, and we have investigated the potential of phycocyanin for generating oxidizing radicals. We report strong activation of phycocyanin with resultant release by oxidizing radicals particularly between the wavelength of 620 and 650 nm. The potential for release of such oxidizing radicals exists at even higher wavelength pending further testing with

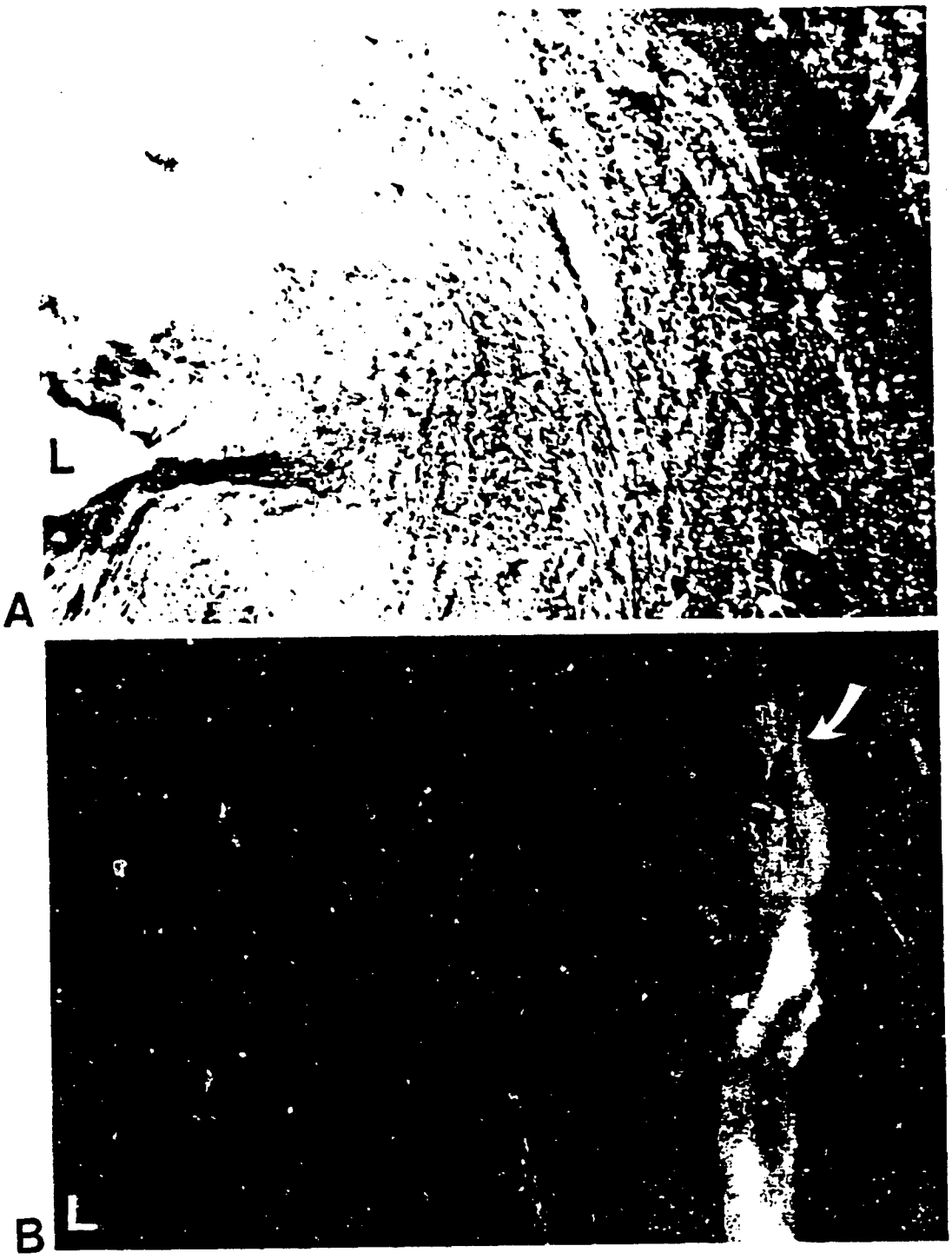

Fig. 6. Light and fluorescence microscopy of the same field in a cross section from a human atherosclerotic coronary artery that was perfused with 0.1 mg/ml phycocyanin in oxygenated Krebs-Ringer bicarbonate solution followed by washout with phycocyanin-free Ringer's solution. A: Light microscopy. B: Fluorescence microscopy. Arrows are internal elastic lamina; L = lumen. ×60.

Fig. 7. Polarized light microscopy of human atherosclerotic coronary artery cross section after perfusion and washout of phycocyanin containing solution (0.1 mg/ml). Polarized light was 577 nm to enhance the shades of areas containing phycocyanin, which absorbs at 620 nm. The lighter band around the periphery represents minimal uptake of phycocyanin in the medial muscle coat. Magnification ×40.

appropriate laser light. The amounts of energies reported in this paper and required for this activation are higher than previously described values for clinically applied photodynamic therapy. It is possible that similar activation levels can be obtained if lower energy levels were used.

In addition to measuring the generation of oxidizing radicals by using a coupled NADPH reaction we have also examined the cytotoxic effect on malignant cells. Mouse myeloma cells in suspension cultures were dramatically killed upon exposure to a combination of laser light and phycocyanin. Effects were observed as early as within the first 10 hours. Such dramatic loss of viability in neoplastic cells may not be similarly observed in atherosclerotic plaque when the parameters measured are based on changes in plaque volume or bulk. The reason for this is that unlike neoplastic cells, plaque components do not have a high turnover rate and that in addition to the cellular components there are structural plaque matrix components such as collagen, which has very low turnover.

We have examined the pattern of uptake of phycocyanin into viable human atherosclerotic plaque on coronary artery segments. Phycocyanin was selectively taken into the plaque, and it was dramatically absent from the medial muscle layer. Within the plaque, phycocyanin was characteristicaly concentrated at several laminae: however, the largest concentration was at the internal elastic lamina. Since phycocyanin is hydrophillic and Kessel and Sykes [1984] described the existence of hydrophillic sites within the plaque, it is therefore possible that these laminae including the internal elastic lamina possess a significant amount of hydrophillic residues. The data presented here suggest that phycocyanin may have potential use as a marker for clinically evaluating atherosclerosis.

The resultant cytotoxicity from activation of phycocyanin, present at those sites within the plaque, using laser at light wavelengths that are minimally absorbed by blood, may have significant clinical implications for regression of plaque and awaits further investigation.

ACKNOWLEDGMENTS

The authors wish to express thanks to the Sheriff-Coroner of Orange County and the Orange County Sheriff-Coroner Forensic Facility and Staff for assistance in obtaining autopsy specimens. This work was supported by grants from Intertherapy Inc. and by National Institute of Health grants NIH RR 01192-08 and NIH HL 31318-04.

REFERENCES

Auler H, Bancer G (1942): Untersuchngen uber die roile der porphine bei geschwulstranken menschem und tieren Z Krebsforch 53:65–68.

Bennett A, Siegelman HW (1979): "Phorphyrins," Vol 6. Dolphine D, ed. New York, Academic Press, pp 493–520.

Boadaness RS, Chan PC (1977): Singlet oxygen as a mediator in the hematoporphyrin-catalyzed photo-oxidation of NADPH to NADP+ in deuterium oxide. J Biol Chem 252:8554–8560.

Dougherty TJ, Grindery GB, Fiel R, Weishaupt KR, and Boyle DB (1975): Photoradiation therapy II. Cure of animal tumors with hematoporphyrin and light. JNCI 55:115–121.

Dougherty TJ, Kaufman JE, Goldfarb A, Weishaupt KR, Boyle D, Mittleman A (1978) Photoradiation therapy for the treatment of malignant tumors. Cancer Res 38:2628–2635

Dougherty TJ, Laurence G, Kaufman JH, Boyle D, Weishaupt KR, Goldfarb A (1979) Photoradiation in the treatment of recurrent breast carcinoma. JNCI 62:231–237

Figge FH, Weiland GS, Manganiello LOJ (1948) Cancer Detection and Therapy. Affinity of neoplastic embryonic and traumatized regenerating tissues for porphyrins and metalloporphyrins. Proc Soc Exp Biol Med 68:640–641

Kessel D, Chan TH (1983) Cancer Res 43:1994–1999.

Kessel D, Sykes E (1984) Porphyrin accumulation by atheromatous plaques of the aorta. Photochem Photobiol 40:59–61

Kvello S, Moan JA, Brunborg G, Eklund T (1980) Photodynamic inactivation of yeast cells sensitized by hematoporphyrin. Photochem Photobiol 32:349

Moreos NC, Stupecky GL, Purdy RE (1985) Effect of arterial endothelium on sensitivity to 5-Hydroxy tryptamine. Proc West Pharmacol Soc 28:77–79

Pollock ME, Eugene J, Hamer-Wilson M, Berns MW (1987) Photosensitization of experimental atheromas by porphyrin. J Am Coll Cardiol 9:639–646

Spears JR, Serum J, Shropshire D, Paulin S (1983) Fluorescence of experimental atheromatous plaques with hematoporphyrin derivative. J Clin Invest 71:395–399

Basic laser physics and tissue interactions

By J. Stuart Nelson, MD, PhD, and Michael W. Berns, PhD

The purpose of this article is to provide a brief understanding of the nature of the laser, how it works, and the fundamental mechanisms of its interaction with matter. It is important to understand these principles because the appropriate and effective medical use of the laser depends on their adequate appreciation.

To start, let us compare the laser with a light bulb (Figure 1). The product of the laser is light, which is composed of packets of energy known as photons. Photons are also produced by the light bulb, and indeed, a photon is a photon whether it comes from the sun or a light bulb, firefly, or laser. Light from the laser and the light bulb differs in how their photons are organized both spatially and temporally. When you look at a light bulb, you see that light radiates in all directions. As you walk away from the light bulb, it gets dimmer and dimmer; there is a direct mathematical relationship between loss of light intensity and the distance that you move from the bulb. In the laser, photons are emitted together in parallel (or near parallel) and in phase with each other. This property is known as coherence; it explains why, when you walk away from a laser, the light intensity does not decrease very much. This property is used by scientists to send a laser beam to the moon and back to measure interplanetary distances.

Another feature that we notice about the light emitted by the light bulb is its white or yellowish-white color, which contains all the colors and wavelengths in the visual portion of the electromagnetic spectrum and hence is polychromatic. If you put a glass prism in front of the light bulb, you will refract the different wavelengths and see the constituent colors. With the laser, a glass prism will produce light of only one wavelength and one color. Laser light is therefore pure or monochromatic.

J. Stuart Nelson, MD, PhD, and Michael W. Berns, PhD,
Beckman Laser Institute and Medical Clinic
University of California, Irvine
Irvine, California, USA

A third difference between the two light sources is their intensity. The number of photons produced by the laser is much greater per unit area of emission than for any other light source. In fact, millions of more photons are emitted by a laser than by a comparable surface area of the sun.

As a result of these three simple differences, the laser produces an enormous number of monochromatic photons. Otherwise, the photons from the laser and light bulb obey the same basic laws and principles that govern their interaction with matter, molecules, and tissues. In summary, the monochromatic, parallel, intense nature of its light beam makes the laser different from conventional light resources.

The word "laser" is an acronym derived from Light Amplification By The Stimulated Emission Of Radiation, which tells us why the laser is what it is. It is obvious that "L" stands for light; amplification by stimulated emission of radiation is the actual physical process that occurs within the device that we call the laser.

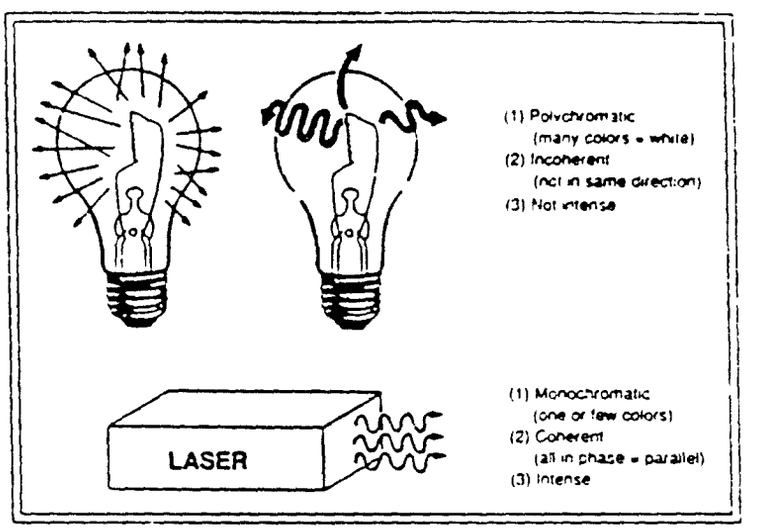

Figure 1: Characteristics of light from the light bulb as opposed to the laser.

Basic laser physics

In Figure 2, there are two atoms in the ground state, the lowest possible energy level. If by some mechanism, we excite these atoms from the ground state by the input of energy, they will move to a higher energy level called the singlet state. The source of this energy can be electrical, chemical, radio frequency, or light. In the first laser that was ever built (1960), the energy that was used to excite the atoms inside the device was derived from a flashlamp.

When these atoms are in the ex-

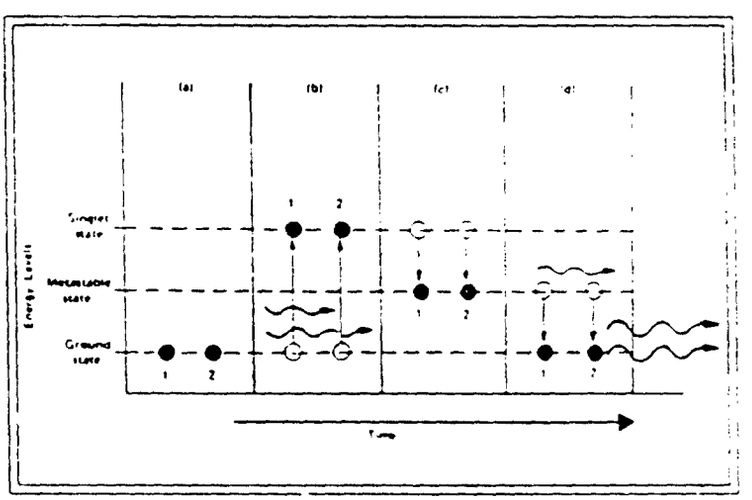

Figure 2: Energy transitions characteristic of atoms in stimulated emissions. **(a)** two ground state atoms 1,2. **(b)** excitation to the singlet state. **(c)** transition to the metastable state. **(d)** atom 1 spontaneously drops to ground state, emitting a photon that stimulates atom 2 to drop to the ground state. Both photons from atom 1 and atom 2 have the same wavelength and are travelling parallel to each other in phase.

Best Available Copy

cited singlet state, they will very quickly drop to an intermediate energy level called the metastable state. This partially explains why some materials can go through the process that we call lasing while others cannot. Only certain types of atoms are capable of the lasing process; those atoms characteristically have a metastable state in their energy structure. This metastable state is unique in that these atoms will stay at this energy level for a relatively long time, perhaps as long as a couple of seconds. The latter may not seem long, but, in photobiology, where most reactions occur in nanoseconds (10^{-9}) or picoseconds (10^{-12}), one second is considered a long period.

What happens next is a spontaneous event. According to the laws of thermodynamics, atoms are always moving. Atoms which exist in the metastable state spontaneously, by random action, return to the ground state with the loss of some energy. This energy loss is in the form of light: the release of a photon. If the photon is in close proximity to another atom which is in the metastable state (remember that the metastable state is long-lived, so there will be many atoms at that energy level), it will actually strike or collide with the other atom. This interaction stimulates the second atom to return to its ground state and, in the process, emit another photon of light. According to the basic principles of physics, since both photons come from identical energy levels, they will be of the same wavelengths (color) and are also moving parallel to and in phase with each other. The simple diagram in Figure 2 really outlines the entire basis of lasing: the stimulated emis-

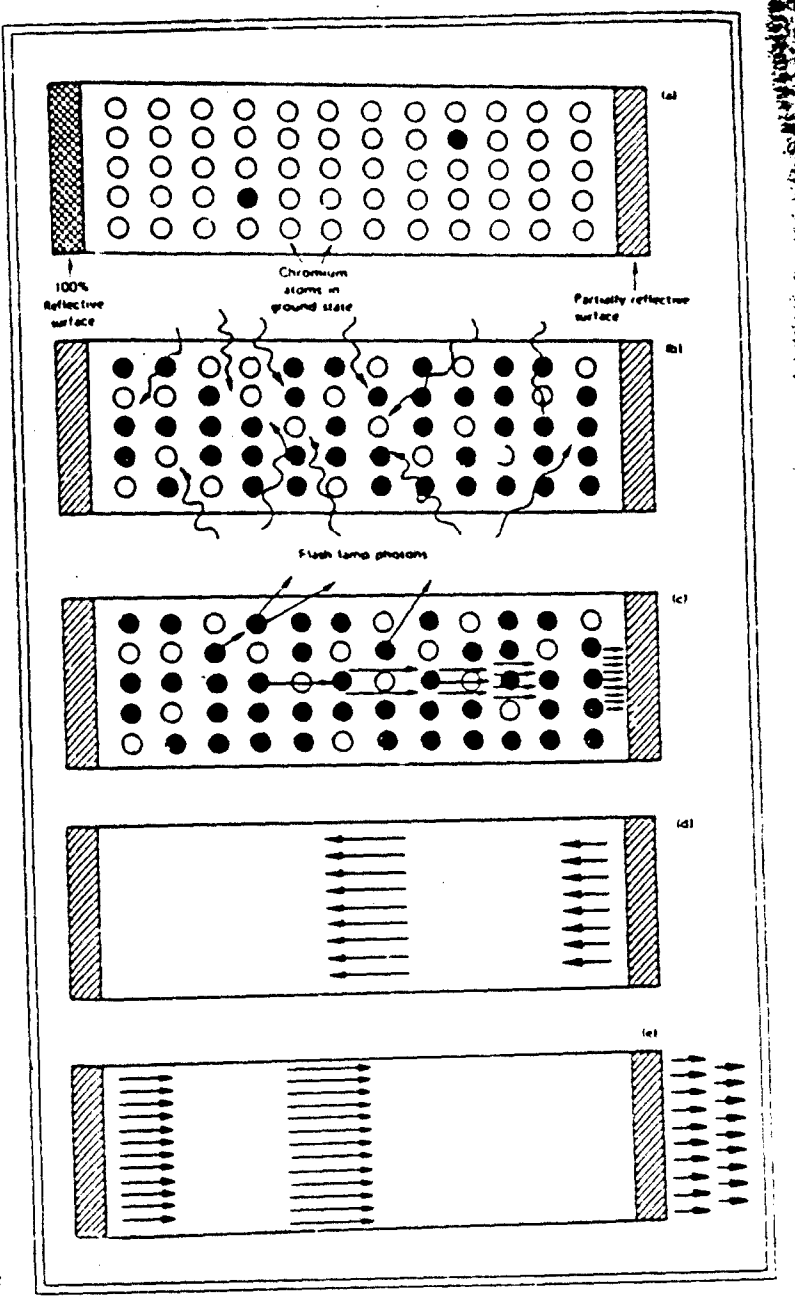

Figure 3: Schematic of ruby laser action illustrating photon cascade. **(a)** unstimulated ruby crystal; a few chromium atoms (closed circles) are spontaneously in the singlet or metastable state, but most are in the ground state (open circles); **(b)** Energy input excites ground state chromium atoms to the singlet state from which they drop to the metastable state (closed circles); **(c)** Stimulated emission of excited atoms by photons of stimulated emitting atoms. **(d)** Photon cascade by reflection of mirrored ends; stimulated emission continues. **(e)** Further photon cascade and passage out of partially reflective end.

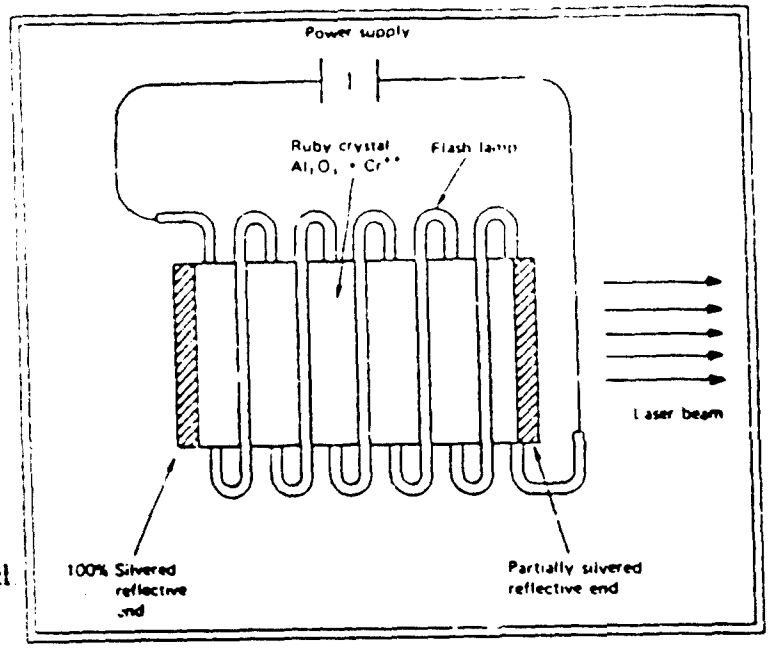

Figure 4: Schematic of a simple ruby laser

Figure 5: Actual components of first ruby laser (1960) pencil indicates ruby crystal, flashlamp to right of crystal

sion of one photon by the action of another photon.

Figure 3 presents the foregoing on a much grander scale. If some kind of suitable material (crystal, gas, or liquid) is within the laser cavity, the atoms are either in the ground state (open circles) or the metastable state (dark circles). The two photons (described above) strike other atoms in the metastable state, causing them to emit photons in parallel and in phase with those already present. Within a fraction of a second, there is an intense buildup of many photons (a "photon cascade"). Within the laser cavity, which has opposing reflective surfaces and contains a suitable lasing material, the released photons will continuously be oscillated through the medium at the speed of light, stimulating the emission of more photons. This is the final physical process in lasing: amplification. By permitting the release of some photons by means of one partially reflective surface at the end of the laser cavity, the result is a bright, intense, monochromatic beam of light.

Figure 4 is a diagram of the first ruby laser built in 1960 by Theodore Maiman. This laser used synthetic red ruby, which is a crystal of aluminum trioxide doped with chromium atoms. It is the chromium atoms inside the crystal lattice that are going through the lasing process to produce the red light. The aluminum trioxide is merely a crystal structure that holds the chromium atoms in place. The Maiman laser (Figure 5) is a notably small apparatus with only three working parts (a ruby crystal, a flashlamp, and a cavity with two reflective mirrors).

BASIC LASER PHYSICS

Figure 6 shows 1988 state-of-the-art technology. Everything in this photograph is a laser except the technician. This device is a free electron laser, which is located at the University of California, Santa Barbara. This laser, which costs many millions of dollars, may be the forerunner of the future. Although much engineering still needs to be done to get this laser to a practical level, research is presently underway on its possible biomedical applications. The real problem of a free electron laser is that it releases an enormous amount of gamma radiation while in use, which potentially can create a serious health hazard.

Figure 7 shows those regions in the electromagnetic spectrum where lasers can be used. Generally and by convention, a medical laser is referred to in terms of its wavelength in either nanometers (nm), microns (um), or millimeters (mm). As you can see, lasers occupy a relatively small portion of the entire electromagnetic spectrum. This portion is expanding, however, with the development of the free electron laser, which eventually may be manipulated from the infrared to the ultraviolet segments of the spectrum.

When discussing different kinds of lasers, identification is made by the type of material inside the device which is going through the lasing process (eg, the argon laser has argon gas as the lasing medium). There are liquid, solid, and gas lasers (Figure 8). It is possible to obtain lasing action from any of these materials, provided their atomic structures have a metastable state that permits the stimulated emission process to occur.

There are also ways to modify the

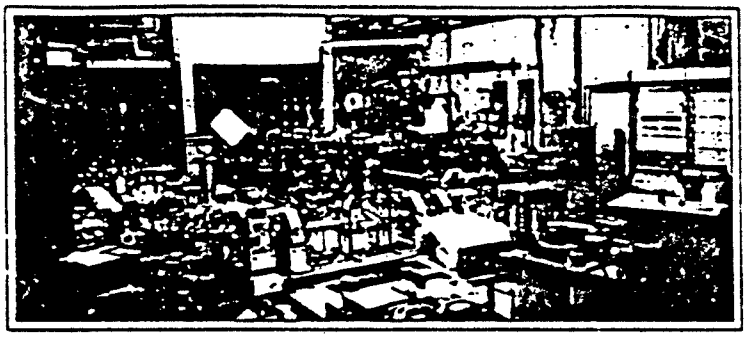

Figure 6: Free electron laser at University of California, Santa Barbara

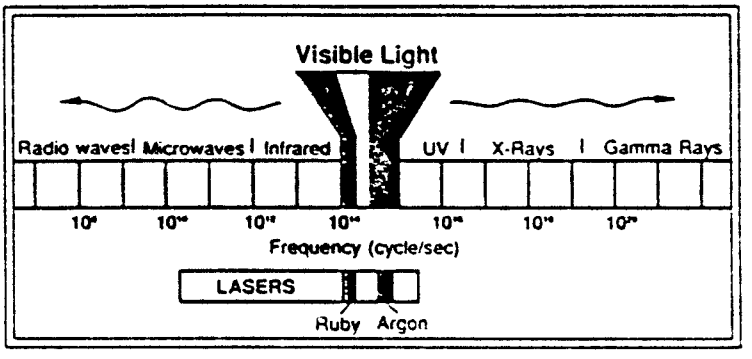

Figure 7: Comparison of various electromagnetic radiation sources

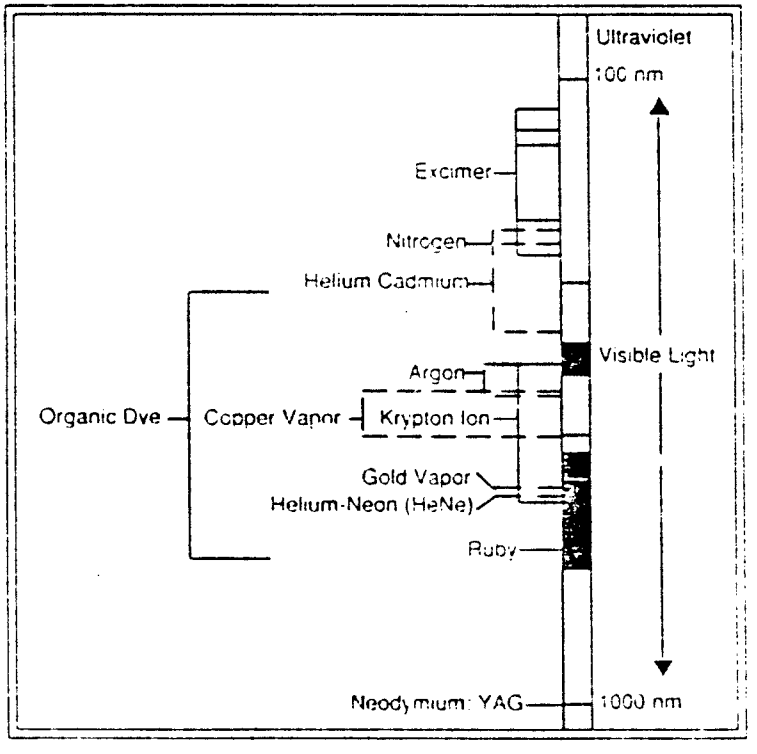

Figure 8: Identification of different types of medical lasers

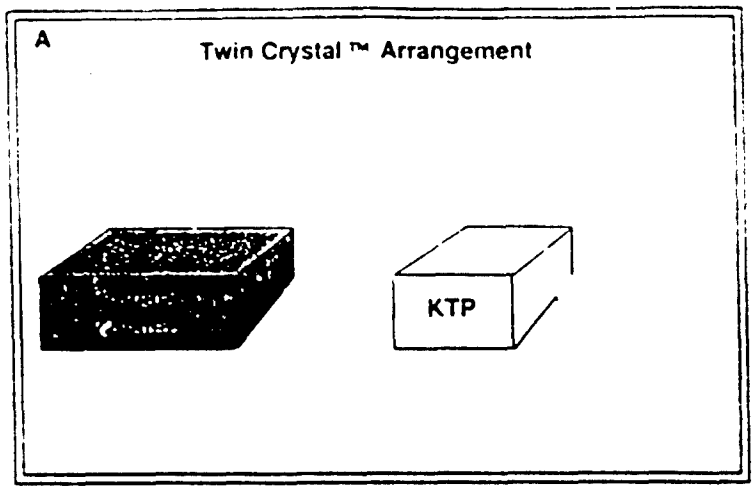

Figure 9: Second harmonic generation by passing a Neodymium- Yag laser beam through the asymmetric crystal potassium trihydrogen phosphate (KTP) (courtesy of Laserscope)

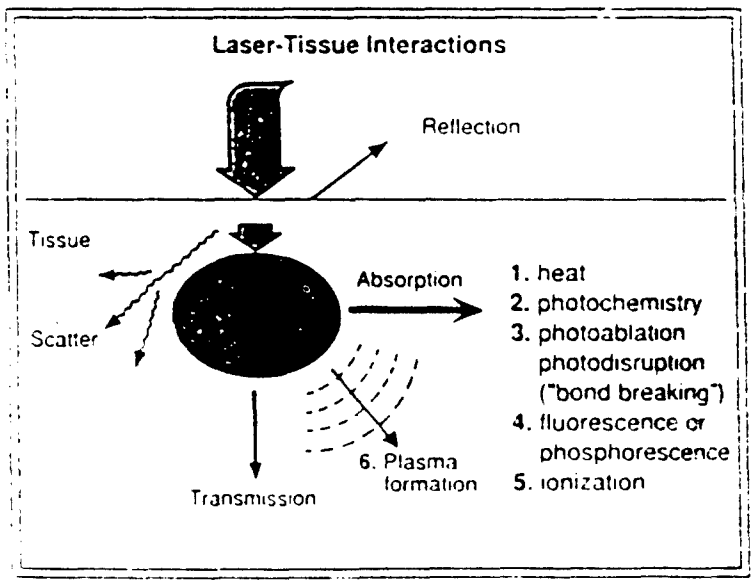

Figure 10: Laser tissue interactions

℞ Nizoral®

ketoconazole cream 2%

TOPICAL ANTIFUNGAL AGENT

ACTION

In vitro studies suggest that the antifungal properties of NIZORAL (keto-conazole) may be related to its ability to impair the synthesis of ergosterol a component of fungal and animal cell membranes. Without the cholesterol of the essential sterol, there are morphological alterations of the fungal and animal cell membranes manifested as abnormal membrane fluid inclusions between the cell wall and the plasma membrane. The inhibition of ergosterol synthesis has been attributed to interference with the reactions involved in the removal of the 14-α methyl group of the precursor of ergosterol, lanosterol.[1]

INDICATIONS

NIZORAL cream 2% may be indicated for the topical treatment of tinea pedis, tinea corporis and tinea cruris caused by *Trichophyton rubrum, T. mentagrophytes* and *Epidermophyton floccosum* and in the treatment of tinea versicolor (pityriasis) caused by *Malassezia furfur (Pityrosporum orbiculare)*.

CONTRAINDICATIONS

NIZORAL cream 2% is contraindicated in persons who have shown hypersensitivity to the active or excipient ingredients of the formulation.

WARNINGS

NIZORAL cream 2% should never be employed for the treatment of infections of the eye.

PRECAUTIONS

If a reaction suggesting sensitivity or chemical irritation should occur use of NIZORAL cream 2% should be promptly discontinued.

Limited short term studies in animals and in human volunteers on whom limited quantities of NIZORAL cream 2% were tested have failed to demonstrate absorption of ketoconazole in detectable amounts. Due to the teratogenic nature of the active ingredient ketoconazole caution should be exercised when NIZORAL cream 2% is administered to pregnant or nursing women.

Cross sensitivity with imidazole and other antibiotics may exist and caution is suggested when NIZORAL cream 2% is employed in patients with known sensitivities to medications.

ADVERSE REACTIONS

Short term studies indicate that NIZORAL cream 2% is well tolerated on the skin. During clinical trials 43 (5.0%) of 867 patients treated with the cream and 311 (8%) of 167 patients treated with placebo reported side effects consisting mainly of severe irritation, pruritus and stinging. One of the patients treated with NIZORAL cream 2% developed a positive allergic reaction, swelling of the foot.

SYMPTOMS AND TREATMENT OF OVERDOSAGE

There has been no experience with overdosage of NIZORAL cream 2%. Treatment should include general supportive measures.

DOSAGE AND ADMINISTRATION

After clinically adequate therapy with NIZORAL cream 2% may be applied once daily for a course and subsequently less frequently. Treatment should be adjusted according to the findings.

NIZORAL cream 2% should be applied to the affected and immediate surrounding areas of patients with the following conditions:

CONDITIONS	FREQUENCY	DURATION
Tinea pedis	once daily	4-6 weeks
Tinea corporis	once daily	3-4 weeks
Tinea cruris	once daily	2-4 weeks
Tinea versicolor	once daily	2-3 weeks

More resistant cases may be treated twice daily depending on adverse response.

The full course of therapy should be followed to reduce the possibility of recurrence. However, there is no response within the recommended treatment period, the diagnosis should be reevaluated.

The safety of NIZORAL cream 2% has not been established with treatment periods exceeding those recommended. Therefore, treatment must not exceed the recommended duration of therapy indicated above.

DOSAGE FORM

NIZORAL cream 2% is a white odourless cream containing 20 mg ketoconazole per gram and is supplied in 30 g tubes.

For Product Monograph and more information please call or write:

REFERENCES 1. Product Monograph 2. Stockel J An Autoradiography Study of the Penetration of a 2% Ketoconazole Cream Formulation in Human Skin Days On Five 3. Swanson N Antimycologic 4. Systemic Absorption following Dermal Application of 2% Ketoconazole Cream Days on Five 5. Adam D Double Blind Comparison of 2% Ketoconazole Cream and Placebo in the Treatment of Fungal Infections of the Skin Days On Five 6. Adam D Double Blind Comparison of 2% Ketoconazole Cream and Placebo in the Treatment of Tinea Corporis and Tinea Cruris Days on Five 7. Adam D Double Blind Comparison of Ketoconazole 2% Cream and Placebo in the Treatment of Tinea Versicolor Days On Five 8. Dockerman [illegible] 9. Topical Ketoconazole [illegible] 10. [illegible]

JANSSEN PHARMACEUTICA

Janssen Pharmaceutica
6705 Mill Creek Dr.
Mississauga, Ont.
L5N [illegible]

wavelengths that are obtainable from lasers (Figure 9). Certain crystals, called nonlinear asymmetric crystals, take photons from very intense light and, through an interaction of these photons with the crystal lattice, generate laser light with twice the frequency (half the wavelength) of the incident radiation. This is known as frequency doubling or harmonic generation. By using these crystals in conjunction with lasers, it is possible to double, triple, or quadruple the wavelengths from the primary laser source. It is also possible to use one laser to excite another and, by using liquid dyes that can go into many different metastable states, to obtain a whole variety of different wave-

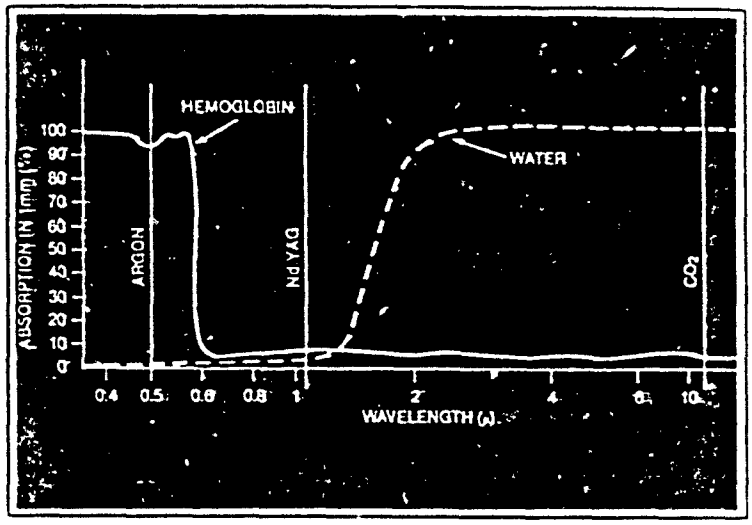

Figure 11: Absorption spectrum of hemoglobin and water

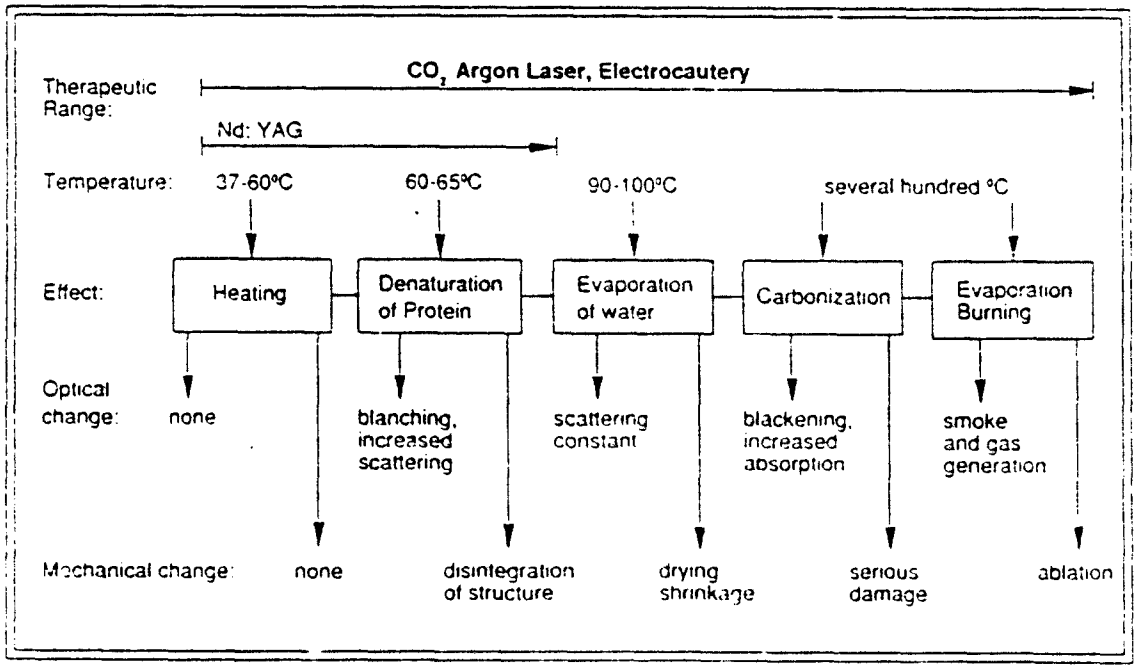

Figure 12: Thermal interaction of laser irradiation with biological tissues

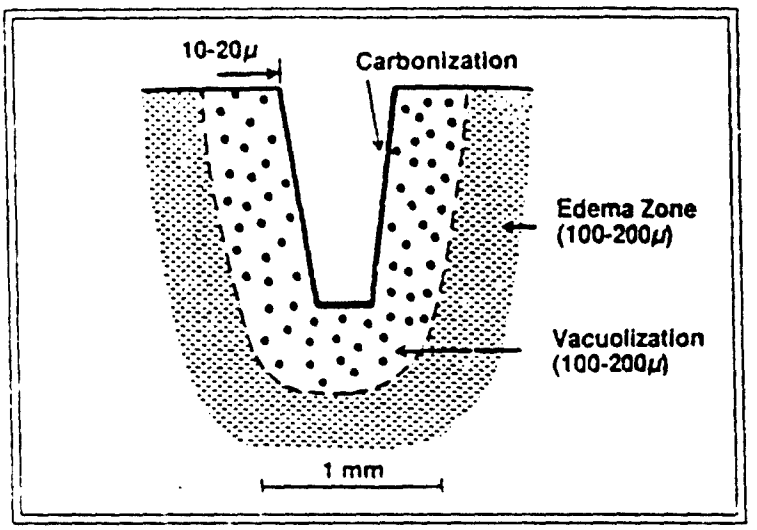

Figure 13: Dissipation of thermal energy in biological tissues

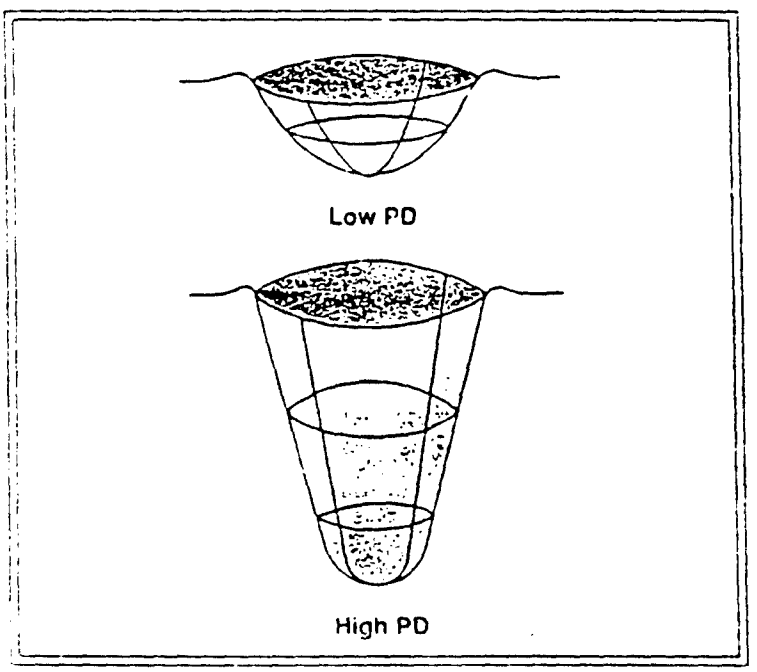

Figure 14: Relative crater configuration and volume as a function of power density

lengths from a single laser device.

In summary, there is considerable flexibility in what wavelengths are available for clinical use. In fact, many newer devices can be precisely tuned to emit photons at the exact wavelength that matches the particular pigment present in body tissues to bring about their selective disruption.

Laser-tissue interactions

Now that this intense, pure beam of light has been generated, how can it be used? Once again, light from lasers follows the basic laws of photobiology. The one exception is for extremely short, intense laser pulses where so-called "nonlinear" events may occur. These effects, such as multiphoton absorption, plasma generation, and ionization occur as a function of photon intensity; they were not possible until extremely short (nanosecond/picosecond) laser pulses were generated.

The first thing to remember is that life is not always as simple as it appears. If a laser beam is directed at a tissue, it may be reflected back to the source or to another undesired surface. Since tissues reflect light, their reflectant properties (reflectance) are important considerations. Furthermore, we must be aware that instruments in the operative field also may reflect the light and may create problems and health hazards for the patient or attending personnel.

When reflectance is adequately controlled and the laser light enters the tissue, the ultimate goal is absorption of light energy to effect tissue change. Two additional complications can occur other than absorption in the tissue. The tissue itself can

scatter the light, which literally bounces off particles and structures within the tissue and "scatters" to places where it is not wanted. Furthermore, the light may be transmitted right through the tissue and only a minimal amount may be absorbed. Since every tissue has reflective, scattering, and transmissive properties, understanding these tissue characteristics is an important aspect of knowing how to use the laser.

The process of absorption is the key to effective laser use. When photons enter the tissue, those that are not reflected, scattered, or transmitted are absorbed. Their energy is transferred to other molecules/groups of atoms within the tissue that is to be altered or changed. Once this photon energy is absorbed, it must go somewhere; this is really the key to produce the different tissue changes. Where and how is this energy dissipated? Normally, we think of lasers as producing heat. Probably 90% of the clinical procedures for which lasers are used involve the production of some kind of local thermal event. Heat, however, is only one way that the photon energy can be dissipated (Figure 10). The important point to remember is that when photons are absorbed, the absorbing structure or tissue must get rid of that energy in some way. The manner in which this energy is dissipated causes the different biological effects that we see clinically.

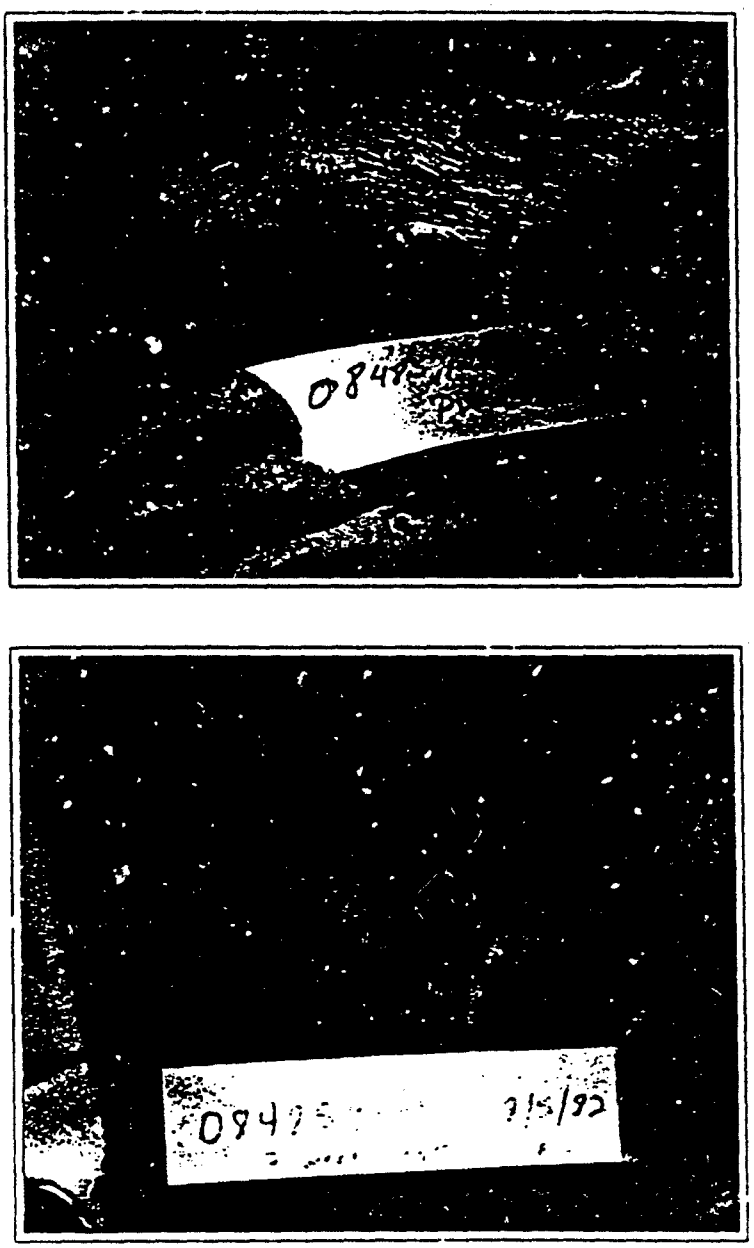

Figure15:Patient with superficial recurrence of breastcancer: (A)before photodynamictherapy;(B) three weeks after treatment

Absorption

Before light energy can be absorbed, there must be some absorbing molecule in the tissue. These molecules are generally referred to as pigments

Figure 11 plots the absorption spectrum of two common body constituents that can function as pigments: hemoglobin and water.

Hemoglobin has a very high absorption in the violet and blue/green portions of the visible spectrum. The absorption starts to decline in the red region of the spectrum, which is why hemoglobin is red (it does not absorb red light). This is the rationale for using an argon laser, which emits blue/green light, as the primary treatment for vascular lesions such as hemangiomas and port-wine stains. Hemoglobin absorbs blue/green light and converts it into heat energy, which destroys the blood vessel; however, this action may not be as selective as anticipated. Even with selective absorption by the hemoglobin molecule, the heat that destroys the blood vessel, unless very precisely controlled and confined just to this area, will radiate in all directions and may destroy the overlying skin layers.

Currently, newer procedures are being developed with short-pulsed lasers, where it is felt that confining the energy to a very short period will reduce the spread of heat to surrounding structures.

Water, on the other hand, does not absorb in the visible, and very minimally in the near infrared portions, of the spectrum. In the far infrared regions, water absorbs maximally. This is why a carbon dioxide laser has a direct effect on any tissue in the body. Water is a major constituent of every tissue in the body. The carbon dioxide laser can be compared clinically to performing a dermabrasion, because the laser gradually removes cell layer

cell layer by the volatilization of

"NIZORAL" 200 mg TABLETS

KETOCONAZOLE

ANTIFUNGAL AGENT

INDICATIONS

Serious or life-threatening systemic fungal infections in normal granulomatous or immunocompromised patients where alternate therapy is considered inappropriate or has been unsuccessful. Systemic Candidosis, chronic mucocutaneous candidosis, coccidioidomycosis and paracoccidioidomycosis, histoplasmosis and chromomycosis. Severe refractory dermatophytoses unresponsive to other forms of therapy.

When clinically warranted, therapy may be initiated prior to identification of the causative organism.

N.B. NIZORAL is not recommended for fungal infections of the CNS.

CONTRAINDICATIONS

Known hypersensitivity. Hepatic dysfunction. In women of childbearing age do not use unless effective forms of contraception are employed.

WARNINGS

Idiosyncratic hepatocellular dysfunction has been reported and can be fatal unless properly recognized and managed. Liver function tests (SGOT, alkaline phosphatase, SGPT, SGOT, bilirubin) should be performed before, and at periodic (monthly or more frequently) intervals during treatment, particularly in patients with a history of significant alcohol consumption. Those expected to be on prolonged therapy and those receiving other potentially hepatotoxic drugs, concurrently. Minor elevations of liver enzymes usually normalize during therapy and do not necessitate discontinuation of therapy. However symptomatic manifestation of hepatotoxicity is an indication for termination of therapy. Deaths have been reported following therapeutic doses of ketoconazole associated with evidence of hepatotoxicity.

In man, single doses of 200, 400 or 600 mg NIZORAL cause a dose related decrease in serum testosterone levels, which returning to baseline values 8 to 24 hours later. During chronic administration of 200 mg daily, testosterone levels were not significantly suppressed. Doses of 1200 mg/day have resulted in reduction of serum testosterone to the castrate level within 24 hours. This was maintained for the duration of therapy. Gynaecomastia and azoospermia have been reported at therapeutic doses and above.

In 6 healthy females receiving 400 mg once in the late follicular phase and once in the luteal phase, NIZORAL produced a 38% drop in 17 β-oestradiol along with a 50% increase in progesterone during the follicular phase as well as a 61% drop in 17 β-oestradiol and a 94% increase in progesterone during the luteal phase. The potential for a deleterious effect on puberty and/or fertility must be carefully considered when long-term NIZORAL therapy is contemplated in children.

A single dose of 200 mg of NIZORAL had no effect on human cortisol levels, however 400 or 600 mg caused a slight non-significant fall in basal cortisol levels and a significant but reversible blunting of cortisol response to ACTH. Chronic administration of 800 or 1200 mg NIZORAL impaired the ability of the adrenals to produce cortisol although evidence of frank adrenal insufficiency was not observed. Cortisol levels should be monitored regularly in patients predisposed to adrenal insufficiency, those with marginal adrenal function or during periods of prolonged stress, such as in the intensive care unit.

In males, 1200 mg/day NIZORAL produced a rapid and significant decline in adrenal androgens (androstenedione and dehydroepiandrosterone). Since the effects on hormonal pathways are incompletely understood, judicious consideration is recommended before prescribing NIZORAL on a long-term basis.

Studies in rats indicate that ketoconazole leads to increased bone fragility in females; therefore doses above 400 mg/day should not be used in susceptible patients (post menopausal women and the elderly). Because of ketoconazole's ability to interfere with steroid synthesis and vitamin D metabolism, careful consideration should be given to use in children. Calcium and phosphorus levels should be monitored during long-term therapy.

Animal studies indicate that NIZORAL crosses the placental barrier and is only eliminated very slowly from fetal membranes. This must be carefully considered in pregnant patients.

PRECAUTIONS

Patients should report any signs and symptoms (abnormal fatigue, anorexia, nausea and/or vomiting, jaundice, dark urine or pale stools) suggesting liver dysfunction so that appropriate biochemical testing can be done. Liver function tests should be performed before and during the initial days of treatment and at monthly or more frequent intervals during treatment in patients with a history of significant alcohol intake or dysfunction of liver. Should therapy be used concurrently with other potentially hepatotoxic drugs, and those designed for long-term therapy (see WARNINGS).

NIZORAL requires acidity for dissolution and absorption. Antacids, anticholinergics or H2 blockers should be given at least 2 hours after NIZORAL. For achlorhydric patients, dissolve each NIZORAL tablet in 4 mL aqueous 0.2 N HCl, drink with a straw to avoid contact with the teeth and follow with a cup of water.

Anaphylactic reactions to NIZORAL with severe angioedema have been reported in 2 cases. Use NIZORAL cautiously in patients with a known sensitivity to miconazole as cross sensitivity may exist.

Use in Women of Child Bearing Age

An effective form of contraception must be used during NIZORAL therapy.

Use in Pregnancy

In rats, NIZORAL is teratogenic, crosses the placental barrier and is eliminated very slowly from fetal membranes. Evidence of maternal toxicity and embryotoxicity was seen at doses of 10 mg/kg. Very careful consideration should be given to the prescription of this medicine and drugs before using NIZORAL in pregnancy.

Use During Lactation

Nursing should be stopped before starting therapy since another patient may be on the same [illegible]

Use in Children

Safety data in children should be examined where NIZORAL is given to children. Carcinogenicity and hematological monitoring is also good NIZORAL

interferes with steroid synthesis, the potential for a deleterious effect on puberty and/or fertility must be carefully considered when long-term therapy is contemplated. Calcium and phosphorus serum levels should be monitored in long-term treatment since NIZORAL interferes with vitamin D metabolism. Hepatic dysfunction developed in a 6 year old during long-term therapy.

DRUG INTERACTIONS

NIZORAL + cyclosporine = increases plasma concentrations of cyclosporine.

Since the occurrence of nephrotoxicity as a side effect of cyclosporine is correlated with high plasma trough levels, additional care is required when they are used concurrently.

NIZORAL + warfarin = potentiation of the action of warfarin.

= short drug in the prothrombin level may occur during concomitant therapy with ketoconazole. Use of oral anticoagulants: More careful monitoring of anticoagulant effects is necessary with appropriate adjustment of the warfarin dose.

NIZORAL + insulin = decreased insulin needs in diabetic patients.

Due to a possible insulin lowering effect, insulin needs should be assessed more frequently when NIZORAL is used concurrently.

NIZORAL + rifampicin and/or isoniazid = reduces NIZORAL levels.

These drugs should not be used concurrently.

NIZORAL + phenytoin = increases or decreases plasma levels of either drug. (Ketoconazole via cytochrome P_{450} enzymes).

ADVERSE REACTIONS

Some deaths occurred in clinical trials which may or may not be drug related.

Gastrointestinal: nausea and/or vomiting (3%), GI haemorrhage (<1%), abdominal pain (1.2%), diarrhea (<1%).

Dermatological: pruritus (1.5%), alopecia, photophobia (<1% in all cases).

Central Nervous System: headache, dizziness, somnolence, tremors, nervousness, paresthesia (<1% in all cases).

Endocrinological: gynecomastia (<1%), dose dependent decrease in sex hormone serum levels, decreased in basal and ACTH induced cortisol levels, increased serum levels of 17 OH progesterone and decreased urinary levels of 17 ketosteroids. Impotence, azoospermia.

Gonadotoxicity: oligospermia and azoospermia, amenorrhea, loss of libido, menstrual irregularities.

Hematological: thrombocytopenia, leucopenia, decreased hematocrit, and rare instances, neutropenia (<1%).

Hepatic: idiosyncratic hepatocellular dysfunction (<0.81%, see WARNINGS), transient increases in liver enzymes. Three patients have died in hepatic coma, two when ketoconazole therapy was continued despite clinical symptoms, and the third despite discontinuation of therapy.

Miscellaneous: fever and chills, photophobia, idiosyncratic allergic reactions, anaphylactic shock, pronounced dyspnea, arthralgia, sensation of detachment, corneal deposits, cataract enlargement (<1%).

DOSAGE AND ADMINISTRATION

The infecting organism should be identified although when clinically warranted therapy may be initiated prior to obtaining these results.

GENERAL GUIDELINES N.B. Refer to WARNINGS AND PRECAUTIONS

CONDITION	RECOMMENDED TREATMENT*	RESPONSE TIME**
DERMAL AND CUTANEOUS MYCOSES		
Dermatomycoses	4-6 weeks	4 weeks
Hair or scalp mycoses	4-8 weeks	4 weeks
Pityriasis versicolor	3-6 weeks	3 weeks
Oral thrush	1-7 weeks	1 week
Chronic mucocutaneous candidosis	6-12 months	6 months
Onychomycosis	6-12 months	3 months
DEEP MYCOSES†		
Systemic candidosis	2-4 weeks	4 weeks
Paracoccidioidomycosis	2-4 months	2 months
Coccidioidomycosis	>6 months	6 months
Histoplasmosis	2-4 months	2 months
Chromomycosis	>6 months	3 months

a Base the duration of therapy on individual clinical and mycological response.

b If no response is seen, biopsy can be repeated up to maximum recommended.

c Continue treatment for at least 1 week after apparent eradication of the infecting fungus.

ADULTS

200 mg once a day. Dose may be increased to 400 mg in severe cases or do not respond (see Table). Dose should not exceed 400 mg.

CHILDREN

< 20 kg: 50 mg; 20-40 kg: 100 mg; over 40 kg: 200 mg. Dose should not exceed 400 mg.

NIZORAL should be taken once a day with a meal. Since NIZORAL requires adequate gastric acidity for dissolution, avoid concomitant use of antacids, anticholinergics and H2 blockers. If administration must be within 2 hours after NIZORAL, in achlorhydric patients, dissolve each tablet in 4 mL 0.2 N HCl. Drink with a straw to avoid contact with the teeth and follow with a cup of water.

AVAILABILITY

Tablets of 200 mg (white, scored, bottles of 100).

Full Product Monograph available on request.

[illegible]

JANSSEN PHARMACEUTICA

[illegible]

water. In a third laser, the Neodymium-Yag, the light energy is very poorly absorbed by hemoglobin, water, and other body pigments. This is why the Neodymium-Yag laser will penetrate much more deeply into tissue.

The selection of the correct laser for a particular clinical procedure requires an understanding of the absorptive as well as the reflective, scattering, and transmissive properties of the target tissue.

Heat

The control of tissue heating is very important. Figure 12 shows the effect of temperature rise in the tissue under irradiation. As the temperature rises to 37-60°C, the tissue starts to retract and conformational changes occur. With a temperature above 60°C, there is protein denaturation and coagulation. From 90-100°C, carbonization and tissue burning occurs. Above 100°C, the tissue is vaporized and ablated. Ideally from a clinical point of view, the physician should be able to stop the heating process at any one of these thermal ranges to produce the desired clinical result. Physicians experienced in laser therapy acquire the ability to discern these tissue changes visually, so that the heating process can be stopped at the desired point. It is therefore important that physicians who plan to use lasers complete a preceptorship with an instructor who has considerable experience in this field and can help them develop the requisite skills.

It is also important to remember that heat radiates in all directions. Around the crater produced by tissue vaporization there will be successive

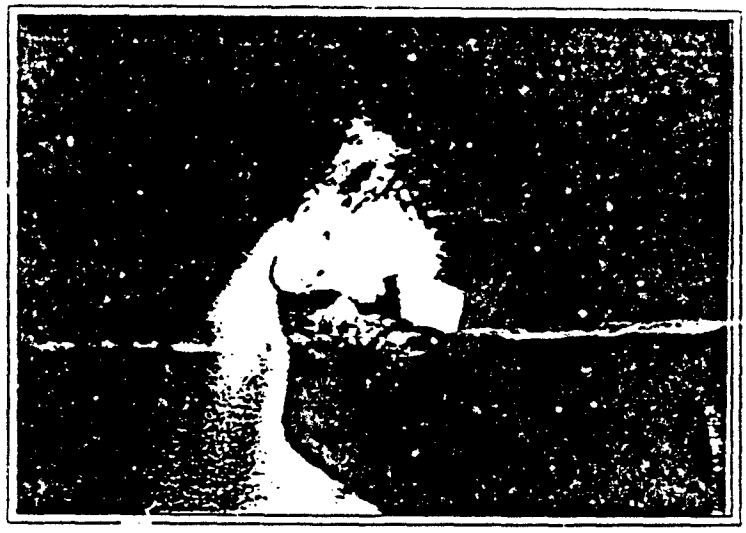

Figure16: Patient with basal cell carcinomas injected previously with hematoporphyrin derivative. Blue/violet, 400-nm light of a krypton laser is used with appropriate filters. Red fluorescence can be observed in malignant cells (Courtesy of Thomas Dougherty)

circumambient zones of carbonization, vacuolization, and edema as the heat is dissipated (Figure 13). The zones of vacuolization and edema may be irreversibly affected and eventually necrose and slough off, or they may be repaired by the host. The laser will not necessarily produce a nice clean cut by vaporization, while leaving other tissue completely unaffected. The objective of laser therapy must be to minimize as much as possible these other zones of thermal injury, while maximizing tissue removal.

Another point that must be emphasized is dosimetry. Obviously, one watt of power (one watt=one joule of energy delivered in one second) delivered over one cm^2 is very different from one watt delivered over one m^2.

As the spot size decreases while the power remains constant, the power density (power per unit area) must necessarily increase. Conversely, as spot size grows from small to large, the power density will diminish. What does this mean in tissues clinically? If the clinical objective is to make a quick incision, the surgeon should use a very small spot with a high power density, because it will penetrate deeply into the tissues. If the intent is to ablate gently from the surface, however, a larger spot size with a lower power density should be used (Figure 14). The operator can therefore control the kind of effect produced in tissue by manipulating either the spot size or power settings on the laser. It is very important to recognize this ability, so that the

operator will be able to get the most out of the device and produce the best clinical results for the patient.

Photochemistry

Photon energy may also be dissipated by photochemistry. The basic concept of photochemistry is that certain molecules (natural and applied) can function as photosensitizers. The presence of these photosensitizers in certain cells makes these cells vulnerable to light of an appropriate wavelength and intensity. The action of these photosensitizers is to absorb photons sufficient to elevate the sensitizer to an excited state. The excited photosensitizer subsequently reacts with a molecular substrate, such as oxygen, to produce singlet oxygen, which causes irreversible oxidation of some essential cellular components. All of this occurs without the generation of heat.

The most common clinical use of this mechanism has been in the treatment of cancer after sensitization with hematoporphyrin derivative (HpD). Although the mechanism of HpD's preferential localization in malignant cells is uncertain, the total time that HpD is retained in malignant tissue is much longer than in nonmalignant tissue, from which it generally clears from 24-72 hours. As a result, there is a "window" of time in which the physician can exploit the differences in HpD concentration to cause the selective photodegradation of malignant tissue.

Clinically, photodynamic therapy (PDT) is carried out by a two-step procedure. HpD is first administered intravenously in the range of 2-5 mg/kg body weight. After a delay of 24-72 hours to allow for its localization in malignant tissue, the tumor is irradiated with visible red light tuned to 630 nm. Shortly after PDT administration, the tumor becomes necrotic (usually within 24 hours) and, when successfully treated, the tumor becomes a nonpalpable scab which is usually sloughed off within a few days (figure 18). The high therapeutic ratio and relative lack of morbidity have made PDT potentially a very attractive form of therapy. Treatment parameters have been selected for the

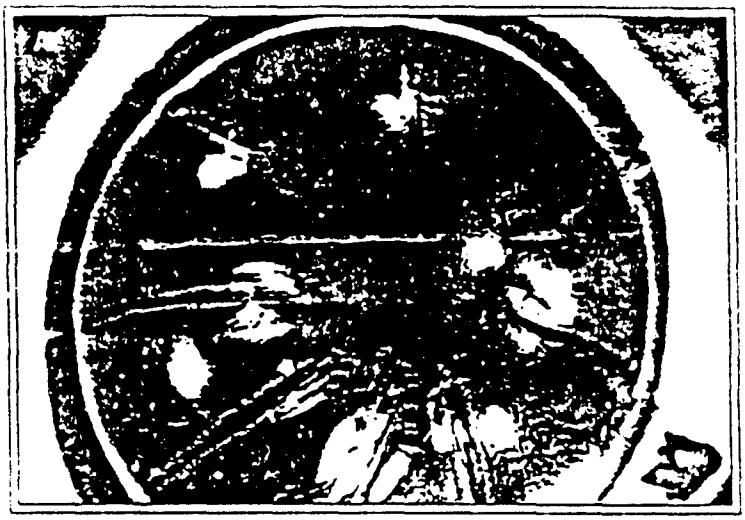

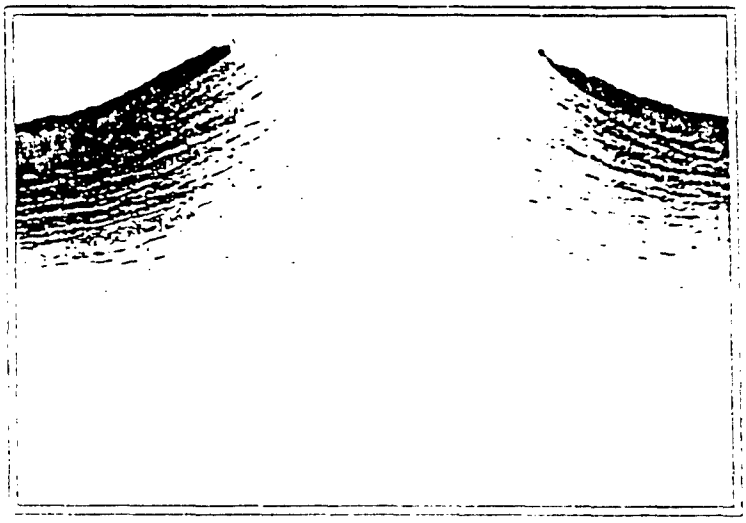

Figure 17: (A) Ablation of corneal stroma with 193-nm radiation of excimer laser (B) Histology reveals clean, non thermal cut

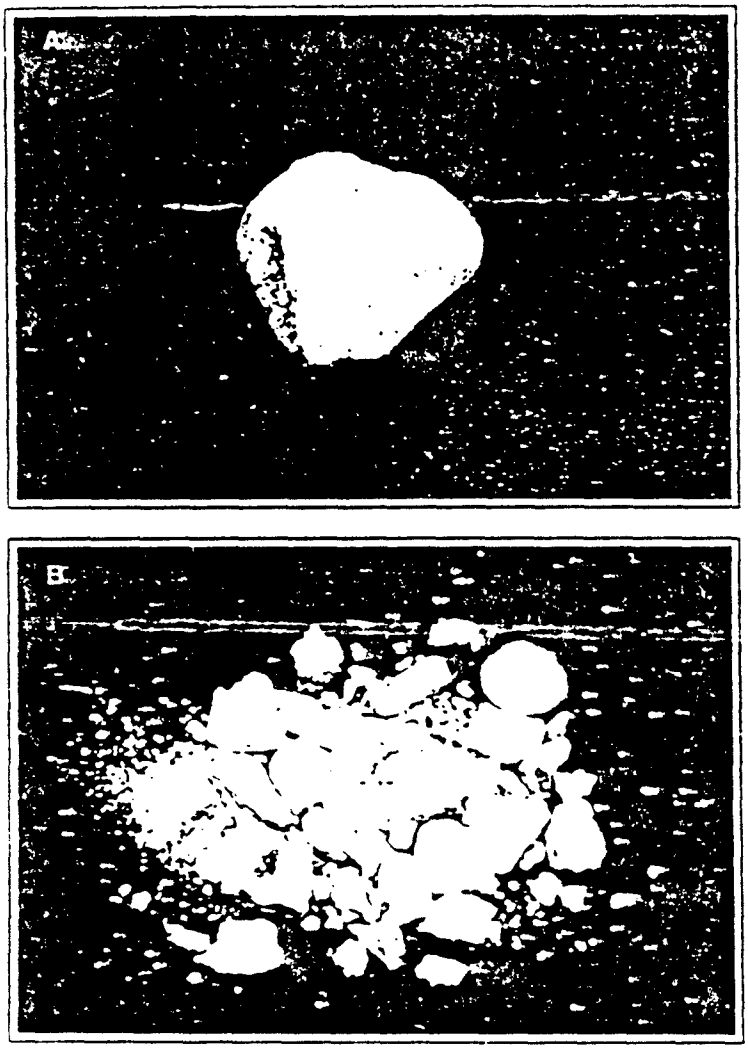

Figure 18: High power density from short-pulsed laser produces acoustical shock wave to destroy urinary calculus

point where therapy can be undertaken with a reasonable expectation of good results in both animal and human trials. While it can be used to eradicate relatively large tumors, PDT appears to be especially advantageous in the patient with a thin superficial tumor that is easily accessible to light.

Fluorescence

Photon energy may be dissipated as the re-emission of light. If this happens within 10^{-8} seconds after absorption, it is called fluorescence.

The fluorescent photon is emitted as the excited atom returns to the ground state. Because excess vibrational energy in the singlet state is dissipated as heat by collisions with other atoms in the excited state, however, the energy of the fluorescent photon is lower (therefore the wavelength is longer) than that of the absorbed photon.

How can this phenomenon be used diagnostically? Many of the photosensitizing dyes used to induce photochemistry (as described above) are also fluorescent. If, in the case of HpD, the 400-nm blue/violet light of a krypton laser is used with an appropriate filter and image intensifier, fluorescence will be observed in malignant tissue (Figure 19). It would then be possible for the physician to switch to a 630-nm red light and bring about the photochemical reaction to kill selectively the cells containing the photosensitizer. This therapy actually has a great deal of promise clinically; it is now used to detect occult lung tumors, to determine the extent of superficial skin tumors, delineating tumors, and to delineate tumors and dysplasia in the bladder.

Potentially, the limit of detection is the ability to detect light, but if the image intensifiers now under development become sensitive enough, it would theoretically be possible to detect just a few photons of light emitted from a single malignant cell. Laser-stimulated fluorescence can also be used analytically to scan large populations of cells that are flowed through a laser beam in a cytofluorometer. Lasers may also be used to excite small microscopic regions

Laser Applications In Biomedicine

Part II: Clinical Applications

J. Stuart Nelson, M.D., Ph.D., and Michael W. Berns, Ph.D
Beckman Laser Institute and Medical Clinic
University of California, Irvine
1002 Health Sciences Road East, Irvine, California 92715

In Vol. 1, No. 1 (Fall 1988) authors Berns and Nelson in Part I: Biophysics, Cell Biology, and Biostimulation, describe the principles of light interaction with tissue and how the successful applications of lasers to biomedicine rely upon an adequate understanding of these principles. The authors explain that many of these applications, such as cell growth stimulation, immunologic response, and wound healing, may be based upon photochemical conversion of absorbed energy.

The purpose of this review, they note, is to place the laser in proper perspective: that is to demonstrate where the laser has had major and minor impact, as well as those areas where the laser is controversial and areas where the laser shows potential for future applications.

Part II: Clinical Applications, continues with a timely review of the various uses of lasers in medicine.

Ophthalmology

THE FIRST LASER built, a ruby laser, was constructed by Theodore Maiman in 1960. In 1961 Zaret et al used this red laser beam to photocoagulate the retinas of experimental animals and by 1964 Zweng et al were using it to treat human patients for retinal tears and other ophtnalmic maladies. Thus, ophthalmology was the first medical specialty to embrace the laser as a therapeutic modality. This was not surprising since ophthalmologists had been using xenon lamp photocoagulators for decades to treat a wide variety of eye disorders. The laser merely provided a more controllable, monochromatic, intense beam of light. Certainly the fact that ophthalmologists fully appreciated the ability of light to produce selective "burns" in the eye, and were able to take advantage of this property to repair visual defects, led to the rapid adoption of the laser in many clinical areas.

The early application of the laser in ophthalmology was for heat welding in the repair of retinal tears. In this treatment, the torn retina is literally heat-fused back down to the other layers of the eye in order to prevent further separation and detachment. The dark pigment of the retina absorbs the intense laser light very effectively resulting in the generation of a small thermal weld. Though the red ruby laser was initially used, it has now been replaced by the blue-green argon laser. The ruby laser is no longer used in ophthalmology because of the technical difficulties in its operation and the fact that it is a higher power pulsed laser that could create some undesirable mechanical shock-wave effects in the tissue. The argon as well as the krypton and new dye lasers are now used in ophthalmic procedures that rely upon thermal photocoagulation. The majority of these cases involve retinal hemorrhage and vascular abnormalities associated with diabetes. This disease is characterized by the excessive growth of blood vessels on the surface of the retina and into the vitreous in response to hypoxia. The result may be major hemorrhage and eventual retinal detachment leading to a drastic reduction in visual acuity. In early studies the laser was used to destroy selectively the newly proliferating blood vessels by focusing the laser directly on the blood vessel itself. The latter has now been replaced by panretinal photocoagulation which involves a grid pattern of laser treatments over the entire ischemic retina rather than the new blood vessels themselves. This treatment results in better oxygenation of the retina and stops further neovascularization. Panretinal photocoagulation has now gained widespread acceptance as a prophylaxis for retinopathy in juvenile onset diabetics. In certain cases where leaking blood vessels can be seen by fluorescein angiography, the laser is still focused on to the leaking vessel to seal it shut, reducing the macular edema and leading to a stabilization of vision. It is also possible to treat more diffuse macular edema (not associated with a specific leaking vessel) with a grid pattern of laser treatments on the macula. While an improvement in vision is not to be expected, the result can be stabilization of vision (1).

The argon laser has been used for a variety of other retinal vascular disorders including central retinal vein occlusion, branch vein occlusion, Eale's disease, sickle cell and other hemoglobinopathies, Coat's disease and leukemia radiation retinopathy (1). As with diabetic retinopathy, these neovascular diseases can be treated effectively with photocoagulation of the ischemic areas. In addition, the direct laser application to leaking vessels can be used to stem immediately the release of fluid and subsequent edema in many of these disorders. Additionally, there is a whole group of neovascular diseases of the choroid that can be treated with either the green argon

Editor's Note:
Review completed Oct.; revised Dec. 28, 1988

(Continued next page)

Best Available Copy

or the red krypton laser. The krypton has been specifically used for choroidal neovascularization because the red beam penetrates through the overlying xanthophyll pigment and also through pigment that may be associated with cataractous changes of the lens (2). Clinical studies are also underway utilizing the krypton yellow and a variety of other wavelengths from the tunable dye laser (3) and the frequency doubled green Nd:YAG laser (4). Thus, through the use of the tunable dye laser, an ever increasing number of eye disorders can be selectively treated by matching structures with a high light absorption to a specific laser wavelength.

Glaucoma is characterized by a buildup of pressure within the eye caused by an interference of the normal outflow of aqueous fluid. The argon laser has been used to photocoagulate selectively portions of the trabecular meshwork which appear to be responsible for the regulation of fluid flow from the eye. Though the precise nature of the argon laser effect on the trabecular meshwork is unknown, it is suspected that the laser may cause a shrinkage or tightening which then permits fluid to pass out of the eye, thus relieving the increased intraocular pressure (5). In a more severe type of glaucoma (angle closure glaucoma), a higher intensity of argon laser radiation may be used to burn a hole directly through the iris (iridotomy) thus permitting the free flow of fluid from the posterior to the anterior chamber of the eye. Because of the large amount of laser energy required, the pulsed Nd:YAG laser may be more effective since it relies upon a shock-wave destructive mechanism rather than thermal photocoagulation although this technique is still experimental (6).

A major advance was the introduction by Aron-Rosa (7) in 1980 of the short pulsed, high peak power Nd:YAG laser for posterior capsule membrane surgery. With the advent of nanosecond (Q-switched) and picosecond (mode-locked) YAG lasers, it has become possible to generate very high power densities (gigawatts/cm^2) in focal spots of 25-50 microns (8). When these lasers are focused precisely on a small spot of tissue, unusual "non-linear" events occur, thereby generating a "plasma", which is a gaseous cloud rich in free electrons. Due to the sudden production of an electrical field in 10^{-9} to 10^{-12} seconds, an intense acoustical shock-wave is generated at the focused spot. When focused just behind the posterior capsule membrane, this acoustic shock-wave moves forward carrying potentially damaging kinetic energy and tears apart the secondary cataract. Primary cataracts are often treated by removal of the clouded lens, followed by implantation of a plastic lens. The surgical procedure, however, all too often causes opacification of the normally transparent posterior membrane behind the implanted lens. Because the membrane is perilously close to the prosthetic lens, this procedure requires a carefully positioned, stable laser beam focus. The technique of posterior capsulotomy now permits non-invasive outpatient treatment for removal of secondary cataract. Early studies demonstrated pitting and cracking in the new lens implants due to laser impact. Later, it was shown that focusing the laser in the vitreous just posterior to the membrane (as opposed to on the membrane itself) eliminated these complications (9). It is very likely that the short pulsed YAG laser will be used in other ophthalmic procedures where a rapid, non-thermal destruction is desired (such as iridotomy).

Currently accepted laser procedures in ophthalmology rely upon the heat producing photocoagulative nature of the light from argon, krypton and tunable dye lasers or the mechanical shock-wave of the pulsed YAG laser. Some new experimental procedures are being developed that utilize non-thermal molecular bond-breaking produced by the excimer laser, and others utilize photochemistry through the interaction of excited porphyrin compounds and the dye laser to produce singlet oxygen. It has been recently demonstrated that the 193 nm ultraviolet wavelength of the ArF excimer laser can ablate corneal tissue by photodissociation of intramolecular bonds without thermal effects. Furthermore, the depth of substrate removal is precisely controllable because, for a fixed energy per pulse (energy per unit area or fluence), there is a linear relationship between etched depth and number of pulses delivered (8). This led to speculation that the excimer laser could be used to produce radial keratotomy incisions of controlled depth and width. Alternatively, the excimer laser has been suggested for use in tangential corneal sculpting instead of as a radial keratotomy device. This technique is more demanding than making radial cuts on the periphery of the cornea, but would allow patients with myopia, hyperopia or astigmatism to be treated. At present, hyperopia or astigmatism cannot be corrected by standard radial keratotomy. However, before these procedures can be accepted clinically, issues surrounding the possible mutagenic and carcinogenic consequences of high intensity ultraviolet radiation as well as questions concerning the non-thermal versus thermal nature of the effects must be resolved.

The photochemical use of porphyrin dyes will be discussed later in this review. Suffice it to say that it is possible to sensitize malignant ocular tumors by the systemic injection of porphyrin compounds, and in combination with 630 nm light, to bring about their selective destruction by photochemistry (10).

Plastic Surgery and Dermatology

Sufficient experience has now been accumulated to determine where the laser has definite applications in plastic surgery and dermatology.

Laser treatment of port-wine stains (PWS) provides an excellent example of the advancement of laser therapy due to an increased understanding of laser-tissue interactions. PWS is a congenital vasculopathy consisting of an abnormal network of capillaries in the outer dermis with an overlying normal epidermis. It occurs most commonly on the face and neck, but may be found anywhere on the body in association with systemic syndromes (11). In the treatment of PWS, the argon laser will pass through the epidermis and then be absorbed by the hemoglobin in the dilated ectatic capillaries in the upper dermis causing thermal damage and thrombosis. Experience has shown that certain types of PWS respond better to this treatment

than others. Increasing age, darker reddish-purple color, location on the face or neck, minimal blanching, and no scarring effect on the test site are all good predictors of improved patient outcome (12). The epidermis is not totally spared and suffers some irreversible damage. Biopsy reveals nonspecific coagulation necrosis of the epidermis and upper dermis which subsequently heals leaving a normal epidermis and diffusely fibrotic upper dermis (13). The test site forms an eschar which is sloughed 10-14 days after treatment leaving the treated site reddened. The latter gradually fades until the final cosmetic result can be assessed in 3-6 months. Results of large clinical studies are encouraging but hypertrophic scarring which occurs in 5-16% of patients remains a worrisome complication (14,15). Good to excellent results with significant color change without scarring occur in 50-80% of cases, and the remaining 20-50% show minimal or no change after treatment (16). In addition, the hypertrophic growth and thickening that these lesions often develop may be smoothed out. One study has suggested that the CO_2 laser may also be of value in the treatment of PWS (17). Interestingly, those patients predicted to respond poorly to argon laser treatment respond best to CO_2 laser therapy (light colored, flat, nonblanchable PWS). Treatment of PWS with the CO_2 laser consists of vaporizing cell layer after layer to reach a depth where the small ectatic vessels are vaporized. Although further studies must be done before this technique is widely accepted, the authors reported good clinical results with the CO_2 laser.

Scarring is the most frequent undesirable result of laser PWS treatments and it appears to be largely related to the degree of epidermal thermal damage (18). Further improvement in treatment results, with reduction in scarring and other side effects may, therefore, depend on the ability to use lasers to induce selective thermal injury of only the abnormal vessels or other targets in the dermis while sparing the normal overlying epidermis. The pulsed dye laser at 577 nm, a wavelength well absorbed by the targeted oxyhemoglobin (HbO_2) molecule relative to other optically absorbing structures, causes highly selective thermal damage to cutaneous blood vessels while minimizing the epidermal melanin absorption (19). Furthermore, the microsecond pulse width produced by the dye laser is on the order of the thermal relaxation time of the tissue. This constant is defined as the time that it takes for a target structure to cool to one half its initial temperature. Thus, if the laser pulse width is suitably brief, the laser energy is invested in the target before much heat is lost by thermal diffusion out of the exposure field. Shorter pulse durations confine the laser energy to progressively smaller targets with more spatial selectivity (20). The pulsed dye laser has been shown to cause selective vascular destruction without damage to the adjacent overlying epidermis and surrounding dermis. Preliminary studies have shown no clinical evidence of hypertrophic scarring, atrophy, induration or hypopigmentation if this laser is used correctly (21-23).

A wide range of other vascular abnormalities such as hemangioma, telangiectasia, lymphangioma, angiofibroma, angiokeratoma and senile angioma have all benefited from treatment with the argon or CO_2 laser (24). Studies employing the argon, CO_2 or Nd:YAG laser for the removal of superficial telangiectasias and varicosities of the lower extremity had previously been discouraging (25), but a recent report using both the superpulsed CO_2 laser and the Nd:YAG laser transmitted through a diffusing sapphire tip did demonstrate significant clinical improvements (26).

Both the argon and CO_2 lasers have been used to treat the decorative tattoo. Successive layers of skin are removed to expose the intradermal pigment which is subsequently vaporized and the wound allowed to heal by re-epithelialization from adjacent skin and undamaged dermal appendages. Because there is no color selective absorption and therefore no epidermal sparing, the treated skin never completely returns to normal and 30-40% of patients have hypertrophic scarring (27,28). Patients must be told what to expect but most are relieved that the original tattoo has been removed.

Skin tumors, both benign and malignant, have been treated with a variety of lasers. The CO_2 laser does have the potential for sealing blood vessels and lymphatics permitting almost a "no touch" tumor removal to be performed. It is possible that the cosmetic results in the treated areas will be superior to those obtained by other methods but conclusive long term studies have not been conducted. Photodynamic therapy (PDT) using red light and photosensitizing dyes has also been successfully used to treat widespread and recurrent head and neck cutaneous malignancies thus precluding the need for multiple, possibly deforming excisions.

Other skin lesions such as papillomatosis, rhinophyma, skin tags, solar keratosis, seborrheic keratosis, xanthelasma, pyogenic granuloma, plantar and hand warts are easily and rapidly vaporized with the CO_2 laser.

Preliminary studies of argon and CO_2 laser treatment of keloid scars have been reported but no long term benefits have been observed (29,30). However, one study did demonstrate that removal of the entire keloid with the CO_2 laser in conjunction with intralesional injections of triamcinolone (40 mg/ml) followed by compression dressings for 3-6 weeks, resulted in 50% of patients achieving an "acceptable" supple, flat scar without recurrence of the keloid (31). This form of therapy may provide a novel treatment modality for a disfiguring and chronic condition.

Gynecology

The laser is increasingly gaining acceptance as the surgical modality of choice for a number of gynecologic clinical entities. Gynecologists have established well defined indications and treatment parameters for the safe use of the CO_2 laser.

(Continued next page)

Best Available Copy

Clinical evidence supports the conclusion that "pre-malignant" cervical intraepithelial neoplasia (CIN) is a progressive disease whose incidence is increasing in young females still in the reproductive stages of life. It is, therefore, critical to preserve the anatomic, sexual, and reproductive integrity of the patient. Results of numerous studies have indicated that the CO_2 laser can be used effectively to eradicate CIN. The treatment includes removal of the entire squamocolumnar transformation zone to a minimum depth of 5-7 mm with a 2-5 mm margin around the lesion. Patients with persistent disease can be retreated without the need for more destructive procedures. The advantages of this technique are outpatient management with little or no local anesthesia, minimal bleeding with rapid wound healing and anatomical and functional conservation. Most series now report 1-5 years follow-up with cure rates of 76-97% (32-34). Intraepithelial neoplasia can involve the vagina (VAIN) or vulva (VIN) and the CO_2 laser has also been found an effective treatment for these sites. Vaporization to eliminate VAIN has resulted in cure rates of 70-90% (35-37). For an upper vaginal lesion, most clinicians vaporize the entire half of the vaginal epithelium. When the disease extends to the lower half of the vagina, the entire vagina is treated to a depth of 1 mm (38). The most undesirable side effects such as scarring, vaginal contracture, and patient discomfort are rare with most patients returning to their pretreatment sexual behavior patterns without dyspareunia. The CO_2 laser has now emerged as the treatment of choice for VIN since cosmetic appearance is of major importance to the patient and it is far less traumatic than the previously used skinning vulvectomy which was frequently painful. Studies show prompt wound healing with no adverse scar formation or dyspareunia (39,40).

Carcinoma in situ of the cervix (CIS) is the precursor to invasive carcinoma and is the most severe form of gynecologic precancer. Laser conization of CIS can now be performed on an outpatient basis under local anesthesia with an average blood loss of 10 ml as compared to 120 ml in the conventionally coned patients (41). Several studies also have shown that laser conization substantially reduces the risk of postconization stenosis as compared to cryosurgery and that the tissue specimens obtained by this method are ample for pathological interpretation (42,43). Vaginal and vulvar carcinoma in situ have both been shown highly responsive to CO_2 laser vaporization which does not produce significant anatomic or functional changes (44,45).

Condyloma acuminata or venereal wart produced by the papilloma virus is a sexually transmitted disease which may be widespread and difficult to treat by conventional techniques. Extensive warts which may cover the vulva and extend into the vagina or anus can be easily and rapidly vaporized by the CO_2 laser which has consistently produced cure rates in excess of 90% (46,47). The major reason for recurrence is inadequate follow-up or failure to examine adequately and treat infected male partners (48).

Recently the Nd:YAG laser has been proposed for the treatment of menorrhagia by endometrial ablation via the hysteroscope in patients with excessive bleeding. The laser was used to vaporize the entire endometrium and was successful in 96% of patients in whom other forms of therapy failed or who were otherwise poor risks for hysterectomy (49).

Adaptation of the CO_2 laser to the operating microscope and laparoscope has now provided surgeons with a technique to ablate, vaporize and excise a wide range of intra-abdominal pathology. Dense adhesive bands can be quickly and bloodlessly lysed by the microscopically directed laser beam. In the treatment of endometriosis, use of a micromanipulator allows the laser beam to be rapidly swept over all endometrial implants with finite accuracy without the need for laparotomy. Numerous investigators have used CO_2 lasers to excise obstructed oviducts with subsequent "welding" of the tissues (50,51). While conflicting reports appear in the literature concerning the incidence of post-operative adhesions using these techniques, studies have documented increased tubal patency rates often in patients who have already failed other treatment modalities for infertility (52,53).

A new surgical laser, the potassium-titanyl-phosphate 532 laser (KTP/532) produces a visible green light beam at a wavelength of 532 nm which can easily be passed through a disposable flexible fiber in the laparoscope, has recently emerged for gynecologic use. Initial investigation of the KTP/532 laser demonstrated the effective laparoscopic vaporization of endometrial implants without complications in ten patients (54). The applicability of the KTP/532 laser has also been recently established in the procedures of fimbrioplasty, pelvic adhesiolysis and transection of the uterosacral ligaments (55). This laser also has the advantage of being used in combination with the hysteroscope in the treatment of septate uteri, submucosal fibroids and benign polyps whereas the CO_2 laser cannot for technical reasons.

General Surgery and Associated Subspecialties

Although surgery is considered to be the most aggressive medical discipline, general surgeons have been the last specialty group to widely embrace the laser. Sufficient experience has been accumulated to determine that the laser can be a useful tool in many general surgical procedures. Certainly in those procedures where major blood loss is expected, the CO_2 laser with its ability to seal intra-operatively blood vessels less than 1 mm in diameter, thus reducing blood loss and post-operative morbidity, is clearly advantageous (56,57). The Nd:YAG laser is now gaining acceptance for use in the debulking of large vascular tumors, partial splenectomies and liver resections (58). Contact probes developed from synthetic sapphire crystals for Nd:YAG laser have been used successfully in liver and pancreatic resections. The optical properties, geometric design, and thermal conductivity of these sapphire probes may be more effective than the current conventional noncontact method of delivering laser energy through a quartz fiber. Potential advantages include greater precision, sterilizability, avoidance of tip melting and a requirement for lower Nd:YAG laser energy with reduced tissue damage (59,60).

In the case of malignant disease where it is highly desirable to perform en bloc excision of the primary tumor including the surrounding lymph nodes, the CO_2 laser's ability to seal lymphatics and tissue planes, makes it possible to perform precise removal of cancerous tissue with maximum normal tissue preservation and minimal mechanical damage. This allows the surgeon, in some cases, to perform a less radical excision while at the same time preventing seeding, dissemination, and recurrence of the tumor (61). Additionally, photodynamic therapy (see below) with porphyrins in combination with 630 nm light can be used to destroy malignant tissue selectively. Furthermore, exposure to blue/violet light will cause these photosensitizers to fluoresce and this property can be used to localize sites of malignancy not identifiable grossly.

A consideration in every surgical subspecialty is the excision of highly infected tissues. The ability of the CO_2 laser to excise gangrene and decubitus ulcers while at the same time sterilizing the surgical field of bacteria and viruses has been particularly well demonstrated (62).

Another area in general surgery where the laser has been shown effective is in the palliative treatment of obstructive endotracheal/bronchial (63,64) and esophageal (65) malignancies, in which the Nd:YAG laser beam passed endoscopically, was used to vaporize the obstructing tumor. Treatments may be repeated and in the case of bronchial malignancy, follow-up bronchoscopy is needed to remove necrotic tumor by suctioning.

Acute bleeding from the upper gastrointestinal tract has been controlled by photocoagulation with the Nd:YAG (66) and argon (56) lasers with a significant reduction in the rate of rebleeding. Bleeding from a variety of lesions including esophageal varices, Mallory-Weiss tears, gastric and duodenal ulcers, and vascular malformations such as the telangiectasia of Osler-Weber-Rendu have been successfully controlled with lasers although further studies are needed to determine the optimum treatment parameters. Laser therapy is especially useful in those patients with massive hemorrhage who are at high risk because of concurrent cardiac, pulmonary or renal pathology. The complication of acute or delayed bowel perforation which may occur 2-4 days post-procedure remains the principal risk. Recently numerous reports on the uses of both the CO_2 and Nd:YAG lasers for hemorrhoidectomy with good results have appeared in the literature (60,67). These studies suggest that there is faster healing, less bleeding, less pain, less scarring and fewer complications following laser surgery. However, results are still very preliminary and not consistent for all patients.

In urology, Nd:YAG lasers have been shown useful in the treatment of superficial malignant bladder tumors. In the management of urethral stricture where recurrence is common after dilatation, results so far have been controversial. The use of the CO_2 laser in the treatment of condyloma acuminata has already been discussed in the section on gynecology, but other premalignant or malignant lesions of the penis such as penile dysplasia, carcinoma in situ and penile cancer can be treated with either the CO_2 or Nd:YAG laser with excellent cosmetic results (68). Patients with ureteral calculi present a difficult and often challenging therapeutic problem. Attempts to use laser generated shock-waves to destroy ureteral stones by conversion of light energy into heat and shock-wave energy at the target surface and thereby fragment them, have to date produced encouraging results (69,70). Detailed studies on fragmentation effectiveness in vivo at various energy levels and pulse durations as well as studies of the secondary effects on the ureter have yet to be reported.

In neurosurgery, a wide range of tumors including gliomas, astrocytomas and metastases have been removed with vaporization of the tumor cavity with either the CO_2 or Nd:YAG laser. It has been shown in most cases that the operative exposure and need for retraction are reduced as are the operative time and intraoperative blood loss (71). Some pituitary tumors have been removed with the CO_2 laser via the transfrontal route or through the transsphenoidal route using the Nd:YAG laser. A small number of cases have been reported where Nd:YAG lasers were helpful in the surgical management of arteriovenous malformations (72). The feeding vessels were initially coagulated, divided, and the malformation removed. The argon laser has been shown useful in the excision of small (less than 3 cm), moderately vascular, critically located lesions such as angiomas, low-flow arteriovenous malformations and hemangioblastomas of the brainstem (73). Results with photodynamic therapy (see below) in neurosurgery have so far been discouraging although removal of the tumor by conventional means followed by PDT of the tumor bed could theoretically be helpful.

In otolaryngology, the CO_2 laser can be used to remove congenital and post-traumatic stenoses of the larynx and upper aerodigestive tract with excellent hemostasis although recurrence of the scar tissue remains a problem. In addition, the CO_2 laser has become the treatment of choice for respiratory papillomatosis. Undoubtedly, the laser's greatest contribution to this field is in the early removal of vocal cord, laryngeal and oropharyngeal carcinomas without the need for more radical surgery. In advanced cases, tumor bulk can be reduced which may contribute to the success of other therapeutic modalities. In removal of leukoplakia and other premalignant lesions of the oral cavity, the laser vaporizes pathological mucosa identified by staining. Post-operative wound healing is slow but subsequent biopsies indicated good removal of the lesions. Small lesions of the mouth and tongue may also be easily excised by the CO_2 laser with minimal blood loss. The Nd:YAG laser can be used to reduce bleeding from extensive hemangiomas and lymphangiomas without great loss of functional tongue mass (74).

In orthopaedics where joint replacement surgery can lead to excessive blood loss, the CO_2 laser's ability to seal vessels as it cuts through muscle tissue is impressive (75). Current research is focused on the development of laser

(Continued next page)

Best Available Copy

systems to cut bone and remove bone cement inserted into artificial joints. A recent study suggested the feasibility of using a mid-infrared Erbium.YAG laser (2.94 um) to ablate both bone and methacrylate with minimal thermal damage to adjacent tissue (76).

Photodynamic Therapy

The attack on cancer with drugs is based upon the thesis that it should be possible to discriminate against cancer cells while having only few or tolerable effects on normal cell populations. While many compounds have been screened for such activity over the past forty years, unfortunately most solid cancers respond either not at all, or to a limited extent only, to these selective agents.

Photodynamic therapy (PDT) by exposure of certain dyes to visible light has been studied since the beginning of this century. The basic concept for the use of PDT in the treatment of malignant tumors is that certain molecules (natural or applied) can function as photosensitizers. The presence of these photosensitizers in certain tumor cells makes the latter vulnerable to light at wavelengths absorbed by the chromophore. The action of photosensitizers is generally to absorb photons of the appropriate wavelength and intensity sufficient to elevate the sensitizer to an excited state. The excited photosensitizer subsequently reacts (transfers its energy) with a molecular substrate, such as oxygen, to produce highly reactive singlet oxygen which causes irreversible oxidation of some essential cellular component. Uncertainty arises as to the exact targets of these excited intermediates responsible for cell death although damage to the cell membrane, mitochondria, lysosomes, microsomes and the nuclear material have all been reported.

While numerous compounds have been tested as selective photosensitizers of malignant cells, considerable interest in the porphyrins was stimulated by early reports on inherent porphyrin fluorescence in large malignant tumors (77). While several porphyrins have been studied, hematoporphyrin derivative (HpD) has received the most attention (78). Although the mechanism of HpD's preferential localization and retention in malignant cells remains uncertain, it is well established that the total time HpD is retained in malignant tissue is much longer than in nonmalignant tissue from which it is generally cleared in 24-72 hours (79). As a result, there is a "window" of time wherein one can exploit the differences in HpD concentration to achieve selective photodegradation of malignant tissue.

Clinically, PDT is carried out by a two-step procedure. HpD is first administered intravenously as a 2-5 mg/kg bolus. After a delay of 24-72 hours (to allow for the accumulation of HpD in the tumor and for the clearing from most normal tissues), the tumor is irradiated with visible red light tuned to 630 nm. The radiation is generally obtained from an argon-pumped dye laser although more conventional light sources have been shown effective. The light may be delivered to the surface of the tumor, interstitially via optical fibers or endoscopically to deep tumors of the digestive, pulmonary, or urogenital tract. Topical application of HpD has also been proposed but only preliminary results have been reported (80). Shortly after PDT, the tumor becomes necrotic (usually within 24 hours) and when effectively treated, forms a nonpalpable scab, sloughed off within a few days. Histologically, the earliest changes occur in and around the tumor vasculature. Apparent internal hemorrhage with red blood cell extravasation is a common finding after PDT, not only in most experimental animal tumors but in tumors in patients as well (81). Furthermore, another study suggests that the effects of PDT are not the result of direct tumor cell kill, but are secondary to destruction of the tumor microvasculature (82). Binding of photosensitizers to collagen and other fibers in the subendothelial zone of the tumor vessel wall, in combination with altered permeability and transport through the endothelial cell layer resulting from erythrocyte swelling and increased intraluminal pressure, may be the key features of the dye-sensitized photodynamic reaction leading to tumor destruction.

HpD-PDT has been shown effective in causing photodegradation of tumor tissue in experimental animal systems since 1972 (83) and in clinical trials since 1976 (78,84,85). A wide variety of tumors with varying histologic types have been treated, including cancers of the skin (86), female genital tract (87), esophagus (88), lung (89), bladder (90), eye (91), breast (92), head and neck squamous cell carcinomas (93). The overall positive response rate as reported in the literature is greater than 70% (88). The high therapeutic ratio and relative lack of morbidity have made this a very attractive form of therapy. Treatment parameters have been refined such that therapy can be undertaken with a reasonable expectation of good results. While PDT can be used to eradicate relatively large tumors, it appears to be especially advantageous to patients with early disease or early recurrence. In some cases this therapy may be a viable alternative to debilitating surgery, and in others, the treatment of choice. In addition, previous surgery, radiation therapy, or chemotherapy do not preclude the use of PDT and many of the clinical studies reported to date have been on patients who have previously failed some, or all other, available therapies.

The fluorescent properties of HpD can also be used in the detection and localization of tumors not detected by more conventional techniques. Studies have shown that HpD fluorescence induced by the blue/violet 405 nm light of the krypton laser can be used successfully to detect occult lung tumors (94) and delineate dysplasia and tumors in the bladder (95). In these clinical trials, the exciting light was delivered via a single quartz fiber in the biopsy channel of a bronchoscope or cystoscope fitted with appropriate filters and an image intensifier to observe the fluorescing (red) light which can be directly observed and recorded. Normal mucosa, and tumors in patients not receiving HpD, were seen not to be fluorescent.

Despite HpD's broad experimental application in clinical oncology, efforts have been hampered by the lack of a complete understanding of what active component in the HpD molecule is responsible for tumor uptake, retention, fluorescence and photosensitization. Even with apparent-

y pure preparations of the individual HpD components, impurities have often complicated the interpretation of data. The active component has been described as a structural isomer of dihematoporphyrin ether (96) or ester (97). Furthermore, the component responsible for photochemistry is not necessarily the same as the component responsible for fluorescence (98). Even though there is an increased tumor neighboring tissue porphyrin content ratio following HpD administration, the amount retained by normal tissues such as skin, liver, spleen and kidney is clinically significant. The major drawback of this therapy is the potential for drug-induced sensitivity to sunlight. This effect is not trivial and may result in complications ranging from slight erythema and edema to extensive skin sloughing and necrosis. The foregoing problems as well as a relatively weak porphyrin absorption band and low tissue transparency a 630 nm, have resulted in considerable effort being devoted to developing new and more effective tumor localizing photosensitizers for PDT.

There is a recent report on the use of a chlorin compound, mono-L-aspartyl chlorin, as a photosensitizer for selective tumor necrosis (99). The chlorins are known to have strong absorption bands with high molar extinction coefficients at wavelengths longer than 650 nm thus providing an advantage over the lower tissue penetrance of 630 nm light used for HpD. Chlorin in combination with light at 664 nm was shown to be an effective tumor localizer and photosensitizer in Balb-C mice inoculated with EMT-6 tumor. Furthermore, it was suggested that this compound may not be retained in high skin concentrations thus minimizing the photosensitivity associated with HpD.

The phthalocyanines, used as industrial dyes and pigments, are porphyrin-like compounds capable of localizing and photosensitizing malignant tumors. These compounds are easily synthesized and purified and exhibit strong absorption in the 650-700 nm range (100). The metal atom complexed with the phthalocyanine ring is critical and studies have demonstrated that aluminum phthalocyanine (AlPc) is the most active photosensitizer (101). AlPc contains a mixture of isomers with varying degrees of sulfonation and the relationship between degree of sulfonation and tumoricidal activity is still under study. AlPc has been shown active in vitro and in vivo and, in at least one study, not to induce skin damage in the presence of ambient light (102).

While the studies on chlorins and phthalocyanines appear promising, they are still at an early stage. Neither of these compounds has been tested in humans and HpD remains the clinical standard for comparison. The greater tissue penetrance of the longer wavelength and the reduced residual skin photosensitivity give these compounds decided advantages over HpD. However, unanswered questions concerning these compounds include delineation of light and drug dosimetry parameters, mechanism of tumor uptake and retention, as well as possible uptake in other organ systems. It is hoped that future investigations will address these critical questions so that the role of other potential photosensitizing compounds in the management of cancer can be fully defined.

Laser-Assisted Microsurgical Anastomosis

Since it had been demonstrated that the laser can seal small blood vessels, lymphatics, alveoli, renal tubules and bile canaliculi, it became a logical clinical extension that if treatment parameters could be refined, the laser might be used to anastomose or "weld" tissues together.

Various techniques have been utilized to perform laser assisted microsurgical anastomosis (LAMSA) and sufficient data has now been generated to make the following general observations. Laser welding occurs at power exposures much lower than those required to coagulate or cut tissue. Grossly apparent tissue changes associated with a good thermal weld include an apparent "drying" of the tissues. Brown discolorization or charring and circumferential constriction of the structure at the anastomotic site should be avoided as they reflect extensive thermal damage. Tight abutment of the severed ends and good apposition of the entire circumference of the structures to be welded are crucial to success. Loose apposition will lead to inadequate fusion which will result in leaks. Precision in the delivery of the laser energy is paramount. Power and the spot size must be well controlled. The power needed to obtain the best anastomosis depends upon the inherent nature of the tissues to be welded and their thickness. Although the mechanism of laser welding is not completely understood, it seems likely that the heat generated by the laser causes protein denaturation allowing the seal of the wound edges. It is also possible that activation of the tissue reactions necessary for normal wound healing such as fibrin clot formation may be involved.

Although numerous researchers have attempted to weld many different kinds of tissue together, the largest volume of data has been published on the laser welding of small blood vessels (103,104,105). Controlled animal studies show that laser assisted microvascular anastomoses have the potential advantages of reduced operative time, less trauma due to less mechanical manipulation of the vessel which should reduce the chance of thrombosis, and elimination of the foreign body response to suture material. Furthermore, laser energy can be delivered precisely through optical fibers via the operating room microscope. The largest published series (106) on vessels with a mean diameter of 1.2 mm show that the wound healing originates in the adventitial and perivascular tissues and progresses towards the lumen. Endothelialization begins about 5 days after welding and is complete at 2-3 weeks. The tensile strength of the laser weld when compared to conventionally sutured anastomoses is weaker in the first 2 weeks after surgery, but by 3 weeks is comparable to the intact vessel and may be stronger than the sutured anastomoses. The overall incidence of aneurysm formation (7%) and patency rates (95%) were comparable to, or even better than, those reported using various conventional suture techniques. The application of laser assisted microsurgical anastomosis to large

(Continued next page)

arteries and veins requires further study to define the surgical techniques and laser parameters necessary to obtain the best results.

Microanastomoses of other structures such as vas deferens (107), bowel (108), skin (109) and fallopian tube (110) have been shown to be practical but conclusive long term studies are not yet available.

Cardiovascular

The nonsurgical approaches to hemodynamically significant cardiovascular obstruction have gained widespread popularity since the advent of percutaneous balloon angioplasty. Although angioplasty is usually effective, there is a significant rate of recurrence that approaches 30-40% in some series (111,112). Furthermore, it is not useful in cases of total obstruction unless the catheter can be passed mechanically through the occluded area. The impetus in the field has, therefore, been redirected at developing new ways to treat such obstructions by debulking and removing atheromatous material. The laser beam, which can be delivered precisely through optical fibers passed via vascular catheters, is theoretically a suitable instrument to open obstructive lesions within the vascular tree. Thus, laser angioplasty may have the following possible roles: (1) to decrease the incidence of restenosis by either removing the bulk of the atheromatous plaque or leaving behind a smoother intimal surface, and (2) to enhance the ability to recanalize lesions that are difficult or impossible to treat by conventional balloon angioplasty. Although the concept of laser angioplasty is relatively new, investigation of potential cardiovascular applications of lasers is being pursued at several centers, but most procedures are still experimental.

Laser radiation generated in the infra-red, visible and ultraviolet regions of the spectrum has been demonstrated to vaporize atherosclerotic plaque both in vitro and in situ in post-mortem specimens (113,114,115). However, where there is plaque ablation, the transfer of heat energy due to thermal conduction and dissipation may occur into the adjacent normal vessel wall. Although the immediate effects of laser induced-arterial wall injury are obvious, the long term effects are unknown. If this technique is to achieve widespread clinical use, this important question must be answered. It is hoped that if the treatment parameters can be refined such that plaque removal can be accomplished without damaging the normal vessel wall, the principal complication of atherolysis, perforation of the underlying wall, might be readily avoided.

One way to improve the therapeutic index might be to sensitize the atheromatous plaque with a photodynamic compound activated by laser light. Several compounds including tetracycline and hematoporphyrin derivative (HpD) have been studied but the results to date have been inconclusive (116,117). One study demonstrated that HpD sensitized atheroma could be surgically excised (endarterectomy) with less laser energy than non-sensitized atheroma (118).

With the development of flexible fiberoptics (119), the argon laser was the first laser to be used both experimentally and clinically for laser angioplasty. It has now been demonstrated in several clinical trials (120,121) that percutaneous transluminal argon laser angioplasty can be safely performed in humans and can establish patency in occluded peripheral vessels, especially in the lower extremities. Despite the fact that the laser fiberoptic was positioned in the center of the arterial lumen inside an angiographic or balloon angioplasty catheter, there was still a 15-20% incidence of vessel perforation. Angioscopy has been proposed as one technique to avoid this hazard. However, in one study (122) with direct angioscopic visualization of peripheral vascular lesions during laser therapy, there was actually a higher incidence of vessel perforation compared to previous studies where the fluoroscopic approach was used.

In addition to the hazard of perforation, in vivo laser angioplasty has been limited by the fact that the recanalized channels produced by the laser were too narrow resulting in poor long term patency. Recently introduced has been a laser-heated metallic-capped fiberoptic device in which the argon laser energy is converted to thermal energy in the enclosed cap of the fiberoptic (123). When brought into contact with atherosclerotic plaque, the laser cap conducts its heat to the plaque, so that no laser light is actually emitted. Studies have shown a lower incidence of perforation and greater angiographic success when compared with direct argon laser vaporization even in patients with lesions that were considered difficult or impossible to treat by conventional means (124,125). In this initial series, the perforation rate was less than 2%. Furthermore, when compared to conventional balloon angioplasty, laser thermal angioplasty resulted in significantly less stenosis and a larger patent vessel lumen documented by angiogram 4 weeks post-procedure.

Even more impressive is a report of laser thermal angioplasty in successfully recanalizing coronary arteries in 7 of 8 patients with severe angina and high grade (80-90%) stenosis in the relatively straight proximal or mid portion of the vessels (126). While this report is promising, it must still be cautioned that no long term benefit has yet been proven and therefore coronary laser angioplasty remains an experimental modality. At this stage, it is only reasonable to suggest that the application of laser technology to recanalize coronary vessels has great potential especially in those patients with medical conditions that would preclude major surgery. Further research is needed to understand the energy ranges required to vaporize plaque and still avoid vessel perforation.

The ability of the excimer laser to remove predictable amounts of surface material with microscopically sharp edges and without associated thermal damage to adjacent tissue, led to the suggestion that this laser could have important cardiovascular applications. In vitro and in vivo studies have demonstrated that excimer lasers at several ultraviolet wavelengths can cut precise craters in vascular atheromatous plaque (127). Of technological importance is the development of a suitable fiber optic to deliver ultraviolet laser energy percutaneously to an obstructed blood vessel. It is very difficult to transmit short laser pulses

produced by excimer lasers through optical fibers: the shorter the pulse, the higher the peak pulse power and the more likely is fiber damage. This problem is compounded with the excimer laser because the shorter and more useful wavelengths are increasingly absorbed by quartz, especially in the presence of impurities. Lengthening the wavelength relaxes the fiber requirements, and it is now possible to transmit up to 40 mJ per pulse through fibers at a wavelength of 308 nm which has been shown to produce ablation of plaque in human cadaver arteries (128). Preliminary reports now indicate that excimer laser recanalization can be achieved in experimentally occluded canine arteries (129) and in human peripheral arterial occlusion (130).

Open laser endarterectomy which allows the investigator to visualize the alignment of the fiber optic with the plaque has also been studied. The optimal site for removal of atherosclerotic plaque is a plane located within the media (after removing the intima and internal elastic lamina) which cannot be accurately determined by transluminal angioplasty. Open laser endarterectomy which allows in vivo evaluation of plaque removal has been shown to leave a smooth, even surface within the media without complications. The open endarterectomy procedure also offers the advantage of allowing the surgeon to "weld" the laser endpoints to the media to ensure a secure and smooth transition zone leading to less thrombus formation (131).

Other cardiovascular applications of the laser have been reported, such as definitive cure of drug resistant tachyarrhythmias with the argon (132) and Nd:YAG (133) lasers by photoablation of abnormal conduction tissue within the heart. The laser has also been used to create atrial septostomy in patients with congenital heart defects, calcified aortic valvuloplasty as well as myotomy to relieve hypertrophic cardiomyopathy and idiopathic hypertrophic subaortic stenosis.

References

1. L'Esperance, F. Ophthalmic laser photocoagulation, photoradiation and surgery. St Louis: Mosby, 1983.
2. Gass, DM. "Present indications and future promise of the krypton laser". In: March, WF, ed. Ophthalmic lasers current clinical uses. Thorofare, NJ: Slack Inc., 97, 1984.
3. L'Esperance, F. "Current use of the dye laser". In: March, WF, ed. Ophthalmic lasers: current clinical uses. Thorofare, NJ: Slack Inc., 273, 1984.
4. Mosier, MA, Champion, J, Liaw, L-H and Berns, MW. "Delayed retinal effects of the frequency-doubled YAG laser (532 nm)". Invest. Ophthal. Vis. Sci. 28:1298, 1987.
5. Wise, JB and Witter, SL. "Argon laser therapy for open angle glaucoma: a pilot study". Arch. Ophthal. 97:319, 1979.
6. Spaeth, G. "Use of YAG laser in performing peripheral iridectomies". In: March, WF, ed. Ophthalmic lasers: current clinical uses. Thorofare, NJ: Slack Inc., 57, 1984.
7. Aron-Rosa, D, Avon, J and Griesermann, J. "Use of the neodymium YAG laser to open the posterior capsule after lens implant surgery". J. Amer. Intraocul. Implant Soc. 6:352, 1980.
8. Trokel, S. Laser ophthalmic microsurgery. Norwalk, CT: Appleton-Century-Crofts, 209, 1983.
9. Gaasterland, DE. "Fundamental aspects of light and lasers for the ophthalmologist". In: Aron-Rosa, D, ed. Pulsed YAG laser surgery. Thorofare, NJ: Slack Inc., 9, 1983.
10. Murphee, AL, Doiron, DR, Gomer, CJ, Szirth, B and Fountain, SW. "Hematoporphyrin derivative photoradiation treatment of ophthalmic tumors". Clayton Foundation Symposium on Porphyrin Localization and Treatment of Tumors, 1983.
11. Esterly, NB and Solomon, NM. "Neonatal dermatology III". J. Pediatr. 81:1003, 1972.
12. Noe, JM, Barsky, SH, Gur, DE and Rose, S. "Port wine stains and the response to argon laser therapy: successful treatment and the predictive role of color, age and biopsy". Plast. Reconstr. Surg. 65:130, 1980.
13. Apfelberg, DB, Maser, MR and Lash, H. "Histology of port wine stains". Plast. Reconstr. Surg. 32:232, 1979.
14. Apfelberg, DB, Maser, MR and Lash, H. "The argon laser for cutaneous lesions". JAMA 245:2073, 1981.
15. Maser, MR, Apfelberg, DB and Lash, H. "Clinical applications of the argon and carbon dioxide lasers in dermatology and plastic surgery". World J. Surg. 7:684, 1983.
16. Silver, L. "Argon laser photocoagulation of port wine stain hemangiomas". Lasers Surg. Med. 6:24, 1986.
17. Ratz, JL and Bailin, PL. "The case for the use of the carbon dioxide laser in the treatment of portwine stains". Arch. Dermatol. 123:74, 1987.
18. Olbricht, SM, Stern, RS, Tang, SV, Noe, JM and Arndt, KA. "Complications of cutaneous laser surgery: a survey". Arch. Dermatol. 123:345, 1987.
19. Anderson, RR and Parrish, JA. "Optical properties of skin". In: Regan, JD and Parrish, JA, eds. The science of photomedicine. New York: Plenum Press, 147, 1982.
20. Anderson, RR and Parrish, JA. "Selective photothermolysis: precise microsurgery by selective absorption of pulsed radiation". Science 220:524, 1983.

(Continued next page)

Best Available Copy

21. Morelli, JG, Tan, OT, Garden, JM, Margolis, R, Sek, Y, Boll, J, Carney, JM, Anderson, RR, Furumoto, H and Parrish, JA. "Tunable dye laser (577 nm) treatment of port wine stains". Lasers Surg. Med. 6:94, 1986.
22. Garden, JM, Tan, OT, Kerschman, R, Boll, J, Furumoto, H, Anderson, RR and Parrish, JA. "Effect of dye laser pulse duration on selective cutaneous vascular injury". J. Invest. Dermatol. 87:653, 1987.
23. Garden JM, Polla, LL and Tan, OT. "The treatment of port-wine stains by the pulsed dye laser". Arch. Dermatol. 124:889, 1988.
24. Kaplan, I. "The CO_2 laser in plastic surgery". Lasers Surg. Med. 6:385, 1986.
25. Apfelberg, DB, Maser, MR, Lash, H, White, DN and Flores, JT. "Use of argon and carbon dioxide lasers for treatment of superficial venous varicosities of the lower extremities". Lasers Surg. Med. 4:221, 1984.
26. Apfelberg, DB, Smith, T, Maser, MR, Lash, H, and White, DN. "Study of three laser systems for treatment of superficial varicosities of the lower extremity". Lasers Surg. Med. 7:219, 1987.
27. Apfelberg, DB, Rivers, J, Maser, MR and Lash, H. "Update on laser usage in the treatment of decorative tattoos". Lasers Surg. Med. 2:269, 1982.
28. Levin, H and Bailin, PL. "Carbon dioxide laser treatment of cutaneous hemangiomas and tattoos". Arch. Otolaryn. 108:236, 1982.
29. Apfelberg, DB, Maser, MR, Lash, H, White, DN and Weston, J. "Preliminary results of argon and carbon dioxide laser treatment of keloid scars". Lasers Surg. Med. 4:283, 1984.
30. Henderson, DH, Cromweil, TA and Mes, LG. "Argon and carbon dioxide laser treatment of hypertrophic and keloid scars". Lasers Surg. Med. 3:271, 1984.
31. Kantor, GR, Wheeland, RG, Bailin, PL, Walker, NPJ and Ratz, JL. "Treatment of earlobe keloids with carbon dioxide laser excision: a report of 16 cases". J. Dermatol. Surg. Oncol. 11:1063, 1985.
32. Bendet, JL, Nickerson, KG and White, GW. "Laser therapy for cervical intraepithelial neoplasia". Obstet. Gynecol. 58:188, 1981.
33. Baggish, MS. "Laser Management of cervical intraepithelial neoplasia". Clin. Obstet. Gynecol. 26:989, 1983.
34. Bellina, JH and Wright VC. "Carbon dioxide laser management of cervical intraepithelial neoplasia". Am. J. Obstet. Gynecol. 141:828, 1981.
35. Pertrilli, ES and Townsend, DE. "Vaginal intraepithelial neoplasia: biological aspects and treatment with topical 5-fluorouracil and the carbon dioxide laser". Am. J. Obstet. Gynecol. 138:321, 1980.
36. Capen, CV, Materson, BJ, Margrina, JF and Calkins, JW. "Laser therapy of vaginal intraepithelial neoplasia". Am. J. Obstet. Gynecol. 142:973, 1982.
37. Jobson, VW and Homesley, HD. "Treatment of vaginal intraepithelial neoplasia with the carbon dioxide laser". Obstet. Gynecol. 62:90, 1983.
38. Baggish, MS. "The state of the art of laser surgery in gynecology". Lasers Surg. Med. 6:390, 1986.
39. Townsend, DE, Levine, RU, Richart, RM, Christopher, RC and Pertrilli, ES. "Management of vulvar intraepithelial neoplasia by carbon dioxide laser". Obstet. Gynecol. 60:49, 1982
40. Ferenczy, A. "Using lasers to treat condyloma and VIN". Cont. Obstet. Gynecol. 20:57, 1982.
41. Meandzija, MP, Locher, G and Jackson, JD. "CO_2 laser conization versus conventional conization: a clinicopathological appraisal". Lasers Surg. Med. 4:139, 1984.
42. Dorsey, JH and Everett, DS. "Microsurgical conization of the cervix by carbon dioxide lasers". Obstet. Gynecol. 54:566, 1979.
43. Larsson, G, Gullberg, B and Grundsell, H. "A comparison of complications of laser and cold knife conization". Obstet. Gynecol. 62:213, 1983.
44. Townsend, DE, Levine, RU, Crum, CP and Richart, RM. "Treatment of vaginal carcinoma in situ with the carbon dioxide laser". Am. J. Obstet. Gynecol. 143:565, 1982.
45. Baggish, MS. "Treatment of vulvar carcinoma in situ". Obstet. Gynecol. 57:371, 1981.
46. Baggish, MS. "Carbon dioxide laser treatment for condylomata acuminata venereal infections". Obstet. Gynecol. 55:711, 1980.
47. Stanhope, CR, Garth, DP, Stuart, GC and Reid, R. "Carbon dioxide laser surgery". Obstet. Gynecol. 61:624, 1983.
48. Baggish, MS. "Improved laser techniques for the elimination of genital and extragenital warts". Am. J. Obstet. Gynecol. 153:545, 1985.
49. Goldrath, M, Futter, T and Segal, S. "Laser photovaporization of endometrium for the treatment of menorrhagia". Am. J. Obstet. Gynecol. 140:14, 1981.
50. Baggish, MS and Chong, CP. "Carbon dioxide laser microsurgery of the uterine horn". Obstet. Gynecol. 58:111, 1981.
51. Bellina, JH. "Microsurgery of the fallopian tube with the carbon dioxide laser: analysis of 230 cases". Lasers Surg. Med. 3:255, 1983.
52. Baggish, MS. "Status of the carbon dioxide laser for infertility surgery". Fertil. Steril. 40:442, 1983.
53. Kelly, RW and Roberts, DK. "Experience with the carbon dioxide laser in gynecologic microsurgery". Am. J. Obstet. Gynecol. 146:586, 1983.
54. Daniell, JF, Miller, W and Tosh, R. "Initial evaluation of the use of the potassium-titanyl-phosphate (KTP/532) laser in gynecologic laparoscopy". Fertil. Steril. 46:373, 1986.
55. Daniell, JF, Meisels, S, Miller, W and Tosh, R. "Laparoscopic use of the KTP/532 laser in nonendometrial pelvic survery". Colposc. Gynecol. Laser Surg. 2:107, 1986.
56. Dixon, JA. Surgical applications of lasers. Chicago: Year Book Medical Publishers, 1983.
57. Bohigian, JM. "Lasers in surgery and medicine: council on scientific affairs". JAMA 256:900, 1987.
58. Joffe, SN. "Lasers in general surgery". Lasers Surg. Med. 7:89, 1987.
59. Daikuzomo, N and Joffe, SN. "Artificial sapphire probe for contact photocoagulation and tissue vaporization with the Nd:YAG laser". Med. Instrum. 19:173, 1985.
60. Joffe, SN. "Contact neodymium:YAG laser surgery in gastroenterology: a preliminary report". Lasers Surg. Med. 6:155, 1986.

61. Aronoff, BL. "The state of the art in general surgery and surgical oncology" Lasers Surg Med 6:376, 1986.
62. Chegin, VM, Skobelkin, OK and Brekhov, EI. "Laser surgery of soft tissue purulent diseases". Lasers Surg. Med. 4:279, 1984.
63. Joyner, LR, Maran, AG, Sarama, R and Yababost, A. "Neodymium YAG laser treatment of intrabronchial lesions: a new mapping technique via the fiberoptic bronchoscope". Chest 87:418, 1985.
64. Kao, SJ, Shen, CY and Hsu, K. "Nd:YAG laser application in pulmonary and intrabronchial lesions". Lasers Surg. Med. 6: 296, 1986.
65. Karlin, DA, Fisher, RS and Krevsky, B. "Prolonged survival and effective palliation in patients with squamous cell carcinoma of the esophagus following endoscopic laser therapy". Cancer 59:1969, 1987.
66. Dwyer, R. "The history of gastrointestinal endoscopic laser hemostasis and management". Endoscopy 18:10, 1986.
67. Sankar, MY and Joffe, SN. "Technique of contact laser hemorrhoidectomy: an ambulatory surgical procedure". Contemp. Surg. 30:9, 1987.
68. Hofstetter, A. "Lasers in urology". Lasers Surg. Med. 6:412, 1986.
69. Dretler, SP, Watson, G, Parrish, JA and Murray, S. "Pulsed dye laser fragmentation of ureteral calculi: initial clinical experience". J. Urol. 137:386, 1987.
70. Benderev, TV, and Martin, DC. "Pulsed dye-laser lithotripsy of ureteral stones". Lasers Surg. Med. 7:112, 1987.
71. Beck, OJ. "The use of the Nd:YAG and CO_2 lasers in neurosurgery". Neurosurg. Rev, 3:261, 1980.
72. Wharren, RE, Anderson, RE and Sundt, TM. "The Nd:YAG laser in neurosurgery: part II, clinical studies". J. Neurosurg. 60:540, 1984.
73. Edwards, MSB, Boggan, JE and Fuller, TA. "The laser in neurological surgery". J. Neurosurg. 59:555, 1983.
74. Ossoff, RH, and Duncavage, JA. "Past, present and future uses of lasers in otolaryngology — head and neck surgery". In: Apfelberg, DA, ed. Evaluation and installation of surgical laser systems. New York: Springer-Verlag, 127, 1986.
75. Horoszowski, H, Heim M and Farine, I. "The carbon dioxide laser in orthopaedic surgery". In: Ben-Hur, E and Rosenthal, I, eds. Photomedicine, Vol. III. Boca Raton, FL: CRC Press Inc., 61, 1987.
76. Nelson, JS, Yow, L, Liaw, L-H, Macleay, L, Zavar, RB, Orenstein, A, Wright, WH, Andrews, JJ and Berns, MW. "Ablation of bone and methacrylate by a prototype mid-infrared erbium:YAG laser". Lasers Surg. Med. 8:494, 1988.
77. Policard, A. "Etudes sur les aspects offerts par des tumeurs experimentales examinee a la lumiere de woods". C. R. Soc. Biol. (Paris) 91:1423, 1924.
78. Dougherty, TJ, Kaufman, JE, Goldfarb, A, Weishaupt, KR, Boyle, DG and Mittelman, A. "Photoradiation for the treatment of malignant tumors". Cancer Res. 38:2628, 1978.
79. Berns, MW, Dahlman, A, Johnson, F, Burns, R, Sperling, D, Guiltinan, M, Siemens, A, Walter, R, Wright, W, Hammer-Wilson, M, and Wile, A. "In vitro cellular effects of hematoporphyrin derivative". Cancer Res 42:2325, 1982.
80. McCullough, J, Weinstein, G, Rettenmaier, M and Berns, MW. "Cutaneous photosensitization by topical hematoporphyrin derivative formulations: potential clinical applications". Proc. Int. Cong. on Applications of Lasers and Electro-Optics, 37:47, 1984.
81. Nelson, JS, Liaw, L-H and Berns, MW. "Tumor destruction in photodynamic therapy". Photochem. Photobiol. 46:829, 1987.
82. Nelson, JS, Liaw, L-H, Orenstein, A, Roberts, WG and Berns, MW. "Mechanism of tumor destruction following photodynamic therapy with hematoporphyrin derivative, chlorin and phthalocyanine". J. Natl. Cancer Inst. 80:1599, 1988
83. Diamond, I, Granelli, SG, McDonagh, AF, Nielson, F, Wilson, CB and Jaenicke, R. "Photodynamic therapy of malignant tumors". Lancet 2:1175, 1972.
84. Forbes, IJ, Cowled, PA, Leong, CY, Ward, AD, Black, RB, Blake, AJ and Jacka, FJ. "Phototherapy of human tumors using hematoporphyrin derivatives". Med. J. Aust. 2:489, 1980.
85. Dahlman, A, Wile, AG, Burns, RG, Mason, GR, Johnson, FM and Berns, MW. "Laser photoradiation therapy of cancer". Cancer Res. 43:430, 1983.
86. Dougherty, TJ. "Photoradiation therapy for cutaneous and subcutaneous malignancies". J. Invest. Dermatol. 77:122, 1981.
87. Rettenmaier, MA, Berman, ML, DiSaia, PJ, Burns, RG, McCullough, J and Berns, MW. "Gynecologic uses of photoradiation therapy". In: Doiron, DR and Gomer, CJ, eds. Advances in experimental medicine and biology, Vol. 170. New York: Liss, 767, 1984.
88. Dougherty, TJ. "Photodynamic therapy (PDT) of malignant tumors". CRC Critical Reviews in Oncology and Hematology 2:83, 1984.
89. Hayata, Y and Kato, H. "Applications of laser phototherapy in the diagnosis and treatment of lung cancer". Jap. Ann. Thoracic Surg. 3:203, 1983.
90. Benson, RC. "Laser photodynamic therapy for bladder cancer". Mayo Clin. Proc. 61:859, 1986.
91. Bruce, BA. "Evaluation of hematoporphyrin photoradiation therapy to treat choroidal melanoma". Lasers Surg. Med. 4:59, 1984.
92. Dougherty, TJ, Lawrence, G, Kaufman, GH, Boyle, D, Weishaupt, KR and Goldfarb, A. "Photoradiation treatment of recurrent breast carcinoma". J. Natl. Cancer Inst. 62:231, 1979.
93. Wile, AG, Dahlman, A, Burns, RG, and Berns, MW. "Laser photoradiation therapy of cancer following hematoporphyrin sensitization". Lasers Surg. Med. 2:163, 1982.
94. Profio, AE, Doiron, DR and King, EG. "Laser fluorescence bronchoscopy for localization of occult lung tumors". Med. Phys. 6:253, 1979.
95. Benson, RC, Farrow, GM, Kinsey, JH, Cortese, DA, Zincke, H and Utz, DC. "Detection and localization of in situ carcinoma of the bladder with hematoporphyrin derivative". Mayo Clin. Proc. 57:548, 1982.
96. Dougherty, TJ. "The structure of the active component of hematoporphyrin derivative". In: Doiron, DR and Gomer, CJ, eds. Porphyrin localization and treatment of tumors. New York: Liss, 301, 1984.
97. Kessel, D, Chang, CK and Musselman, B. "Structure of the tumor-localizing derivative of hematoporphyrins". In: Kessel, D, ed. Methods of porphyrin photosensitization. New York: Plenum Press, 213, 1986.

(Continued next page)

98. Nelson, JS and Berns, MW. "Biological studies on the main fractions of hematoporphyrin derivative". Cancer Res. 47:1027, 1987.

99. Nelson, JS, Roberts, WG and Berns, MW. "In vivo studies on the utilization of mono-L-aspartyl chlorin (NPe6) in photodynamic therapy". Cancer Res. 47:4681, 1987.

100. Ben-Hur, E and Rosenthal, I. "The phthalocyanines: a new class of mammalian cell photosensitizers with a potential for cancer phototherapy". Int. J. Radiat. Biol. 47:145, 1985.

101. Ben-Hur, E and Rosenthal, I. "Photosensitized inactivation of chinese hamster cells by phthalocyanines". Photochem. Photobiol. 42:129, 1985.

102. Bown, SG, Traulau, CJ, Coleridge-Smith, PD, Akdemir, D and Wieman, TJ. "Photodynamic therapy with porphyrin and phthalocyanine sensitization: quantitative studies in normal rat liver". Br. J. Cancer 54:717, 1986.

103. Sartorius, CJ, Shapiro, SA, Campbell, RL, Klatte, EC and Clark, SA. "Experimental laser-assisted end-to-side microvascular anastomosis". Microsurg. 7:79, 1986.

104. Quigley, MR, Bailes, JE, Kwaan, HC, Cerullo, LJ, Brown, JT and Fitzsimmons, J. "Comparison of bursting strength between suture and laser anastomosed vessels". Microsurg. 6:229, 1985.

105. White, RA, Kopchok, G, Donayre, C, Lyons, R, White, G, Klein, SR, Abergel, RP and Uitto, J. "Laser welding of large diameter arteries and veins". TASAIO 32:181, 1986.

106. Neblett, CR, Morris, JR, and Thomsen, S. "Laser-assisted microsurgical anastomosis". Neurosurg. 19:914, 1986.

107. Lynne, CM, Carter, M, Morris, J, Dew, D, Thomsen, S and Thomsen, C. "Laser-assisted vas anastomosis: a preliminary report". Lasers Surg. Med. 3:261, 1983.

108. Mercer, CD, Minich, P and Pauli, B. "Sutureless bowel anastomosis using the Nd:YAG laser". Lasers Surg. Med. 7:90, 1987.

109. Abergel, RP, Lyons, R, Dwyer, R, White, RA and Uitto, J. "Use of lasers for closure of cutaneous wounds: experience with Nd:YAG, argon and CO_2 lasers". J. Dermatol. Surg. Onc. 12:1181, 1986.

110. Choe, JK, Darwood, MY and Andrews, AH. "Conventional versus laser reanastomosis of rabbit ligated uterine horns". Obstet. Gynecol. 61:689, 1983.

111. Meier, B, King, SB, Gruentzig, AR, Douglas, JS, Hollman, J, Ischinger, T, Galen, K and Tankersley, R. "Repeat coronary angioplasty". J. Am. Coll. Cardiol. 4:463, 1984.

112. Levine, S, Ewels, CJ, Rosing, DR and Kent, KM. "Coronary angioplasty: clinical and angiographic follow-up". Am. J. Cardiol. 55:673, 1985.

113. Abela, GS, Normann, S, Cohen, D, Feldman, RL, Geiser, EA and Conti, CR. "Effects of carbon dioxide, Nd:YAG and argon laser radiation on coronary atheromatous plaques". Am. J. Cardiol. 50:1199, 1982.

114. Geschwind, H, Boussignac, G and Teisseire, B. "Percutaneous transluminal laser angioplasty in man". Letter to the editor. Lancet 1:844, 1984.

115. Isner, JM, Donaldson, RF, Deckelbaum, LI, Clarke, RH, Laliberte, SM, Ucci, AA, Salem, DN and Konstam, MA. "The excimer laser: gross, light microscopic and ultrastructural analysis of potential advantages for use in laser therapy of cardiovascular disease". J. Am. Coll. Cardiol. 5:1102, 1985.

116. Murphy-Chutorian, D, Kosek, J, Mok, W, Quay, S, Huestis, W, Mehigan, J, Profitt, D and Ginsburg, R. "Selective absorption of ultraviolet laser energy by human atherosclerotic plaque treated with tetracycline". Am. J. Cardiol. 55:1293, 1985.

117. Spears, JR, Serur, J, Shropshire, D and Paulin, S. "Fluorescence of experimental plaques with hematoporphyrin derivative". J. Clin. Invest. 71:395, 1983.

118. Pollock, ME, Eugene, J, Hammer-Wilson, M and Berns, MW. "Photosensitization of experimental atheromas by porphyrin". J. Amer. Coll. Card. 9:639, 1987.

119. Choy, DSJ, Stertzer, S, Rotterdam, HZ, Sharrock, N and Kaminow, I. "Transluminal laser catheter angioplasty". Am. J. Cardiol. 50:1206, 1982.

120. Ginsberg, R, Wexler, L, Mitchell, RS and Profitt, D. "Percutaneous transluminal laser angioplasty for treatment of peripheral vascular disease: clinical experience with 16 patients". Radiol. 156:619, 1985.

121. Cumberland, DC, Taylor, DI and Procter, AE. "Laser-assisted percutaneous angioplasty: initial clinical experience in peripheral arteries". Clin. Radiol. 37:423, 1986.

122. Abela, GS, Seeger, JM, Barbieri, E, Franzini, J, French, A, Pepine, CJ and Conti, CR. "Laser angioplasty with angioscopic guidance in humans". J. Amer. Coll. Cardiol. 8:184, 1986.

123. Hussein, H. "A novel fiberoptic laser probe for treatment of occlusive vessel disease". Optical Laser Technol. Med. 605:59, 1986.

124. Sanborn, TA, Greenfield, AJ, Guben, JK, Menzoian, J and LoGerto, FW. "Human percutaneous and intraoperative laser thermal angioplasty: initial clinical results as an adjunct to balloon angioplasty". J. Vascular Surg. 5:83, 1987.

125. Sanborn, TA, Cumberland, DC, Greenfield, AJ, Welsh, CL and Guben, JK. "Percutaneous laser thermal angioplasty: initial results and one year follow-up of 129 femoropopliteal lesions". Radiol. 168:121, 1988.

126. Sanborn, TA, Faxon, DP, Kellett, MA, Jacobs, AK and Ryan, TJ. "Percutaneous coronary laser thermal angioplasty with a metallic capped fiber". J. Amer. Coll. Cardiol. 9:104A, 1987.

127. Grundfest, WS, Litvak, F, Goldenberg, T, Sherman, T, Morgenstern, L, Carroll, R, Fishbein, M, Forrester, J, Margitan, J, McDermid, S, Pacala, TJ, Rider, DM and Laudenslager, JB. "Pulsed ultraviolet lasers and the potential for safe laser angioplasty". Am. J. Surg. 150:220, 1985.

128. Litvak, F, Grundfest, WS, Papaioannou, T, Mohr, FW, Jakubowski, T and Forrester, JS. "Role of laser and thermal ablation devices in the treatment of vascular diseases". Am. J. Cardiol. 61:81G, 1988.

129. Forrester, JS, Litvak, F and Grundfest, WS. "Laser angioplasty and cardiovascular disease". Am. J. Cardiol. 57:990, 1986.

130. Wollenek, G, Laufer, G and Grabenwoger, F. "Percutaneous transluminal excimer laser angioplasty in total peripheral artery occlusion in man". Lasers Surg. Med. 8:464, 1988.

131. Eugene, J, McColgan, SJ, Pollock, ME, Hammer-Wilson, M, Moore-Jeffries, EW and Berns, MW. "Experimental arteriosclerosis treated by conventional and laser endarterectomy". J. Surg. Res. 39:31, 1985.

132. Saksena, S and Gadhoke, A. "Laser therapy for tachyarrhythmias: a new frontier". PACE 9:531, 1986.

133. Selle, JG, Svenson, SH, Sealy, WC, Gallagher, JJ, Zimmern, SH, Fedor, JM, Marroum, MC and Robicsek, F. "Successful clinical laser ablation of ventricular tachycardia: a promising new therapeutic model". Ann. Thorac. Surg. 42:380, 1986.

▲ End

ABSTRACT FORM

AMERICAN SOCIETY FOR LASER MEDICINE AND SURGERY, INC.

313 Second Street, Suite 200
Wausau, WI 54401
Phone (715) 845-9283

APRIL 11-13, 1987 - SAN FRANCISCO, CALIFORNIA - SEVENTH ANNUAL MEETING

Type name, address and telephone of author who receives correspondence in box A and complete boxes B, C, D, E, F
ABSTRACTS MUST BE POSTMARKED NO LATER THAN OCTOBER 20, 1986

Michael W. Berns

Beckman Laser Institute and Medical Clinic
1002 Health Sciences Road East
Irvine, California 92717

PHONE (714) 856-6996

B. PAPER PRESENTATION (Not Required)

X 35 mm. Slides ___ 3/4" U-Matic
(Must be requested in advance)

F. FILM SESSION Time Requested ___
Maximum 10 Min.

___ 16 mm. ___ 3/4" U-Matic
___ Beta 1/2" ___ VHS 1/2"

TYPE ABSTRACT BELOW - BE SURE TO STAY WITHIN BORDER

CATEGORIES (Check one)

Basic Science & Safety	X
Biostimulation, Pain Control (Low Dose Effects)	___
Cardiovascular	___
Endoscopic Applications (GI,GU,ENT,Pulmonary)	___
General Surgery	___
Gynecology	___
New Devices & Instrumentation	___
Nursing	___
Oncology	___
Ophthalmology	___
Plastic/Dermatology	___
Podiatry	___
Film Session	___
Poster (4 x 8)	___
Scientific Exhibit	___

The principal author affirms that all persons named in this abstract have agreed to submission for presentation and that material herein will not have been published in an abstract or article by April 1987.

Michael W. Berns
Signature of Author

I hereby give permission for my abstract to be published in LASERS IN SURGERY AND MEDICINE and for my presentation to be taped by the Society with the understanding that tapes will subsequently be offered for sale.

Michael W. Berns
Signature of Author

BIOLOGICAL STUDIES ON THE FREE ELECTRON LASER. Michael W. Berns*, William Bewley**, Luis R. Elias**, and Vincent Jaccarino**. *Beckman Laser Institute, University of California, Irvine, Irvine, CA 92717 and **Department of Physics, University of California, Santa Barbara Santa Barbara, CA 93106.

Preliminary biological experiments have been performed on the free electron laser at UCSB. The biological system was rat kangaroo kidney epithelial cells growing in Rose culture chambers on 0.3 mm thick fused silica or quartz windows. The cells were exposed to the laser beam entering from the window surface with no water interface between the cells and the window. All initial experiments were conducted with FEL operating at 200 um, 2 usec pulse duration, and 0.5 - 3 kW per pulse. Beam profiles for the laser emission was determined prior to each experiment and revealed an energy profile that demonstrated that 75% of the energy was contained in a .5 cm diameter spot in the center of an overall 2.5 cm diameter spot at the culture surface. Transmission through the silica and quartz windows were 65% and 95% respectively. Cultures were exposed to from 1-200 pulses, and followed for up to 48 hours during which time cells were incubated in tritiated thymidine (concentration 2.5 uCi/ml with specific activity 60 Ci/mmole for 48 hours), and tritiated uridine (concentration 1.0 mCi/ml with specific activity 17 Ci/mmole for 18 hours). Autoradiography was performed and the degree of labeling compared to controls (no FEL) was determined. The results of three series of experiments involving irradiation of 100 culture chambers has revealed that the FEL at the wavelength, power and energy densities used results in a consistent reduction by 3-8% in the number of cells exibiting a high degree of tritiated thymidine incorporation. Similarly there was reduction by 5-10% in the number of cells incorporating a high amount of tritiated uridine. These experiments do indicate an inhibition of both DNA and RNA synthesis in a fraction of the cell population exposed to the FEL. The nature of this alteration and the reason why other cells are unaffected are currently under invescigation.

Supported by Office of Naval Research grant N00014-86-K-0115

AMERICAN SOCIETY FOR LASER MEDICINE AND SURGERY, INC.

813 Second Street, Suite 200
Wausau, WI 54401
Phone (715) 845-9283

APRIL 11-13, 1987 - SAN FRANCISCO, CALIFORNIA - SEVENTH ANNUAL MEETING

Type name, address and telephone of author who receives correspondence in box A and complete boxes B,C,D,E, & F.
ABSTRACTS MUST BE POSTMARKED NO LATER THAN OCTOBER 20, 1986

A. NAME Michael W. Berns

ADDRESS Beckman Laser Institute

1002 E. Health Sciences Rd.

Irvine, Ca 92715

TELEPHONE (714) 856-6291

E. PAPER PRESENTATION Time Requested 10 min. (Maximum 10 Min.)

XX 35 mm. Slides ___ 3/4 " U-Matic (Must be requested in advance)

F. FILM SESSION Time Requested ___ (Maximum 10 Min.)

___ 16 mm. ___ 3/4 " U-Matic

___ Beta 1/2" ___ VHS 1/2"

B. CATEGORIES (Check one)

Basic Science & Safety	___
Biostimulation, Pain Control (Low Dose Effects)	___
Cardiovascular	___
Endoscopic Applications (GI,GU,ENT,Pulmonary)	___
General Surgery	___
Gynecology	___
New Devices & Instrumentation	___
Nursing	___
Oncology	XX
Ophthalmology	___
Plastic/Dermatology	___
Podiatry	___
Film Session	___
Poster (4 x 8)	___
Scientific Exhibit	___

C. The principal author affirms that all authors named in this abstract have agreed to its submission for presentation and that the material herein will not have been published in an abstract or article by April, 1987.

Signature of Author

D. I hereby give permission for my abstract to be published in LASERS IN SURGERY AND MEDICINE and for my presentation to be taped by the Society with the understanding that the tapes will subsequently be offered for sale.

Signature of Author

IN VITRO CHARACTERIZATION OF MONO-L-ASPARTYL CHLORIN(NPe6) FOR PHOTODYNAMIC THERAPY. W. Gregory Roberts, Chung-Ho Sun and Michael W. Berns. Dept. of Surgery, Beckman Laser Institute and Medical Clinic, Univ. of CA-Irvine, Irvine, CA. 92715. The cellular characteristics of Mono-L-Aspartyl Chlorin (NPe6) have been studied by determining the amount of phototoxicity, subcellular localization and physical characteristics in vitro and were compared to Dihematoporphyrin Ester (DHE). Cell killing efficiency was determined by dose response curves and subcellular localization was determined by using fluorescent microscopy. The absorption and fluorescent spectra were also determined. The cell lines used were the PTK_2 and the Balb/3T3 clone A31. Laser irradiation was performed with an argon dye laser system tuned to emit radiation at 630nm for DHE treated cells, and at 664um for NPe6 treated cells. The fluorescence emission spectrum of NPe6 in PTK_2 cells shows a single peak at 665nm. Cells incubated with NPe6 for 48 hrs show discrete brightly staining particles in the cytoplasm under the fluorescent microscope Cells treated with acridine orange, a known lysosome staining fluorochrome, show the same discrete particles, whereas DHE stains the nucleus, membrane and cytoplasm. Dose response studies reveal that virtually all of the cells treated with 3.0 ug/ml DHE for 24 hrs are killed and only 70% are killed with 12.5ug/ml NPe6 (24 hrs). However, there is an increased killing efficiency with 72 hrs treatment with NPe6, whereas, DHE shows decreased killing efficiency with 72 hrs of treatment. Photodynamic therapy with HPD or DHE has been limited in its effectiveness to treat cancers due to the low level of tissue penetrance at 630nm. The emission spectrum peak at 665nm is a useful wavelength for photodynamic therapy due to increased tissue penetrance. The fluorescent micrographs show specific localization of NPe6 solely into lysosomes suggesting a different mechanism of cellular uptake and subcellular specificity in comparison to DHE. Although DHE appears more potent, the dose response curves for NPe6 show that it is an effective phototoxic agent in vitro with PTK_2 and 3T3 cells. It is also important to note that none of the control cells which received NPe6 without light were adversly affected by the drug alone, suggesting NPe6 is not cytotoxic unless photoactivated.

Funded by NIH 3 R01 CA 32248-03S1

ABSTRACT FORM

AMERICAN SOCIETY FOR LASER MEDICINE AND SURGERY, INC.

813 Second Street, Suite 200
Wausau, WI 54401
Phone (715) 845-9283

APRIL 11-13, 1987 - SAN FRANCISCO, CALIFORNIA - SEVENTH ANNUAL MEETING

Type name, address and telephone of author who receives correspondence in box A and complete boxes B,C,D,E, & F
ABSTRACTS MUST BE POSTMARKED NO LATER THAN OCTOBER 20, 1986

A. NAME J. Stuart Nelson

ADDRESS Beckman Laser Institute and Medical Clinic

1002 Health Sciences Road East

Irvine, California 92717

TELEPHONE (714) 856-6996

D. PAPER PRESENTATION Time Requested 10 Minutes Maximum

X 3/4 " U-Matic Video

___ 3/4 " U-Matic
(Must be requested in advance)

E. FILM SESSION Time Requested ____ Maximum 10 Min

___ 16 mm.

___ 3/4 " U-Matic

___ Beta 1/2"

___ VHS 1/2"

TYPE ABSTRACT BELOW - BE SURE TO STAY WITHIN BORDER

MECHANISM OF TUMOR DESTRUCTION IN PHOTODYNAMIC THERAPY.

J. Stuart Nelson, L.-H. Liaw and Michael W. Berns.
Beckman Laser Institute and Medical Clinic, University of California, Irvine, Irvine, CA 92717.

One of the major unanswered questions of PDT is the precise mechanisms of tumor destruction. In order to fully appreciate the potential of HpD-PDT, it is necessary to characterize the role of the vasculature in bringing about the tumoricidal effect. Because of the complex nature of the tumor vasculature in HpD-PDT, we have undertaken a series of experiments aimed at elucidating the effects of HpD-PDT on the tumor microvasculature during the first few hours after phototherapy. DBA/2Ha mice bearing SMT-F tumors received intraperitoneal injections of 10 mg/kg of Photofrin II and 24 hours later tumors were treated with 100 J/cm^2 of light (630 nm). Animals were sacrificed and their tumors removed at time 0, 30 min, 1 hr, 2 hrs, 8 hrs, 16 hrs and 24 hrs after treatment. The effects of HpD-PDT on the tumor vasculature were examined at the light microscope (LM) and electron microscope (EM) levels. Our study demonstrates that the first observable changes occur in the elastic fibers and endothelial cells lining the tumor microvasculature. These structural subunits of the vasculature lose their functional integrity and are ultimately destroyed within the first 2-4 hrs after phototherapy. This is followed by diffuse hemorrhage into the surrounding perivascular stroma with subsequent tumor cell death. The results indicate that the effects of PDT are primarily initially direct destruction of the tumor microvasculature with subsequent tumor cell death.

Supported by NIH grants CA 32248 and RR 01192.

C. CATEGORIES (Check one)

Basic Science & Safety	___
Biostimulation, Pain Control (Low Dose Effects)	___
Cardiovascular	___
Endoscopic Applications (GI,GU,ENT,Pulmonary)	___
General Surgery	___
Gynecology	___
New Devices & Instrumentation	___
Nursing	___
Oncology	X
Ophthalmology	___
Plastic/Dermatology	___
Podiatry	___
Film Session	___
Poster (4 x 8)	___
Scientific Exhibit	___

F. The principal author affirms that all authors named in this abstract have agreed to its submission for presentation and that the material herein will not have been published in an abstract or article by April, 1987.

Signature of Author

G. I hereby give permission for my abstract to be published in LASERS IN SURGERY AND MEDICINE and for my presentation to be taped by the Society with the understanding that the tapes will subsequently be offered for sale.

Signature of Author

Post Available

ABSTRACT FORM

AMERICAN SOCIETY FOR LASER MEDICINE AND SURGERY, INC.

313 Second Street, Suite 200
Wausau, WI 54401
Phone (715) 845-9283

APRIL 11-13, 1987 - SAN FRANCISCO, CALIFORNIA - SEVENTH ANNUAL MEETING

Type name, address and telephone of author who receives correspondence in box A and complete boxes B,C,D,E, & F.
ABSTRACTS MUST BE POSTMARKED NO LATER THAN OCTOBER 20, 1986

A.
NAME Kenton W. Gregory, M.D.

ADDRESS Beckman Laser Institute and Medical Clinic
1002 Health Sciences Road East
Irvine, California 92715

TELEPHONE (714) 856-6996

E. PAPER PRESENTATION Time Requested 10 Maximum 10 Min.

x 35 mm. Slides ___ 3/4 " U-Matic (Must be requested in advance)

F. FILM SESSION Time Requested ___ Maximum 10 Min.

___ 16 mm. ___ 3/4 " U-Matic

___ Beta 1/2" ___ VHS 1/2"

B. CATEGORIES (Check one)

Basic Science & Safety	___
Biostimulation, Pain Control (Low Dose Effects)	___
Cardiovascular	x
Endoscopic Applications (GI,GU,ENT,Pulmonary)	___
General Surgery	___
Gynecology	___
New Devices & Instrumentation	___
Nursing	___
Oncology	___
Ophthalmology	___
Plastic/Dermatology	___
Podiatry	___
Film Session	___
Poster (4 x 8)	___
Scientific Exhibit	___

C. The principal author affirms that all authors named in this abstract have agreed to its submission for presentation and that the material herein will not have been published in an abstract or article by April, 1987.

Kenton W. Gregory
Signature of Author

D. I hereby give permission for my abstract to be published in LASERS IN SURGERY AND MEDICINE and for my presentation to be taped by the Society with the understanding that the tapes will subsequently be offered for sale.

Kenton W. Gregory
Signature of Author

TYPE ABSTRACT BELOW - BE SURE TO STAY WITHIN BORDER

CORONARY LASER ANGIOPLASTY IN AN ATHEROSCLEROTIC HUMAN XENOGRAFT-SWINE MODEL. Kenton W. Gregory, Warren D. Johnston, Roger A. Nahais, John A. Mallory, Peter Grandaw, Michael W. Berns, and Walter L. Henry, Division of Cardiology and Beckman Laser Institute and Medical Clinic, University of California, Irvine, Irvine, CA. The application of laser energy to human coronary angioplasty has great promise but concern remains regarding adverse vascular consequences such as vessel perforation or thrombosis. Design limitations of laser catheters and fibers have revolved around the lack of a suitable animal model of human atherosclerosis. We have developed a xenograft model using atherosclerotic human coronary arteries (C.A.) microdissected within hours of donor expiration. The left main, anterior descending (L.A.D.) and circumflex (L.C.X.) C.A. are then available for implantation as a unit. 200 lb. swine undergo general anesthesia, thoracotomy and anastomosis of the left main C.A. xenograft into the proximal aorta. A 'Y' graft into the swine left anterior descending (L.A.D.) C.A. receives the distal segments of the human LAD/LCX C.A. Human C.A. branches are attached to the swine pericardium to provide realistic anatomical position and cardiac motion. It is then possible to cannulate the human xenograft by percutaneous catheterization to evaluate laser fiber/catheter systems in a realistic in vivo setting as well as the study of the downstream effects of laser angioplasty of human atherosclerosis on swine myocardial contractility, hemodynamics and electrical stability. Human and swine tissues are subsequently available for gross and microscopic study. We conclude that this model provides a relatively inexpensive, expedient and versatile method to evaluate the clinical utility of various interventions and devices such as laser angioplasty catheters on human atherosclerotic lesions. Supported by NIH grants HL 31318 and RR 01192.

1.6 - Burstein 4yr Project

also Short file on Arvo ARVO meeting / abstract

WOUND HEALING AFTER CORNEAL ABLATION BY 193 nm EXCIMER LASER IN RABBITS

Neal L. Burstein[1],

Ronald N. Gaster[1],

Perry Binder[2],

and

Michael Berns[1]

From: [1]The University of California, Irvine, California, and [2]The University of California, San Diego, California

*Reprint Requests: Neal L. Burstein, Ph.D., Department of Ophthalmology, University of California, Irvine, California 92717

ABSTRACT

The 193 nm argon fluoride excimer laser was used to ablate corneal tissue over a wide area at the center of the rabbit cornea. The ablations had no detectable effect on endothelium even when made to 80% depth through the stroma Epithelium rehealed over the ablated areas slightly slower than over intact basal lamina, and more rapidly than over a lamellar keratectomy. The results indicate that a reshaping of the corneal surface involving less than 30% of the corneal thickness could result in optical correction of both spherical and astigmatic problems, with greater accuracy of correction than is presently available. Further development of the optical system is necessary, together with the determination of short and long-term epithelial wound healing in primates, before human studies are attempted.

FEL Contractors Meeting
Washington, DC
5/22 - 5/23/88

ABSTRACT

A CENTRALIZED LASER FOR MEDICINE: PRINCIPLES AND PRACTICE AT THE BECKMAN LASER INSTITUTE. Michael W. Berns. Department of Surgery, Beckman Laser Institute and Medical Clinic, University of California, Irvine, Irvine, CA 92717.

The impetus for much of the biomedical work on the FEL has been the desire to build a laser that can be centralized in a treatment facility. Such a device should be tunable over a broad region of the "laser" spectrum and relatively easy to use. In designing and building the Beckman Laser Institute and Medical Clinic, we have been confronted with many of the same issues. The idea of centralized lasers has required the consideration of multiple user, room, and laser devices as well as efficient fiber optic delivery systems. Of particular concern was the consideration of simultaneous use of the same laser system at different power outputs. In addition, the consideration of different users at different locations requiring different wavelengths at the same time must be considered. All of these issues have been considered (but not necessarily solved) in developing our facility. These same considerations should not be lost sight of in the early developlment and justification of the FEL for medical use.

used to report last - full w
Heart part fill

60th Scientific Sessions Abstract Form

American Heart Association

Medical Research
Nursing Research

November 16-19 '987
Anaheim Convention Center, Anaheim California

Number _____
Please do not fill in!

Please read instructions before typing abstract.

Deadline Date: Abstracts must be postmarked no later than Monday, May 11, 1987.

For review and grading, assign this abstract to the grading category listed below:

Choice 1 Number 41

Choice 2 Number 9

Identify two key words or phrases from the abstract indexing list to be used for indexing in the supplement to *Circulation*, an AHA journal

1. 1380 Laser
2. 1143 Coronary Vessels

Properties of Atherosclerotic Coronary Arteries Exposed to Laser Heated Tip

N. Charle Morcos, Michael Berns and Walter L. Henry, University of California, Irvine, CA

Effects of Laser heated tip angioplasty on arteries is not fully understood. We report histology, ultrasound properties and vasoreactivity of human atherosclerotic coronary arteries after exposure to hot tip catheter. Segments of isolated human coronary arteries were obtained within 5 hours post mortem, side branches ligated and perfused with Krebs solution. Coronary artery segments with high grade stenosis and occlusion were recanalyzed using a 1.5 mm tip heated twice with 10 W Argon laser for 10 seconds while two-dimensional 12 MHz ultrasound images were recorded. Images documented vessel recanalization and an increase in ultrasound refractile properties of vessel walls adjacent and 5 mm distal to the heated tip. Histologic studies showed charring along the neolumen and extensive coagulation pattern within the plaque. Vasoreactivity was assessed by measuring flow rate changes during perfusion with 100 ml of 10-5M seratonin followed by washout with serotonin free solution. Re-canalized arteries showed a 50% increase in magnitude of vasospasm which was persistent for 5 hours compared to control atherosclerotic vessels which relaxed within 30 minutes. In conclusion, laser heated tip irradiated vessels demonstrated plaque coagulation, increased ultrasound refractile properties of plaque and increased vasospasm which persisted for several hours.

The author affirms that the material herein will not have been published as a manuscript prior to presentation or presented at any national meeting or world congress held in the United States, that any animal studies conform with the "Position of the American Heart Association on Research Animal Use" (*Circulation* 71:349 A, 1985) and that any human experimentation has been conducted according to a protocol approved by the institutional committee on ethics of human investigation or — if no such committee exists — that it conforms with the principles of the Declaration of Helsinki of the World Medical Association (*Clinical Research* 14:193, 1966).

Author's signature N. Charle Morcos MD

The undersigned certifies that all authors named in this abstract have agreed to its submission for presentation at the AHA Scientific Sessions, and are familiar with the ten-author rule (see "Rules for Submitting Abstracts").

N. C. Morcos

Best Available Copy

60th Scientific Sessions Abstract Form

American Heart Association

Medical Research
Nursing Research

November 16-19, 1987
Anaheim Convention Center, Anaheim, California

Number _____
Please do not fill in!

Please read instructions before typing abstract.

Deadline Date: Abstracts must be postmarked no later than Monday, May 11, 1987.

Laser-Assisted Angioplasty of Human Peripheral Arteries.

Jonathan Tobis, John Mallery, Michael Berns, Warren D Johnston, Walter L Henry; University of California, Irvine, CA

Laser energy has recently been used to recanalize completely occluded peripheral arteries. This study of laser angioplasty was performed with digital angiographic acquisition for quantitative analysis to determine the characteristics that might affect outcome of the procedure. Recanalization of completely occluded peripheral arteries was performed in 16 patients using an Argon laser heated tip fiberoptic probe. Mean length of total occlusion was 11.7cm (range 0.5-26.0 cm). Mean diameter of the normal segment was 4.4mm and mean diameter of the narrowest segment post laser and balloon dilatation was 4.2mm by edge detection and 3.6mm by videodensitometry ($p < 0.05$). Mean Doppler ankle/ arm index was 0.61 before and 0.93 post procedure. There were 11 (69%) primary successful procedures. Parameters that affected success were length of the obstruction and vessel tortuosity. Artery diameter distal to the occlusion did not affect outcome. Early reocclusion occurred in 2 pts due to poor runoff or intimal disruption. In one of these 2, collateral vessels did not disappear after apparently successful recannalization. Thus, laser assisted angioplasty is useful for re-establishing a patent lumen in long, completely occluded peripheral arteries that might otherwise require bypass surgery.

For review and grading, assign this abstract to the grading category listed below:

Choice 1 Number 31

Choice 2 Number 30

Identify two key words or phrases from the abstract indexing list to be used for indexing in the supplement to *Circulation*, an AHA journal:

1. 1380 Laser
2. 1019 Angioplasty, transluminal

The author affirms that the material herein will not have been published as a manuscript prior to presentation or presented at any national meeting or world congress held in the United States, that any animal studies conform with the "Position of the American Heart Association on Research Animal Use" (*Circulation* 71:849 A, 1985) and that any human experimentation has been conducted according to a protocol approved by the institutional committee on ethics of human investigation or — if no such committee exists — that it conforms with the principles of the Declaration of Helsinki of the World Medical Association (*Clinical Research* 14:193, 1966).

Author's signature Jon Tobis

The undersigned certifies that all authors named in this abstract have agreed to its submission for presentation at the AHA Scientific Sessions, and are familiar with the ten-author rule (see "Rules for Submitting Abstracts").

ASCB
11/16/87 -
11/20/87
St. Louis

Presentation Preference: CHOOSE ONE ONLY

Category Code: B3
Category Name: Micro Dynam Assem

☒ POSTER ONLY — do not consider for minisymposium

☐ CONSIDER FOR MINISYMPOSIUM Abstract not selected for minisymposium will be placed in poster presentation

☐ MINISYMPOSIUM ONLY — Abstract will be **automatically withdrawn** if not selected for minisymposium

☐ FILM SESSION — (16mm, ¾" VHS & BETA will be available and will handle all formats If film is used, specify type of projector and length of presentation. _____

OFFICE USE ONLY

Category code must be designated above
MINISYMPOSIUM CODE: ____ ____ ____
MINISYMPOSIUM TITLE: _____

INSTRUCTIONS

For Typing

IMPORTANT: TYPE-SIZE must be equal to, or larger than, EXAMPLE below.

- **Symbols and letters not available in type should be hand-printed in black ink with fine pen.**
- **Type single space, use clean type and new BLACK silk or carbon ribbon.**
- **Abstracts prepared on a word processor are acceptable if printed on a high quality impact printer, such as a daisy wheel, which produces typewriter-quality print. Abstracts printed on a low-quality impact printer, such as a dot matrix, are not acceptable.**

For Corrections

- **DO NOT ERASE: Use correction tape or fluid, or correcting typewriter.**
- **PROOFREAD ABSTRACT: Each Abstract is printed exactly as you prepare it.**
- **Photo-copies of Abstract form or Abstract forms from previous years are not acceptable.**

For Title

- **Type title in upper and lower case letters. Underline title.**
- **Use INITIALS ONLY for authors' names; use same initials on every Abstract.**
- **Underline names and initials of authors.**
- **If Sponsor is not an author, type "Intr. by (Sponsor's name.)" after the address.**

For Text

- **Indent five spaces: type Abstract in one paragraph; leave no top or left margins.**

Start here: TITLE and TEXT MUST fit within the lines

Dynamics of Microtubule Assembly in Vivo. W. Tao and M. W. Berns. Beckman Laser Institute and Medical Clinic, University of California, Irvine, CA 92717.

Microtubules are one of the major cytoplastic elements of the eucaryotic cell's cytoskeleton and are involved in many cell functions. However, in most cases, the mechanism of microtubule assembly in vivo is unclear. To address the question of assembly and disassembly in vitro, we used the focused fourth harmonic wavelength (266 nm) of the short-pulsed YAG laser to shear microtubules in interphase PTK_2 cells in pre-defined regions. The laser shearing zone within a cell was accurately determined by projecting the microscopic image onto a TV monitor interfaced with an image array processor and superimposing a cursor box on the desired area. At different time points after irradiation, the cells were stained with monoclonal anti-tubulin and the growth and shrinkage of individual microtubules in the cutting zone were examined under an epi-fluorescent microscope. The results show that sheared microtubules grow back in the cutting zone individually and that growing and shrinking microtubules coexist. The half-time of replacement of cut microtubules was observed to be 15-20 min. The simultaneous growth or shrinkage of all microtubules was never observed under the experimental conditions. From these data, we conclude that most microtubules, if not all, in interphase cells exhibit the property of dynamic instability. Supported by NIH grants RR01192 and ONR grant N00014-86-0115.

Michael W. Berns
Print or type member's name

(714) 856-6291
Phone number

Member's signature

A member (as author or sponsor) MUST sign the Abstract

ASCB member ☐ FASEB member ☐

Check here if you are a Student ☒

Example: TYPE-SIZE and STYLE for typing Abstract. **DO NOT FOLD ABSTRACT FORM**

Text starts new line; indent 5 spaces

Microtubules and Movement in the Foraminifer, Allogromia. J.L. Travis and R.D. Allen, Dartmouth College, Hanover (Intr. by M. Lubin).

The Reticulopodial networks (RPN) of the foraminifera provide excellent models for the study of the role of cytoplasmic microtubules (MT) in the structure and function of motile systems. Allogromia latticollaris, a benthic foram.

ABSTRACT FORM FOR THE SIXTEENTH ANNUAL MEETING
Deadline: Abstracts must be received by November 16, 1987

AMERICAN SOCIETY FOR PHOTOBIOLOGY

(Member) Sponsor's or Presenter's Name (legible) _____ and
Signature _____

TOP

PLEASE NOTE RULE (OTHER SIDE) REGARDING NUMBER OF ABSTRACTS THAT MAY BE SUBMITTED

OXYGEN CONSUMPTION IN PHOTOSENSITIZATION OF CHO CELLS WITH VARIOUS DRUGS

S.Kimel*, W.G.Roberts, R.Senz[1]*, and M.W.Berns, introduced by J.McCullough
Beckman Laser Institute and Medical Clinic, Univ. of California-Irvine, Irvine, CA 92715

In order to elucidate the mechanism of photosensitization at the cellular level we have investigated the role of O_2 in conditions normally used for in vitro viability studies. CHO cells were incubated for 24 hours with DHE (Dihematoporphyrin Ether) or MACE (Mono-Aspartyl Chlorin e_6). The cell suspensions (10^6 cells/ml) were irradiated at 630 nm (for DHE) or at 664 nm (for MACE). The oxygen concentration in the suspension was monitored with Clark-type oxygen microelectrodes, calibrated in PBS solutions containing known amounts of O_2. At the onset of laser irradiation we observed a decrease of O_2 content of approximately 10%, occurring over a time interval ranging from 10 s to 100 s, depending on the initial O_2 and drug concentrations and on the laser power density (mW/cm^2). After the initial rapid decrease steady-state conditions prevailed which were, however, influenced by the aggregation of irradiated cells in the suspension. The results show differences in O_2 consumption between DHE and MACE.

[1]R.S. is a Visiting Scholar from Laser-Medizin-Zentrum, D-1000 Berlin 45, FRG.

March
1988
Colorado

TYPE YOUR ABSTRACT W[illegible] OT fold across abstract)

THE INSTRUCTIONS BELOW MUST BE FOLLOWED EXACTLY. READ ALL INSTRUCTIONS BEFORE YOU BEGIN TYPING ON THIS SPECIAL FORM.

1. Use a typewriter (preferably electric) with ELITE type. Clean the type THOROUGHLY before using. Use a carbon ribbon or a new black silk ribbon. Practice typing the abstract on a rectangle [illegible] on plain paper before using this special form. Letters crossing the blue lines will not be printed. Have print in BLACK INK. Greek letters and symbols not on your typewriter. If you use a word processor a letter quality printer must be employed.
2. Your entire abstract (including title, author(s), location, text and acknowledgements must be completely contained within the [illegible] rectangle. *LEAVE NO TOP OR LEFT MARGINS WITHIN THE RECTANGLE. SINGLE SPACE ALL TYPING.* Place entire abstract in one paragraph with a 5-space indentation. This rectangle holds 250-300 words of typing. Invited lecturers and Symposium Speakers should submit abstracts on SPECIAL FORMS which will be sent to them.
3. DO NOT ERASE. Corrections may be made using correction fluid (thinly applied) or correction tape. The block will be photographed and appear in the Abstract Book just as you prepare it. Extra forms are available upon request.)
4. Type the title of the abstract in FULL CAPS. *Underline the name and initials of the person PRESENTING the paper. Place an asterisk (*) after each non-member's name* (see reverse side for example). *If all authors are non-members do NOT use an asterisk (*) but include "state," by* and the name of the sponsoring society after the last author. The introducer is the sponsor who signs the abstract. Invited nonmember participants in Symposia do not require a sponsor. *If the authors are from different departments or institutions, first list ALL authors, and then ALL addresses.*
5. Two (2) extra copies of the abstract are required. DO NOT try to make carbons when typing on this special form. Either [illegible] photoreproductions on [illegible] (single spaced, double spaced, using carbons for the second copy).
6. Mail this form with [illegible] to American Society for Photobiology, 5000 Westpark Drive, Suite 1001, McLean, VA [illegible]. Use care when [illegible] Cannot be responsible for [illegible] in the mail.

ABSTRACTS MUST BE RECEIVED BY 16 NOVEMBER 1987.

IMPORTANT! Check One: X Poster Session presentation

[illegible] presentation

CATEGORY (Check One)
(See [illegible])

PLEASE NOTE: THE RESPONSIBLE SPONSORING AUTHOR DOES NOT COMPLETE THE UPPER RIGHT HAND CORNER OF THIS FORM. THE ABSTRACT WILL BE RETURNED.

IMPORTANT! Please [illegible] appropriate

[illegible] author should [illegible] abbreviations [illegible] [illegible] address [illegible] telephone [illegible] [illegible]

PLEASE [illegible] NUMBER [illegible]

Abstract of paper to be considered for presentation at the
37th Annual Scientific Session

AMERICAN COLLEGE OF CARDIOLOGY

March 27–31, 1988, Atlanta, Georgia

Submit to: American College of Cardiology
Meeting Services Department
9111 Old Georgetown Road
Bethesda, Maryland 20814

DEADLINE DATE: Must be postmarked no later than September 4, 1987.

ABSTRACT CATEGORIES

1 Angioplasty & Other Interventional Techniques
2 Cardiac Function—Basic
3 Cardiac Function—Clinical
4 Cardiac Pacing and Implantable Antiarrhythmic Devices
5 Cardiac Surgery
6 Cardiovascular Disease Among the Elderly
7 Cardiovascular X-Ray NMR CT
8 Coronary Artery Disease—Basic
9 Coronary Artery Disease—Clinical
10 Echocardiography Doppler
11 Electrocardiography Ambulatory Monitoring
12 Electrophysiology—Basic
13 Electrophysiology—Clinical
14 Epidemiology Prevention
15 Exercise Physiology & Testing
16 Heart Failure
17 Hypertension
18 Myocardial & Pericardial Disease
19 Myocardial Infarction—Clinical
20 Myocardial Infarction—Experimental
21 Myocardial Metabolism
22 Nuclear Cardiology Single Photon Radionuclides PET
23 Pediatric Cardiology
24 Pharmacology—Antiarrhythmic Drugs—Basic
25 Pharmacology—Antiarrhythmic Drugs—Clinical
26 Pharmacology—Basic
27 Pharmacology—Clinical
28 Thrombosis & Thromboembolism
29 Valvular Disease
30 Other Adult Cardiology

CATEGORY SELECTION

CHOICE #1—Category Number 1
CHOICE #2—Category Number 10

Please Read Instructions Carefully Before Typing Abstract

ABSTRACT REPRODUCTION SPACE

CHANGES IN ULTRASOUND CHARACTERISTICS OF HUMAN ATHEROSCLEROTIC ARTERY WALLS DURING LASER ANGIOPLASTY AS VIEWED FROM AN INTRAVASCULAR ULTRASOUND IMAGING CATHETER

John A. Mallery M.D., James Gessert, James Griffith Ph.D., N. Charle Morcos M.D., Ph.D., Michael Berns Ph.D., Orhan Nalcioglu Ph.D., Walter L. Henry M.D., FACC,
University of California, Irvine CA

Intravascular ultrasound imaging may provide a useful method for evaluating the effect of laser energy on the vascular wall during laser angioplasty. In the present study, we evaluated a newly developed 1.4 mm diameter intravascular ultrasound imaging catheter in 11 human atherosclerotic iliac segments in a saline bath before and after injuring the arterial wall with an argon-driven hot-tip laser fiber. Before lasing, artery walls showed relatively low amplitude echos. After lasing for 10-30 sec. at 10 W output, the same arterial sites showed a strikingly different pattern in all 11 specimens, with a very bright specular echo at the intimal-lumen border, which represented an approximately 10 fold increase in amplitude from the pre-lasing image. In 6 segments, a charred and viable crater was formed. In these 6 segments, wall thickness measurements averaged 3.5 mm before lasing and 1.7 mm after lasing ($p<0.05$). In the other 5 segments, the marked increase in reflection from the intimal-lumen border was not due to grossly visable charring or measurable tissue ablation. We conclude that laser thermal injury results in a marked increase in echogenicity of the lumenal surface, which is not due simply to charring or ablation of tissue. Moreover, evaluation of the artery wall before and after lasing with an intravascular ultrasound imaging catheter allows evaluation not only of changes in artery wall thickness, but also of changes in the ultrasound characteristics of the thermally damaged tissue.

1. Has this or a similar abstract been submitted for presentation at another scientific meeting? ☐ Yes X No If yes, please specify: _____

2. Has this abstract or manuscript been accepted for publication? ☐ Yes X No If yes, please specify: _____

3. Check only if this abstract has also been submitted in the YIA Competition ☐ Yes

4. The author affirms that any animal studies conform with the ACC Annual Scientific Session Program Committee's position on responsible use of animals in research.

Abstract of paper to be considered for presentation at the
37th Annual Scientific Session

AMERICAN COLLEGE OF CARDIOLOGY

March 27–31, 1988, Atlanta, Georgia

Submit to: American College of Cardiology
Meeting Services Department
9111 Old Georgetown Road
Bethesda, Maryland 20814

DEADLINE DATE: Must be postmarked no later than September 4, 1987.

ABSTRACT CATEGORIES

1. Angioplasty & Other Interventional Techniques
2. Cardiac Function—Basic
3. Cardiac Function—Clinical
4. Cardiac Pacing and Implantable Antiarrhythmic Devices
5. Cardiac Surgery
6. Cardiovascular Disease Among the Elderly
7. Cardiovascular X-Ray NMR CT
8. Coronary Artery Disease—Basic
9. Coronary Artery Disease—Clinical
10. Echocardiography Doppler
11. Electrocardiography Ambulatory Monitoring
12. Electrophysiology—Basic
13. Electrophysiology—Clinical
14. Epidemiology Prevention
15. Exercise Physiology & Testing
16. Heart Failure
17. Hypertension
18. Myocardial & Pericardial Disease
19. Myocardial Infarction—Clinical
20. Myocardial Infarction—Experimental
21. Myocardial Metabolism
22. Nuclear Cardiology Single Photon Radionuclides PET
23. Pediatric Cardiology
24. Pharmacology—Antiarrhythmic Drugs—Basic
25. Pharmacology—Antiarrhythmic Drugs—Clinical
26. Pharmacology—Basic
27. Pharmacology—Clinical
28. Thrombosis & Thromboembolism
29. Valvular Disease
30. Other Adult Cardiology

CATEGORY SELECTION

CHOICE #1—Category Number 1
CHOICE #2—Category Number 9

Please Read Instructions Carefully Before Typing Abstract

ABSTRACT REPRODUCTION SPACE

LASER-WIRE: A NEW DEVICE FOR REOPENING COMPLETE ARTERIAL OCCLUSIONS

Jonathan M. Tobis, M.D. FACC; John Mallery, M.D.; Michael Crocker, B.S.; Hany Hussein, Ph.D.; Michael W. Berns, Ph.D.; Walter L. Henry, M.D. FACC.
University of California, Irvine.

Percutaneous transluminal coronary angioplasty has not been very successful in reopening complete occlusions especially if they are greater than 3 months old. Although laser technology holds promise as a technique which may be useful in reestablishing a lumen through complete obstructions, current devices are difficult to maneuver and may cause large perforations. In the present study, we evaluated a new device called a Laser-wire which is 200 microns in diameter and which is designed to create a small diameter channel. The wire is a coated quartz optic-fiber with a metal tip attached to the end. The fiber was connected to an Argon laser at 0.5-2 watts and was tested in isolated human atherosclerotic artery segments and in vivo in a pig model of acute embolic occlusion. The Laser-wire could be manipulated easily through a standard angioplasty balloon catheter and successfully recanalized 6 acutely occluded peripheral arteries. The Laser-wire was also used in vivo in 2 coronary arteries to recanalize complete embolic occlusions to the LAD and RCA. When the laser-wire was applied to long segments of the coronary arteries, the Laser-wire perforated the artery but did not create a hemopericardium. Although the Laser-wire is still in a developmental stage, this study demonstrates the feasibility of using this approach to reopen complete arterial occlusions which could then permit balloon dilatation to be performed over the Laser-wire.

1. Has this or a similar abstract been accepted for presentation at another scientific meeting? ☐ Yes X No If yes, please specify: _____

2. Has this abstract or manuscript been accepted for publication? ☐ Yes X No If yes, please specify: _____

3. Check only if this abstract has also been submitted in the YIA Competition. ☐ Yes

4. The author affirms that any animal studies conform with the ACC Annual Scientific Session Program Committee's position on responsible use of animals in research.

T. J. M. T. M. D.

Abstract of paper to be considered for presentation at the
37th Annual Scientific Session

AMERICAN COLLEGE OF CARDIOLOGY

March 27–31, 1988, Atlanta, Georgia

Submit to: American College of Cardiology
Meeting Services Department
9111 Old Georgetown Road
Bethesda, Maryland 20814

***DEADLINE DATE:** Must be postmarked no later than September 4, 1987.*

ABSTRACT CATEGORIES

1 Angioplasty & Other Intervention Techniques
2 Cardiac Function—Basic
3 Cardiac Function—Clinical
4 Cardiac Pacing and Implantable Antiarrhythmic Devices
5 Cardiac Surgery
6 Cardiovascular Disease Among the Elderly
7 Cardiovascular X-Ray NMR CT
8 Coronary Artery Disease—Basic
9 Coronary Artery Disease—Clinical
10 Echocardiography Doppler
11 Electrocardiography Ambulatory Monitoring
12 Electrophysiology—Basic
13 Electrophysiology—Clinical
14 Epidemiology Prevention
15 Exercise Physiology & Testing
16 Heart Failure
17 Hypertension
18 Myocardial & Pericardial Disease
19 Myocardial Infarction—Clinical
20 Myocardial Infarction—Experimental
21 Myocardial Metabolism
22 Nuclear Cardiology Single Photon Radionuclides PET
23 Pediatric Cardiology
24 Pharmacology—Antiarrhythmic Drugs—Basic
25 Pharmacology—Antiarrhythmic Drugs—Clinical
26 Pharmacology—Basic
27 Pharmacology—Clinical
28 Thrombosis & Thromboembolism
29 Valvular Disease
30 Other Adult Cardiology

CATEGORY SELECTION

CHOICE #1—Category Number 1
CHOICE #2—Category Number 9

Please Read Instructions Carefully Before Typing Abstract

ABSTRACT REPRODUCTION SPACE

LASER-ASSISTED ANGIOPLASTY OF HUMAN PERIPHERAL ARTERIES.

Jonathan M. Tobis, M.D. FACC; Michael Smolin, M.D.; Michael Berns, Ph.D.; Warren D. Johnston, M.D.; John A. Mallery, M.D.; Walter L. Henry, M.D., FACC.
University of California, Irvine, CA

Laser energy has recently been used to recanalize completely occluded peripheral arteries. This study of laser angioplasty was performed to determine the characteristics that might predict outcome of the procedure. Recanalization of completely occluded peripheral arteries was performed in 16 patients using an Argon laser heated tip fiberoptic probe. Mean Doppler ankle/arm index was 0.61 before and 0.93 post procedure. Quantitative measurements of lesion length before and arterial diameter after the procedure were obtained from digital angiograms. Mean length of total occlusion was 11.7cm (range 0.5-26.0 cm). Mean diameter of the angiographically normal segment by edge detection was 4.4mm and mean diameter of the narrowest segment post laser and balloon dilatation was 4.2mm. There were 11 (69%) primary successful procedures. Parameters that affected success were length of the obstruction and vessel tortuosity. Neither artery diameter after dilatation nor the diameter distal to the occlusion correlated with outcome. Early reocclusion occurred in 2 pts due to poor runoff or intimal disruption. In one of these 2, collateral vessels did not disappear after apparently successful recanalization. Thus, laser assisted angioplasty is useful for re-establishing a patent lumen in completely occluded peripheral arteries that might otherwise require bypass surgery. Factors that influence primary success or failure include the length of the lesion and the degree of vessel tortuosity.

1 Has this or a similar abstract been accepted for presentation at another scientific meeting? Yes XX No If Yes, please specify: _____

2 Has this abstract or manuscript been accepted for publication? Yes XX No If Yes, please specify: _____

3 Check only if this abstract has also been submitted in the YIA Competition Yes

4 The author affirms that any animal studies conform with the ACC Annual Scientific Session Program Committee's position on responsible use of animals in research.

Best Available Copy

61st Scientific Sessions

American Heart Association

November 14-17, 1988
Washington Convention Center, Washington, DC

Abstract Form

Medical Research
Nursing Research

Avoid disqualification.
Read instructions.

Number _____
Please do not fill in!

Deadline Date: Abstracts must be postmarked no later than Monday, May 9, 1988, and received by May 12, 1988.

Name of corresponding author:

Mallery John A.
Cardiology/Medicine
U.C. Irvine Medical Center
101 City Dr. So., Orange, CA
92668 Orange
714/634-6545

Names of authors (last name, first name, M.I.):

1. Mallery, John A.
2. Tobis, Jonathan M.
3. Berns, Michael ✓
4. Griffith, James
5. Gessert, James M.
6. Bessen, Matthew
7. Macleay, Lachlan
8. Morcos, N. Charle
9. Henry, Walter L.
10.
11.
12.

For review and grading, assign this abstract to the grading category listed below:

Choice 1 **Number** 41

Choice 2 **Number** 30

Identify two key words or phrases from the abstract indexing list to be used for indexing in the supplement to *Circulation*, an AHA journal. Enter the numbers and key words or phrases here.

1. 1380 Laser
2. 1700 Ultrasonic diagnosis

VISUALIZATION OF HUMAN ATHEROMA IN VITRO BY AN INTRAVASCULAR ULTRASOUND CATHETER BEFORE AND AFTER LASER ABLATION

John A Mallery, Jonathan M Tobis, Michael Berns, James Griffith, James M Gessert, Matthew Bessen, Lachlan Macleay, N Charle Morcos, Walter L Henry, University of California, Irvine, CA

Perforation of the arterial wall remains a major problem of intra-arterial laser catheters. Catheter guidance with angiography is limited because it shows lumen contour, but not atheroma thickness. We evaluated the ability of a 1.2 mm diameter, 20 MHz intravascular ultrasound imaging catheter to guide the effectiveness of laser angioplasty in vitro. . ive severely atherosclerotic human artery segments were imaged before and after ablation of plaque by bare fiber argon laser therapy. The ultrasound imaging catheter was hand rotated to generate a 360° cross-sectional image of the artery wall. Atheroma thickness was well visualized before laser treatment in all artery segments. The mean plaque thickness in the laser treated area decreased from 1.83 ± 0.12 mm to 0.73 ± 0.26 mm following laser treatment ($p<.05$). Regions of the arterial wall shadowed by calcified atheroma became visible following laser removal of the calcified tissue matrix near the lumen surface. ultrasound imaging of diseased human arteries before and after laser therapy is feasible in vitro and holds promise as a method to guide laser therapy.

The author affirms that the material herein will not have been published as a manuscript prior to presentation or presented at any national meeting or world congress held in the United States, that any animal studies conform with the "Position of the American Heart Association on Research Animal Use" *(Circulation* 1985;71:849) and that any human experimentation has been conducted according to a protocol approved by the institutional committee on ethics of human investigation or — if no such committee exists — that it conforms with the principles of the Declaration of Helsinki of the World Medical Association *(Clinical Research* 1966;14:103).

The submitting author also certifies that all authors named in this abstract have agreed to its submission for presentation at the AHA Scientific Sessions, and are familiar with the ten-author rule (see "Rules for Submitting Abstracts").

Submitting author's signature

Abstract of paper to be considered for presentation at the
37th Annual Scientific Session

AMERICAN COLLEGE OF CARDIOLOGY

March 27-31, 1988, Atlanta, Georgia

Submit to: American College of Cardiology
Meeting Services Department
9111 Old Georgetown Road
Bethesda, Maryland 20814

DEADLINE DATE: Must be postmarked no later than September 4, 1987.

Abstract to C.C. / put in below in Heart part removed

ABSTRACT CATEGORIES

1. Angioplasty & Other Interventional Techniques
2. Cardiac Function—Basic
3. Cardiac Function—Clinical
4. Cardiac Pacing and Implantable Antiarrhythmic Devices
5. Cardiac Surgery
6. Cardiovascular Disease Among the Elderly
7. Cardiovascular X-Ray NMR CT
8. Coronary Artery Disease—Basic
9. Coronary Artery Disease—Clinical
10. Echocardiography Doppler
11. Electrocardiography Ambulatory Monitoring
12. Electrophysiology—Basic
13. Electrophysiology—Clinical
14. Epidemiology Prevention
15. Exercise Physiology & Testing
16. Heart Failure
17. Hypertension
18. Myocardial & Pericardial Disease
19. Myocardial Infarction—Clinical
20. Myocardial Infarction—Experimental
21. Myocardial Metabolism
22. Nuclear Cardiology Single Photon Radionuclides PET
23. Pediatric Cardiology
24. Pharmacology—Antiarrhythmic Drugs—Basic
25. Pharmacology—Antiarrhythmic Drugs—Clinical
26. Pharmacology—Basic
27. Pharmacology—Clinical
28. Thrombosis & Thromboembolism
29. Valvular Disease
30. Other Adult Cardiology

CATEGORY SELECTION

CHOICE #1—Category Number 8
CHOICE #2—Category Number 1

Please Read Instructions Carefully Before Typing Abstract

ABSTRACT REPRODUCTION SPACE

PHYCOCYANIN: CYTOTOXIC EFFECTS AND UPTAKE IN HUMAN ATHEROSCLEROTIC PLAQUE.

N. Charle Morcos, M.D., Ph.D., Michael Berns, Ph.D., and Walter L. Henry, M.D., FACC, University of California, Irvine, CA.

Hematoporphyrin derivative (HPD) has been proposed for use in photodynamic therapy of atherosclerosis. Phycocyanin (PHYCO) is a phycobiliprotein with many properties similar to HPD. However, unlike HPD, PHYCO has an activation wavelength that is minimally absorbed by blood. As a result, we studied its laser activation, cytotoxic effects and uptake into atherosclerotic plaque. Optimal activation of PHYCO was produced by laser energy at 620 and 650nm as evidenced by reduction of optical density due to NADPH oxidation in a buffered reaction solution containing 0.1mg/ml of PHYCO. Cytotoxicity was evaluated by measuring viability of mouse myeloma cells in culture 72 hours post-treatment. After incubation with PHYCO (2.5mg/ml) followed by irradiation with laser energy, cell viability was 15% compared to 69 and 71% for control cells exposed to laser only or PHYCO only, respectively. Uptake into atherosclerotic plaque was assessed in atherosclerotic artery segments obtained within 5 hours post mortem and perfused with 0.1 mg/ml PHYCO in oxygenated Krebs Ringer solution for 5 minutes followed by washout with PHYCO-free Krebs for 10 minutes. Artery sections examined histologically by fluorescence and light microscopy showed specific florescence localization within the plaque particularly at the elastic laminea but not in the medial muscle layer. In conclusion, phycocyanin is a cytotoxic photosensitizer that exhibits specific binding to atherosclerotic plaque and is activated at a wave length minimally absorbed by blood. These properties suggest potential therapeutic use of phycocyanin for plaque regression.

1. Has this or a similar abstract been accepted for presentation at another scientific meeting? ☐ Yes ☒ No If yes please specify

2. Has this abstract or manuscript been accepted for publication? ☐ Yes ☒ No If yes please specify

3. Check only if this abstract has also been submitted in the YIA Competition ☐ Yes

4. The author affirms that any animal studies conform with the ACC Annual Scientific Session Program Committee's position on responsible use of animals in research

N. Charle Morcos
Signature of Senior Author

ABSTRACT FORM

AMERICAN SOCIETY FOR LASER MEDICINE AND SURGERY, INC.

813 Second Street, Suite 200
Wausau, WI 54401
Phone (715) 845-9283

APRIL 28-31, 1988 - DALLAS, TEXAS - EIGHTH ANNUAL MEETING

Type name, address and telephone of author who receives correspondence in box A and complete boxes B,C,D,E, & F.
ABSTRACTS MUST BE POSTMARKED NO LATER THAN OCTOBER 20, 1987

A.
NAME Sol Kimel

ADDRESS Beckman Laser Institute
1002 E. Health Sciences Rd.
Irvine, CA 92715

TELEPHONE (714) 856-6291

B. CATEGORIES (Check one)

Basic Science & Safety	XX
Biostimulation, Pain Control (Low Dose Effects)	___
Cardiovascular	___
General Surgery	___
GI	___
Gynecology	___
Neurosurgery	___
New Devices & Instrumentation	___
Nursing	___
Oncology	XX
Ophthalmology	___
Otolaryngology/Pulmonary	___
Plastic/Dermatology	___
Podiatry	___
Urology	___
Veterinary Medicine	___
Film	___
Poster (4 x 8)	___
Scientific Exhibit	___

C. The principal author affirms that all authors named in this abstract have agreed to its submission for presentation and that the material herein will not have been published in an article or abstract by April, 1988.

S. Kimel
Signature of Author

D. I authorize the American Society for Laser Medicine and Surgery Inc., to publish my abstract in Lasers in Surgery and Medicine and to include it in a compilation that it may register and/or transfer copyright ownership to. I also authorize the Society to electronically record my presentation and to sell the recordings.

S. Kimel
Signature of Author

E. PAPER PRESENTATION Time Requested 10 min
Maximum 10 Min.

XX 35. mm. Slides ___ 3/4" U-Matic

F. FILM SESSION Time Requested ___
Maximum 10 Min.

___ 16 mm. ___ 3/4" U-Matic

___ Beta 1/2"* ___ VHS 1/2"*

*Designate Standard ___ Pal ___ Secam ___ NTSC

TYPE ABSTRACT BELOW - BE SURE TO STAY WITHIN BORDER

OXYGEN CONSUMPTION AND THE PHOTOSENSITIZATION EFFICIENCY OF DIHEMATOPORPHYRIN ETHER AND CHLORINS

S.Kimel, W.G.Roberts and M.W.Berns
Beckman Laser Institute, Univ. of Cal-Irvine.

We have irradiated photosensitizers in buffer solutions containing either imidazole or cell suspensions as acceptors for singlet oxygen ($^1O_2$). The disappearance of total oxygen (O_2) can be used to determine the relative efficiency of various photosensitizers to produce $^1O_2$. Dihematoporphyrin ether (DHE) and the compounds Mono-L-Aspartyl Chlorin e_6 (MACE) and Di-Aspartyl Chlorin (DACE) were chosen because they represent two extremes with respect to cellular localization and photosensitizing properties: DHE is lipophilic, highly aggregated in solutions and becomes interralized in cells via diffusion, while MACE and DACE are hydrophilic, monomeric and are pinocytotically internalized. A Clark type oxygen microelectrode was calibrated by irradiating a sensitizer/imidazole solution containing known amounts of dissolved O_2. The solutions were irradiated using a dye laser tuned to 630 nm or 664 nm for DHE and the chlorins, respectively. The measured consumption of O_2 was used to arrive at the quantum yields of $^1O_2$ production for the different photosensitizers at various concentrations and irradiation doses. In an effort to mimic in vitro conditions we also measured the O_2 consumption in solutions containing 1% Fetal Calf Serum (FCS) with and without imidazole. Changes in the quantum yield of DHE in the presence of FCS were studied. In an additional set of measurements we used Chinese Hamster Ovary (CHO) cell suspensions as an acceptor for monitoring consumption in vitro. Identical conditions of incubation and irradiation were then employed to determine cell viability, with a standard clonogenic assay. The relationship between O_2 consumption and cell [illegible] was examined for each photosensitizer.

Supported by NIH Grant CA36240.

ABSTRACT FORM

AMERICAN SOCIETY FOR LASER MEDICINE AND SURGERY, INC.

[illegible], Suite 253
Wausau, WI 54401
Phone (715) 845-6243

APRIL 23-27, 1988 - DALLAS, TEXAS - EIGHTH ANNUAL MEETING

Type name, address and telephone of author who receives correspondence in box A and complete boxes B, C, D, E, F.
ABSTRACTS MUST BE POSTMARKED NO LATER THAN OCTOBER 23, 1987

A.
NAME J. Stuart Nelson, M.D., Ph.D.

ADDRESS Beckman Laser Institute and Medical Clinic, University of California Irvine, 1002 Health Sciences Road East, Irvine, California 92715

TELEPHONE ( ) (714) 856-6996

B. CATEGORIES (Check one)

Basic Science & Safety	___
Biostimulation, Pain Control (Low Dose Effects)	___
Cardiovascular	
General Surgery	XX
GI	___
Gynecology	___
Neurosurgery	___
New Devices & Instrumentation	___
Nursing	___
Oncology	___
Ophthalmology	___
Otolaryngology/Pulmonary	___
Plastic/Dermatology	___
Podiatry	___
Urology	___
Veterinary Medicine	___
Film	___
Poster (4 x 8)	___
Scientific Exhibit	___

C. The principal author affirms that all authors named in this abstract have agreed to its submission for presentation and that the material herein will not have been published in an article or abstract by April, 1988.

J. Stuart Nelson
Signature of Author

I authorize the American Society for Laser Medicine and Surgery Inc., to publish this abstract in Lasers in Surgery and Medicine and to include it in a compilation that it may register and/or transfer copyright ownership to. I also authorize the Society to electronically record my presentation and to sell the recordings.

J. Stuart Nelson
Signature of Author

D. PAPER PRESENTATION Time Requested 10 Minutes
Maximum 10 Min.
XX 35 mm. Slides ___ 3/4" U-Matic

E. FILM SESSION Time Requested _____
Maximum 15 Min.
___ 16 mm. ___ 3/4" U-Matic
___ Beta 1/2"* ___ VHS 1/2"*
*Designate Standard ___ Pal ___ Secam ___ NTSC

TYPE ABSTRACT BELOW - BE SURE TO STAY WITHIN BORDER

ABLATION OF BONE AND ORGANIC POLYMERS BY MID-INFRARED AND ULTRAVIOLET LASERS. J.S. Nelson, L. Yow and M.W. Berns. Beckman Laser Institute and Medical Clinic, University of California, Irvine, Irvine, CA 92715.

The various techniques presently employed for the intra-operative cutting of bone and removal of bone cement typically involve mechanical force and the generation of considerable heat. Damage to the surrounding bone frequently occurs due to the large forces needed to free polymethyl methacrylate (PMMA) embedded in artificial hip prostheses. In experiments reported here, fresh rabbit long bones (humerus, femur and tibia) and PMMA templates were treated with the mid-infrared Erbium:YAG (2.94 um) and the ultraviolet excimer laser (193 nm and 308 nm). Histopathological analyses were performed to examine the areas of vaporization, charring and peripheral necrosis. The results show that both the mid-infrared Erbium:YAG and ultraviolet excimer lasers are able to spontaneously etch away bone and organic polymer such as PMMA. In this process there is no detectable thermal damage to the adjacent substrate that remains behind. It is anticipated that the importance of these two laser systems to medicine will grow with increasing availability of dependable lasers and sophisticated laser delivery systems. Supported by the Office of Naval Research #N00014-86-K-0015.

Best Available Copy

ABSTRACT FORM

AMERICAN SOCIETY FOR LASER MEDICINE AND SURGERY, INC.

813 Second Street, Suite 200
Wausau, WI 54401
Phone (715) 845-9233

APRIL 25-27, 1988 - DALLAS, TEXAS - EIGHTH ANNUAL MEETING

Type name, address and telephone of author who receives correspondence in box A and complete boxes B,C,D,E, & F.
ABSTRACTS MUST BE POSTMARKED NO LATER THAN OCTOBER 20, 1987

Arie Orenstein, M.D.
ress Beckman Laser Institue and Medical
inic, University of California, Irvine
02 Health Sciences Road East, Irvine
EPHONE ( ) California 92715
(4) 856-6996

CATEGORIES (Check one)

Basic Science & Safety	___
Biostimulation, Pain Control (Low Dose Effects)	___
Cardiovascular	
General Surgery	XX
GI	___
Gynecology	___
Neurosurgery	___
New Devices & Instrumentation	___
Nursing	___
Oncology	___
Ophthalmology	___
Otolaryngology/Pulmonary	___
Plastic/Dermatology	___
Podiatry	___
Urology	___
Veterinary Medicine	___
Film	___
Poster (4 x 8)	___
Scientific Exhibit	___

E. PAPER PRESENTATION Time Requested 10 Minutes
Maximum 12 Min.

XX 35. mm. Slides ___ 3/4" U-Matic

F. FILM SESSION Time Requested ___
Maximum 10 Min.

___ 16 mm. ___ 3/4" U-Matic

___ Beta 1/2"* ___ VHS 1/2"*

*Designate Standard ___ Pal ___ Secam ___ NTSC

TYPE ABSTRACT BELOW - BE SURE TO STAY WITHIN BORDER

COMPARISON BETWEEN THE TISSUE EFFECTS OF THE ARGON AND COPPER VAPOR LASERS ON CHICKEN COMBS

A. Orenstein, M. W.Berns and Haggai Tsur. Beckman Laser Institute and Medical Clinic, University of California, Irvine, Irvine, CA 92715. We report a tissue effect comparison between the argon and copper vapor lasers on highly vascularized chicken combs. This serves as a model for human vascular lesions. The argon laser was used as a CW laser providing light at 488 nm, and 514 nm. The copper vapor laser is a pulsed laser providing a green 510 nm and a yellow 578 nm which can be used separately or as a mixture of both beams. The effects of the different copper vapor laser wavelengths were compared to those of the argon laser wavelengths in all of the possible six options (combined wavelength or single wavelength). Each chicken was anesthetized and 4 parallel lines of the selected laser beam were placed on one side of the comb. The beam delivery optics and working distance were set in such a way that when using both lasers, the spot size on tissue and the linear scanning speed were the same. The spot size on tissue was 2 mm, the power 0.9 W and the energy density was 65 J/cm^2. Samples were taken immediately post radiation, 3 days, 7 days and 14 days post radiation. Tissue was fixed in 10% formalin and processed for histological analysis using standard H & E procedures. Histological analysis indicate that the yellow light of the copper vapor laser provides the most efficient capillary vessel occlusion and long term blanching with the least epidermal damage. Supported by Grant #N00014-86-K-0119 from the U.S. Navy SDI program.

The principal author affirms that all hors named in this abstract have agreed its submission for presentation and that material herein will not have been lished in an article or abstract by il, 1988.

Signature of Author

I authorize the American Society for er Medicine and Surgery Inc., to publish abstract in Lasers in Surgery and Medicine to include it in a compilation that it may ister and/or transfer copyright ownership to. lso authorize the Society to electronically ord my presentation and to sell the ordings.

Signature of Author

ABSTRACT FORM

AMERICAN SOCIETY FOR LASER MEDICINE AND SURGERY, INC.

414 So. 2nd Street, Suite 210
Mauston, WI 53948
Phone (608) 847-4283

APRIL 25-27, 1988 - DALLAS, TEXAS - EIGHTH ANNUAL MEETING

Type name, address and telephone of author who receives correspondence in box A and complete boxes B,C,D,E, & F
ABSTRACTS MUST BE POSTMARKED NO LATER THAN OCTOBER 20, 1987

A. PAPER PRESENTATION Time Requested 10 Minutes
Maximum 15 Min.

XX 35 mm. slides 3/4" U-Matic

F. FILM SESSION Time Requested
Maximum 10 Min.

___16 mm. ___3/4" U-Matic

___Beta 1/2"* ___VHS 1/2"*

*Designate Standard ___PAL ___Secam ___NTSC

NAME Arie Orenstein, M.D.

ADDRESS Beckman Laser Institute and Medical Clinic, University of California, Irvine 1002 Health Sciences Road East, Irvine,

TELEPHONE ( ) California 92715
(714) 856-6906

B. **CATEGORIES (Check one)**

Basic Science & Safety	___
Biostimulation, Pain Control (Low Dose Effects)	___
Cardiovascular	___
General Surgery	___
GI	___
Gynecology	___
Neurosurgery	___
New Devices & Instrumentation	___
Nursing	___
Oncology	___
Ophthalmology	___
Otolaryngology/Pulmonary	___
Plastic/Dermatology	XX
Podiatry	___
Urology	___
Veterinary Medicine	___
Film	___
Poster (4 x 8)	___
Scientific Exhibit	___

TYPE ABSTRACT BELOW - BE SURE TO STAY WITHIN BORDER

AN ACUTE AND CHRONIC STUDY OF THE HISTOLOGICAL EFFECTS OF PULSED AND CW MODES OF THE CO_2 LASER

A. Orenstein, Jean Champion, J.S. Nelson, M.W. Berns. Beckman Laser Institute and Medical Clinic, University of California, Irvine, Irvine, CA 92715. Using the Sharplan 1060 CO_2 laser, we have looked at the tissue effects of three available modes: continuous wave, pulsed mode at 60 Hz., and pulsed mode at 300 Hz. The average power in all three modes was 10 watts and the tissue was moved under the beam at 15 mm/sec using a mechanical drive platform. The spot size was 0.2 mm and cuts were made in the skin on the back of a rabbit. Samples were taken for histological evaluation at 0', 24 hour, 72 hours and 1 week. H & E staining of paraffin sections was performed to examine areas of vaporization, charring and peripheral necrosis. Using computer imaging we have compared quantitatively the variations in the areas of damage between the available modes. Supported by Grant #N00014-86-K-0115 from the U.S. Navy SDI program.

. The principal author affirms that all uthors named in this abstract have agreed o its submission for presentation and that he material herein will not have been ublished in an article or abstract by pril, 1988.

Signature of Author

. I authorize the American Society for aser Medicine and Surgery Inc., to publish y abstract in Lasers in Surgery and Medicine nd to include it in a compilation that it may egister and/or transfer copyright ownership to. also authorize the Society to electronically ecord my presentation and to sell the ecordings.

Signature of Author

Best Available Copy

ABSTRACT FORM

AMERICAN SOCIETY FOR LASER MEDICINE AND SURGERY, INC.

613 Second Street, Suite 200
Wausau, WI 54401
Phone (715) 845-9283

APRIL 25-27, 1988 - DALLAS, TEXAS - EIGHTH ANNUAL MEETING

Type name, address and telephone of author who receives correspondence in box A and complete boxes B,C,D,E, & F.
ABSTRACTS MUST BE POSTMARKED NO LATER THAN OCTOBER 20, 1987

ME Michael W. Berns
DRESS Beckman Laser Institute and Medical Clinic
1002 Health Sciences Road East
Irvine, California 92715
LEPHONE (714) 856-6291

CATEGORIES (Check one)

Basic Science & Safety	✓
Bicstimulation, Pain Control (Low Dose Effects)	
Cardiovascular	
General Surgery	
GI	
Gynecology	
Neurosurgery	
New Devices & Instrumentation	
Nursing	
Oncology	
Ophthalmology	
Otolaryngology/Pulmonary	
Plastic/Dermatology	
Podiatry	
Urology	
Veterinary Medicine	
Film	
Poster (4 x 8)	
Scientific Exhibit	

The principal author affirms that all uthors named in this abstract have agreed o its submission for presentation and that he material herein will not have been ublished in an article or abstract by pril, 1988.

Signature of Author

D. I authorize the American Society for Laser Medicine and Surgery Inc., to publish my abstract in Lasers in Surgery and Medicine and to include it in a compilation that it may register and/or transfer copyright ownership to. I also authorize the Society to electronically record my presentation and to sell the recordings.

Signature of Author

E. PAPER PRESENTATION Time Requested 10 min. Maximum 10 Min.

X 35. mm. Slides ___3/4" U-Matic

F. FILM SESSION Time Requested ___ Maximum 10 Min.

___16 mm. ___3/4" U-Matic

___Beta 1/2"* ___VHS 1/2"*

*Designate Standard ___Pal ___Secam ___NTSC

TYPE ABSTRACT BELOW - BE SURE TO STAY WITHIN BORDER

DIFFERENTIAL INHIBITION OF NUCLEIC ACID SYNTHESIS IN TISSUE CULTURE USING THE FAR INFRARED WAVELENGTHS OF THE FREE ELECTRON LASER. Michael W. Berns and William Bewley, Beckman Laser Institute and Medical Clinic, University of California, Irvine, CA and Department of Physics, University of California, Santa Barbara, CA. We have previously reported the inhibition of DNA synthesis in cultured cells following exposure to the 200 μm wavelength of the FEL (Berns and Bewley, Photochem. Photobiol. 46: 165-168, 1987). In those experiments only 3% of the cells exposed to the radiation were affected. It was felt that this small percent of cells affected may have been due to either the wavelength being at a weak point on the absorption curve or that only a small proportion of the cells were in a susceptible phase of the cell cycle. In order to investigate this question, cells were exposed to the FEL beam at 160 μm under the following parameters: 1 mJ per pulse; 50 - 100 pulses; 1 μsec duration pulses; 4 mm diameter focused spot. The cells were exposed in culture chambers with the beam passing through a fused silica window (transmission 65 - 70%) before impinging directly on the cells. Twenty replicate chambers at two different light doses (50 and 100 pulses) were used and the cells were subsequently incubated in either tritiated thymidine or uridine for analysis of DNA or RNA synthesis. The results indicated that there was no effect on DNA synthesis but a definite effect on RNA synthesis ($p = 0.001$). In combination with our previous results using 200 μm, the observed effect on RNA synthesis at 160 μm suggests a definite wavelength specific effect on the different classes of nucleic acid. The results support the prediction of other authors that there are specific rotational and vibrational modes of biological molecules in the far infrared regions of the spectrum. Our results would suggest that radiation at these frequencies may be used to alter and probe the structure and function of these molecules. Supported by Grant #N00014-86-K-0115 from the U. S. Navy SDI program.

Method of Presentation: CHOOSE ONE ONLY

ABSTRACT DEADLINE: AUGUST 15, 1988

[x] **POSTER ONLY** -- do not consider for afternoon symposium

[ ] **CONSIDER FOR AFTERNOON SYMPOSIUM** -- Abstract not selected for afternoon symposium will be placed in poster presentation

[ ] **AFTERNOON SYMPOSIUM ONLY** -- Abstract will be automatically withdrawn if not selected for afternoon symposium

[ ] **FILM SESSION** -- (16 mm, 3/4" VHS & BETA will be available and will handle all formats.)
If film is used, specify type of projector and length of presentation: (See Page 3) _____

OFFICE USE ONLY

SELECT CATEGORY NUMBER & TITLES
Afternoon Symposia Preference (See list on Page 9)

1. _____ _____
No. Title

Poster Preference (See list on Page 10)

1. B17 Cell motility
No. Title

2. _____ _____
No. Title

Note: **ASCB Members:** *This year only, you may sponsor as many abstracts as you wish, but you may be "first author" on only one abstract.*
ASBMB Members: *Underscore title as well as author. (See sample below.)*

DO NOT FOLD ABSTRACT FORM

Mail to: ASCB/ASBMB Meeting Office
Beaumont House, Room B-206
9650 Rockville Pike
Bethesda, MD 20814

Start here: TITLE and TEXT MUST fit within the lines

MAILING ADDRESS OF FIRST AUTHOR

(Please Print or Type. Provide full name rather than initials.)

Beckman Laser Institute
1002 Health Sciences Rd

Irvine, CA 92715

Phone: Office (714)856-6291

Home/Holiday (714)240-8326

Each abstract form submitted must be signed by an ASCB/ASBMB or FASEB Member. Signature provides assurance of adherence to the rules and the scientific validity of the presentation.

Michael W. Berns
Member's Name (Print or Type)

Member's Signature

(714) 856-6291
Member's Phone Number

Member's Affiliation:

[x] ASCB [ ] ASBMB [ ] FASEB

Is first author a grad student?
[ ] YES [x] NO

Optical Trapping with a Laser Microbeam: A New Method to Study Cell Motility. Michael W. Berns, Dept. of Surgery, Beckman Laser Institute and Medical Clinic, University of California, Irvine, CA 92715.

Visible and infrared light can be scattered (refracted) by inanimate as well as living objects with the creation of a substantial amount of force. This force is created as a result of momentum transfer from the refracted photons to the object. As a result, the object is "pulled" back towards the focal point of the beam. We report here experiments in which an infrared neodymium YAG laser (1.06 microns) has been focused using a 100X phase contrast objective to a spot diameter of 1-2 microns at a power of between 10-100 milliwatts. The beam has been focused adjacent to and onto several different biological objects: single red blood cells, isolated chromosomes, chromosomes and centrioles in the mitotic spindle. This "optical tractor beam" can be shown to move individual blood cells and chromosomes in saline suspensions. Inside the living cell, force can be generated at the centriole region leading to inhibition of spindle formation but not inhibition of further chromosome condensation during mitosis. When the beam is focused onto a chromosome that is lagging off of the metaphase plate, enough force can be generated to hold the chromosome away from the spindle even though spindle forces eventually will try to move the chromosome towards the metaphase plate. The results suggest that a non-destructive beam of light can be focused inside living cells to generate a known amount of force which can then be applied selectively to study and manipulate specific cellular functions. Supported by NIH grant RR01192 and DOD SDI084-88-C-0025.

Example: TYPE SIZE and STYLE FOR TYPING ABSTRACT

Text starts new line; indent 5 spaces

[ ] Microtubules and Movement in the Foraminifer, Allogromia. J.L. Travis and R.D. Allen, Dartmouth College, Hanover (Spon. by M. Lubin).

The Reticulopodial networks (RPN) of the foraminifera provide excellent models for the study of the role of cytoplasmic microtubules (MT) in the structure and function of motile systems. Allogromia laticollaris, a benthic foram,

ABSTRACT FORM

AMERICAN SOCIETY FOR LASER MEDICINE AND SURGERY, INC.

313 Second Street, Suite 200
Wausau, WI 54401
Phone (715) 845-9283

APRIL 25-27, 1988 - DALLAS, TEXAS - EIGHTH ANNUAL MEETING

Type name, address and telephone of author who receives correspondence in box A and complete boxes B,C,D,E, & F
ABSTRACTS MUST BE POSTMARKED NO LATER THAN OCTOBER 20, 1987

AME Ronald E. Rasmussen

DDRESS Dept. of Community & Environmental Med.
College of Medicine
University of California, Irvine CA 92717

ELEPHONE (714) 856-5816

. CATEGORIES (Check one)

Basic Science & Safety	X
Biostimulation, Pain Control (Low Dose Effects)	___
Cardiovascular	___
General Surgery	___
GI	___
Gynecology	___
Neurosurgery	___
New Devices & Instrumentation	___
Nursing	___
Oncology	___
Ophthalmology	___
Otolaryngology/Pulmonary	___
Plastic/Dermatology	___
Podiatry	___
Urology	___
Veterinary Medicine	___
Film	___
Poster (4 x 8)	___
Scientific Exhibit	___

C. The principal author affirms that all authors named in this abstract have agreed to its submission for presentation and that the material herein will not have been published in an article or abstract by April, 1988.

Signature of Author

D. I authorize the American Society for Laser Medicine and Surgery Inc., to publish my abstract in Lasers in Surgery and Medicine and to include it in a compilation that it may register and/or transfer copyright ownership to. I also authorize the Society to electronically record my presentation and to sell the recordings.

Signature of Author

E. PAPER PRESENTATION Time Requested 10 Maximum 10 Min.

X 35. mm. Slides ___ 3/4" U-Matic

F. FILM SESSION Time Requested ___ Maximum 10 Min.

___ 16 mm. ___ 3/4" U-Matic

___ Beta 1/2"* ___ VHS 1/2"*

*Designate Standard ___ Pal ___ Secam ___ NTSC

TYPE ABSTRACT BELOW - BE SURE TO STAY WITHIN BORDER

GENERATION OF MUTATIONS AND OZONE FROM PULSED UV LASER SOURCES. Ronald E. Rasmussen*, Marie J. Hammer-Wilson**, and Michael W. Berns**. *Department of Community and Environmental Medicine and **Beckman Laser Institute and Medical Clinic, University of California, Irvine, CA. Because ultraviolet radiation below 200 nm is capable of producing ozone by ionization of atmospheric oxygen, we measured the ozone concentration in the vicinity of the radiation target when using the 193 nm excimer laser. At a repetition rate of 50 Hz and energy of approximately 1 mJ per pulse we found amounts of ozone up to 6.0 ppm (600 times background level). Since ozone is highly toxic and also may have mutagenic potential we are investigating the possible effects of ozone using the conditions and concentrations which may be produced during therapeutic applications of UV lasers. To avoid possible interference by ozone in tests for the mutagenic potential of 193 nm laser radiation, we carried out the exposures in a nitrogen atmosphere. The mutagenic potential of UV light produced by 2 pulsed excimer lasers (193 and 308 nm) was compared to that of low-intensity continuous 254 nm UV. All radiations were mutagenic to strains TA98 and TA100 in the Ames Salmonella test system. Pulsed laser radiation at 193 or 308 nm was about 100-fold less mutagenic than 254 nm continuous UV. At doses below 100 J/m^2 no mutagenic activity was seen with 193 or 308 nm pulsed radiation. Sister chromatid exchanges (SCEs) were induced by all radiations in Chinese hamster ovary (CHO) cells. Pulsed 308 nm UV induced SCEs in a dose-dependent manner with an efficiency of about 0.01 that of 254 nm UV. Pulsed 193 nm UV also increased the SCE incidence, but the incidence was not dose related over the range examined (25-1500 J/m^2). The latter result may be due to the overriding cytotoxicity of this laser and also to the limited penetration of this wavelength into the cell nucleus. These results demonstrate that genotoxic effects can be produced by pulsed UV lasers operating in the range of energies used for therapeutic purposes. Mutagenesis tests in CHO cells are in progress using the HGPRT point mutation assay.

ABSTRACT FORM

AMERICAN SOCIETY FOR LASER MEDICINE AND SURGERY, INC.

313 Second Street, Suite 200
Wausau, WI 54401
Phone (715) 845-9283

APRIL 25-27, 1988 - DALLAS, TEXAS - EIGHTH ANNUAL MEETING

Type name, address and telephone of author who receives correspondence in box A and complete boxes B,C,D,E, & F.
ABSTRACTS MUST BE POSTMARKED NO LATER THAN OCTOBER 20, 1987

ME J. Stuart Nelson, M.D., Ph.D.

DRESS Beckman Laser Institute and Medical
.inic, University of California, Irvine

)02 Health Sciences Road East, Irvine

LEPHONE ( ) California 92715

714) 856-6996

E. PAPER PRESENTATION Time Requested 10 Minutes
Maximum 10 Min.

XX 35. mm. Slides ___ 3/4" U-Matic

F. FILM SESSION Time Requested _____
Maximum 10 Min.

___16 mm. ___3/4" U-Matic

___Beta 1/2"* ___VHS 1/2"*

*Designate Standard ___Pal ___Secam ___NTSC

CATEGORIES (Check one)

Basic Science & Safety	___
Biostimulation, Pain Control (Low Dose Effects)	___
Cardiovascular	___
General Surgery	___
GI	___
Gynecology	___
Neurosurgery	___
New Devices & Instrumentation	___
Nursing	___
Oncology	XX
Ophthalmology	___
Otolaryngology/Pulmonary	___
Plastic/Dermatology	___
Podiatry	___
Urology	___
Veterinary Medicine	___
Film	___
Poster (4 x 8)	___
Scientific Exhibit	___

The principal author affirms that all
thors named in this abstract have agreed
) its submission for presentation and that
ie material herein will not have been
iblished in an article or abstract by
)ril, 1988.

Signature of Author

. I authorize the American Society for
ase~ Medicine and Surgery Inc., to publish
y abstract in Lasers in Surgery and Medicine
nd to include it in a compilation that it may
egister and/or transfer copyright ownership to.
also authorize the Society to electronically
ecord my presentation and to sell the
ecordings.

Signature of Author

TYPE ABSTRACT BELOW - BE SURE TO STAY WITHIN BORDER

MECHANISM OF TUMOR DESTRUCTION BY MONO-L-ASPARTYL CHLORIN DURING PHOTODYNAMIC THERAPY. J.S. Nelson, L.H. Liaw, W.G. Roberts and M.W. Berns. Beckman Laser Institute and Medical Clinic, University of California, Irvine, Irvine, CA 92715. One of the major unanswered questions in PDT is the precise mechanism of tumor destruction. Presumably any photosensitizer would first have to interact with the vascular endothelium of the tumor tissue before passing into the surrounding perivascular tumor stroma. The effectiveness of tumor destruction is dependent upon a complete understanding of the parameters involved in this process. This effect may be direct, such as destruction of the vasculature that nourishes the tumor as has been shown with hematoporphyrin derivative. We have previously demonstrated that mono-l-aspartyl chlorin is an effective tumor localizing photosensitizer in vivo (Cancer Research 47:4681-4685, 1987). Because of the complex nature of the tumor vasculature in PDT, we have undertaken a series of experiments aimed at elucidating the effects of PDT with mono-l-aspartyl chlorin during the first few hours after phototherapy. Balb-c mice bearing EMT-6 tumor received i.p. injections of 10 mg/kg of chlorin and 24 hours later tumors were treated with 100 J/cm² of light (664 nm). Animals were sacrificed and their tumors removed at time 0, 30 min., 1 hr., 2 hrs., 4 hrs. and 8 hrs. after treatment. The effects of PDT on the microvasculature were examined at the LM and EM levels. The results indicate the initial effects of PDT with chlorin are primarily direct destruction of the tumor microvasculature with subsequent tumor cell death. Supported by NIH grants CA 32248 and RR 01192.

Best Available Copy

ABSTRACT FORM

AMERICAN SOCIETY FOR LASER MEDICINE AND SURGERY, INC.

813 Second Street, Suite 200
Wausau, WI 54401
Phone (715) 845-9283

APRIL 25-27, 1988 - DALLAS, TEXAS - EIGHTH ANNUAL MEETING

Type name, address and telephone of author who receives correspondence in box A and complete boxes B,C,D,E, & F.
ABSTRACTS MUST BE POSTMARKED NO LATER THAN OCTOBER 20, 1987

A.
NAME W. Gregory Roberts
ADDRESS 1002 E. Health Sciences Rd.
Irvine, CA 92715
Beckman Laser Institute
TELEPHONE (714) 856-6291

B. CATEGORIES (Check one)

Basic Science & Safety	___
Biostimulation, Pain Control (Low Dose Effects)	___
Cardiovascular	___
General Surgery	___
GI	___
Gynecology	___
Neurosurgery	___
New Devices & Instrumentation	___
Nursing	___
Oncology	XX
Ophthalmology	___
Otolaryngology/Pulmonary	___
Plastic/Dermatology	___
Podiatry	___
Urology	___
Veterinary Medicine	___
Film	___
Poster (4 x 8)	___
Scientific Exhibit	___

C. The principal author affirms that all authors named in this abstract have agreed to its submission for presentation and that the material herein will not have been published in an article or abstract by April, 1988.

Signature of Author

D. I authorize the American Society for Laser Medicine and Surgery Inc., to publish my abstract in Lasers in Surgery and Medicine and to include it in a compilation that it may register and/or transfer copyright ownership to. I also authorize the Society to electronically record my presentation and to sell the recordings.

Signature of Author

E. PAPER PRESENTATION Time Requested 10min
Maximum 10 Min.

XX 35. mm. Slides ___ 3/4" U-Matic

F. FILM SESSION Time Requested ___
Maximum 10 Min.

___ 16 mm. ___ 3/4" U-Matic

___ Beta 1/2"* ___ VHS 1/2"*

*Designate Standard ___ Pal ___ Secam ___ NTSC

TYPE ABSTRACT BELOW - BE SURE TO STAY WITHIN BORDER

MECHANISM OF IN VITRO UPTAKE AND DESTRUCTION OF VARIOUS PHOTOSENSITIZERS W. Gregory Roberts[1], F.Y.Shiau[2], K.Smith[2], M.W.Berns[1].[1]Beckman Laser Institute and Medical Clinic, Univ. of CA-Irvine, Irvine, CA 92715;[2]Dept. of Chemistry, Univ. of CA-Davis, Davis, CA 925616. The mechanism of cellular uptake of photosensitizers used in photodynamic therapy (PDT) has never been clearly elucidated. Different cellular uptake mechanisms for various sensitizers will lead to unique subcellular localizations. Thus, upon irradiation they will yield different subcellular destruction loci. The study of in vitro uptake of sensitizers could provide valuable insight to the in vivo uptake mechanism. In addition, different tissue localization and sensitivity of a photosensitizer could be due, in part or totally, to cellular uptake and destruction mechanisms specific for that drug. We have studied the cellular uptake and destruction mechanisms of Dihematoporphyrin ether (DHE), Mono-L-Aspartyl Chlorin e_6 (MACE) and Di-Aspartyl Chlorin (DACE). MACE and DACE are new chlorin compounds which show promise for use in PDT. Both compounds are pure and absorb substantially at 664nm. These chlorin compounds have generated significant attention due to their lack of skin photosensitization and very good tumor eradication properties. Our results show that DHE enters the cell primarily through diffusion, and the chlorins enter solely by endocytosis. Endocytosis can be completely and reversibly inhibited by incubating cells at 4°C. Cells were incubated with DHE or the chlorins at 4°C for 24 hrs with no adverse effects to the cells. Fluorescent micrographs were then taken to determine the extent of cellular uptake of the sensitizers. These different cellular uptake mechanisms yield unique subcellular localizations, which eventually with irradiation may cause different primary sites of subcellular destruction. The differences in cellular uptake can be explained by the lipophilic and hydrophilic nature of DHE and the chlorins, respectively. Supported by NIH grant #CA32248 and U. S. Navy SDI program grant #N00014-86-K-0115.

CALEO 1988
Oct. 1988
Santa Clara, CA

ABSTRACT

EXCIMER LASER EFFECTS ON TISSUE. Michael W. Berns, Ph.D., J. Stuart Nelson, M. D., Ph.D., Lindy Yow, Marie Wilson and Ronald Rasmussen,* Ph.D. Beckman Laser Institute and Medical Clinic, Dept. of Surgery, University of California, Irvine, and Dept. of Community and Environmental Medicine,* University of California, Irvine, Irvine, CA 92717.

Excimer lasers (ArFl, 193 nm, and XeCl, 308 nm) are being actively investigated with respect to their application in a variety of medical areas. The 193 nm excimer laser is being most actively pursued for non-thermal photoablation of corneal tissue in the eye with the hope of eventual application to correct for refractive disorders. Light and electron microscopic examination of ablated corneal tissue suggests that this laser can be used to precisely remove corneal tissue either in an incisional mode or in a shallow ablative mode. However, thermal camera measurements do demonstrate that there is a thermal component in the ablation process. Mutagenesis studies indicate that this wavelength does produce a high level of cellular toxicity and a level of mutation induction 1-2 orders of magnitude less than a conventional 254 nm mutation source. The 308 nm excimer laser is being examined with respect to its potential for removal of hard tissue, such as bone, and for the selective ablation of vascular plaque. Histologic studies will be presented as well as mutation studies that elucidate mutation frequencies in bacterial and vertebrate cell cultures.

Lasers in Surgery and Medicine 8:494–500 (1988)

Ablation of Bone and Methacrylate by a Prototype Mid-Infrared Erbium:YAG Laser

J. Stuart Nelson, MD, PhD, Lindy Yow, MS,EE, L.-H. Liaw, MS, Lachlan Macleay, MD, Rhonda B. Zavar, BS, Arie Orenstein, MD, William H. Wright, BS, Jeffrey J. Andrews, BA, and Michael W. Berns, PhD

Beckman Laser Institute and Medical Clinic (J.S.N., L.Y., L.-H.L., R.B.Z., A.O., W.H.W., J.J.A., M.W.B.) and Departments of Surgery (J.S.N., M.W.B.) and Pathology (L.M.), University of California, Irvine

An erbium:YAG laser was used to generate 200-μs pulses of mid-infrared 2.94-μm light in both the single and multimode configurations. Laser pulses were focused on the surfaces of both rabbit long bones and methacrylate blocks, and the tissue response was examined histologically. The depth of thermal injury was determined by ocular micrometry.

Over all energy levels tested, the erbium:YAG laser produced ablation of bone and methacrylate with minimal thermal damage to adjacent tissue. Increasing the laser energy per pulse produced increasingly wider and deeper grooves in both bone and methacrylate. However, such increase in laser energy produced a proportionately greater increase in the zone of thermal injury in methacrylate as compared with bone.

These studies suggest the feasibility of a surgical erbium:YAG laser in orthopaedics and other forms of ablative surgery.

Key words: orthopaedics, ablation, erbium:YAG laser

INTRODUCTION

In 1973, Moore reported the first attempt at laser use in orthopaedics [1]. Since that time, the number of investigations using the laser as an orthopaedic surgical tool has been steadily increasing. Carbon dioxide lasers have been used advantageously in the removal of malignant and benign bone tumors, in the excision of infected tissue, and in patients with bleeding diatheses [2].

Specific to orthopaedics are the problems of cutting bone and removal of bone cement in patients who have had artificial joints inserted. Carbon dioxide lasers have been used in both the continuous wave and superpulsed modes to perform experimental osteotomies, but carbonization because of thermal injury to bone immediately adjacent to the irradiated areas has been described [3–5]. Additionally, one study reported that the presence of this carbonized debris persisted up to 4 weeks after surgery and stimulated a foreign body inflammatory response with a retarded rate of bone healing [6].

There is no specific way of removing bone cement (a methacrylate polymer) with lasers, and each surgeon has developed his/her own techniques and instruments to remove such cement. These techniques have involved cement chisels, high-speed burrs, intramedullary reamers, and cement drills. However, the torque and mechanical force generated by these devices may lead to numerous untoward complications. A method for clean removal of cement without mechanical trauma would have distinct advantage over existing techniques.

The present study describes the use of the mid-infrared erbium:YAG laser (2.94 μm) to ablate both bone and methacrylate.

MATERIALS AND METHODS

Laser Light Delivery System

Laser irradiations were performed with a Quantronix (Smithtown, NY) Model 294 erbium:YAG laser operating at a wavelength of 2.94

Accepted for publication July 8, 1988

Address reprint requests to Michael W. Berns, Ph.D., Beckman Laser Institute and Medical Clinic, 1002 Health Sciences Road East, Irvine, CA 92715.

© 1988 Alan R. Liss, Inc.

μm. This laser produces a 200-μs pulse with a repetition rate variable from 0 to 9.9 Hz in both the single mode (TEM_{oo}) and multimode form (TEM_{mn}) of operation.

The laser beam was deflected down to the operating stage using a standard silver front surfaced mirror and focused with a 50-mm calcium fluoride lens to a spot diameter of 150 μm for the single mode and 287–325 μm for the multimode form of operation. The spot diameter was determined at all pulse energy levels tested. Briefly, a 480-μm slit was attached to a x-y-z stage and moved across the incident beam. The relative intensity vs. position of the detector was then plotted Beam waist was defined as the radius of the intensity profile at an amplitude of $1/e^2$ of the maximum intensity. Calculations using the theory of Gaussian beam transfc mation were performed for the spot diameter at the focal point of the lens, taking into account the focal properties of the lens as well as the divergence and path length of the beam. The theoretical parameters were then compared to actual burns on laser and thermographic paper, which were measured by ocular micrometry. Since the spot diameter increased with increasing pulse energy in the TEM_{mn} mode, the radiant exposure (J/mm^2) was not a linear function of the pulse energy level.

Since the mid-infrared light is invisible to the human eye, a low-power (2 mW) He-Ne laser (PMS Electro-Optics, Boulder, CO) generating orange light was aligned with the erbium:YAG laser beam for aiming purposes. Laser irradiation was monitored with a Coherent Model 201 (Auburn, CA) power meter before and after treatment at the tissue surface.

Study parameters varied from 0.1 to 0.2 J per pulse (5.7–11.3 J/mm^2) single mode and 0.1 to 1.0 J per pulse (1.6–12.1 J/mm^2) multimode at both 5 and 7 Hz for each mode. The samples were placed on a mobile operating stage that passed underneath the laser beam at a constant velocity of 1.8 mm/s. Bone and methacrylate ablations were produced by moving the substrate underneath the laser beam six times.

Animal System

Adult New Zealand white rabbits were sacrificed, and their long compact bones (humerus, femur, and tibia) were removed and immediately frozen at −20°C. On the day of the experiment, the bones were thawed and kept in fresh normal saline at room temperature until laser irradiation was performed. Samples were cut with a saw to a 0.8 × 2.0-cm surface size for easy manipulation under the laser beam, and the bone marrow was removed. The bone samples were positioned under the laser such that a flat bone surface was exposed to the laser.

Immediately after treatment, specimens were fixed in fresh 10% formalin in phosphate buffer, pH 7.4. For decalcification, bones were suspended in Surgipath Decalcifier II (Grayslake, IL) at room temperature for 48 h. Samples were then dehydrated in graded alcohols, cleared in xylene, and embedded in paraffin. Six-micron sections were cut, stained with hematoxylin and eosin, cleared of paraffin in xylene, and dried. Sections were examined with an Olympus microscope and photographed with Panatomic-X film (Eastman Kodak). The depth of thermal injury as a function of energy per pulse was measured for bone by ocular micrometry.

Methacrylate

Surgical Simplex P Radiopaque Bone Cement (Howmedica, Rutherford, NJ) containing a mixture of polymethyl methacrylate (15%), methyl methacrylate-styrene-copolymer (75%), and barium sulfate (10%) was prepared as described in the package insert. Methacrylate was placed into a 0.6 × 1.4-cm embedding mold and allowed to solidify overnight at room temperature.

After laser irradiation, samples were cut perpendicular to the laser cuts to obtain a cross-sectional view. Six-micron thin sections were cut with a ultramicrotome, magnified, and photographed as described above. The depth of thermal injury as a function of energy per pulse was measured for methacrylate by ocular micrometry.

RESULTS

Gross inspection of both bone and methacrylate specimens revealed no visual evidence of thermal injury (Fig. 1a,b). These photographs illustrate the excellent edge definition obtained with erbium:YAG laser ablation together with the absence of any significant gross charring or burning of the surrounding material. The bright white discoloration in methacrylate in Figure 1b is caused by reflection off the ablated edge and is not due to thermal injury. Histologically, the erbium:YAG laser is capable of producing deep narrow cuts in both bone (Fig. 2a,b) and methacrylate (Fig. 2c) in both TEM_{oo} and TEM_{mn} modes. Review of all slides demonstrated that increasing the laser energy per pulse produced increasingly wider and

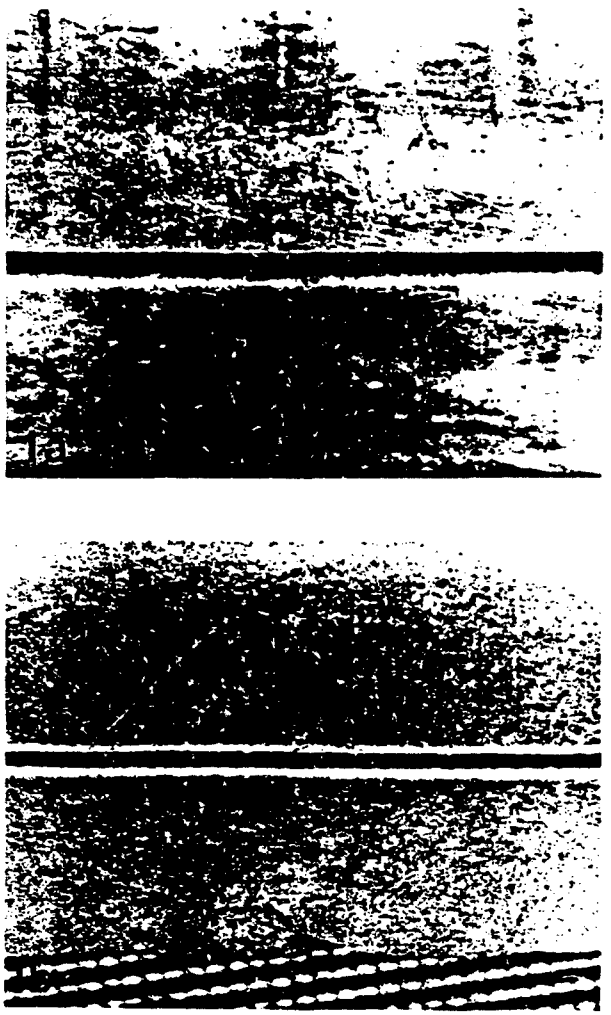

Fig. 1. Gross photomicrographs of cuts made with the erbium:YAG laser in (a) bone and (b) methacrylate. These cuts were produced by moving the substrate underneath the laser beam six times. ×9.

deeper grooves in both bone (Fig. 2a,b) and methacrylate (Fig. 3a,b). As the laser energy per pulse was increased, the zone of thermal damage in bone, consisting of coagulation necrosis immediately adjacent to the area of ablation, increased from 5 to 11 μm (Table 1). No signs of thermal injury or distortion were seen in areas not immediately adjacent to the ablated zone (Fig. 4a,b). However, for methacrylate, as the laser energy per pulse was increased, the zone of thermal injury also increased from 90 to 375 μm. Although there was no histological evidence of charring or carbonaceous material, methacrylate polymer adjacent to the zone of ablation appeared to have undergone thermal decomposition and distortion (Fig. 3a,b). The repeating individual, small, monomeric subunits of methacrylate can no longer be clearly distinguished microscopically.

DISCUSSION

The objective of any laser-assisted surgical procedure is to perform precise ablation of targeted tissue with minimal damage to the remaining tissue. Most present surgical applications of lasers primarily affect tissue change by the controlled burning and volatilization of tissue. This is based on the conversion of electromagnetic radiation into thermal energy. Unfortunately, this thermal energy will radiate in different directions with successive circumferential zones of carbonization, vacuolization, and edema as the heat is dissipated.

In order to have radiant energy absorbed, it is necessary to have some absorbing molecule or chromophore in the target tissue. Water absorbs minimally in the visible and near infrared portions of the electromagnetic spectrum. However, in the mid- and far-infrared regions of the spectrum, water absorbs strongly. The erbium:YAG laser has a maximal emission in the mid-infrared region at 2.94 μm, which corresponds to a large absorption band for water. The photophysical parameter of interest is the absorption coefficient, α, which is specific to the material of interest at a particular wavelength. The characteristic absorption length of a material is the reciprocal of the absorption coefficient, α^{-1}. Water has an absorption length of 3.3 μm at a wavelength of 2.94 μm [7]. A large number of photons being absorbed in such a small volume produces a rapid rise in the temperature of the substrate. When the boiling point of water is reached, some vapor will escape through tiny cracks in the surface of the irradiated material. However, other vapor produced by the laser energy will build up internal pressure until a microexplosion occurs with part of the substrate being ejected in the form of microscopic particles [8]. The major part of the incident energy is consumed in the ablative process, and only a small fraction of the energy remains in the tissue. Therefore, ablation of the exposed material can, in principle, be performed more precisely. Any thermal damage will be confined to a small region immediately adjacent to the ablated zone with little or no disruption of the remaining substrate.

The results of this study suggest that the erbium:YAG laser will effectively ablate bone and methacrylate by the microexplosive removal of substrate with minimal thermal damage adjacent to the cut. Additionally, as the laser energy per

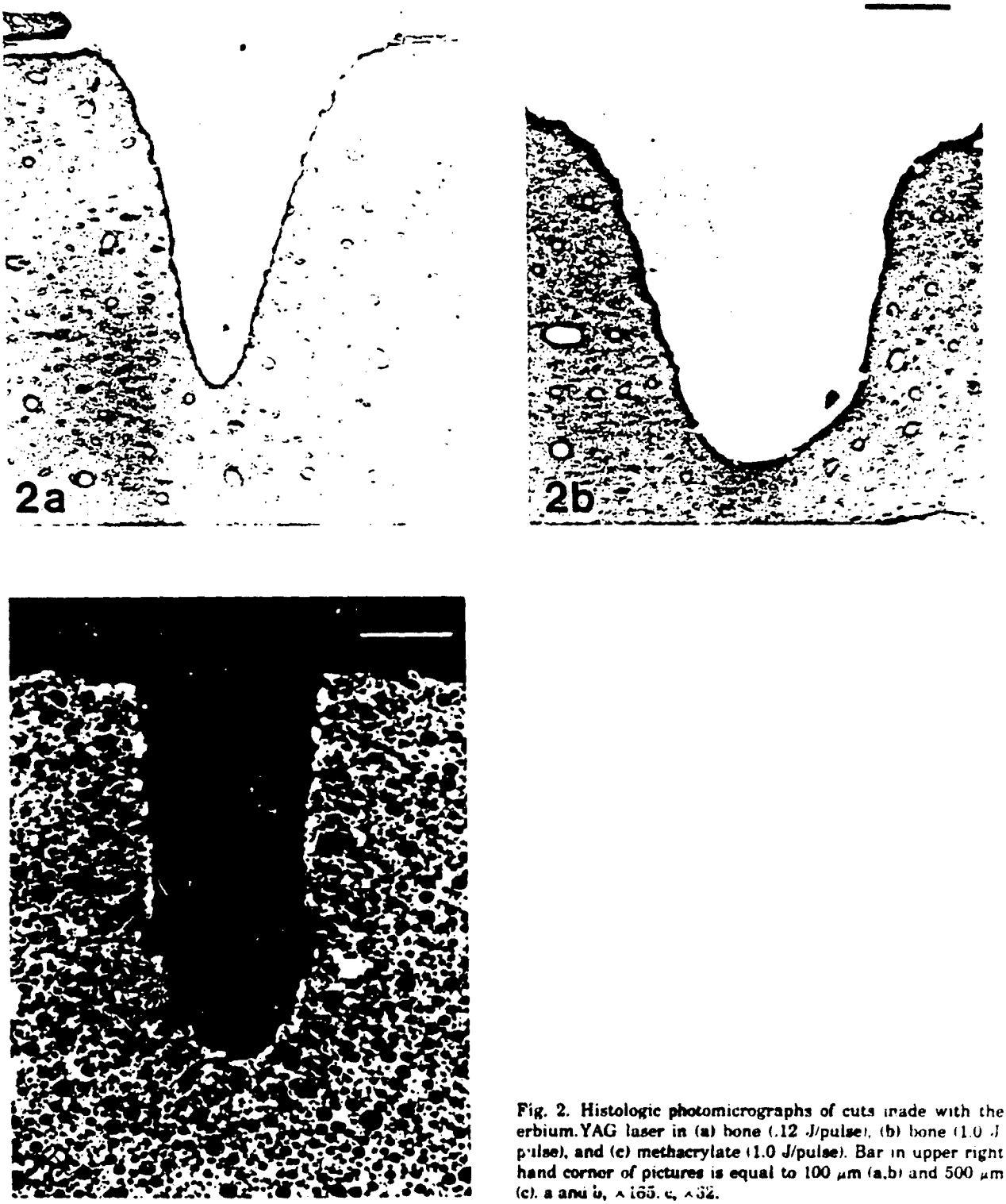

Fig. 2. Histologic photomicrographs of cuts made with the erbium:YAG laser in (a) bone (.12 J/pulse), (b) bone (1.0 J/pulse), and (c) methacrylate (1.0 J/pulse). Bar in upper right hand corner of pictures is equal to 100 μm (a,b) and 500 μm (c). a and b, ×165. c, ×32.

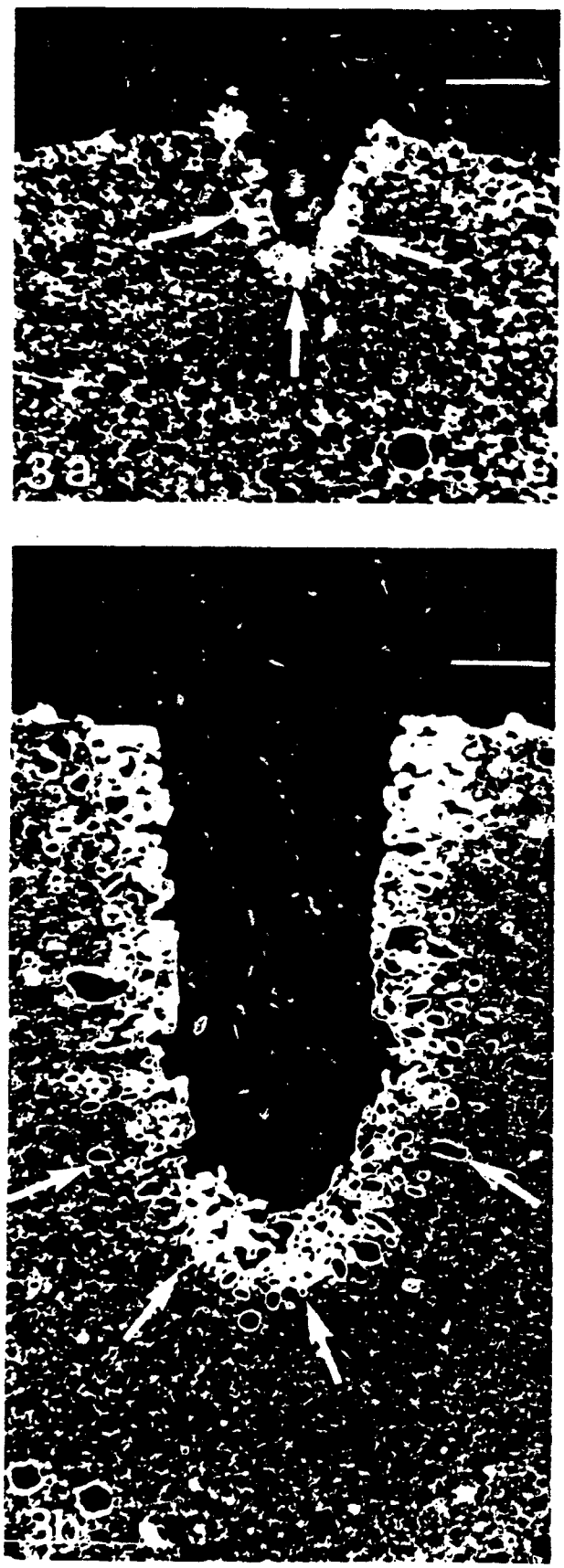

pulse is increased, deeper and wider cuts are obtained. However, such increases in laser energy per pulse produced a proportionately greater increase in the zone of thermal injury in methacrylate as compared with bone. Since these increases occurred at the highest energy per pulse levels in the TEM_{mn}, they were most probably related to the increased energy at the tails of the quasi-Gaussian profile, which now have enough energy to cause thermal damage but not enough energy to cause ablation. When the amount of energy per pulse was equal in both the TEM_{oo} and TEM_{mn} modes, the zones of thermal damage were comparable (Table 1).

The reason for the large increase in the zone of thermal injury for methacrylate as opposed to bone is most likely related to the physical parameters of the two substrates. Although little experimentation has been done to determine the thermal conductivity, specific heat, heat capacity, and heat of fusion for methacrylate, those values that have been reported are significantly lower than those for the cortical and cancellous bone typically found in the rabbit femur [9]. Extrapolation of these physical constants to our system does involve some uncertainties, but these parameters could be useful in developing a temperature profile that could facilitate prediction of the zone of thermal damage in both bone and methacrylate.

The histopathology of the ablation produced by the erbium:YAG laser resembles that produced by the pulsed ultraviolet radiation of excimer lasers but for a different reason. With the excimer laser, "ablative photodecomposition" results in the breakup of materials by high-energy ultraviolet photons with the expulsion of atoms and small molecular fragments at supersonic velocities [10]. As discussed previously, the erbium:YAG laser ablates tissue by a buildup of internal pressure caused by heat until a microexplosion occurs with part of the substrate being ejected in the form of microscopic particles.

The main problem with the 2.94-μm wavelength of the erbium:YAG laser is the difficulty in devising a suitable fiber optic delivery system. The transmission of this wavelength through zirconium fluoride and fluoride glass fibers has been shown to be possible but requires stringent glass-

Fig. 3. Phase-contrast histologic photomicrographs of cuts made in methacrylate with the erbium:YAG laser: a) .15 J/pulse, b) 1.0 J/pulse. Note the deeper, wider cut produced in b with the increased energy per pulse and the fourfold increase in the zone of thermal injury (outlined by arrows). Bar in upper right hand corner of pictures is equal to 500 μm. ×32.

Fig. 4. Histologic photomicrographs of cuts made in bone with the erbium:YAG laser: a) .15 J/pulse, b) 1.0 J/pulse. Note the twofold increase in the zone of coagulation necrosis (outlined by arrows) as the energy per pulse is increased. Bar in upper right hand corner of pictures is equal to 10 μm. ×725.

TABLE 1. Zone of Thermal Injury in Bone and Methacrylate Produced by the Erbium:YAG Laser

Laser energy (J/pulse)	Fluence (J/mm^2)	TEM	Average zone of thermal injury[a] (μm)
Bone			
.10	5.7	oo	5.1
.15	8.5	oo	5.4
.20	11.3	oo	5.7
.10	1.6	mn	5.2
.15	2.3	mn	5.1
.20	3.0	mn	5.4
.25	3.7	mn	5.6
.40	5.7	mn	5.2
.55	7.5	mn	6.5
.70	9.2	mn	7.2
.75	9.8	mn	8.3
.85	10.8	mn	9.4
1.00	12.1	mn	11.3
Methacrylate			
.10	5.7	oo	91.2
.15	8.5	oo	92.5
.20	11.3	oo	97.9
.10	1.6	mn	90.2
.15	2.3	mn	93.7
.20	2.9	mn	97.2
.40	5.7	mn	115.1
.60	8.1	mn	200.8
.80	10.3	mn	240.4
1.00	12.1	mn	374.8

[a]Average taken from ten individual measurements made around crater produced by erbium:YAG laser irradiation.

processing techniques to avoid laser-induced damage [7,11]. In addition, the fibers are very brittle and susceptible to mechanical damage. When a clinically useful fiber with a high reliability against laser-induced and mechanical damage becomes available, the mid-infrared lasers should play a wider role in human ablative orthopaedic and ear surgery.

ACKNOWLEDGMENTS

This study was supported by NIH grants RR01192 and CA 32248 and Department of Defense grant SDI084-88-C-0025. The authors wish to thank Ms. Elaine Kato for her assistance in the preparation of the manuscript.

REFERENCES

1. Moore YH: Laser energy in orthopaedic surgery. In "Proc Int Congr Orthopaedic Surgeons." Amsterdam: Exerpta Medica, 1973: 1077 (abstract).
2. Horoszowski H, Heim M, Farine I: The carbon dioxide laser in orthopaedic surgery. In Ben-Hur E, Rosenthal I (eds): "Photomedicine," Vol. 3. Boca Raton, FL: CRC Press, Inc., 1987: 61–65.
3. Clayman L, Fuller T, Beckman H: Healing of continuous wave and rapid superpulsed carbon dioxide laser induced bone defects. J Oral Surg 1978; 36:932–937.
4. Smail I, Osborn T, Fuller T, Hussain M, Kobernick S: Observations of carbon dioxide laser and bone burr in the osteotomy of the rabbit tibia. J Oral Surg 1979; 37:159–166.
5. Gertzbein SD, deDemeter D, Cruickshank B, Kaparsouri A: The effect of laser osteotomy on bone healing. Lasers Surg Med 1981; 1:361–373.
6. Allen G, Adrian J: Effects of carbon dioxide laser radiation on bone: An initial report. Milit Med 1981; 146:120–123.
7. Bonner RF, Smith PD, Leon M: Quantification of tissue effects due to pulsed Er:YAG laser at 2.9 um with beam delivery in a wet field in zirconium fluoride fibers. SPIE 1986; 713:2–5.
8. Biyikli S, Modest MF: Energy requirements for osteotomy of femora and tibiae with a moving CW CO_2 laser. Lasers Surg Med 1987; 7:512–519.
9. Nelson CG, Krishnan EC, Neff JR: Consideration of physical parameters to predict thermal necrosis in acrylic cement implants at the site of giant cell tumors of bone. Med Phys 1986; 13:462–468.
10. Srinivasan R: Ablation of polymers and biological tissue by ultraviolet lasers. Science 1986; 234:559–565.
11. Tran DC, Levin KH: Zirconium fluoride fiber requirements for mid-infrared laser surgery applications. SPIE 1986; 713:36–37.

Photochemistry and Photobiology Vol. 46, No. 2, pp. 165–167, 198
Printed in Great Britain. All rights reserved

0031-8655/87 $03.00+0.00
Copyright © 1987 Pergamon Journals Ltd

INHIBITION OF NUCLEIC ACID SYNTHESIS IN CELLS EXPOSED TO 200 MICROMETER RADIATION FROM THE FREE ELECTRON LASER

Michael W. Berns[1] and William Bewley[2]
[1]Department of Surgery, Beckman Laser Institute and Medical Clinic, University of California, Irvine, California 92717
[2]Department of Physics, University of California Santa Barbara, California 93106

(Received 4 May 1987; accepted 20 may 1987)

Abstract--Vertebrate tissue culture cells were exposed to 200 μm wavelength radiation (100 W/cm^2) from a free electron laser (FEL) of the electrostatic generator type. Cell cultures demonstrated no morphological alterations but a statistically significant ($P \leq .05$) proportion of the cells exhibited inhibition of DNA synthesis. This study demonstrates the first biological effects of the FEL and the feasibility of performing biological investigations with this device.

INTRODUCTION

Free electron lasers (FEL) can provide tunable, intense monochromatic electromagnetic radiation extending all the way from ultraviolet to the far infrared. As such, they could have great potential in biological, chemical and medical research and applications, insofar as they could be used to access regions of the spectrum not now available by fixed frequency sources. In this study we report the first series of biological experiments utilizing a FEL at 200 μm.

MATERIALS AND METHODS

The biological samples were cells from an established cell line from the rat kangaroo kidney (PTK_2). These are standard cells grown in many cell biology laboratories, and are particularly useful as a biological assay system because of their flat morphology, hardy nature, and low chromosome number (Berns et al., 1977). The cells used in these studies were grown in Rose culture chambers which were comprised of two optical windows separated by a silicone gasket that provided an enclosed sterile chamber capable of holding a volume of 2-3 ml of fluid. One of the two windows was made of either fused silica or crystalline quartz. The former had 65% transmission and the latter 95% transmission for the FEL wavelength (200 μm) used in these studies. The cells were injected into the culture chambers 24-48 hours prior to FEL exposure and maintained in standard MEM culture medium at 37°C in 5% CO_2 and air. The chambers were positioned in the incubator such that the cells settled onto the window surface that was transparent to the FEL wavelength. The cells attached to this surface where they multiplied and underwent normal physiological and biochemical activity (Berns et al., 1981). For exposure to the FEL, the culture chamber was positioned (described later) so that the FEL radiation passed through the highly transmissive window directly on to the cells before passing into the culture medium. This was possible because the cells attached tightly to the window surface with little or no liquid interface between the cell and the surface. The windows were 2.5 cm in diameter and had a thickness of 0.01 mm.

The FEL was the Van deGraff electrostatic accelerator system at the University of California, Santa Barbara. For the studies reported here the laser was operated at a wavelength of 200 um with a pulse duration of 2 μs. Laser power varied from 0.5 - 4 kW per pulse. Pulse repetition frequency varied from 3 - 6 seconds between pulses. The FEL beam was collected and focused to a spot at the culture chamber window surface.

The beam profile at the sample position was measured by mechanically scanning a pyroelectric detector perpendicularly across the sample beam in two orthogonal directions (X and Y). The detector used was a Molectron model P3-01 with a 1 mm diameter detection element. Measurements were made over 25 mm intervals with the final scans made through the center of the beam. The 1/e half-width of the beam was measured to be between 7 and 8 mm. The power density at the center of the sample beam was measured and the reference signal calibrated for use in monitoring the power per pulse during the experiment. The power density per pulse was typically 100 W/cm^2. The transmission of the

fused silica and quartz windows was determined from the ratios of the sample and reference signals with the windows alternately placed into and removed from the sample beam path.

The experimental protocol involved placement of 10 culture chambers in a remotely controlled rotating assembly that positioned each individual chamber in the FEL beam path for a preselected number of FEL pulses. The entire assembly plus culture chambers was surrounded by lead bricks in order to shield the cells from high energy ionizing radiation generated during FEL operation. Control culture chambers were placed within the assembly, but did not rotate into the path of the FEL beam. Prior to and immediately after placement of the culture chambers into the rotating assembly, the chambers were stored at 37°C in an adjacent room. All exposures to the FEL occurred at room temperature (18-20°C). Cells were examined cytologically through an inverted phase contrast microscope at 30 minute intervals following removal of the chambers from the rotating assembly. Individual culture chambers were exposed to a range of 1-100 laser pulses. In all experiments at least 5 replicate chambers were exposed to each pulse regime.

Two methods were used to assay FEL effects: (1) observation of cell cytology by phase contrast light microscopy, (2) incubation in radioactive ^{3}H-thymidine (specific activity 40-60 Ci/mmole at concentration of 5 uCi/ml for 48 hrs) followed by light microscope autoradiographic analysis of DNA synthesis. For autoradiographic analysis, the cells within the 5mm FEL irradiation zone were scored either "heavy" or "light" for the amount of radioactive labeling (Fig. 1). Either 100 or 500 cells were scored in each culture chamber by a person who was unaware of the treatment parameters of the individual samples being scored. An additional control population of cells were those cells within the irradiation chamber but outside the FEL exposure zone. Comparison of the experimental and control cell populations was made by using two different statistical tests: (1) one way analysis of variance and (2) the Kruskal-Wallis nonparametric test.

RESULTS AND DISCUSSION

Cytological observation immediately (within 30 minutes) and up to 3 hours following laser exposure did not reveal any evidence of FEL effects. At 20 hours following FEL exposure, cells were scored cytologically: dead; normal cytology in interphase; normal cytology in mitosis. A cell that was categorized as dead had a dark, pyknotic nucleus; a refractile appearing nucleolus; a phase darkened nuclear envelope; and cytoplasmic vacuolation. Scoring of 5000 cells (500 cells per chamber in 10 replicate chambers) for each of the FEL exposures revealed only a slight increase in dead cells for the chambers receiving 100 pulses of FEL radiation: 7% of the experimental cells exhibited "cell death" cytology as compared to 4% for the controls. Though the cytological results suggested that there was an effect on a small proportion of the cells in the cell populations exposed, the statistical tests used did not provide the level of statistical significance needed to conclude that the FEL inhibited cell growth. Subsequent DNA synthesis studies were undertaken to more precisely determine if the results of the cytological study were statistically significant at the biochemical level.

Three separate experiments (each a month apart) were conducted using ^{3}H-thymidine autoradiography. In each experiment five hundred cells were scored in at least five replicate chambers for each laser power exposure. The results of the three experiments are presented in Table 1. It should be noted that in each experiment there was always an increase when compared to the controls in the mean number of cells that were scored as "light" with respect to radioactive labeling (see Figure 1 for an example of cells exhibiting "light" and "heavy" labeling). The levels of statistical significance for each of these experiments was $p \leq 0.05$ using both statistical methods. The total number of laser pulses was 100 for each culture chamber in the first two experiments. In the third experiment chambers were exposed to 10, 20, or 100 laser pulses. When compared to the non-laser control, only the cells receiving 100 laser pulses were statistically different.

Figure 1. Autoradiogram of PTK$_2$ cells exhibiting "light" and heavy radioactive labeling. Large arrows indicate heavily labeled nuclei and small arrows indicate "lightly" labeled cells.

The results of these studies are interesting not only because they are the first biological studies with the FEL, but also because the observed effects appear to be on only a small subpopulation of cells within the cultures. Even though there have been some studies demonstrating raman bands for B-DNA at 12 cm^{-1} (Lindsey et al, 1984) and low lying vibrational modes for oriented films of DNA at 3-450 cm^{-1} (Wittlin et al, 1986), there seems to be a general lack of literature on the biological effects of radiation in the 100 micron to one millimeter wavelength range. The present study suggests that there may be vibrational modes in heterogeneous living biological systems in this wavelength range that lead to either thermal or non-thermal effects in the cells. It is interesting that only a small proportion of the cells appear to be affected. It is possible that the cells exhibiting inhibited DNA synthesis represent either a unique genetic subpopulation or a fraction of cells that were in a "susceptible" phase of the cell cycle at the time of irradiation. Furthermore, it is known that there are sharp resonances in the microwave region that result in a stimulation of growth in yeast (Grundler and Keilmann, 1983) that have been shown to be non-thermal. In conclusion, the FEL provides a unique source of intense monochromatic radiation for studies in a region of the spectrum that has not been well characterized in biological systems. In addition, it does appear feasible to perform biological and medical studies with the technologically complex FEL.

Table 1: Cells Exhibiting "Light" ^{3}H-Thymidine Label

	Exp. I	Exp. II	Exp. III
Control	43*	92	43
**100 laser pulses	70	114	74
20 laser pulses	-	-	61+
10 laser pulses	-	-	50+

*All values are means based upon 500 cells tabulated per culture chamber with 5-10 replicate chambers to obtain each mean. Each group receiving 100 laser pulses is statistically different from the control value with $p = \leq .05$.

+These values are not statistically different from the control value.

**Each laser pulse power density was 100 W/cm^2 with a duration of 2 μs per pulse.

ACKNOWLEDGEMENTS

We wish to thank Chung-Ho Sun, John Mellott and Marie Wilson for their technical assistance. Professors Vincent Jaccarino and Luis Elias are gratefully acknowledged for their intellectual input and for making the Santa Barbara FEL available for this study. This work has been supported by grant #N00014-86-K-0115 from the ONCR SDI program.

REFERENCES

Berns, M. W., J. B. Rattner, S. Brenner and S. Meredith (1977) The role of the centriolar region in animal cell mitosis: a laser microbeam study. J. Cell Biol. 72, 351-367.

Berns, M. W., J. Aist, J. Edwards, K. Strahs, J. Girton, M. Kitzes, M. Hammer-Wilson, L.-H. Liaw, A. Siemens, M. Koonce, P. Walter, D. van Dyk, J. Coulombe, T. Cahill and G. S. Berns (1981) Laser microsurgery in cell and developmental biology. Science 213:505-513.

Grundler, W. and F. Keilmann (1983) Sharp resonances in yeast growth prove nonthermal sensitivity to microwaves. Physical Review Letters 51: 1214-1216, The American Physical Society.

Lindsay, S. M., J. W. Powell and A. Rupprecht (1984) Observation of low-lying raman bands in DNA by tandem interferometry. Physical Review Letters 53:1853-1855, The American Physical Society.

Wittlin, A., L. Genzel, F. Kremer, S. Haseler and A. Poglitsch (1986) Far-infrared spectroscopy on oriented films of dry and hydrated DNA. Physical Review A 34:493-500, The American Physical Society.

CANCER RESEARCH 47, 4681–4685, September 1, 1987]

In Vivo Studies on the Utilization of Mono-L-aspartyl Chlorin (NPe6) for Photodynamic Therapy

I. Stuart Nelson, W. Gregory Roberts, and Michael W. Berns[1]

Department of Surgery, Beckman Laser Institute and Medical Clinic, University of California, Irvine CA 92717

ABSTRACT

The *in vivo* photosensitizing efficacy of mono-L-aspartyl chlorin has been studied by determining the percentage of BALB/c mice cured at varying doses of drug. Using an EMT-6 tumor model, animals received i.p. injections of mono-L-aspartyl chlorin (0.5–100 mg/kg) and then were subsequently exposed to light at 664 nm. Tumor biopsies were taken from selected animals sacrificed at 24 h after treatment and routine histopathological sections made. The other animals remained in the dark for a period of 6 weeks to determine the cure rate.

Our results show that mono-L-aspartyl chlorin is an effective tumor localizer that brings about the selective degradation of tumor tissue following light exposure.

INTRODUCTION

The attack on cancer with drugs has been based on the thesis that it should be possible to target cancer cells while having only little or tolerable effects in normal cell populations. Many compounds have been screened for such activity during the past 40 years. Unfortunately, most common solid cancers respond either not at all or to a limited extent to these selective agents.

Several photosensitizing porphyrins are selectively retained in solid tumors and other rapidly growing tissues in humans and other animals. During the past several years, there has been an increasing interest in the use of porphyrins for tumor localization and therapy. Effective use of porphyrin photosensitizers for antitumor therapy has been documented at several clinical centers and has been used on several thousand patients with generally encouraging results (1–4). Although the history of porphyrins and their role as a diagnostic and therapeutic modality is relatively recent, a wide variety of human tumors with varying histological types have been treated. Good results with PDT[2] have been reported with cancers of the skin (5), female genital tract (6), lung (7), esophagus (8), bladder (9), eye (10), breast (11), and oropharynx (12).

This photochemotherapeutic procedure which has become known as photodynamic therapy is based on the conclusion that some porphyrins, including HpD, are to some degree selectively retained by tumor tissue (13). On subsequent illumination with light of the appropriate wavelength absorbed by the porphyrin, tumors can be destroyed with relatively little damage to the surrounding normal tissue.

The properties of tumors that result in selective accumulation and retention of porphyrins remain to be elucidated. In cell culture, there appears to be no preferential uptake of porphyrins by either neoplastic *versus* normal cells (14–16) or as a function of malignancy in different cell lines (17). What is clear is that porphyrins are potent photosensitizers which result in the rapid necrosis of tumor tissue upon exposure to red light at 630 nm (the longest wavelength absorption peak of the porphyrin).

The major limitation of HpD-PDT is that it is primarily restricted to thin superficial tumors readily accessible to light. The attenuation of a light beam propagating in tissue is determined by the scattering and absorption characteristics of the tissue being exposed. It has been demonstrated that the efficiency for excitation of a drug molecule in a collimated beam of 630 nm light will be reduced to 10% at a location less than 1 cm from the tissue surface (18). Generally, absorption, which depends on specific chromophores in the absorbing molecules, increases with increasing wavelength. Furthermore, compounds with higher molar extinction coefficients may have a significant advantage in capturing any photons that penetrate into the tissue. It is anticipated that the development of other photosensitizers that utilize longer wavelengths with stronger absorption bands in the red and higher extinction coefficients will enhance the versatility of PDT.

In the present study, we have examined the effectiveness of NPe6 as a photosensitizer for selective tumor necrosis (Fig. 1). This compound has a strong absorption band at 664 nm, a wavelength that has a greater depth of tissue penetration than the 630 nm wavelength used with HpD.

MATERIALS AND METHODS

NPe6 and Photofrin II. NPe6 (Porphyrin Products, Logan, UT) was received as a dark blue-green powder and was stored in the dark at −70°C. The powder was reconstituted in Dulbecco's PBS (final pH 7.0–7.20) to a final concentration of 2.5 mg/ml and stored at −20°C until used. Photofrin II was obtained from Photomedica Inc., (Raritan, NJ) as an aqueous solution at a concentration of 2.5 mg/ml and stored in the dark at −20°C until used. An absorption spectrum of NPe6 was obtained with a Beckman DV-7 Spectrophotometer on PTK_2 cells (rat kangaroo epithelial, American Type Culture Collection no. 56, kidney marsupial, *Potorus tridactylis*) incubated for 24 h with 25 μg/ml NPe6. Cells were washed three times in PBS and sonicated prior to being scanned from 350 to 700 nm.

Animal and Tumor System. Ten- to 12-week old BALB/c mice were used. They weighed between 30 and 35 g at the time of treatment. The tumor system used was the EMT-6 undifferentiated sarcoma obtained from the Frederick Cancer Research Institute, Frederick, MD. The EMT-6 tumor was obtained as an *in vitro* culture. Tumor cells were harvested from tissue culture flasks and a heavy inoculum was injected into the right flank of the mice. When the tumors attained a size of 1–2 cm in diameter, they were excised and minced in PBS. The resulting suspension of tumor cells was filtered through sterile fine-mesh gauze, washed twice in PBS and resuspended in RPMI media (GIBCO, Grand Island, NY) at a concentration of 5×10^5 viable cells/ml. Cell viability was assessed by the ability to resist cell lysis and exclude Trypan Blue dye (GIBCO). Tumors were initiated by injecting 0.1 ml of fresh tumor inoculum into the right flank of the mouse. The mouse tumors were generally palpable at 5 days and reached a size of 5–7 mm at 10–14 days at which time treatment was started. At this size, the small tumor was homogeneously white, and spontaneous tumor necrosis was minimal or absent.

Light Exposure. When tumors were of the appropriate size (as indicated above), the animals were shaved in the tumor area and given i.p. injections of NPe6 in doses of 0.5–100 mg/kg body weight. The

Received 7/17/86; revised 1/12/87, 4/14/87; accepted 6/8/87.

The costs of publication of this article were defrayed in part by the payment of page charges. This article must therefore be hereby marked *advertisement* in accordance with 18 U.S.C. Section 1734 solely to indicate this fact.

[1] To whom requests for reprints should be addressed, at University of California, Irvine, Beckman Laser Institute, Department of Surgery, 1002 Health Science Road East, Irvine, CA 92715.

[2] The abbreviations used are: PDT, photodynamic therapy; HPD, hematoporphyrin derivative; NPe6, mono-L-aspartyl chlorin; PBS, phosphate buffered saline; EMT-6, experimental-mammary-tumor.

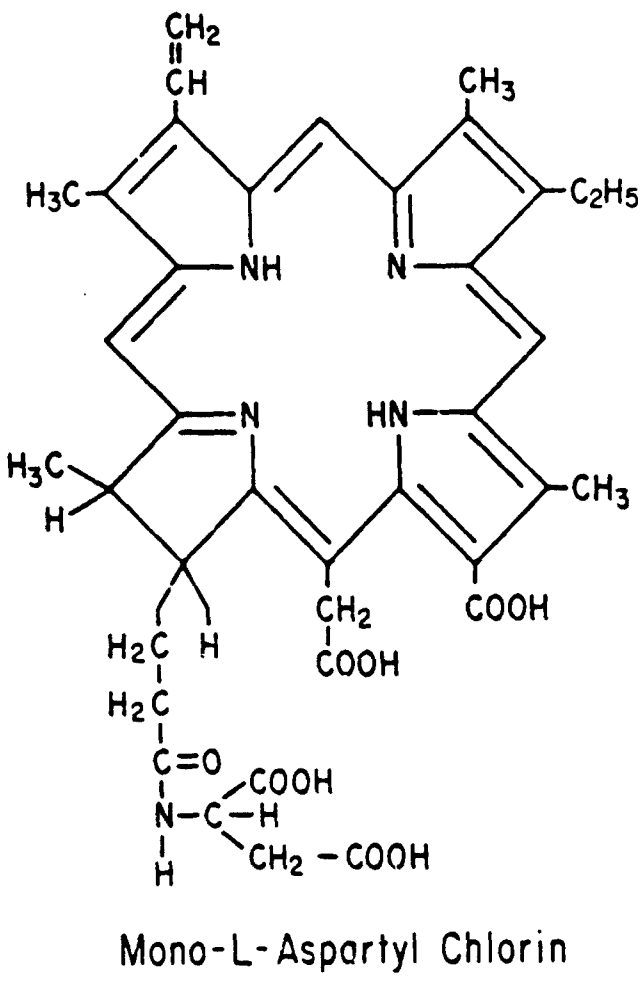

Fig. 1. Chemical formula of mono-L-aspartyl chlorin.

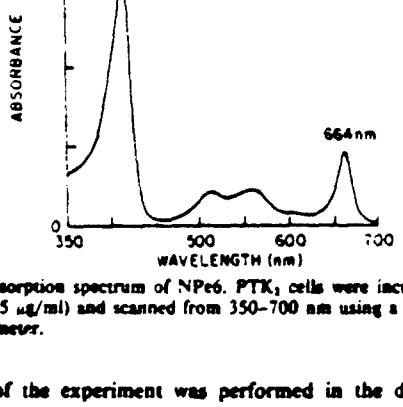

Fig. 2. Absorption spectrum of NPe6. PTK$_2$ cells were incubated for 24 h with NPe6 (25 μg/ml) and scanned from 350–700 nm using a Beckman DV-7 spectrophotometer.

remainder of the experiment was performed in the dark including housing of the animals. Control tumor-bearing animals received light without NPe6 as well as NPe6 without light. The experimental animals were treated with the laser light delivery system at 664 nm described below. Prior to illumination, the mouse was anesthetized with Ketamine HCl (Parke-Davis), and covered with a metal shield with a circular hole exposing only the tumor. Tumor biopsies were taken from selected animals sacrificed at 24 h after treatment. The other animals remained in the dark for a period of 6 weeks. Biopsy tissue was immediately fixed in 3% glutaraldehyde:5% formalin in phosphate buffer, pH 7.4. Samples were then dehydrated in graded alcohols, cleared in xylene, and embedded in paraffin. Six-μm sections were cut, stained with hematoxylin and eosin, cleared of paraffin in xylene, and dried. Sections were examined with a Zeiss Axiomat microscope, and photographed with Panatomic X film (Eastman Kodak).

Table 1 *NPe6 dose response*

Animals treated with 100 J/cm^2 at a power density of 100 mw/cm^2 24 h after injection with NPe6.

Dose of NPe6 (mg/kg)	Complete response (cured)	Partial response	No response	% Cured
100	10			100
80	10			100
60	10			100
40	10			100
20	10			100
10	10			100
9	10			100
8	10			100
7	5	5		50
6	3	7		30
5	3	7		30
4		10		0
3		10		0
2		7	3	0
1			10	0
.5			10	0

Laser Light Delivery System. Laser irradiation was performed with a Cooper Lasersonics (Santa Clara, CA) 770DL Argon dye laser system. The dye used in the dye laser was DCM Premixed Laser Dye (Cooper Lasersonics) with a tuning range of 610–690 nm. The dye laser was tuned to emit radiation at 664 ± 1 nm for the entire experiment. The wavelength was verified using a Jobin Yvon no. 5/354 UV monochromator (Longjumeau, France). The radiation from the dye laser was coupled into a 400-μm fused silica fiber optic. The output end of the fiber optic was terminated with a microlens that focused the laser radiation into a circular field of uniform light intensity. Laser irradiation emanating from the fiber was monitored with a Coherent Model 210 power meter before and after treatment.

Mice were placed underneath an aperture that controlled the area of light illumination on the tumor site. The area of illumination was 1 cm^2. Total laser energy density was 100 J/cm^2 with a power density of 100 mw/cm^2.

Dose Response Study. A total of 192 light-treated tumors were examined: 12 animals each at NPe6 doses of 0.5, 1, 2, 3, 4, 5, 6, 7, 8, 9, 10, 20, 40, 60, 80, and 100 mg/kg. Two animals were sacrificed at 24 h after treatment and their tumors removed for histopathological analysis as described above. The remaining 10 animals in each group were returned to the dark for a period of 6 weeks to determine the percentage of animals cured. Control experiments were also carried out: 12 animals with NPe6 (100 mg/kg) without light and 12 animals with 100 J/cm^2 light without NPe6.

Skin Photosensitivity Study. Animals were given i.p. injections of 10 mg/kg of either NPe6 or Photofrin II. An isolated patch of skin on the right hind leg of the animal measuring 1 cm^2 was subsequently exposed to light (664 nm for NPe6; 630 nm for Photofrin II) 24 h later. A total of 60 light-treated animals were examined: three animals each for NPe6 and Photofrin II at doses of 100, 200, 300, 400, 500, 600, 700, 800, 900, and 1000 J/cm^2. Control experiments were also carried out: three animals with 664 nm light at 1000 J/cm^2 and three animals with 630 nm light at 1000 J/cm^2 without drugs. The animals were returned to the dark and a clinical evaluation of the skin photosensitivity was made daily for 10 days posttreatment.

RESULTS

The absorption spectrum of NPe6 in cells demonstrated the main absorption peaks at 202, 284, 400, 502, and 664 nm (Fig. 2). The 664-nm peak was selected for treatment because of the improved tissue transmittance of light at this longer wavelength.

The effect of NPe6 and activating red light at 664 nm on 192

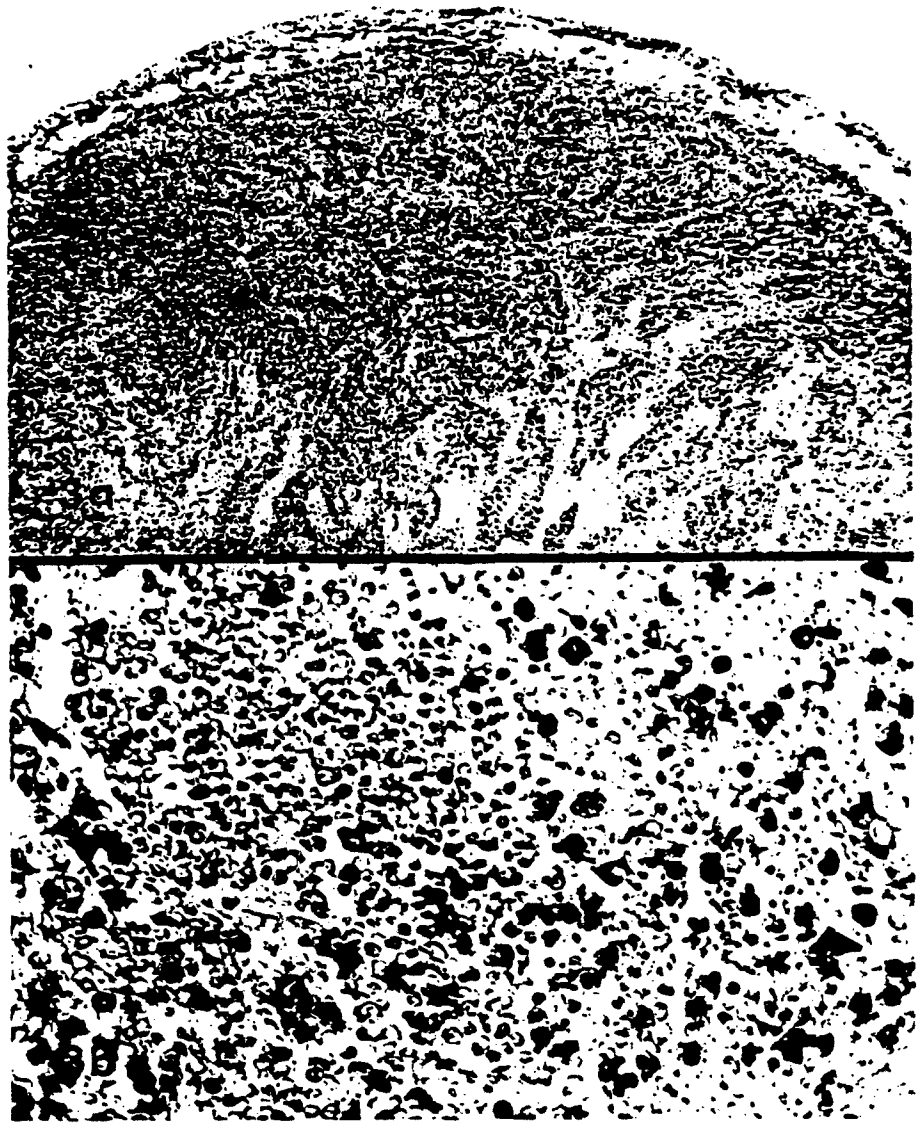

Fig. 3. Photomicrographs of EMT-6 tumor treated with NPe6 (8 mg/kg) and 100 J/cm² light at 24 h postinjection. Biopsies shown were taken 24 h after laser irradiation. In *a*, note the vast areas of hemorrhagic necrosis throughout the entire tumor; *b*, high power magnification of *a* showing tumor cells in varying stages of cell death and disintegration in a sea of red blood cells. *a*, 100 ×; *b*, 570 ×.

Table 2 *Photofrin II versus NPe6 skin photosensitivity*

Animals treated with 10 mg/kg of each drug and irradiated 24 h later at a power density of 100 mw/cm².

Dose of light (J/cm²)	Clinical evaluation[a]	
	Photofrin II (630 nm)	NPe6 (664 nm)
100	++	0
200	++	0
300	++++	0
400	++++	0
500	++++	0
600	++++	0
700	++++	0
800	++++	0
900	++++	0
1000	++++	0

[a] 0, no response; +, erythema; ++, blistering; +++, crusting/erosion; ++++, necrosis.

tumors in mice is summarized in Table 1. With 100 J/cm² of light exposure at a power density of 100 mw/cm², we obtained a 100% cure rate at NPe6 doses of 8–100 mg/kg. Cure is defined as no palpable tumor mass at least 6 weeks after treatment. Without treatment, 100% of these animals died within 1 month of tumor inoculation. In the experimental animals, there was complete disappearance of palpable tumor mass with biopsy confirmed tumor necrosis beginning 24 h after light treatment. Tumor tissue biopsy of these animals at 24 h posttreatment revealed massive hemorrhagic necrosis with frank extravasation of red blood cells into the surrounding tumor stroma. The tumor cell architecture is characterized by nuclear pyknosis and karyorrhexis, with only minimal preservation of the basic cellular shape permitting recognition of the cellular outline in a sea of amorphous granular debris (Fig. 3). The entire tumor mass disintegrated into a nonpalpable scab within a few days after treatment and eventually, the skin completely healed with varying degrees of hair regrowth. At NPe6 doses of 5–7 mg/kg, all animals responded to the treatment with varying results of partial to complete necrosis. However, regrowth of the noncured tumors (partial necrosis) generally was apparent within 7–8 days and usually occurred around the periphery of the original tumor. These tumors grew as rapidly as the nontreated tumors and these animals subsequently died of tumor bulk at the same time as the untreated controls. Between doses of NPe6 (2–4 mg/kg) there was partial necrosis with no cures and at doses of 0.5–1 mg/kg no response.

Additionally, we attempted to determine the isolated skin

photosensitivity of animals receiving NPe6 (10 mg/kg) *versus* Photofrin II (10 mg/kg) at light doses of 100–1000 J/cm^2. Animals that received Photofrin II (10 mg/kg) and light up to 1000 J/cm^2 (630 nm) showed severe blistering with subsequent skin slough at 100–200 J/cm^2 and frank skin necrosis at 300 J/cm^2 or more. Animals that received NPe6 (10 mg/kg) and light to doses as high as 1000 J/cm^2 (664 nm) showed no signs of erythema (Table 2). Control animals with 1000 J/cm^2 of light at either the 630 nm or 664 nm wavelengths showed no signs of erythema.

DISCUSSION

During the past 10 years, the selective photodegradation of malignant tissue by hematoporphyrin derivative has proved to be a promising new therapeutic modality in the treatment of cancer. In some cases, it may be a viable alternative to debilitating surgery, while in others, it may be the treatment of choice. However, despite its broad experimental application in clinical oncology, efforts have been hampered by the lack of a complete understanding of what active component in the HpD complex is responsible for tumor uptake and retention. The most active component has been described as a dihematoporphyrin ether by Dougherty (19) or as a dihematoporphyrin ester by Kessel (20). Even though there is an increased tumor:neighboring tissue porphyrin content ratio following HpD administration, the amount retained by normal tissues such as the skin, liver, spleen, and kidney is significant. This is sufficient to cause nonspecific skin necrosis following PDT of cutaneous malignancies as well as photocutaneous side effects which can persist up to 4 to 6 weeks after HpD administration. These problems as well as a relatively weak porphyrin absorption band and low tissue transparency at 630 nm resulting in inefficient phototoxicity have resulted in considerable effort being devoted to developing new and more efficient tumor localizing photosensitizers for PDT.

The chlorins are known to have strong absorption bands with high molar extinction coefficients at wavelengths greater than 650 nm thus providing an advantage over the lower tissue penetrance of 630 nm used for HpD. Our study was undertaken to evaluate the photosensitizing potential of NPe6 with a significant absorption band located at 664 nm.

This study describes the first successful "cures" resulting in long term animal survival with NPe6 and light. The results of our study suggest that NPe6 is an effective tumor photosensitizer *in vivo*. Our study shows that 100% cure rates can be obtained at an NPe6 dose as low as 8 mg/kg. In no animals has the tumor reappeared after 6 weeks following treatment. We can expect a 30–50% cure in animals receiving 5–7 mg/kg. Animals that received 2–4 mg/kg of NPe6 exhibited no cures but did have some observable response. Animals that received NPe6 (0.5–1 mg/kg) showed no response. The amounts of light energy used in this experiment have been shown by our group (21–23) and others (24) to effectively destroy the EMT-6 tumor in conjunction with HpD. Further studies on the uptake and excretion of NPe6 by proliferating tumor cells are needed to determine the optimal time for light exposure after injection.

As mentioned previously, a major drawback of this form of therapy is the potential for drug-induced sensitivity to sunlight. These effects are not trivial and may result in symptoms ranging from slight erythema and edema to extensive skin damage and necrosis. Ideally, the photosensitizer should be modified to avoid the deleterious effects on normal skin tissue upon light exposure. In the experiment reported here, animals that received NPe6 (10 mg/kg) and 100–1000 J/cm^2 of light showed no deleterious side effects whereas the HpD animals suffered adverse skin reactions such as blistering with subsequent skin slough and necrosis. This lack of skin photosensitivity which minimizes undesired side effects is clearly an advantage of NPe6. These results suggest that NPe6 may provide a realistic approach to the treatment of tumors where exposure to sunlight is unavoidable or even desirable.

While our study is promising, the studies on NPe6 are still at an early phase. Unanswered questions include delineation of light and drug dosimetry parameters, mechanisms of tumor localization, possible uptake in other organs such as liver, intestine, spleen, and kidney as well as determination of PDT cytotoxicity. It is hoped that future investigation will address these questions so that the role of NPe6 in the management of cancer can be fully defined.

ACKNOWLEDGMENTS

We thank William Wright and Jeffrey Andrews for technical assistance and Beverly Byadman for her assistance in the preparation of the manuscript. This research was supported by NIH Grants RR-01192 and CA-32248.

REFERENCES

1. Cortese, D. A., and Kinsey, J. H. Endoscopic management of lung cancer with hematoporphyrin derivative phototherapy. Mayo Clin. Proc., *57:* 543–547, 1982.
2. Dahlman, A., Wile, A. G., Burns, R. G., Mason, G. R., Johnson, E. M., and Berns, M. W. Laser photoradiation therapy of cancer. Cancer Res., *43:* 430–434, 1983.
3. Dougherty, T. J., Boyle, D. G., Weishaupt, K. R., Henderson, B. A., Potter, W. R., Bellnier, D. A., and Wityk, K. E. Photoradiation therapy—clinical and drug advances. *In:* D. Kessel and T. J. Dougherty (eds.), Porphyrin Photosensitization, pp. 3–13. New York: Plenum Publishing Co., 1983.
4. Hayata, Y., Kato, H., Konaka, C., Ono, J., and Takizawa, N. Hematoporphyrin derivative and laser photoradiation in the treatment of lung cancer. Chest, *81:* 269–277, 1982.
5. Dougherty, T. J., Kaufman, J. E., Goldfarb, A., Weishaupt, K. R., Boyle, D., and Mittleman, A. Photoradiation therapy for the treatment of malignant tumors. Cancer Res., *38:* 2628–2635, 1978.
6. Rettenmaier, M. A., Berman, M. L., DiSaia, P. J., Burns, R. G., McCullough, J., and Berns, M. W. Gynecologic uses of photoradiation therapy. *In:* D. R. Doiron and C. J. Gomer (eds.), Advances in Experimental Medicine and Biology, Vol. 170, pp. 767–775. New York: Alan R. Liss, 1984.
7. Hayata, Y., and Kato, H. Applications of laser phototherapy in the diagnosis and treatment of lung cancer. Jpn. Ann. Thoracic Surg., *3:* 203–210, 1983.
8. Dougherty, T. J. Photodynamic therapy (PDT) of malignant tumors. CRC Crit. Rev. Oncol./Hematol., *2:* 83–116, 1984.
9. Benson, R. C., Farrow, G. M., Kinsey, J. H., Cortese, D. A., Zinke, H., and Utz, D. C. Detection and localization of *in situ* carcinoma of the bladder with hematoporphyrin derivative. Mayo Clin. Proc., *57:* 548–555, 1982.
10. Murphee, A. L., Doiron, D. R., Gomer, C. J., Szirth, B., and Fountain, S. W. Hematoporphyrin derivative photoradiation treatment of ophthalmic tumors. Clayton Foundation Symp. Porphyrin Localization and Treatment of Tumors, 1983.
11. Dougherty, T. J., Lawrence, G., Kaufman, G. H., Boyle, D., Weishaupt, K. R., and Goldfarb, A. Photoradiation in the treatment of recurrent breast carcinoma. J. Natl. Cancer Inst., *62:* 231–236, 1979.
12. Wile, A. W., Dahlman, A., Burns, R. G., and Berns, M. W. Laser photoradiation therapy of cancer following hematoporphyrin sensitization. Lasers Med. Surg., *2:* 163–168, 1982.
13. Evenson, J. F., Mann, J., Hindar, A., and Sommer, S. Tissue distribution of ^{3}H-hematoporphyrin derivative and its main components, ^{67}G and ^{125}I-albumin in mice bearing Lewis lung carcinoma. *In:* D. R. Doiron and C. J. Gomer (eds.), Porphyrin Localization and Treatment of Tumors, pp. 541–562. New York: Alan R. Liss, 1984.
14. Chang, C., and Dougherty, T. J. Photoradiation therapy: kinetics and thermodynamics of porphyrin uptake and loss in normal and malignant cells in culture. Radiat. Res., *74:* 498–506, 1978.
15. Henderson, B. W., Bellnier, D. A., Zirling, B., and Dougherty, T. J. Aspects of the cellular uptake and retention of hematoporphyrin derivative and their correlation with the biologic response to PRT *in vitro*. *In:* D. Kessel and T. J. Dougherty (eds.) Porphyrin Photosensitization, pp. 279–292. New York: Plenum Publishing Co., 1983.
16. Berns, M. W., Hammer-Wilson, M., Walter, R. J., Wright, W., Chow, M. H., Nahabedian, M., and Wile, A. Uptake and localization of HpD and active fractions in tissue culture and in serial biopsied human tumors. *In:* D.

R. De[illegible] and C. J. Gomer (eds.), Porphyrin Localization and Treatment of Tumors, pp. 501–520. New York: Alan R. Liss, 1984.
17. Moan, J., Steen, H. B., Øeren, K., and Christensen, T. Uptake of hematoporphyrin derivative and sensitized photoinactivation C3H cells with different oncogenic potential. Cancer Lett., *14:* 291–295, 1981.
18. Svaasand, L. O. Optical dosimetry for direct and interstitial photoradiation therapy of malignant tumors. *In:* D. R. Doiron and C. J. Gomer (eds.), Porphyrin Localization and Treatment of Tumors, pp. 91–114. New York: Alan R. Liss, 1984.
19. Dougherty, T. J. The structure of the active component of hematoporphyrin derivative. *In:* D. R. Doiron and C. J. Gomer (eds.), Porphyrin Localization and Treatment of Tumors, pp. 301–314. New York: Alan R. Liss, 1984.
20. Kessel, D., Chang, C. K., and Musselman, B. Structure of the tumor-localizing derivative of hematoporphyrins. *In:* D. Kessel (ed.), Methods in Porphyrin Photosensitization, pp. 213–227. New York: Plenum Publishing Co., 1986.
21. Nelson, J. S., Wright, W. H., and Berns, M. W. Histopathological comparison of the effects of hematoporphyrin derivative on two different murine tumors using computer enhanced digital video fluorescence microscopy. Cancer Res., *45:* 5781–5786, 1985.
22. Nelson, J. S., Wright, W. H., and Berns, M. W. Histopathological and fluorescence analysis of the photodynamic activity of whole hematoporphyrin derivative and its enriched active components. J. Natl. Cancer Inst., *75:* 1135–1140, 1985.
23. Nelson, J. S., Sun, C. H., and Berns, M. W. A study of the *in vivo* and *in vitro* photosensitizing capabilities of uroporphyrin I as compared to HpD. Lasers Surg. Med., *6:* 131–136, 1986.
24. Henderson, B. W., Waldow, S. M., Mang, T. S., Potter, W. R., Malone, P. B., and Dougherty, T. J. Tumor destruction and kinetics of tumor cell death in two experimental mouse tumors following photodynamic therapy. Cancer Res., *45:* 572–576, 1985.

Reprinted from: OPHTHALMOLOGY, Vol. 95, No. 10, October 1988
Copyright © 1988 by the American Academy of Ophthalmology

An Acute Light and Electron Microscopic Study of Ultraviolet 193-nm Excimer Laser Corneal Incisions

MICHAEL W. BERNS, PhD,[1] L.-H. LIAW, MS,[1] ALLISON OLIVA, BS,[1]
JEFFREY J. ANDREWS, BA,[1] RONALD E. RASMUSSEN, PhD,[2] SOL KIMEL, PhD[1]

Abstract: The 193-nm ultraviolet beam from an argon fluoride excimer laser was focused on the corneas of rabbits to produce incisions of the type necessary for radial keratotomy. The energy densities used were in two ranges, 1.0 to 2.1 J/cm^2 per pulse and 200 to 700 mJ/cm^2 per pulse. The eyes were enucleated and fixed for histologic and electron microscopic examination immediately after exposure. Structural analysis of the higher energy density exposures showed ridging on the surface of the cornea, micro-pitting on the stromal surface inside the cut, and denudation of the endothelium under the ablation zone. The lower energy density incisions did not exhibit significant surface ridging or endothelial cell loss but did exhibit significant stromal swelling during the laser exposure thus making it difficult to produce incisions of a precisely controlled depth. Beam profile measurements and infrared thermal measurements of the cornea surface during laser exposure were made. [Key words: cornea, electron microscope, laser, ultraviolet.] Ophthalmology 95:1422–1433, 1988

The use of the ultraviolet 193-nm excimer laser for surgical use on the cornea has been suggested in several studies since the first study by Trokel et al[1] in 1983 and others.[2–6] The apparent athermal removal of corneal tissue by a process termed *ablative photodecomposition* is common in all of these investigations.[7] Despite the original excitement generated by the possibility of producing precisely controlled, athermal laser surgery on the cornea, this approach is moving very slowly toward clinical application. The reasons for this are the many variables and contraindications that must be taken into consideration before acceptance of a new modality as complex as an ultraviolet laser beam. Some of the issues that remain unresolved are: (1) the levels of mutagenesis and carcinogenicity of the beam; (2) wound healing after tissue removal; (3) geometry of laser incidence on the cornea; and (4) determination of the best dosimetry for maximal rate of tissue removal with minimal effects on the epithelium and endothelium.[2,8]

In the current study, we have investigated some of the above-mentioned factors with particular emphasis on (1) dosimetry for optimal and consistent tissue removal, (2) characterization of the structural alteration of the cornea, and (3) possible contraindications caused by corneal swelling during laser exposure.

Originally received: December 28, 1987.
Revision accepted: March 22, 1988.

[1] Beckman Laser Institute and Medical Clinic, Department of Surgery, Irvine.
[2] Community and Environmental Medicine, University of California, Irvine.

Supported by NIH grant RR01192 and Department of Navy grant N00014-86-K-0115, and Coherent Radiation.

Reprint requests to Michael W. Berns, PhD, Beckman Laser Institute and Medical Clinic, 1002 Health Sciences Rd East, Irvine, CA 92717

MATERIALS AND METHODS

Experimental corneal ablations at 193 nm were conducted with a Lambda Physik EMG 103-MSC excimer laser (Gottingen, FRG). It contained helium, fluorine,

Best Available Copy

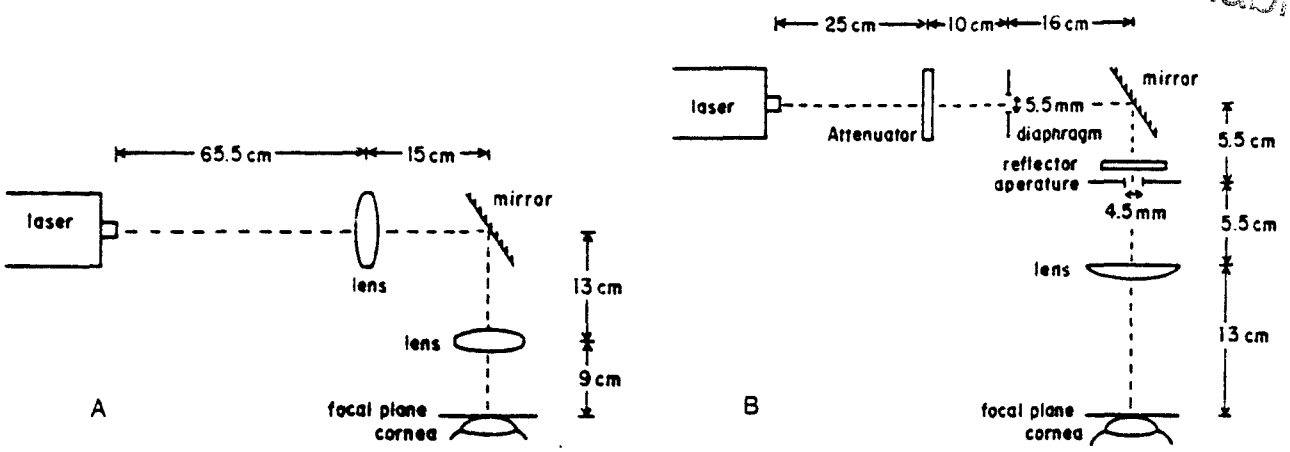

Fig 1. A, laser system using 50-mm spherical lens and 150-mm cylindrical lens. B, laser system similar to one used by Dehm et al[4] in 1986.

and argon gases to a total pressure of 2200 millibars and was operated in the stable configuration.

In the initial studies, the laser operating at 5 to 10 Hz output was focused through a 50-mm spherical lens, a 193-nm reflecting mirror, and a 150-mm cylindrical lens (Fig 1A). The beam image was either passed through a copper mask or imaged directly onto the corneal surface. In later studies, a lens configuration was employed similar to that used by Dehm et al.[4] Laser output operating at 10 to 50 Hz was shaped through an attenuator, a 5.5-mm diaphragm, a reflecting mirror, and a 150-mm planocylindrical lens. The beam was imaged directly onto the corneal surface with dimensions of 6.0 × 0.2 mm (Fig 1B). Pulse energies were measured at the laser head and at the corneal surface with Gentec #ED500 (Quebec, Canada) and Coherent #201 (Palo Alto, CA) meters. A Spiricon Model #LMP-32 × 16 matrix array detector (Logan, UT) was used to make beam profile energy measurements of the laser output in the configuration depicted in Figure 1B. Energy per pulse ranged from 0.2 to 2.1 J/cm^2. Total energy ranged from 120 to 1216 J/cm^2 with exposure times from 9 to 180 seconds. An Inframetrics thermal camera #600 with a close-up lens (Bedford, MA) was used to measure the temperature rise at the incision site during laser exposure.

A total of 25 male, Dutch Cross rabbits were used. Rabbits weighing 2 to 5 kg were anesthetized with Acepromazine (plegicil) (0.8 ml/kg) and a mixture of Rompum (xylazine):ketamine (0.25:0.49 ml/kg). Two animals were euthanatized with an intravenous injection of 0.5 ml euthanol, and the eyes were enucleated. After immersion in a Millonig's buffer rinse, each eye was placed on a specimen stage for irradiation. In the remaining 23 animals, the eyes were treated with Opthetic (0.05% proparacine HCl) as a topical anesthetic. Animals were immobilized in a holder and carefully positioned on their side to expose one eye which was held open for irradiation.

Twenty-two animals were assumed to have normal corneal thicknesses of 380 to 400 μm. Irradiation times were calculated from experimental ablation rates (microns of tissue removed/second) at a known energy density. In three rabbits, central corneal depths were measured with a Polkington specular microscope before irradiation. Exposure times were set using calculated average ablation rates from previous experiments. Within 30 minutes of irradiation, the animals were euthanatized and eyes were enucleated and rinsed in 0.2 M sodium phosphate buffer (pH 7.2). In all eyes, a small slit was made in the lateral globe to facilitate immersion fixation in a buffered 4% glutaraldehyde solution. After 24 hours in glutaraldehyde, eyes were again rinsed in buffer and the cornea dissected out and photographed using an Olympus AD camera system (La Palma, CA) through a Wild Heerburg dissecting microscope (Heerbrugg, Switzerland). One eye was processed for both light and transmission electron microscopic examinations. The other eye was processed for scanning electron microscopic examination.

Light and transmission electron microscopic samples were postfixed in a 1% buffered osmium tetroxide solution for 1 hour. After a buffer rinse, the eyes were stained in Kellenberger/UA pH 6.0 for 2 hours, dehydrated in an ethanol series and ethanol/propylene oxide mixture, and embedded in Medcast 800 epoxy resin. For light microscopic examination, 0.5 μm sections were cut on glass knives using a Reichert NR321820 or Sorvall MT6000 ultramicrotome. Sections were stained with Richardson's stain and photographed on an Olympus BH compound microscope. Sections for transmission electron microscopic study were made with a Dupont diamond knife and were stained with a standard uranyl acetate/methanol and lead counterstain. Transmission electron microscopy was performed on either a JEOL 100C (Peabody, MA) or Philips EM300 microscope (Mahwah, NJ) at 80 KV. Micrographs were taken to examine ultrastructural levels of disruption at the ablation site. Samples obtained from scanning electron microscopy were also postfixed in 1% osmium tetroxide.

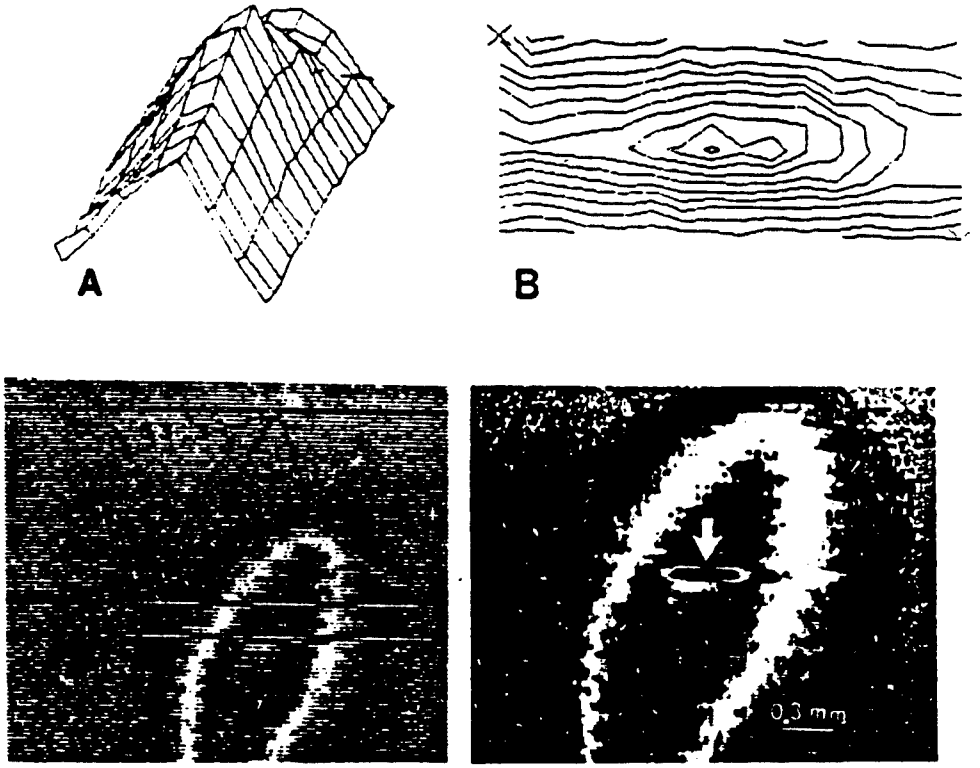

Fig 2. A, frontal and longitudinal beam profile of a 193-nm beam exiting the laser cavity in the stable configuration. B, top view of beam profile. C, thermal camera image of corneal surface during laser ablation at 193 nm, 400 mJ/cm^2 per pulse, 50 Hz. Graph superimposed on the image is the thermal profile across the ablation site at the bottom horizontal line (arrow). This thermal profile is from the plume immediately following laser exposure (see text). The ambient temperature on the corneal surface is 18.4°C. D, higher magnification than C. The width of the central peak temperature zone is 300 μm. Notice that the temperature of the adjacent surface drops to 38°C (light zone) almost immediately.

Fig 3. Rabbit cornea with incisions placed radially using energy densities of 1.0 to 2.1 J/cm^2 per pulse (original magnification, ×13.75).

dehydrated in acetone, critical point dried, and sputter coated with gold palladium on a Technics Hummer II (San Jose, CA) or gold on a Pelco PAC-1 evaporating system (Redding, CA). Micrographs were taken on either a Hitachi S500 (Mountain View, CA) or a Philips 515 (Mahwah, NJ) scanning electron microscope.

Best Available Copy

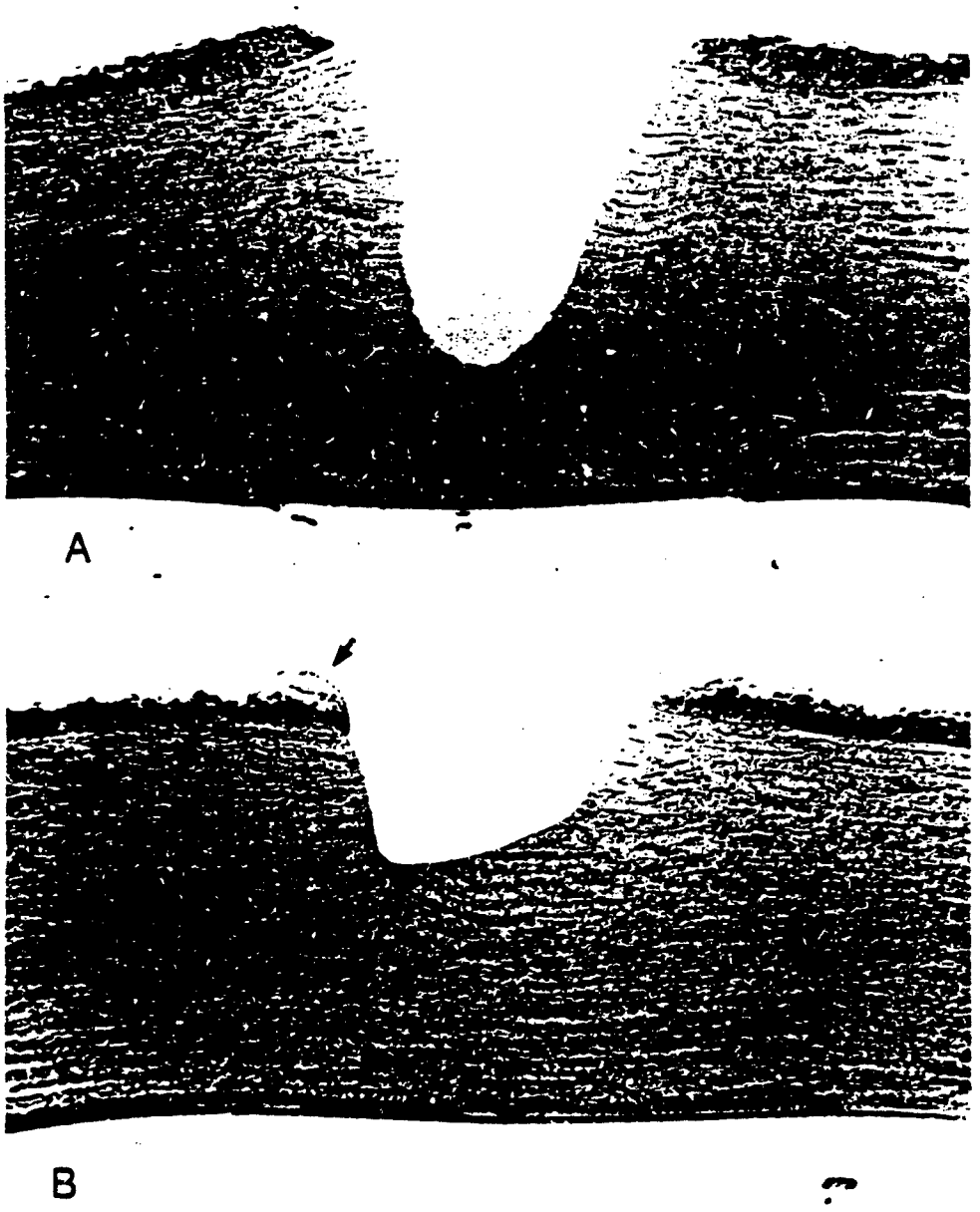

Fig 4. A, an 80% incision produced with 315 J/cm^2 over a 30-second irradiation period (2.1 J/cm^2 per pulse). B, a 40% incision with the same irradiation parameters as A, notice the epithelial ridge (arrow) (original magnification, ×180).

RESULTS

BEAM PROFILE AND THERMAL MEASUREMENTS

Energy profiles of the 193-nm excimer laser beam are presented in Figure 2 A and B. Figure 2A is a three-dimensional frontal view illustrating a gaussian-like profile in cross-section. Notice that the sides of the gaussian are rather steep with a minimal area of low-energy intensity. Figure 2B is a contoured energy profile from a dorsal view.

An infrared thermal profile across the ablation zone in a dorsal view is presented in Figure 2, C and D. The different gray levels represent temperature differences around the central ablation site. The average temperature profile across the ablation zone during exposure (laser operating at 50 Hz; 400 mJ/cm^2 per pulse) demonstrates a background (ambient) temperature of 18.4°C with average temperatures at the corneal surface immediately adjacent to the ablation zone of 38°C. Because of the characteristic scan rates of the thermal camera (horizontal 8000 Hz, vertical 60 Hz), the readout position of the scanner, for most pulses will not be near the point of laser impact at the time of incidence. Thus, the average temperature of the cornea at a later time (within the time interval 1/60 second = 16.6 msecond)

Fig 5. A, high-power magnification light micrograph of Figure 4B (original magnification, ×525). B, Scanning electron micrograph of corneal ridge (original magnification, ×260).

is recorded. However, for some laser pulses, the scanner will be at a position such that when it crosses the image field it coincides with the laser pulse (to within 1/8000 second = 125 μsecond). For this case, a higher temperature is recorded during one single scan line. This can be understood by noting that on impact, each laser pulse produces an ablation plume which lasts up to 150 μseconds.[9] This plume consists of a varified plasma and although it is characterized by a high temperature it does not emit strongly within the 8- to 12-μm response of the thermal camera, thus giving rise to a temperature reading (53°C) that is considerably lower than the actual plume temperature. The arrow in Figure 2C indicates the line across the corneal surface of this temperature profile. A higher magnification image depicting that thermal scan line is presented in Figure 2D. The arrow points to the peak temperature at the center of the incision. The scale indicates that the width of this peak temperature zone is 200 to 300 μm. The temperature rise of the corneal surface in between individual pulses at a 50-Hz pulse rate demonstrated a maximum temperature of 38°C (Fig 2, C and D).

HIGH ENERGY PER PULSE

In order to maximize the rate of tissue removal and minimize the total procedure time, energy densities from 1.0 to 2.1 J/cm^2 per pulse at 5 Hz were tried. In a typical experiment, a series of radial incisions were placed in eyes that had their central zone protected by a shield (Fig 3). Pairs of incisions were produced at 15, 20, 25, and 30 seconds of focused laser exposure. Upon sectioning and examination, it was obvious immediately that seemingly identical total energy densities produced different results. At maximum exposure (30 seconds, 315 J/cm^2) one incision extended 80% through the cornea (Fig 4A), whereas another extended only 40% (Fig 4B). In addition, in the 80% incision the endothelium was denuded from Descemet's membrane. In the 40% incision, no effect was detected in the endothelium but there was a definite folding over or "ridging" of the surface epithelium along the incision on the surface of the cornea. The cells in the folded-up ridge stained much less and appeared sharply altered from those in the adjacent, unaffected epithelium (Fig 5A). When a large number of incisions were examined with the scanning electron microscope, this ridging phenomenon was frequently observed (Fig 5B).

Analysis of the damaged endothelium by transmission electron microscopy (Fig 6A) showed a progression from total cellular destruction with fragmented external and internal membranes and organelles (Fig 6B) to a relatively intact endothelial cell with disruption primarily in the internal membranous organelles (Fig 6C). The cell closest to the denuded zone exhibited the former characteristics and the next cell moving away from the denuded zone exhibited the latter characteristics. This cell had normal-appearing nuclear chromatin and nuclear envelope. Results of the low-power micrographic examination showed a normal Descemet's membrane (Fig 6A).

Transmission electron microscopic images of the

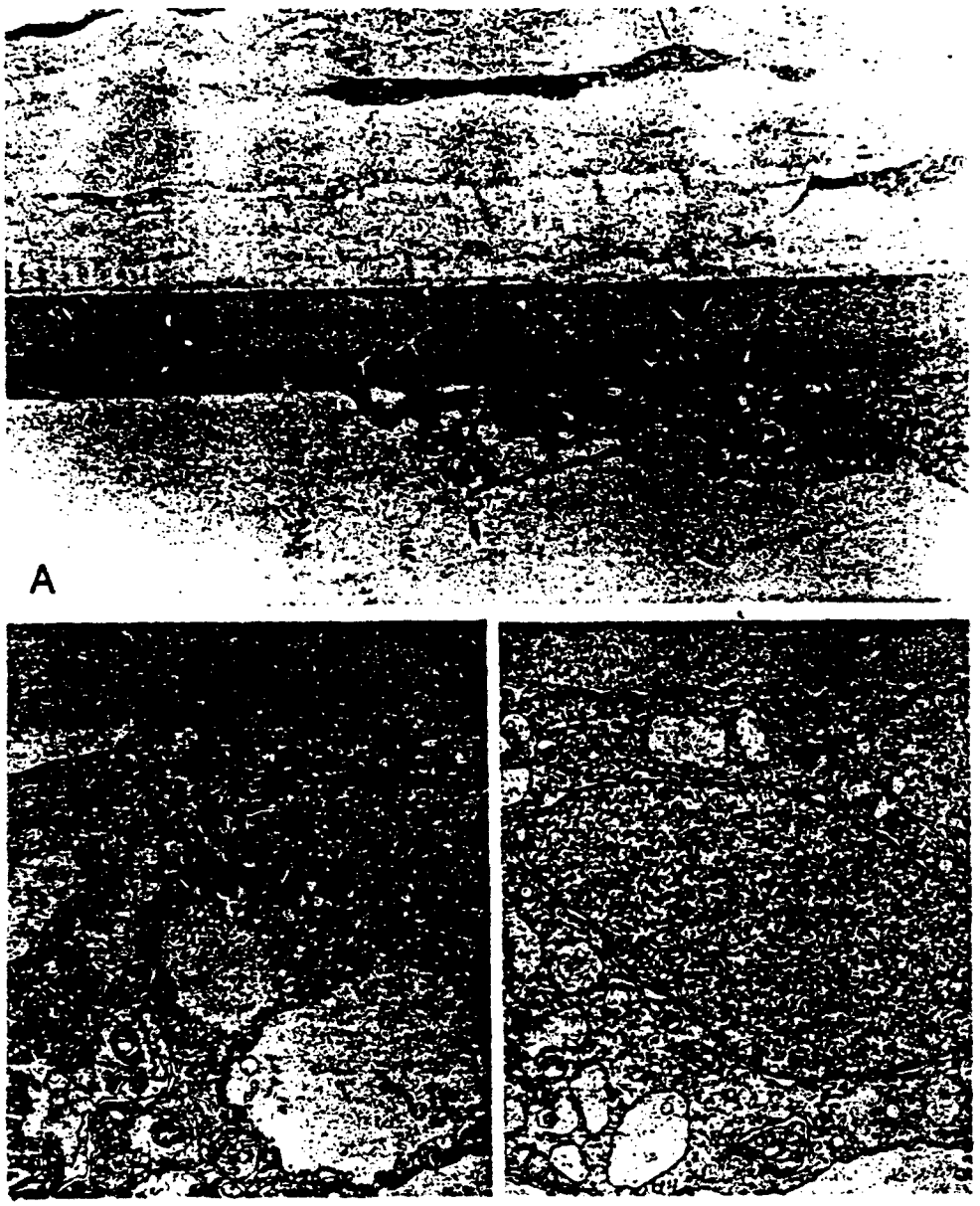

Fig 6. Transmission electron micrographs of the cornea base underneath the incision in Figure 4A. A, low-power magnification of the denuded Descemet's membrane and two adjacent endothelial cells with progressive damage (original magnification, ×2700). B, higher magnification of the endothelial cell immediately adjacent to the denuded portion of Descemet's membrane (original magnification, ×13,200). C, next cell distal to the denuded region (original magnification, ×13,200).

stromal surface inside the incision showed areas of micro-pitting (Fig 7A, arrows). A higher magnification demonstrated that there was some lightly staining particulate material in these micro-pits. In addition, an electron-dense pseudomembrane, approximately 25 nm in width, extended over the entire ablated stromal surface as well as into the micro-pits. Normal-appearing collagen fibers could be seen in both longitudinal and cross-section closely apposed to the pseudomembrane (Fig 7B).

LOW ENERGY PER PULSE

At lower energy densities (200–700 mJ/cm^2) and higher pulse rates (10–50 Hz), incisions were made that varied from 10 to 100% through the cornea (Table 1). The higher pulse rates were used in order to reduce the length of time that was required to make the incisions. It was evident that there was little correlation between the total energy and the depth of the cut. For example, two identical total energies of 158 J/cm^2 at 220 mJ/cm^2 per pulse resulted in 53 and 61% cuts. Similarly, 800 J/cm^2 at 670 mJ/cm^2 per pulse resulted in incisions of 100 and 50%.

In addition to the variation in incision depth, considerable swelling of the cornea was observed during the actual procedure. The average swelling in the ablation region was 26% for the 208- to 246-mJ/cm^2 lesions and 48% for the 670-mJ/cm^2 lesions (Table 1). The swelling was clearly in the region of the laser exposure as evidenced by scanning electron microscopic examination

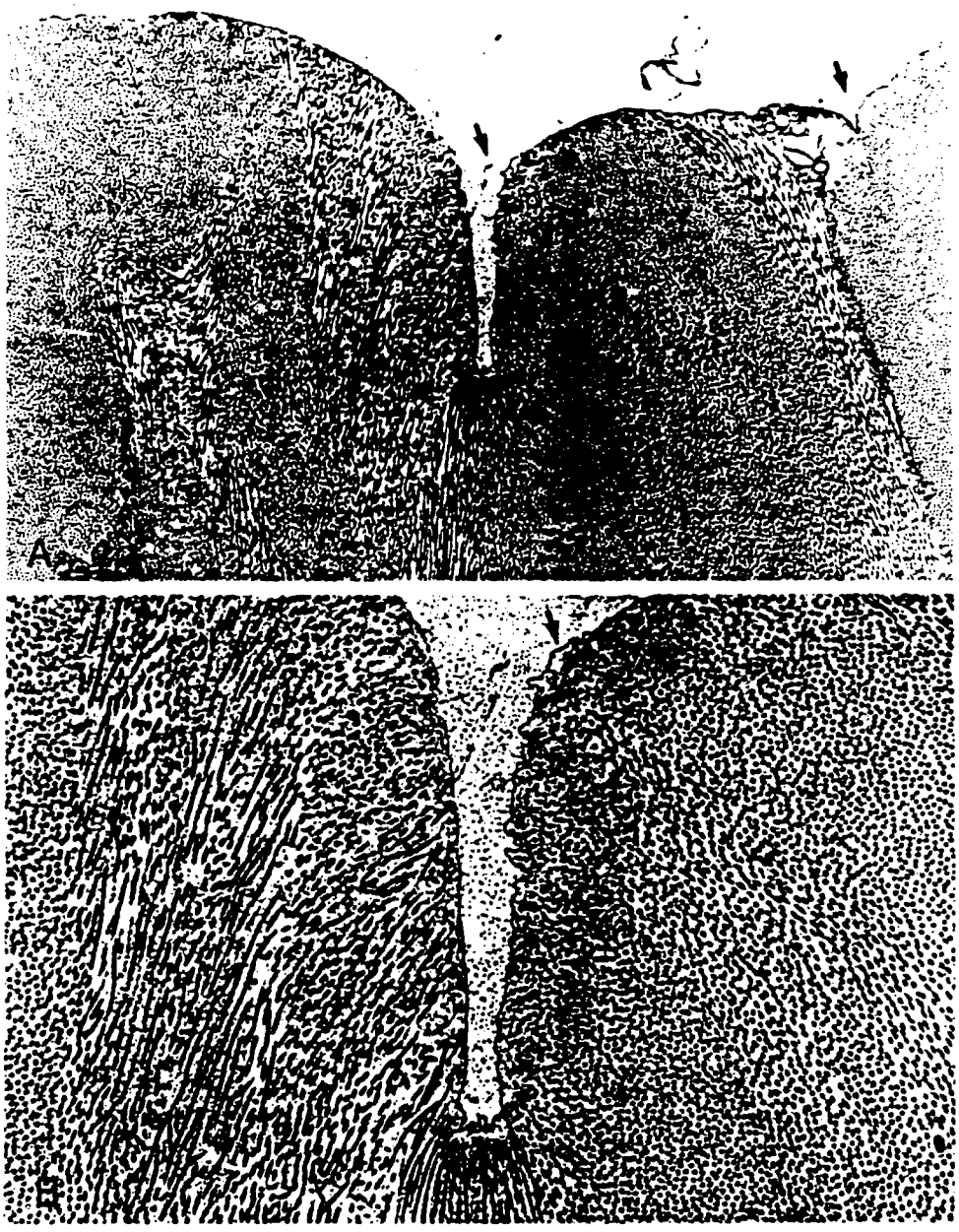

Fig 7. Transmission electron micrographs of the stromal surface inside the ablation zone of the incision in Figure 4A. A, low power magnification illustrating micro-pitting (arrows) (original magnification ×10,000). B, higher magnification illustrating granular material within the micro-pits and pseudomembrane along the entire ablated surface. Notice collagen fibers in cross-section and longitudinal section (original magnification, ×23,000).

(Fig 8) and light microscopic examination (Fig 9). Results of light microscopic examination did not show any piling up of cells on the surface at the incisions as observed with the higher energy densities (previous section). However, the epithelial cells immediately adjacent to the incision lines did stain less intensely than the normal surface epithelium (Fig 10A).

Transmission electron microscopic analysis confirmed that there was no evident damage to the endothelium or Descemet's membrane. By contrast, considerable ultrastructural damage was evident in the epithelial cells that were closest to the incision line on the surface of the cornea. The damage extended in a two-to-four cell margin along the length of the incision. Ultrastructurally, these cells exhibited very weak cytoplasmic staining (Fig 10 B, C) with gross damage to the cell membrane on the exposed surface of the cornea. The rest of the cytoplasm exhibited vacuolation, scattered electron-dense material, and general disorganization. In one cell (Fig 10C), a nucleus adjacent to the ablated surface had a ruptured nuclear envelope with the chromatin extruded extracellularly.

Best Available Copy

Table 1. Laser Parameters for Corneal Ablation

Pulse Energy Density (mJ/cm² per pulse)	Time of Experiment (seconds)	Total Energy Density (J/cm²)	Corneal Ablation (%)	Corneal Thickness		Corneal Swelling (%)	
				Pre-ablation (mm)	Post-ablation (mm)		
50 Hz							
258	9.0	120	51	440	550	25	
246	10.5	123	77	470	530	13	
246	12.8	158	53	470	600	28	$\bar{x}$ = 26
246	12.8	158	61	470	620	32	
246	17.9	220	60	450	620	38	
246	20.4	251	82	410	490	20	
10 Hz							
670	30	201	100	400	610	53	
670	60	402	17.5	450	570	27	
670	60	402	89	530	720	36	
670	120	804	100	520	940	81	$\bar{x}$ = 48
670	120	804	50	420	610	45	
670	180	1216	50	430	600	40	
670	180	1216	70	430	660	53	

The damage along the ablated stromal surface within the ablation zone was different than that observed with the higher energy density exposures. No micro-pitting was observed either at the bottom of the cut (Fig 11A) or along the sides (Fig 11B). The surfaces were smooth and more undulating than in the higher energy density situation. The electron-dense "pseudomembrane" appeared either broken, not as smooth, or not evident at all. In the latter case, the cut ends of the collagen fibers were directly exposed along the ablation surface. Blood cells were evident at the bottom of the ablation zone (Fig 11A).

DISCUSSION

The results of the high-energy density experiments (1.0–2.1 J/cm² per pulse) confirm the work of others with respect to an apparent clean removal of corneal stroma with minimal thermal damage to adjacent structures. However, it is also clear that despite the relatively low pulse repetition rate of 5 Hz, there is considerable damage produced on the surface of the cornea. The "ridging" phenomenon may be caused by the force of the ejected material. As illustrated by Puliafito et al,[9] using high-speed photography, the ejection of this material from the surface can be graphically documented over a 500-ns to 150-μsecond period after laser exposure. Those studies used energy densities of up to 900 mJ/cm², and it was estimated that the material was ejected from the corneal surface with supersonic velocities. It is conceivable that material hitting the side of the laser incision at the corneal surface could result in the surface being "pushed up" as the material is ejected. The damage observed in the endothelium below Descemet's membrane is reminiscent of that described by Marshall et al.[5] As in their study, we observed endothelial cell loss in the zone under the region of laser exposure even though Descemet's membrane remained intact. This was particularly evident in samples that had ablation depths greater than 50%. It is possible that this resulted either from penetration of some 193-nm photons to the endothelium or from a shock wave that generated from the point of laser focus in the cornea.[10] However, in the latter case, one might expect to see damage in Descemet's membrane. The nature of the endothelial cell damage would suggest a nonshock wave effect. Though the first detectable damaged cell was completely disrupted with respect to its outer and inner membranous components (Fig 6B), the second cell was intact except for its inner membranous components (Fig 6C). This observation plus the intact nature of Descemet's membrane would argue against a shock wave.

Transmission electron microscopic pictures of the stromal surface in the ablation zone showed an electron-dense "pseudomembrane" along the entire ablation surface that appeared identical to that described by other investigators.[2,5] However, unlike both of these previous studies, we have observed small micro-pits or fissures, extending into the stroma from the ablation surface. These fissures are not due to splitting of the stroma caused by a stretching or tension as evidenced by the fact that the pseudomembrane extended unbroken along the surface of the pits. It is possible that the pitting was caused by uneven distribution of the photons in the beam resulting in high-intensity microfluences that resulted in deeper ablation points along the incision surface. However, our beam profile data indicate a relatively uniform gaussian photon distribution. Since no other published studies provide beam profile data, it is not possible to make direct comparisons with our studies. It is possible that some of the effects we have ob-

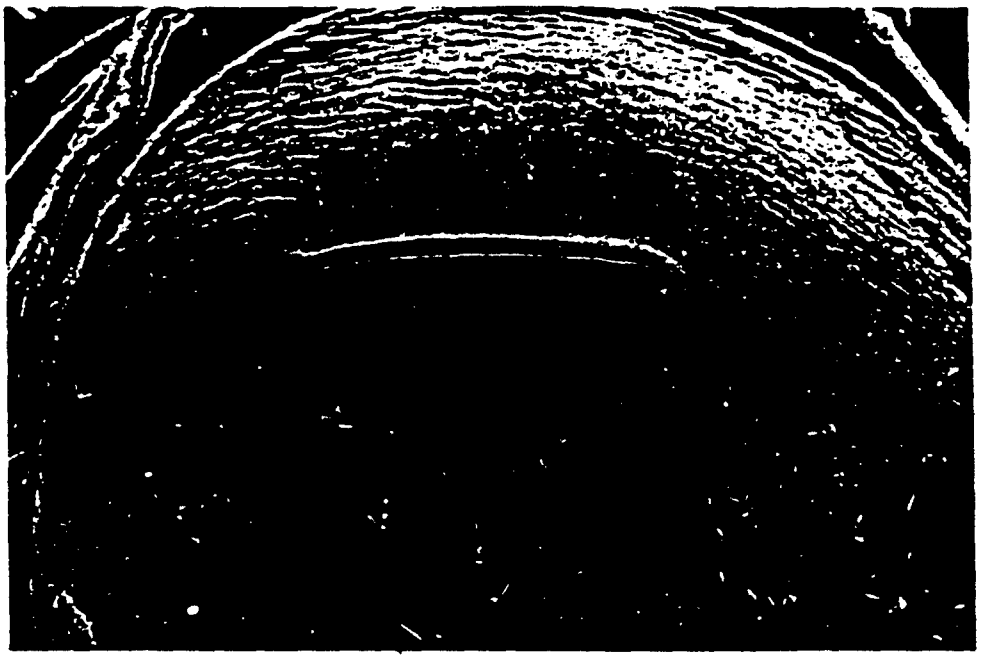

Fig 8. Low-power scanning electron micrograph of corneal surface after exposure to 280 mJ/cm² per pulse for 10 seconds at 15 Hz. Notice swelling along the incision line (original magnification, ×42).

Fig 9. Light micrograph illustrating stromal swelling after exposure to 246 mJ/cm² per pulse at 50 Hz for 12.8 seconds (original magnification, ×164).

served may be due to thermal ablation in the portion of our focused beam that is below threshold for photoablation. This, presumably, would be in the low-intensity margin of the gaussian beam profile (Fig 2). However, we do not believe that this is consistent with the mechanism of bond breaking by the high-energy, 193-nm photons since the individual photon energy is the same regardless of the beam profile. The sharp edges of the gaussian profile of the excimer beam used in these studies indicate that there is little "tailing off" (gradual decrease) of energy toward the edges of the focused excimer beam. At worst, this type of profile would predict an ablation zone that is slightly deeper in the center than in the periphery. Moreover, the thermal camera data indicate a temperature rise that is not sufficient to cause major structural damage such as charring and coagulation (see subsequent discussion).

The structural results using energy densities of 200 to 700 mJ/cm² per pulse were comparable with the studies of other investigators with respect to the absence of ridging along the corneal surface, smoothness of the ablation inside the cut zone, and a lack of micro-fissures.

Best Available Copy

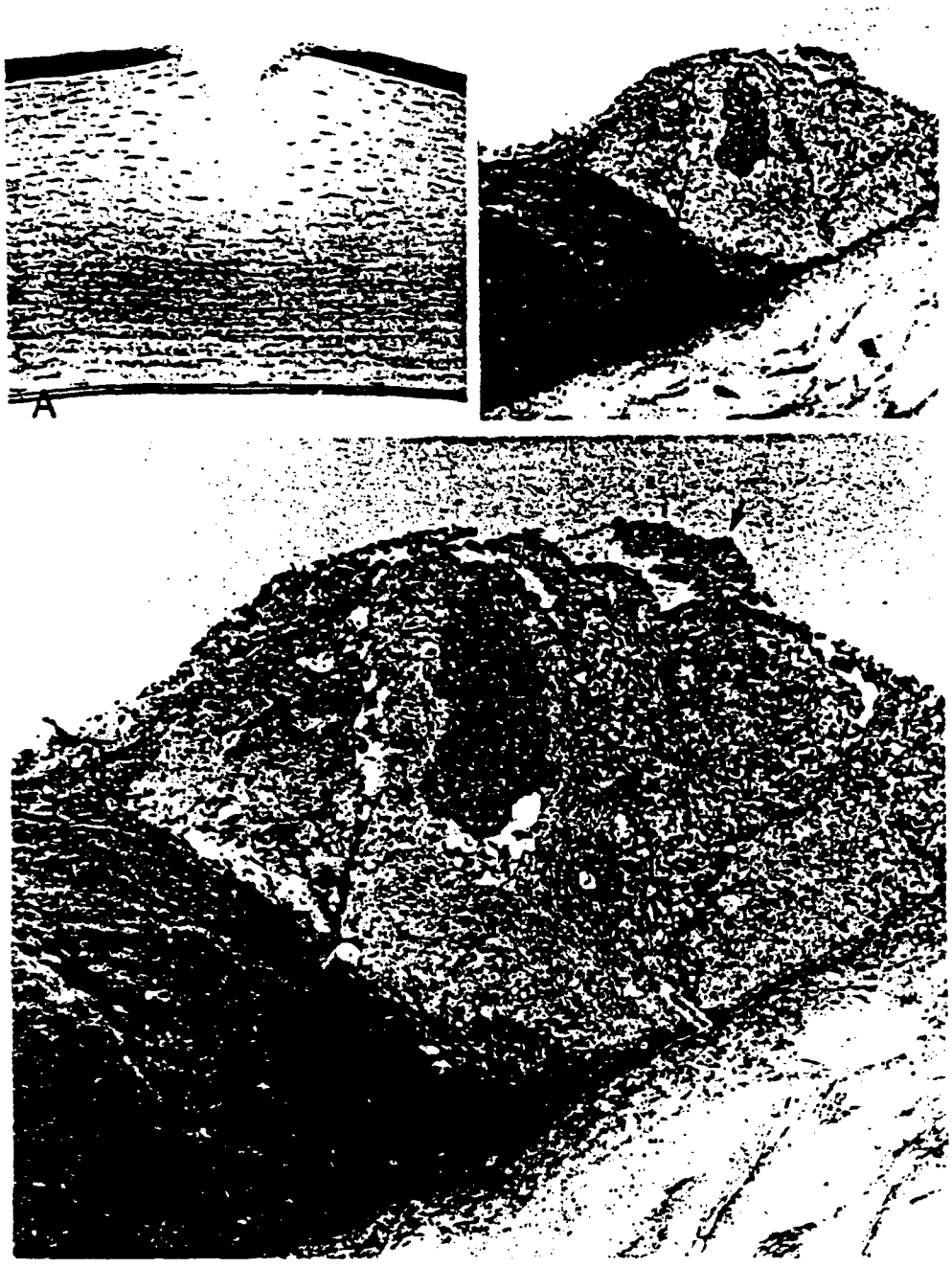

Fig 10. Light and transmission electron micrographs of corneal incision produced with 268 mJ/cm^2 per pulse at 50 Hz for 9 seconds. **A**, low-power light micrograph illustrating incision depth of 50% and minimal stromal swelling (original magnification, ×150). **B**, moderate-power electron micrograph illustrating disrupted and vacuolated cytoplasm, nuclear extrusion, and general cellular damage (original magnification, ×5800).

In addition, there was no apparent structural effect on the endothelial layer. This is consistent with the findings of Puliafito et al[3] and Dehm et al.[4] Substantial swelling of the corneal stroma was observed immediately after the laser exposure. This swelling appeared to be unrelated to the total energy density but clearly was related to the energy density per pulse. At 200 to 250 mJ/cm^2 per pulse, the average swelling was 26% as compared with 48% at 670 mJ/cm^2 per pulse. Furthermore, at identical pulse energy densities and total densities (Table 1) not only was there considerable variation in the amount of swelling, but the ablation depth varied as well. The variation in ablation depth with identical dosimetric parameters is not surprising since the swelling could be observed occurring during the actual laser exposure. In order to have precise control over ablation depth, it would be necessary to monitor changes in corneal thickness during the actual laser treatment since the corneal thickness changes during the treatment. Our results clearly document substantial stromal swelling simi-

Fig 11. Electron micrographs of the surface of the incision 'groove) illustrated in Figure 10. A, micrograph of the bottom of the incision Notice the undulating surface, broken pseudomembrane (compared with Fig 7, A and B), and blood cells (original magnification, ×5800). B, micrograph along the side of the incision. Notice the broken nature of the pseudomembrane. Also notice the absence of micro-pits; collagen fibers can be seen in both longitudinal and cross-section (original magnification, ×5800).

lar to that depicted by Seiler and Wollensak[11] (Fig 4) and pointed out by Marshall et al.[5]

Another noteworthy structural aspect of the lower energy density incisions was the appearance of lightly stained ultrastructurally damaged epithelial cells on the surface immediately adjacent to the incision. This would suggest that these cells were affected either by the beam directly or by the material being ejected from the ablation zone. Alternative explanations could be (1) an ozone effect on the epithelium in close proximity to the incision line (ozone levels at the surface of the cornea during irradiation were measured at 200–300 times the background levels, unpublished data), and (2) the possibility of secondary fluorescence in the ultraviolet region of the spectrum that is damage producing.[12] A major thermal effect such as charring, coagulation, or vaporization is unlikely because the thermal camera data demonstrated that the corneal surface experiences a 20°C rise in temperature (from 18°–38°C). Thermal denaturation of biological molecules does not occur until temperatures of 40° to 60°C are attained. Because, at 50 Hz, most of the heat of an individual pulse is

Best Available Copy

dissipated before the next pulse arrives, the corneal surface immediately adjacent to the ablation zone only reached a maximum temperature of 38°C. We conclude that even though there is a thermal component to 193-nm laser ablation of tissue, it probably does not have a major contribution to tissue damage under the parameters used.

In conclusion, the current study confirms certain aspects of the mechanism of 193-nm excimer laser ablation for corneal surgery. However, effects such as corneal ridging, epithelial cell damage, stromal swelling, and difficulty in making incisions to predictable depth argue for caution in human application.

REFERENCES

1. Trokel SL, Srinivasan R, Braren B. Excimer laser surgery of the cornea. Am J Ophthalmol 1983; 96:710–5.
2. Krueger RR, Trokel SL. Quantitation of corneal ablation by ultraviolet laser light. Arch Ophthalmol 1985; 103:1741–2.
3. Puliafito CA, Wong K, Steinert, RF. Quantitative and ultrastructural studies of excimer laser ablation of the cornea at 193 nm and 248 nm. Lasers Surg Med 1987; 7:155–9.
4. Dehm EJ, Puliafito CA, Adler CM, Steinert RF. Corneal endothelial injury in rabbits following excimer laser ablation at 193 and 248 nm. Arch Ophthalmol 1986; 104:1364–8.
5. Marshall J, Trokel S, Rothery S, Schuber H. An ultrastructural study of corneal incisions induced by an excimer laser at 193 nm. Ophthalmology 1985; 92:749–58.
6. Marshall J, Trokel S, Rothery S, et al. Photoablative reprofiling of the cornea using an excimer laser: Photorefractive keratectomy. Lasers Ophthalmol 1986; 1:21–48.
7. Puliafito CA, Steinert RF, Deutsch TF, et al. Excimer laser ablation of the cornea and lens: experimental studies. Ophthalmology 1985; 92:741–8.
8. Green H, Boll J, Parrish JA, et al. Cytotoxicity and mutagenicity of low intensity, 248 and 193 nm excimer laser radiation in mammalian cells. Cancer Res 1987; 47:410–3.
9. Puliafito CA, Stern D, Krueger RR, Mandel ER. High-speed photography of excimer laser ablation of the cornea. Arch Ophthalmol 1987; 105:1255–9.
10. Krauss JM, Puliafito CA, Steinert RF. Laser interactions with the cornea. Surv Ophthalmol 1986; 31:37–53.
11. Seiler T, Wollensak J. In vivo experiments with the excimer laser—technical parameters and healing processes. Ophthalmologica 1986; 192:65–70.
12. Marshall J, Trokel S, Rothery S, Krueger RR. A comparative study of corneal incisions induced by diamond and steel knives and two ultraviolet radiations from excimer laser. Br J Ophthalmol 1986; 70:482–501.

Today's Microscopy

Recent developments in light and acoustic microscopy for biologists

Edwin S. Boatman, Michael W. Berns, Robert J. Walter, and John S. Foster

During the past 300 years, the optical microscope has changed from a simple device to a sophisticated research instrument. Although the instrument's resolution reached its practical limit decades ago, improved glass manufacturing processes and computer and laser technology have improved the precision of light microscope optical components. In the future, it is likely that the resolution limit of the optical microscope will be bypassed by other systems of "optics," such as ultrasound. Here, we review recent developments in microscope technology and use, particularly in biology.

Light microscopy's limit of resolution is likely to be bypassed by other systems of "optics," such as ultrasound

Microscopes and components

In 1673, Anton van Leeuwenhoek designed and built a hand-held device (Figure 1) containing planoconvex and biconvex lenses that had a 30–275 magnification range, capable of resolving certain forms of bacteria. In the late 1800s, Carl Zeiss, Ernst Abbe, Otto Schott, and August Koehler formulated and expanded the theoretical basis of optical microscopy and made improvements on the optical components as well. Much later, more complex instruments, such as those in Figure 2, were developed.

A microscope's components are generally dictated by the nature of the specimen (e.g., biological, metallurgical, or mineral), the magnification desired, and the form of the final image (photograph, projection, or video display). The heart of the instrument is the lens system—the eyepiece, objective, and condenser—and the source and alignment of the illumination (Figure 3).

The design of each component varies markedly according to the type of microscopy. These include transmitted illumination, Zernike phase-contrast observation, Nomarski differential interference contrast, dark-field illumination, low-power optics with oblique lighting, or ultraviolet illumination (Allen et al. 1969, Bradbury 1984, Gupta and Hinsch 1983, Needham 1958, Smith 1984, 1985a,b, Spencer 1982, Zernike 1942).

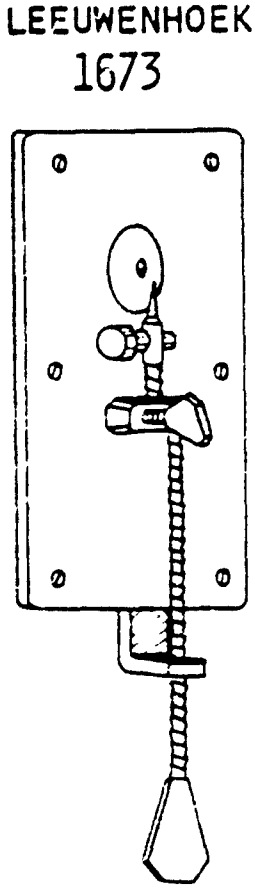

Figure 1. Anton van Leeuwenhoek's (1673) microscope. The object to be viewed is placed on the sharp point, the observer's eye is close to the lens, and the sun is the light source.

Edwin S. Boatman is a professor of environmental health and pathobiology in the School of Public Health and Community Medicine, University of Washington, Seattle, WA 98195. His areas of research are morphology and morphometry of the lungs; microorganisms; and environmental fibers. Michael W. Berns is a professor of cell biology and surgery and Robert J. Walter is a computer image processing specialist in the Department of Developmental and Cell Biology, School of Biological Sciences, University of California, Irvine, CA 92717. Their research interests are laser microbeam microscopy and computer imaging. John S. Foster is a physicist at the IBM Almaden Research Center, 6650 Harry Road, San Jose, CA 95120. His research interest is in scanning acoustic microscopy design and applications and scanning tunneling microscopy.
© 1987 American Institute of Biological Sciences.

Optical lenses. Over the years, the major aberrations inherent in optical lenses—spherical aberration, chromatic aberration, astigmatism, and coma—have been practically eliminated, at least in the most expensive systems. Light diffraction by the image and optical system, however is likely to remain for some time the major factor limiting resolution.

When a source of coherent light illuminates an object or an aperture, a series of fringes known as an Airy disc, forms around the object's image (Figure 4). These fringes significantly affect the ability to resolve two objects that are very close to each other. The limit of resolution is the minimum distance at which two objects can be distinguished as separate entities. The formulas for determining resolving power vary slightly but may be generalized as:

$$d = \frac{\lambda}{2NA} \text{ at } \frac{0.550\ \mu}{2 \times 1.3} = 0.21\ \mu$$

where d = the minimum resolvable distance between two luminous points; λ = wavelength of light; and NA (numerical aperture) = n sin (half the angular aperture), where n = refractive index of the medium between front lens and cover glass.

Spherical aberration is corrected by combining positive and negative lens elements made of different refractive indices and dispersions so that axial and peripheral light rays are focused to the same point on the axis of the lens. Chromatic aberration in microscope objectives was (and still is in some cases) corrected with compensating eyepieces (such oculars are marked by *K* or *COMP*).

Today, many objective and ocular (eyepiece) lenses are corrected individually by use of low-dispersion glass. Depending on the degree of correction, objectives are classified as achromats, hemiapochromats and apochromats. A planapochromat objective is corrected for four wavelengths of spherical and chromatic aberration and produces a flat field. The body of this objective (e.g., Zeiss, 100× oil immersion, NA 1.3) contains a train of 12 separate lenses (Figure 5) and requires no fewer than 481 steps to manufacture.

A variety of objectives with a number of special features is now available, such as planachromat 100× oil-immersion objectives that require no cover glass. Nikon makes a 40× objective especially for inverted microscopes; this objective has a variable long-working distance from 0.18–2.39 mm. Nikon has also a new color-free 60× planapochromat oil immersion objective with a numerical aperture of 1.40, which is ideal for epifluorescence work, as are their improved phase-contrast objectives. Zeiss now makes so-called plan-neofluar multi-immersion objectives of 16, 25, and 40× that may be used with water, immersion oil, glycerine, paraffin oil, and silicone oils. Some objectives are corrected for infinite tube length and give excellent image quality, especially with automatic focusing devices.

Whereas eyepieces in earlier microscopes contained two lenses, some modern oculars contain four or five; magnifications range from 2–25×; field-of-view numbers (field of view in millimeters multiplied by ocular magnification) from 6.3–26.5×. Also available are high-point oculars designed specifically for people who wear glasses and multiviewing attachments that can accommodate up to ten observers. But because most oculars and objectives are matched to give the best optical performance, it is unwise to mix oculars and objectives

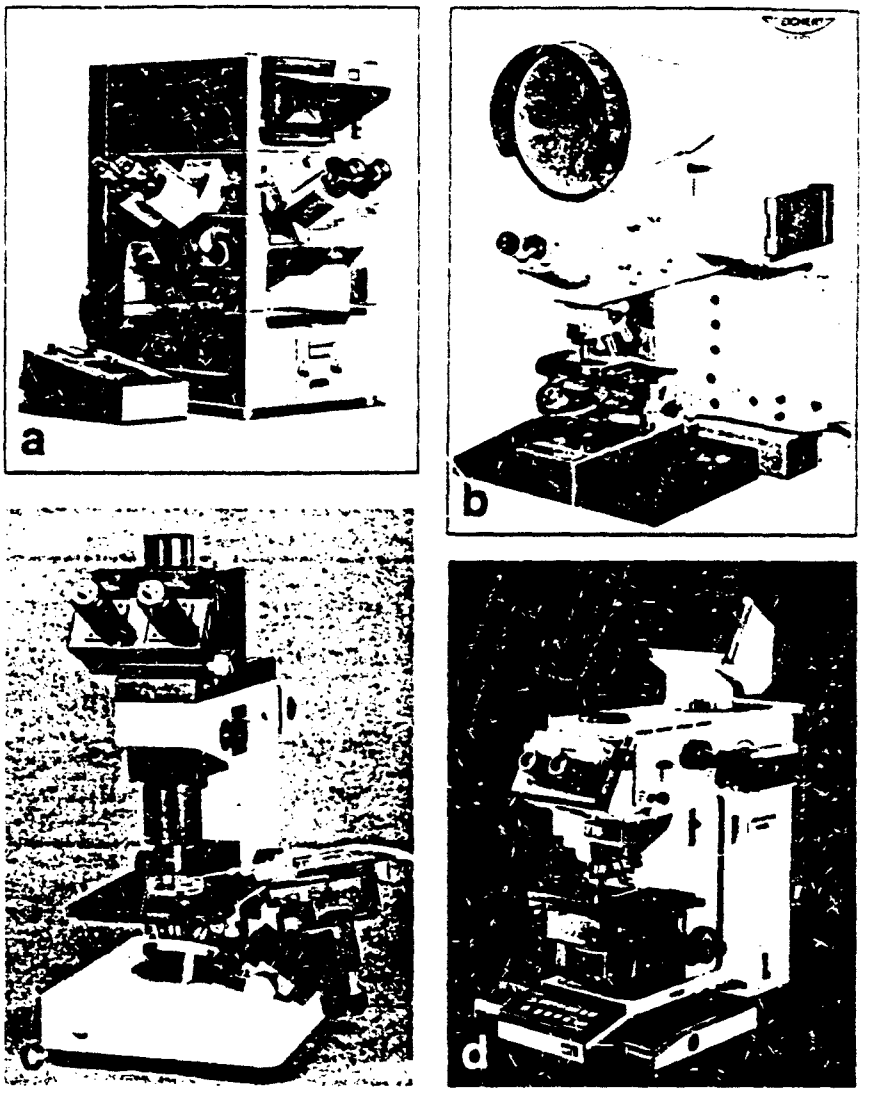

Figure 2.a. Zeiss "Axiomat" multipurpose microscope. b. Reichert "Univar" multipurpose microscope. c. Leitz inverted microscope with micromanipulator. d. Advanced Olympus Vanox-T microscope with automated features.

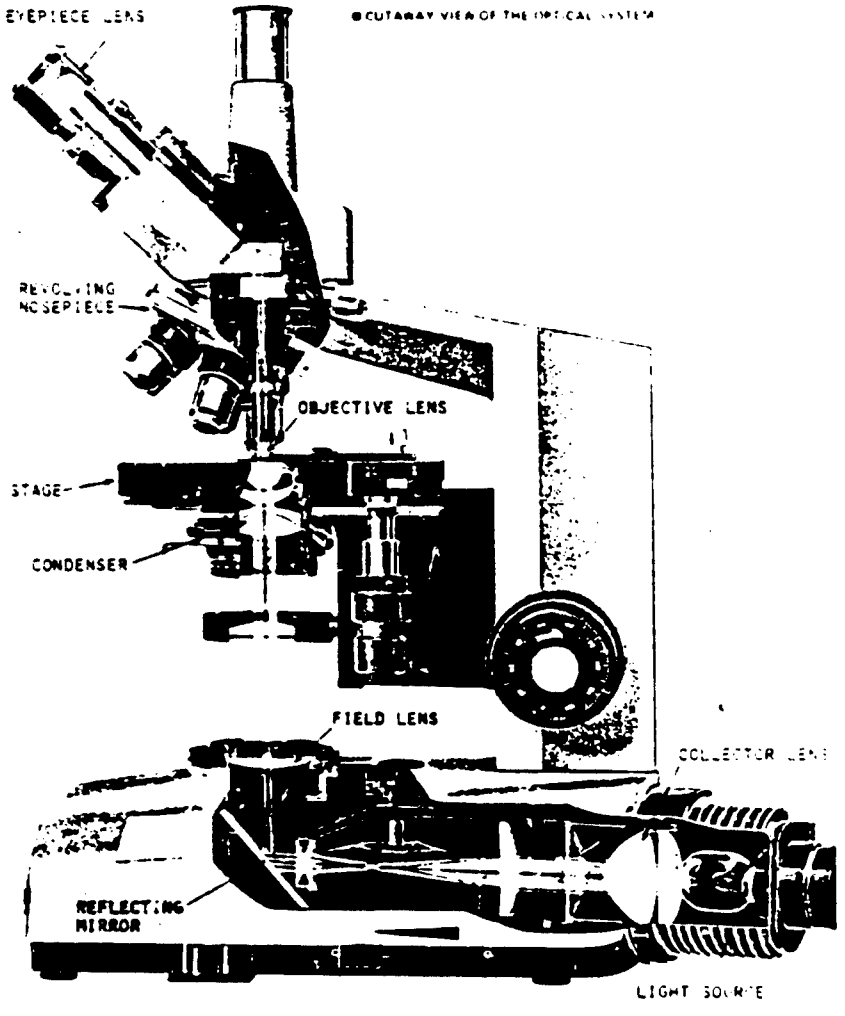

Figure 3. Optical components and approximate light path of a standard binocular microscope (OLYMPUS, BH Series).

from different manufacturers on the same microscope.

Condensers. The purpose of a substage condenser is to deliver as much illumination as possible to the specimen and ultimately to the front lens of the objective. Highly corrected objectives require highly corrected condensers. Some condensers have either a swing-out or removable front lens to reduce the numerical aperture of the condenser for low-power objectives; substage condensers may contain an appropriate range of annular rings for Zernike phase-contrast and wollaston prisms for Nomarski differential interference contrast effects.

Dark-field condensers can be oil immersion (in which the corresponding oil immersion objective contains an iris diaphragm to reduce glare) or dry, used at lower magnifications. They are constructed so that no direct light enters the objective, and hence only the specimen's own luminosity appears on the dark background. Many small objects (e.g., bacterial flagella) not observable by transmitted light, can be detected this way. Dark-field illumination requires a high-intensity light source, such as a 12-volt, 100-watt quartz halogen lamp. Dark-field illumination is also useful in stereomicroscopy.

Light sources. Twelve-volt quartz halogen lamps are preferred for light microscopy because they can be stabilized at 3200K color temperature for good photographic color reproduction. Light intensity can be controlled by placing neutral-density filters in the light path instead of changing the voltage control. It is important at all times to maintain even (Koehler) illumination; on some microscopes, this is done automatically following a change in objective magnification.

Photography. Automatic camera systems under microcomputer control are now the rule. Exposure can be measured either integrally over the entire picture field or, with a movable spot, from any desired object detail. Camera formats vary in size from 35-millimeter roll film to 8 × 10-inch sheets, and shutter speeds range from about 1/100 second to more than an hour. Electronic control ensures ease of use and reliable results. Nikon has a microscope adapter with a double camera so that black-and-white and color pictures of the same area can be taken one after the other.

Modern microscopes tend to be cubic or angular in structure and modular, offering increased stability and strength. These microscopes present a wide choice of techniques: the usual bright-field, dark-field, and phase-contrast as well as differential interference contrast, fluorescence, polarized light, reflected light, micro- to macrocapabilities, and various means of image projection and TV image analysis. Photography is automatically controlled, and many components formerly adjusted by hand are now motorized and automated, including objectives and condensers, coarse and fine focusing, and automatic focus for low magnifications. Examples of advanced microscopes include Olympus's Vanox-T (Figure 2d; Smith 1984), Nikon's Microphot-FX with twin-mounted 35-millimeter cameras (Smith 1985a), and Reichert's Polyvar microscope (Smith 1985b). The tandem scanning reflected light microscope (Petran et al. 1985) is designed to overcome the problems associated with observing living tissue by reflected light. Further advances in light microscope design will come largely through automation. At the same time, laser-beam microscopy, video image enhancement, and acoustic microscopy will receive increasing attention.

Computer applications

Video cameras and computers coupled to a microscope have been used

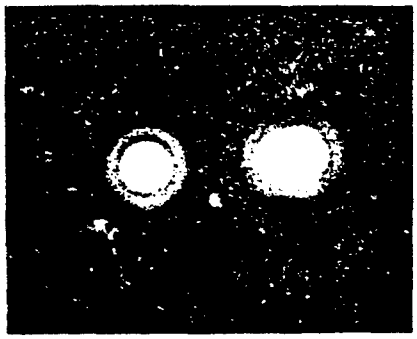

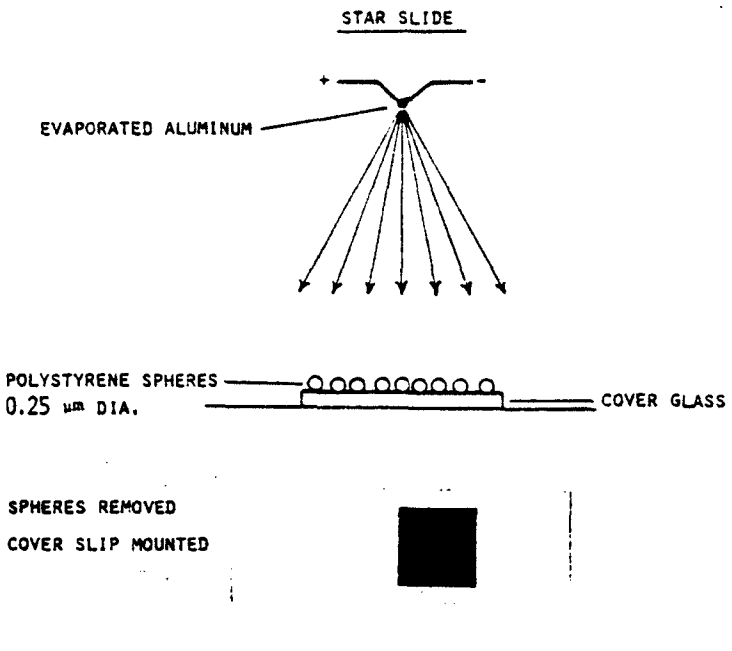

Figure 4.a. Single aperture (top left) shows uniform diffraction fringes (Airy disc). Two apertures (top right) are shown too close together to permit detection as distinct entities. (Planapochromat 1.25 NA. 9000×.) b. Aberrations in medium- and high-power objectives (40–100×) can be detected by a star slide preparation. Star slides are made by depositing 0.25-micron diameter polystyrene spheres on a cover glass, coating the glass with evaporated aluminum, and then removing the spheres with a solvent. Removing the spheres leaves discrete areas, which act as small apertures for light to pass through, devoid of aluminum. Viewed through a high-quality objective whose performance is limited only by diffraction, each aperture will be surrounded by circular diffraction rings (as in a.) Viewed through lower-quality objectives, the diffraction rings are often distorted into a comet shape and may be marred by colored fringes.

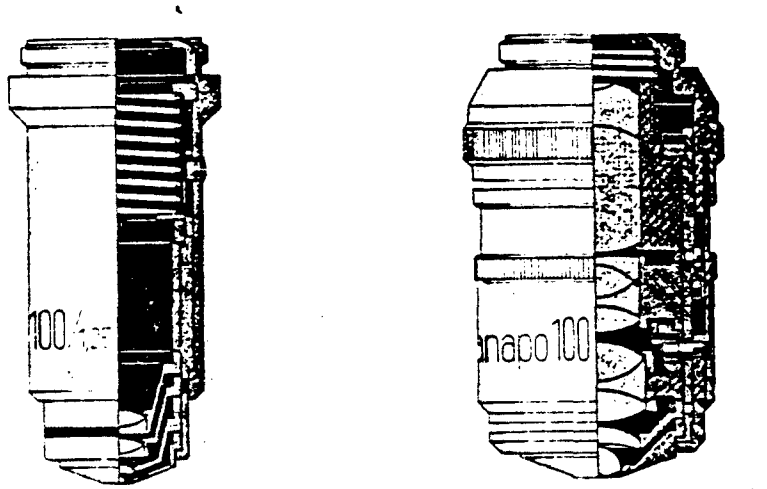

Figure 5. Cut-away diagrams of an achromat and a planapochromat objective. The planapochromat contains twice the number of lenses (Zeiss).

in a variety of applications, including the analysis of cell locomotion (Bartels et al. 1981, Berns and Berns 1982), automated analysis of clinical blood specimens (Bradbury 1983), and measurement of fluorescent intensity in specially labeled biological material (Arndt-Jovin et al. 1985). The use of computer techniques can also help correct degradation in a microscope image or otherwise change the image to make it more useful to the observer. The applications, which are listed in Table 1, indicate how computer technology makes the most of an image, transforming the microscope from a device used primarily for description into a truly analytical research tool.

Image-processing equipment. A microscope's normal output, an optical image that is either viewed directly or captured on photographic film, is unsuitable for a computer, which can only handle discrete numerical information. An optical digitizer (Figure 6) can help overcome this difficulty by scanning the optical image and then converting it into an array of coded values called the digital image. Many devices can be coupled with a microscope to produce digital images, including scanning photomultipliers, digitizing tablets, or photodiode arrays. Although each one of these devices has its advantages (Walter and Berns 1986), most computer microscopy relies on another device, called the video camera, to produce an electronic image that can then be digitized.

The greatest advantage of video technology in computer microscopy is the speed with which it produces images, typically 30 full frames per second in a standard format camera. The output from the video camera is directed to a high-speed video digitizer that converts the video signal into an array of individual picture elements (called pixels) that are stored in the memory of the computer as quickly as the electronic signal can be produced

able 1. Uses of computer image processing in microscopy.

Application	Description
lorphometry	Calculating the size and shape of objects.
ensitometry	Calculating density as a measure of concentration, staining, etc.
lotion analysis	Describing speed, direction, and variability in the motion of objects.
ligh-speed processing	Real time processing of the microscope image so that a raw image and a processed image of the specimen can be viewed simultaneously.
nage enhancement	Routines used to increase contrast in an image or otherwise improve its appearance, e.g., pseudocoloring, noise reduction, shading correction, digital filtering.
mage decalibration	Manipulating the image to correct for distortion in the microscope or video system, e.g., correcting geometric distortion, nonlinear camera response, and out-of-focus images.
\utomation	Repeated performance of routine tasks such as particle counting and area measurement.
Decision making	Using processing routines to make statistical decisions about the microscope image, e.g., classifying abnormal blood smears.

by the video camera. This speed is necessary for many video microscope applications where computer processing must be performed on quickly moving objects, or where instantaneous (real time) processing of the microscope image is required. This speed advantage outweighs the potential disadvantages of a video camera, which include uneven sensitivity, geometric distortion, and lag (Castleman 1979).

A potential problem in computer processing of microscope images is the digital image size in computer memory and the processing time needed to manipulate it. A typical digital image might consist of 512 rows of 512 individual pixels each, where each pixel represents one of 256 possible shades of gray in the original optical image. Using standard formats, this digital image must be stored in 262,144 bytes of computer memory before it can be processed. The size of this digital image may exceed all the available memory in a small laboratory computer, especially if several images must be stored in computer memory simultaneously for purposes of comparison. This memory requirement may also limit the speed at which the host computer can manipulate such a digital image. A delay of even a few seconds may be unacceptable if a processed image is required for high-speed or real-time applications.

These limitations are overcome by use of special ancillary devices known as array processors (Figure 6). These devices have separate memories for storing one or more digital images as well as special microprocessors for manipulating the digital image at high speeds. The various array processors available commercially for laboratory use can differ by a number of properties such as the number and size of the images they can store, the number of different manipulations they can perform on the digital image, or such features as image zoom, false color displays, and joystick controlled cursors (Walter and Berns 1986).

Array processors can greatly reduce the time required for many image processing applications, and are an absolute requirement for high-speed applications. However, array processors by themselves are currently not sophisticated enough to perform many of the more complex applications used in microscopy, such as the detection and characterization of a tissue culture cell, without some additional processing being performed on the digital image by a host computer. In such applications, small sections of the digital image must be transferred from the array processor to the memory of the host computer for subsequent processing using specifically designed algorithms. This additional processing is often the time-limiting step in image processing applications. Furthermore, the algorithms used to process digital images are often unique for a given application and must be custom-designed in the laboratory. Few image processing devices are now available commercially that can be used for research applications without additional in-house programming. As the use of computers in microscopy continues to grow, it is

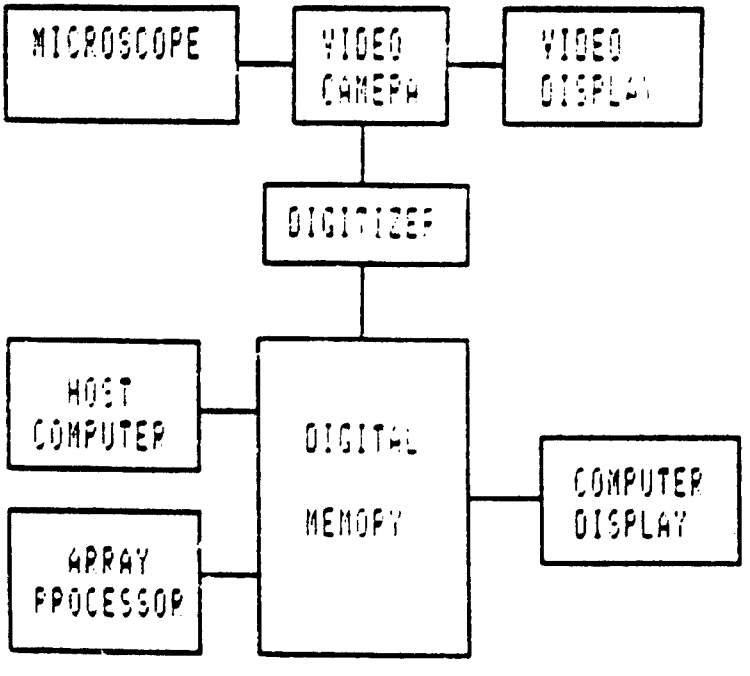

Figure 6. Block diagram of a microscope digital image-processing system.

Best Available Copy

likely that this situation will be corrected.

Examples of computer processing. Computer manipulations of microscope images can be arbitrarily divided into two classes; image analysis and image processing. In image analysis, the purpose of the computer processing is to obtain descriptive numerical values, for example, the number of cells in a microscope field or the average density of a stained nucleus. These quantities are fairly easy to obtain from the digital image (Pavlidis 1982), and are limited only by the speed of the computer processor and the ability of the video camera to accurately reproduce the size and density of the actual object. Figure 7 shows an example of this type of processing, and other examples are given in recent reviews (Arndt-Jovin et al. 1985, Bradbury 1983, Sklansky et al. 1987).

A problem frequently encountered in image analysis is the computer's inability to discriminate among regions that are known to be different by the computer operator. Typical examples are the ability to trace a cell boundary in a phase-contrast image or to accurately recognize all cell nuclei in a stained section. These problems can often only be overcome by having the computer work interactively with a computer operator who uses a lightpen or joystick device to discriminate ambiguous regions that cannot be recognized by the computer alone.

Alternatively, some success has been achieved either through the use of custom-designed algorithms (Sklansky 1978) or by carefully controlling the preparation of the sample and/or the image acquisition procedures in such a way that ambiguous objects are less likely to appear. Even when these extra procedures are used, the time saving between computerized analysis and strictly manual techniques is great enough to justify the additional effort.

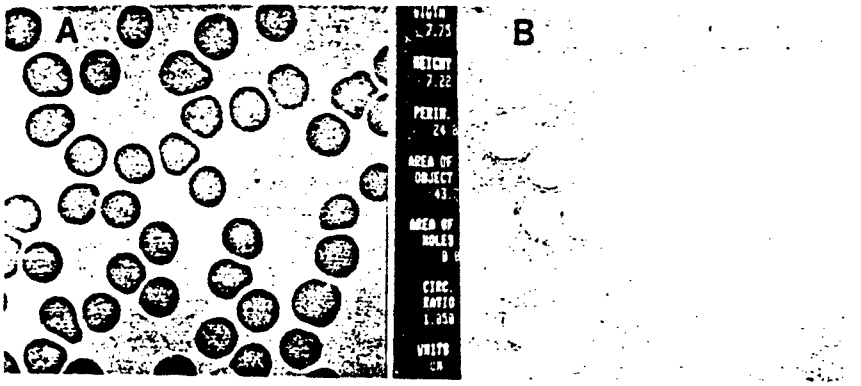

Figure 7. Image analysis. a. Original video image. b. Results of an automated analysis routine used to characterize red blood cells from a peripheral blood smear.

The second type of computer manipulation of microscope images is called image processing, which makes the image more meaningful to the observer. Examples of image processing applications are image subtraction procedures to remove unwanted background or false coloring routines to increase the apparent contrast of a monochrome image. Examples of image processing routines are given in Figure 8.

Noteworthy image processing routines correct for various sources of distortion in a microscope image, such as "barrel" or "pincushion" distortion. Once corrected, the displayed image represents the true shape of the microscope specimen. Various digital filtering routines can be used to improve the sharpness of an image, as shown in Figure 8, or can be used to correct for other sources of degradation in an image, such as out-of-focus fluorescence (Agard and Sedat 1983). It is important to note that these types of manipulations would be difficult or impossible to perform without the use of an image processing computer.

Laser and computer microscopy in biology

Laser microscopy has been combined with computer image processing to study fundamental problems in cell biology (Berns et al. 1981). In these studies, a laser is used to selectively alter subcellular processes or to excite

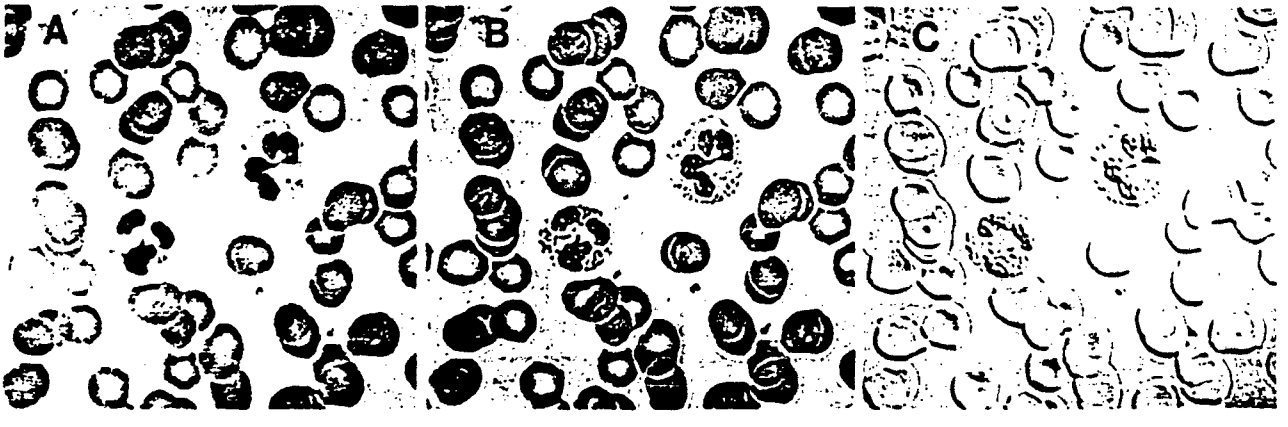

Figure 8. Image enhancement. a. Original video image of two polymorphonuclear leukocytes within a peripheral blood smear. b. Same image after digital filtering with a sharpening mask to accentuate cell boundaries. c. Original image after digital filtering with horizontal gradient filter.

fluorescence at a particular subcellular site.

Subcellular microsurgery. Berns et al. (1969) used an argon laser in conjunction with the vital dye, acridine orange, to selectively alter submicron regions of dividing vertebrate cells in culture. They passed a pulsed green argon laser beam through a standard phase-contrast microscope, which focused the beam to a small spot on a selected chromosome. Over the last 15 years, this form of genetic microsurgery has been extensively developed to study specific genes in ribosomal DNA (Berns et al. 1979) and to remove and manipulate whole chromosomes (Berns 1974). In addition to genetic applications, the laser microbeam has been applied to other cell organelles—the nucleolus (Berns et al. 1970a), mitochondria (Berns et al. 1970b), centrioles (Berns et al. 1977), chloroplasts (McBride et al. 1974), myofibrils (Strahs et al. 1978), cell membrane (Burt et al. 1979), cytoplasmic fibers and filaments (Strahs and Berns 1979), and kinetochores (McNeill and Berns 1981). These studies involved analysis of the structural and functional alterations produced in the cell, as well as the mechanisms of laser interaction with the natural and/or applied light-absorbing molecules (Calmettes and Berns 1983).

The instrumentation available for laser microsurgery has expanded to involve a wider variety of lasers and laser wavelengths, as well as computer imaging technology. The current system of the NIH Biotechnology Laser Resource (LAMP) is comprised of a variety of ytrium aluminum garnet (YAG) and dye lasers that can be used with a Zeiss Axiomat microscope and an image array processor driven by an LSI 11/23 computer (see Figures 9 and 12). This system is undergoing further modification to include a wavelength-tunable, continuous wave argon laser, a pumped dye laser system, and a high power ultraviolet wavelength Excimer laser. These added technical capabilities will permit the application of subcellular laser microsurgery to an even broader set of biological problems.

Computer imaging arose out of the need to follow a large number of cells for days after laser exposure. This long period of observation was necessary to analyze altered function as well as, in the case of the genetic deletion experiments, to isolate and clone cells and their descendants. For these experiments, a series of pattern recognition and tracking programs was developed (Berns and Berns 1982). Now a computer image processing system can control the microscope stage so that as a cell moves over time, it is continually held in the center of the optical field. This capa-

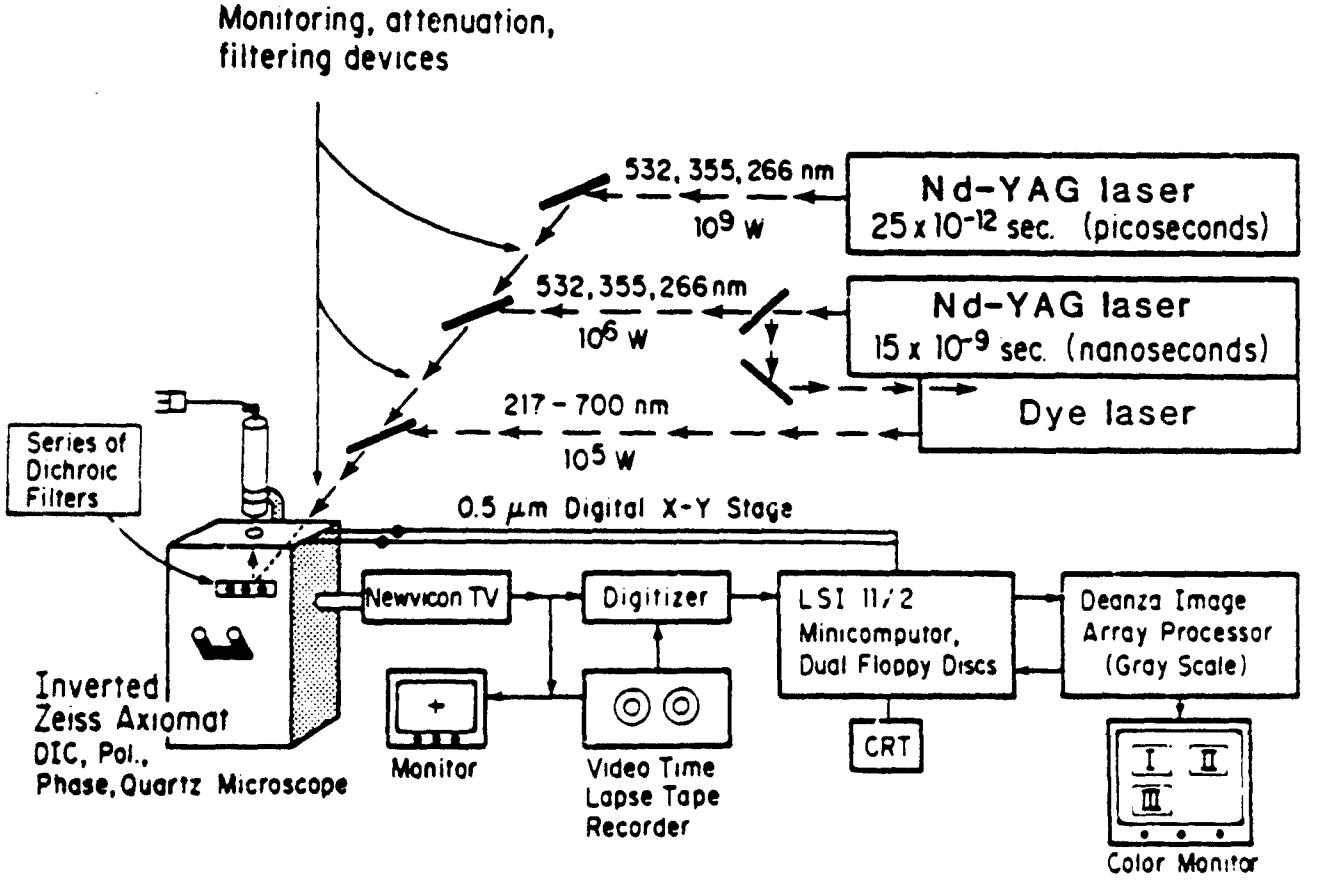

Figure 9. Diagram of laser microbeam system. The three basic components of the system are the lasers (Quantel YAG 400 and 481/TDL III), the microscope (Zeiss inverted Axiomat equipped for phase contrast, bright field, polarization, and differential interference contrast), and the television computer system (DeAnza 5000 image array processor, Sierra L T-1 television camera, and GYYR DA 5300 MKIII videotape system). An LSI-11 minicomputer is used to drive the image array processor. In addition, the image processor-LSI combination is connected to the X-Y digital microscope stage in order to provide cell tracking capabilities.

Best Available Copy

bility facilitated studies on the mechanism and control of cell movement (Koonce et al. 1984). For example, salamander white blood cells maintained in vitro were laser irradiated in their centriolar region, which was suspected to be the migration control site. The resulting migration patterns (as determined by computer tracking) of cells that had been moving in a straight line prior to irradiation, became haphazard and random. The researchers thus concluded that the centriolar region does indeed have a control function in determining the direction of cell migration. Both the number of cells analyzed and the time period that the individual cells were tracked were far greater than what could have been performed by non-computer methods.

Laser-stimulated microfluorescence. Instead of being used to destroy a subcellular region, the laser can be used to excite fluorescence at desired subcellular locations. Early studies were centered on the technique called fluorescence recovery after photobleaching or FRAP, which is now widely applied to study the mobility of specific molecules in the plasma membrane. Here, the laser excites fluorescence in micron-diameter spots on the surface of fluorescent-tagged cells. The power is momentarily increased about 1000-fold, which causes an irreversible photobleaching of the fluorescent molecules under the focused beam. However, over a period of seconds to minutes, fluorescence recovers as nonirradiated fluorescent molecules diffuse into the previously bleached site. By careful quantitation, the recovery of fluorescence can be related to the mobility of the molecules in the cell membrane and, therefore, membrane fluidity. Recent addition of sophisticated low-light detection systems and computer imaging into this technique should greatly expand its applications (Kapitza et al. 1985).

The application of laser-stimulated microfluorescence has extended from use at the cell surface to regions within the cell. Studies are being conducted on the mitotic apparatus with the goal of elucidating the kinetics and distribution of fluorescently tagged mobile molecules during the cell division process (Salmon et al. 1984). Other studies are being conducted on individual mitochondria of contracting myocardial cells *in vitro* (Siemens et al. 1982). In these studies, the beam of a blue helium cadmium laser is focused on a micron-diameter spot on individual mitochondria that have been tagged with the fluorescent molecule, rhodamine. Oscillating patterns of fluorescence intensity can be monitored over time within single mitochondria; thus, it may be possible to relate the respiratory activity of individual mitochondria to specific cell regions and overall cell activity. These fluorescent patterns can be further related to cell fluorescence by low-light video imaging, enhanced and analyzed by real-time computer image array processing (Berns et al. 1984).

Scanning acoustic microscopy

Although light waves have been used for microscopy for centuries, the use of sound waves is just over a decade old (Quate 1979). Imaging with sound may not at first seem comparable with light; sound waves involve vibrational motion of matter, whereas light involves electric and magnetic field fluctuations. Yet sound and light waves can each be focused with an appropriate lens and used for imaging with similar resolution.

The acoustic microscope uses sound waves focused in a liquid, usually water or superfluid helium. The sound waves are typically high frequency, between 0.1 and 10 gigahertz (1 GHz = 10^9 cycles/sec). These are typical microwave-radar frequencies, so we can use available microwave technology for acoustic microscopy.

The wavelength of the radiation used by a microscope is a major factor in determining resolution. Although the frequencies used in acoustic microscopy are much lower than in optical microscopy, the acoustic wavelengths turn out to be in the optical range because sound is much slower than light, and the wavelength equals the speed divided by the frequency. For example, the sound wavelength in water at 3 GHz is the same as the wavelength of (550 nm) green light. In helium at 8 GHz, the sound wavelength is only 30 nm, which is in the soft x-ray part of the electromagnetic spectrum.

Principles of the acoustic microscope. To image with sound waves, one must be able to generate sound, focus it onto the sample, and receive the echo. While work on generating sound waves is still progressing, we rely principally on a very old concept—piezoelectricity. Piezoelectric material either expands or contracts when a voltage is applied. Therefore, an oscillating voltage across a piezoelectric plate forces the plate to vibrate mechanically. If this plate, now a transducer, is pressed against a bulk material, sound waves will be launched into the bulk. In the same manner, if sound waves from the bulk cross into the transducer, an oscillating voltage will result in response to the squeezing and expanding of the sound. Thus a piezoelectric transducer, coupled to conventional electronics, can both generate and receive coherent sound waves.

Focusing sound waves is in principle very similar to focusing light, that is, the radiation is passed through a curved interface between two media and refraction causes the beam to converge to a small spot. A typical acoustic lens configuration is shown in Figure 10. Electric signals are applied to the transducer, generating plane sound waves that propagate into sapphire (Al_2O_3). As the plane waves pass from the sapphire lens into the liquid, they refract inward because the speed in liquids is generally much slower than in solids. This refraction also occurs in optics because the speed of light is less in glass than in air or vacuum. However, in optics, the refraction is not very strong because the speed of light usually changes by less than a factor or two. In contrast, the ratio of sound speeds between sapphire and water is greater than 7 and between sapphire and superfluid helium is 47.

This speed difference between solids and liquids has important consequences for acoustic microscopy. As the sound refracts into the slow liquid, the waves propagate almost perpendicular to the curved surface. Thus, a spherical interface will produce a very nearly spherical converging wave and a diffraction-limited focus. The strong refraction of sound into the liquid eliminates the spherical aberration of optical lenses, where a single convex spherical lens does not

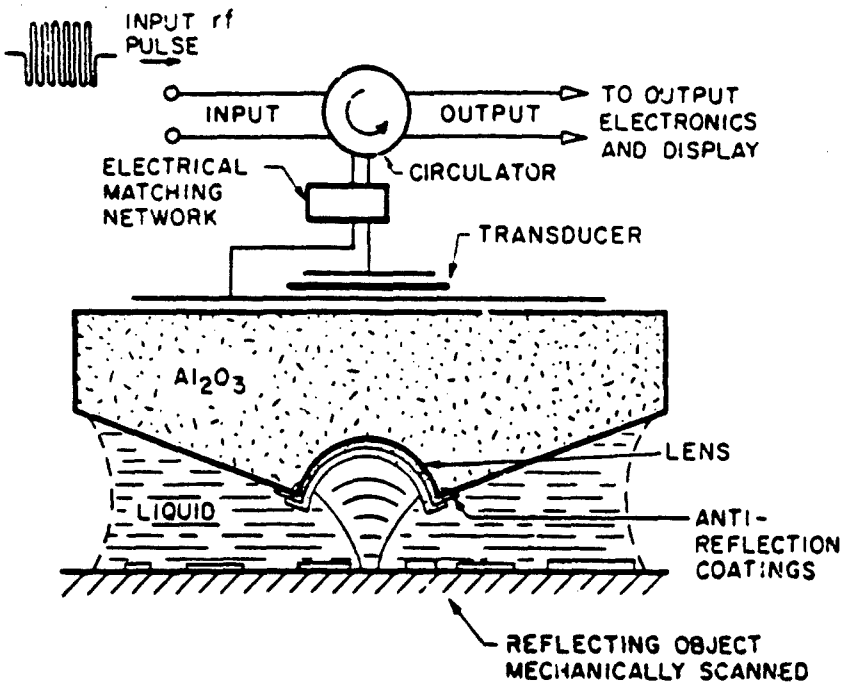

Figure 10. Configuration of the scanning reflection acoustic microscope. Microwave frequency electrical signals are applied to a zinc-oxide piezoelectric transducer, launching plane sound waves into the solid (Al_2O_3). The sound refracts into the liquid, focuses on the sample, and the echo returns to the transducer. The echo intensity is recorded as a function of the lens position as it is mechanically scanned across the sample.

give a good focus and more complicated lens shapes and/or multiple lenses are required.

One problem with the large change in sound speed between solids and liquids is the corresponding large reflection of sound at the interface. This problem can be solved, as in optics, by using quarter-wave-thick, antireflection coatings. We are currently coating lenses with a single layer of carbon.

Now that we can generate high frequency sound waves and focus them to a diffraction limited spot on a sample, how can we form an acoustic image? The answer is to receive the acoustic signal, the echo, from the focus while mechanically scanning the lens across the sample. The echo intensity is recorded for every lens position, and the resulting image is displayed on a cathode ray tube (CRT). This imaging system is similar to a scanning electron microscope, although the scanning is done mechanically instead of electronically.

The lateral resolution of the acoustic microscope is determined by the focal spot size, and is approximately equal to the lens f-number (focal length divided by the aperture diameter) multiplied by the acoustic wavelength (λ) in the liquid. Since $\lambda = c/f$ where c is the sound speed and f is the frequency, it is desirable to operate with low sound-speed liquids at high frequencies to achieve higher resolution. But high frequency operation of the microscope is limited to a few gigahertz, because in the liquid the acoustic attenuation—which increases with the square of the frequency—becomes so large that no echo can be received.

The standard liquid used for acoustic microscopy is water. A typical resolving power is 1 μ, although a resolution of 200 nm has been achieved (Hadimioglu and Quate 1983). Water is easy to handle, readily available, and offers reasonable acoustic attenuation compared with other liquids. The water acoustic microscope is able to image living biological specimens (Figure 11).

There is one liquid, however, that has negligible sound attenuation at microwave frequencies: superfluid helium at temperatures less than 0.2 K. Moreover, the sound speed in helium is quite low, so that x-ray wavelength sound is available at reasonable frequencies (10–200 GHz). A refrigerated microscope has been built using helium in the liquid path. Its present operating frequency is 8.0 GHz, and the sound wavelength is 30 nm. The lateral resolution is 20 nm, giving the superfluid helium acoustic microscope a much higher resolving power than other acoustic microscopes.

Most of the contrast for the superfluid helium acoustic microscope comes from the surface topography, although some information from inside biological cells may be obtained. Because the microscope uses short, coherent radiation, it is sensitive to slight changes in height, for example, a 1-nanometer step on a surface. In addition, because of the wide-angle lens used, the depth of focus is generally less than 100 nm. Because the bacteria in Figure 12 are about 0.4 μ thick, it is not possible to focus on all parts of the cell as well as on the substrate. Figure 12a is actually a composite image formed by combining the images from three different focal positions. The image can be viewed assigning a different color to each plane to provide a three-dimensional image.

The acoustic microscope's future. The scanning acoustic microscope operating with water-immersed material is now available commercially from several sources around the world, notably in West Germany (Hoppe and Bereiter-Hahn 1985), England (Smith et al. 1985), and Japan. These instruments are finding application in science and industry in areas that include subsurface imaging, imaging elastic properties, and nondestructive imaging. The resolution available in these instruments is slightly better than 1 μ, and the cost is comparable with that of a scanning electron microscope. As the commercial products become common, there should be a large increase in the understanding of contrast mechanisms and use of the microscope for detailed quantitative measurements. Because of the sound attenuation in water, however, the resolution of the water microscope will never be much better than 200 nm.

Figure 11. Living chicken heart fibroblast imaged by a water acoustic microscope. The pair of cells was viewed continuously for 2 hr, during which the cells appeared to exhibit normal mobility patterns. Intracellular organelles, such as nuclei, mitochondria, and lipid or lysosomal bodies, are visible (Hildebrand et al. 1981). The images were taken 27 and 69 min apart. The acoustic microscope was operated at a frequency of 1.7 GHz, giving an acoustic wavelength in water of 0.9 μ and a resolution of 0.72 μ using an f/0.75 lens. The water was heated to 37° C to lessen the acoustic attenuation in the liquid path, and no apparent damage was seen during the two-hour imaging. Image (b) is shown at twice the magnification of (a) and (c). The scale bar is 20 μ.

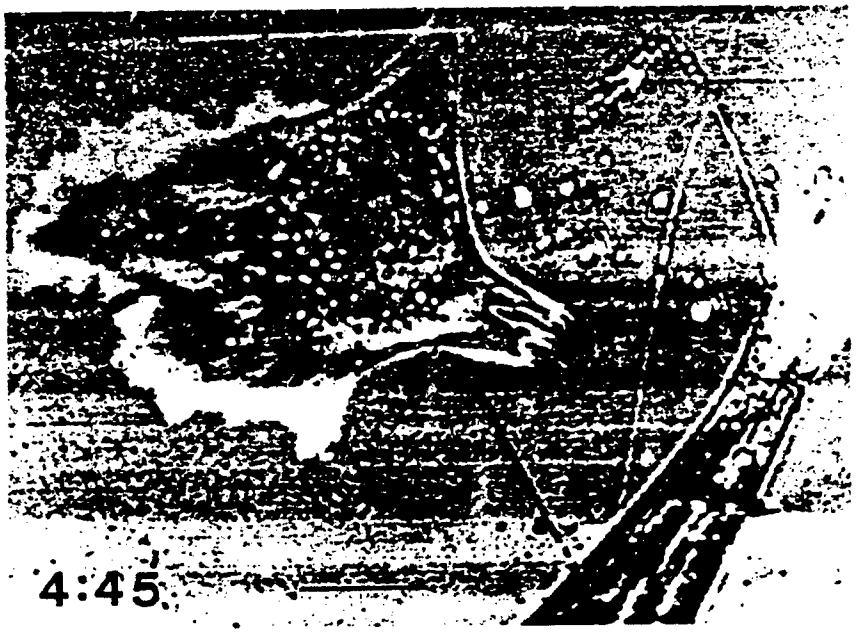

With the superfluid helium acoustic microscope, sound attenuation is not a problem and lateral resolution of 20 nm has already been demonstrated. Perhaps more importantly, there appear to be no physical limits to increasing the frequency and bringing the resolution down to near atomic distances, 1–2 nm (Foster 1984). Combining this resolution with acoustic contrast mechanisms and the low damage of the acoustic beam should result in a formidable microscopy tool, particularly for biology.

The design, efficiency, and wide applicability of present day optical and acoustic microscopes are products of the significant advances in glass, computer, laser beam, and acoustic technologies.

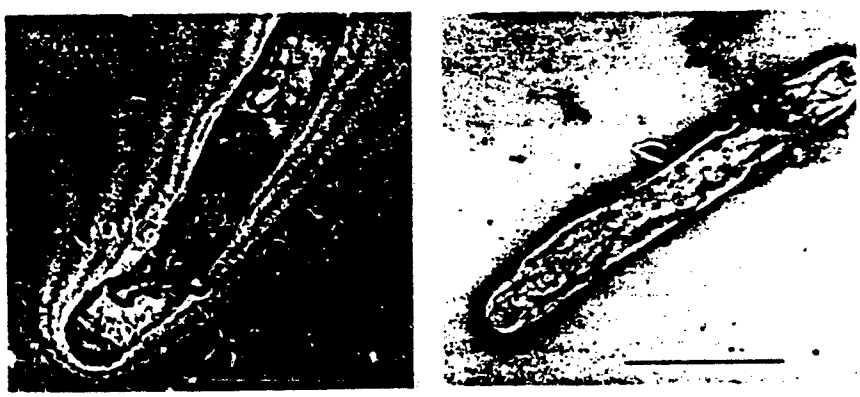

Figure 12. Myxobacteria imaged by (a) a superfluid helium acoustic microscope at 0.1° K and (b) a transmission electron microscope (TEM). The sample is of unsectioned Myxobacteria fixed with uranyl acetate, as prepared by Professor Dale Kaiser and Karl Stevens of the Biochemistry Department at Stanford University. The operating frequency of the acoustic microscope is 8 GHz, corresponding to an acoustic wavelength of 30 nm in helium, and the resolution is 20 nm. The "wake" in the acoustic image is due to topography generated during the fixing procedure. The TEM image for whole cells has markedly limited resolution. The scale bar is 1 μ.

References cited

Agard, D., and J. W. Sedat. 1983. Three dimension architecture of polytene nucleus. *Nature* 302: 676–681.

Allen, R. D., G. B. David, and G. Nomarski. 1969. The Zeiss-Nomarski differential equipment for transmitted-light microscopy *Zeitschrift für Wissenschaftliche Mikroskopie und Mikroskopische Technik*. 69: 193–221.

Arndt-Jovin, D. J., M. Robert-Nicoud, S. J. Kaufman, and T. M. Jovin. 1985. Fluorescence digital imaging microscopy cell biology. *Science* 230: 247–255.

Bartels, P. H., G. B. Olson, H. G. Bartels, D. E. Brooks, and G. V. Seaman. 1981. The automated analytic electrophoresis microscope. *Cell Biophys.* 4: 371–388.

Berns, M. W. 1974. Directed chromosome loss by laser microirradiation. *Science* 186: 700–705.

Berns, M. W., J. Aist, J. Edwards, K. Strahs, J. Girton, J. Kirzes, M. Hammer-Wilson, L. H. Liaw, A. Siemens, M. Koonce, R. Walter, D. van Dyk, J. Coulombe, T. Cahill, and G. S. Berns. 1981. Laser microsurgery in cell and developmental biology. *Science* 213: 505–513.

Berns, G. S., and M. W. Berns. 1982. Computer-based tracking of living cells. *Exp. Cell Res.* 142: 103–109.

Berns, M. W., L. K. Chong, M. Hammer-Wilson, K. Miller, and A. Siemens. 1979. Genetic microsurgery by laser: establishment of a clonal population of rat kangaroo cells (PTK_2) with a directed deficiency in a chromosomal nucleolar organizer. *Chromosoma* 73: 1–8.

Berns, M. W., Gamaleja, C. Duffy, R. Olson, and D. E. Rounds. 1970b. Argon laser microirradiation of mitochondria in rat myocardial cells in tissue culture. *J. Cell Physiol.* 76: 207–214.

Berns, M. W., Y. Ohnuki, D. E. Rounds, and R. S. Olson. 1970a. Modification of nucleolar expression laser microirradiation of chromosomes. *Exp. Cell Res.* 60: 133–138.

Berns, M. W., R. S. Olson, and D. E. Rounds. 1969. *In vitro* production of chromosomal lesions using an argon laser microbeam. *Nature* 221: 74–75.

Berns, M. W., J. B. Rattner, S. Brenner, and S. Meredith. 1977. The role of the centriolar region in animal cell mitosis: a laser microbeam study. *J. Cell Biol.* 72: 351–368.

Berns, M. W., A. E. Siemens, and R. J. Walter. 1984. Mitochondrial fluorescence patterns in rhodamine 6G-stained myocardial cells *in vitro*. Analysis by real time computer video microscopy and laser microspot excitation. *Cell Biophys.* 6: 263–277.

Bradbury, S. 1983. Commercial image analyzers and the characterization of microscope images. *J. Microsc.* 131: 203–210.

———. 1984. *An Introduction to the Optical Microscope*. Oxford University Press, New York.

Burt, J. M., K. R. Strahs, and M. W. Berns. 1979. Correlation of cell surface alterations with contractile response in laser microbeam irradiated myocardial cells: a scanning electron microscope study *Exp. Cell Res.* 118: 341–351.

Calmettes, P. P., and M. W. Berns. 1983. Laser-induced multiphoton processes in living cells. *Proc. Natl. Acad. Sci.*, 80: 7197–7199.

Castleman, K. R 1979. *Digital Image Processing*, Prentice-Hall, Englewood Cliffs, NJ.

Foster, J. S. 1984. High resolution acoustic microscopy in superfluid helium. *Physica* 126B: 199–205.

Gupta, P. K. and J. Hinsch. 1983. Essentials of light microscopy and photomicrography. Pages 331–358 in S. C. Sommers and P. P. Rosen, eds. *Pathology Annual*, vol. 18, part 1, Appleton-Century-Crofts, East Norwalk, CT.

Hadimioglu, B., and C. F. Quate. 1983. Water acoustic microscopy at sub-optical wavelengths. *Appl. Physics Lett.* 43: 1006–1007.

Hildebrand, J. A., D. Rugar, R. N. Johnston, and C. F. Quate. 1981. Acoustic microscopy of living cells. *Proc. Natl. Acad. Sci.* 78: 1656–1660.

Hoppe, M., and J. Bereiter-Hahn. 1985. Applications of scanning acoustic microscopy—survey and new aspects. *IEEE Trans. Sonics and Ultrasonics*, SU-32: 289–301.

Kapitza, H. G., G. McGregor, and K. A. Jacobson. 1985. Direct measurement of lateral transport in membranes by using time resolved spatial photometry. *Proc. Natl. Acad. Sci.* 82: 4122–4166.

Koonce, M. P., R. J. Cloney, and M. W. Berns. 1984. Laser irradiation of centrosomes in newt eosinophils: evidence of centriole role in motility. *J. Cell Biol.* 98: 1999–2010.

McBride, G., J. LaBounty, J. Adams, and M. Berns. 1974. The totipotency and relationship of seta-bearing cells to thallus development in the green alga *Coleochaete scutata*. A laser microbeam study. *Dev. Biol.* 37: 90–99.

McNeill, P. A., and M. W. Berns. 1981. Chromosome behavior following laser microirradiation of a single kinetochore in mitotic PTK$_2$ cells. *J. Cell Biol.* 88: 543–553.

Needham, G. 1958. *The Practical Use of the Microscope*. Charles C. Thomas. Springfield, IL.

Pavlidis, T. 1982. *Algorithms for Graphics and Image Processing*. Computer Science Press, Rockville, MD.

Petran, M., M. Hadravsky, J. Benes, R. Kucera, and A. Boyde. 1985. The tandem scanning reflected light microscope. Part I—the principle and its design. *Proc. R. Microsc. Soc.* 20: 125–129.

Quate, C. F. 1979. The acoustic microscope. *Sci. Am.* 241: 62–70.

Salmon, E. D., W. M. Saxton, R. J. Leslie, M. L. Karow, and J. R. McIntosh. 1984. Diffusion coefficient of fluorescein-labeled tubulin in the cytoplasm of embryonic cells of the sea urchin: video image analysis of fluorescence redistribution after photobleaching. *J. Cell Biol.* 99: 2157–2164.

Siemens, A., R. J. Walter, L. H. Liaw, and M. W. Berns. 1982. Laser stimulated fluorescence of submicron regions within single mitochondria of Rhodamine treated myocardial cells in culture. *Proc. Natl. Acad. Sci.* 79: 466–470.

Sklansky, J. 1978. Image segmentation and feature extraction. *IEEE Transactions on Systems Man and Cybernetics* 8: 237–247.

Sklansky, J., P. Sankar, and R. J. Walter. 1986. Biomedical image processing. Pages 629–647 in T. S. Young and K. S. Fu, eds. *Biomedical Image Analysis*. Academic Press, Orlando, FL.

Smith, R. F. 1984. Olympus revolutionary microscope. *Funct. Photogr.* 19(4): 22–24.

———. 1985a. The microscopist's microscope. *Funct. Photogr.* 20(5): 23–25.

———. 1985b. A unique instrument (Reichert Polyvar). *Funct. Photogr.* 20(1): 18–20.

Smith, I. R., R. A. Harvey, and D. J. Fathers. 1985. An acoustic microscope for industrial applications. *IEEE Trans. Sonics and Ultrasonics*, SU-32: 274–288.

Spencer, M. 1982. *Fundamentals of Light Microscopy*. Cambridge University Press, New York.

Strahs, K. R., and M. W. Berns. 1979. Laser microirradiation of stress fibers and intermediate filaments in non-muscle cells from cultured rat heart. *Exp. Cell Res.* 119: 31–45.

Strahs, K. R., J. M. Burt, and M. W. Berns. 1978. Contractility changes in cultured cardiac cells following laser microirradiation of myofibrils and the cell surface. *Exp. Cell Res.* 113: 75–83.

Walter, R. J., and M. W. Berns. 1986. Digital image processing and analysis. Pages 327–386 in S. Inoue, ed. *Video Microscopy* Plenum Press, New York.

Zernike, F. 1942. Phase-contrast, a new method for microscopic observation of transparent objects. *Physica* 9: 686–698.

Proc. Natl. Acad. Sci. USA
Vol. 84, pp. 4180–4184, June 1987
Genetics

Direct gene transfer into human cultured cells facilitated by laser micropuncture of the cell membrane

(transformation/microbeam)

WEN TAO*†, JOYCE WILKINSON‡, ERIC J. STANBRIDGE‡, AND MICHAEL W. BERNS*†

*Beckman Laser Institute and Medical Clinic and ‡Department of Microbiology and Molecular Genetics, University of California, Irvine, CA 92717

Communicated by Peter M. Rentzepis, January 29, 1987

ABSTRACT **The selective alteration of the cellular genome by laser microbeam irradiation has been extensively applied in cell biology. We report here the use of the third harmonic (355 nm) of an yttrium–aluminum garnet laser to facilitate the direct transfer of the *neo* gene into cultured human HT1080-6TG cells. The resultant transformants were selected in medium containing an aminoglycoside antibiotic, G418. Integration of the *neo* gene into individual human chromosomes and expression of the gene were demonstrated by Southern blot analyses, microcell-mediated chromosome transfer, and chromosome analyses. The stability of the integrated *neo* gene in the transformants was shown by a comparative growth assay in selective and nonselective media. Transformation and incorporation of the *neo* gene into the host genome occurred at a frequency of 8×10^{-4}–3×10^{-3}. This method appears to be 100-fold more efficient than the standard calcium phosphate-mediated method of DNA transfer.**

The introduction of exogenous genes into the cells of multicellular organisms using different techniques has proven to be a powerful approach for the study of gene regulation and function in bacteria, fungi, animal, and plant cells. Any efficient method for direct gene transfer could be of considerable value in continued progress in genetic engineering. The frequently used methods for direct gene transfer involve either chemical methods such as uptake of calcium phosphate-precipitated DNA enhanced by treatment with glycerol, dimethyl sulfoxide, or polyethylene glycol (1–3) or the manual microinjection of DNA into individual cells (4–6). DNA sequences introduced by these transformation procedures can become associated with high molecular weight DNA (7) and integrate into host chromosomes by unknown mechanisms. However, these techniques have their limitations. Although the chemical method is simple and can be performed easily, transformation frequencies are low (most protocols yield 1–5 transformants per 10^5–10^7 cells), and toxicity of the chemicals may result in cell damage. Furthermore, some cell lines are not transformed by chemical methods. The manual microinjection method yields higher transformation frequencies (1–3 in 10^3 cells) but is a very tedious technique requiring considerable skill on the part of the person performing the procedure. The microinjection method has worked very poorly in isolated protoplasts for plant transformation (8, 9). These problems might be solved by a new method for cell transformation.

Over the past 15 years the laser has steadily developed as a method to perform selective subcellular microsurgery. Numerous cell structures such as individual chromosomes, mitotic organelles, mitochondria, and the cell membrane have been selectively altered by using a variety of lasers. These alterations can be in a specific class of molecules confined to an area of less than a micrometer in diameter (10–14). In addition, interfacing a laser system with a microscope and an image array processing computer permits the exposure of single cells or individual organelles within single cells to a variety of wavelengths at various power densities. These laser microscope systems can be used to perform state-of-the-art optical and photometric examinations of the biological sample. It has been suggested that a highly focused laser beam could be used as an "optical" microbeam to produce tiny submicrometer holes in the cell membrane to facilitate uptake of exogenous DNA into cultured mouse cells (15, 16). In the present study a technique of direct gene transfer into human cells is described. We focused a 355-nm beam of a frequency-tripled neodymium–yttrium–aluminum garnet laser onto the cell membrane of human cells in culture medium containing pSV2-neo plasmid DNA. Apparently DNA entered the cell prior to the membrane alteration rehealing. Transformants were selected in media containing an amino glycoside antibiotic, G418 (Fig. 1). Southern blot analyses demonstrate the physical presence of the *neo* gene in these transformants. The integration and expression of the *neo* gene were further characterized by microcell-mediated chromosome transfer and chromosome analyses. The stability of the integrated *neo* gene in the transformants was shown by a comparative growth assay in selective and nonselective media.

MATERIALS AND METHODS

Cell Lines and Plasmid. HT1080-6TG, a hypoxanthine phosphoribosyltransferase (HPRT)-deficient human fibrosarcoma (17, 18), was used for transformation. HT1080-6TG cells were grown in minimal essential medium (MEM) supplemented with nonessential amino acids and 10% fetal calf serum. A9, a HPRT-deficient line derived from mouse L cells (19), was used as the recipient for microcell-mediated chromosome transfer. Rodent cells were maintained on Dulbecco's modified Eagle's medium (DMEM) supplemented with 10% fetal calf serum. The transformants were selected and maintained in MEM alpha modification (αMEM) containing 10% fetal calf serum and G418 at the concentrations indicated. Microcell hybrids were selected and maintained in DMEM supplemented with 10% fetal calf serum, 800 μg of G418 (GIBCO) per ml, and 5 μM ouabain (Sigma).

The plasmid vector pSV2-neo containing the *neo* gene for phosphotransferase, APH (3')II derived from transposon Tn*5*, was described by Southern and Berg (20).

Transformation of HT1080-6TG Cells. *Laser microsurgery in cells.* Laser microsurgery was conducted on cells in Rose chambers using the third harmonic 355-nm wavelength from a short-pulsed Quantel model YG 481a neodymium–yttrium–aluminum garnet laser (10). Laser pulse duration was 10 nsec. Laser energy was controlled by a KLC model K1174

The publication costs of this article were defrayed in part by page charge payment. This article must therefore be hereby marked "*advertisement*" in accordance with 18 U.S.C. §1734 solely to indicate this fact.

†To whom reprints should be addressed.

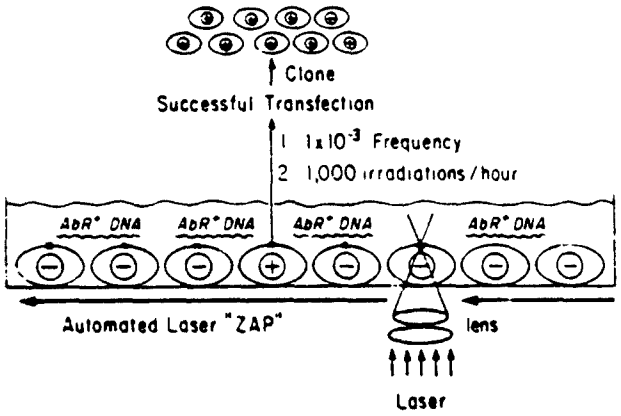

FIG. 1. Schematic representation of laser-mediated gene transfer. The cells (−) are irradiated with the focused laser beam in the presence of the plasmid DNA. The plasmid DNA, contained in the culture medium, is thought to be introduced into the cells through a very small hole momentarily made in the membrane by the laser. The transformants (+) are then selected and expanded to stable cell lines in selective medium.

continuously adjustable optical attenuator (Karl Lambrecht, Chicago) placed in the light path. Pulse energies were in the range of 23–67 μJ. All of the laser energy measurements were made with a Scientech no. 362 energy power meter at the level of the rear aperture stop of an inverted Zeiss Axiomat microscope. The laser was diverted by a series of optical mirrors and a dichroic filter into the microscope and focused to a spot of about 2.0 μm in diameter using a Zeiss 32× Ultrafluar objective. The laser beam was carefully focused onto the cell membrane of individual cells using the method described earlier (10). Single pulses were obtained by an electronic shutter synchronized with the laser. Imaging the cells and targeting the laser using the motorized microscope stage, video camera, TV monitor, and computer have been described (21). With this configuration of equipment, 1000 cells could easily be irradiated per hour.

DNA transfection and selection of transformants. The cells were seeded in standard Rose culture chambers at a density of 1×10^5 per chamber 36 hr before addition of the pSV2-neo plasmid DNA. The plasmid DNA was first sterilized and precipitated by adding sodium acetate to 0.3 M and 2 vol of ethanol. The DNA was resuspended in 1× TE buffer (10 mM Tris·HCl/1 mM EDTA, pH 7.5). The DNA suspension was added to MEM growth medium to give a final concentration of 12 μg/ml, which was injected into the Rose chambers. The cells were incubated at 37°C for 1 hr and then subjected to laser irradiation as described above. About 6 hr after the irradiation, the Rose chamber was disassembled in a sterile laminar flow hood. The coverslip containing the cells was washed twice with MEM growth medium and transferred to a 100 × 20 mm Petri dish with 10 ml of MEM growth medium. After incubation at 37°C for 24–36 hr, the cells were trypsinized and replated into two 100-mm Petri dishes. Within 12–16 hr the medium was replaced with MEM containing G418 at a concentration of 800 μg/ml. The G418-supplemented medium was changed every 3–4 days. Independent colonies that arose were trypsinized in cloning rings and transferred to 24-multiwell plates after 14–18 days. The cells were then grown in nonselective medium for 1 day. Once established, the clones were subsequently maintained in MEM containing 600 μg of G418 per ml.

Genomic Blot Hybridization Analysis of Transformants. High molecular weight cellular DNAs were extracted and digested with individual restriction enzymes, *Eco*RI or *Xba* I. The digests were then subjected to electrophoresis in a 1.0% agarose gel, and DNA fragments in the gel were transferred to nitrocellulose filters by the method of Southern (22). After prehybridization, DNA on the filters was hybridized with ^{32}P-labeled pSV2-neo DNA at 65°C overnight. The labeling was done using the oligo-labeling method according to the procedure of Feinberg and Vogelstein (23, 24). Filters were washed, air dried, and autoradiographed (ref. 25, p. 141).

Microcell-Mediated Chromosome Transfer and Chromosome Analysis. HT1080 *neo* transformants were used as microcell donors. The microcells were prepared and introduced to recipient A9 cells as described (ref. 25, pp. 140–146) except that the concentration of colcemid was 0.02 μg/ml and that the selection medium was DMEM with 800 μg of G418 per ml and 5 μM ouabain.

The chromosome constitutions of the microcell hybrids were analyzed by using the alkaline Giemsa staining method (26). The single human chromosome in the mouse background was identified by this technique. At least 12 metaphase spreads were analyzed for each microcell hybrid.

Stability Analysis of the Transformants. The analyses were performed as described (27). Briefly, each transformant was switched to growth in nonselective medium for at least 42 days. Every 6 days, 1500 cells were plated in duplicate 25-cm^2 culture flasks; one flask contained selective medium (600 μg of G418 per ml) and the other contained nonselective medium. After 11–12 days the resulting colonies were stained and counted. Stability was calculated as the ratio of colonies formed in selective medium versus nonselective medium.

RESULTS

Cell Transformation and Selection of G418-Resistant Cell Lines. The transformation experiments were initiated to determine whether the transfer of DNA contained in the culture medium into human cells could be mediated through self-healing holes in the cell membranes produced by laser and to establish the efficiency of laser-mediated DNA transformation.

The experimental system chosen for these studies was the transfer of the *neo* gene into human fibrosarcoma cells, HT1080-6TG. HT1080-6TG cells were cultured in Rose chambers and irradiated in the presence of pSV2-neo plasmid DNA using a neodymium–yttrium–aluminum garnet laser at 355-nm wavelength as described in *Materials and Methods*. The colonies were detected and isolated in αMEM containing 800 μg of G418 per ml after 14–18 days. Fig. 2 shows the morphologies of dead cells from the control experiments and of three representative independent colonies from the transformation experiments. HT1080-6TG cells were transformed to G418 resistance at a relatively high frequency with pSV2-neo DNA using this method (on average, a frequency of about 1.6 transformants in 10^3 treated cells). This is in contrast to the lower frequencies of G418-resistant transformation using the calcium phosphate precipitation technique (about 2 transformants in 10^5 treated cells). The transformation frequencies using the laser method are in the range of $0.8–3.0 \times 10^{-3}$ based on a number of separate transformation experiments (Table 1). Control experiments (nontreated cells, cells irradiated without DNA or treated with DNA without laser irradiation) have not yielded G418-resistant colonies under these conditions. The sensitivity of HT1080-6TG cells to G418 was tested by plating cells at low cell density in multiwell plates in αMEM supplemented with various concentrations of G418. We found that 100% cell killing could be achieved at concentrations of G418 as low as 400 μg/ml (unpublished data).

Genomic Analysis of the Transformants. Molecular analyses for the presence of the transforming *neo* gene were carried out on five G418-resistant colonies as well as on control cells. High molecular weight DNA from each trans-

Best Available Copy

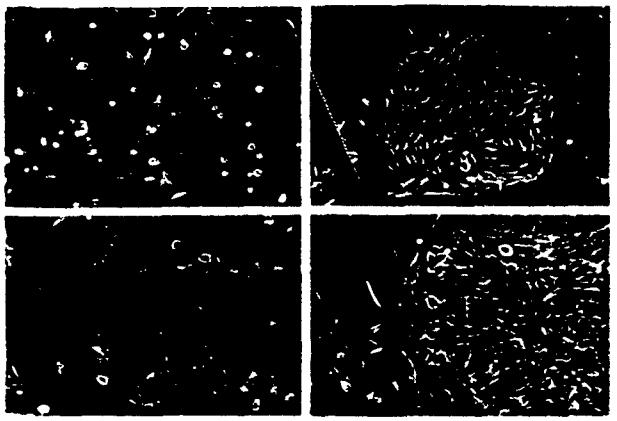

FIG. 2. Microscopic photographs of nontreated and transformed HT1080-6TG cells growing on the αMEM containing 800 μg of G418 per ml. (*A*) Control (nontreated cells). No resistant colonies developed under the experimental conditions. (*B* and *C*) Two independent G418-resistant colonies. (*D*) A large resistant colony after 15 days on the selective medium. (×100.)

formant was digested with *Eco*RI or *Xba* I, electrophoresed in an agarose gel, transferred to nitrocellulose filters, and probed with ^{32}P-labeled pSV2-neo DNA (Fig. 3). The results revealed that the untreated HT1080-6TG cells do not contain the pSV2-neo plasmid-related sequences; however, cell DNA obtained from G418-resistant transformants contained DNA sequences homologous to the pSV2-neo DNA. Moreover, the hybridization patterns of DNA isolated from individual transformants were not identical. This indicates that each independent transformant has its own organization of the integrated pSV2-neo DNA sequences with probable variation in the locations of integration and gene copy number among these transformants. Since the pSV2-neo plasmid contains a single *Eco*RI restriction site and no *Xba* I site, each integrated plasmid copy should produce two hybridizing fragments when digested with *Eco*RI but only one hybridizing fragment when digested with *Xba* I if there is no rearrangement of the plasmid DNA (20). From the number of hybridizing fragments on the autoradiogram, we infer that transformants 1:C4 and dS each contain a single copy of pSV2-neo plasmid DNA. Transformants 3, 2, and 7 appear to contain two copies of pSV2-neo plasmid; however, the hybridization pattern of DNA obtained from transformant 3 differs from that expected, which may be due to modification of the input pSV2-neo DNA during transformation. Expression of the *neo* gene in pSV2-neo-transformed cells can be inferred from the fact that all of the transformants tested are resistant to a high concentration of G418 (900 μg/ml).

Table 1. Transformation of HT1080 cells with pSV2-neo plasmid DNA

Conc of pSV2-neo DNA, μg/ml	Irradiated cells, no.	Isolated and clonal G418-resistant colonies, no.	Transformation frequency
0	0	0	--
12	0	0	—
0	1250	0	—
12	1250	1	8×10^{-4}
12	1250	1	8×10^{-4}
12	1000	2	2×10^{-3}
12	1000	3	3×10^{-3}
12	1000	2	2×10^{-3}
12	1000	1	1×10^{-3}

Transformation frequency is expressed as the fraction of cells irradiated in the presence of DNA that produces viable colonies in selective medium that have been isolated and expanded. All colonies were further characterized by Southern blot analyses to confirm that they were truly independent clones.

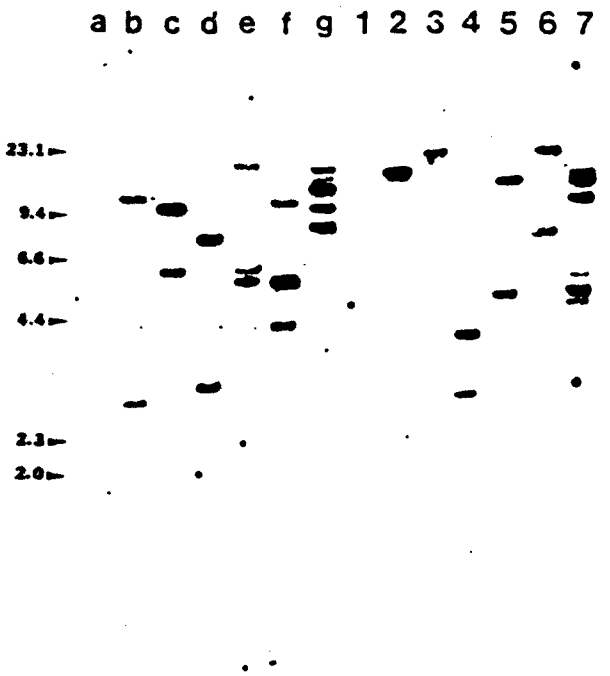

FIG. 3. Southern blot analysis of laser-mediated G418-resistant transformants. High molecular weight DNA was isolated from nontreated HT1080-6TG cells and from representative G418-resistant cell lines that had been transformed with pSV2-neo DNA and digested with either restriction endonuclease *Eco*RI or *Xba* I. After separation on a 1% agarose gel, DNA was transferred onto a nitrocellulose filter and hybridized with ^{32}P-labeled pSV2-neo DNA. Lanes a–g, DNA restricted with *Eco*RI; lanes 1–7, DNA restricted with *Xba* I. Lanes a and 1, DNA isolated from nontreated HT1080-6TG cells (negative control); lanes b and 2, c and 3, d and 4, e and 5, and f and 6, DNA isolated from transformants 1:C4, dS, 3, 2, and 7, respectively; lanes g and 7, DNA isolated from cells that had been shown to contain multiple integrated pSV2-neo DNA sequences previously (positive control). There is a single recognition site in pSV2-neo DNA for *Eco*RI cleavage and no recognition site in pSV2-neo DNA for *Xba* I cleavage. The numbers beside the arrowheads refer to the molecular sizes of DNA in kilobase pairs, and marker molecular sizes were derived from *Hin*dIII DNA restriction fragments in an adjacent lane on the gel.

Microcell Hybridization and Chromosome Analysis. Although the genomic blot hybridization data suggest that exogenous pSV2-neo DNA was integrated into host chromosomes, it was still possible that the exogenous neo DNA somehow rearranged and replicated independently as an extrachromosomal unit (7). To confirm that the exogenous pSV2-neo DNA in the transformants was actually integrated into chromosomes, the two transformants shown to contain a single copy of pSV2-neo plasmid DNA, dS and 1:C4, were used as microcell donors. Microcells were prepared as described in *Materials and Methods* and fused to mouse A9 cells. Microcell hybrids were selected on DMEM containing 800 μg of G418 per ml and 5 μM ouabain, and the colonies were isolated and expanded. The presence of human chromosomes in these hybrids was examined by using the alkaline Giemsa differential staining technique: the human chromosomes stain blue, whereas mouse chromosomes stain magenta with blue centromeric regions. The single lighter-staining human chromosome (Fig. 4, arrow) was observed in

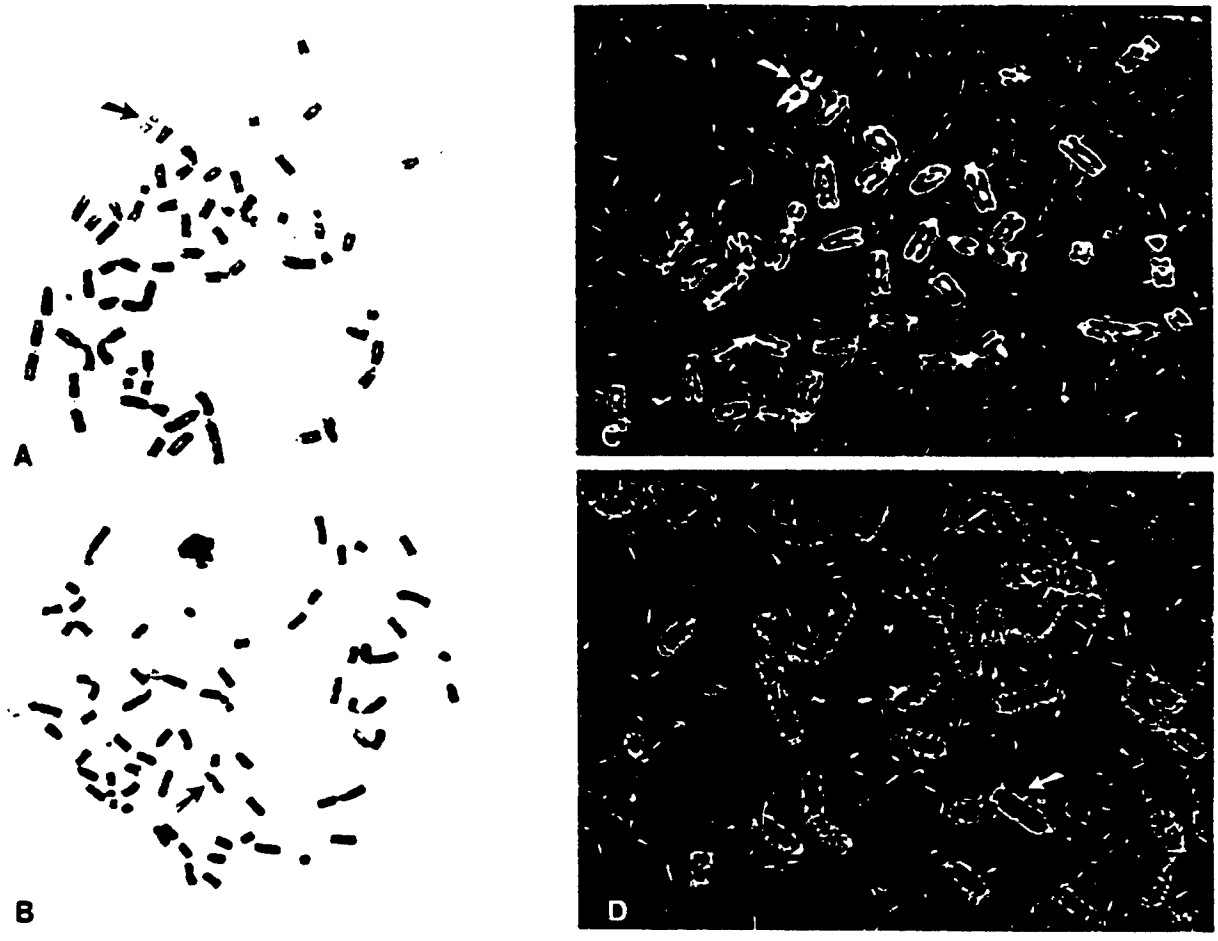

FIG. 4. Alkaline Giemsa-stained metaphase spreads of human–mouse microcell hybrids containing single human chromosomes (arrow). (*A*) Hybrid 1:C4/A9. (*B*) Hybrid dS/A9. Each hybrid represents a mouse A9 fusion to a different human transformant containing singly integrated pSV2-neo DNA. (*C* and *D*) Computer enhancement of *A* and *B*. (×1050 for *A* and *B*.)

each microcell hybrid derived from transformants 1:C4 (Fig. 4*A*) and dS (Fig. 4*B*), respectively. A computer enhancement (Fig. 4 *C* and *D*) of the mitotic spreads facilitates identification of the human chromosome. These results demonstrate that the pSV2-neo plasmid DNA has indeed integrated into host chromosomes. From these data alone, we cannot determine the identities of the human chromosomes. However, it appears that the human chromosome in hybrid dS/A9 belongs to the D group, whereas the human chromosome in hybrid 1:C4/A9 belongs to the C group, judging by the chromosomal morphologies.

Stability of Transformants. The stability of the transferred G418-resistant phenotype was analyzed by growing each transformant on nonselective medium for at least 42 days and then plating an aliquot of each cell line in selective medium and nonselective medium at various times. The number of colonies arising in both media was scored and the ratios were plotted versus the time in nonselective medium. Most of the transformants tested were found to be stable, showing no loss of the resistant phenotype. The results obtained from three representative independent transformants were shown in Fig. 5.

During the course of the experiments, we found that the ratios obtained from a couple of transformants did vary (data not shown). However, after being grown in nonselective medium for 42 days, these cells when replated at 1/12th the cell density and challenged in selective medium still remained fully resistant to a high concentration of G418 (900 μg/ml). Thus, these transformants also appear to be stable.

DISCUSSION

We have developed an efficient method to transfer plasmid DNA into human fibrosarcoma HT1080-6TG cells. Our data demonstrate that a short pulsed laser of 355 nm can be focused on the surface of cells, thus facilitating the uptake of

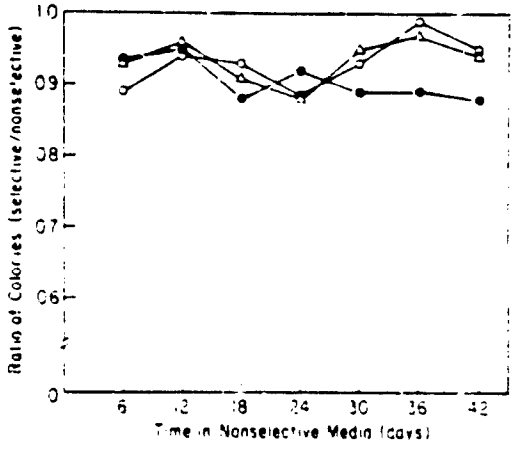

FIG. 5. Stability data for G418-resistant transformants when grown in nonselective medium. The number of colonies formed in αMEM containing G418 versus nonselective medium is taken as a measure of the fraction of cells retaining the G418-resistant phenotype.

plasmid DNA from the medium. The transferred *neo* gene was incorporated into host chromosomes and expressed. Most of the transformants that have been examined appear to contain the nonrearranged introduced *neo* gene and have a low plasmid copy number, generally one to two copies per cell. Transformant 3 is exceptional in that restrictions with either *Eco*RI or *Xba* I produce two bands and the sizes of the fragments produced by digestion with *Xba* I are substantially smaller than that of pSV2-neo plasmid (5.7 kilobase pairs in size). Rearrangement or deletions of the introduced DNA molecules may explain this result. The majority of the transformants is shown to stably maintain the transferred phenotype for at least 42 days without selective pressure. This method is nearly 100-fold more efficient than the standard calcium phosphate technique. Even though the transformation frequency ($0.8–3 \times 10^{-3}$) is comparable with that of microinjection, the laser method has the advantage of simplicity of operation. At present, the gene transfer experiments have been conducted with the ultrasophisticated laser system described; however, this by no means implies that this hardware is absolutely necessary for transformation. A more simplistic type of laser interfaced with a standard microscope and TV system will be expected to allow one to perform gene transfer experiments using this method. Thus, when compared to the microinjection technique, the number of cells treated in a given time by an "unskilled" operator will be much greater. In addition, the actual transformation frequency achieved using this method may be higher than 3×10^{-3} since there is no evidence indicated that we have reached the optimum transformation frequency. Many factors need to be examined that could affect the transformation frequency, such as cell viability after laser treatment and the percentage of successful cell-surface "perforations." Furthermore, it is likely that laser beam intensity and wavelength can be readily modulated to achieve the optimum frequency for transformation and to accommodate various cell types, such as plant cells whose walls cannot be easily penetrated by the microinjection capillary pipette.

Although the experiments presented here have been carried out with HT1080-6TG cells, theoretically there is no reason to expect that this system should not work with other given cell types, animal or plant. This method could be of considerable value in genetic engineering, especially in plants. Direct gene transfer to isolated protoplasts using the calcium phosphate method has been reported to be a successful method in many cases (28–30); however, it requires protoplasts, and the regeneration of whole plants from isolated protoplasts is still a severe problem for many monocots. Transformation experiments with the Ti plasmid of *Agrobacterium tumefaciens* (31–33) are restricted to dicots due to the natural host range of *A. tumefaciens*. Taken together, new techniques for plant transformation are absolutely needed. The laser method might be a candidate since it does not require protoplasts and circumvents the problem of host range. Furthermore, it might be possible to facilitate gene transfer directly into pollen. Another application of this method might be its use in transforming cell types that are too fragile or sensitive to chemical techniques, such as the keratinocytes. These cells cannot be transformed with the calcium phosphate method due to initiation of terminal differentiation in the presence of calcium.

The mechanism of action of laser-mediated DNA transfer is not yet completely understood; the suggested cell-surface perforation by the laser with DNA entry into the cell followed by rapid self-sealing of the hole can only be hypothesized at this time. Determination of the structural and physiological nature of this interaction requires further investigation.

This work is supported by National Institutes of Health Grants RR 01192, CA 32248, and CA 19401 and by grants from the Council for Tobacco Research–U.S.A. and the Office of Naval Research (86 K-015).

1. Graham, F. L. & Van der Eb, A. J. (1973) *Virology* **52**, 457–467.
2. Wigler, F. L., Silverstein, S., Lee, L. S., Pellicer, A., Chen, Y. C. & Axel, R. (1977) *Cell* **11**, 223–232.
3. Wold, B., Wigler, M., Lacy, E., Maniatis, T., Silverstein, S. & Axel, R. (1979) *Proc. Natl. Acad. Sci. USA* **76**, 5687–5689.
4. Cappechi, M. R. (1980) *Cell* **22**, 479–488.
5. Palmiter, R. D., Brinster, R. L., Hammer, R. E., Trumbauer, M. E., Rosenfeld, M. G., Birnberg, N. C. & Evans, R. M. (1982) *Nature (London)* **300**, 611–615.
6. Graessmann, M. & Graessman, A. (1976) *Proc. Natl. Acad. Sci. USA* **73**, 366–370.
7. Perucho, M., Hanahan, D. & Wigler, M. (1980) *Cell* **22**, 309–317.
8. Steinbiss, H., Stabel, R., Topfer, R., Hirtz, R. D. & Schell, J. (1985) in *Experimental Manipulation of Ovule Tissue*, eds. Chapman, G. P., Mantell, S. H. & Daniels, R. W. (Longman, London), pp. 64–75.
9. Griesbach, R. (1985) *Bio/Techniques* **3**, 348–350.
10. Berns, M. W., Aist, J., Edwards, J., Strahs, K., Girton, J., Kitzes, M., Hammer-Wilson, M., Liaw, L.-H., Siemens, A., Koonce, M., Peterson, S., Brenner, S., Burt, J., Walter, R., Bryant, P. J., Van Dyk, D., Coulombe, J., Cahill, T. & Berns, G. S. (1981) *Science* **213**, 505–513.
11. Berns, M. W. (1974) *Science* **186**, 700–705.
12. Berns, M. W., Chong, L. K., Hammer-Wilson, M., Miller, K. & Siemens, A. (1979) *Chromosoma* **73**, 1–8.
13. Peterson, S. P. & Berns, M. W. (1978) *J. Cell Sci.* **34**, 289–301.
14. Kitzes, M., Twiggs, G. & Berns, M. W. (1977) *J. Cell Biol.* **72**, 368–379.
15. Tao, W. & Berns, M. W. (1986) *Am. Soc. Laser Med. Surg.* **6**, 168–169 (abstr.).
16. Tsukakoshi, M., Kurata, S., Nomiya, Y., Ikawa, Y. & Kasuya, T. (1984) *Appl. Phys. B* **35**, 135–140.
17. Croce, C. M. (1976) *Proc. Natl. Acad. Sci. USA* **73**, 3248–3252.
18. Rasheed, S., Nelson, W. A., Toth, E. M., Arnstein, P. & Gardner, M. B. (1974) *Cancer* **33**, 1027–1033.
19. Littlefield, J. (1966) *Exp. Cell Res.* **41**, 190–196.
20. Southern, P. J. & Berg, P. (1982) *J. Mol. Appl. Genet.* **1**, 327–341.
21. Walter, R. J. & Berns, M. W. (1981) *Proc. Natl. Acad. Sci. USA* **78**, 6927–6931.
22. Southern, E. M. (1975) *J. Mol. Biol.* **98**, 503–517.
23. Feinberg, A. P. & Vogelstein, B. (1983) *Anal. Biochem.* **132**, 6–13.
24. Feinberg, A. P. & Vogelstein, B. (1984) *Anal. Biochem.* **137**, Addendum, 266–267.
25. Saxon, P. J., Srivatsan, E., Leipzig, G. V., Sameshima, J. H. & Stanbridge, E. J. (1985) *Mol. Cell. Biol.* **5**, 140–146.
26. Friend, K. K., Chen, S. & Ruddle, F. H. (1976) *Somatic Cell Genet.* **2**, 183–188.
27. Klobutcher, L. A., Miller, C. L. & Ruddle, F. H. (1980) *Proc. Natl. Acad. Sci. USA* **77**, 3610–3614.
28. Potrykus, I., Saul, M. W., Petruska, J., Paszkowski, J. & Shillito, R. D. (1985) *Mol. Gen. Genet.* **199**, 183–188.
29. Hain, R., Stabel, P., Czernilofsky, A. P., Steinbiss, H. H., Herrera-Estrella, L. & Schell, J. (1985) *Mol. Gen. Genet.* **199**, 166–168.
30. Lorz, H., Baker, B. & Schell, J. (1985) *Mol. Gen. Genet.* **199**, 178–182.
31. Schell, J. & Montagu, M. V. (1983) *Bio/Technology* **1**, 175–180.
32. Schoffl, F. & Baumann, G. (1985) *EMBO J.* **4**, 1119–1124.
33. Zambrgski, P., Joos, H., Genetello, C., Leemans, J., Montagu, M. V. & Schell, J. (1983) *EMBO J.* **2**, 2134–2150.

[CANCER RESEARCH 47, 1027–1030, February 15, 1987]

Biological Studies on the Main Fractions of Hematoporphyrin Derivative[1]

J. Stuart Nelson and Michael W. Berns

Beckman Laser Institute and Medical Clinic, University of California, Irvine, Irvine, California 92717

ABSTRACT

The four main fractions of hematoporphyrin derivative were separated by high-pressure liquid chromatography. Each fraction was studied with respect to photosensitizing capabilities, fluorescence, and tumor tissue uptake in mice bearing EMT-6 tumors.

Animals received i.p. injections of 10 mg/kg of each fraction, and 24 h later tumors either were treated with 100 J/cm² of light (630 nm) to evaluate photosensitizing capabilities, or the animals were sacrificed and tumors removed for fluorescence and fraction uptake determination.

The results indicate that the fraction responsible for photosensitization has the highest tumor tissue uptake and retention. Furthermore, this fraction demonstrates the highest overall fluorescence localization in neoplastic tissue. The other poorly photosensitizing fractions have a lower overall fluorescence *in vivo* due to their poor tumor tissue localization.

INTRODUCTION

Due to their selective retention in tumors and their efficiency as photosensitizers, porphyrins are being evaluated by numerous groups for their effectiveness in the diagnosis and treatment of cancer (1–4). Recent work with HpD[2] has shown great promise in treating a wide variety of animal and human tumors with little damage to the adjacent normal tissues and host. This high therapeutic ratio and relative lack of morbidity of HpD-PDT have made this form of therapy very attractive.

HpD, whose tumor localizing properties were first described by Lipson (5) over 20 yr ago, is defined as the product resulting from the alkaline hydrolysis of a mixture of hematoporphyrin acetates (6). After the i.v. administration of labeled HpD, there is a gradual accumulation of radioactivity in tumor tissue (7). Although the mechanism of HpD's preferential retention is uncertain, it is known that soon after injection HpD localizes in most normal tissues. What is clear is that the total time the HpD is being retained in the malignant tissue is much longer than in the nonmalignant tissue from which it is generally cleared between 24 and 48 h (8). The recent development of instrumentation for exploring the localization of porphyrins in malignant tissues has provided the incentive for continued research into porphyrin photochemistry.

Singlet oxygen ($^1O_2$), the metastable excited state of triplet molecular oxygen, has been identified as the cytotoxic agent that is probably responsible for the photodynamic destruction of malignant cells exposed to light of the appropriate wavelength and intensity (9). This short-lived highly reactive molecule subsequently catalyzes the destruction of numerous cellular loci including mitochondria (10), microsomes (11), lysosomes (12), and transport and permeability factors associated with the cell membrane (13).

HpD is a complex mixture of porphyrins, and it is not always clear which of the components are responsible for cellular photosensitization *in vitro* or *in vivo*. Several investigators have attempted to determine which of these components is active with respect to fluorescence, photosensitization, and tumor localization using thin-layer chromatography (14), high-pressure liquid chromatography (15–19), and reverse-phase chromatography (20). Attempts to ascertain which of the porphyrins is active have been frustrated by difficulty in determining the relative purity of the various fractions. Even with apparently pure preparations of the individual HpD components, impurities have often complicated the interpretation of data.

In the present study, we have studied the four major fractions of HpD with respect to photosensitizing ability, fluorescence, and porphyrin localization in tumors of BALB/c mice bearing EMT-6 tumor. These comparisons were performed in order to further clarify which of the fractions are responsible for fluorescence as well as those responsible for sensitization and localization *in vivo*. An analysis of the individual chemical species was not carried out because they were too numerous and present in too low concentrations to make such analysis possible with our equipment.

MATERIALS AND METHODS

Hematoporphyrin Derivative. Photofrin II was obtained from Photofrin, Inc., Cheektowaga, NY, as an aqueous solution at a concentration of 2.5 mg/ml and stored in the dark at −70°C until used. For *in vivo* experiments, Photofrin II was diluted 1:4 with 0.9% NaCl solution and injected i.p.

HPLC. Analytical HPLC studies were carried out with a Beckman 324 gradient liquid chromatography system using a Beckman Ultrasphere Octyl C_8 column (5-μm particle size, 4.6 × 150-mm column dimension). The column was eluted at a constant flow rate of 2.5 ml/min. Photofrin II was applied directly to the column by injecting 2 ml at a concentration of 2.5 mg/ml for each run. The porphyrins were then eluted with a linear gradient application of 30% methanol:70% water, 30% methanol:70% isopropyl alcohol for 200 min. The column was then eluted with a linear gradient application of 30% methanol:70% isopropyl alcohol and 100% isopropyl alcohol for an additional 40 min. The four principle fractions were all separated on the column within 4 h. The fractions were collected at the following time intervals: Fraction I, 60 to 80 min; Fraction II, 95 to 110 min; Fraction III, 125 to 210 min; and Fraction IV, 210 to 240 min. Each band was collected, and the solvent was removed with a rotary evaporator and freeze dried. To determine the concentration, each fraction was dissolved in 0.1 N NaOH for 1 h at room temperature, and its absorbance was measured at 400 nm in comparison to a known concentration of Photofrin II. After the concentration was calculated, proper dilution was carried out with saline to obtain a final concentration of 2.5 mg/ml used for *in vivo* studies.

Animal and Tumor System. All mice were 14 to 16 wk old and weighed between 30 and 35 g at the time of treatment. The following tumor system was used: a EMT-6 (experimental mammary tumor) undifferentiated sarcoma obtained from the Frederick Cancer Institute, Frederick, MD, arising in the flank of a BALB/c mouse (21). Tumors were harvested fresh from mice and minced using fine scissors. Transplanted tumors were initiated intradermally in the right flank of each mouse by injecting 0.1 ml of fresh tumor inoculum prepared with a concentration of 5×10^5 viable tumor cells/ml suspended in RPMI (GIBCO, Grand Island, NY). Cell viability was assessed by the ability to resist cell lysis and exclude trypan blue dye (GIBCO). The mouse tumors were generally palpable at 5 days and reached a size of 5 to 7

Received 8/25/86; revised 11/4/86; accepted 11/6/86.

The costs of publication of this article were defrayed in part by the payment of page charges. This article must therefore be hereby marked *advertisement* in accordance with 18 U.S.C. Section 1734 solely to indicate this fact.

[1] This research was supported by NIH Grants RR 01192 and CA 32248.

[2] The abbreviations used are: HpD, hematoporphyrin derivative; HPLC, high-pressure liquid chromatography; PDT, photodynamic therapy; Hp, hematoporphyrin; HVD, 2(4)-hydroxyethyl-4(2)-vinyldeuteroporphyrin; DVFM, digital video fluorescence microscopy; DHE, dihematoporphyrin ether.

plasmid DNA from the medium. The transferred *neo* gene was incorporated into host chromosomes and expressed. Most of the transformants that have been examined appear to contain the nonrearranged introduced *neo* gene and have a low plasmid copy number, generally one to two copies per cell. Transformant 3 is exceptional in that restrictions with either *Eco*RI or *Xba* I produce two bands and the sizes of the fragments produced by digestion with *Xba* I are substantially smaller than that of pSV2-neo plasmid (5.7 kilobase pairs in size). Rearrangement or deletions of the introduced DNA molecules may explain this result. The majority of the transformants is shown to stably maintain the transferred phenotype for at least 42 days without selective pressure. This method is nearly 100-fold more efficient than the standard calcium phosphate technique. Even though the transformation frequency ($0.8–3 \times 10^{-3}$) is comparable with that of microinjection, the laser method has the advantage of simplicity of operation. At present, the gene transfer experiments have been conducted with the ultrasophisticated laser system described; however, this by no means implies that this hardware is absolutely necessary for transformation. A more simplistic type of laser interfaced with a standard microscope and TV system will be expected to allow one to perform gene transfer experiments using this method. Thus, when compared to the microinjection technique, the number of cells treated in a given time by an "unskilled" operator will be much greater. In addition, the actual transformation frequency achieved using this method may be higher than 3×10^{-3} since there is no evidence indicated that we have reached the optimum transformation frequency. Many factors need to be examined that could affect the transformation frequency, such as cell viability after laser treatment and the percentage of successful cell-surface "perforations." Furthermore, it is likely that laser beam intensity and wavelength can be readily modulated to achieve the optimum frequency for transformation and to accommodate various cell types, such as plant cells whose walls cannot be easily penetrated by the microinjection capillary pipette.

Although the experiments presented here have been carried out with HT1080-6TG cells, theoretically there is no reason to expect that this system should not work with other given cell types, animal or plant. This method could be of considerable value in genetic engineering, especially in plants. Direct gene transfer to isolated protoplasts using the calcium phosphate method has been reported to be a successful method in many cases (28–30); however, it requires protoplasts, and the regeneration of whole plants from isolated protoplasts is still a severe problem for many monocots. Transformation experiments with the Ti plasmid of *Agrobacterium tumefaciens* (31–33) are restricted to dicots due to the natural host range of *A. tumefaciens*. Taken together, new techniques for plant transformation are absolutely needed. The laser method might be a candidate since it does not require protoplasts and circumvents the problem of host range. Furthermore, it might be possible to facilitate gene transfer directly into pollen. Another application of this method might be its use in transforming cell types that are too fragile or sensitive to chemical techniques, such as the keratinocytes. These cells cannot be transformed with the calcium phosphate method due to initiation of terminal differentiation in the presence of calcium.

The mechanism of action of laser-mediated DNA transfer is not yet completely understood; the suggested cell-surface perforation by the laser with DNA entry into the cell followed by rapid self-sealing of the hole can only be hypothesized at this time. Determination of the structural and physiological nature of this interaction requires further investigation.

This work is supported by National Institutes of Health Grants RR 01192, CA 32248, and CA 19401 and by grants from the Council for Tobacco Research–U.S.A. and the Office of Naval Research (86 K-015).

1. Graham, F. L. & Van der Eb, A. J. (1973) *Virology* **52**, 457–467.
2. Wigler, F. L., Silverstein, S., Lee, L. S., Pellicer, A., Chen, Y. C. & Axel, R. (1977) *Cell* **11**, 223–232.
3. Wold, B., Wigler, M., Lacy, E., Maniatis, T., Silverstein, S. & Axel, R. (1979) *Proc. Natl. Acad. Sci. USA* **76**, 5684–5689.
4. Cappechi, M. R. (1980) *Cell* **22**, 479–488.
5. Palmiter, R. D., Brinster, R. L., Hammer, R. E., Trumbauer, M. E., Rosenfeld, M. G., Birnberg, N. C. & Evans, R. M. (1982) *Nature (London)* **300**, 611–615.
6. Graessmann, M. & Graessman, A. (1976) *Proc. Natl. Acad. Sci. USA* **73**, 366–370.
7. Perucho, M., Hanahan, D. & Wigler, M. (1980) *Cell* **22**, 309–317.
8. Steinbiss, H., Stabel, R., Topfer, R., Hirtz, R. D. & Schell, J. (1985) in *Experimental Manipulation of Ovule Tissue*, eds. Chapman, G. P., Mantell, S. H. & Daniels, R. W. (Longman, London), pp. 64–75.
9. Griesbach, R. (1985) *Bio/Techniques* **3**, 348–350.
10. Berns, M. W., Aist, J., Edwards, J., Strahs, K., Girton, J., Kitzes, M., Hammer-Wilson, M., Liaw, L.-H., Siemens, A., Koonce, M., Peterson, S., Brenner, S., Burt, J., Walter, R., Bryant, P. J., Van Dyk, D., Coulombe, J., Cahill, T. & Berns, G. S. (1981) *Science* **213**, 505–513.
11. Berns, M. W. (1974) *Science* **186**, 700–705.
12. Berns, M. W., Chong, L. K., Hammer-Wilson, M., Miller, K. & Siemens, A. (1979) *Chromosoma* **73**, 1–8.
13. Peterson, S. P. & Berns, M. W. (1978) *J. Cell Sci.* **34**, 289–301.
14. Kitzes, M., Twiggs, G. & Berns, M. W. (1977) *J. Cell Biol.* **72**, 368–379.
15. Tao, W. & Berns, M. W. (1986) *Am. Soc. Laser Med. Surg.* **6**, 168–169 (abstr.).
16. Tsukakoshi, M., Kurata, S., Nomiya, Y., Ikawa, Y. & Kasuya, T. (1984) *Appl. Phys. B* **35**, 135–140.
17. Croce, C. M. (1976) *Proc. Natl. Acad. Sci. USA* **73**, 3248–3252.
18. Rasheed, S., Nelson, W. A., Toth, E. M., Arnstein, P. & Gardner, M. B. (1974) *Cancer* **33**, 1027–1033.
19. Littlefield, J. (1966) *Exp. Cell Res.* **41**, 190–196.
20. Southern, P. J. & Berg, P. (1982) *J. Mol. Appl. Genet.* **1**, 327–341.
21. Walter, R. J. & Berns, M. W. (1981) *Proc. Natl. Acad. Sci. USA* **78**, 6927–6931.
22. Southern, E. M. (1975) *J. Mol. Biol.* **98**, 503–517.
23. Feinberg, A. P. & Vogelstein, B. (1983) *Anal. Biochem.* **132**, 6–13.
24. Feinberg, A. P. & Vogelstein, B. (1984) *Anal. Biochem.* **137**, Addendum, 266–267.
25. Saxon, P. J., Srivatsan, E., Leipzig, G. V., Sameshima, J. H. & Stanbridge, E. J. (1985) *Mol. Cell. Biol.* **5**, 140–146.
26. Friend, K. K., Chen, S. & Ruddle, F. H. (1976) *Somatic Cell Genet.* **2**, 183–188.
27. Klobutcher, L. A., Miller, C. L. & Ruddle, F. H. (1980) *Proc. Natl. Acad. Sci. USA* **77**, 3610–3614.
28. Potrykus, I., Saul, M. W., Petruska, J., Paszkowski, J. & Shillito, R. D. (1985) *Mol. Gen. Genet.* **199**, 183–188.
29. Hain, R., Stabel, P., Czernilofsky, A. P., Steinbiß, H. H., Herrera-Estrella, L. & Schell, J. (1985) *Mol. Gen. Genet.* **199**, 166–168.
30. Lorz, H., Baker, B. & Schell, J. (1985) *Mol. Gen. Genet.* **199**, 178–182.
31. Schell, J. & Montagu, M. V. (1983) *Bio/Technology* **1**, 175–180.
32. Schoffl, F. & Baumann, G. (1985) *EMBO J.* **4**, 1119–1124.
33. Zambrgski, P., Joos, H., Genetello, C., Leemans, J., Montagu, M. V. & Schell, J. (1983) *EMBO J.* **2**, 2134–2150.

of 10 mg/kg of each fraction, and the total fluorescence was measured by computer-enhanced DVFM. Relative to tumor-bearing non-HpD control animals, the increase in total tumor tissue fluorescence was 2.12 and 2.26 times control for Fractions I and II, respectively. Animals that received Fractions III and IV had a total tumor fluorescence of 3.42 and 2.58 times control (Table 1).

Tumor Localization and Uptake. Animals were sacrificed at 24 h postinjection of 10 mg/kg of each fraction, and the porphyrins were extracted, expressed in terms of μg of porphyrin per g of tumor (wet weight), and compared in terms of their increase over control non-HpD tumors. Control animals had an average of 1.02 μg of porphyrin/g of tumor. Animals that received Fractions I and II had an average of 1.68 and 1.54 μg of porphyrin, respectively, or 1.65 and 1.51 times control animals. Animals that received Fraction III and Fraction IV had an average of 7.07 and 3.60 μg of porphyrin, respectively, or 6.93 and 3.51 times control animals (Table 2).

DISCUSSION

Photofrin II, the commercially available "enriched" fraction of HpD, was separated into four main fractions by HPLC. Our HPLC chromatographic analysis of Photofrin II agrees with the previously published work of others (24–27). Furthermore, our photosensitization studies document that the fraction responsible for photochemistry lies in the broad band containing protoporphyrin (Fraction III) also in agreement with the work of previous investigators. The exact chemical structure of this photosensitizing fraction is still under considerable debate at the present time. Studies by Dougherty *et al.* (28) in 1983 with fast atom bombardment, mass spectrometry, and nuclear magnetic resonance spectra led to the conclusion that the active ingredient was most likely a structural isomer of DHE. Kessel (29) has recently reported on a series of hydrolysis experiments conducted in solvents inhibiting porphyrin aggregation, and he found the hydrolysis pattern to be most consistent with the presence of a diporphyrin ester structure.

Table 1 *Total tumor fluorescence using computer-enhanced DVFM*

Component	Mean absolute fluorescence (pixels)[a]	Av.	Increase from control (times)
Control (non-HpD)	2367, 2459	2354	1.0
	2280, 2313		
	2357, 2347		
	2325, 2345		
	2347, 2401		
Fraction I	5053, 5042	4996	2.12
	4779, 5377		
	4904, 4956		
	4953, 5011		
	4953, 4932		
Fraction II	5356, 5380	5312	2.26
	5304, 5242		
	5311, 5368		
	5255, 5256		
	5347, 5300		
Fraction III	8067, 8059	8065	3.42
	8080, 8113		
	8057, 8047		
	8025, 8045		
	8068, 8092		
Fraction IV	6160, 6110	6076	2.58
	6104, 6042		
	6053, 6050		
	6068, 6068		
	6063, 6050		

[a] The image is divided into small regions called picture elements or pixels for short. At each pixel location, the image brightness is sampled and quantized. This step generates an integer value or Gy level at each pixel representing the brightness or darkness of the image at that point. The computer divides the image into 256 different Gy levels from which a threshold value is chosen. All brightness above the threshold Gy level is counted by the computer.

Table 2 *Tumor localization and uptake of the individual fractions*

Component	Uptake of porphyrin (μg/g tumor)	Av. porphyrin (μg/g tumor)	Increase from control (times)
Control (non-HpD)	1.05	1.02	1.0
	1.02		
	0.98		
	1.07		
	0.99		
Fraction I	1.64	1.68	1.65
	1.73		
	1.92		
	1.55		
	1.57		
Fraction II	1.31	1.54	1.51
	1.54		
	1.56		
	1.66		
	1.62		
Fraction III	7.19	7.07	6.93
	6.93		
	7.14		
	7.07		
	7.02		
Fraction IV	3.64	3.60	3.51
	3.57		
	3.33		
	3.64		
	3.74		

Using the methodology described by Kessel (23), we found that the total porphyrin accumulation by EMT-6 tumors 24 h after injection of Fraction III, as described above, to be on the average approximately 7.07 μg of porphyrin per g of tumor tissue. This is an approximate 7-fold increase from control animals. This would seem to confirm this fraction as being the major tumor localizing fraction of HpD. Our study shows that the relative efficiencies of the individual fractions in sensitizing tumors to photoinactivation follow the same pattern as tumor uptake and retention. It is important to optimize localization as well as sensitizing effect, and it therefore appears necessary that these two quantities should be studied independently. Other investigators have reported that the uptake of the HpD components increased with decreasing polarity (13, 24). The excellent tumor uptake of the more hydrophobic Fraction III shown in our study is consistent with these observations. Another factor which has been shown to be of importance for the cellular uptake and photosensitizing properties of porphyrin is their tendency to dimerize and aggregate in aqueous solutions. This tendency to aggregate has also been shown by other investigators to increase with decreasing polarity (15, 30). Thus we conclude that the photosensitizing effect of HpD is primarily due to this fraction.

The relative fluorescence yield of the individual fractions is shown in Table 1. Data shown in Table 1 indicate that Fraction III results in the greatest overall tumor fluorescence *in vivo* (approximately 3.42 times control animals). This is interesting in light of the fact that other investigators have shown the predominant fluorescent species *in vitro* (15) to correspond with Hp and HVD. Kessel and Cheng (31) examined the HpD fraction containing DHE and reported that this material had the lowest quantum fluorescent yield of all HpD components

Best Available Copy

mm at 10 to 14 days, at which time treatment was started. At this size, the small tumor was homogeneously white, and spontaneous tumor necrosis was minimal or absent.

Procedure for Photosensitization Studies. When tumors were of the appropriate size (as indicated above), the animals were shaved in the tumor area and given i.p. injections of the individual fractions in doses equal to 10 mg/kg of body weight. The remainder of the experiment was done in the dark, including housing of the animals. Control tumor-bearing animals were those that received light without porphyrin and porphyrin without light. Twenty-four h postinjection of material, the experimental animals were treated with the laser light delivery system (see below). The mouse was anesthetized with ketamine hydrochloride (Parke-Davis) and covered with a metal shield with a circular hole exposing the tumor. Animals were sacrificed 24 h after photodynamic therapy by halothane (Halocarbon Laboratories, Inc., Hackensack, NJ) anesthesia. Tissue was excised immediately and fixed in 3% glutaraldehyde:5% formalin in phosphate buffer, pH 7.4. Samples were then dehydrated in graded alcohols, cleared in xylene, and embedded in paraffin. Six-μm sections were cut, stained with hematoxylin:eosin, cleared of paraffin in xylene, and dried. Sections were examined with an Axiomat microscope (Zeiss) and photographed with Panatomic X film (Eastman Kodak).

Laser Light Delivery System. Laser irradiations were performed with a Coherent (Palo Alto, CA) Innova 20 argon ion laser stimulating a Coherent PRT-95 dye laser. The dye laser was tuned to emit radiation at 630 nm. The wavelength was verified using a Jobin Yvon No. 5/354 UV monochromator (Longjuneau, France). The radiation was then coupled into a 400-μm fused silica fiber optic using a Spectra-Physics (Mountain View, CA) Model 316 fiber optic coupler. The output end of the fiber was terminated with a microlens that focused the laser radiation into a circular field of uniform light intensity. Laser irradiation emanating from the fiber was monitored with a Coherent Model 210 power meter before and after treatment.

Mice were placed underneath an aperture that controlled the area of light illumination on the tumor site. The area of illumination was 1 cm^2. Total light dose was 100 J/cm^2 with a power density of 150 milliwatts/cm^2. The intensity of light on the tumor surface was calculated by measuring the intensity of the light emitted from the laser and dividing this number by the area treated in cm^2. The total light dose was calculated as intensity in W/cm^2 multiplied by the treatment time in s and expressed in J/cm^2.

Fluorescence Studies. Animals destined for fluorescence studies were sacrificed 24 h postinjection of 10 mg/kg of the individual fractions. Tumors were excised, immediately embedded in Tissue Tek II (Miles Laboratories, Inc., Naperville, ILL), and frozen at −70°C. Six-μm sections were cut on a cryostat, placed on acid-cleaned slides, and stored at −70°C until fluorescence microscopy was performed.

Fluorescence Microscopy. Frozen histological sections of tumor were viewed and recorded using epifluorescence. Light from a 100-W mercury lamp was filtered through a G 546 band pass (530 to 570 nm) exciter filter (Zeiss) and directed to the tissue by a chromatic beam splitter. The fluorescence was filtered through a LP-590 long pass barrier filter and then directed to a low light level video camera, Venus Scientific No. TV2M (Zeiss). The video signal was recorded on video tape by a GYYR DAS-MkII video tape recorder.

Image Processing. The image processing system used to analyze the fluorescence recorded above has been described earlier (22). The signal from the video tape recorder in playback mode was fed into an image array processor with synchronization between the two units provided by a time base corrector. A LSI-11/23 minicomputer was used to control the image processor.

The video signal was acquired by the image processor under control of software loaded in the computer. Thirty-two frames were acquired from each video scene and then averaged to give an increase in the signal:noise ratio. This acquired image was used by the computer for measurement of the average Gy level (corresponding to fluorescence) within a zone defined by a cursor on the image display monitor. Measurements were made in all areas of the tumor tissue. Generally, the tumor was arbitrarily divided into 4 equal areas, and within each area 10 measurements were made. The average of the 40 measurements is presented in the tables. Tumors from 50 animals were examined: 10 animals received each of the individual 4 fractions, and 10 animals were used as controls.

Localization and Uptake Studies. Animals destined for localization and uptake studies were sacrificed 24 h postinjection of 10 mg/kg of individual fractions. Tumors were excised and immediately frozen at −70°C until extraction procedures were performed. The extraction procedure used has been previously well described by Kessel (23). Briefly, tumor tissue was quickly thawed and weighed (approximately 300- to 600-mg wet weight). Extractions were carried out by disrupting tumor tissue in 2.5 ml of sodium phosphate buffer (pH 3.5) using a glass homogenizer. The homogenate was shaken for 5 min at 22°C with 2.5 volumes of methanol:chloroform (1:1) and subsequently centrifuged (1000 × *g*, 10 min, room temperature). The lower fluorescent phase was removed and evaporated under nitrogen, the residue was taken up in 100 μl of methanol, and insoluble materials were removed by brief centrifugation (12,000 × *g*, 30 s, room temperature). Porphyrin uptake was estimated from the absorbance of a 2-ml aliquot of the methanol extract scanned from 350 to 650 nm using a Beckman DU-7 spectrophotometer. The concentration of each fraction was determined by comparing its absorbance at 400 nm with a known concentration of Photofrin II (20). Absorption spectra were obtained in solution for each fraction which showed a broad peak of maximal absorption between 380 and 420 nm. Values listed in Table 2 are expressed in terms of μg of porphyrin per g of tumor tissue (wet weight).

RESULTS

Our HPLC analysis (Fig. 1) shows that HpD (Photofrin II) contains the same main fractions reported by other investigators (24–27). Fraction I is obviously Hp based on its location on the chromatogram. Fraction II is composed of the isomers of HVD. Fraction III contains a large number of components (Moan has previously reported in Ref. 17) including protoporphyrin. Fraction IV contains all components eluted after Fraction III. Reanalysis of Fraction IV results in a chromatogram almost identical to that of Photofrin II and probably includes small amounts of all the previous fractions strongly bound to the column.

Photosensitizing Efficiency. Inspection of the tumors 24 h post-PDT revealed no evidence of necrosis in control animals which received 100 J/cm^2 of light. In those animals that received either Fraction I or II, gross inspection of the tumors revealed no visual evidence of necrosis and only minimal superficial necrosis at the surface of the tumor upon histological examination. In contrast, those animals that received Fraction III had 100% destruction of their tumor. Histologically, these tumors were completely hemorrhagic with all tumor cells destroyed. Those tumors that received Fraction IV demonstrated hemorrhagic and coagulation necrosis in over 75% of the tumor.

Fluorescence. Animals were sacrificed at 24 h postinjection

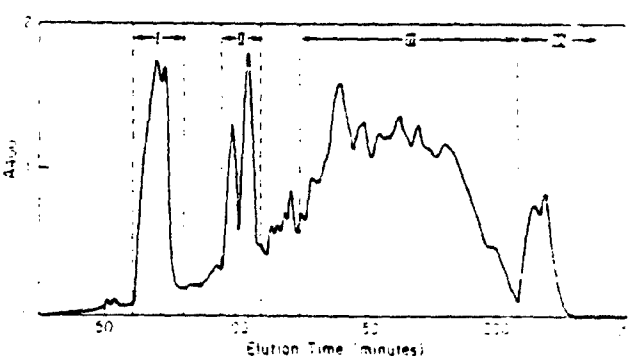

Fig. 1. HPLC elution profile of Photofrin II on a C_4 column. Absorbance at 400 nm was monitored.

Our experiments show that Fractions I and II which correspond to Hp and HVD are more fluorescent when one considers their fluorescence in terms of μg of porphyrin taken up in the tumor. Our data show that these fractions are able to more than double the total tumor fluorescence with only minor increases in tumor uptake (1.65 and 1.51 times control for Fractions I and II). It would appear that the reason for Fractions I and II resulting in such poor overall fluorescence in tumors is due to the poor uptake and retention of these fractions *in vivo*.

Use of Fraction III results in an increase in tumor fluorescence 3.42 times control desite the fact that the total porphyrin content of the tumor increases almost 7 times the control. We are thus left with the question of how a poorly fluorescent porphyrin results in the greatest overall tumor fluorescence. Kessel (23) has recently proposed a sequence of events which appears to answer this question. He suggested that the administration of HpD *in vivo* leads to the accumulation at the tumor loci of the DHE (Fraction III). Subsequently, gradual intracellular hydrolysis yields the highly fluorescent Hp and HVD components which are responsible for the overall tumor fluorescence. These conclusions were based on an experiment where Kessel (23) injected pure DHE into mice and subsequently used the extraction procedure described above and found the resulting HPLC analysis to include large amounts of the highly fluorescent Hp and HVD isomers. An almost identical HPLC profile was obtained when HpD was administered. Dougherty (6) has also described experiments in which Hp and HVD were found in neoplastic tissue even though these components are not tumor localizers. He also concluded that these fractions must therefore result from the degradation of the tumor-localizing component of HpD, which is by itself in the unhydrolyzed form, a poorly fluorescent porphyrin. It is clear that the hematoporphyrin derivtive is a complex mixture of porphyrins, and models which treat this material as a single compound are incomplete.

ACKNOWLEDGMENTS

We thank William Wright and Jeffrey Andrews for technical assistance and Dr. Chung-Ho Sun and John Mellot for their assistance in the preparation of the fractions.

REFERENCES

1. Wile, A. W., Dahlman, A., Burns, R. G., and Berns, M. W. Laser photoradiation therapy of cancer following hematoporphyrin sensitization. Lasers Med. Surg., *2:* 163–168, 1982.
2. Dahlman, A., Wile, A. G., Burns, R. G., Mason, G. R., Johnson, F. M., and Berns, M. W. Laser photoradiation therapy of cancer. Cancer Res., *43:* 430–434, 1983.
3. Dougherty, T. J., Boyle, D. G., Weishaupt, K. R., Henderson, B. A., Potter, W. R., Bellnier, D. A., and Wityk, K. E. Photoradiation therapy—clinical and drug advances. *In*: D. Kessel and T. J. Dougherty (eds.), Porphyrin Photosensitization, pp. 3–13. New York, NY: Plenum Publishing Corp., 1983.
4. Hayata, Y., Kato, H., Konaka, C., Onom, J., and Takizawa, N. Hematoporphyrin derivative and laser photoradiation in the treatment of lung cancer. Chest, *81:* 269–277, 1982.
5. Lipson, R., Baldes, E., and Olen, A. The use of a derivative of hematoporphyrin in tumor detection. J. Natl. Cancer Inst., *26:* 1–8, 1961.
6. Dougherty, T. J. Photodynamic therapy (PDT) of malignant tumors. Crit. Rev. Oncol. Hematol., *2:* 83–116, 1984.
7. Gomer, C. J., and Dougherty, T. J. Determination of [^{3}H]- and [^{14}C]hematoporphyrin derivative distribution in malignant and normal tissue. Cancer Res., *39:* 146–151, 1979.
8. Berns, M. W., Dahlman, A., Johnson, F., Burns, R., Sperling, D., Guiltinan, M., Siemens, A., Walter, R., Wright, W., Hammer-Wilson, M., and Wile, A. *In vitro* cellular effects of hematoporphyrin derivative. Cancer Res., *42:* 2325–2329, 1982.
9. Weishaupt, K. R., Gomer, C. L., and Dougherty, T. J. Identification of singlet oxygen and the cytotoxic agent in photoinactivation of a murine tumor. Cancer Res., *36:* 2316–2319, 1976.
10. Moan, J., Johnanssen, J. V., Christensen, I., Espevik, T., and McGhie, J. B. Porphyrin-sensitized photoinactivation of human cells *in vitro*. Am. J. Pathol., *109:* 184–192, 1982.
11. Bickers, D. R., Dixit, R., and Mukhtar, R. Hematoporphyrin photosensitization of epidermal microsomes results in destruction of cytochrome P-450 and decreased monooxygenase activities and heme content. Biochem. Biophys. Res. Commun., *108:* 1032–1039, 1982.
12. Torinuki, W., Miora, T., and Seiji, M. Lysosome destruction and lipoperoxide formation due to active oxygen generated from hematoporphyrin or UV radiation. Br. J. Dermatol., *102:* 17–27, 1980.
13. Kessel, D. Effects of photoactivated porphyrins at the cell surface of leukemia L1210 cells. Biochemistry, *16:* 3443–3449, 1976.
14. Berenbaum, M. C., Bonnett, R., and Scourides, P. A. *In vivo* biological activity of the components of haematoporphyrin derivative. Br. J. Cancer, *45:* 571–581, 1982.
15. Moan, J., and Sommer, S. Fluorescence and absorption properties of the components of hematoporphyrin derivative. Photochem. Photobiol., *3:* 93–103, 1981.
16. Evenson, J. F., Moan, J., Hindbar, A., and Sommer, S. Tissue distribution of ^{3}H-hematoporphyrin derivative and its main components. ^{67}Ga and ^{125}I-albumin in mice bearing Lewis lung carcinoma. *In*: D. R. Doiron and C. J. Gomer (eds.), Porphyrin Localization and Treatment of Tumors, pp. 541–562. New York, NY: Alan R. Liss, Inc., 1984.
17. Hilf, R., Leakey, P. B., Sollott, S. J., and Gibson, S. L. Photodynamic inactivation of R3230AC mammary carcinoma *in vitro* with hematoporphyrin derivative: effects of dose, time, and serum on uptake and phototoxicity. Photochem. Photobiol., *37:* 633–642, 1983.
18. Christensen, T., Moan, J., McGhie, J. B., Waksvik, H., and Stigum, H. Studies of HpD: chemical composition and *in vitro* photosensitization. *In*: D. Kessel and T. J. Dougherty (eds.), Porphyrin Photosensitization, pp. 63–76. New York, NY: Plenum Publishing Corp., 1983.
19. Swincer, A. G., Trenerry, V. C., and Ward, A. D. The analysis and some chemistry of haematoporphyrin derivative. *In*: D. R. Doiron and C. J. Gomer (eds.), Porphyrin Localization and Treatment of Tumors, pp. 285–300. New York, NY: Alan R. Liss, Inc., 1984.
20. Kessel, D., and Cheng, M. L. Biological and biophysical properties of the tumor localizing component of hematoporphyrin derivative. Cancer Res., *45:* 3053–3057, 1985.
21. Rockawell, S. C., and Kallman, R. F. Cellular radiosensitivity and tumor radition response in the EMT-6 tumor cell system. Radiat. Res., *53:* 281–294, 1973.
22. Walter, R. J., and Berns, M. W. Computer-enhanced video microscopy: digitally processed microscope images can be produced in real time. Proc. Natl. Acad. Sci. USA, *7:* 6927–6931, 1981.
23. Kessel, D. *In vivo* fluorescence of tumors after treatment with derivatives of hematoporphyrin. Photochem. Photobiol., *44:* 107–108, 1986.
24. Moan, J., Christensen, T., and Sommer, S. The main photosensitizing components of hematoporphyrin derivative. Cancer Lett., *15:* 161–166, 1982.
25. Evenson, J. F., Sommer, S., Moan, J., and Christensen, T. J. Tumor-localizing and photosensitizing properties of the main components of hematoporphyrin derivative. Cancer Res., *44:* 482–486, 1984.
26. Kessel, D., and Chou, T. C. Tumor-localizing components of the porphyrin preparation hematoporphyrin derivative. Cancer Res., *43:* 1994–1999, 1983.
27. Bennett, R., Ridge, R. J., and Scourides, P. A. On the nature of hematoporphyrin derivative. J. Chem. Soc. Perkin Trans., *1:* 3135–3140, 1981.
28. Dougherty, T. J. The structure of the active component of hematoporphyrin derivative. *In*: D. R. Doiron and C. J. Gomer (eds.), Porphyrin Localization and Treatment of Tumors, pp. 75–87. New York, NY: Alan R. Liss, Inc. 1984.
29. Kessel, D., Chang, C. K., and Musselman, B. Structure of the tumor localizing derivative of hematoporphyrins. *In*: D. Kessel, (ed.), Methods in Porphyrin Photosensitization, pp. 213–227. New York, NY: Plenum Publishing Corp., 1986.
30. White, W. I. Aggregation of porphyrins and metalloporphyrins. *In*: D. Dolphin (ed.), The Porphyrins, pp. 303–308. New York, NY: Elsevier Scientific Publishing Corp., Inc., 1978.
31. Kessel, D., and Cheng, M. L. On the preparation and properties of dihematoporphyrin ether, the tumor-localizing component of HpD. Photochem. Photobiol., *41:* 277–282, 1985.

Photochemistry and Photobiology Vol. 46, No. 1, pp. 77–82, 1987
Printed in Great Britain All rights reserved

0031-8655/87 $03.00+0.00
Copyright © 1987 Pergamon Journals Ltd

PHOTOSENSITIZERS IN DERMATOLOGY*

JERRY L. MCCULLOUGH[1]†, GERALD D. WEINSTEIN[1], JANET L. DOUGLAS[1] and MICHAEL W. BERNS[2]

Departments of [1]Dermatology and [2]Surgery, University of California, Irvine, Irvine, CA 92717, USA

(*Received* 16 *September* 1986; *accepted* 2 *December* 1986)

Abstract—Systemic injection of hematoporphyrin derivative (HpD) in combination with visible light (red or blue–green) delivered by laser was used to treat a patient with psoriasis. The psoriatic lesions responded vigorously to laser treatments, forming eschars by 1 week post irradiation. In contrast, only minimal erythema was observed in the noninvolved, clinically normal appearing skin. Two approaches for localized HpD administration were investigated in the guinea-pig and minipig models as a means of achieving local photodynamic effects. Intracutaneous injection of HpD produced localized cutaneous photosensitization with either UVA or red light. Azone increased percutaneous penetration of HpD in human skin *in vitro*. Topical application of HpD and irradiation with UVA produced localized cutaneous photosensitivity and inhibition of epidermal DNA synthesis.

INTRODUCTION

Photosensitizers have been used for centuries to enhance the therapeutic effects of light in treating skin disorders (Urbach *et al.*, 1976). As early as 1400 BC crude psoralen preparations derived from plants were used in combination with sunlight to restore skin pigmentation in vitiligo. With the development of artificial light sources, compounds which sensitize to UVB and UVA have come to play an important role in the phototherapy of skin diseases.

Recently there has been renewed interest in the photoactive porphyrins, particularly hematoporphyrin derivative (HpD),‡ in the treatment of a variety of human malignancies, including skin cancers (Dougherty, 1981; Tomio *et al.*, 1984; Tse *et al.*, 1984). In the present report we examine the selectivity of systemic HpD photosensitization in psoriatic skin and present basic studies to establish the rationale for local drug delivery to minimize the generalized photosensitivity of normal skin.

MATERIALS AND METHODS

Light delivery systems

Human studies. The blue–green light source was a 12-W argon ion laser (Spectra-Physics Model No. 171) emitting 6 W at 488, 514 nm. The red light source (630 nm) was a rhodamine B dye laser (Spectra-Physics Model No. 375) excited by the argon ion laser. The dye laser beam was focused into a 400-μm quartz fiber optic. The output from the fiber-optic tip was measured with a Scientech No. 354 colorimeter and the dye laser wavelength determined using a JY 5-354 monochrometer.

Animal studies. Two different light sources were used for irradiation. The UVA irradiation source was provided by a high-intensity UVA point source (National Biological Corp., Cleveland, OH) (peak emission level 360–365 nm) placed 3 cm from the skin surface. The light intensity measured by a LM301 light-meter (National Biological Corp., Cleveland, OH) was approximately 25 mW/cm² at the skin surface. Laser irradiation was performed with a Coherent (Palo Alto, CA) Innova 20 argon ion laser stimulating a Coherent 599-01 dye laser. The dye laser was tuned to emit radiation at 630 nm for HpD. The radiation was coupled to a 400-μm fused silica fiber optic using a Spectra-Physics (Mountain View, CA) Model 316 fiber-optic coupler. The output end of the fiber was terminated with a microlens which focused the laser radiation into a circular field of uniform light intensity of approximately 2-cm diameter. Laser irradiation from the fiber was monitored with a Coherent Model 210 power-meter before and after treatment.

Hematoporphyrin derivative (HpD)

Photofrin II (Photomedica, Raritan, NJ) was used in both human and animal studies.

Psoriasis photodynamic therapy (PDT)

A patient receiving PDT for a malignancy, and having psoriasis as a secondary malady, was injected intravenously with HpD at a dose of 3 mg/kg 72 h prior to laser irradiation. Four treatment sites of psoriasis and 4 sites of noninvolved clinically normal skin each approximately 2-cm diameter were irradiated with red and blue–green laser for 2–4 min with a power density of 159 mW/cm² (i.e. of 20 and 40 J/cm²). The patient returned to the outpatient clinic for follow-up examination at 24 h and at 1, 2, 4, and 8 weeks following laser exposure.

Animal PDT studies

Mature female albino guinea-pigs (Charles River Laboratories, Inc., N. Wilmington, MA) were housed under natural light and dark conditions until administration of photosensitizers, at which time they were placed in the dark. Neet, a commercial hair depilatory preparation (Whitehall Laboratories, Inc., New York, NY) was used

*Presented at a Symposium on Medical Applications of Photosensitizers, Annual Meeting of the American Society for Photobiology, 22–26 June 1986, Universal City (Los Angeles). Chairman, C. J. Gomer.

†To whom correspondence should be addressed.

‡Abbreviations: HpD, hematoporphyrin derivative; PDT, photodynamic therapy.

Best Available Copy

to depilate the backs of the guinea-pigs 24 h prior to drug administration.

To identify which of the porphyrin components of HpD confers photosensitivity to skin, we injected HpD (Photofrin II), hematoporphyrin (Dr. T. J. Dougherty, Roswell Park Memorial Institute, Buffalo, NY), protoporphyrin and hydroxyethylvinyldeuteroporphyrin (Porphyrin Products, Logan, UT) at increasing doses (5, 50, 500 μg) intracutaneously in guinea-pigs, followed by UVA (20 J/cm²) irradiation 6 h post drug treatment. Photosensitization as manifested by delayed erythema was graded at 24 h post irradiation using the following scale: 0: no reaction; 1+: minimal erythema with sharp borders; 2+: more pronounced, bright erythema without edema; 3+: marked erythema with edema; 4+: violaceous erythema with vesiculation.

Minipigs (Miles Laboratories, Inc., Shawnee, KS) were injected intradermally with 0.1 ml isotonic saline solution containing 0, 10, 25, or 50 μg HpD. During the light exposure animals were restrained and lightly anesthetized with xylazine and ketamine HCL (Parke-Davis, Morris Plains, NJ). Twenty-four h after HpD injection the injected sites were treated with UVA (20 J/cm²) or red laser (100 J/cm²) and erythema evaluated at different time intervals after irradiation using the scale above.

Autoradiographic studies

Autoradiographic techniques were used to study the effects of topical 1% HpD in 10% Azone [1-dodecylazacycloheptan-2-one (Nelson Research, Irvine, CA)] in combination with UVA irradiation on epidermal DNA synthesis in minipigs. Drug was applied to dorsal skin as a single application or applied every 12 h for a total of 3 or 5 applications. Six h after the last application, sites were irradiated with 20 J/cm² UVA. Skin biopsies were taken prior to irradiation to examine HpD fluorescence in cryostat sections. At 24, 48, and 72 h after UVA, treatment sites were injected with 0.1 ml methyl[³H]thymidine (25 Ci/mmol; Amersham, Arlington Heights, IL). One h after isotope administration, sites were biopsied with a 4-mm punch and prepared histologically for autoradiography (Weinstein, 1965), and exposed for 6 weeks. The labelling index was determined as a measure of epidermal DNA synthesis by counting the number of labeled basal cells per 1000 interfollicular basal cells. The autoradiographic results were expressed as per cent of control (saline-injected sites).

In vitro percutaneous penetration

The percutaneous penetration of HpD through excised full-thickness human cadaver skin was measured in Franz glass diffusion cells using the technique previously described (McCullough *et al.*, 1983). Hematoporphyrin derivative at a concentration of 1% in various concentrations of Azone was applied to the epidermal surface (3.5 cm²) of the skin. HpD percutaneous penetration into the lower saline-containing reservoir was quantitated by fluorometric analysis (McCullough *et al.*, 1983) and expressed as μg/h per cm². Cryostat sections of the full-thickness skin specimens removed from the diffusion chambers at the end of the study were examined for HpD red fluorescence.

RESULTS

Systemic HpD photosensitization in psoriasis

The cutaneous photosensitizing effects produced by irradiation with red and blue-green light were compared in a psoriatic patient who received HpD (3 mg/kg) given intravenously 72 h prior to irradiation. At 1 week post-laser (Fig. 1A) all of the psoriasis sites treated with red and blue-green light exhibited increased reddening, and tissue necrosis with eschar formation. In contrast, the clinically normal skin was relatively unaffected, with only the high dose (40 J/cm²) of the blue-green light producing a noticeable erythema (Fig. 1B). By 14 days the psoriatic sites had begun re epithelization around the central region, with extensive re-epithelization by 1 month. At 2 months all psoriatic lesions had healed normally.

Local HpD administration

Intracutaneous injection. Hematoporphyrin derivative and its various porphyrin components were injected intradermally in guinea-pigs to determine the minimum dose required to produce skin photosensitization when irradiated with UVA (Table 1). Hematoporphyrin derivative produced marked erythema and edema at the lowest dose of 5.0 μg. Hematoporphyrin produced only minimal erythema at 50.0 μg, with no effect at the 5.0-μg dose. The highest dose (500 μg) of protoporphyrin and hydroxyethylvinyldeuteroporphyrin did not produce cutaneous photosensitization. Likewise, control injections of saline and UVA irradiation did not cause cutaneous photosensitivity.

The swine model (Sambuco, 1985) was used to compare HpD cutaneous photosensitivity with UVA (20 J/cm²) and red light (630 nm laser) (100 J/cm²) (Fig. 2). Various doses of HpD or saline (control) were injected intradermally into different skin sites. Laser treatment of the HpD sites produced an immediate erythema (3+) response, in contrast to mild (1+) erythema with UVA. With both light sources the erythema response was dependent on HpD dose, and peaked at 48–72 h, with the maximum response (4+) obtained with laser. There was no photosensitivity in the saline-injected sites.

Topical delivery of HpD. Azone increased the penetration of 1% HpD through human skin *in vitro* (Fig. 3). Maximum HpD penetration (0.5 μg/cm² per h) was obtained with 10% Azone.

The effect of topical HpD in combination with UVA on epidermal DNA synthesis was determined in the minipig (Fig. 4). No effect was seen with either a single application or 3 consecutive applications at 12-h intervals. A total of 5 consecutive HpD applications at 12-h intervals followed by UVA irradiation was required to effectively inhibit epidermal DNA synthesis. These results are consistent with skin fluorescence measurements which showed that a minimum of 5 applications was necessary to achieve detectable HpD fluorescence in the epidermis.

DISCUSSION

The present study confirms our previous observation (Berns *et al.*, 1984c) that in psoriasis, UVA

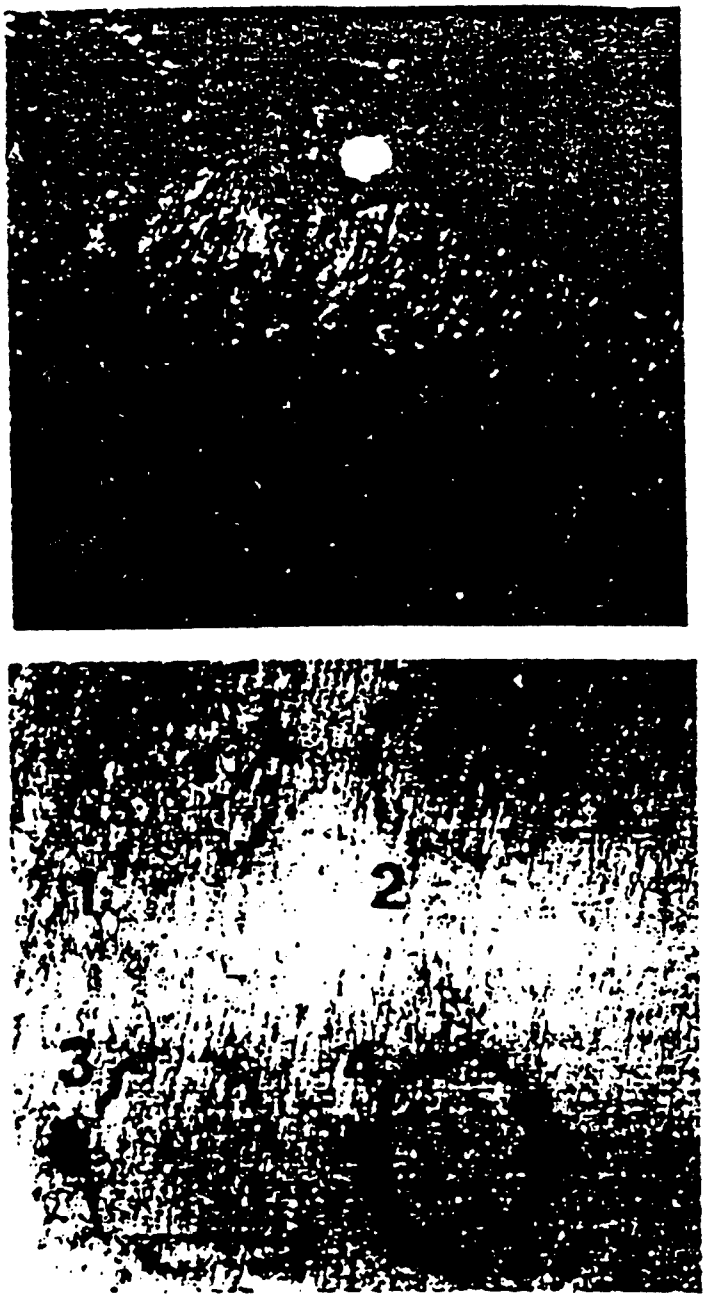

Figure 1 PDT of psoriasis: psoriatic lesion (A) and clinically normal (noninvolved) skin (B), 7 days postirradiation with blue-green laser: (1) 20 J/cm², (2) 40 J/cm² (2); red laser: (3) 20 J/cm², (4) 40 J/cm²

temic HpD in combination with visible light delivered by laser produces a selective destruction of lesional skin without damaging the clinically normal skin. It may be postulated that the basis of the enhanced photosensitivity of psoriatic skin is a selective retention of HpD in the hyperproliferative psoriatic tissue. Hematoporphyrin derivative has been shown to have an affinity for tissues with a rapid cellular turnover, such as neoplastic, embryonic and regenerative cells (Carpenter *et al.*, 1977, Berns *et al.*, 1984b). Heat as a single modality at temperatures of 45°C or above has been shown to produce beneficial effects in psoriasis (Orenberg, 1984). These temperatures would not have been achieved with the low power density used in the present study (Berns *et al.*, 1984a). Thus, it is unlikely that hyperthermia contributed significantly to the clinical changes of the psoriatic lesion. Future efforts to develop this regimen for the photodynamic therapy of psoriasis must examine lower

Best Available Copy

Table 1. Cutaneous photosensitization in guinea-pigs by intradermal injection of HpD porphyrin components and UVA irradiation

Porphyrin	Dose (μg)	Erythema at 24 h
HpD	5.0	+4
Hematoporphyrin	50.0	+1
Protoporphyrin	500.0	0
Hydroxyethylvinyl deuteroporphyrin	500.0	0

UVA (20 J/cm²) irradiation 6 h post drug treatment.

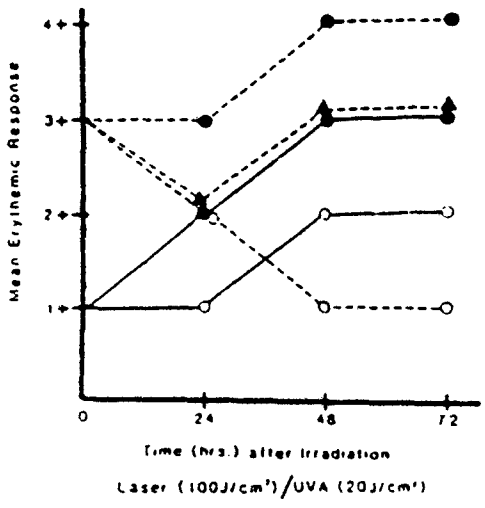

Figure 2. Photosensitization by intracutaneous injection of HpD in combination with UVA and pulsed laser irradiation in minipigs. Laser (100 J/cm²) (----), UVA (20 J/cm²) (——) HpD: 50 μg (●); 25 μg (▲); 10 μg (○).

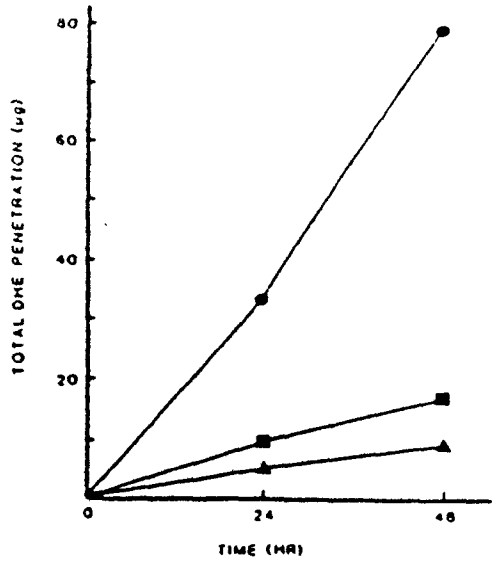

Figure 3. Effect of Azone concentration on percutaneous penetration of 1% HpD in human skin *in vitro*. Azone concentration: 0% (▲); 2% (■), 10% (●).

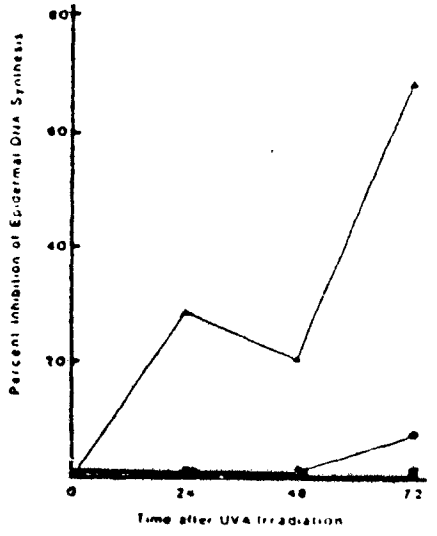

Figure 4. Effect of topical application of 1% HpD in 10% Azone and UVA (20 J/cm²) irradiation on epidermal DNA synthesis in minipigs. One application (●); 3 applications (■), 5 applications (▲)

doses of HpD and/or light to achieve beneficial therapeutic effects without producing tissue necrosis. In contrast to the known carcinogenic effects of psoralen-UVA (PUVA) (Stern, 1984), HpD is thought to be nonmutagenic (Gomer *et al.*, 1983; Kessel and Dougherty, 1983). Hematoporphyrin derivative PDT may, therefore, have substantial advantage over conventional PUVA therapy.

The major disadvantage of porphyrin PDT by the standard systemic route of administration is the prolonged generalized sensitivity of the normal skin to visible and UV light, which lasts for at least 30 days post drug administration (Zalar *et al.*, 1977). In an effort to eliminate systemic exposure to HpD, intracutaneous injection and topical delivery were investigated as approaches for localized drug delivery.

Intracutaneous injection of low dose (5 μg) HpD in guinea-pigs produced a vigorous cutaneous photosensitivity which was localized to the injection site. Hematoporphyrin derivative contains dihematoporphyrin ether dimers/oligomers and a complex mixture of porphyrins (Dougherty *et al.*, 1984). The results of the present study show that the porphyrin monomers (hematoporphyrin, protoporphyrin, hydroxyvinyldeuteroporphyrin) are not potent photosensitizers when injected intracutaneously. These findings are consistent with other studies

showing that these porphyrin components are photosensitizers *in vitro*, but *in vivo* do not accumulate sufficiently to mediate phototoxic effects (Moan *et al.*, 1984, Dougherty *et al.*, 1983). The tumor-localizing dihematoporphyrin ethers are thought to be responsible for conferring photosensitivity *in vivo* (Dougherty *et al.*, 1984).

Hematoporphyrin derivative can be activated by far-UV wavelengths and nearly all wavelengths of the visible spectrum. In the present investigation the phototoxic response with intracutaneous HpD was more intense with visible light than with UVA. However, UVA which is limited to more superficial tissue depths, may be more useful for the treatment of diseases localized to the skin and mucosa. UVA has been shown to be effective in HpD PDT of psoriasis (Diezel *et al.*, 1980).

Topical delivery of HpD would be useful for the treatment of psoriasis and other non-neoplastic hyperproliferative diseases of the skin. The limiting factor in topical therapy is the ineffective percutaneous penetration of HpD (McCullough *et al.*, 1983). In the present study Azone, a penetration enhancer (Stoughton, 1982) increased percutaneous penetration of HpD in human skin *in vitro*. However, *in vivo* several consecutive HpD applications were required to achieve epidermal levels necessary to inhibit DNA synthesis with UVA. Topical HpD may also be useful in the PDT of premalignant and malignant hyperproliferative diseases in mucosal tissues including the oral cavity, bladder, and intestine. HpD should more readily penetrate these nonkeratinized mucosal tissues. Topical delivery of HpD with laser has been used with some success in a limited trial for PDT of intraepithelial neoplasia of the female genital tract (Rettenmaier *et al.*, 1983).

CONCLUSIONS

Photosensitizers provide a unique approach for the selective photodynamic therapy of diseases localized to the skin and mucosa. The local delivery of photosensitizers by topical application and intracutaneous or intralesional injection should enhance the selectivity and minimize the normal skin photosensitization produced by systemic administration. Considerable progress has already been made in understanding the photodynamic actions of the porphyrins leading to more effective clinical applications. The addition of new chemicals that sensitize diseased cells and tissues to electromagnetic radiation in the near-UV and visible regions of the spectrum remains of considerable interest for dermatologic therapy.

Acknowledgements—We gratefully acknowledge the collaborative efforts of Dr. Alan Wile and clinical assistance of Joan Heinemann, R.N. This work was supported in part by USPHS Grants AM27110, CA32248 and RR01192 from the National Institutes of Health and by the Southern California Dermatology Foundation.

REFERENCES

Berns, M. W., J. Coffey and A. G. Wile (1984a) Laser photoradiation therapy of cancer: possible role of hyperthermia. *Lasers Surg. Med.* **4**, 87–89.

Berns, M. W., M. Hammer-Wilson, R. J. Walter, W. Wright, M. H. Chow, M. Nahabedian and A. Wile (1984b) Uptake and localization of HPD and "active fraction" in tissue culture and in serially biopsied human tumors. In *Porphyrin Localization and Treatment of Tumors*, pp. 501–520. (Edited by D. R. Doiron and C. J. Gomer). Alan R. Liss, New York.

Berns, M. W., M. A. Rettenmaier, J. L. McCullough, J. Coffey, A. G. Wile, M. L. Berman, P. J. DiSaia and G. D. Weinstein (1984c) Response of psoriasis to red laser light (630 nm) following systemic injection of hematoporphyrin derivative. *Lasers Surg. Med.* **4**, 73–77.

Carpenter, R. J., H. B. Neel, R. J. Ryan and D. R. Sanderson (1977) Tumor fluorescence with hematoporphyrin derivative. *Ann. Otol. Rhinol. Laryngol.* **86**, 661–666.

Diezel, W., H. Meffert and N. Sonnichsen (1980) Therapie der Psoriasis mit Hamatoporphyrin und Licht. *Dermatol. Monatsschr.* **166**, 793–797.

Dougherty, T. J. (1981) Photoradiation therapy for cutaneous and subcutaneous malignancies. *J. Invest. Dermatol.* **77**, 122–124.

Dougherty, T. J., D. G. Boyle, K. R. Weishaupt, B. A. Henderson, W. R. Potter, D. A. Bellnier and K. E. Wittyk (1983) Photoradiation therapy—clinical and drug advances. *Adv. Exp. Med. Biol.* **160**, 3–13.

Dougherty, T. J., W. R. Potter and K. R. Weishaupt (1984) The structure of the active component of hematoporphyrin derivative. In *Porphyrin Localization and Treatment of Tumors*, pp. 301–314. Alan R. Liss, New York.

Gomer, C. J., N. Rucker, A. Banerjee and W. F. Benedict (1983) Comparison of mutagenicity and induction of sister chromatid exchange in Chinese hamster cells exposed to hematoporphyrin derivative photoradiation, ionizing radiation, or ultraviolet radiation. *Cancer Res.* **43**, 2622–2627.

Kessel, D. and T. J. Dougherty (Editors) (1983) Porphyrin photosensitization. In *Advances in Experimental Medicine and Biology*, pp. 53–62. Plenum, New York.

McCullough, J. L., G. D. Weinstein, L. L. Lemus, W. Rampone and J. J. Jenkins (1983) Development of a topical hematoporphyrin derivative formulation: characterization of photosensitizing effects *in vivo*. *J. Invest. Dermatol.* **81**, 528–532.

Moan, J., T. Christensen and P. B. Jacobsen (1984) Porphyrin-sensitized photoinactivation of cells *in vitro*. *Prog. Clin. Biol. Res.* **170**, 419–422.

Orenberg, E. K. (1984) Use of hyperthermia as an experimental treatment for psoriasis. *Cutis* **34**, 115–116.

Rettenmaier, M. A., M. L. Berman, P. J. DiSaia, R. G. Burns, J. L. McCullough and G. D. Weinstein (1983) Gynecologic uses of photoradiation therapy. *Prog. Clin. Biol. Res.* **170**, 767–775.

Sambuco, C. P. (1985) Miniature swine as an animal model in photodermatology: factors influencing sunburn cell formation. *Photodermatology* **2**, 144–150.

Stern, R. S. (1984) Carcinogenic risk of psoralen plus ultraviolet radiation therapy: evidence in humans. *Nat. Cancer Inst. Monogr.* **66**, 211–216.

Stoughton, R. B. (1982) Enhanced percutaneous penetration with 1-dodecylazacycloheptan-2-one (Azone). *Arch. Dermatol.* **118**, 474–477.

Tomio, L., F. Calzavara, P. L. Zorat, L. Corti, C. Polico, E. Reddi, G. Jori and G. Mandolini (1984) In *Porphyrin Localization and Treatment of Tumors*, pp. 829–840. Alan R. Liss, New York.

Best Available Copy

Tse, D. T., R. C. Kersten and R. L. Anderson (1984) Hematoporphyrin derivative photoradiation therapy in managing nevoid basal-cell carcinoma syndrome. *Arch. Ophthalmol.* **102**, 990–994.

Urbach, F., P. D. Forbes, R. E. Davis and D. Berger (1976) Cutaneous photobiology: past, present and future. *J. Invest. Dermatol.* **67**, 209–224.

Weinstein, G. D. (1965) Autoradiographic studies of turnover time and protein synthesis in pig epidermis. *J. Invest. Dermatol.* **44**, 413–419.

Zalar, G. L., M. P. Fitzpatrick, D. L. Krohn, R. Jacobs and L. C. Harber (1977) Induction of drug photosensitization in man after parenteral exposure to hematoporphyrin. *Arch. Dermatol.* **113**, 1392–1397.

JOURNAL OF SURGICAL RESEARCH 42, 153–158 (1987)

The Thrombogenic Potential of Argon Ion Laser Endarterectomy[1,2]

MARC E. POLLOCK, M.D., JOHN EUGENE, M.D.,[3] MARIE HAMMER-WILSON, M.S., AND MICHAEL W. BERNS, PH.D.

Department of Surgery, VA Medical Center, Long Beach, California 90822; University of California, Irvine, California 92717; and The Beckman Laser Institute and Medical Clinic, Irvine, California 92715

Submitted for publication November 22, 1985

The surface thrombogenicity of atheromas, conventional endarterectomy (CE), laser endarterectomy (LE), and laser angioplasty (LA) were compared in the rabbit arteriosclerosis model. Normal ($N = 6$) and arteriosclerotic ($N = 15$) rabbits underwent thoracoabdominal exploration. Multiple CEs and LEs were performed in 12 arteriosclerotic rabbits leaving a segment of intact atheroma between each endarterectomy. Multiple LAs were performed in three arteriosclerotic rabbits. Argon ion laser radiation was used for all laser procedures. Blood (0.05 ml) from normal rabbits was placed on the CE surface, LE surface, LA surface, atheroma, and normal intima and clotting times were determined. Surface thrombogenicity was calculated as the ratio of the clotting time of the CE, LE, LA, or atheroma to normal intima. Surface thrombogenicity was 1.0 ± 0.03 for normal intima (control), 0.58 ± 0.06 for atheromas ($P < 0.001$), 0.46 ± 0.08 for CE ($P < 0.001$ from atheromas), 0.46 ± 0.08 for LE (P = NS from CE), and 0.27 ± 0.09 for LA ($P < 0.001$ from CE and LE). The thrombogenicity of LE is the same as the thrombogenicity of CE. Both forms of endarterectomy are less thrombogenic than LA in the rabbit model. © 1987 Academic Press, Inc.

Argon ion laser radiation of arteriosclerotic plaques has been shown to leave carbonized debris and thermal disruption of several cell layers beneath the luminal surface [1, 5, 9, 12, 13]. Since atheromas and atheromatous debris (also known as atheromatous gruel), as well as disruption of the endothelial surface predispose to thrombosis [3, 16], the vascular surface following laser angioplasty of arteriosclerosis may be highly thrombogenic. We have attempted to minimize thermal injury to the arterial surface by performing open laser endarterectomy rather than closed laser angioplasty with the argon ion laser [4, 5, 6, 7]. The initial results of laser endarterectomy are comparable, and in some ways superior, to conventional surgical endarterectomy [6]. Yet the influence of laser radiation upon the atheroma–platelet interaction and the endothelial response to injury may cause the laser surface to be more thrombogenic than the surgical surface. This report evaluates the surface thrombogenicity [19, 23] of argon ion laser endarterectomy in an experimental rabbit arteriosclerosis model.

MATERIALS AND METHODS

Normal and arteriosclerotic New Zealand white rabbits were used in this study. They received humane care in compliance with the Animal Care Committee of the University of California, Irvine and the *Guide for the Care and Use of Laboratory Animals* prepared by the National Academy of Sciences and published by the National Institutes of Health (NIH publication No. 80-23, revised 1978). Under general anesthesia (im acepromazine 0.5 mg/kg, xylazine 30 mg/kg, ketamine 50 mg/kg), 15 rabbits underwent balloon catheter trauma to the thoracoabdominal aorta. They were fed a 2% cholesterol diet for 20 weeks. This regimen pro-

[1] Presented at the Annual Meeting of the Association for Academic Surgery, Cincinnati, Ohio, November 10–13, 1985.

[2] This work was supported by NIH Grants HL 31318 and RRO 1192.

[3] To whom reprint requests should be addressed at 5901 East Seventh Street (112), Long Beach, Calif. 90822.

0022-4804/87 $1.50
Copyright © 1987 by Academic Press, Inc.
All rights of reproduction in any form reserved.

duces significant arteriosclerosis in 86% of rabbits [4]. The disease is uniform throughout the traumatized aorta. Grossly the intima appears markedly thickened and discolored. Microscopically the atheromas are surrounded by a fibrous cap. They show inflammation, fatty infiltration, and microcalcification with extension into the superficial layers of the media [4].

Argon ion lasers (Coherent INNOVA 20 or Spectra Physics Model 171) with mixed wavelengths 488 and 514.5 nm were used for laser procedures. Laser light was delivered through a 400 μm quartz fiber optic at a power of 1.0 W. Power was measured from the fiber optic output end (Coherent power meter, Model 210) at the beginning and conclusion of each procedure and was continuously monitored from the laser head during laser operation. The ends of the fiber optic were freshly cut and polished for each experiment. The delivery of laser energy was controlled by the duration of exposure and this ranged from 1.0 to 30 sec (1.0 to 30 J). The energy density was approximately 770 W/cm^2 and the spot diameters were approximately 0.5 mm^2. Six normal rabbits and 15 arteriosclerotic rabbits were anesthetized (im acepromazine 0.5 mg/kg, xylazine 3.0 mg/kg, ketamine 50 mg/kg), intubated, and ventilated with a small animal respirator. Additional ketamine (50 mg/kg iv) was administered during the procedure to maintain anesthesia. A thoracoabdominal exploration was performed. The aorta was isolated and major branches were controlled. No anticoagulants were administered. In the normal rabbits and in 12 arteriosclerotic rabbits, proximal and distal vascular control of the thoracoabdominal aorta was obtained and the aorta was opened longitudinally. Multiple conventional surgical endarterectomies and laser endarterectomies [4] were performed in each of the arteriosclerotic rabbits leaving a segment of intact atheroma between each endarterectomy. Conventional endarterectomy was performed in the standard fashion [20] using an endarterectomy dissector and vascular instruments. A cleavage plane was developed just beneath the internal elastic lamina to dissect the atheroma from the arterial wall and the end points were sharply divided. Laser endarterectomy was performed by using individual laser exposures (1.0 to 5.0 J) to create a line of laser craters at the proximal and distal ends of an atheroma. These lines of laser craters were connected by continuous wave laser light (multiple exposures of 10 to 20 J) to loosen the atheroma. The cleavage plane was dissected within the media by continuous wave laser radiation (multiple exposures of 10 to 30 J). When the plaque was dissected free from the atheroma, the end points were welded by continuous wave laser radiation (10 to 20 J).

In the remaining three arteriosclerotic rabbits, vascular control of the common iliac arteries was obtained, an arteriotomy was made in the left common iliac artery, and a balloon catheter was inserted for proximal control. A 5 Fr. catheter was introduced and advanced proximally until an obstructing atheroma was encountered. The exact site of the lesion could be marked for future study because the rabbits were open. The quartz fiber optic was passed through the catheter and 1.0 sec laser exposures were delivered until the plaques were ablated and the catheter could be advanced. Multiple laser angioplasties were performed in each rabbit. Upon completion of laser angioplasties, proximal vascular control was obtained, the fiber optic and the catheters were withdrawn and the aorta was opened longitudinally.

Upon completion of the procedures (endarterectomy or angioplasty), the aortas were rinsed with saline (37°C) to remove blood. Local humidification was provided to the open thorax and abdomen to prevent dessication of the arterial surface. Blood was drawn from normal donor rabbits and 0.05 ml of normal rabbit blood was applied immediately to normal intima (control), intact atheroma, conventional endarterectomy surface, laser endarterectomy surface and laser angioplasty surface. A fresh wood applicator stick was applied to the blood–surface inter-

face every 15 sec and clotting times were determined as the time at which a reproducible strand of fibrin attached to the applicator stick and pulled away from the surface. Each applicator was used only once. Six donor rabbits were used. A total of 2.0 ml of blood was withdrawn from each donor rabbit so that progressive exsanguination and subsequent changes in the coagulability of the donor rabbit blood did not occur. Prior to use as a donor, a 0.05 ml sample of blood was applied to a glass slide to assure that the donor blood had not been activated. None of the donors were found to be hypercoagulable by this method. There were 12 experiments performed on normal intima (control), 26 experiments performed on atheromas, conventional endarterectomy surfaces, and laser endarterectomy surfaces, and 8 experiments on laser angioplasty surfaces.

Following the determination of surface clotting time, the aortas were harvested from the rabbits and the rabbits were sacrificed (barbiturate injection). The aortas were examined under a dissecting microscope. No perforations were seen. The laser endarterectomy and laser angioplasty sites were measured to determine the surface area irradiated. Energy fluence (J/cm^2) was calculated from the energy necessary to perform each laser procedure and the surface area of each laser procedure. Surface thrombogenicity was calculated as the ratio of the clotting time of the atheroma, conventional endarterectomy, laser endarterectomy, or laser angioplasty surface to normal intima. The values of surface thrombogenicity were evaluated by the F statistic for a single factor analysis of variance [21] and the Kruskal–Wallis test for equality of means [14]. Differences amounting to a value of $P < 0.05$ were considered significant.

RESULTS

The results are reported as the mean ± SD for the rabbits in each group (Table 1). Atheromatous plaque was found to have a clotting time of 247 ± 35 sec for a surface thrombogenicity of 0.58 ± 0.06. This was highly significant ($P < 0.001$) from control clotting time, 425 ± 51 sec. The clotting times of the conventional and laser endarterectomy surfaces were 193 ± 40 and 192 ± 36 sec, respectively, for identical surface thrombogenicity values of 0.46 ± 0.08 ($P < 0.001$ from atheroma). The laser angioplasty surface achieved a clotting time of 117 ± 13 sec for a surface thrombogenicity value of 0.27 ± 0.03 ($P < 0.001$ from endarterectomy). The laser endarterectomy required an average energy density of 112 ± 12 J/cm^2 and the laser angioplasty required an average energy density of 92 ± 30 J/cm^2.

DISCUSSION

The purpose of intraluminal angioplasty is recanalization of a stenotic or occluded arteriosclerotic artery. The procedure does not remove atheromas or reconstruct a diseased artery. Open laser endarterectomy is a reconstructive procedure for the removal of atheromatous plaques like a conventional surgical endarterectomy. Since arteriosclе-

TABLE 1
SURFACE CLOTTING TIME AND THROMBOGENICITY[a]

Surface	Number of rabbits	Clotting time (sec)	Surface thrombogenicity
Normal intima	6	425 ± 51	1.0 ± 0.03
Atheroma	12	247 ± 35	0.58 ± 0.06
Conventional endarterectomy	12	193 ± 40	0.46 ± 0.08
Laser endarterectomy	12	192 ± 36	0.46 ± 0.08
Laser angioplasty	3	117 ± 13	0.27 ± 0.03

[a] All values are means ± SD.

rotic plaques have a fibrous cap, the laser angioplasty procedure will remove the cap and leave an exposed atheroma. Lyford *et al.* [16] have homogenized atheromas to create atheromatous gruel and demonstrated that this atheromatous gruel is a highly thrombogenic substance. When atheromatous gruel was injected into rats, thrombocytopenia, intravascular coagulation, and thromboembolic phenomena ensued. The exposed atheroma following intraluminal laser angioplasty, therefore, may be highly thrombogenic.

Our data support this hypothesis. The laser angioplasty surface, denuded of its fibrous cap, had the fastest clotting time of the surfaces studied and the surface thrombogenicity of laser angioplasty was significantly greater than the surface thrombogenicity of laser endarterectomy. The endarterectomy clotting times (laser versus conventional) were nearly identical. This is not unexpected because both procedures remove the atheroma from beneath the internal elastic lamina. The surfaces were significantly more thrombogenic than normal intima or undisturbed atheroma but this occurs because endarterectomy leaves exposed collagen fibers and eliminates the fibrinolytic system of the intact vascular endothelium [2, 10, 11]. In the present study, atheromas were also found to be thrombogenic. This is in agreement with previous studies that have shown that atheromas are preferential sites for platelet adhesion and thrombus formation [17, 18].

Grundfest and associates have questioned the quality of the argon ion laser angioplasty surface because of carbonization and cellular vacuolization [9]. They have proposed the excimer laser (308 nm) for laser angioplasty because the excimer laser angioplasty surface appears free of carbon and "blast" injury. Since it may be the exposed atheroma rather than the carbonization that is responsible for thrombosis following photoradiation, the excimer laser surface may be just as thrombogenic as the argon ion lase. surface. Certainly if the argon ion effects alone were responsible for increased thrombogenicity, the laser endarterectomy surface should be more thrombogenic than the conventional endarterectomy surface. Our data do not support this. The only other study of the thrombotic potential of a photoradiated arterial surface was performed by Van Stiegmann *et al.* [22]. They photoradiated segments of normal porcine carotid arteries with a Nd-YAG laser (1.06 μm) and implanted these segments in an aortic window. They reported a lack of thrombus formation in these segments, but they qualified their results by noting that the experiments were not analogous to laser radiation of arteriosclerotic arterial segments. They performed chronic experiments, however, as opposed to our acute experiments. We could not perform chronic endarterectomy experiments in the arteriosclerotic rabbits. By the time the lesions were advanced enough for study, the rabbits were too ill to routinely survive thoracoabdominal exploration. They had coronary artery disease as well as peripheral vascular disease. They also had fatty infiltration of the liver and approximately 20% had lipid ascites. If chronic investigations of thrombogenicity following laser treatment of arteriosclerosis are to be performed, a different animal model must be used.

Thrombosis is one of the major complications of intraluminal laser use [1, 8, 13]. Ginsburg and co-workers have shown that thrombotic complications increase as the amount of argon ion laser energy delivered increases [8]. Of course, the patients with the most severe disease would probably require the highest levels of energy for recanalization, so their results may be a reflection of the severity of disease rather than increased thrombotic potential due to laser energy. In the present study, comparable energy fluence was used to perform both laser endarterectomy and laser angioplasty. Since laser light was delivered in perpendicular and tangential directions for laser endarterectomy and in a coaxial direction for laser angioplasty, the laser endarterectomy surface probably received more direct laser energy than the

laser angioplasty surface. Hence, the greater thrombotic potential of laser angioplasty cannot be attributed to greater energy fluence. Livesay has recommended the liberal use of anticoagulants and antiplatelet medications following carbon dioxide laser (10.6 μm) radiation of coronary artery arteriosclerosis [15]. Lyford *et al.* showed that blood from patients receiving heparin retained its anticoagulant properties when exposed to atheromatous gruel whereas blood from patients receiving coumadin did not [16]. He did not study the effect of antiplatelet medications on the coagulant response to atheromatous gruel, however. Since we have shown that laser-irradiated atheromas are highly thrombogenic, we agree with Livesay's recommendation for anticoagulation following laser recanalization.

The surface clotting time measures the thrombogenicity of a blood flow surface. Although it is a static measurement which does not reflect the fibrinolytic capability of high velocity blood flow or the coagulant effects of neointima formation, it does provide a reliable measure of the relative thrombogenicity of arterial surfaces [19, 23]. Various arterial prostheses have been evaluated by this technique and subsequent clinical results have confirmed the experimental results. Based upon the surface thrombogenicity, we would expect better patency following laser endarterectomy than laser angioplasty. Since it may be the exposed atheroma rather than the laser–atheroma interaction which is responsible for increased thrombogenic potential, the laser angioplasty surface may be highly thrombogenic no matter which laser is used.

ACKNOWLEDGMENTS

The authors thank Jeffrey J. Andrews, B.A., Regina Reyes, and Shannon Smith for technical assistance in this work. The authors thank Arline Nakanishi, B.S., and Howard G. Tucker, Ph.D., for statistical consultation. R. L. Maxwell prepared the manuscript.

REFERENCES

1. Abela, G. S., Normann, S. J., Cohen, D. M., Franzini, D., Feldman, R. L., Crea, F., Fenech, A., Pepine, C. J., and Conti, C. R. Laser recanalization of occluded atherosclerotic arteries in vivo and in vitro. *Circulation* **71**: 403, 1985.
2. Benditt, E. P. Implications of the monoclonal character of human atherosclerotic plaques. *Amer. J. Pathol.* **86**: 693, 1977.
3. Constantinides, P. Plaque fissures in human coronary thrombosis. *J. Atheroscler. Res.* **6**: 1, 1966.
4. Eugene, J., McColgan, S. J., Hammer-Wilson, M., and Berns, M. W. Laser endarterectomy. *Lasers Surg. Med.* **5**: 265, 1985.
5. Eugene, J., McColgan, S. J., Hammer-Wilson, M., Moore-Jeffries, E. W., and Berns, M. W. Laser applications to arteriosclerosis: Angioplasty, angioscopy, and open endarterectomy. *Lasers Surg. Med.* **5**: 309, 1985.
6. Eugene, J., McColgan, S. J., Pollock, M. E., Hammer-Wilson, M., Moore-Jeffries, E. W., and Berns, M. W. Experimental arteriosclerosis treated by conventional and laser endarterectomy. *J. Surg. Res.* **39**: 31, 1985.
7. Eugene, J., McColgan, S. J., Pollock, M. E., Hammer-Wilson, M., Moore-Jeffries, E. W., and Berns, M. W. Experimental arteriosclerosis treated by argon ion and neodymium-YAG laser endarterectomy. *Circulation* **72**(Suppl. II): 200, 1985.
8. Ginsburg, R., Wexler, L., Mitchell, R. S., and Profitt, O. Percutaneous transluminal laser angioplasty for treatment of peripheral vascular disease: Clinical experience with 16 patients. *Radiology* **156**: 619, 1985.
9. Grundfest, W. S., Litvack, I. F., Goldenberg, T., Sherman, T., Morgenstern, L., Carroll, R., Fishbein, M., Forrester, J., Morgitan, J., McDermid, S., Pacela, T. J., Rider, D. M., and Laundenslager, J. B. Pulsed ultraviolet lasers and the potential for safe laser angioplasty. *Amer. J. Surg.* **150**: 220, 1985.
10. Huttner, I., and Gabbiani, G. Vascular endothelium: recent advances and unanswered questions. *J. Lab. Invest.* **47**: 409, 1982.
11. Jaffe, E. A. (Ed.) *Biology of Endothelial Cells*. Boston: Martinus' Nijhoff, 1984.
12. Lee, G., Ikeda, R., Herman, I., Dwyer, R. M., Bass, M., Hussein, H., Kozina, J., and Mason, D. T. The qualitative effects of laser irradiation on human arteriosclerotic disease. *Amer. Heart. J.* **105**: 385, 1983.
13. Lee, G., Ikeda, R. M., Theis, J. H., Chan, M. C., Stobbe, D., Ogata, C., Kumagi, A., and Mason, D. T. Acute and chronic complications of laser angioplasty: Vascular wall damage and formation of aneurysms in the atherosclerotic rabbit. *Amer. J. Cardiol.* **53**: 290, 1984.
14. Lehmann, E. L. *Nonparametrics: Statistical Methods Based on Ranks*. San Francisco: Holden–Day, 1975. P. 202.
15. Livesay, J. J., personal communication.
16. Lyford, C. L., Connor, W. E., Hoak, J. C., and

Best Available Copy

Warner, E. D. The coagulant and thrombogenic properties of human atheroma. *Circulation* **36:** 284, 1967.

17. Prentice, C. R. M., McNichol, G. P., and Douglas, A. S. Effect of normal and atheromatous aortic tissue on platelet aggregation in vitro. *J. Clin. Pathol.* **19:** 343, 1966.
18. Powers, W., Mathias, C. J., Welch, M. J., Sherman, L. A., Siegel, B. A., and Clarkson, T. B. Scintigraphic detection of platelet deposition in atherosclerotic macaques: A new technique for investigation of antithrombic drugs. *Thromb. Res.* **25:** 137, 1982.
19. Roon, A. J., Moore, W. S., Goldstone, J., Towan, H., and Campagna, G. Comparative surface thrombogenicity of implanted vascular grafts. *J. Surg. Res.* **22:** 165, 1977.
20. Stoney, R. J. The technique of thromboendarterectomy. In R. B. Rutherford (Ed.), *Vascular Surgery*, 2nd ed. Philadelphia: Saunders, 1984. P. 357.
21. Tucker, H. G. *An Introduction to Probability and Mathematical Statistics*. New York: Academic Press, 1962. P. 200.
22. Van Stiegmann, G., Kahn, D., Rose, A. G., Borrman, P. C., and Terblanche, J. Endoscopic laser endarterectomy. *Surg. Gynecol. Obstet.* **158:** 529, 1984.
23. Yates, S. G., Nakagawa, Y., Berger, K., and Sauvage, L. R. Surface thrombogenicity of arterial prostheses. *Surg. Gynecol. Obstet.* **136:** 12, 1973.

Laser-transected Microtubules Exhibit Individuality of Regrowth, However Most Free New Ends of the Microtubules Are Stable

Wen Tao, Robert J. Walter, and Michael W. Berns

Beckman Laser Institute and Medical Clinic, University of California at Irvine, Irvine, California 92717

Abstract. To study the possible mechanism of microtubule turnover in interphase cells, we have used the 266-nm wavelength of a short-pulsed Nd/YAG laser to transect microtubules in situ in PtK_2 cells at predefined regions. The regrowth and shrinkage of the transected microtubules have been examined by staining the treated cells with antitubulin mAb at various time points after laser irradiation. The results demonstrate that microtubules grow back into the transected zones individually; neither simultaneous growth nor shrinkage of all microtubules has been observed. The half-time of replacement of laser-dissociated microtubules is observed to be ~10 min. On the other hand, exposure of the core of the microtubule, which is expected to consist almost completely of GDP-tubulin, by transecting the internal regions of the microtubule does not render the remaining polymer catastrophically disassembled, and most transected microtubules with free minus ends do not quickly disappear. Taken together, these results suggest that most microtubules in cultured interphase cells exhibit some properties of dynamic instability (individual regrowth or shrinkage); however, other factors in addition to the hydrolysis of GTP-tubulin need to be involved in modulating the dynamics and the stability of these cytoplasmic microtubules.

MICROTUBULES (MTs)[1] are one of the three major fibrillar systems of the cytoskeleton and play an important role in cell movement, determination of cell shape, organization of the internal architecture of the cell, and segregation of chromosomes in mitosis (10, 34). For a better understanding of these fundamental cellular processes it is essential to understand the mechanism of assembly of the MT polymer.

MTs were initially postulated to be polymers in a simple equilibrium with the free tubulin subunits (18, 30). Subsequently, evidence indicated that this view was overly simple. Experimental as well as theoretical explorations of the role of nucleotide hydrolysis in assembly led to the treadmilling model which proposes that, at steady state, there may be a net tubulin addition at one end of the polymer and a net loss from the other end, resulting in a unidirectional flux of tubulin through MTs (9, 25; reviewed in reference 26). More recently, based on observations of individual MT behavior under conditions in which the free monomer concentration is equal to or below the steady-state concentration and on modeling of dynamics of theoretical MTs using hypothetical values for the rate constants, an alternative "dynamic instability" model was proposed. This model asserts that over a wide tubulin concentration range, a slow growing phase and rapid shrinking phase may coexist in a population of MTs; growing MTs are postulated to have tubulin subunits with bound GTP at the polymer ends, while the terminal subunits in shrinking MTs are thought to have bound GDP. The two phases interconvert stochastically and infrequently (15, 16, 23, 27, 28).

At present, it appears that more is known about the assembly of tubulin dimers into MTs under various artificial conditions in vitro than in living cells. Microinjection of fluorescently labeled tubulin into living cells and subsequent immunocytochemistry or measurement of fluorescence redistribution after laser photobleaching has demonstrated that intracellular MTs must be in a dynamic steady state (5, 36, 38, 40), although the mechanism of MT assembly in cells is not well understood. One recent study suggested that dynamic instability may be the mechanism of MT turnover in living fibroblasts; however, the lack of overall high resolution of individual MTs made the interpretation of the experiments difficult (37). There are several other possible drawbacks associated with microinjection experiments: an increase in intracellular tubulin concentration and in total cell volume, mixture of labeled and endogenous tubulins, and differences of behavior between the labeled and unmodified subunits.

Selective subcellular microsurgery on many cell structures using a variety of focused laser beams has been well developed (reviewed in reference 2). Furthermore, it has been shown that a short-pulsed UV laser can be used to ablate an

1 *Abbreviation used in this paper*: MT, microtubule.

© The Rockefeller University Press, 0021-9525/88/09/1025/11 $2.00

organic polymer or biological tissue with no detectable thermal damage to the substrate (41).

We have combined the techniques of laser microsurgery and immunocytochemistry, and designed a series of experiments to examine the mechanism of assembly and disassembly of cytoplasmic MTs in interphase cells. The results show that MTs grow back into the transected zones individually after laser transection. The half-time of MT replacement was observed to be ~10 min. The simultaneous growth or shrinkage of all transected MTs predicted by the treadmilling model was never observed under the experimental conditions. This suggests that the majority of cytoplasmic MTs exhibit some properties of dynamic instability. But most transected MTs with free new ends generated by laser irradiation do not immediately disassemble to completion, and the free minus ends of these MTs are relatively stable for a period of >10 min. This suggests that the presence of other factors besides the hydrolysis of GTP-tubulin modulates the dynamics and stability of the cytoplasmic MTs.

Materials and Methods

Cell Culture

PtK_2 cells (rat kangaroo kidney epithelium) were originally obtained from the American Type Culture Collection (ATCC; Rockville, MD), and have the advantage in that they are thin and remain relatively flat throughout their cell cycle. The cells were grown as monolayers in minimal essential medium (Gibco Laboratories, Grand Island, NY) containing 10% FCS without antibiotics. Cultures were maintained at 37°C in a humidified atmosphere of 5% CO_2.

Laser Transection of MTs

The laser microbeam system was similar to that described previously (42). Laser transection of MTs was performed on cells in Rose culture chambers using the fourth harmonic 266-nm wavelength from a short-pulsed Nd/YAG laser (model YG 481A; Quantel Corp., Tempe, AZ). The pulse energy of the unfocused laser beam was found to be 63–144 microjoules before attenuation, with a pulse duration of 10 ns. Laser energy was controlled with neutral density filters (Oriel Corp. of America, Stanford, CT) placed in the light path. For each individual experiment, the laser pulse energy was carefully monitored and controlled so that it remained constant throughout the experiment. The laser was diverted by a series of optical mirrors and a dichroic filter into an inverted Axomat microscope (Carl Zeiss, Inc., Thornwood, NY), and focused through a 100× Ultrafluar objective (Carl Zeiss, Inc.). The effective spot size of the focused laser beam was estimated to be 5 μm in diameter. Frequency of the pulses was controlled by an electronic shutter synchronized with the laser.

The cells were seeded in Rose culture chambers with quartz coverslips, as one chamber window, 36–40 h before the experiments. To minimize cell-to-cell variability, the cells with a similar size (~100 μm long) and elliptic shape were selected for this study. The positions of the selected cells were marked by scribing small circles (1.0 mm in diameter) around them on the outside surface of the quartz coverslips using a diamond marking objective. Observation of the target cells and accurate determination of predefined regions were accomplished by projecting the cell images, through a Newvicon tube video camera (Sierra Scientific Corp., Mountain View, CA), onto a video monitor interfaced with an image array processor, and superimposing a rectangular cursor box at a preselected area on the real-time image of a cell. Transection of cytoplasmic MTs was achieved by moving the xy motorized stage with a joystick controller so that the focused laser beam raster-scanned in straight lines through the entire cursor box-outlined cytoplasm of a target cell. The scan lines were parallel to the long axis of the cursor box. On average, it took ~8 s to transect MTs and produce a transected zone in a given cell. The predefined regions were always 19–23 μm away from the leading edges of the cells and had a width of 5 μm across the cells. For each experiment, several cells in a Rose chamber were selected, marked, and MTs in the transected zones within these cells were dissociated at various time points by the laser as described above. The microscope stage was kept at 37°C using an air stream incubator. Photographs were taken before and after irradiation. After treatment of the last selected cell, the cells were immediately fixed and then processed for immunofluorescence.

Immunofluorescence

About 20 s after the last laser transection, the cells were fixed for 10 min in 3.7% formaldehyde in PBS with three changes by injecting the fixative into the Rose chambers. The Rose chambers were then disassembled, the cells on the quartz coverslips were permeabilized for 1 min in 0.1% Triton X-100 in PBS, further fixed for 30 min with the same fixative, and extracted again for 15 min in 0.1% Triton X-100 in PBS. This treatment not only rapidly fixed the cells, resulting in good preservation of MTs, but also gave very good permeabilization. The fixed and permeabilized cells were incubated for 1 h at 37°C with anti-α-tubulin mAb (Amersham Corp., Arlington Heights, IL) diluted 1:100 in PBS. The cells were then freed of excess primary antibody by three washes with PBS and incubated for 30 min at 37°C with fluorescein-conjugated goat anti-mouse IgG+IgM (Boehringer Mannheim Biochemicals, Indianapolis, IN) diluted 1:70 in PBS. After fluorescent labeling, coverslips were washed in three changes of PBS for a total of 10 min, rinsed with double-distilled water, and mounted in Aquamount (Lerner Labs, New Haven, CT). Cells were subsequently examined with an epifluorescence microscope (Carl Zeiss Inc.) equipped with the appropriate excitation and barrier filters (Zeiss filter set No. 487710). All immunofluorescence micrographs were taken on Tri-X Pan film (Eastman Kodak Co., Rochester, NY) using 1-min exposures, and developed in Kodak Microdol-X.

Electron Microscopy

The cells were treated with the laser under the conditions identical to those described above. Immediately after the treatment, the cells were fixed for 10 min in 3% glutaraldehyde in medium, washed with PBS twice, and further fixed for another 50 min with the same fixative. Subsequently, the Rose chambers were disassembled, and the locations of the treated cells were marked using a diamond pen. Fixed cells on the quartz coverslips were washed twice with PBS, postfixed for 1 h with 1% osmium tetroxide in Millonig's phosphate buffer (pH 7.0), and rinsed in the same buffer. The cells were critical point dried after dehydration in a graded series of acetone (30–100%). Critical point-dried samples were then gold coated, and examined with a scanning EM (model SEM 515; Philips Electronic Instruments, Inc., Mahwah, NJ).

Viability Assay

Groups of cells in a Rose chamber were marked in 2-mm-diam circles as described. All cells inside the circles were treated with the laser under the same conditions described above. At various times after the treatment, the cells were rinsed with PBS and stained with 0.08% trypan blue in PBS for 10 min. The cells inside the circles were counted and the viability was expressed as the ratio of cells retaining the stain vs. total number of cells examined.

Data Analyses

The image processing system was described previously (44). For analyses, negatives were imaged with a Newvicon tube camera (model LST-1; Sierra Scientific Corp.); the images were digitized, processed with a Plessey 6200 computer system (Plessey Peripheral Systems, Irvine, CA) equipped with IP-512 image processing boards (Imaging Technology Inc., Woburn, CA), and displayed on a video monitor.

To determine accurately the location of transection on a phase-contrast or fluorescence micrograph, we collected an image from a phase-contrast or fluorescence micrograph, stored the image in the image processor, and subsequently superimposed it with another image of the same cell with the cursor box showing the predefined region.

Average gray value measurements were performed as follows. Images of fluorescence micrographs (negatives) were positioned in such a way that the longitudinal directions of transection aligned with the vertical axis of the video images. An interactive mouse-controlled cursor box, with the length corresponding to the length of the cell, was then displayed on the video monitor. The location and width of the cursor box was determined by the criteria that the cursor box should cover as much of the cellular region as possible while minimizing background regions. The average gray values within the

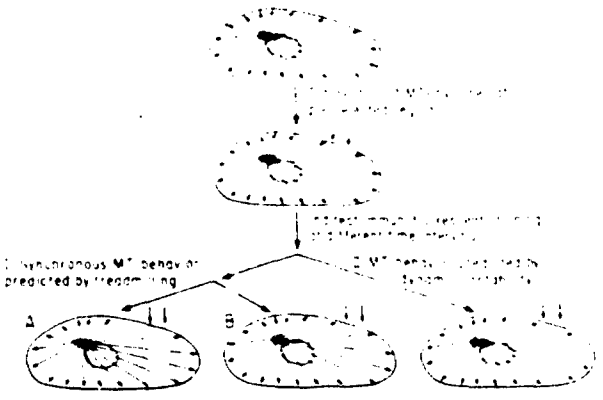

Figure 1. Schematic representation of the experimental design. Two arrows outside each cell indicate the transected zones within which MTs are dissociated by laser. MTs are depicted as lines inside the cells and the polarity of MTs is indicated by the arrows. See Results for details.

box were measured, integrated in a vertical direction, and displayed as a summed histogram showing the variation in average gray value vs. horizontal position in a cell. The displayed histograms were recorded on Kodak Panatomic-X film and traced onto transparent paper from enlarged prints made from the original negatives. The background average gray values were normalized with respect to those measured from a cell fixed 20 s after laser transection.

To quantitate MTs within the transected zones, we performed the following analysis. Micrographs (negatives) of tubulin-stained cells were imaged and processed as described, and the image contrast was optimized using system software. A mouse-controlled cursor box with a width of 10 μm and length corresponding to the width of the cell was then superimposed on the image to outline the transected zone; MTs within the cursor box were counted directly from the video monitor and calculated as MT density (number of MTs/500 μm^2). The surface area of 500 μm^2 was chosen because it was about the average of the surface areas of the cursor boxes. Quantification of MTs outside the transected zones was performed in the same way except that the cursor box was placed between the transected zones and the cell edges adjoining the transected zones.

Results

Experimental Design and Rationale

Most cytoplasmic MTs in tissue culture cells have been shown to originate from a centrosome or MT organizing center and to extend radially towards the cell periphery (31). Moreover, it is known that MT assembly both in living cells and in vitro experiments in crude lysates is initiated at the MT organizing center and that virtually all the MTs have the same polarity—their fast-growing ends distal to the site of initiation (1, 11, 14).

To test the possible models of MT assembly, we used a short-pulsed laser beam to transect MTs in situ in interphase PtK_2 cells at predefined regions followed by indirect immunofluorescent staining at various time points with antitubulin mAb to examine the behavior of transected MTs. Under these conditions, the treadmilling and dynamic instability models give distinct predictions with respect to the patterns of regrowth or shrinkage of the transected MTs. The rationale of the experiments is diagrammed in Fig. 1.

According to the treadmilling model, one would predict two different situations under steady-state conditions. In the first instance, if MTs are attached to a centrosome or a structural matrix by lateral linkages near their ends, in such a way that the ends remain free for subunit exchange (22, 26), the new plus end generated by transection would add subunits and the minus end at the centrosome would lose subunits at the same rate; similarly, the loss of subunits from the new minus end would be balanced by the addition of subunits from the plus end of the MT fragment. Therefore, the lengths of the MTs would not change and the transected zone would remain stationary with time (Fig. 1 *A*). Secondly, if the anchored minus ends of MTs are blocked by attaching to a centrosome (20), the new plus end would grow; but the loss of subunits from the new minus end would be balanced by the addition of subunits from the plus end. Thus, the transected zone would be filled in with time from the side in proximity to the centrosome (Fig. 1 *B*). In either case, the treadmilling model would predict synchronous behavior of MTs.

Under the experimental conditions, dynamic instability would predict that (*a*) MTs grow back into the transected zone individually—thus, the replacement of laser-dissociated MTs should occur MT by MT; and (*b*) the number of MTs found in the transected zone would increase gradually at certain time intervals after laser transection. Furthermore, the GTP cap model, which has been proposed as the mechanism of dynamic instability, would predict that transecting the internal regions of MTs would cause all the transected MTs with free exposed ends to be in the rapid-shrinking phase, and that a majority of these shrinking MTs would catastrophically depolymerize to completion since the phase transitions are expected to be low probability events (7, 16, 28). Therefore, according to the GTP cap model, one would expect a drastic decrease in the number of MTs in regions proximal from the transected zones in relation to the cell nuclei and almost complete lack of MTs in regions distal from the transected zones soon after laser transection.

Transection of Cytoplasmic MTs In Situ Using Laser at Accurately Predefined Regions

One of the prerequisites for our experiments is that there must be a means to transect MTs in living cells at desired regions which must be accurately relocated on subsequent analyses. To determine whether the short-pulsed UV laser can actually be used to dissociate MTs in a controlled manner, we focused the 266-nm wavelength of the short-pulsed Nd/YAG laser into the cytoplasm of interphase PtK_2 cells and manually raster-scanned the focused laser beam through the entire cytoplasmic area outlined by a superimposed cursor box as described in Materials and Methods. The computer-generated cursor box on a live video image of the living cell determined the scan zone. The cells were then fixed, and processed for immunofluorescence ~20 s after the laser treatment. The typical results (Fig. 2) show that the UV laser indeed could uniformly dissociate the cytoplasmic MTs in situ at selected regions and that such a transection is a localized reaction because the cytoplasmic regions outside the irradiated zone showed normal patterns of antitubulin labeling (Fig. 2 *c*). These observations have been confirmed using high voltage electron microscopy (Rieder, C. L., personal communication).

Surprisingly, the actual transected zone on the immunofluorescent image was ~10 μm in width, which was wider than the predefined region (Fig. 2 *c*). Such discrepancy is likely

Best Available Copy

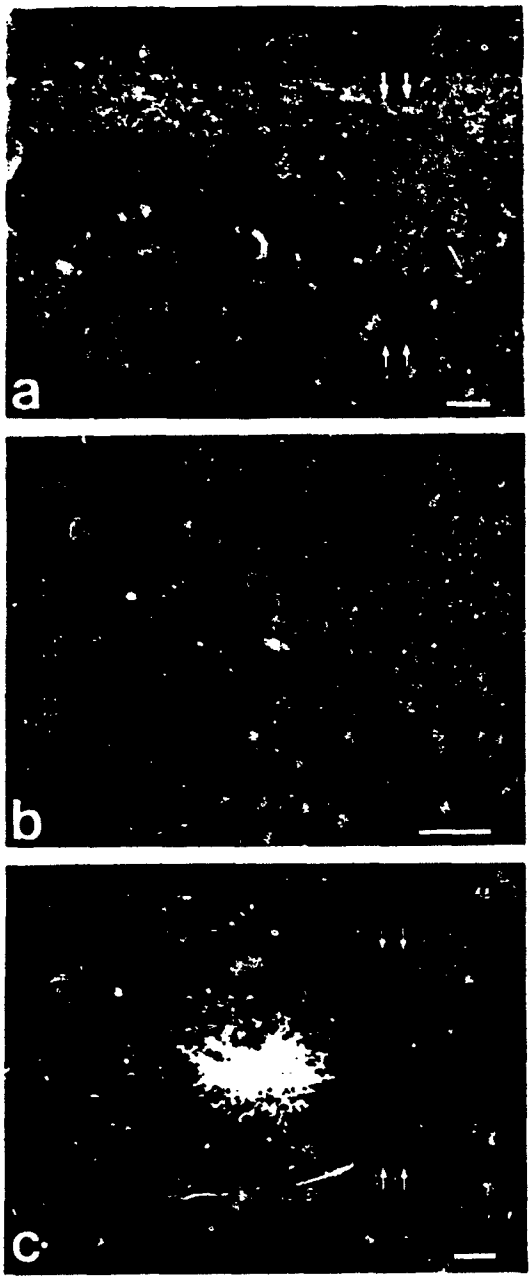

Figure 2. Local dissociation of cytoplasmic MTs by laser at predefined regions. (*a*) Phase-contrast image of an interphase PtK_2 cell. (*b*) Image of the same cell photographed from the video monitor showing that the predefined region is determined by the superimposed rectangular cursor box. (*c*) Corresponding tubulin staining of the same cell shows the lack of MTs in the transected zone and normal distribution of MTs elsewhere. *Arrows*, predefined regions. Bars, 10 μm.

due to the large effective spot size of the laser beam. This is inferred from the following facts. (*a*) The cells fixed 20, 40, and 50 s after laser transection under the identical conditions exhibited almost the same width of the transected zones. This argues against the possibility that the discrepancy could have resulted from the rapid transient depolymerization at the ends during the time interval between transection and fixation since it predicts that the widths of the transected zones would drastically vary with the time interval. (*b*) When the predefined region was narrowed, the width of the transected zone was observed to be proportionally reduced. (*c*) When a low magnification (32×) objective was used instead of the 100× objective, the widths of the transected zones were reduced, indicating that the aperture angles of the objectives play a role in determination of effective spot sizes of the laser microbeam.

Table I. Cell Viability after Laser Transection

Time after laser treatment	Cells stained	Cells treated	Survival
	n	*n*	%
20 s	1	172	99
	0	124	100
2 h	2	132	99
	0	107	100
4 h	0	118	100
	1	147	99
6 h	2	105	98
	1	131	99

Effects of Laser Irradiation on Cells

To estimate the effects of laser irradiation on cells other than on the cytoplasmic MTs, cell viability after laser treatment was assayed using the trypan blue dye exclusion method. The results (Taole I) show that almost all the irradiated cells survived ≥6 h after irradiation.

Scanning EM on the treated cells was performed to determine whether laser irradiation might have damaged the cell membrane. The typical data (Fig. 3) reveal that there is no difference between the cell surface over the irradiated regions and that over control regions (Fig. 3, *b* and *c*). Therefore, to the limits of scanning EM, there is no detectable laser-induced damage to the cell membrane.

The effect of laser irradiation on cell morphology is shown in Fig. 4, *a* and *b*. The results demonstrate that laser transection of MTs did not induce remarkable changes in the overall cell morphology; however, some subtle morphological changes after irradiation did occur, as shown by changes in the phase-contrast images at the cell margins (*open arrows*, Fig. 4 *b*). Fig. 4 *c* reveals that the cytoplasmic MTs had indeed been transected and some of the MTs grew back into the transected zone since the cell was irradiated 10 min before fixation.

Furthermore, the laser-dissociated MTs were completely replaced by 40 min after laser irradiation (Figs. 5 and 7). Interestingly, a couple of cells were observed under the phase-contrast microscope to undergo mitosis within 1 h after laser irradiation. This indicates that the laser irradiation under the experimental conditions did not interfere with the cellular processes of transition from interphase to M phase (not shown). General observations of time-lapse video tape images of the cells after irradiation revealed normal-appearing cytoplasmic particle transport in nonirradiated regions (our unpublished data).

All these results strongly suggest that any possible pertur-

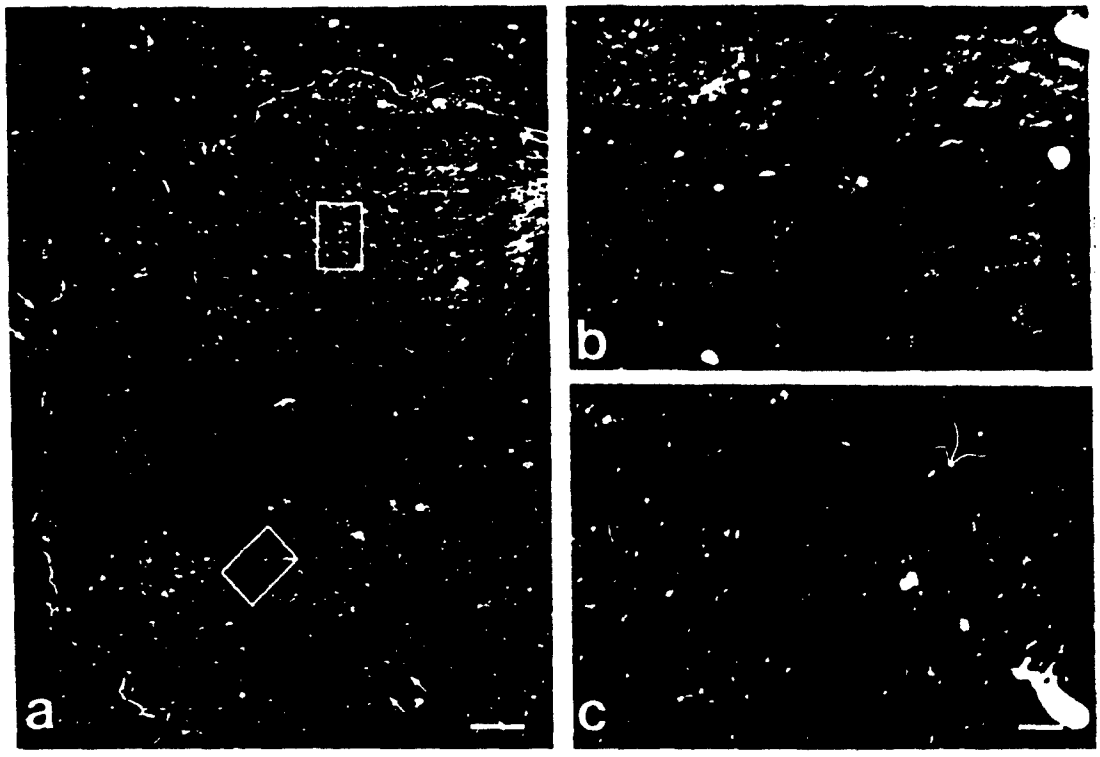

Figure 3. Scanning electron micrographs of a laser irradiated PtK_2 cell showing no detectable membrane damage. (*a*) Low magnification view of the PtK_2 cell in which the cytoplasmic MTs were dissociated using the laser at the region indicated by arrows. The upper and lower boxes in *a* indicate the boundaries of the field shown at higher magnification in *b* and *c*, respectively. (*b*) High magnification view of the cell surface at an untreated region. (*c*) High magnification view of the cell surface over the irradiated region. Bars: (*a*) 10 μm; (*b* and *c*) 1 μm.

bative effects of the laser irradiation on the cells is minimal under the experimental conditions used.

Replacement of Laser-dissociated MTs Occurs Individually with No Synchronous Behavior of MTs

To address the question whether the transected MTs behave individually or synchronously, we have fixed and stained the cells with monoclonal antitubulin at various time points after the laser transection of the cytoplasmic MTs. Representative results from such experiments are shown in Fig. 5. At 20 s after irradiation, the earliest time at which we are able to inject the fixative into the Rose culture chambers, we detect no MTs in transected zones with a width of ~10 μm, and the new MT ends created by transecting the internal regions of the MTs are evident (Figs. 2 and 5 *a*). The cells fixed 9, 13, and 19 min after laser transection (Fig. 5, *b–d*) show a progressive increase in the number of MTs in the transected zones, indicating that the transected and newly initiated MTs grow back into the transected zones individually. Some ends of the MTs can be easily seen in the area within or across the transected zones and in the area distant from the transected zones. Since all the free new MT ends produced by the transection were initially in line at the edges of the transected zone, we refer to the MTs with ends that lay within or across the transected zones as growing MTs, and to MTs with ends that lay distant from the transected zones as shrinking MTs. The growing and shrinking MTs can be found from both sides of the transected zones. At 28 and 35 min after laser transection, almost all the MT-depleted zones are replaced by newly grown MTs and the ends of the MTs near the transected zones can only be seen occasionally (Fig. 5, *e* and *f*). By 55 min after the transection, there is no difference between the MT distribution of treated cells and those of control cells (Fig. 5 *g*).

To determine the average properties of the regrowth or shrinkage of transected MTs, we have used computerized image analysis to measure the average gray values in digitized tubulin-stained images. In any given cell, the average density of tubulin staining should be proportional to the average number of MTs, and the average staining density can be reflected by the average digitized gray values. The normalized average gray values were measured as a function of horizontal position in the cells, integrated in the vertical direction, and plotted as a summed histogram. Fig. 6 is typical of these measurements and shows that there is no synchronous regrowth or shrinkage of the transected MTs. Cells fixed and stained 20 s after laser transection showed 10-μm-wide troughs in the transected zones in the summed histograms (Fig. 6, $T = 20$ *s*), indicating the depletion of MTs in those regions. With time the troughs gradually shallowed, indicating an increase in the number of MTs in those regions. This is contrary to the two predictions of the treadmilling model (Fig. 1, *A* and *B*), which in this case would predict that with time the trough would either remain unchanged or

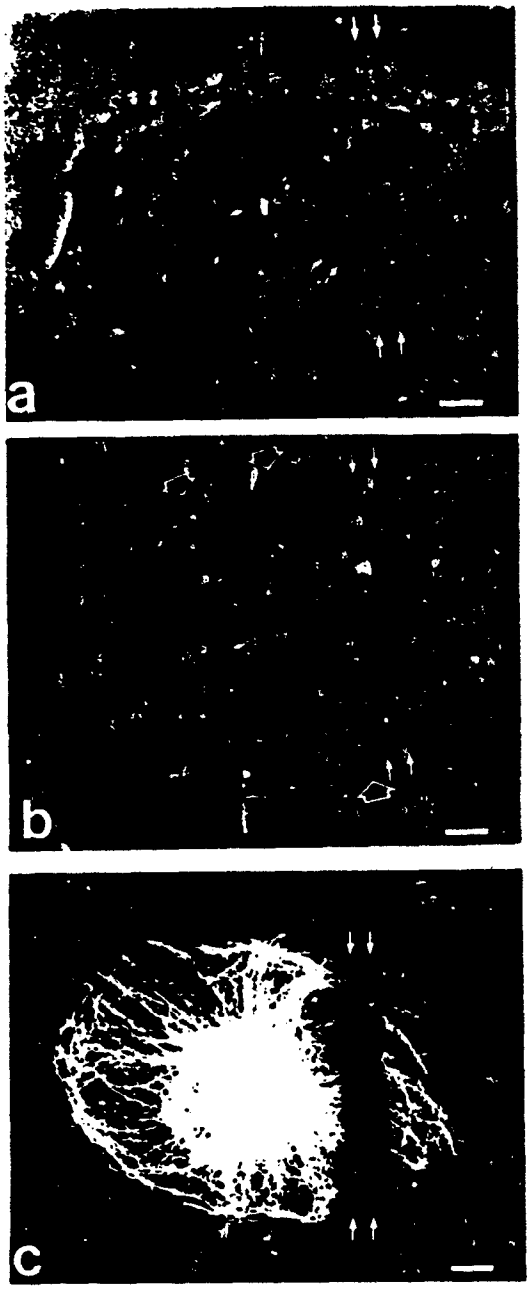

Figure 4. Effects of laser irradiation on cell morphology. Phase-contrast micrographs of a PtK_2 cell (*a*) before and (*b*) 2 min after irradiation. Open arrows in *b* depict the morphological changes that occurred after irradiation. The corresponding tubulin staining of the same cell fixed 10 min after irradiation (*c*) shows the transection of MTs. The predefined regions were indicated by small arrows outside the cells. Bars, 10 μm.

get narrower. On the other hand, such behavior of the MTs can be explained by dynamic instability.

Transected MTs With Free New Ends Do Not Quickly Disappear

Another result from the above experiments is that the majority of MTs with free new ends generated by in situ laser transection do not immediately depolymerize to completion, and the free minus ends of these MTs are relatively stable. If shrinking MTs rapidly disassemble to completion and the free minus ends of these MTs were unstable, a drastic decrease in the number of MTs in regions proximal from transected zones in relation to the cell nuclei, and a total lack of MTs in regions distal from transected zones soon after the transection would be expected because transecting the internal regions of MTs would result in all the transected MTs entering the shrinking phase. Fig. 5, *b–d*, along with Fig. 4 *c*, shows that most transected MTs do not disappear for periods of more than 10 min, and there is no drastic decrease in the number of MTs or MT density on both sides of transected zones, indicating that most transected MTs do not rapidly depolymerize to completion. This is more obvious for the MTs with free minus ends, and some of the free minus ends can be detected in cells fixed 19 min after transection (Fig. 5 *d*).

Quantitative Analyses of Transected MTs

To further confirm the above results, we have examined negatives for 84 cells and quantitated the number of MTs both in transected zones and in regions on the distal side (toward the leading edges of the cells) of the transected zones as a function of time. Although the cells selected for this study had similar size and morphology, relatively small variations in cell sizes and in MT density were observed. The variations in cell sizes were overcome by converting the number of MTs to MT density, and variability in MT density was estimated by conducting the same measurements on untreated cells. To facilitate tracking of individual MTs, the immunofluorescent images were digitized and processed as described in Materials and Methods. The digital processing enhanced the contrast in MT and nonMT regions. Individual MTs in regions from several micrometers away from the side of a transected zone in proximity to the nucleus all the way to the cell leading edge can be readily tracked on the video monitor. Fig. 7 confirms that the number of MTs in transected zones increases progressively with time and that by ~30 min after transection of MTs, the laser-dissociated MTs are completely replaced by newly grown MTs; consequently, the half-time of such a replacement is calculated to be ~10 min. When quantitating the number of MTs in the regions between the transected zones and cell edges, however, we have again found that most transected MTs do not catastrophically disassemble and these MTs which have free new minus ends persisted, although the number of MTs slightly decreases at the beginning (20 s to 7 min) and then increases with time in comparison with control cells (Fig. 8).

Discussion

We have developed a new approach to study the mechanism of cytoplasmic MT turnover by combining laser microsurgery with immunocytochemistry. This method avoids some of the possible drawbacks of other techniques such as an increase in intracellular tubulin concentration and total cell volume. The data presented here show that the majority of cytoplasmic MTs in interphase cells exhibit individuality of growth and shrinkage after transection of the MTs, and the half-time of complete MT replacement after laser transection

is estimated to be ~10 min, compatible with other in vivo and in vitro studies of end-dependent MT assembly (17, 37-39). Simultaneous growth or shrinkage of all MTs was never observed under the experimental conditions. These results are contrary to the predictions of the treadmilling model, and suggest that a majority of cytoplasmic MTs in cultured cells exhibit some properties of dynamic instability (individual regrowth and shrinkage). On the other hand, our results also show that the exposure of the core of the MTs, which is expected to consist almost completely of GDP-tubulin subunits according to the GTP cap model, by transecting the internal regions of the MTs does not render the remaining polymer catastrophically disassembled, and most transected MTs with exposed free minus ends do not quickly disappear. This is not in agreement with the predictions of GTP cap model, and suggests that under in vivo conditions, other factors in addition to the hydrolysis of GTP need to be involved in modulating the dynamics and stability of these dynamic cytoplasmic MTs.

It has been demonstrated that MT-associated proteins bind to the outside surface of MTs, altering the energetics and kinetics of their assembly and disassembly. In addition, certain divalent cations such as Mg^{2+} and Ca^{2+}, etc., have been shown to affect MT assembly and disassembly. Based on the fact that most transected MTs with free new ends in PtK_2 cells do not quickly disappear, we propose that in vivo the hydrolysis of GTP-tubulin may not cause a rapid disassembly. Rather it would change the interactions between the subunits in the polymer only to such a degree as to permit the GDP polymer to exist in a metastable state. This structurally stable GDP polymer may then be further stabilized or induced to rapidly disassemble by other factors such as MT-associated proteins, and Ca^{2+} etc., and it may exchange with either free GDP-tubulin or free GTP-tubulin at an MT end with different rates. Under certain conditions, more than one kind of factor may simultaneously act on MTs, and some of them may even act randomly. One recent study has also suggested the presence of factors in Madin-Darby canine kidney cells which stabilize the noncentrosomal cytoplasmic MTs (4). These factors may play important functional roles in modulating the dynamics and stability of MTs in vivo. Although the hypothesis discussed above can well explain the stability of MTs with exposed free ends in cells, the possibility could exist that the laser somehow "cauterized" the transected MT ends so that they were no longer reactive. However, the following observations argue against this possibility: (*a*) the laser-dissociated MTs are completely replaced, and the time course of such replacement is compatible with other in vivo and in vitro studies of MT assembly using different methodologies; and (*b*) irradiated cells incubated at 4°C for periods of 15-30 min show a complete loss of fibrillar MT staining even in the irradiated regions, suggesting that the MT ends are able to undergo a net loss of tubulin subunits under depolymerizing conditions.

The observed replacement of laser-dissociated MTs in the transected zone is unlikely to be explained by some form of active sliding of the MTs. First, if the transected MTs actively slid into the transected zone, then a number of short MTs with both ends free would be present in regions around the transected zone soon after the transection, and these short MTs would be accumulated with time while the transected zone gradually refilled with MTs. However, when we performed our quantitative analyses, individual MTs in regions around the transected zones were traced from a video monitor after computer enhancement, and no such short MTs with both ends free were found. Second, the observed time course of replacement of laser-dissociated MTs in the transected zone is much too slow to be explained by the active sliding of MTs. As our data showed, it took about 30 min to completely refill the 10-μm-wide transected zone with MTs; but, the reported rate of active sliding of MTs of the same polarity ranges from 0.2–16 $\mu m/s^{-1}$ (21, 29, 32, 33, 35, 43). Apparently, the expected time course of refill of the MT-depleted zone by some form of active sliding of the MTs would be much faster than the observed time course, even when the lowest reported rate of MT sliding is considered.

It is necessary to emphasize that our results may be limited to cultured interphase cells whose MTs are dynamic and undergoing constant remodeling. It is known that MTs in some terminally differentiated cells, such as neurons and mature chicken erythrocytes, have distinct properties which differ from those of MTs in cultured cells. These MTs are more stable and lack MT organizing centers (6, 19). In these cases, the stability and possible lateral interactions of MTs appear to be more important than the dynamic aspects of MTs in order for the MTs to perform their functions. Different mechanisms may be needed to be involved to achieve such stability and spatial organization.

In mammals, the α and β tubulins are encoded by multigene families (reviewed in reference 8), and it seems that more than one gene for the tubulins are expressed in any cell type at any time, which results in the presence of multiple tubulin isotypes in a cell. The existence of different tubulin isotypes led to speculation that distinct kinds of MTs might be assembled from or enriched in one or more tubulin isotypes (12). Therefore, it raises the possibility that there might exist subsets of MTs with different properties in cultured cells due to the structural difference in isotype contents. However, very recent studies have demonstrated that in cultured cells these isotypes form mixed copolymers and appear to function interchangeably (3, 24). It has been shown that the coexistence of two populations of MTs in cells with different stabilities which could probably result from post-translational modification(s) or binding of MT-associated proteins along their length is possible. However, not only do the dynamic MTs represent 80% of all MTs while stable MTs only represent 20% but also the overall shapes and spatial distributions of these two populations are quite different from one another. The stable MTs are curly or kinky, compared to the dynamic MTs which are usually straight and cluster around the nucleus and centrosome. In addition, the stable MTs rarely extend to the cell periphery, as opposed to the dynamic MTs many of which reach the cell's edge (4, 13, 39). Since the transected zones chosen for this study are located relatively far away from the nuclei, the stable MTs which would be found within the transected zones represent a very small fraction of all the MTs in those regions. Therefore, any possible diversity in MT assembly resulting from the coexistence of stable and dynamic populations of MTs would make a very small contribution to the observed MT behavior after laser transection in situ. It is possible that mechanisms for the turnover of such a small percent of stable MTs may be different from that for the turnover of dynamic MTs. It is not surprising, however, if we come to think these

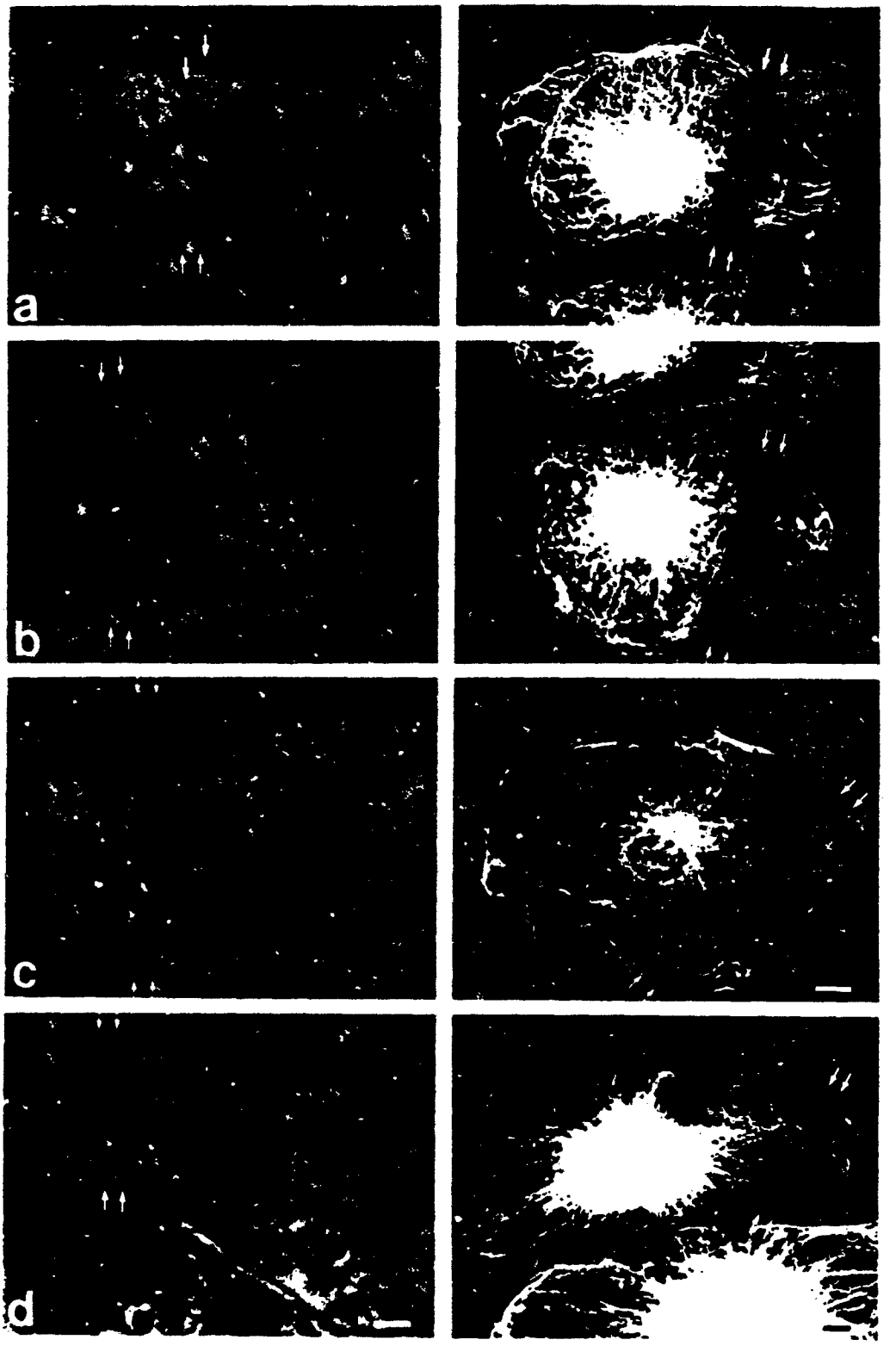
a
b
c
d

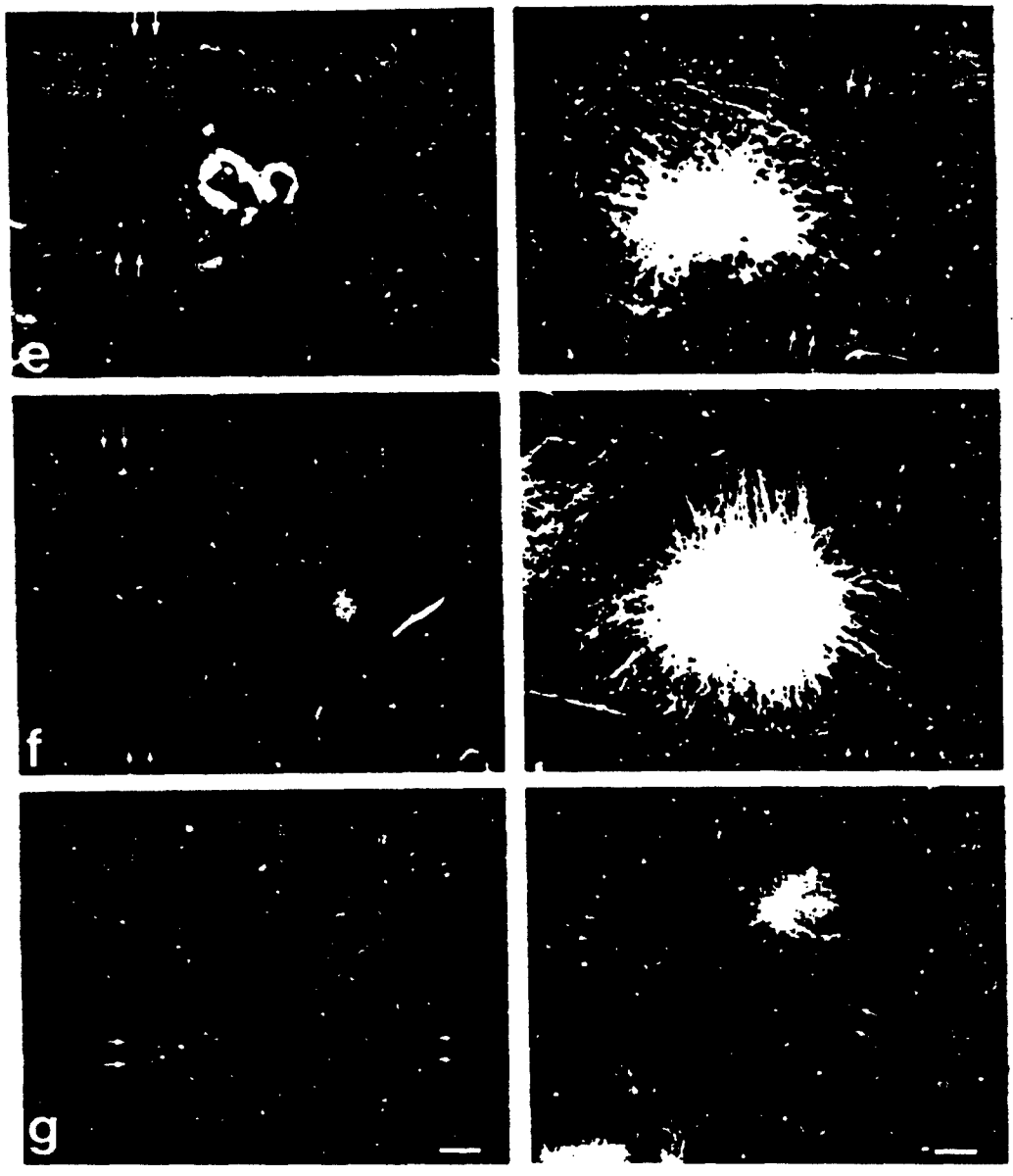

Figure 5. **Regrowth of MTs after transection. Phase contrast and corresponding antitubulin fluorescence of cells whose MTs were laser dissociated in the transected zones. *Arrows*, predefined regions. The cells (fluorescent micrographs) were fixed 20 s and 9, 13, 19, 28, 35, and 55 min after laser transection, respectively, and then stained with antitubulin mAb. Bars, 10 μm.**

MTs may have specialized functions and be involved in such diverse processes as intracellular transport or sensing of environmental changes coupled with communication of the signal to the nucleus.

At present, the exact identities of the factors that regulate the dynamics and stability of MTs in vivo and the molecular mechanism by which they would function are still unclear. Elucidation of these factors is fundamental to achieving a better understanding of cell function.

We would like to thank Drs. E. D. Salmon and C. L. Rieder for stimulating discussion and helpful suggestions. We are also grateful to Drs. Frank Solomon and James Aist for their helpful comments on the manuscript.

This work was supported by National Institutes of Health grants RR 01192 and CA-22248, and by a grant from the Office of Naval Research (N 00014-86-K-0115).

Received for publication 25 April 1988

References

1. Bergen, L., R. Kuriyama, and G. G. Borisy. 1980. Polarity of microtubules nucleated by centrosomes and chromosomes of Chinese hamster ovary cells in vitro. *J. Cell Biol.* 84:151–159.
2. Berns, M. W., J. Aist, J. Edwards, K. Strahs, J. Girton, M. Kitzes, M. Hammer-Wilson, L. H. Liaw, A. Siemens, M. Koonce, S. Peterson, S. Brenner, J. Burt, R. Walter, P. J. Bryant, D. Dyk Van, J. Coulombe, T. Cahill, and G. S. Berns. 1981. Laser microsurgery in cell and developmental biology. *Science (Wash. DC).* 213:505–513.
3. Boyd, J. F., J. L. Frydenvang Keil, L. Pillus, R. C. Mulligan, and F. Solomon. 1986. A chicken-yeast chimeric β-tubulin protein is incorporated into mouse microtubules in vivo. *Cell.* 44:461–468.
4. Bre, M.-H., T. E. Kreis, and E. Karsenti. 1987. Control of microtubule nucleation and stability in Madin Darby canine kidney cells: the occurrence of noncentrosomal, stable detyrosinated microtubules. *J. Cell Biol.* 105:1283–1296.

Best Available Copy

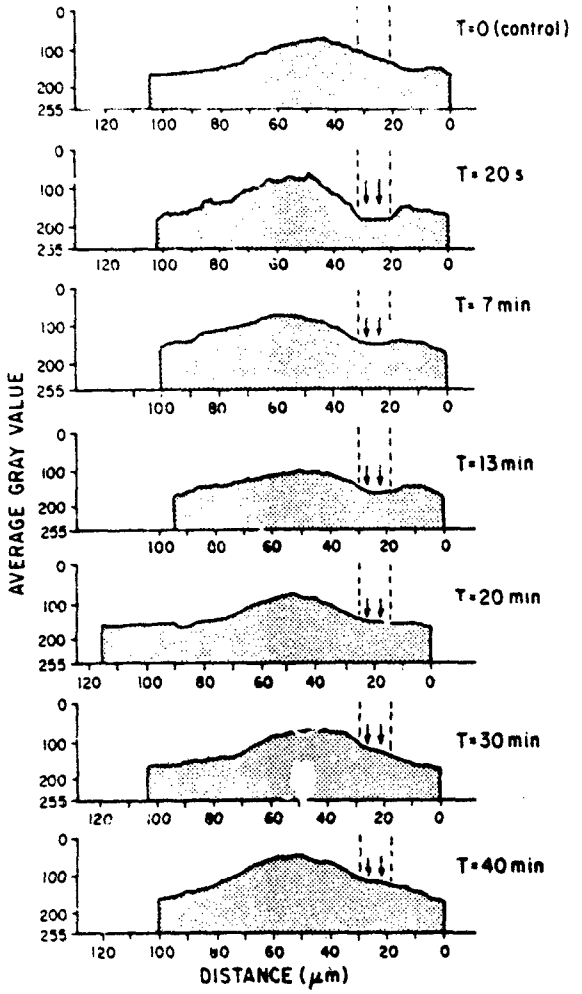

Figure 6. Average properties of the MT behavior as a function of time. The distributions of measured average gray values in each histogram correspond to the average variations in MT staining in the digital image of a cell. Distance was measured from one side of a cell edge to the other. *Arrows*, predefined regions; *dashed lines*, the actual transected zones on the fluorescence micrographs. *T*, the time intervals between irradiation and fixation; $T = 0$, untreated control cells.

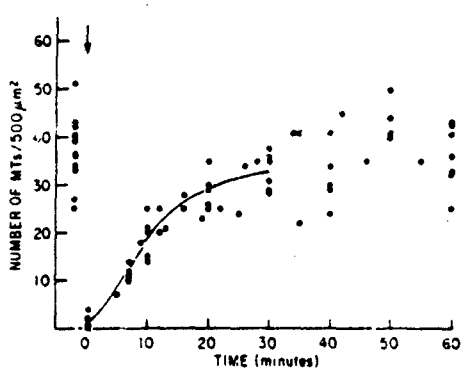

Figure 7. Increase in the number of MTs in transected zones with time. The MT density in both control cells (on the left side of the arrow) and experimental cells (on the right side of the arrow) was measured. The data points are collected from one (*solid circle*), six (*open triangle*), and nine cells (*open square*), respectively. *Arrow*, the time at which MTs were transected in situ.

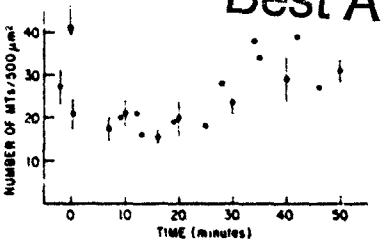

Figure 8. Quantification of MTs in regions distal from the transected zones. The MT density in both control cells (on the left side of the arrow) and experimental cells (on the right side of the arrow) was measured. *Arrow*, the time at which MTs were transected in situ. *Solid circles*, data from single cells; *error bars*, SDs.

5. Cassimeris, L. U., P. Wadsworth, and E. D. Salmon. 1986. Dynamics of microtubule depolymerization in monocytes. *J. Cell Biol.* 102:2023–2032.
6. Chalfie, M., and J. Thompson. 1979. Organization of neuronal microtubules in the nematode *Caenorhabditis elegans*. *J. Cell Biol.* 82:278–291.
7. Chen, Y.-D., and T. L. Hill. 1985. Theoretical treatment of microtubules disappearing in solution. *Proc. Natl. Acad. Sci. USA.* 82:4127–4131.
8. Cleveland, D. W., and K. F. Sullivan. 1985. Molecular biology and genetics of tubulin. *Annu. Rev. Biochem.* 54:331–365.
9. Cote, R. H., and G. G. Borisy. 1981. Head to tail polymerization of microtubules in vitro. *J. Mol. Biol* 150:577–602.
10. Dustin, P. 1984. Microtubules. Springer-Verlag New York, Inc., New York. 482 pp.
11. Euteneuer, U., and J. R. McIntosh. 1981. Structural polarity of kinetochore microtubules in PtK1 cells. *J. Cell Biol.* 89:338–345.
12. Fulton, C., and P. A. Simpson. 1976. Selective synthesis and utilization of flagellar tubulin: the multitubulin hypothesis. *Cell Motil.* 3:987–1005.
13. Gundersen, G., M. H. Kalnoski, and J. C. Bulinski. 1984. Distinct populations of microtubules: tyrosinated and nontyrosinated alpha tubulin are distributed differently in vivo. *Cell.* 38:779–789.
14. Haimo, L. T., J. R. Telzer, and J. L. Rosenbaum. 1979. Dynein binds to and crossbridges cytoplasmic microtubules. *Proc. Natl. Acad. Sci. USA.* 76:5759–5763.
15. Hill, T. L., and M.-F. Carlier. 1983. Steady-state theory of the interference of GTP hydrolysis in the mechanism of microtubule assembly. *Proc. Natl. Acad. Sci. USA.* 80:7234–7238.
16. Hill, T. L., and Y.-D. Chen. 1984. Phase changes at the end of a microtubule with a GTP cap. *Proc. Natl. Acad. Sci. USA.* 81:5772–5776.
17. Horio, T., and H. Hotani. 1986. Visualization of the dynamic instability of individual microtubules by dark-field microscopy. *Nature (Lond.).* 321:605–607.
18. Johnson, K. A., and G. G. Borisy. 1977. Kinetic analysis of microtubule self-assembly in vitro. *J. Mol. Biol.* 117:1–131.
19. Kim, S., M. Magendantz, W. Katz, and F. Solomon. 1987. Development of a differentiated microtubule structure: formation of the chicken erythrocyte marginal band in vivo. *J. Cell Biol.* 104:51–59.
20. Kirschner, M. 1980. Implications of treadmilling for the stability and polarity of actin and tubulin polymers in vitro. *J. Cell Biol.* 86:330–334.
21. Koonce, M. P., J. Tong, U. Euteneuer, and M. Schliwa. 1987. Active sliding between cytoplasmic microtubules. *Nature (Lond.).* 328:737–739.
22. Koshland, D. E., T. Mitchison, and M. Kirschner. 1988. Polewards chromosome movement driven by microtubule depolymerization in vitro. *Nature (Lond.).* 331:499–504.
23. Kristofferson, D., T. Mitchison, and M. Kirschner. 1986. Direct visualization of steady-state microtubule dynamics. *J. Cell Biol.* 102:1007–1019.
24. Lewis, S. A., W. Gu, and N. J. Cowan. 1987. Free intermingling of mammalian β-tubulin isotypes among functionally distinct microtubules. *Cell.* 49:539–548.
25. Margolis, R. L., and L. Wilson. 1978. Opposite end assembly and disassembly of microtubules at steady state in vitro. *Cell.* 13:1–8.
26. Margolis, R. L., and L. Wilson. 1981. Microtubule treadmills—possible molecular machinery. *Nature (Lond.).* 293:705–711.
27. Mitchison, T., and M. Kirschner. 1984. Microtubule assembly nucleated by isolated centrosomes. *Nature (Lond.).* 312:232–237.
28. Mitchison, T., and M. Kirschner. 1984. Dynamic instability of microtubule growth. *Nature (Lond.).* 312:237–242.
29. Okagaki, T., and R. Kamiya. 1986. Microtubule sliding in mutant *Chlamydomonas* axonemes devoid of outer or inner dynein arms. *J. Cell Biol.* 103:1895–1902.
30. Oosawa, F., and S. Asakura. 1975. Thermodynamics of the polymerization of protein. Academic Press, New York. 194 pp.
31. Osborn, M., and K. Weber. 1976. Cytoplasmic microtubules in tissue culture cells appear to grow from an organizing structure towards the plasma membrane. *Proc. Natl. Acad. Sci. USA.* 73:867–871.

32 Paschal, B. M., S. M. King, A. G. Moss, C. A. Collins, R. B. Vallee, and G. B. Witman. 1987. Isolated flagellar outer arm dynein translocates brain microtubules in vitro. *Nature (Lond.)*. 330:672–674.
33 Paschal, B. M., H. S. Shpetner, and R. B. Vallee. 1987. MAP 1C is a microtubule activated ATPase which translocates microtubules in vitro and has dynein like properties. *J. Cell Biol.* 105:1273–1282.
34 Roberts, K., and J. S. Hyams. 1979. Microtubules. Academic Press, New York. 595 pp.
35 Sale, W. S. 1986. The axonemal axis and Ca^{2+}-induced asymmetry of active microtubule sliding in sea urchin sperm tails. *J. Cell Biol.* 102:2042–2052.
36 Salmon, E. D., R. J. Leslie, W. M. Saxton, M. L. Karow, and J. R. McIntosh. 1984. Spindle microtubule dynamics in sea urchin embryos: analysis using a fluorescent-labeled tubulin and measurement of fluorescence redistribution after laser photobleaching. *J. Cell Biol.* 99:2165–2174.
37 Sammak, P. J., G. J. Gorbsky, and G. G. Borisy. 1987. Microtubule dynamics in vivo: a test of mechanisms of turnover. *J. Cell Biol.* 104:395–405.
38 Schulze, E., and M. Kirschner. 1986. Microtubule dynamics in interphase cells. *J. Cell Biol.* 102:1020–1031.
39 Schulze, E., and M. Kirschner. 1987. Dynamic and stable populations of microtubules in cells. *J. Cell Biol.* 104:277–288.
40 Soltys, B. J., and G. G. Borisy. 1985. Polymerization of tubulin in vivo: direct evidence for assembly onto microtubule ends and from centrosomes. *J. Cell Biol.* 100:1682–1689.
41 Srinivasan, R. 1986. Ablation of polymers and biological tissue by ultraviolet lasers. *Science (Wash. DC)*. 234:559–565.
42 Tao, W., J. Wilkinson, E. J. Stanbridge, and M. W. Berns. 1987. Direct gene transfer into human cultured cells facilitated by laser micropuncture of the cell membrane. *Proc. Natl. Acad. Sci. USA*. 84:4180–4184.
43 Vale, R. D., T. S. Reese, and M. P. Sheetz. 1985. Identification of a novel force-generating protein, kinesin, involved in microtubule-based motility. *Cell*. 42:39–50.
44 Water, R. J., and M. W. Berns. 1981. Computer enhanced video microscopy: images can be produced in real time. *Proc. Natl. Acad. Sci. USA*. 78:6927–6931.